

OKINAWA INSTITUTE OF SCIENCE AND TECHNOLOGY  
GRADUATE UNIVERSITY

Thesis submitted for the degree

Doctor of Philosophy

---

**Micro- and Nanoplastics in Okinawa -  
Potential Impacts on Planktonic Microalgae  
and Endosymbiotic Dinoflagellates**

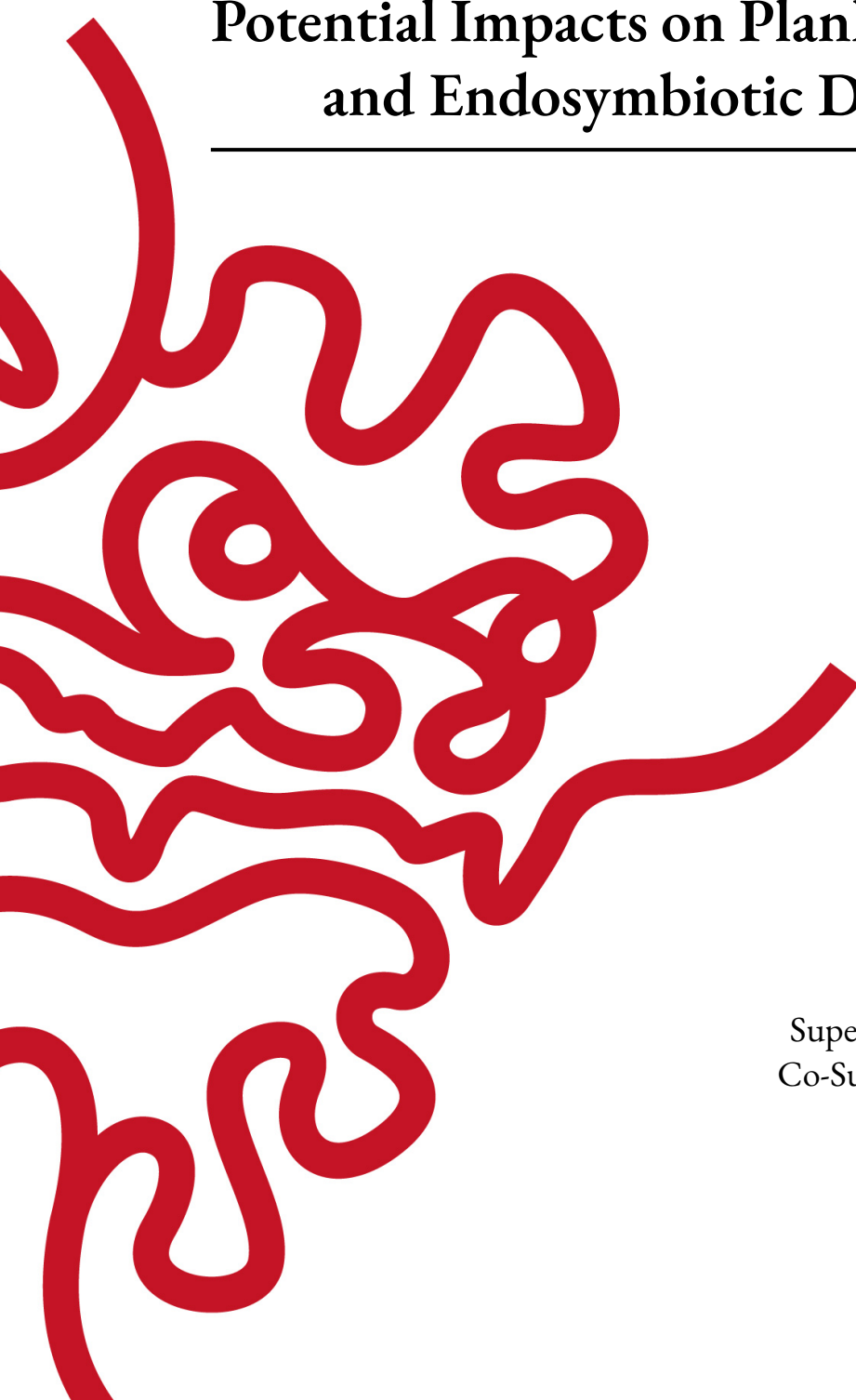
---

by

**Christina Helen Ripken**

Supervisor: **Prof. Síle Nic Chormaic**  
Co-Supervisor: **Prof. Noriyuki Satoh**

November 24th 2020







# Declaration of Original and Sole Authorship

I, Christina Helen Ripken, declare that this thesis entitled *Micro- and Nanoplastics in Okinawa - Potential Impacts on Planktonic Microalgae and Endosymbiotic Dinoflagellates* and the data presented in it are original and my own work. I confirm that:

- No part of this work has previously been submitted for a degree at this or any other university.
- References to the work of others have been clearly acknowledged. Quotations from the work of others have been clearly indicated, and attributed to them.
- In cases where others have contributed to part of this work, such contribution has been clearly acknowledged and distinguished from my own work.
- None of this work has been previously published elsewhere, with the exception of the following:
  - 1. Gregory S. Gavelis, Kevin C. Wakeman, Urban Tillmann, Christina Ripken, Satoshi Mitarai, Maria Herranz, Suat Özbek, Thomas Holstein, Patrick J. Keeling, Brian S. Leander, “Microbial arms race: Ballistic ‘nematocysts’ in dinoflagellates represent a new extreme in organelle complexity”, *Science Advance* (2017) e1602552
  - 2. Gregory S. Gavelis, Maria Herranz, Kevin C. Wakeman, Christina Ripken, Satoshi Mitarai, Gillian H. Gile, Patrick J. Keeling, Brian S. Leander, “Dinoflagellate nucleus contains an extensive endomembrane network, the nuclear net” *Scientific Report* 9, 839 (2019)

Date: November 24th 2020

Signature:

A handwritten signature in black ink, appearing to read 'Chr Ripken', written in a cursive style.



# Abstract

From coast to gyre, from surface to deep sea, the study of marine plastic pollution takes us on a journey of potential harm through our marine ecosystems, where man-made plastics break down into ever smaller pieces along their way. Studying micro- and nanoplastic pollution in field and laboratory work, new insights into microalgae interactions, and these smallest plastic particles were gathered. Mimicking two different environments in the laboratory - reef and open ocean water - an effect assessment of four different microalgae species (Diatoms *Skeletonema grethae* and *Odontella aurita*, cyanobacterium *Synechococcus elongatus*, endosymbiotic dinoflagellates *Symbiodinium tri-dacnidorum* and *Cladocopium* sp.) and their interaction with micro- and nanoplastics at different sizes, types, and concentrations was conducted. Aggregation, sedimentation, photosynthesis, extracellular substance production, and RNA expression patterns were all found to be affected. Specifically, hetero-aggregation with nanoplastic led to neutrally buoyant marine snow, differentially expressed genes, and reduced photosynthesis. Furthermore, an exposure assessment around Okinawa, an isolated subtropical island with fringing reefs, found that microplastic pollution follows the island's population gradient. Polyethylene was the most abundant polymer found 45%, and of the ubiquitous sub 20  $\mu\text{m}$  plastics, the majority was embedded in organic matter.



# Acknowledgment

I would like to start thanking my supervisors Profs. Síle Nic Chormaic and Noriyuki Satoh for their continuing personal and material support and kind encouragement throughout the thesis. I also want to thank my host at the University of Santa Barbara, Prof. Uta Passow for her support and help.

Throughout the thesis, I got help in the lab from various people. I want to specifically thank Thummanoon Jenarewong for his help with the TEP related lab work; Haruhi Narisoko and Megan Lowry for helping me with culturing of the microalgae; Girish Beedessee for teaching me about RNA extraction; Julia Sweet for helping with filtration and experimental set up and for teaching me how to handle aggregates with the care they deserve.

I want to thank Nigel D'souza, Eiichi Shoguchi, Konstantin Khalturin and Domna Kotsifaki for help with the data analysis and writing, proofing, or copy-editing of the corresponding manuscript. I want to thank Georg Fischer for copy-editing. For technical support, I want to thank Metin Ozer for helping with MATLAB and Fabien Benureau for Latex and MATLAB support.

I want to thank Thea Hamm and Angela Ares Pita for work discussion and Stefanie Kemp for refreshing my mind with talks of microplastic unrelated things.

I also thank the captain and crew of the Okinawa Prefectural Fisheries and Ocean Research Center ship, Tonan Maru, and the on-board team of Akinori Murata.

I am grateful to OIST DNA sequencing section for RNA preparation and sequencing. I also want to thank the OIST Imaging Section, the OIST Engineering Support Section and the OIST Research Support Division, as well as the University of Santa Barbara NRI-MCDB Microscopy Facility.

Last, but certainly not least, I am very grateful to my parents, Hartmut and Marcia, and my brother Alex for their unwavering support and help throughout this difficult and nerve-wrecking time. My kids, Kiki and Lucas, helped me through this, always ready to take my mind of work but also being very understanding when I was busy and stressed, in particular during the writing process. I want to thank Karim for his enduring support even when we were living oceans apart.



# Abbreviations

aMF	Acrylic microfiber
ANOVA	Analysis of variation
BPA	Bisphenol-A
BPC	Bisphenol-C
DDT	Dichlorodiphenyltrichloroethane
DEG	Differentially expressed genes
DOC	Dissolved organic matter
EPS	extracellular polymeric substances
ESD	Equivalent spherical diameter
ESP	Expanded polystyrene
FTIR	Fourier-transform infrared spectroscopy
μP	Microplastic
MF	Microfiber
microPS <sub>2</sub>	Micro Polystyrne beads at 2 μm diameter
MSFD	Marine strategy framework directive of the European Union
nP	Nanoplastic
NanoPS <sub>42</sub>	Nano Polystyrne beads at 42 nm diameter
NanoPS <sub>194</sub>	Nano Polystyrne beads at 194 nm diameter
PA	Polyamide
PAM	Pulse amplitude modulation
PCB	Polychlorinated biphenyl
PCR	Polymerase chain reaction
PE	Polyethylene
PET	Polyethylene terephthalate
pMF	Polyester microfiber
PMMA	Polymethyl methacrylate
POM	Particulate organic matter
POP	Persistent organic pollutants
PP	Polypropylene
PS	Polystyrene
PUR	Polyurethane
PVC	Polyvinyl-chloride
RNA	Ribonucleic acid
TEP	Transparent exopolymer particles
UV	Ultraviolet radiation
XRF	X-ray fluorescence spectroscopy

---

aMF	Acrylic microfiber
ANOVA	Analysis of variation
BPA	Bisphenol-A
BPC	Bisphenol-C
DDT	Dichlorodiphenyltrichloroethane
DEG	Differentially expressed genes
DOC	Dissolved organic matter
EPS	extracellular polymeric substances
ESD	Equivalent spherical diameter
ESP	Expanded polystyrene
FTIR	Fourier-transform infrared spectroscopy
µP	Microplastics
MF	Microfiber
microPS <sub>2</sub>	Micro Polystyrne beads at 2 µm diameter
MSFD	Marine strategy framework directive of the European Union
nP	Nanoplastic
NanoPS <sub>42</sub>	Nano Polystyrne beads at 42 nm diameter
NanoPS <sub>194</sub>	Nano Polystyrne beads at 194 nm diameter
PA	Polyamide
PAM	Pulse amplitude modulation
PCB	Polychlorinated biphenyl
PCR	Polymerase chain reaction
PE	Polyethylene
PET	Polyethylene terephthalate
pMF	Polyester microfiber
PMMA	Polymethyl methacrylate
POM	Particulate organic matter
POP	Persistent organic pollutants
PP	Polypropylene
PS	Polystyrene
PUR	Polyurethane
PVC	Polyvinyl-chloride
RNA	Ribonucleic acid
TEP	Transparent exopolymer particles
UV	Ultraviolet radiation
XRF	X-ray fluorescence spectroscopy



For  
Shohei Suzuki  
30.09.1979 - 14.11.2016  
for his love of the ocean



# Contents

<b>Declaration of Original and Sole Authorship</b>	<b>iii</b>
<b>Abstract</b>	<b>v</b>
<b>Acknowledgment</b>	<b>vii</b>
<b>Abbreviations</b>	<b>ix</b>
<b>Contents</b>	<b>xiii</b>
<b>List of Figures</b>	<b>xvii</b>
<b>List of Tables</b>	<b>xxi</b>
<b>1 General Introduction and Outline</b>	<b>1</b>
1.1 Anthropogenic Effects: The Origin of Marine Microplastics . . . . .	2
1.2 From Micro to Nanoplastic – It is Still Plastic . . . . .	8
1.3 From Plastic to Marine Habitats . . . . .	12
1.4 From Habitats to Risk Assessment . . . . .	16
1.5 Conclusions and Objectives . . . . .	17
<b>2 Micro- and Nanoplastic Particles in Marine Snow Formation</b>	<b>19</b>
2.1 The Carbon Cycle and Marine Snow . . . . .	19
2.1.1 Hetero-aggregation and its Implications . . . . .	22
2.1.2 Micro- and Nanoplastic in the Open Ocean Ecosystem . . . . .	24
2.2 Materials and Methods . . . . .	25
2.2.1 Roller Tanks . . . . .	25
2.2.2 Biological Materials . . . . .	27
2.2.3 Plastic Fibers and Beads characterization . . . . .	28
2.2.4 Exposure . . . . .	33
2.2.5 Aggregate Characterization: Sampling and Analysis . . . . .	33
2.3 Overview of the Experiments . . . . .	37
2.4 Results and Discussion . . . . .	46
2.4.1 Sinking Velocities . . . . .	47
2.4.2 Transparent exopolymer particles (TEP) concentration . . . . .	57

2.4.3	Photophysiology . . . . .	66
2.4.4	3D images reveal internal structure of aggregates . . . . .	71
2.5	Conclusions . . . . .	75
<b>3</b>	<b>Micro- and Nanoplastic around Okinawa</b>	<b>77</b>
3.1	Environmental Risk Assessments of Micro- and Nanoplastic in Okinawa . . . . .	77
3.2	Materials and Methods . . . . .	80
3.2.1	Study Region . . . . .	80
3.2.2	Field Sampling . . . . .	80
3.2.3	Laboratory Analysis . . . . .	82
3.2.4	X-ray fluorescence (XRF) spectroscopy for trace metal detection . . . . .	82
3.2.5	Micro-Raman Raman Spectroscopy . . . . .	84
3.2.6	Risk Assessment . . . . .	86
3.3	Results and Discussion . . . . .	89
3.3.1	Distribution and Abundance on Microplastics . . . . .	89
3.3.2	Trace Metal Distribution and Abundance on Microplastic . . . . .	96
3.3.3	Distribution and Abundance of sub-20 $\mu\text{m}$ and Nanoplastic . . . . .	104
3.3.4	Risk Analysis . . . . .	111
3.4	Conclusion . . . . .	112
<b>4</b>	<b>Nanoplastic Toxicity in Endosymbiotic Dinoflagellates</b>	<b>115</b>
4.1	Nanoplastic Pollution in Coral Reef Environments . . . . .	115
4.2	Coral Reef Environments - Not Just Corals . . . . .	117
4.3	Materials and Methods . . . . .	119
4.3.1	Roller tanks . . . . .	120
4.3.2	Biological materials . . . . .	120
4.3.3	Exposure . . . . .	121
4.3.4	Aggregate characterization: sampling and analysis . . . . .	122
4.4	Results and Discussion . . . . .	127
4.4.1	NanoPS <sub>42</sub> exposure influences the size and number of cell aggregates . . . . .	128
4.4.2	Photophysiology . . . . .	132
4.4.3	Suppression of Algal Growth under nanoPS <sub>42</sub> Exposure . . . . .	135
4.4.4	Composition, 3D imaging for Internal Structure . . . . .	137
4.4.5	NanoPS <sub>42</sub> Effects on Gene Expression . . . . .	142
4.5	Conclusion . . . . .	146
<b>5</b>	<b>Conclusion and Outlook</b>	<b>149</b>
5.1	Open Ocean - Plankton Communities Under Change . . . . .	149
5.2	Coastal Waters - Plastics around Okinawa . . . . .	150
5.3	Inside the Reef - Impacts on Endosymbionts . . . . .	150
<b>A</b>	<b>Articles under review</b>	<b>183</b>

---

<b>B</b>	<b>Genes that responded to nanoplastic exposure in <i>Symbiodinium tridacnidorum</i> and <i>Cladocopium</i> sp.</b>	<b>215</b>
<b>C</b>	<b>Tables of Microplastics found and analyzed, with optical images</b>	<b>231</b>
<b>D</b>	<b>3D images for species in Chapter 2</b>	<b>245</b>
D.1	3D images in <i>Synechococcus elongatus</i> . . . . .	249
D.2	3D images of <i>Skeletonema grethae</i> . . . . .	257
D.3	3D images in <i>Odontella aurita</i> . . . . .	273



# List of Figures

1.1	Thermosets vs thermoplastics . . . . .	3
1.2	Where does the plastic pollution originate? . . . . .	7
1.3	Plastic debris sizing . . . . .	9
1.4	Leaching, adsorption and desorption . . . . .	11
1.5	Potential pathways . . . . .	13
1.6	Plankton-plastic aggregate formation . . . . .	15
2.1	Oceanic carbon pump . . . . .	21
2.2	Buoyancy of different polymer types . . . . .	23
2.3	Oceanic carbon pump with plastic infiltration . . . . .	24
2.4	Pictures of tank series used . . . . .	26
2.5	Optical image polystyrene beads . . . . .	28
2.6	$\zeta$ -potential . . . . .	30
2.7	3D image of nanoPS <sub>194</sub> agglomerate . . . . .	31
2.8	Raman spectra acrylic . . . . .	32
2.9	Raman spectra polyester . . . . .	32
2.10	Glass cylinder image . . . . .	34
2.11	Optical images of filters prepared for cell counting . . . . .	35
2.12	3D imaging program ‘Imaris’ spot tool . . . . .	36
2.13	Light curve for PAM measurements . . . . .	37
2.14	<i>Skeletonema grethae</i> setup in climate chamber . . . . .	39
2.15	Optical image of <i>Odontella aurita</i> infection . . . . .	41
2.16	Optical images of <i>Odontella aurita</i> aggregates . . . . .	42
2.17	Bubbles in nanoPS <sub>42</sub> experiment on <i>Synechococcus elongatus</i> . . . . .	43
2.18	Sampling set up polyester MF experiment on <i>Synechococcus elongatus</i> . . . . .	44
2.19	Sampling set up acrylic MF experiment in <i>Synechococcus elongatus</i> . . . . .	45
2.20	<i>Synechococcus elongatus</i> rolling table set-up . . . . .	46
2.21	Comparison of sinking velocities over all experiments . . . . .	48
2.22	<i>Skeletonema grethae</i> sinking velocities . . . . .	49
2.23	Dense aggregates in <i>Skeletonema grethae</i> nanoPS <sub>194</sub> experiment . . . . .	50
2.24	nanoPS <sub>42</sub> experiment in <i>Skeletonema grethae</i> tank image comparison . . . . .	51
2.25	Polyester MF in <i>Skeletonema grethae</i> aggregates . . . . .	52
2.26	<i>Odontella aurita</i> sinking velocities . . . . .	54
2.27	<i>Synechococcus elongatus</i> sinking velocities . . . . .	55
2.28	Transparent exopolymer particles (TEP) in <i>Skeletonema grethae</i> . . . . .	58
2.29	Aggregates numbers microPS <sub>2</sub> <i>Skeletonema grethae</i> experiment . . . . .	59

2.30	Aggregates numbers in nanoPS <sub>194</sub> <i>Skeletonema grethae</i> experiment . . . . .	59
2.31	Number of aggregates in pMF <i>Skeletonema grethae</i> experiment . . . . .	60
2.32	Different aggregate size distribution in <i>Synechococcus elongatus</i> nanoPS <sub>194</sub> exp. . . . .	61
2.33	Different aggregate size distribution in <i>Synechococcus elongatus</i> nanoPS <sub>42</sub> exp. . . . .	62
2.34	Comparison between nanoPS <sub>194</sub> and pMF TEP . . . . .	63
2.35	<i>Synechococcus elongatus</i> acrylic MF dust aggregation . . . . .	64
2.36	Comparison between nanoPS and aMF TEP . . . . .	65
2.37	Photophysiology – <i>Skeletonema grethae</i> F <sub>0</sub> measurements . . . . .	67
2.38	Photophysiology – <i>Skeletonema grethae</i> QY <sub>max</sub> measurements . . . . .	68
2.39	3D images for the nanoPS <sub>42</sub> experiments in <i>Synechococcus elongatus</i> . . . . .	72
2.40	3D images of microPS <sub>2</sub> aggregates in <i>Skeletonema grethae</i> . . . . .	73
2.41	3D image of <i>Odontella aurita</i> . . . . .	74
3.1	Map of Okinawa and Kuroshio Current . . . . .	78
3.2	Sampling and analysis of marine pollution found around Okinawa . . . . .	79
3.3	Map of field study area . . . . .	81
3.4	Biota on sampled $\mu$ P . . . . .	84
3.5	Micro-Raman optical tweezers setup . . . . .	85
3.6	Optical image of micro particle trapping process . . . . .	86
3.7	Correlation Population density to $\mu$ P distribution . . . . .	92
3.8	Raman spectrum of three $\mu$ P . . . . .	93
3.9	Optical images of 8 $\mu$ P particles . . . . .	94
3.10	Raman of 8 $\mu$ P particles . . . . .	95
3.11	Trace metal distribution on PP $\mu$ P particle 46 . . . . .	96
3.12	Trace metal distribution on PE $\mu$ P particle 24 . . . . .	97
3.13	Trace metal distribution on PE $\mu$ P particle 12 . . . . .	98
3.14	Optical image and trace metal distribution of PE $\mu$ P particle 4 . . . . .	99
3.15	Trace metal distribution on $\mu$ P particle 21 . . . . .	100
3.16	Trace metal distribution on PE $\mu$ P particle 69 . . . . .	101
3.17	Trace metal distribution on PS $\mu$ P particle 31 . . . . .	102
3.18	Trace metal distribution on $\mu$ P particle 35 of unknown polymer type. . . . .	103
3.19	Plastic particle composition . . . . .	104
3.20	Correlation population density to sub-20 $\mu$ m distribution . . . . .	106
3.21	Raman spectrum of sub-20 $\mu$ m PVC particle . . . . .	107
3.22	Raman spectrum of microscope slide and organic matter found in the samples . . . . .	108
3.23	Raman spectra of optically trapped $\mu$ P/nPs . . . . .	109
3.24	Raman spectra of optically trapped minerals . . . . .	110
3.25	Summary of all particles analysed . . . . .	112
4.1	Endosymbiotic dinoflagellates experimental set up . . . . .	119
4.2	Images of host animals . . . . .	121
4.3	Symbiodiniaceae aggregate size classes . . . . .	123
4.4	Photophysiology – Light curve . . . . .	124
4.5	Photophysiology – Spacing of measuring points in light curve . . . . .	125
4.6	Photophysiology – Reference for Symbiodiniaceae . . . . .	126
4.7	Symbiodiniaceae sinking velocity . . . . .	128



4.8	3D image of medium aggregate under high nanoPS <sub>42</sub> exposure . . . . .	129
4.9	Altered aggregate size distribution in Symbiodiniaceae . . . . .	130
4.10	Enhanced aggregation under NanoPS <sub>42</sub> exposure in Symbiodiniaceae . . . . .	131
4.11	rETR correlation to QY <sub>max</sub> under nanoPS <sub>42</sub> exposure in Symbiodiniaceae . . . . .	133
4.12	Changes in QY <sub>max</sub> in Symbiodiniaceae . . . . .	134
4.13	Changes in rETR in Symbiodiniaceae . . . . .	134
4.14	Cell abundance changes in daily comparison in Symbiodiniaceae . . . . .	136
4.15	Cell abundance changes under nanoPS <sub>42</sub> exposure in Symbiodiniaceae . . . . .	137
4.16	3D image of aggregate under control nanoPS <sub>42</sub> . . . . .	139
4.17	3D image of aggregate under low nanoPS <sub>42</sub> exposure . . . . .	140
4.18	3D image of aggregate under medium nanoPS <sub>42</sub> exposure . . . . .	141
4.19	3D image of aggregate under high nanoPS <sub>42</sub> exposure with nanoPS <sub>42</sub> clusters . . . . .	142
4.20	Heatmap and clustering in <i>Symbiodinium tridacnidorum</i> . . . . .	143
4.21	Heatmap and clustering in <i>Cladocopium</i> sp. . . . .	144
4.22	Changes in symbiotic dinoflagellate cell under nanoPS <sub>42</sub> exposure . . . . .	147
D.1	Lightsheet internal view and schematic of the set-up of the light sheet . . . . .	245
D.2	Method of measuring internal structure through 3D fluorescent microscopy . . . . .	246
D.3	Method of visualizing internal structure through 3D fluorescent microscopy . . . . .	247
D.4	Method for cell counting in 3D images . . . . .	248
D.5	Method for plastic counting in 3D images . . . . .	249
D.6	3D images of a <i>Synechococcus elongatus</i> control aggregate . . . . .	250
D.7	Optical and 3D images of <i>Synechococcus elongatus</i> agg. with 0.01 mg/L nanoPS <sub>194</sub> . . . . .	251
D.8	Optical and 3D images of <i>Synechococcus elongatus</i> agg. with 1 mg/L nanoPS <sub>194</sub> . . . . .	252
D.9	3D images of <i>Synechococcus elongatus</i> control agg. in the nanoPS <sub>42</sub> experiments . . . . .	253
D.10	3D image collage for <i>Synechococcus elongatus</i> in nanoPS <sub>42</sub> exp. at 1 mg/L . . . . .	254
D.11	3D images for the dust aggregates in aMF experiments of <i>Synechococcus elongatus</i> . . . . .	256
D.12	3D images of microPS <sub>2</sub> aggregate in <i>Skeletonema grethae</i> control . . . . .	258
D.13	3D images of microPS <sub>2</sub> aggregate in <i>Skeletonema grethae</i> 0.01 mg/L treatment . . . . .	259
D.14	3D images of microPS <sub>2</sub> aggregate in <i>Skeletonema grethae</i> in 10 mg/L treatment . . . . .	260
D.15	3D images of nanoPS <sub>194</sub> control aggregate in <i>Skeletonema grethae</i> . . . . .	262
D.16	3D images of nanoPS <sub>194</sub> 0.01 mg/L treatment aggregate in <i>Skeletonema grethae</i> . . . . .	263
D.17	3D images of nanoPS <sub>194</sub> 1 mg/L treatment aggregate in <i>Skeletonema grethae</i> . . . . .	264
D.18	3D images of nanoPS <sub>194</sub> 10 mg/L treatment aggregate in <i>Skeletonema grethae</i> . . . . .	265
D.19	3D images of nanoPS <sub>42</sub> control aggregate in <i>Skeletonema grethae</i> . . . . .	266
D.20	3D images of nanoPS <sub>42</sub> 0.01 mg/L treatment aggregate in <i>Skeletonema grethae</i> . . . . .	267
D.21	3D images of nanoPS <sub>42</sub> 1 mg/L treatment aggregate in <i>Skeletonema grethae</i> . . . . .	268
D.22	3D images of nanoPS <sub>42</sub> 10 mg/L treatment aggregate part in <i>Skeletonema grethae</i> . . . . .	269
D.23	3D images of pMF aggregate A in <i>Skeletonema grethae</i> . . . . .	271
D.24	3D images of pMF aggregate B in <i>Skeletonema grethae</i> . . . . .	272
D.25	Method for cell counting in 3D images in <i>Odontella aurita</i> . . . . .	273
D.27	3D Image of infected control aggregate of <i>Odontella aurita</i> . . . . .	274
D.26	Images of a clean control aggregate of <i>Odontella aurita</i> . . . . .	275
D.28	Images of <i>Odontella aurita</i> under microPS <sub>2</sub> exposure . . . . .	276
D.29	Images of <i>Odontella aurita</i> under nanoPS <sub>194</sub> exposure . . . . .	277
D.30	Images of <i>Odontella aurita</i> under acrylic MF exposure . . . . .	278

D.31 Images of infected <i>Odontella aurita</i> under nanoPS <sub>42</sub> exposure . . . . .	279
---	-----

# List of Tables

1.1	Thermoplastics chemical structure . . . . .	4
1.2	Raman modes of polystyrene (PS) . . . . .	5
2.1	Tank measurements . . . . .	27
2.2	Plastic particle details . . . . .	29
2.3	$\zeta$ -potential . . . . .	30
2.4	Experiment overview . . . . .	38
2.5	<i>Odontella aurita</i> treatment distribution . . . . .	41
2.6	Color coding for results in chapter 2 . . . . .	47
2.7	Aggregate volume comparison for <i>Skeletonema grethae</i> . . . . .	53
2.8	Aggregate volume comparison for <i>Odontella aurita</i> . . . . .	54
2.9	Aggregate volume comparison for <i>Synechococcus elongatus</i> . . . . .	57
2.10	T-tests for fraction comparison of TEP in pMF <i>Synechococcus elongatus</i> . . . . .	63
2.11	T-tests for fraction comparison on TEP in aMF <i>Synechococcus elongatus</i> . . . . .	65
2.12	Photophysiology – measurements of $F_0$ in a negative control . . . . .	66
2.13	Photophysiology – $F_0$ statistics . . . . .	66
3.1	Log book data for the field research . . . . .	83
3.2	Risk level categories . . . . .	87
3.3	Polymer types found around Okinawa . . . . .	89
3.4	Micro- and nanoplastic particles found around Okinawa . . . . .	90
3.5	Nanoplastics distribution around Okinawa . . . . .	105
3.6	Raman modes of polyvinyl chloride (PVC) . . . . .	107
3.7	Raman modes of polyethylene (PE) . . . . .	109
3.8	Pollution load index for the stations around Okinawa for $\mu\text{P}$ . . . . .	112
4.1	Sampling schedule for biological replicas . . . . .	122
4.2	Aggregate volume comparison for Symbiodiniaceae . . . . .	138
4.3	Domains encoded by more than three upregulated genes in <i>Cladocopium</i> sp. . . . .	145
4.4	Domains encoded by more than three downregulated genes in <i>Cladocopium</i> sp. . . . .	146
B.1	Genes that responded to nanoplastic exposure in <i>Symbiodinium tridacnidorum</i> . . . . .	215
B.2	Genes that responded to nanoplastic exposure in <i>Cladocopium</i> sp. . . . .	220
B.3	Differentially expressed genes with 2-fold difference between the controls and nP exposure in <i>Symbiodinium tridacnidorum</i> . . . . .	224
B.4	Differentially expressed genes with 2-fold difference between the controls and nP exposure in <i>Cladocopium</i> . . . . .	225

---

C.1	Optical image and description of 8 $\mu$ P from Station 1, Nakagusku . . . . .	232
C.2	Optical image and description of 9 $\mu$ P from Station 2, Nakagusku . . . . .	233
C.3	Optical image and description of 6 $\mu$ P from Station 3, Kin . . . . .	235
C.4	Optical image and description of 5 $\mu$ P from Station 4, Kin . . . . .	236
C.5	Optical image and description of 2 $\mu$ P from Station 5, Oura . . . . .	237
C.6	Optical image and description of 4 $\mu$ P from Station 6, Cape Hedo . . . . .	238
C.7	Optical image and description of 2 $\mu$ P from Station 8, Nago . . . . .	239
C.8	Optical image and description of 6 $\mu$ P from Station 9, Nago . . . . .	240
C.9	Optical image and description of 24 $\mu$ P from Station 10, Naha . . . . .	241
C.10	Optical image and description of 7 $\mu$ P from Station 11, Naha . . . . .	244

# Chapter 1

## General Introduction and Outline

### Arriving in the Age of Plastic

In ancient times, raw materials were found in nature and used to produce tools and objects that humans need in their daily lives. When these objects were worn out, they were either repaired or repurposed. This first recycling of artifacts has been observed within multiple industries during the Paleolithic period [1], ranging further into the Neolithic [2], all the way into the Bronze and Iron Ages [3]. In the literature, recycling has been mentioned in the context of studying human use of resources as early as 1906 [4] and, notwithstanding that recycling has different goals and mechanisms within different cultural landscapes, the concept displays a respect for the limits of resources [5, 6]. Recycling ranges from simple repurposing (old hand axes to smaller flint tools) to repairing (Kintsugi technique is the Japanese art of repairing broken pottery by mending with urushi lacquer and highlighting the seam with a mixture of powdered gold, silver, or platinum) to reinventing (reclaiming post-industrial building structures for new purposes, changing factories into lofts) and ultimately leads to a circular economy (emphasizing the benefits of recycling residual waste materials and by-products through the development of complex economic cycles). Today, this sustainable resource recovery and product life-extension is seen as something new and many countries and cultures take time to integrate recycling. But looking back in time recycling is clearly a long-standing best practice by humans.

The use of moldable polymers also dates back until at least the late Bronze Age, as organic materials such as latex-based rubbers and shellacs (resin secreted by the female lac bug) were used for containers and water-proofing coatings [7]. These natural occurring polymers are compostable in their original state. In the 20th century, our modern world and our attitude towards consumption was largely shaped by one single and apparently limitless natural resource: oil [8]. Derived from oil and even more influential in the 21st century, plastic challenges our intuition about natural resources. If we consider ecosystem-derived materials that humans have traditionally used for tools and housing such as stone (can be shaped with time and effort, heavy and breakable), metal (can be molded with special techniques, heavy and only durable when well-preserved) and natural polymers (can be molded, high in production costs and therefore often unsuitable at industrial scale), each of those come with preexisting conditions making them less suitable for the task. Plastic, on the other hand, has the advantages of being cheap, abundant, durable, lightweight and moldable.

One of the main advantages of plastic, its durability, has proven detrimental in combination with modern single-use applications. Traditionally seen as a drawback, decomposing materials become part of the elemental cycle of the earth after being discarded into nature. Plastics can last

centuries in the environment [9], all the while releasing toxins and chemicals, such as Bisphenol-A (BPA) [10].

Using our planet's limited resources sustainably depends to a great deal on using plastic in a more responsible way, conserving limited fossil fuel resources, as well as reducing environmental pollution - in this case marine plastic pollution. Plastic, either still in use or as waste, often ends up in the ocean, as the lightweight polymer is easily transported via wind and rain. The resulting marine plastic pollution comes in all shapes and sizes, from big plastic sheets used for soil cover and dragged away by wind to the tiny plastic beads used in toothpaste.

## 1.1 Anthropogenic Effects: The Origin of Marine Microplastics

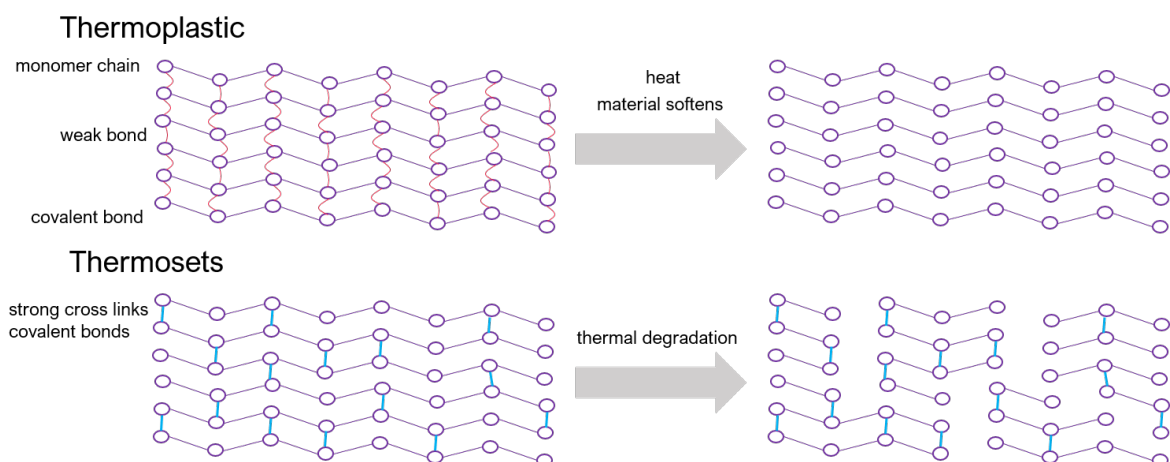
The Anthropocene has been nicknamed the “age of plastic”, making it the first period in the history of our planet which is shaped more by one single species - humans - than by the combination of all other species [11]. Particles made of plastic can be found in every part of the planet, from the higher layers of the atmosphere [12] to the deepest oceanic trenches [13](see Figure 1.2). Plastic will leave a geological imprint in fossil records [14] and marine plastic pollution, being irreversible and globally ubiquitous [15], is considered to be a potential planetary boundary threat [16]. A planetary boundary threat is defined as disruption of our plants vital ecosystems functions on a global scale that when crossed cannot be reversed. [17]. Should plastic pollution, in particular microplastic ( $\mu\text{P}$ ) pollution turn out to be such a planetary boundary threat, the plastic-induced shift in the earth's ecosystems function will generate rising risks for our societies. Boundaries should be set in a way to prevent such shifts, but for that, more information about  $\mu\text{P}$  effects in the global ecosystem is needed.  $\mu\text{P}$  is found at all levels of the marine food web, from krill to whales, and in many terrestrial life forms, including humans [18]. Assessing the possible changes induced by plastic in the environment is important for the future, especially in the light of other imminent threats to our plant's ecosystems.

### Synthetic Polymers

Plastic is ubiquitous and there is no way of eliminating it from daily use, nor is there a viable replacement for most of its applications. On the opening page of their book ‘Plastics’, Yarsley & Couzens [19] consider that ‘the possible applications [of plastics] are almost inexhaustible’. Unmatched flexibility is the reason for the usage of plastic reaching an indispensable status, with extensive industrial, medicinal, commercial, as well as municipal and research applications in modern society [20].

Plastic - being a durable, cheap, and lightweight material, making its application extremely versatile and ideal for mass production - is an integral part of our society. There are two categories of polymers that are used in plastic production. Thermoplastics melt when heated and harden when cooled. This process is reversible, and materials can be reheated and reshaped repeatedly. Most of our everyday plastics belong to this group, including polyethylene (PE), polypropylene (PP), polyvinyl-chloride (PVC), polyethylene terephthalate (PET), polystyrene (PS), expanded polystyrene (ePS), poly-amid (PA), polymethyl methacrylate (PMMA) (see Table 1.1). These plastics are often polymerized into pre-production pellets for easier transport. Additives are added to stabilize these plastics from softening under normal use conditions, as temperatures at which they are rigid

can easily be exceeded (see Figure 1.1). The second category is called thermosets. They undergo a chemical change when heated, preventing the possibility of being reheated and reshaped, they are “set” once they cool. This category includes polyester, acrylic and vinyl.



**Figure 1.1: Why can some plastics be reshaped?** In order to recycle a material efficiently, it has to be reheatable and reformable, as for instance glass. Thermoplastics only form weak links when cooling in their desired form between the monomer chains. These weak bonds break when the material is reheated which both increases thermal degradation but also makes recycling possible. In contrast, the thermosets form strong cross-links between the monomer chains when cooling, creating a three dimensional network. This makes them more heat resistant and not remoldable, heat application will lead to thermal degradation, breaking the monomer chains before the cross-linkages.

The common term “plastic” refers to synthetic organic polymers, derived from the polymerization of monomers which are extracted from fossil oil and gas [21, 22]. Although they might look the same to the naked eye, plastic polymers vary widely in their molecular structure. This difference in structure leads to problems, e.g. being able to recycle them efficiently, but also has the advantage of making polymers easily identifiable via their spectral footprint. Spectral analysis techniques such as Raman spectroscopy or Fourier-transform infrared spectroscopy (FTIR) display the unique spectrum of each material which makes identification of plastics without a label possible (see Table 1.2).

**Table 1.1: Chemical structure of thermoplastic polymers [23].** The difference in chemical structure makes identification via Raman spectroscopy possible through a difference in vibrations in the molecule. Density is included to illustrate differences in buoyancy behavior when introduced into the marine environment.

Thermoplastics	Abbreviation	Density (g/cm <sup>3</sup> )	Chemical Structure
Polyethylene	PE	0.91 – 0.96	$\left[ \text{CH}_2 - \text{CH}_2 \right]_n$
Polypropylene	PP	0.90 – 0.91	$\left[ \begin{array}{c} \text{CH}_3 \\   \\ \text{CH} - \text{CH}_2 \end{array} \right]_n$
Polystyrene	PS	0.96 – 1.05	$\left[ \begin{array}{c} \text{C}_6\text{H}_5 \\   \\ \text{CH} - \text{CH}_2 \end{array} \right]_n$
Polyamid	PA	1.01 – 1.42	$\left[ \begin{array}{c} \text{H} \\   \\ \text{N} - \text{C} - \text{R} \\    \\ \text{O} \end{array} \right]_n$
Polyvinyl Chloride	PVC	1.16 – 1.58	$\left[ \begin{array}{c} \text{Cl} \\   \\ \text{CH}_2 - \text{CH} \end{array} \right]_n$
Polymethyl methacrylate	PMMA	1.18 – 1.20	$\left[ \begin{array}{c} \text{CH}_3 \\   \\ \text{CH}_2 - \text{C} \\   \\ \text{C} \\ / \quad \backslash \\ \text{O} \quad \text{O} \\ \backslash \quad / \\ \text{CH}_3 \end{array} \right]_n$
Polyethylene Terephthalate	PET	1.37 – 1.45	$\text{H} \left[ \begin{array}{c} \text{O} \\ // \\ \text{C} - \text{C}_6\text{H}_4 - \text{C} \\ // \quad \backslash \\ \text{O} \quad \text{O} \end{array} \right] \text{O} - \text{CH}_2 - \text{CH}_2 \left. \right]_n \text{OH}$

FTIR and Raman spectroscopy have different detection mechanism for vibrations within the molecule after absorption of the radiation required to excite the molecule. Vibrations modifying the dipole moment of a molecule are detected by FTIR, whereas Raman scattering detects vibrations modifying the polarizability of a molecule. Some vibrations can modify both polarizability and dipole moment, and are determined by both FTIR and Raman spectroscopy. Raman spectroscopy can also detect rotational and low-frequency modes of a system, so it is commonly used to provide a structural fingerprint of molecules for identification. Symmetric stretches and bends in a molecule tend to be more Raman active and vibrations detected by Raman spectroscopy do not change the center of symmetry in the molecule (see Table 1.2). Vibrations of the backbone of long



polymer chains cause no change in the dipole moment due to canceling out of adjacent dipoles by repeating units, but cause significant changes in polarizability. Hence, polymer backbone structure and conformation can be analyzed using Raman spectroscopy (for chemical structure of common plastics see Table 1.1). In this thesis Raman analysis was used for the identification of the environmental polymer samples.

**Table 1.2: Raman modes of polystyrene (PS):** while this polymer displays all these modes, not all of them are always observed. Differences in the exact wavelength of the peaks are due to different excitation (laser) wavelength as well as the purity of the material. As seen in the Raman modes below, only the peak at about 1437 nm refers to the backbone of the polymer, while the other peaks refer to the aromatic ring structure [24].

$\nu$ (cm <sup>-1</sup> )	Vibration
1588	Aromatic C=C stretching
1437	CH <sub>2</sub> deformation
1183	Aromatic ring stretching
1152	Aromatic CH in plane deformation
1026	Aromatic CH in plane deformation
998	Aromatic ring breathing mode
793	Aromatic C=C out of plane deformation
622	Aromatic C=C in plane ring deformation

## History of Synthetic Polymers

As “plastic” refers to this wide range of materials, there is no single discovery date. Different plastics were discovered at different times by different people. Many chemists contributed to the material science of plastics, including Nobel laureate Hermann Staudinger who has been called “the father of polymer chemistry” and Herman Mark, known as “the father of polymer physics”. One notable discovery was that of polystyrene by a German apothecary Eduard Simon in 1839 [25]. The first fully synthetic plastic was discovered in 1907 - Bakelite, a thermoset [7]. Because of its electrical non-conductivity and heat-resistant properties, it gained wide use in electrical insulators, radio and telephone casings as well as kitchenware, children’s toys, and firearms. Old Bakelite products are nowadays considered collectibles. By 1910, Bakelite was in mass production [26].

From 1920 to 1940 there was a shift from using thermosets to thermoplastics, as the sites of plastic production disassociated from the sites of production of the end product. Companies such as DuPont and BASF went into mass production of nylon and PS, respectively. The 1950s saw a massive increase in mean annual production of over 1.5 millions tons [27] and expansion of plastic use into increasingly more parts of human society (packaging, construction, car production). In 2020, plastic production was expected to surpass 370 million tons [28] and to supply over 1.6 million jobs in Europe alone. Asia produces over 51% of all plastics worldwide with 30% of the production in China alone. It accounts for more than 8% of global oil production [12]. Development of new plastics continues until today [29].

Plastic has invaded every aspect of life in the 100 years since mass production started. In this relatively short time, plastic is viewed by some as a massive global problem with an unclear outcome that needs monitoring [30]. Clothing, worn directly on our skin or used to create a waterproof

second outside layer of protection, often contain various degrees of plastic polymers [31]. From cheap to expensive, from casual to business and formal, from designer to mass-produced and in every local industry, plastic has a great functional, color and tactile impact on the fabrics used [32]. It is ever-present in our houses, from carpets to wall paints and from flooring to ceiling covers, plastic is an integral part of our housing industry [28]. Interior designs products such as beds linens, shower curtains, heat resistant gloves in the kitchen, microfiber (MF) cleaning cloth; the list of applications goes on and is nearly inexhaustible. We do not just have a plastic solution for every household and clothing item, all our modern comforts are plastic-made as well, from cell phones to food packaging.  $\mu$ P and additives leach from the packaging into the food, creating a potential estimated source of chemical exposure [18]. We add  $\mu$ P to beauty products and household cleaners. With the increasing world population and expanding industrialization of societies, the yearly plastic production increases as well [28]. This is a worldwide phenomenon, spanning all economic and social classes across all continents.

## Marine Plastic Pollution

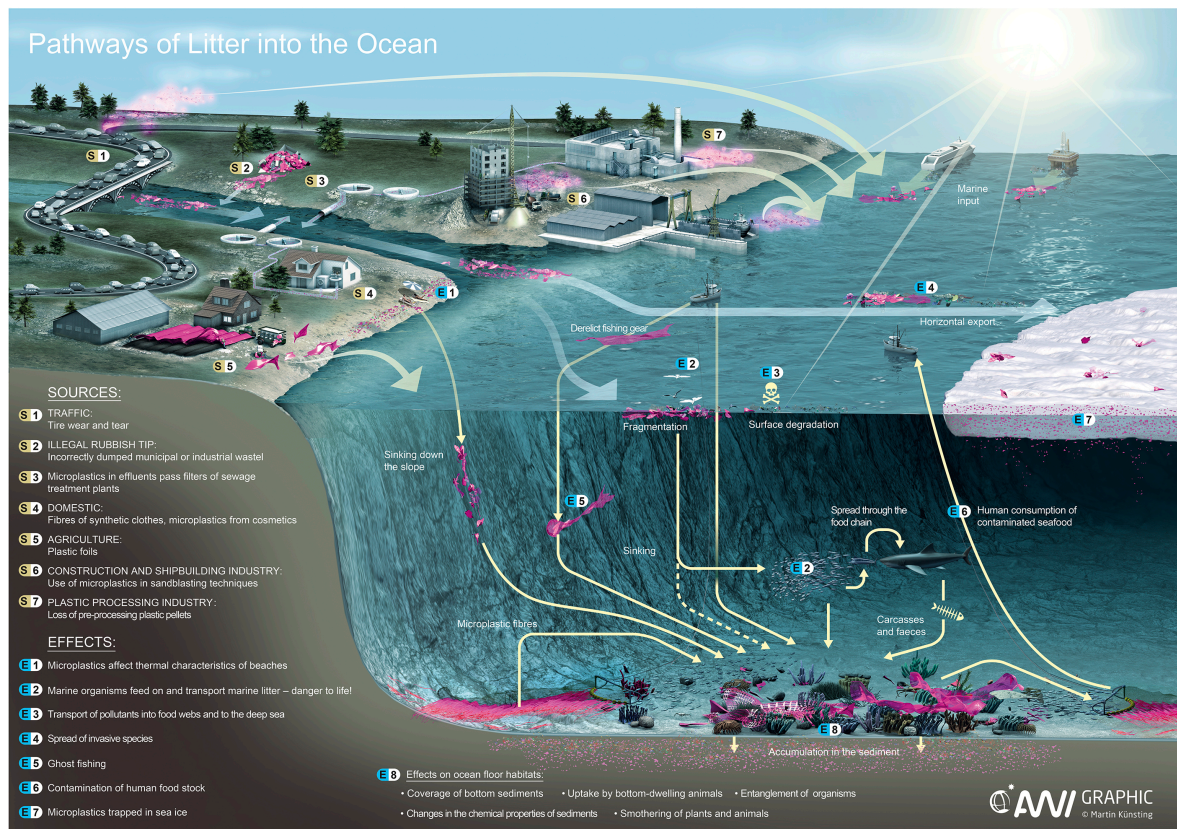
Plastic debris is accumulating at a rapid rate in coastal and marine ecosystems worldwide [33](see Figure 1.2). Only roughly 10% of marine plastic pollution originates at sea [27]. Most plastic is positive buoyant when first introduced into the marine environment, making it easily dispersible over long distances via wind and wave action [21]. Undergoing diverse processes in the marine environment, many plastic types become negatively buoyant and are found throughout the water column, accumulating in sea floor substrates [34]. This creates an artificial partition that can inhibit benthic gas and nutrient exchanges, leading to anoxic and hypoxic conditions in affected areas [35]. In addition, plastic can leach additives and dyes (both of which can contain heavy metals) into the water column, while at the same time absorbing hydrophobic compounds and nutrients from the water. Plastic also transports sessile invasive species [36] and acts as a vector for pathogenic microorganisms and parasites (e.g., *Escherichia coli*, *Bacillus cereus* and *Stenotrophomonas maltophilia*) [37].

The impact of large macroplastic (maP) debris has been reviewed and researched numerous times [38, 39, 40, 41, 42, 43] with big clean-up research and application programs under way [44]. However,  $\mu$ P and nanoplastics (nP) have been less of a focus [20, 22]. The term microplastic was coined in 2004 by Thompson et al. [45] in a Science article “Lost at Sea: Where Is All the Plastic?” although they were first observed in 1972 by Carpenter and Smith [46].

Especially important is research about the nP scale, as much is yet unknown about effects of the smallest sizes of marine plastic pollution. Combining regional surveys and previously unpublished reports [47] correlates the collected plastics with their sizes as well as normalized values to volume. It shows that  $\mu$ P make up the largest fraction of plastics in the ocean. More importantly, it reveals that the observed plastic debris values are lower than expected and do not correspond to models of fragmentation. This effect increases with decreasing particle size, raising the question where those tiny particles have disappeared to. Four possible sinks are suggested: Shore deposition, nano fragmentation, biofouling<sup>1</sup>, and ingestion - none of which have been researched to their full extent in any size-class. Looking at the amount found on the shores around the world, it is important not just to notice that the plastic particle abundance differs around the planet but also that there are no

---

<sup>1</sup>Accumulation of bacteria and algae on the plastics surface, causing the polymer matrix to degrade



**Figure 1.2: The question of the origin of marine plastic pollution is not easily answered, for there are a wide variety of sources distributed across land and sea. Yellow numbers show sources of marine plastic pollution, blue numbers show the effects of marine plastic pollution in the oceans. Plastic is highlighted in red and arrows display the route the plastic takes to reach the ocean. Marine plastic pollution is up to 90 % land-based. It reaches the ocean via the atmosphere, river and land runoff. The pollution is produced in different sizes. Grand scale  $\mu$ P input into the ocean includes abrasions of tires, sandblasting/abrasion of plastic paints, pre-production plastic pellets and microfiber from domestic and commercial fabric washing. (Graphic: Alfred-Wegener-Institut / Martin Künsting (CC-BY 4.0))**

uniform sampling and reporting standards. This problem of non-standardized sampling methods is discussed by Hidalgo-Ruz et al. [48].  $\mu$ P from pre-production pellets have been sampled since the 1970s [46, 49], standardization in sampling and reporting of  $\mu$ P should be a priority by now. To address the problem of marine plastic pollution, policymakers need comparable abundance numbers and risk assessments [50, 30].

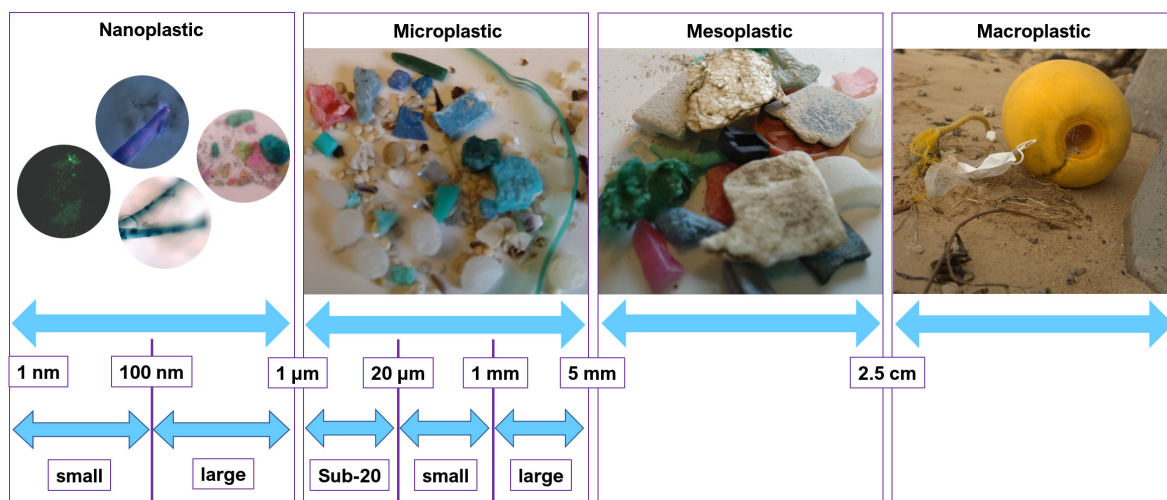
In addition to the unanswered question of the fate of  $\mu$ P/nPs, the first study of the negative effects of nPs on aquatic microorganisms was published in 2014. Besseling et al. [51] reported that the algae population of *Scenedesmus obliquus* displayed an inhibition of growth and reduced chlorophyll-a levels after exposure. The demonstrated negative effects of nPs on algae combined with the potential manifold increase of the nano fraction of the plastic pollution (via secondary or primary input) calls for immediate research into this topic. The need to act to prevent further harm to the marine ecosystem was also pointed out in Science Perspectives, “Micoplastics in the Sea” by Law and Thompson [52]. Besides scientists pointing out the need for research, the EU adopted the Marine Strategy Framework Directive [53] in 2008. This framework was discussed by scientists in 2010 and they agreed on a list of open questions [54] in three categories, “*emission, transport, and fate*”, “*physical effects*” and “*chemical effects*”. In this thesis, all three categories will be addressed in the different chapters.

## 1.2 From Micro to Nanoplastic – It is Still Plastic

The terminology for sizing marine plastic pollution initially followed the traditional plankton sizing categories [55] for  $\mu$ P/nP ( $\mu$ P between 5 - 1 mm and nP from below 20  $\mu$ m), with arbitrary boundaries defined for macro- and mesoplastics. There is still no consensus about the size classes, but after decades of research, the categories are now expanded to include a wider range of particles. Arthur et al. [56] proposed  $\mu$ P to include all fragments smaller than 5 mm, a definition which has subsequently been adopted by the National Oceanic and Atmospheric Administration (NOAA). Since then,  $\mu$ P have been separated into two fractions, large (5 - 1 mm) and small (1 mm - 20  $\mu$ m), with a sub-micron category added (20  $\mu$ m - 1  $\mu$ m) [24]. The definition for nP still lacks consensus and is defined by each author, with the most commonly used definitions being either the traditional plankton one (<20  $\mu$ m from [57]) and more accurate to the name of nPs (<100 nm from [58]). In this thesis, the following definitions were adopted for all size classes of marine plastic pollution as shown in Figure 1.3):

- Macroplastic (maP): > 2.5 cm
- Mesoplastic (meP): 2.5 cm - 5 mm
- Microplastic ( $\mu$ P): large (5 - 1 mm), small (1 mm - 20  $\mu$ m), sub-20 (20  $\mu$ m - 1  $\mu$ m)
- Nanoplastic (nP): large (1  $\mu$ m - 100 nm), small (100 nm - 1 nm)





**Figure 1.3: Size categories for marine plastic pollution.** Consequences of the marine plastic pollution, to the extent that it is known, is size dependent. Both in mechanisms and impact, different sizes of plastic vary. While  $\mu$ P/nPs, and to some extent meP possess the ability to travel through the food chain and bio-accumulate toxins in living organisms, meP and maP have a greater influence on habitats through preventing gas-exchange on sea-beds and creating artificial surfaces [7].

Since being initially observed over four decades ago, these small plastic particles have decreased in average size, as archived plastic samples show a mean particle size decrease from 10.66 mm in the 1990s to 5.05 mm in the 2000s [20]. In 2010, 69% of the fragments were only 2-6 mm [59]. Recently, the particles of the nano fraction have been reported from surface waters of the North Atlantic Subtropical Gyre [60]. As mean plastic particle size in the ocean has been decreasing over the last decades, one possible explanation in tandem with better sampling techniques is fragmentation into secondary micro- and nano-sized plastic particles. In the marine environment, fragmentation involves an interplay of many different processes. Plastic degrades by a shortening of its long polymer chains, often a combination of wind, currents and tidal action can mechanically degrade the plastic and start fragmentation processes [45]. This kind of fragmentation, fueled by the forces of the water forcefully breaking the still intact polymer chains, leads to sharp breaks that get rounded over time. Photochemical degradation (photodegradation) initiated by UV radiation (UV-B radiation ( $\sim 295$  -  $315$  nm) and UV-A radiation ( $\sim 315$  -  $400$  nm)) on the other hand affects the polymer structure, leading to discoloration and loss of mechanical stability which in turn leads to the characteristic photodegradation cracks, brittleness and disintegration [29]. Centers of attack for direct photodegradation are tertiary carbon bonds in PP and PE, as they require a low amount of energy to scission. As these saturated hydrocarbons give PP and PE their chemical and biological stability, photodegradation is the most common degradation in these polymers [61]. Another center of attack sensitive to UV radiation is aromatic rings as found in PS and PET. UV radiation interacts with these bonds to form free radicals, which in turn react further with the surrounding oxygen leading to carbonyl groups in the main chain - the polymer chain is broken and with it the stability. Fragmentation occurs. As photodegradation is actually a process of oxidation and hydrolysis jump-started by UV radiation, it occurs most frequently in the surface layer of the ocean, where UV radiation and oxygen levels are high. Once plastic debris exits the layer of the ocean where UV radiation can reach, this kind of degradation is stopped. To prevent photodegradation, light stabilizers are often added to plastics. They work through preferentially absorbing the UV

radiation, dissipating the energy as low-level heat and by doing so preventing the formation of free radicals. The specific chemical used depends on the polymer needing the protection [62]. The visible part of sunlight (400-760 nm) leads to polymeric degradation by heating and infrared radiation (760-2500 nm) accelerates thermal oxidation [29]. Thermal degradation works through the same mechanism as photodegradation, providing the molecule with more energy, leading to a kinetically unstable version of the polymer which, in the presence of oxygen or water, will be oxidized or hydrolyzed [63]. An increasing field of study is the biodegradation of plastic. This degradation, and subsequent fragmentation, are mediated by microorganisms secreting exo-enzymes that break down the plastics to low chain molecules which can be used by the organisms to fuel their metabolism. By-products often enter the sulfur, nitrogen and carbon cycle. Biodegradation happens under both aerobic and anaerobic conditions, leading to different products: while aerobic degradation produces CO<sub>2</sub> and H<sub>2</sub>O, anaerobic degradation produces CO<sub>2</sub> and CH<sub>4</sub>. Biodegradation takes place in the “plastisphere” [64] as the hydrophobic surface of plastics of all sizes attracts bacterial and microalgae communities, creating a biofilm. Different plastic types have different communities on them and these communities are distinct from the surrounding sea water [65, 64].

Both  $\mu$ P/nP can be of primary (originally of micro- and nano-size) or secondary (fragmentation of maP/meP) origin [66, 20]. Primary  $\mu$ P/nP can come from a variety of sources we use in our daily life.  $\mu$ P/nP beads in detergents, scrubs and medical applications as well as makeup and lotion fillers enter the marine ecosystem via the water system and are often not removed in treatment plants [67]. Unintentional primary  $\mu$ P/nP are by-products of 3D printing [68] and Styrofoam [58], for example. Pre-production pellets and flakes are often lost during transport, storage, loading and cleaning, and enter the environment at high rates [69]. Secondary  $\mu$ P/nPs are caused by photochemical (UV radiation) and mechanical degradation of larger maP/meP leading to fragmentation within the marine environment, but also by tire wear and tear and removal of paints from buildings and ships, and fibers from clothes and carpets [66, 20, 70, 31].

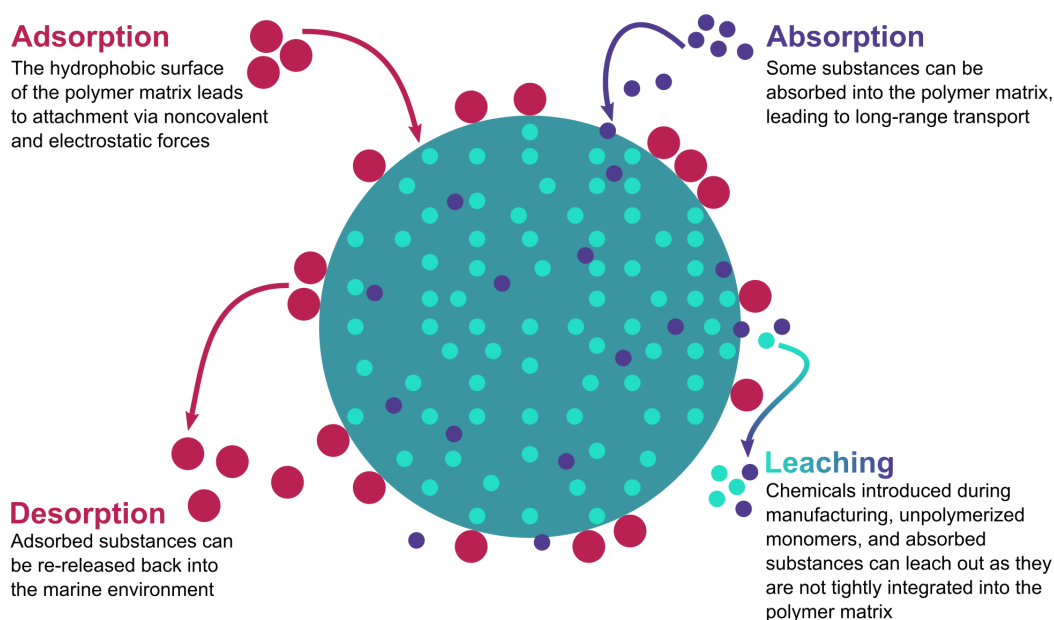
Another possible reason for an increase in micro- and nano-sized plastic particles in the marine environment is the increased release of plastic particles primarily of that size. Recent reviews of pre-production pellet release in Sweden estimate an annual release between a minimum of 3 million and a worst-case scenario of 36 million pellets from the study area [69]. If the fraction smaller than 300  $\mu$ m had been included, the total plastic particle count in the hourly runoff would have exceeded 500,000 particles [69].

While the increase in smaller particles has been observed [59, 45], changes in chemical composition, color, polymer structure and, consequently, the leaching of chemicals from the plastic into the ocean has not been studied to its full extent (Figure 1.4). Due to the higher surface to volume ratio, the smaller pieces of  $\mu$ P/nP are bound to lose higher quantities of chemicals to the surrounding environment, thus this process is in urgent need of quantification.

## Leaching and Sorption of Chemicals in Micro- and Nanoplastic

During production additional chemicals or additives, are added to improve the desired qualities of the pure polymer, e.g. UV stabilizers against UV radiation-induced degradation. These also are largely derived from non-renewable crude oil. Although the plastic itself, when polymerized, is said to be biochemically inert due to its large molecular size, residual monomers and additives to the plastic are hazardous for human health and the environment [71]. Additives can be divided into four categories, functional additives (e. g. stabilizers/UV stabilizers, antistatic agents, flame

retardants, plasticizers, lubricants, slip agents, curing agents, foaming agents, biocides and smoke suppressors), colorants (e.g. pigments, soluble azocolorants), fillers (e.g. mica, talc, kaolin, clay, calcium carbonate, barium sulphate), and reinforcements (e.g. impact modifiers, glass fibres, carbon fibre) [10]. All non-polymeric components of plastic, including heavy metals dyes, are often of lower molecular weight and may, therefore, migrate from the plastic matrix [72] to air, water or other contact media (e.g., food) [71]. They may be released during production, use or after disposal, in a process called leaching (see Figure 1.4). Leaching of plasticizers (e.g., phthalates), have shown to be teratogenic and endocrine disrupting in amphibian and fish [73]. In addition to leaching of toxins from the polymer matrix, chemicals can also sorb onto the plastic surface. Two different processes interplay, adsorption to the surface and absorption into the polymer matrix (see Figure 1.4). Adsorption happens through hydrophobic interactions, electrostatic forces, and noncovalent interactions. Adsorption of a chemical has three stages, attaching and distributing on the particle until an equilibrium stage is reached [74].



**Figure 1.4: Leaching and sorption processes in  $\mu\text{P}/\text{nPs}$ .** Monomers (see Table 1.1), additives (e.g., stabilizers, plasticizers, flame retardants, pigments, fillers) and dyes are not bound within the polymer matrix and can leach from the plastic into the surrounding seawater. Many monomers are carcinogenic. Persistent organic pollutants (such as polychlorinated biphenyls (PCBs), pesticides (e.g., DDT) and polycyclic aromatic hydrocarbons (PAHs)) and heavy metals sorb on to the surface of the plastic. Different polymer types attract different toxins as well as different amounts of toxins. These toxins can sorb onto the hydrophobic surface but also release easily. Adsorbed toxins can be released easily from the surface into the surrounding media or tissue (in bio-accumulation) but absorbed chemicals tend to travel with  $\mu\text{P}/\text{nP}$  for longer and leach at a later point.

Several papers explore the different sorption processes in laboratory experiments [73, 75] and field studies on the amount of persistent organic pollutants (POP) and heavy metals on  $\mu\text{P}/\text{nPs}$  have been conducted with alarming findings [37, 76, 10, 77]. Model analysis also contributes to the knowledge about this problem in  $\mu\text{P}/\text{nPs}$  [78, 30].

The alteration of  $\mu\text{P}$  and  $\text{nP}$  surface properties in the marine environment explains the affin-

ity of the exposed and eroded particles for chemicals that the virgin plastics would not sorb [79]. Erosion of plastic increases the surface porosity, thereby increasing the surface area through unevenness. Changes in surface charges via chemical alteration of the plastic due to erosion make the particles more favorable to interaction with polar compounds, whereas virgin plastic particles have a neutral surface [79]. Many dyes, surfactance and metals are more easily sorped to the surface of eroded plastics. Adsorbed to the surface they can be transported over great distances, as well as through the food chain by being released inside an organism that ingested the particle. Through this process of bio-accumulation even small amounts can travel all the way through the trophic levels.

Various types of  $\mu\text{P}/\text{nPs}$ , including fibers, pre-production pellets and fragments, are now commonly found in organisms [80, 81, 82]. When plastic is confused for food or accidentally ingested by filter feeders [83], these toxins can be released into organisms and can bio-accumulate to higher trophic levels [75, 84]. Toxic heavy metals are generally found absorbed to all types of plastics in the marine environment, with the concentrations of all metals increasing over time. However, none of the heavy metals found have reached saturation [75]. Trace metals, such as cadmium, zinc, and lead can also leach from additives such as heat stabilizers and slip agents and can comprise up to 3% of the polymer composition [10]. Whether inherent or accumulated, these metals add to the risk that  $\mu\text{P}/\text{nP}$  pose to the environment [85], a risk that needs better evaluation.

### 1.3 From Plastic to Marine Habitats

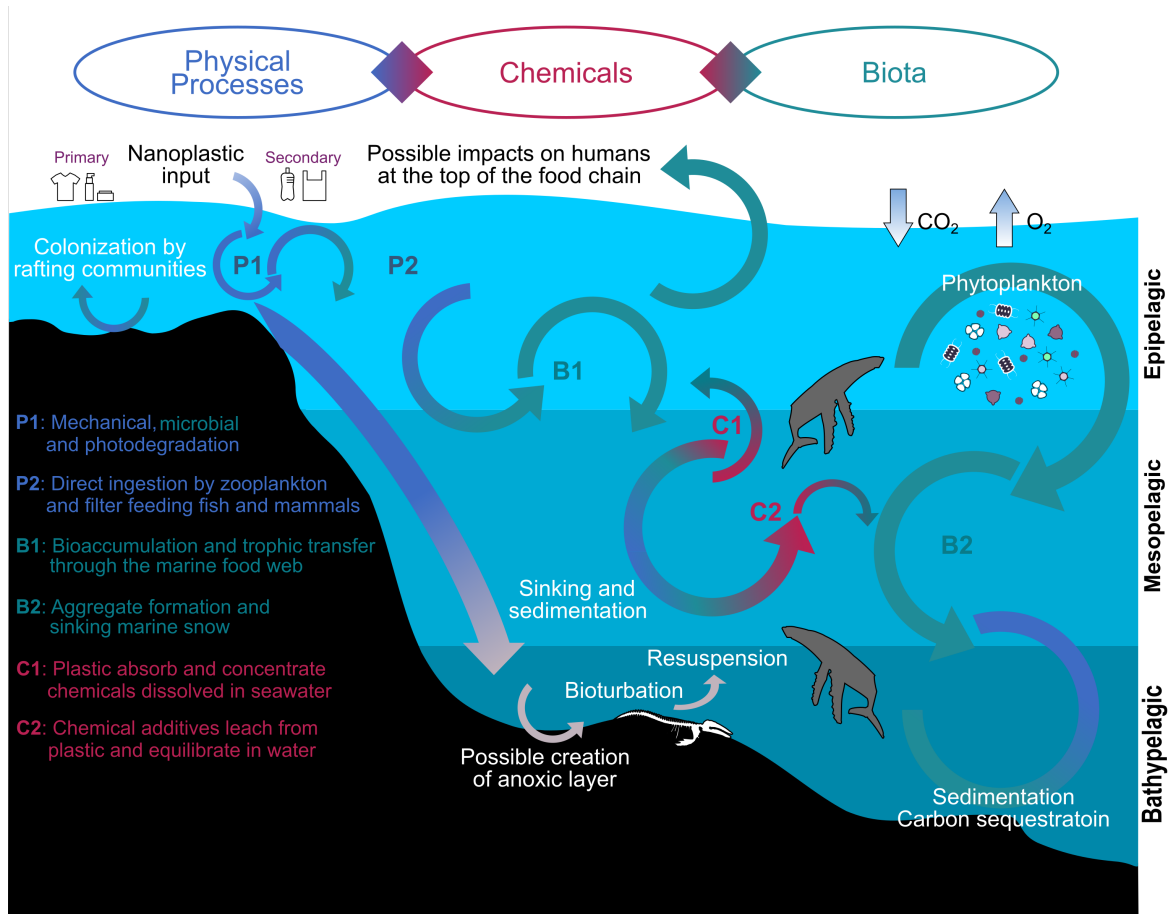
The theory of the fate of marine plastic pollution is well documented and the different components of Figure 1.5 are all part of different investigations, in environmental ecology, food sciences, and material sciences. As shape, color, and composition of plastic changes over time during exposure to marine conditions, so does the impact on organisms growing on or ingesting these particles.

As floating debris, plastic is harmful to the ecosystem nutrient cycle and marine wildlife [86]. High concentrations of floating plastic debris are reported from all marine ecosystems, but exact abundances and distributions of plastic litter remain unknown [47]. In addition, such research has mainly focused on the center of oceanic gyres, an accumulation zone for marine litter, especially plastic. Gyres are very old biomes; the North Pacific Subtropical Gyre present-day boundaries have persisted since the Pliocene. They also constitute the largest contiguous biomes on earth [87]. Created by wind-driven circulation patterns [88], gyres account for most of the oceanic primary production. Plastic is lightweight, buoyant, and thus prone to wind movement, getting trapped at the gyres center. Due to prolonged exposure of larger plastic litter to UV radiation and wave action, gyres have particularly high concentrations of secondary  $\mu\text{P}$  and presumably  $\text{nPs}$ . Concentrations in the largest ecosystem on our planet, the North Pacific Subtropical Gyre, have been reported with 32.76 particles/ $\text{m}^3$  and 250mg/ $\text{m}^3$  [89] or 334 pieces/ $\text{m}^2$  in the Northeast Pacific [86]<sup>2</sup>. The South Pacific gyre has been found to contain up to 396 pieces/ $\text{m}^2$  [90]. Gyres are considered oligotrophic because they are far from terrestrial runoff [91]. Still they support one half of the world's primary production [87]. Phytoplankton and their predating zooplankton have adapted to these stable conditions. For example, through the reduction of their genome, they have reduced the need

---

<sup>2</sup>It should be noted that there are no reporting standards for  $\mu\text{P}/\text{nP}$  pollution, so some of the reported values are concentrations to unit volume and others are per area.





**Figure 1.5: Potential pathways of  $\mu\text{P}/\text{nP}$  in the marine environment.**  $\mu\text{P}/\text{nP}$  debris is transported and interacts with the marine biota, the complexity of interactions and spatial dimensions making the problem hard to tackle for scientists and policymakers alike. Touching on every marine habitat, the potential problems arising from these particles' presence are in great need of being quantified and qualified. Uncertainty in the potential risks of  $\mu\text{P}/\text{nP}$  is one of the greatest problems. Physical processes are shown in blue arrows (fragmentation and sinking), chemical processes in red (leaching and accumulation) and interactions with biota in green.

for nutrient elements as these have become limited. This results in particularly vulnerable stratigraphy, as the smallest changes can prove disastrous. With global warming and ocean acidification stressing these communities, the introduction and prevalence of  $\mu\text{P}/\text{nPs}$  into this ecosystem as another stressor needs to be studied in more detail. Other regions of the ocean have lower reported concentrations: 1.414 pieces/ $\text{m}^2$  in the Caribbean Sea [59]; 1.534 pieces/ $\text{m}^2$  in the Gulf of Maine [59] and on a fringing reef on Mo'orea 0.74 pieces/ $\text{m}^2$  [92]. At the surface of the Kuroshio Current only 0.0176/ $\text{m}^2$  items can be found [93].

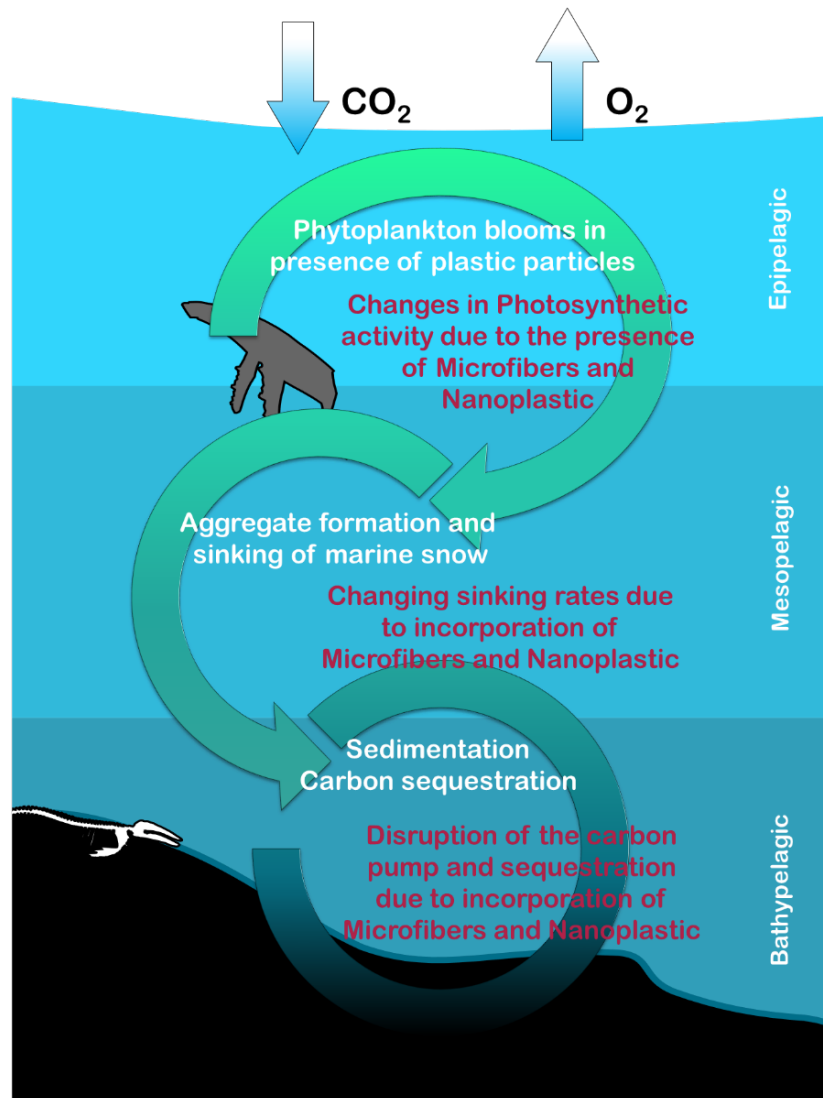
Plastic of all sizes is detrimental not just on the surface or in the water column where the problem is visible to us but also throughout the entire ocean, having been found throughout the water column [34, 94]. Once it settles on the ocean floor, it can accumulate and create a barrier in the substrate, limiting gas and nutrient exchange. This can lead to anoxia and hypoxia for benthic organisms (Figure 1.5) [35]. In addition to the effects plastic itself has on the animals, toxic chemicals and heavy metals that are adsorbed to the plastic surface and into the polymer matrix are leaching from the particles once they are ingested. In addition, these chemicals bio-accumulate in organisms and will be transferred through the food web to higher trophic levels (Figure 1.5) [84, 75].

The ingestion of plastic particles of differing sizes by various marine organisms - from zooplankton to whales - is well-reported [95, 96, 80]. While there are studies and research expeditions about the macroplastic pollution of the open ocean and especially the gyres, giving a general overview and detailed quantification of the problem,  $\mu\text{P}/\text{nP}$  are just starting to be investigated on an ocean wide basis. In particular, the impact on plankton communities needs more research. One study reports on the aggregation processes between  $\mu\text{Ps}$  and plankton [97]. Another study correlates  $\text{nPs}$  to a reduction in Chlorophyll A levels and growth rate of fresh water algae [51] which could imply that the same holds true for marine planktonic primary producers.

As the effects of human activity increase and change to more synthetic pollution, both  $\mu\text{P}/\text{nPs}$  themselves, as well as associated pollutants, will keep increasing. Quantification of the underlying processes and relationships of  $\mu\text{P}/\text{nP}$  pollution with plankton is important in order to understand the changes in the marine environment that might result from this pollution (Figure 1.6). Besides the direct impact of  $\mu\text{P}/\text{nPs}$  on the plankton communities, there are additional effects. Adsorbed pollutants on the  $\mu\text{P}/\text{nPs}$  are another factor directly affecting the communities. Changes in the aggregation processes and sinking behavior of plankton derived marine snow due to  $\mu\text{P}/\text{nP}$  incorporation has an indirect effect on these communities but a direct effect on the ocean's biological carbon pump. Marine snow consists of aggregates composed of organic detritus, such as bacteria, extracellular polymeric substances (EPS), phytoplankton, or zooplankton faeces [98] and inorganic particles such as minerals, and more recently oil [99] and  $\mu\text{P}/\text{nP}$  [100].

The marine ecosystems (and plankton communities) play a critical role in the planet's carbon cycle (Figure 1.6). The vertical downward transport of organic carbon is called the biological pump; the pumping referring to the transport against the dissolved inorganic carbon gradient (highest in the deep sea). This happens via the biological part of the ocean carbon pump. Photosynthetically fixed carbon in the form of organic matter is transported from the upper oceans, where photosynthesis is possible, to the ocean's depth, thus sequestering carbon from the atmosphere for months up to millennia. This process mitigates climate change. Plankton communities are the basis of the food web and biological carbon pump, with phytoplankton doing the crucial job of fixing inorganic dissolved carbon in organic matter [101], although higher trophic levels contribute as well [102].

As the upper oceans are missing predicted amounts of  $\mu\text{P}$  pollution to one order of magnitude [47], the vertical transport through marine snow has been proposed to explain these low con-



**Figure 1.6: Studying plankton-plastic aggregate formation in the presence of microfibers (MF) and  $\mu\text{P}/\text{nP}$  is important to understand the effects that these particles have on the oceanic carbon pump.** At the lowest level of the marine food web, phytoplankton is the main  $\text{O}_2$  producer and drives  $\text{CO}_2$  assimilation to mitigate climate change. Preliminary results have shown that the process of aggregate formation is not influenced by the presence of plastic particles, but through incorporation the physical characteristics change. This results in changed sinking rates (increased for microfiber incorporation, decreased for nanospheres). Photosynthesis rates decrease with the amount of  $\mu\text{P}/\text{nPs}$  present, making the plankton less efficient in  $\text{CO}_2$  assimilation. Both of these effects can potentially lead to a disruption of the oceanic carbon pump and as such limit carbon sequestration. Sinking rates and photosynthetic efficiency is influenced by abiotic factors.

centrations [103, 97]. As Choy et al. [34] point out, we lack a comprehensive understanding of concentrations, cycling and fate of plastics in subsurface waters, these deep pelagic waters being the largest ecosystems on Earth. In their study of the protected marine area of Monterey Bay, they conclude that a large pool of  $\mu$ P can be found throughout the water column, in some case matching and exceeding those found in other areas. Considering the enormous spatial (both horizontal and vertical) and ecological scale of the problem [34], new sampling technologies are necessary to tackle the problem.

The vertical transport of plastic through various pathways eventually ends at the sea floor. Although studies on a global scale are lacking, regional studies find a ubiquitous distribution of  $\mu$ P in marine sediments [104]. This study found that hydrological/sediment-matrix properties are important for deposition/retention (positive correlations between  $\mu$ P filaments and wave exposure, and  $\mu$ P particles with finer sediments). They further found that there is no higher concentration of  $\mu$ P associated with any other pollutants (heavy metals/sewage). They conclude that the “impacts of marine  $\mu$ P at the individual, population, and community levels of sea floor flora and fauna need to be assessed through broader surveys and mechanistic studies involving laboratory and, ultimately, field settings.”

Coral reefs are productive, biologically diverse ecosystems [105, 106]. They cover less than 1% of the ocean floor, while containing around one third of all described marine species [107]. Millions of people along the ocean’s coast depend on coral reefs for food and livelihood [108]. Anthropological effects, on local and global scales, threaten coral reefs, including increased sedimentation by runoff from rivers originating in agricultural and industrial removal of soil cover, increasing temperatures from global climate change, and changes in sea water chemistry [109, 110, 111]. Meso- and macroplastics such as fishing nets and buoys are a known source of coral degradation [112], and  $\mu$ P contaminate reefs around the world [92, 113, 114]. Negative effects on coral health (i.e. bleaching and tissue necrosis) from the exposure to  $\mu$ P have been reported [115]. Ling et al. [104] do not find that neighboring reef biota have any impact on amounts of  $\mu$ P found in sediments.

As Okinawa is surrounded by fringing reef, understanding how the magnitude of plastic pollution found in coastal waters can impact the reef-building community is important. Our knowledge of the biological impact of  $\mu$ P/nP/MF pollution on coral is limited and risk assessments do not exist.

## 1.4 From Habitats to Risk Assessment

Risk assessments of ecosystems involves different concepts and metrics. While the study of the resilience, vulnerability and reorganization of ecosystems has been ongoing since the 1970s, risk assessments in the field of marine plastic pollution is less than a decade old [50, 116, 30]. To understand how resilient the different marine ecosystems are to this new pollution, more data on how plastic influences biodiversity and the resulting ecosystem functions is needed. The potential of  $\mu$ P/nP to influence the plankton communities that drive the oceanic carbon pump gives this pollution an immense importance in the global oceanic ecosystem. To correctly assess these potentially adverse effects, complex ecological studies in combination with exact laboratory studies are needed. These can give data input for models but also show if there are any risks from  $\mu$ P/nP to individual species. Resilience to plastic pollution can operate at different scales and times [117]. The ability for reorganization and renewal of a desired ecosystem state after disturbance and the degree of change will strongly depend on “past exposure to perturbations” [118]. Exposure is

not a part of resilience itself [119], but a history of past similar disturbances may be important to build resilience [120, 121]. There have been no past exposures to  $\mu\text{P}/\text{nP}$  to develop resilience, but other marine algae communities are exposed to floating inorganic particles (minerals such as clay, sand, silt, silica and oil) and organic particles (cellulose, chitin, amber, etc.[122]) on a regular basis. It stands to reason, but has to be explored in more detail, that plankton communities could also adapt to  $\mu\text{P}/\text{nP}$  presence, and reorganize depending on the extent of the effects to continue to provide the essential ecosystem services we depend on (e.g., oxygen production and carbon sequestration as well as the basis of the marine food web). Such cross-scale aspects of resilience are captured in the notion of a panarchy, a set of dynamic systems nested across scales [120]. Human actors can also manage cross-scale interactions to avoid or instigate loss of resilience at larger and more catastrophic scales [120]. Managing resilience of the plankton communities would reduce the risk of  $\mu\text{P}/\text{nP}$  as a potential planetary boundary threat [16]. Being present throughout the water column, on beaches and in surface waters, and within the benthos [123, 86, 45, 34],  $\mu\text{P}/\text{nPs}$  have invaded the most remote marine ecosystems [124]. On Okinawa, sources of marine pollution have increased in the last 30 years [125, 126] leading to more calls for marine protection [127]. Increasing knowledge on  $\mu\text{P}/\text{nP}$  distribution, abundance and influence on the Okinawan marine environment can help take into better consideration all the different stakeholders in this problem and lead to more efficient creation of marine protection [128]. A Choice Experiment [129] conducted on Okinawa about marine protection in 2014/2015 revealed that residents of Okinawa are supportive of increasing the coral coverage and marine biodiversity while restricting coastal development [130]. As in many coastal communities, Okinawans have an interdependence with the marine ecosystem. Understanding the specific vulnerabilities of the reef ecosystem to  $\mu\text{P}/\text{nP}$  comes from a synergy between laboratory experiments on specific reef community species as well as a knowledge of the environmental conditions presently found on the reef. Conducting more detailed risk analysis will help us understand the resilience ecosystems have to  $\mu\text{P}/\text{nP}/\text{MF}$  and the vulnerability they express towards this pollution.

## 1.5 Conclusions and Objectives

In conclusion, the yearly increasing plastic production, combined with the decrease in average particle size and the missing micro- and nano-sized plastic particle fractions indicate an immediate need to investigate marine plastic pollution. The risk and challenge that the presence of micro- and nano-particles and -fibers pose to the various marine ecosystems are diverse and largely unquantified. There is a clear need to research the topic of marine  $\mu\text{P}/\text{nP}$  pollution so that we can understand, predict, and potentially mitigate its effect on the marine environment. As this is such a complex problem, building on available methods and techniques used by the community is essential to close the knowledge gaps. In addition, the Okinawan Prefectural Government has signaled that input about  $\mu\text{P}/\text{nP}$  pollution will be helpful to their policy making as they want to preserve the marine ecosystem

Given the potentially substantial threat to Pacific Island communities, who often depend on the ocean as a direct or indirect source of income, this thesis aims to answer two of the problems raised above - nano fragmentation and biofouling - in the context of Okinawa. The unique location along the Kuroshio Current with mainly fringing reefs will create an entirely new data set for the questions concerning emission, transport, and fate in the environment. This study aims to increase the knowledge about the interactions of these particles with microalgae of two different ecosystems,

the plankton communities of the open oceans and fringing reef habitats. In addition, an initial assessment of the presence and distribution of  $\mu\text{P}/\text{nPs}$  around Okinawa is given.

To build on the available data and extend the knowledge in several different directions, the main foci of this thesis will be (I) micro- and nanoplastics effects on microalgae and (II) micro- and nanoplastics abundance and distribution around Okinawa. The layout of the thesis is as follows:

## Chapter 2

This chapter investigates the aggregate formation processes between  $\mu\text{P}/\text{nPs}/\text{MF}$  with marine planktonic primary producers which leads to the potential introduction of plastics into the carbon pump.

- How does the presence of plastic particles affect aggregation and sedimentation of key phytoplankton species (physical effects)?
- Are biological carbon pump pathways infiltrated by  $\mu\text{P}/\text{nPs}/\text{MF}$  through incorporation into aggregates (connection to environmental data)?

## Chapter 3

In this chapter the results of a field study around Okinawa are presented. An initial assessment of abundance, type and pollution status of micro- and nano-sized plastic particles in the coastal environment of Okinawa is given to evaluate the local emission, transport, and fate of  $\mu\text{P}/\text{nPs}$ .

- How many plastic particles are found in the surface waters around Okinawa and does this reflect human population and industrial distribution?
- What type of plastic particles can be found?
- What kind of heavy metals can be found on the plastic particles?
- Is there a potential risk posed by  $\mu\text{P}/\text{nP}$ ?

## Chapter 4

Chapter 4 investigates the effects of polystyrene nanoplastic ( $\text{nanoPS}_{42}$ ) on endosymbiotic dinoflagellates isolated from Okinawa reef environment and relates to potential effects on the symbiont-host dynamic and for the fringing reefs of Okinawa.

- Does the presence of  $\text{nanoPS}_{42}$  inhibit *Symbiodinium tridacnidorum* and *Cladocopium* sp. ability to do photosynthesis and reduce its growth rates?
- Which genes show a change in expression patterns?

## Chapter 5

The last chapter of this thesis gives an overview of the results and conclusions. The outlook discusses which further research could build onto the work presented in this thesis.



## Chapter 2

# Micro- and Nanoplastic Particles in Marine Snow Formation<sup>1</sup>

### 2.1 The Carbon Cycle and Marine Snow

Between 50% and 80% of the photosynthetic oxygen produced on Earth each year comes from the ocean, and 90% of that is generated by phytoplankton through photosynthesis [131]. By the same process, phytoplankton are a major contributor to the oceanic carbon cycle. They assimilate dissolved carbon dioxide into organic matter, forming the basis of the marine food web. A wide range of physico-chemical and biological processes contribute to the oceanic carbon cycle, connecting different carbon reservoirs in the atmosphere and ocean.

One hundred gigatons of carbon (GtC) in the form of CO<sub>2</sub> are exchanged between the ocean and atmosphere reservoir each year, while our oceans also retain and store CO<sub>2</sub> through carbon sequestration<sup>2</sup>. Organically fixed carbon from the atmosphere and, as such, from anthropogenic origins, can be sequestered into the ocean's depth. If buried in sediments, the carbon can remain there for millions of years, a major mechanism to lower atmospheric carbon levels. This process depends on the biological side of the carbon cycle. When phytoplankton, or other living organisms in the oceanic food web, die, their organic matter sinks downward in the water column (see Figure 2.1). The export of carbon in the form of biomass from the light-filled upper ocean to lower levels where it gets sequestered and removed from the present-day carbon cycle is called the *biological carbon pump*. This pump has a direct effect on climate stability as the oceans absorb around 2.6 GtC, amounting to 30% of anthropogenic output [132, 133], with the biological carbon pump sequestering ~0.2 GtC/year out of the present day cycle.

Anthropogenic actions, including fossil fuel burning, deforestation, and increase in agricultural land and urban areas, have led to an increase in the amount of CO<sub>2</sub> released into the atmosphere and the increase keeps growing year by year. Atmospheric CO<sub>2</sub> increased from below 300

---

<sup>1</sup>The work presented in this chapter was conducted at the University of California, Santa Barbara, in the [laboratory of Professor Uta Passow](#). It was financed in part by the Passow Lab (UCSB Marine Science Institute) and the Marine Biophysics Unit of OIST Graduate University.

<sup>2</sup>The oceans contain 38,000 gigatons of carbon (GtC), 16 times more than the terrestrial biosphere, and 50 times that of the atmospheric reservoir.

ppm to more than 400 ppm, in the last 200 years [134]<sup>3</sup>. Without the oceans as carbon sink, this increase would have been even larger. The absorption of this greenhouse gas considerably contributes to slowing down anthropogenic climate change.

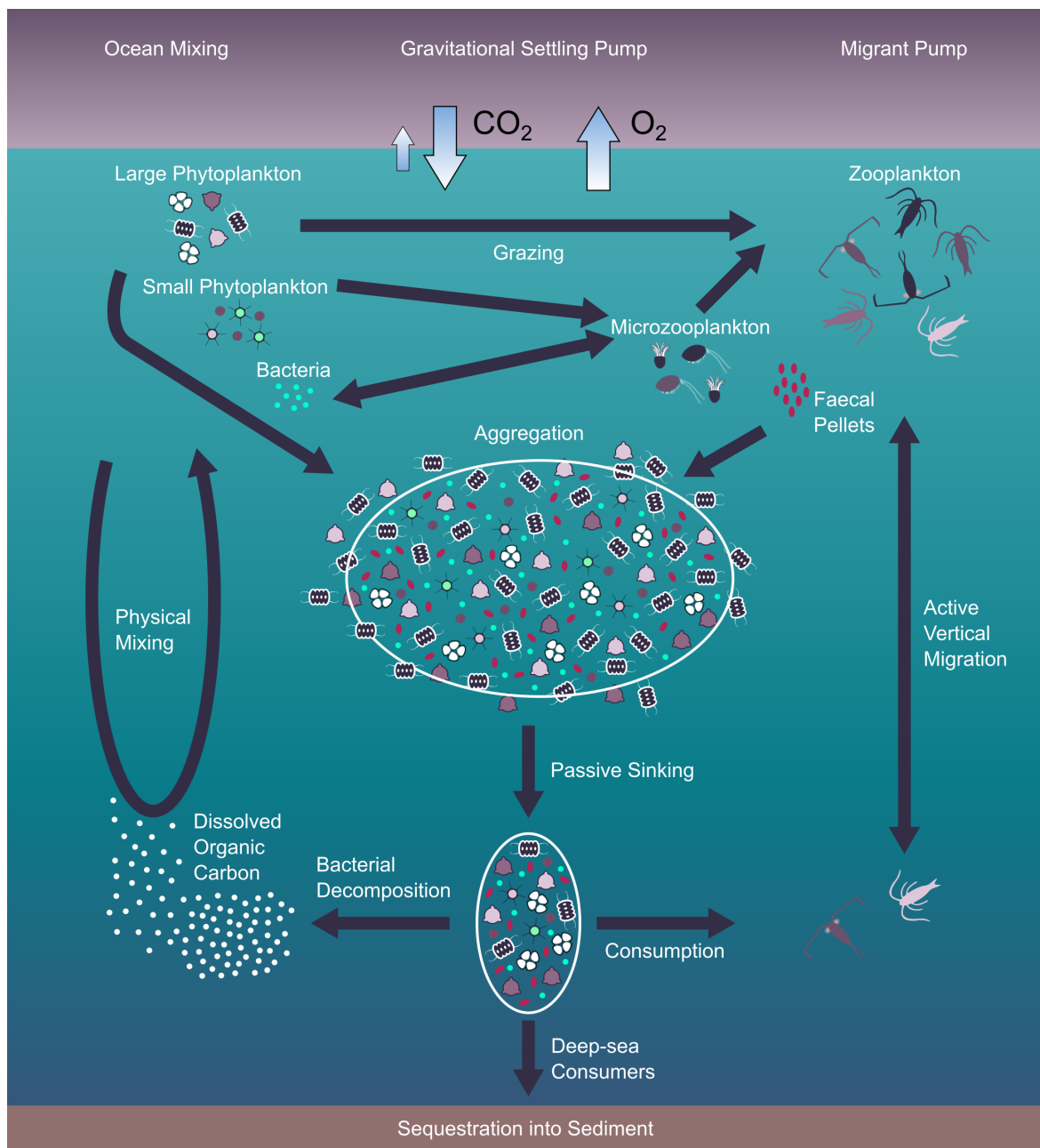
Interestingly, the plankton communities performing the primary production, which extract CO<sub>2</sub> from the atmosphere into organic matter, only represent a small organic carbon pool (~3 GtC), but they are capable of generating large amounts of dissolved organic carbon (~700 GtC) [133]. This fuels the marine food web, as phytoplankton turnover is high.

So-called *marine snow* particles (see Figure 2.1), consisting of organic and inorganic matter, aggregate and sink, sometimes for days, to the bottom of the ocean. Various types of marine snow exist, being in part determined by the plankton community they originate from. These particles have different sinking velocities and carbon content. As these aggregates descend, the particulate organic matter gets biodegraded by bacteria, reaching the deep sea and forming the basis of the food web in many of those areas.

---

<sup>3</sup>While it has been shown that CO<sub>2</sub> levels fluctuate over time, the highest level of CO<sub>2</sub> over the last 800,000 years was around 300 ppm





**Figure 2.1: Biological oceanic carbon pump transports organic carbon to the ocean floor.** Phytoplankton communities in the upper, light-filled ocean absorb dissolved CO<sub>2</sub> and fix it in organic carbon through photosynthesis. Zooplankton are always there to graze on these tiny organisms. Plankton detritus and extracellular polymeric substances (EPS) coagulate with other particulate organic matter and each other to form marine snow. These aggregates travel through the water column to the ocean floor. This process is called a gravitational settling pump because it is a sun-fueled pump that works against the unequal spatial distribution of carbon in the ocean. Dissolved carbon levels are higher at depth than at the top of the ocean. In addition, ocean mixing and active vertical migration by zooplankton are part of the oceanic carbon cycle.

Different marine snow aggregations have implications for the marine food web [135]. During aggregation, inorganic materials such as sand and silt (depending on geographical location and

time of year) get trapped in marine snow particles. More recently, anthropogenic oil and plastics floating in the water column have been found in marine snow. The incorporation (also called hetero-aggregation<sup>4</sup>) of these particles changes marine snows aggregation and sedimentation behavior. Hetero-aggregation with potentially toxic micro- and nanoplastics ( $\mu\text{P}/\text{nP}$ ), as well as plastic microfibers (MF) is well-documented [97, 136, 137] and can lead to changes in the growth rates of phytoplankton. Combined, this infiltration of the plankton communities and carbon pump has implications for the marine food web well before the aggregates ever reach the ocean floor.

### 2.1.1 Hetero-aggregation and its Implications

Through the incorporation of plastics into marine snow,  $\mu\text{P}/\text{nP}/\text{MF}$  can become available to parts of the food web that would not recognize them as food otherwise. Ingestion of  $\mu\text{P}/\text{nP}/\text{MF}$ , has shown to be problematic in many marine vertebrates, especially fish species which become food for other animals including mammals [138, 139, 140]. This facilitates the transport of plastic particles and related toxins through the food web, leading to bio-accumulation and increased effects at each stage [139].

More direct implications resulting from incorporation of  $\mu\text{P}/\text{nP}/\text{MF}$  are effects on the phytoplankton communities themselves. Natural plankton communities are very diverse; more than most models can account for [141]. Biochemical cycling and the marine food web crucially depend on this diversity. Plankton communities in the open ocean are oligotrophic due to their spatial distance from terrestrial runoff. Resource limitation leads to vulnerability of these communities, which might be counteracted by high levels of ecological diversity with large degrees of overlap and redundancy. However, the introduction of  $\mu\text{P}/\text{nP}/\text{MF}$  into this ecosystem could lead to drastic changes in the plankton communities, potentially getting the whole system out of balance. It has been discovered that the microorganism found in the “plastisphere” of  $\mu\text{P}$  is markedly different from the microorganisms communities in the surrounding seawater [64] attached via EPS [65]. In the same way, the incorporation of  $\mu\text{P}/\text{nP}/\text{MF}$  could lead to a shift in the plankton communities.

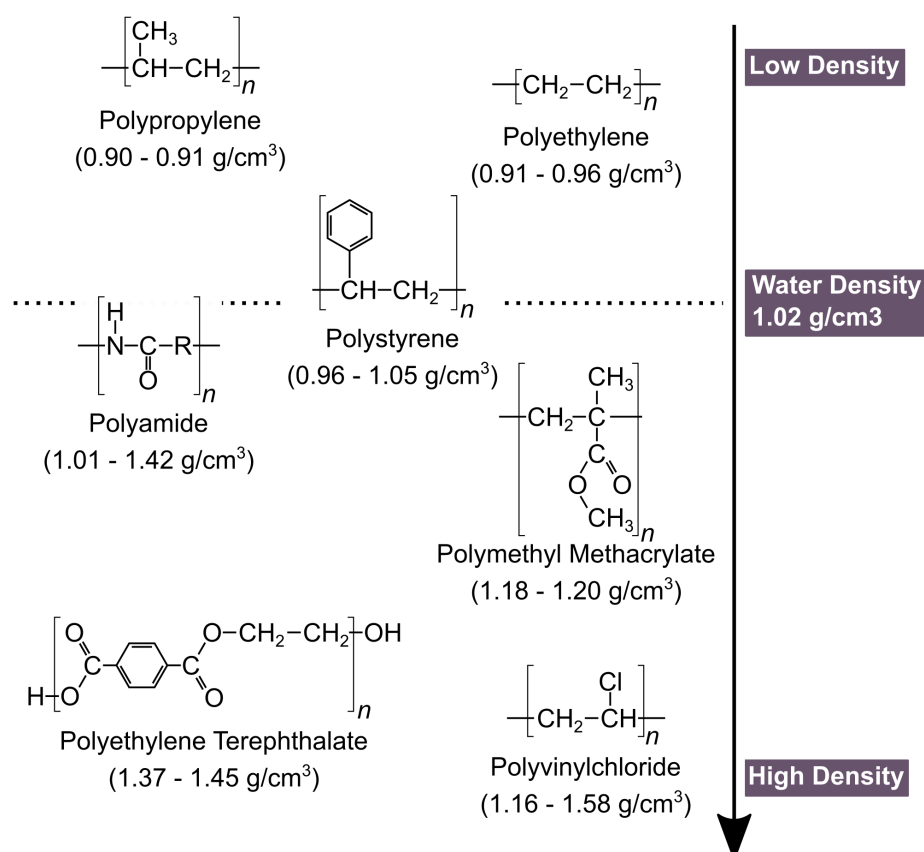
Our society depends on the stable ecosystem services the oceans provide [142]. Especially the carbon cycle and carbon sequestration is a major ecosystem service provided by the plankton communities and contributes strongly to natural climate change mitigation. Carbon sequestration is achieved in the ocean ecosystem in large parts through aggregation and subsequent sedimentation of marine snow. While part of the cycle involves mineralization of carbon, e.g. by microbial activity, and a subsequent return into the cycle through up-welling of water and biological processes, most marine snow particles reach the sea floor where they either serve as food or get sedimented. Changes in sedimentation of plankton have led to the reorganization of plankton communities and oxygenated zones in the oceans in the history of our planet well before human involvement [143]. This reorganization involves changes in marine element cycles, such as carbon and sulphur [143]. Presently,  $\mu\text{P}/\text{nP}/\text{MF}$  induced shifts in sedimentation could well prove to be catastrophic [144].

Changing sedimentation of marine snow, through incorporation of  $\mu\text{P}/\text{nP}/\text{MF}$ , can be due to several factors. One factor is the mere presence of  $\mu\text{P}/\text{nP}/\text{MF}$  in marine snow which increases the aggregates' physical density (see Figure 2.2). Different plastic polymers have different densities

---

<sup>4</sup>e.g. marine snow aggregates that have inorganic particles incorporated.

(see Section 1.1, Table 1.1), some being more buoyant and others less which makes them distribute differently in seawater (see Figure 2.2) and potentially influencing the buoyancy of marine snow.



**Figure 2.2: Buoyancy of different polymer types.** Most plastic found at the surface of the oceans are the more buoyant ones – PE, PP and PS. These polymers have recently been reported throughout the water column [94]. Other polymers are also found in the upper oceans, but material density of the polymers plays a role in where they are found within the water column.

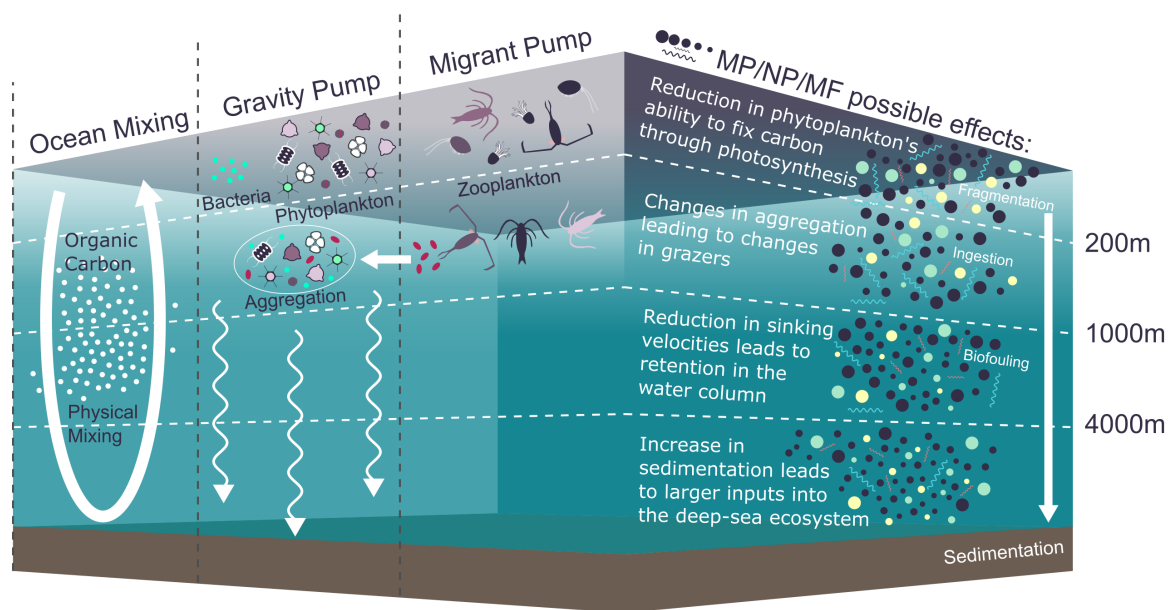
The majority of  $\mu$ P found around Okinawa were embedded into aggregates (see Chapter 3). Since this hetero-aggregation leads to a wider availability of  $\mu$ P/nP/MF in the marine food web and a wider spatial distribution of the  $\mu$ P/nP/MF [94], increasing our understanding of aggregation effects is very important to understand future implications of this marine pollutant.

To this day, little is known about the effects of  $\mu$ P/nP/MF on plankton communities. A critical review of the topic by Prata et al. [145] showed the effects of different sizes of  $\mu$ P/nP/MF on multiple food web levels. Most notable among these effects on microalgae are growth inhibition [51, 146, 147, 148, 149, 150, 151, 152, 137] and decrease in photosynthesis rates and chlorophyll content [153, 150, 51, 154, 137, 145]. Affecting growth and photosynthetic ability would directly influence the atmospheric O<sub>2</sub> content and the basis of the marine food web. Potentially changing the sedimentation would affect the carbon cycle and climate change mitigation.

### 2.1.2 Micro- and Nanoplastic in the Open Ocean Ecosystem

The yearly increasing plastic production [155], combined with the decrease in mean plastic particle size sampled in the ocean [59] and missing micro- and nano-sized plastic particle fractions [47] from the upper oceans samplings and an undersampling of ocean surface and subsurface waters [156], indicate an urgent need to investigate the fate of  $\mu\text{P}/\text{nP}/\text{MF}$  in the open ocean ecosystem. A recent study show that much of the  $\mu\text{P}/\text{nP}/\text{MF}$  is found at intermediate (50 – 170 m below sea surface) and mesopelagic depths (100 – 270 m below sea surface) [94]. Incorporation into marine snow particles is one way for buoyant plastic types to get to those depths.

The proposed sinks for  $\mu\text{P}$  are shore deposition, (nano) fragmentation, biofouling, and ingestion (see Figure 2.3). The relevant literature explores the possibility of  $\mu\text{P}$ s infiltrating the ocean carbon pump through incorporation into sinking marine snow particles [97, 103], but the ultimate fate of  $\mu\text{P}/\text{nP}/\text{MF}$  in the water column of the open ocean is not as well studied as in the shallow waters near the continents [94]. Exposure of deep-sea organisms to the pollution [157] and changes to the water column ecosystem [17] are just the most notable problems caused by  $\mu\text{P}$ s.



**Figure 2.3: Oceanic carbon pump infiltration by  $\mu\text{P}/\text{nP}/\text{MF}$ .** The results of our study show effects on aggregation, sedimentation, transparent exopolymer particles (TEP) and potentially photophysiology, all to varying extends.

The work in this Chapter investigates the aggregate formation processes between  $\mu\text{P}/\text{nP}/\text{MF}$  and three marine planktonic microalgae species, two diatoms *Skeletonema grethae* and *Odontella aurita* and one cyanobacterium *Synechococcus elongatus*. The formation process, with a special focus on transparent exopolymer particles (TEP), and resulting changes to sinking velocities of the hetero-aggregates, were studied over a 6-day period in the dark, mimicking the fall of marine snow particles through the water column. Observed effects can give information about the possible pathways through which the biological carbon pump might be infiltrated and altered extensively due to the particles' presence. The question of how shape, size, amount of particles, and surface area play a role is also addressed. "Do  $\mu\text{P}/\text{nP}/\text{MF}$  all have the same potential impact?" is an important part of

this research field, as the fragmentation of plastic particles to nano-size through photo-oxidation, mechanical action, and bio-degradation is a well-established fact [76, 45, 38, 158].

## 2.2 Materials and Methods<sup>5</sup>

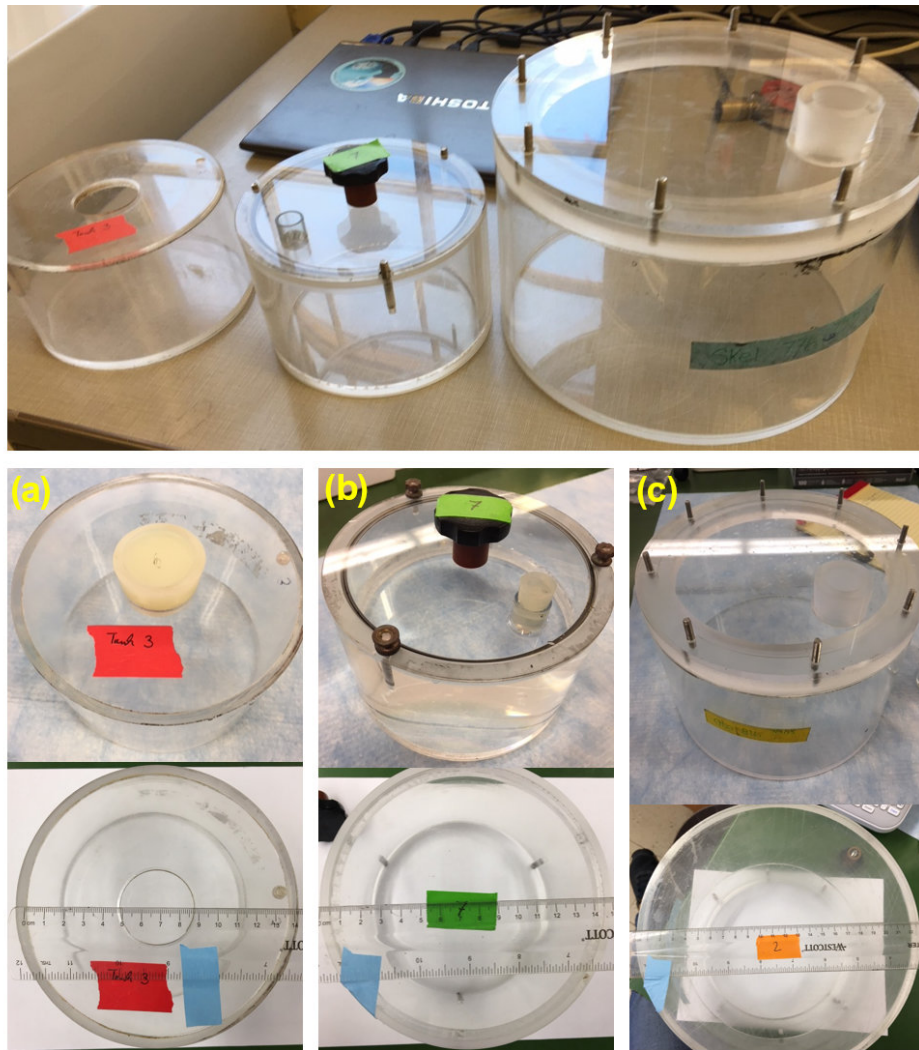
To address the question of the incorporation of  $\mu\text{P}/\text{nP}/\text{MF}$  into phytoplankton aggregates, a series of 9 roller tank experiments were conducted for an average of 6 days in the dark. There were five different densities of plastics used (see Figures 2.4 and 2.2), with between 2 and 4 used for each of the five different plastic types.

### 2.2.1 Roller Tanks

Roller tables [159] and roller tanks (see Figure 2.4) were used to simulate the natural environment in which marine snow formation occurs [160]. Rolling tanks are commonly used to promote aggregation since Shanks and Edmondson's work [159, 97]. In addition, the tanks ensured that no plastic particles were lost during the experiments [161], and exposure levels remained constant throughout. The rotation speed varied for different species to ensure continued aggregate suspension and collision of particles with different sinking velocities [160] (see Table 2.1). The tanks were closed without bubbles to simulate the marine environment in which this aggregation process takes place [97].

---

<sup>5</sup>Some methods are explained in greater detail than traditionally done within the methods section. Especially methods that were developed, failed or could not be conducted (although they were included in the thesis proposal) are elucidated to give a better overview of the work done. The author feels this is better presented in the respective method sections than under results.



**Figure 2.4:** Images of tank series used for different microalgae experiments. (a) 9 tanks used for *Synechococcus elongatus*. (b) 15 tanks used for *Skeletonema grethae*. (c) 8 tanks used for *Odontella aurita*. Pictures taken by T. Jenarewong.

Exact measurements of height and volume for all tanks used are found in Table 2.1. As experiments were run simultaneously, different rolling tables were used as well (see Figure 2.20 for *Synechococcus elongatus* set-up and Figure 2.14 for *Skeletonema grethae* set-up).



**Table 2.1: Measurements of the tanks used.** Two tanks were measured per tank series. The approximate volume is included for the tank series derived from  $V = \pi r^2 h$ . The rotating speed of the tanks varied for different species to ensure continuous aggregate suspension and collision of particles with different sinking velocities, mimicking the continued fall of the marine snow particles through the water column to the ocean floor. [rpm] stands for revolutions per minute. Measurements taken by T. Jenarewong.

	Tank measurements	cm	volume	rpm
	<i>Synechococcus elongatus</i> tanks (Tank (a) in Figure 2.4)		1154 mL	6.6
Tank 3:	inner (outer) diameter	14 (15)		
	wall thickness when measuring diameter from above or bottom	0.5		
	inside (outside) height	7.5 (8.6)		
	wall thickness when measuring height from the side	0.5		
Tank 8:	inner (outer) diameter	14.1 (15.1)		
	wall thickness when measuring diameter from above or bottom	0.5		
	inside (outside) height	7.5 (8.5)		
	wall thickness when measuring height from the side	0.5		
	<i>Skeletonema grethae</i> tanks (Tank (b) in Figure 2.4)		1057 mL	3.0
Tank 1:	inner (outer) diameter (same as the lid)	13.4 (15.2)		
	wall thickness	0.9		
	inside (outside) height	7.5 (9.3)		
Tank 7:	inner (outer) diameter (same as the lid)	13.4 (15.2)		
	wall thickness	0.9		
	inside (outside) height	7.5 (9.3)		
	<i>Odontella aurita</i> tanks (Tank (c) in Figure 2.4)		5000 mL	2.0
	For the bottom portion of the cylinder:			
	inner (outer) diameter	21.9 (22.9)		
	wall thickness	0.5		
	For the top portion of the cylinder and the lid:			
	inner (outer) diameter	17.8 (22.9)		
	Heights:			
	Total height of bottom portion	12.8		
	Total height of Top portion	2.2		
	Total height of whole cylinder+lid	15.05		

### 2.2.2 Biological Materials

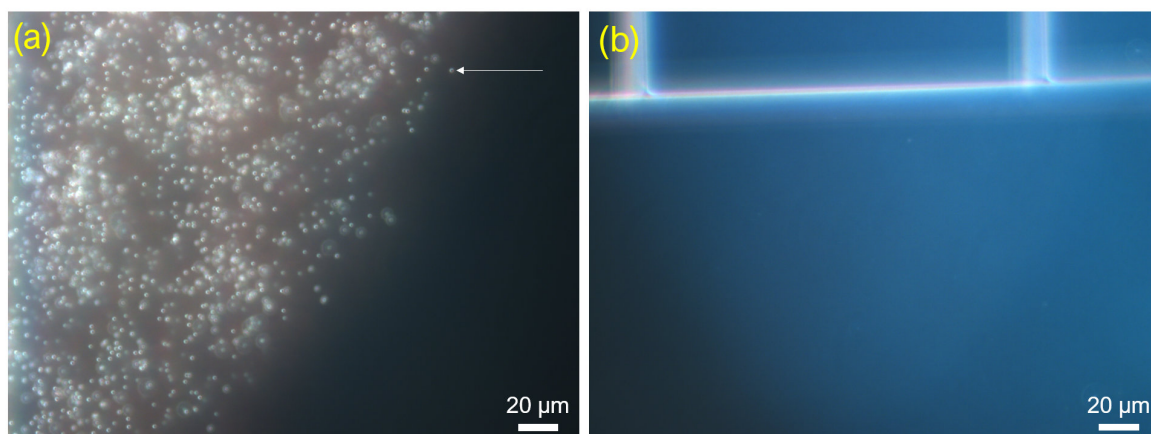
Three phytoplankton cultures were used in the experiments, the diatoms *Skeletonema grethae* CCMP 776 and *Odontella aurita* CCMP 816, as well as the cyanobacteria *Synechococcus elongatus*. All were grown in 1× Guillard’ s (F/2) marine-water enrichment solution (Sigma-Aldrich) made from 0.2 µm filtered and autoclaved natural seawater. *Skeletonema grethae* was cultivated at 13°C under a 12h /12h photoperiod (80 µmol photons m<sup>-2</sup> sec<sup>-1</sup>) and *Synechococcus elongatus* and *Odontella aurita* were cultivated at 22°C under a 12h/12h photoperiod (120 µmol photons m<sup>-2</sup> sec<sup>-1</sup>). All cultivation took place in 2.5 L covered glass flasks. For the experiments, phytoplankton cultures were at the end of the stationary growth phase.

### 2.2.3 Plastic Fibers and Beads characterization

In the experiments, three different types of plastics were used, consisting of two fibers and three different sized beads. Characterizing the  $\mu\text{P}/\text{nP}/\text{MF}$  is important, as the surface properties, size, surface area and shape play a direct role in the observed interactions between  $\mu\text{P}/\text{nP}/\text{MF}$  and microalgae. The potential ecological impacts depend on these properties [17]. As Bhattacharjee notes in a 2016 review [162], adequate characterization of nP (and by extension  $\mu\text{P}$  and MF) is paramount to understanding interactions of these particles with their surroundings. Many studies have been done on how different particle sizes and surfaces charge affect microalgae [151, 51, 163, 164, 165, 166] and even smaller organisms like marine bacteria [167, 168, 169, 170]. The physico-chemical properties of the bead determine their behavior in the environment, in this case (artificial) seawater with growth medium. In order to correctly interpret results from these exposure experiments, certain characteristics need to be known. In addition to the physico-chemical properties, weathering and organic matter precipitation will also change the surface properties [171, 172]. When virgin plastic enters the marine environment, photooxidation and mechanical abrasion modifies its surface. This enhances the acquisition of charged ions and organic matter [173, 174], leading to the formation of an ecocorona [17]. Some of the components found in the ecocorona could influence the behavior of the  $\mu\text{P}$  – such as stabilizing and dispersing particles [17].

#### Beads –

Three different sizes, 42 nm (nanoPS<sub>42</sub>), 194 nm (nanoPS<sub>194</sub>) and 2  $\mu\text{m} \pm 0.15 \mu\text{m}$  (microPS<sub>2</sub>), of pristine fluorescent polystyrene beads (in 0.1% Tween 20 solution) from Bang Labs (catalogue number FSDG001) were used (see Figure 2.5 for optical image). Fluorescent “Dragon Green” color was selected to give contrast in 3D imaging. The polystyrene has a material density of 1.03 mg/cm<sup>3</sup>, making it practically neutrally buoyant in seawater. Different particle concentrations of each bead size were used in different experiments (see Section 2.3 Table 2.4). For surface area per L see Table 2.2.



**Figure 2.5: Optical images of polystyrene beads.** (a) shows the microPS<sub>2</sub> beads. The white arrow points to a single bead. The nanoPS<sub>194</sub> and nanoPS<sub>42</sub> are too small to be seen in these images. (b) shows the milky fluid of the nanoPS<sub>194</sub> beads displacing the water.



**Table 2.2: Relationship between mass concentration, particle concentration and surface area of used PS beads in solution.** The mass concentration will be referred to as ‘concentration’ through the thesis.

	Concentration (mg/L)	Particle Concentration (n/L)	Surface Area ( $\mu\text{m}^2/\text{L}$ )
<b>microPS<sub>2</sub></b>			
	10 mg/L	$2.05 \times 10^6$	$2.76 \times 10^7$
	1 mg/L	$2.05 \times 10^5$	$2.76 \times 10^6$
	0.1 mg/L	$2.05 \times 10^4$	$2.76 \times 10^5$
	0.01 mg/L	$2.05 \times 10^3$	$2.76 \times 10^4$
<b>nanoPS<sub>194</sub></b>			
	10 mg/L	$2.54 \times 10^9$	$2.95 \times 10^8$
	1 mg/L	$2.54 \times 10^8$	$2.95 \times 10^7$
	0.1 mg/L	$2.54 \times 10^7$	$2.95 \times 10^6$
	0.01 mg/L	$2.54 \times 10^6$	$2.95 \times 10^5$
<b>nanoPS<sub>42</sub></b>			
	10 mg/L	$2.46 \times 10^{11}$	$1.36 \times 10^9$
	1 mg/L	$2.46 \times 10^{10}$	$1.36 \times 10^8$
	0.1 mg/L	$2.46 \times 10^9$	$1.36 \times 10^7$
	0.01 mg/L	$2.46 \times 10^8$	$1.36 \times 10^6$

Particle concentrations between different sizes were adjusted by mass per volume (mg/L). This led to an introduction of up to five orders of magnitude difference in particle concentration and two orders of magnitude difference in surface area between treatments of the same concentration with different particle sizes (see Figure 2.4). At the time of the experiment design, this was the method used (and still often today) to set-up these experiments [175]. This leads to the problem that the particle concentration and surface area across experiments are only directly comparable between the same plastics, but it becomes more complicated between particle concentration of different bead sizes. It has been reported that changes in the phytoplankton exposed to  $\mu\text{P}/\text{nP}$  are based on nutrient deficiencies [151]. The theory is that nutrients and multivalent metals, which the microalgae need to grow and function, attach to the surface of the plastics [151]. A higher surface area would automatically lead to a larger impact, regardless of size. In this case, basing used particle concentrations on the surface area would lead to more accurately comparable results. While in a lab setting, nutrients are often supplied in overflow to not add nutrient deficiency stress to the plastic exposure, the natural environment of plankton is oligotrophic [176]. Through trace element depletion, plastic toxicity may be found even at low particle concentrations, as trace element concentrations are low and association constants with plastics high [151]. The highest particle concentration of microPS<sub>2</sub> beads was matched to the dilution phase of Long et al. [97] of 2000 beads/mL, making the results comparable. In addition to knowing the available surface area for interactions (see Table 2.2), the potential of that surface determines the behaviour of the particle in the media. Smaller particles have lower binding energy per surface atom, due to lower number of surrounding surface atoms per atom.

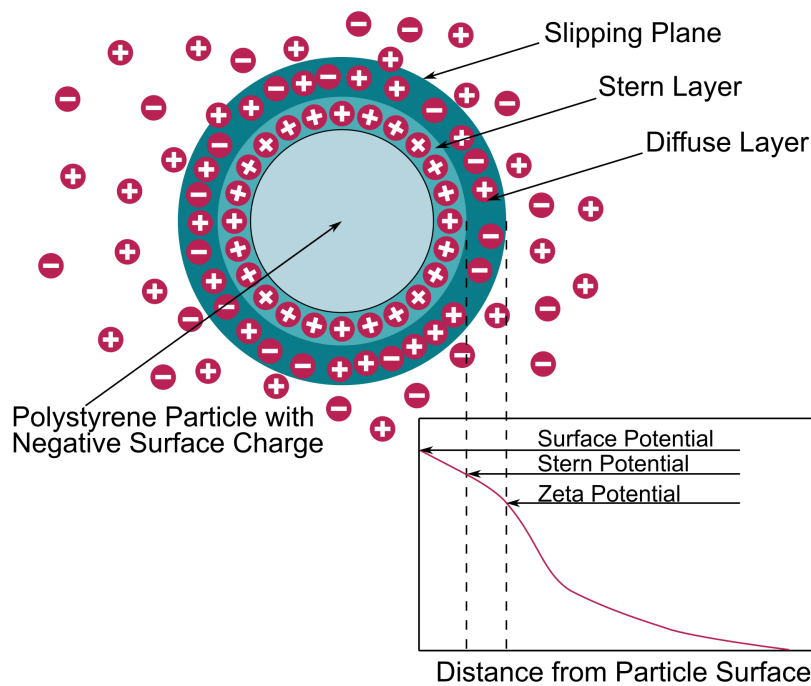
**Surface Charge and Zeta Potential** – While beads without surface functionalization were bought, suspension in seawater leads to a negative surface potential [79]. The negative surface potential will adsorb positively charged ions present in the water, forming what is called the Stern layer. A sec-

ond diffuse layer of both positive and negative ions will form around the Stern. The boundaries of this double layer, called the slipping plane, leads to the particle having an effective potential, the  $\zeta$ -potential (see Figure 2.6). The zeta ( $\zeta$ ) potential is influenced by different properties, including pH, ionic strength, and concentration [162, 177]. Our media has a pH of  $\sim 8$  and according to the literature this would lead to a negative  $\zeta$ -potential [178, 177, 179] for polystyrene nano-particles.

Since the  $\zeta$ -potential could not be measured with the available resources, values for each bead size were estimated from the literature and behavior observed in the media (see Table 2.3).

**Table 2.3:  $\zeta$ -potential of the beads.**

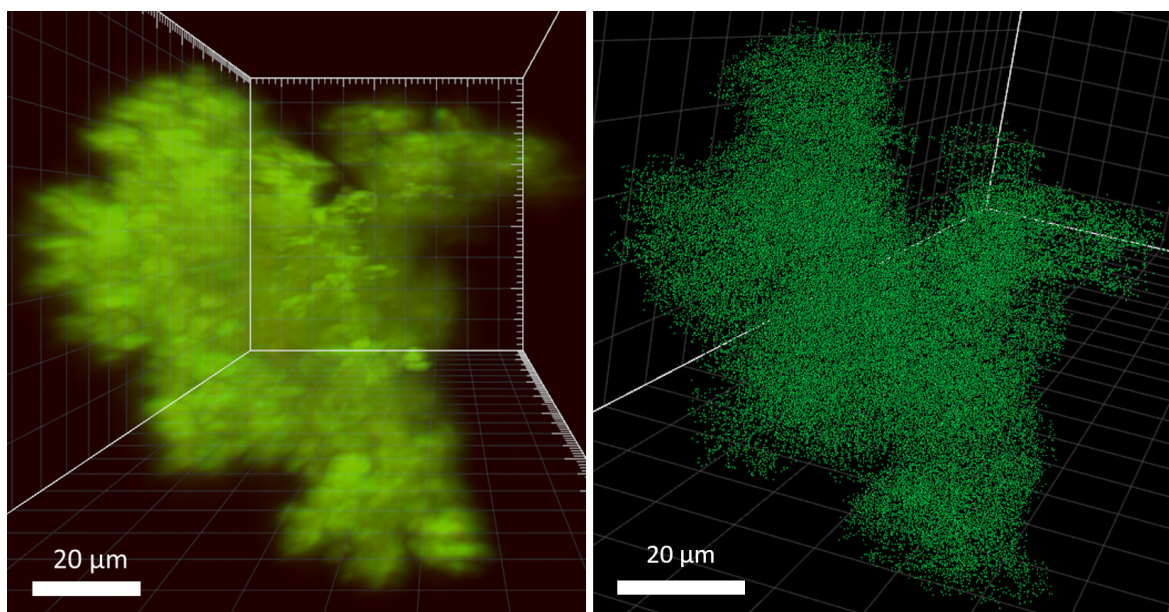
	$\zeta$ -potential (mV)	Source
microPS <sub>2</sub>	-15 to -5	[179, 177]
nanoPS <sub>194</sub>	-40 to -20	[179, 178, 162]
nanoPS <sub>42</sub>	-40 to -20	[179, 178, 162]



**Figure 2.6:  $\zeta$ -potential is a measure of the “effective” electric charge on the nanoparticle surface.** A layer of oppositely charged ions surrounds the polystyrene particle. The ions are adsorbed on the surface via chemical interactions. This layer moves with the particle, the effective electric potential at the boundary of this layer is the Stern Potential. A second diffuse layer with mixed charges gets attracted to the particle via a Coulomb interaction, and it screens the first layer. The ions in this second layer are more loosely associated with the polystyrene particle, so the layer is called diffuse. Both the Stern and diffuse layers are referred to as the electrical double layer. The  $\zeta$ -potential is a measure of the difference in potential between the media and the layer containing the oppositely charged ions associated with the nanoparticle surface. The  $\zeta$ -potential determines if the particle will bind positive or negative nutrient ions from the media.

It is essential to know the  $\zeta$ -potential of the beads in the medium to understand the observed interactions and effects on the microalgae. Note that the  $\zeta$ -potential is not the surface charge, but results from the surface charge interactions with the surrounding medium.

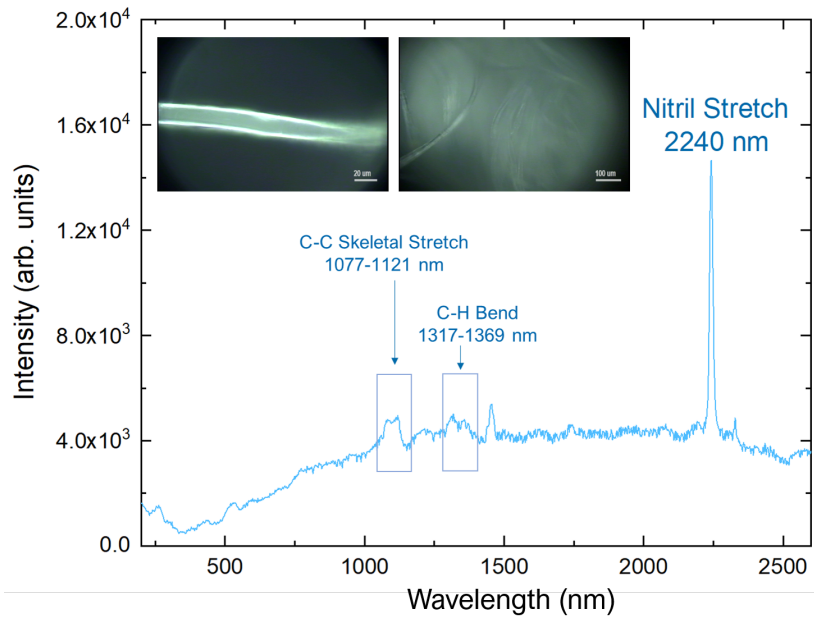
Agglomerates of nanoPS<sub>194</sub> and nanoPS<sub>42</sub> were observed. Figure 2.7 shows a plastic-only agglomerate at 10 mg/L bead concentration. These agglomerates have been reported in literature [179].



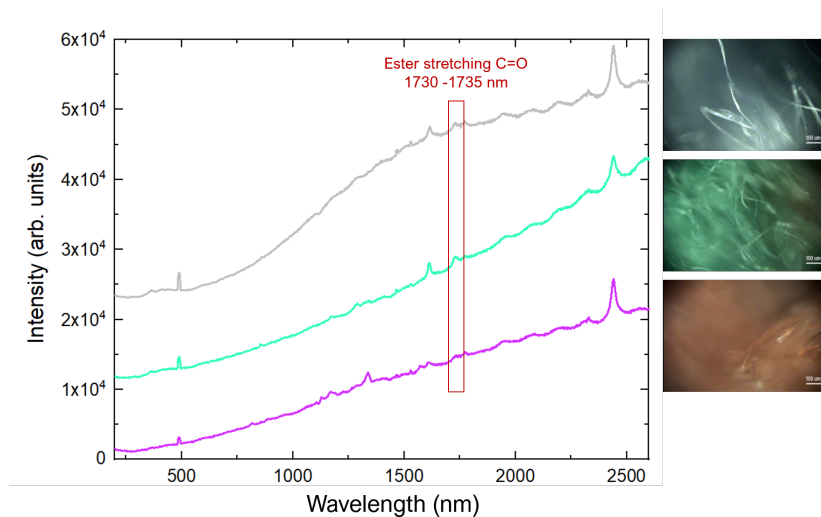
**Figure 2.7: 3D image of nanoPS<sub>194</sub> agglomerate.** This agglomerate of nanoPS<sub>194</sub> polystyrene beads was formed in a negative control tank, *i.e.* without any cells. There are  $8.75 \times 10^4$  beads in the agglomerate. Each bead has a volume of  $3.8 \mu\text{m}^3$  leading to a total plastic volume of  $334.5 \mu\text{m}^3$ . With the agglomerate volume of  $2.13 \times 10^5 \mu\text{m}^3$  (height 76.8  $\mu\text{m}$ , width 70.2  $\mu\text{m}$ , depth 75.5  $\mu\text{m}$  and equivalent spherical diameter (ESD) 74.11  $\mu\text{m}$ ), the ratio of the plastic in the agglomerate is 0.16%.

### Microfibers –

Microfibers (MF) were obtained by washing and drying fabrics. Polyester and acrylic (Polymethyl methacrylate) fabrics (see Figures 2.8 and 2.9 for optical images) were washed in two cycles with detergent and two without to remove any surface dyes and surfactants from the MF. After washing, the fabrics were dried, and the lint was collected for the experiments. The plastic lint was disentangled in 0.1 % Tween 20 solution and diluted to the following densities: 0.01 mg/L, 0.1 mg/L, 1 mg/L, 10 mg/L (see Figure 2.8 and Figure 2.9 for Raman spectra). The fibers were left in their original state, not cut into smaller sizes as proposed by Cole [180]. The reasoning was that these are the fibers that would enter the Okinawan environment, should it not be removed by the decentralized wastewater treatments used on the island. Polyester MF (pMF) had an average diameter of  $8 \pm 2 \mu\text{m}$  and lengths of 4 mm to 16 mm, while acrylic MF (aMF) had an average diameter of  $20 \pm 2 \mu\text{m}$  and a length range of 2 mm to 12 mm (see Figures 2.8 and 2.9). This corresponds well to sampled MF found around the world [180, 181, 182] and isolated from wastewater [183] and washing experiments [31]. Both MFs are none buoyant in our experiments, as they settle in 0.1 % Tween 20 solution as well as in the culture media.



**Figure 2.8: Raman spectrum and optical images of acrylic fibers used.** This fiber is made from polyacrylonitrile and polymethyl methacrylate, with possibly more than 85% polyacrylonitrile (see nitril stretch peak at 2240 nm) [184]. Exposure time was 25 sec ( $5 \times 5$  sec) with a 523 nm laser.



**Figure 2.9: Raman spectra and optical images of polyester fibers used in the experiment.** Polyester refers to a wide group of polymers used primarily for clothing and fiber production which all contain a function ester group on the polymer backbone. The different colors of the fibers show slightly different spectra due to the dyes used, but the functional ester groups are visible in all three spectra (red box). Exposure time was 25 sec ( $5 \times 5$  sec) with a 523 nm laser.

Leachates – Although not pre-prepared in this experiment, the assumption is that the surrounding seawater in the tanks will contain leachates. Literature calls ‘leachates’ the is leached

from the plastics, monomers and additives, often toxic [81]. Leachates of the MF will be discussed in the relevant result sections [185].

### 2.2.4 Exposure

Plastic and phytoplankton inoculation were done simultaneously after filling roller tanks to 50% with filtered (0.2  $\mu\text{m}$ ) and autoclaved natural seawater. By filling the rest of the tanks with the cell culture, cell concentrations at inoculation were equal in all treatment and control tanks. We filled the tanks bubble-free to minimize turbulence, mimicking the fall through the water column.

In addition to treatment tanks (plankton culture + plastic) and control tanks (plankton culture), negative control tanks of just plastic in seawater were run. Tanks were rotated for 5 to 7 days in the dark under the respective cultivation temperatures.

### 2.2.5 Aggregate Characterization: Sampling and Analysis

For the harvest of the aggregates, the tanks were placed on their sides and carefully opened. Aggregates ( $> 1\text{mm}$ , by visual observation) were manually collected and labeled as Aggregate fraction (Agg), while the rest was surrounding seawater fraction (SSW). When relevant, samples of both fractions were collected for individual measurements. Aggregates were picked up one by one for the different measurements with a cut-off pipette. When no clear aggregates could be distinguished, SSW and slurry (the settled portion of aggregated material not forming collectible aggregates) were collected instead. This is stated in the introduction to each experiment. It has to be noted that sampling of the aggregates leads to the unintentional collection of SSW. For logistical reasons, the biological replica were harvested on consecutive days, as indicated in the introduction of each experiment. In order to have a full overview of how  $\mu\text{P}/\text{nP}/\text{MF}$  affect aggregate formation, different parameters were measured at the end of each experiment. The following measurements were taken on collection day, in order of tasks:

- Total aggregate count
- Samples for photosystem efficiency measurements (both fractions)
- Samples for plastic and cell concentrations ratio (both fractions)
- Aggregate sample 3D imaging
- Aggregate sinking velocity measurements
- Aggregate size measurements
- Samples for transparent exopolymer particles (TEP) analysis (both fractions)

To quantify the exposure effects of the different plastics on microalgae, different measurements were taken. As growth inhibition is qualified as a less sensitive endpoint [175], photosynthesis was measured in addition. Aggregate sinking velocity tied back to the incorporation of plastics into the carbon pump and was not used as a measure of plastic effects on the algae, but on the ecosystem at large. The measurements are explained in detail below.



**Total aggregate count** Enumerating of the total number of aggregates in each tank, counted clockwise. As the determining triggers of aggregate formation are still opaque, it is important to have controls in each individual experiment [99]. Counting and describing the physical appearances of the aggregates and their number within each tank adds to understand if the measured effects are caused by the plastic exposure of the cell culture itself.

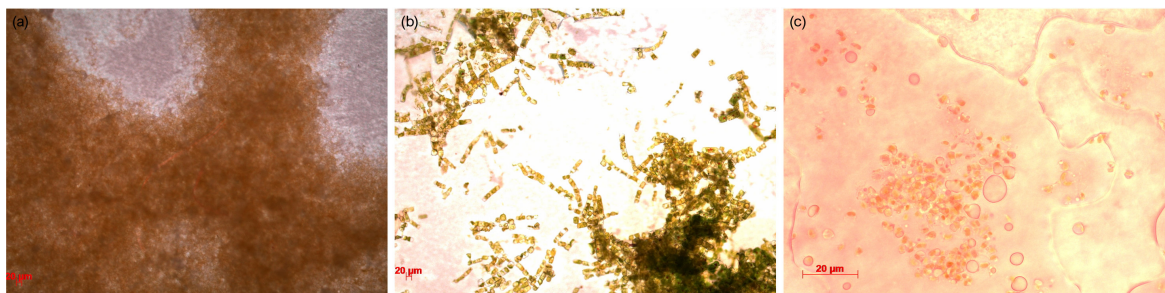
**Sinking velocity** Three aggregates per size class were measured for their sinking velocity over 29.3 cm in a 100 mL glass graduated cylinder. The sinking velocity of aggregates of each tank were measured at the same temperature as the experiment was conducted. Water to fill the cylinder came from the same seawater batch that was used to fill the tanks and was stored in the dark in the same room to keep salinity and temperature constant.



**Figure 2.10: Images of glass cylinder with sinking aggregate of *Odontella aurita*.** The sinking distance was measured in the same water that was used for the experiments and at the same temperature.

**Size** Aggregate size (diameter and height) was measured using an Carson eFlex 75x/300x microscope in a petri dish. This data is not included in the thesis and will be analyzed at a later date. Although the size of all aggregates is not included, the aggregates that were imaged in 3D have size measurements (height, depth, width), and the equivalent spherical diameter (ESD) is given for those aggregates. If possible, the ratio between cell volume and aggregate volume is given for those aggregates.

**Growth rates** The original method planned was described in the proposal to this experiment. The plastic to cell ratio was to be measured via filtration and subsequent counting to use available resources and established methods. The samples were vortexed before filtration. White polycarbonate filters (Millipore, GTTP02500, 0.22  $\mu\text{m}$ ) were stained to make the cells more visible on the filters. Stained filters were checked on Zeiss Axio Imager Z1 microscope (Zeiss, Jena, Germany). The problem with this method was that through the aggregation process, cells lumped together unevenly, and a cell count could not be established (see Figure 2.11).



**Figure 2.11: Optical images of filters prepared for cell counting.** Through the aggregation in the rolling tanks, this method was unsuitable for cell counting to identify the per mL count or growth rates. (a) *Synechococcus elongatus* was too dense in places and no cells in others, (b) *Odontella aurita* and (c) *Skeletonema grethae* stayed in aggregates and did not separate after vortexing. The same was observed in *Symbiodinium tridacnidorum* and *Cladocodium* sp. (see Section 4.3.4). Images were taken with Zeiss Axio Imager Z1 microscope.

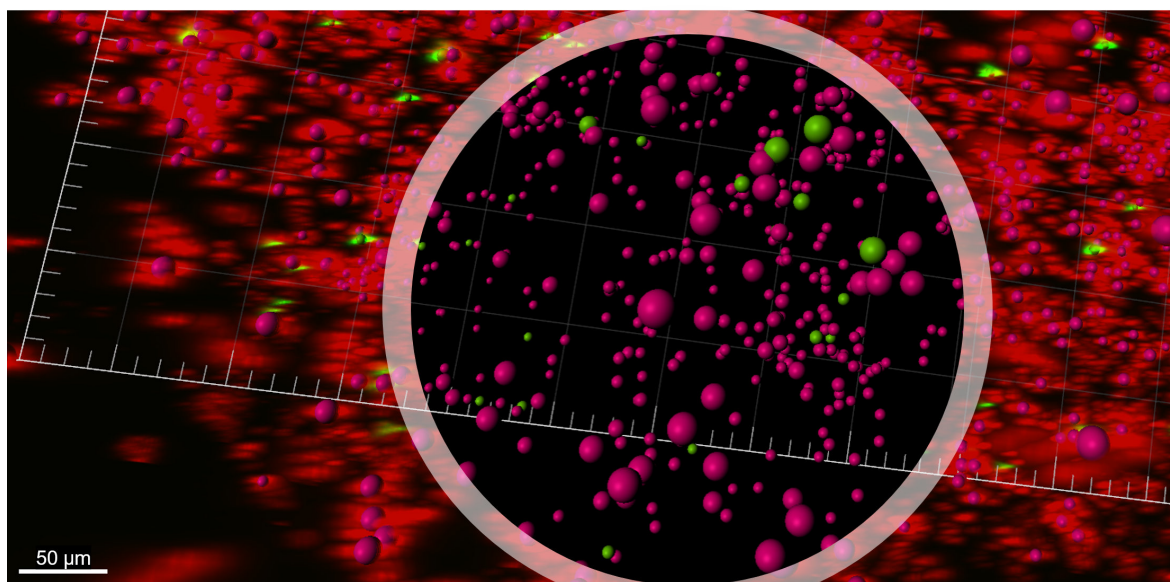
To still use the obtained samples for cell counts, cell counting via flow cytometry was tried. The Flow Cytometer Accuri C6 4523 had problems counting the cells correctly for *Skeletonema grethae* and *Odontella aurita*, most likely due to the same problem as with the aggregates not breaking up correctly. This was also observed in *Symbiodinium tridacnidorum* and *Cladocodium* sp. (see Section 4.3.4). For *Synechococcus elongatus*, the flow cytometry worked well for the  $T_0$  measurements, and the Agg and SSW fraction showed significant differences in cell counts (Kruskal-Wallis,  $p < 0.001$ ), but variances were too high to use the data for any growth rate analysis. Overall, a recount by hand in a hemocytometer will be needed for all three species to establish growth rates. In this thesis's time frame, it was not possible to recount by hand, but, where possible, the plastic/cell ratio was calculated for the 3D imaged aggregates.

**Transparent exopolymer particles (TEP)** TEP can be defined as particles rich in acidic polysaccharides [186], although they are a chemically heterogenic substance group [187]. They are a subgroup of extracellular polymeric substances (EPS) and are used as a proxy for stickiness [99]. Aggregate formation in diatoms [188] and cyanobacteria [189] is a function of collision frequency, cell concentration, and stickiness, which can be measured via TEP. Measuring the TEP in Agg and SSW fractions will give a better understanding of the origin of potential changes in aggregation induced by the exposure to  $\mu\text{P/nP}$ . Triplicates of the Agg and SSW fractions were taken from each treatment for the TEP analysis using the colorimetric method with Alcian blue [186]. Following the samples' filtration over  $0.4 \mu\text{m}$  polycarbonate (Poretics) filters, Alcian blue was used to stain the filters. The spectra of the filters were measured with a UV-vis spectrophotometer. The results were expressed in gum xanthan equivalents ( $\text{GX}_{eq}$ ) in  $\mu\text{g/L}$  and were determined from the absorption of the sample.

TEP dynamics are variable, depending on the microalgae culture and interactions with bacteria, inorganic substances (oil, plastic, minerals), and nutrient and light availability [190]. The role that TEP plays in aggregate formation makes it important to measure the concentration changes caused by plastic exposure [191].

**Internal structure through 3D fluorescent microscopy** To check the distribution of plastic in the aggregates and to get some insight into the cell packaging differences at different concentrations, 3D images were obtained using Zeiss Lightsheet Z.1. The fluorescent polystyrene beads were

observed with band pass filter (excitation: 405 nm; emission: 505-545 nm), and chloroplasts were visible using a long pass red filter (excitation: 488 nm, emission: 660 nm). Z-stacks were analyzed using Imaris software (see Figures 2.12). For a detailed method, see Appendix D.

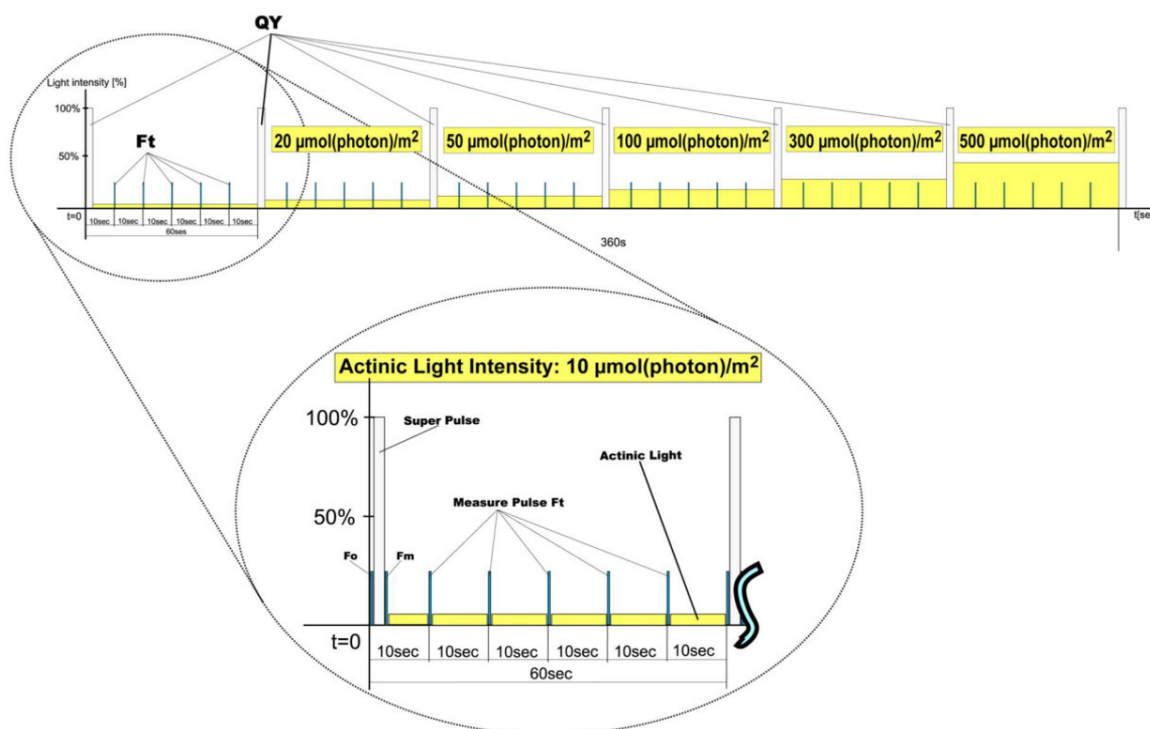


**Figure 2.12: Imaris spot tool.** The image displays a *Skeletonema grethae* aggregate with microPS<sub>2</sub> at a concentration of 0.01 mg/L. The outside shows how the laser lights up the cell (red) and microPS<sub>2</sub> (green). The “spot tool” displays cells in pink and the microPS<sub>2</sub> in green. The comparison between the pink spots and the red laser ellipsoids shows that this technique stretches the image of the cells in the z-direction. The spot tool allows in addition to counting cells and plastic to remove this stretching. Spot diameter can be adjusted to match the cells or plastics diameter; in this image, the microPS<sub>2</sub> is displayed with a 6 μm diameter for better visualization. The inner circle of the image shows the image without the laser created volume for better analysis of the plastics’ location within the aggregate. Not all red laser cells in this image have a complimentary spot, as spots are generated per laser and in this image only two laser channels are displayed for illustrative purposes, making the image better suited for 2D representation.

**Pulse amplitude modulation chlorophyll fluorometer measurement (PAM)** Changes in the efficiency of the photosystem were measured using a handheld pulse amplitude modulated fluorometer (AquaPen-C AP-C 100<sup>6</sup>). A light curve was measured after 30 min of dark adaptation (see Figure 2.13). This included measurements for changes in the effective quantum yield  $QY_{max}$ , or  $F_v/F_m$ , maximum quantum yield of Photosystem II (PSII) in the dark-adapted state and the proxy of *in-vivo* chlorophyll autofluorescence  $F_0$ , the minimum fluorescence in the dark-adapted state. This was done using the reprogrammed light curve 3 (LC3) program of the AquaPen 2.13. Blue light (455 nm) was used as actinic light for *Skeletonema grethae* and *Odontella aurita*, while red light (630 nm) was used as actinic light for cyanobacteria *Synechococcus elongatus* [192].

<sup>6</sup>PSI (Photon Systems Instruments), spol. s r.o. Drasov 470, 664 24 Drasov, Czech Republic, <http://www.psi.cz>





**Figure 2.13:** Light Curve (LC) protocol designed to acquire  $QY_{\max}$  and  $F_0$ . Picture taken from AquaPen Manual.

The LC3 protocol has 7 phases, with each phase lasting 60 s. The actinic illumination (Actinic Light Intensity or A-pulse) intensities increase in the following steps: 10; 20; 50; 100; 300; 500; 1000 ( $\mu\text{mol}(\text{photons})/(\text{m}^2\text{s})$ ). This method is based on the successive measurement of the sample exposed to a stepwise increase of light intensity and can relate the rate of photosynthesis to photon flux density. Displayed in Figure 2.13 is the LC1 protocol, missing the 1000  $\mu\text{mol}(\text{photons})/(\text{m}^2\text{s})$  step. Measuring illumination (Measure Pulse or f-pulse) intensity was at 0.03  $\mu\text{mol}(\text{photons})/(\text{m}^2\text{s})$ , while a saturating (Super Pulse or F-pulse) illumination of 2100  $\mu\text{mol}(\text{photons})/(\text{m}^2\text{s})$  was used.

Testing the functionality of the photosystem as well as the efficiency of the electron transport between photosystem I and II (PSI and PSII) will give an indication of the damage done to the cell by plastic exposure. Potentially, a reduction in chlorophyll-a and growth rate could be better explained.

## 2.3 Overview of the Experiments

The incorporation of  $\mu\text{P}/\text{nP}/\text{MF}$  into phytoplankton aggregates was studied in a series of 9 roller tank experiments. There were five different densities of plastics used, with between 2 and 4 treatments for each of the five different plastic types (see Figure 2.4).

**Table 2.4: Overview of experiments with different plankton species.** The experiments were done on 2 or 3 types of microalgae. 5 different plastic particle concentrations were used, with not every particle concentration present in each experiments. Tanks represent biological replica for each experiment. From Figure 2.4, Tank (a), (b) and (c) are ⊙, ○ and ⊖ respectively.

Experiment	Species	Tanks				
		10 mg/L	1 mg/L	0.1 mg/L	0.01 mg/L	control
microPS <sub>2</sub>	<i>Skeletonema grethae</i>	○○○	○○○	-	○○○	○○○
	<i>Odontella aurita</i>	-	-	-	⊙	⊙⊙
nanoPS <sub>194</sub>	<i>Synechococcus elongatus</i>	-	⊙⊙	-	⊙⊙	⊙⊙
	<i>Skeletonema grethae</i>	○○○	○○○	-	○○○	○○○
	<i>Odontella aurita</i>	-	-	-	⊙	⊙⊙
nanoPS <sub>42</sub>	<i>Synechococcus elongatus</i>	-	⊙⊙	-	⊙⊙	⊙⊙
	<i>Skeletonema grethae</i>	○○○	○○○	-	○○○	○○○
	<i>Odontella aurita</i>	-	-	-	⊙⊙	⊙⊙
Polyester MF	<i>Synechococcus elongatus</i>	-	⊙⊙	⊙⊙	-	⊙⊙
	<i>Skeletonema grethae</i>	○○○	○○○	-	○○○	○○○
Acrylic MF	<i>Synechococcus elongatus</i>	-	⊙⊙	⊙⊙	-	⊙⊙
	<i>Odontella aurita</i>	-	-	⊙⊙	-	⊙⊙

***Skeletonema grethae* Experiments** Four roller tank experiments were performed (see Figure 2.14), with two polymer types: polystyrene of the sizes 42 nm (nanoPS<sub>42</sub>), 194 nm (nanoPS<sub>194</sub>) and 2 μm (microPS<sub>2</sub>), and polyester fibers. Temperature varied between experiments (15° and 20°). Within each experiment, replication was achieved through having three tanks per different plastic particle concentration (low, medium, and high: 0.01 mg/L, 1 mg/L, 10 mg/L, respectively). The four experiments thus provide insight into the aggregation process under three particle concentrations plus controls.

#### MicroPS<sub>2</sub> Experiment on *Skeletonema grethae* –

This experiment was conducted from the 8th to 22nd of June 2018, at 15°C in the dark. At filling, the control and treatment tanks all had 200,000 cells/mL. Since no aggregate formation was observed for seven days, the cell count was increased to 400,000 cells/mL, and aggregate formation started the same day. The tanks were allowed to rotate for another six days, and tank harvest of the biological replica was done on three consecutive days (20th, 21st and 22nd of June). Sinking velocities and PAM measurements were taken on the same day, 3D imaging was done on 23rd and 24th of June, and TEP was filtered on 1st of August.

#### NanoPS<sub>194</sub> Experiment on *Skeletonema grethae* –

This experiment was conducted from the 22nd to 29th of June 2018, at 15°C in the dark. At filling, the control and treatment tanks all had 400,000 cells/mL. Aggregate formation started after two days. The tanks were allowed to rotate for six days, and tank harvest of the biological replica was done on three consecutive days (June 27/28/29). Sinking velocities and PAM measurements were taken on the same day, and 3D imaging was done on 30th of June and 1st of July.



Figure 2.14: Rolling table for *Skeletonema grethae* in the climate chamber at 15°C in the dark.

#### NanoPS<sub>42</sub> Experiment on *Skeletonema grethae* –

This experiment was conducted from the 29th of June to 5th of July 2018, at 15°C in the dark until the 3rd of July. Due to a breakdown in the climate chamber, the temperature was higher than in the other experiments, reaching up to 23°C. Unfortunately, the duration of the temperature stress could not be determined. Only one biological replica of each treatment was obtained from this experiment. The photochemistry data were likely affected by this change in temperature. At filling the control and treatment tanks, all had 400,000 cells/mL. Aggregate formation started on the first day and the tanks were allowed to rotate for six days. Sinking velocities and PAM measurements were taken on the same day and 3D imaging was done on the following weekend. Tank 2 (0.01 mg/L) was kept rolling at 15°C after the climate chamber was restored until 20th of July and the aggregate number did not change during that time.

#### Polyester MF Experiment on *Skeletonema grethae* –

This experiment was conducted from the 20th to 26th of July 2018, at 15°C in the dark. At filling the control and treatment tanks, all had 400,000 cells/mL. Aggregate formation started after two days, and overall there were fewer aggregates than in previous experiments with *Skeletonema grethae*. The tanks were allowed to rotate for another six days, and tank harvest of two biological replicas was done on 26th of July. One set of tanks of each concentration was allowed to continue rolling until the 31st of July. No additional aggregation was observed, making the aggregate formation more likely a function of the culture and the plastic rather than time. Sinking velocities and PAM measurements were taken on the harvesting days, and 3D imaging was done on the following weekend.

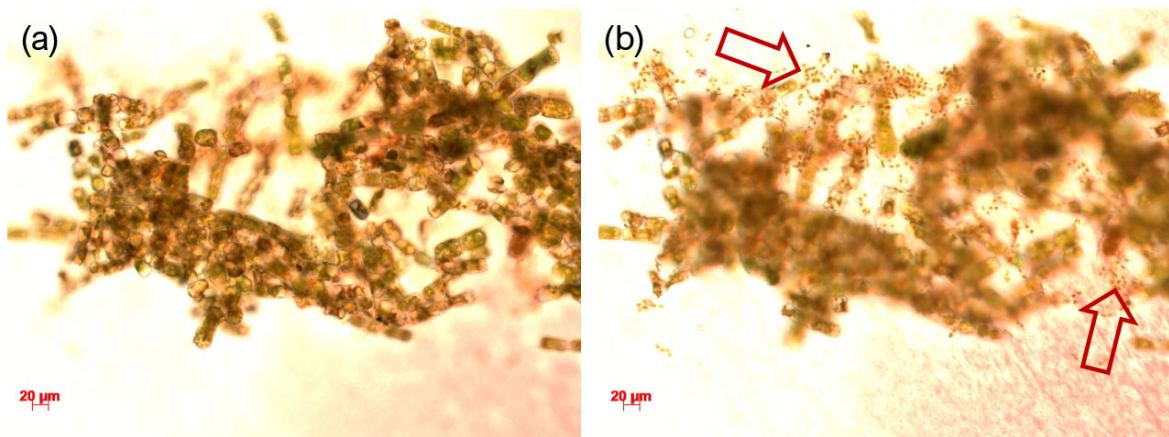
***Odontella aurita* Experiments** *Odontella aurita*, a centric planktonic bloom-forming diatom, is found along the northern coast of Japan and the European Atlantic coast [193]. In addition to being part of the plankton communities, and thus part of the oceanic carbon cycle, it is now widely cultivated in open ponds for human nutrition and pharmaceutical formulations [194]. As open cultivation ponds have the potential of atmospheric  $\mu\text{P}/\text{nP}/\text{MF}$  pollution input, understanding the implications of this kind of pollution can also help prevent production losses. As *Odontella aurita* is a slow-growing diatom and as 5 L rolling tanks had to be used, only one experiment was performed. There were eight treatment tanks in total (see Table 2.5), and the negative control was taken from the third *Synechococcus elongatus* experiment (see Section 2.3). This was possible since they were run at the same time under the same conditions. One-third of the cultures had an infection with a highly mobile ciliate (see Figures 2.15 and D.27), and the differences between those (one control tank and two treatment tanks) and the uninfected treatments (one control tank and four treatment tanks) are discussed.



Table 2.5: Distribution of treatments in the *Odontella aurita* experiments.

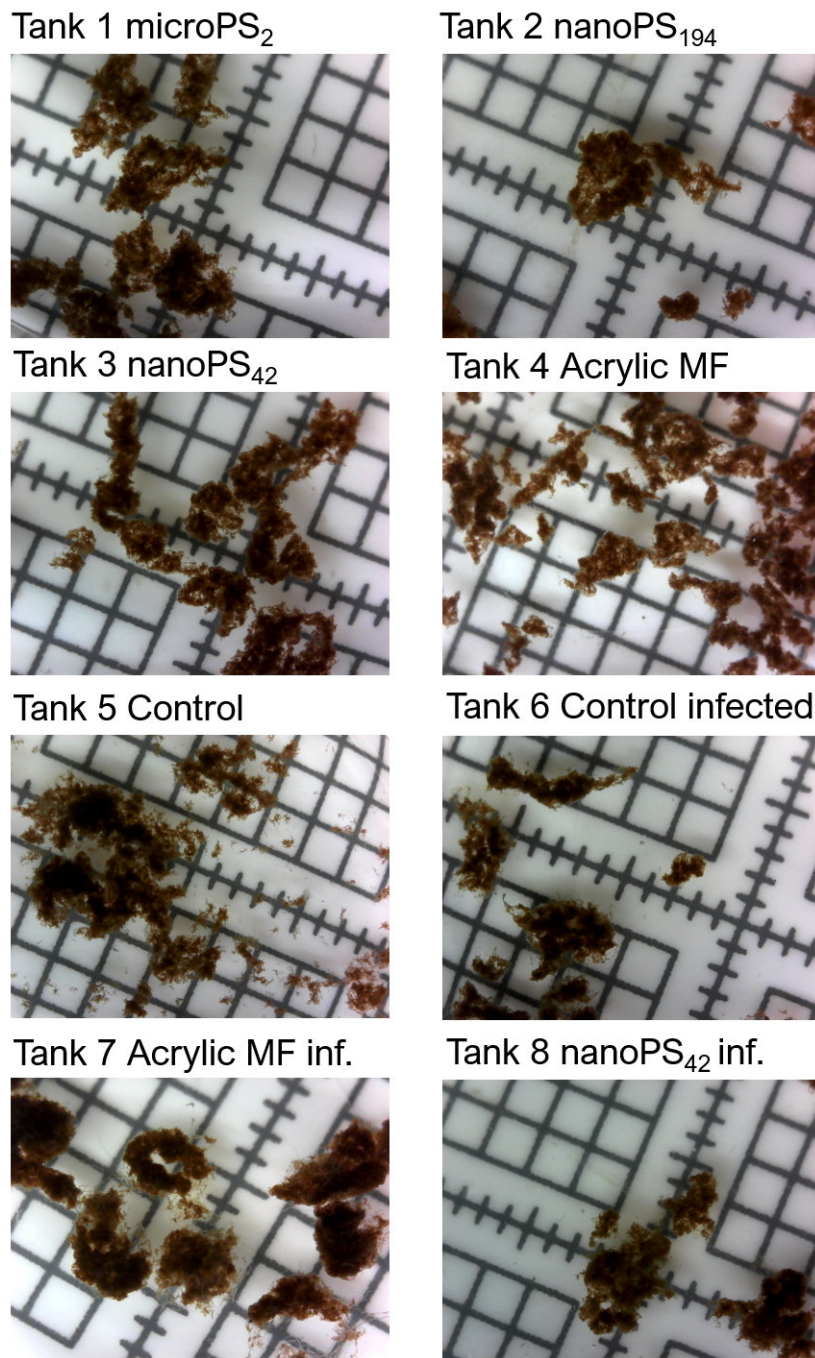
Tank	Concentration	Plastic Type	Infection
1	0.01 mg/L	microPS <sub>2</sub>	no
2	0.01 mg/L	nanoPS <sub>194</sub>	no
3	0.01 mg/L	nanoPS <sub>42</sub>	no
4	1 mg/L	Acrylic fibers	no
5	Pos. Control	none	no
6	Pos. Control	none	yes
7	1 mg/L	Acrylic fibers	yes
8	0.01 mg/L	nanoPS <sub>42</sub>	yes
9	Neg. Control	none	no

The experiment was run from 23rd to 30th of July, 2018, at 20°C in the dark with 2 rpm. Aggregates formed on the first day. Sinking velocities, TEP, and PAM measurements were taken on the sampling day, and 3D imaging was done on 1st and 2nd of August. The data shows preliminary results, as no biological replicas were performed.



**Figure 2.15: Infection of the *Odontella aurita* culture.** (a) *Odontella aurita* cells in the Agg fraction of the control tank. When focusing on the lower plane (b), the ciliate infection becomes visible. The cells are much smaller than the *Odontella aurita* chains on top. While the *Odontella aurita* chains are entangled, staying in some form of aggregate even after homogenization and filtration, the infection does not stick together. Images were taken with Zeiss Axio Imager Z1 microscope.

Some visual differences between aggregates of different treatments could be observed on harvest day (see Figure 2.16).



**Figure 2.16:** Visual differences in *Odontella aurita* aggregates on harvesting day. One square is 5 times 5 mm. Pictures were taken with Carson eFlex microscope under experimental temperature conditions and in SSW from corresponding tanks.

The visual differences include the density of infected aggregates (Tank 6, 7, and 8) in contrast to uninfected aggregates (Tank 1 – 5). The uninfected control (Tank 5) had many aggregates smaller than one mm and the uninfected treatments looked similar, even for the aMF.

***Synechococcus elongatus* Experiments** Four experiments were run on the cyanobacteria *Synechococcus elongatus*, with two different nano polystyrene (nanoPS) plastic sizes (42 nm (nanoPS<sub>42</sub>))

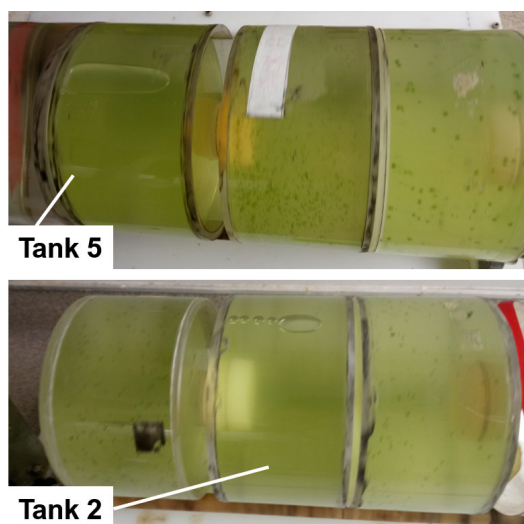
and 194 nm (nanoPS<sub>194</sub>), two different fiber types (polyester and acrylic) and a trial with 2  $\mu\text{m}$  polystyrene (microPS<sub>2</sub>) (data not displayed). All experiments were run in the same climate chamber at 20°C in the dark. Within each experiment, replication was achieved through having two tanks for each of the concentrations (control with 0 mg/L, low plastic at 0.01 mg/L in beads and 0.1 mg/L in fibers, high plastic at 1 mg/L). The four experiments thus provide insight into aggregation processes under four different conditions. For the set up, see Figure 2.20.

#### NanoPS<sub>194</sub> Experiment in *Synechococcus elongatus* –

This experiment was conducted from June 23rd to 28th of June 2018. It was run at 20°C in the dark. Aggregate formation started the same day. On 26th of June, the tanks were transferred to a faster rotation table because the formed aggregates kept hitting the bottom of the tank. The revolutions per min were increased from 3 rpm to 6.6 rpm. The tanks were allowed to rotate for a total of 6 days, and tank harvest of the biological replica was done on 6th of July. Sinking velocities and PAM measurements were taken the same day, and 3D imaging was done on 30th of June and 1st of July. Cell count at  $T_0$  was about  $22.65 \times 10^6$  cells/mL. The analysis of the photometer data for this experiment did not show any differences between the treatment and the control. However, not all data were taken with the same Aquapen and the same settings, which is important for comparison of the data. This makes the results inconclusive. Data is not displayed.

#### NanoPS<sub>42</sub> Experiment on *Synechococcus elongatus* –

This experiment was conducted from 29th of June to 6th of July 2018. It was run at 20°C in the dark. Aggregate formation started the same day. The tanks were allowed to rotate for another six days, and harvest of the biological replica was done on 6th of July. Sinking velocities and PAM measurements were taken the same day, and 3D imaging was done on 7th and 8th of July. Cell count at  $T_0$  was about  $24.84 \times 10^6$  cells/mL.



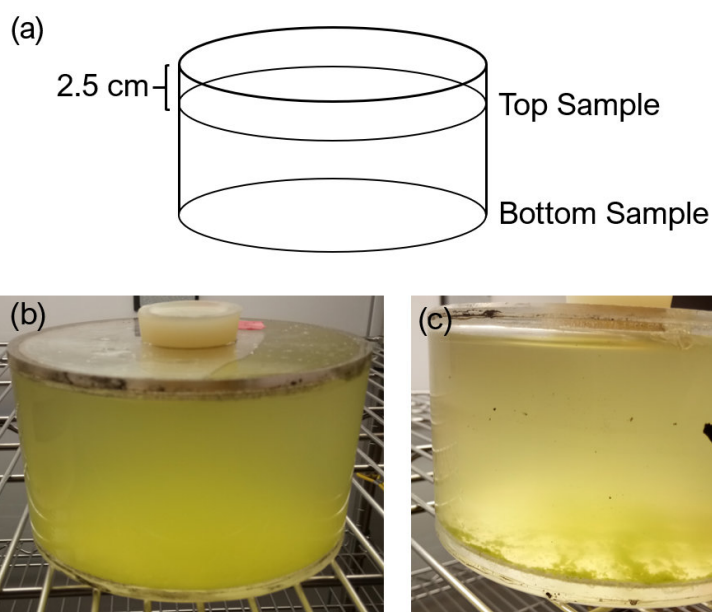
**Figure 2.17: Bubbles found in Tank 5 and Tank 2.** In comparison to the other tanks, bubbles present in Tank 5 and Tank 2 could have caused missing aggregation of cells in those tanks. There was not even a slurry fraction to sample after settling time. All cells remained freely suspended.

Bubbles formed within two tanks (see Figure 2.17) and could have caused missing cell aggregation. As exposure to nanoPS has recently been shown to increase hetero-aggregation [169] in *Synechococcus elongatus* PCC 7002 and the lack of even a settling slurry fraction could likely be due to increased turbulence caused by the formed bubbles. This bubble formation in two of the treatment tanks introduced unevenness into the statistical analysis of the sinking velocities, TEP concentration, and photosystem measurements.

#### Polyester MF Experiment on *Synechococcus elongatus* –



This experiment was conducted from 20th to 27th of July, 2018. It was run at 20°C in the dark. The tanks were allowed to rotate for six days, and harvest of the biological replica was done on 27th of July. There was no aggregation during the experiment time, but a fine dust was observed in the high plastic treatment (1 mg/L) (see Figure 2.18 (c)). This will be referred to as “dust aggregation” from here on, referring to the fine cell aggregates < 1 mm that settled at the bottom of the tank. None of them included fibers. Due to the lack of traditional aggregates, a different sampling technique was applied. The tanks were laid on their side and were allowed to settle for 1.5 hours (see Figure 2.18 (a)). After, the bottom part was deemed to be slurry, as all cell aggregates not buoyant accumulated on the bottom of the tank. The SSW fraction was taking 2.5 cm below the top. While the control and 0.1 mg/L treatment did not show any accumulation of cell dust on the tank bottom (see Figure 2.18 (b)), the 1 mg/L plastic treatment did (see Figure 2.18 (c)). Cell count at  $T_0$  was about  $39.08 \times 10^6$  cells/mL.



**Figure 2.18:** The MF treatments in *Synechococcus elongatus* did not lead to any aggregation, as in the other experiments. (a) Location of the samples in the treatment without aggregation. Tanks were laid on the side and after 1.5 h were sampled for TEP and Aquapen measurements. (b) No aggregation in Tank 5 (control) and (c) dust aggregation in Tank 4 (1 mg/L treatment).

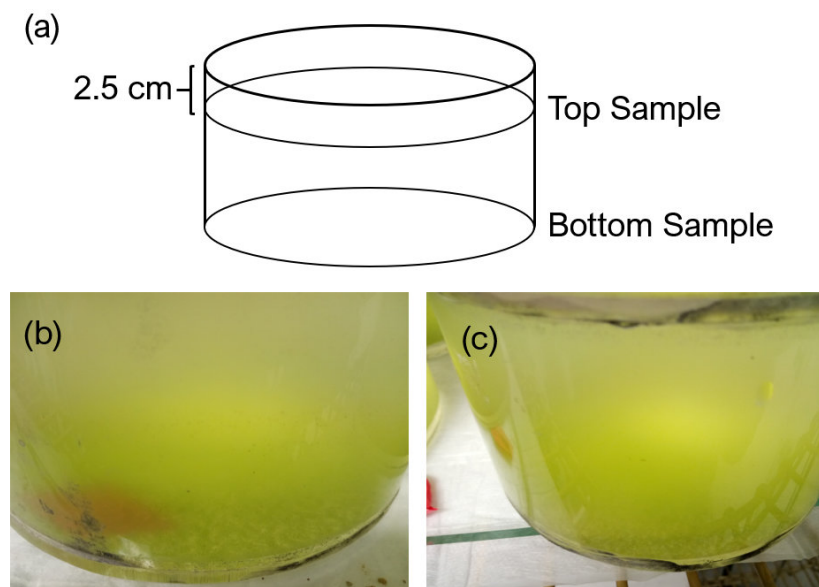
TEP and PAM measurements were taken the same day, but no 3D imaging samples were taken. No sinking velocities could be measured due to only dust aggregation. So far, there are no studies on *Synechococcus elongatus* and plastic MF. These are the first reports on changes in *Synechococcus elongatus* due to the exposure to such anthropogenic stressors. As no aggregation was observed in the controls of this experiment, it is clear that the lack of aggregates is not due to the presence of plastic. In fact, the dust aggregation seen in the 1 mg/L treatment tanks supports the theory that if *Synechococcus elongatus* does not aggregate, the presence of plastic leads to increased aggregation, forming dust aggregates that sink faster than unaggregated cells. To better understand the reason for this, we compared TEP and PAM measurements between the fractions.

#### Acrylic MF Experiment on *Synechococcus elongatus* –

This experiment was conducted from 27th of July to 3rd of August 2018. It was run at 20°C



in the dark. The tanks were allowed to rotate for six days, and tank harvest of the biological replica was done during one day (3rd of August). Again, there was no aggregation during that time, but a fine dust was observed in all tanks. This dust aggregation was different in color and size from the previous experiment (compare Figure 2.18 to Figure 2.19). Sampling was done in top and bottom fractions, as explained in the previous section (see Figure 2.19). The low plastic treatment was at 0.1 mg/L. Cell count at  $T_0$  was about  $32.75 \times 10^6$  cells/mL.



**Figure 2.19: The aMF treatments in *Synechococcus elongatus* only yielded dust aggregation.** (a) Location of the samples in the treatment without aggregation. Tanks were laid on the side, and after 1.5 h were sampled for TEP and Aquapen measurements. (b) Dust aggregation in treatment Tank 2 (0.1 mg/L) and (c) in control Tank 5.

TEP and PAM measurements were taken the same day, and 3D imaging was done on the following weekend. No sinking velocities could be measured due to only dust aggregation.

As mentioned above, besides this study, no other aggregation studies with *Synechococcus elongatus* and plastic MF are reported. The results of this aMF experiment were to be compared to the pMF experiment. Again, only a dust aggregation was observed in all tanks (see Figure 2.19) irrespective of treatment. Aggregation in this experiment was different from the pMF, where dust aggregation of different color and size was only observed in the highest plastic concentration.


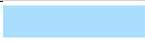








**Figure 2.20: Rolling table setup for *Synechococcus elongatus*.** To avoid artifacts in the data due to placement, one tank of each treatment was placed on the top and bottom levels.

## 2.4 Results and Discussion

Results and discussion are presented together, divided into sections about sinking velocity (Section 2.4.1), transparent exopolymer particles (TEP) concentration (Section 2.4.2), photophysiology (Section 2.4.3), and 3D images (Section 2.4.4). Each section is divided to address species separately. For easy comparison, the same color coding for the different treatments are used throughout the section (see Figure 2.6).

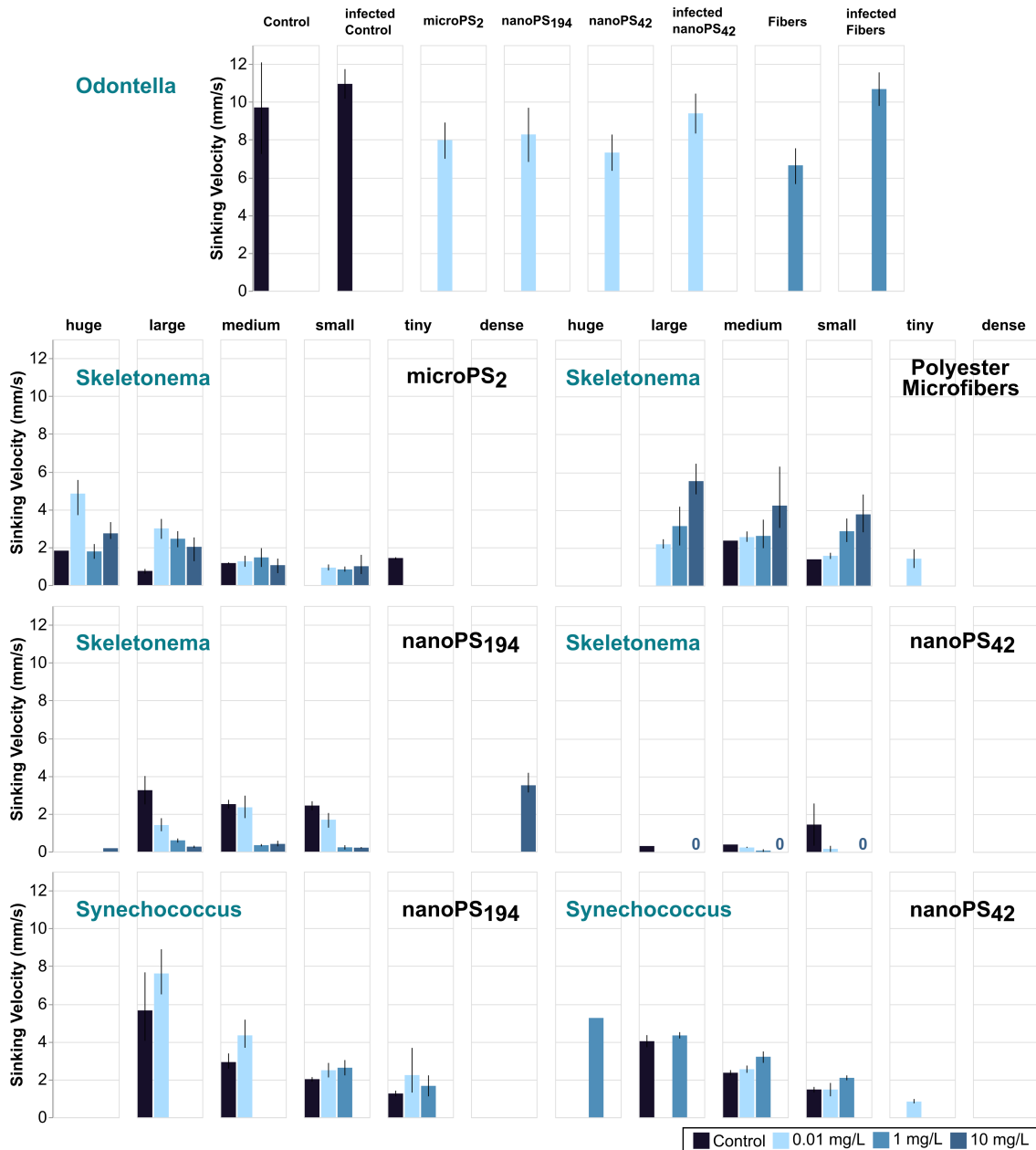
**Table 2.6:** Color coding in the different sections is consistent to make figures and graphs comparable:

Fraction	0 mg/L	0.01 mg/L	0.1 mg/L	10 mg/L
Aggregate (Agg) fraction				
Seawater (SSW) fraction				

### 2.4.1 Sinking Velocities

Three aggregates per size class were measured for their sinking velocity over 29.3 cm in a 100 mL glass graduated cylinder (see Section 2.2.5 for details). In a comparison between all species, *Odonotella aurita* has by far the fastest sinking velocities with 1234 meters per day (14.29 mm/s) (see Figure 2.26). The slowest sinking velocities were found in the *Skeletonema grethae*, where nanoPS<sub>42</sub> incorporation led to neutrally buoyant aggregates (see Figure 2.4.1).

From the direct comparison of all sinking velocities and aggregate size distributions (see Figure 2.21) the direct and indirect (via aggregate size distribution) effect of  $\mu\text{P}/\text{nP}/\text{MF}$  on aggregation and sedimentation becomes evident.



**Figure 2.21: Comparison of sinking velocities over all experiments.** The y axis was scaled to the fastest sinking *Odontella aurita*, to make a direct comparison possible. The error bars display confidence intervals.

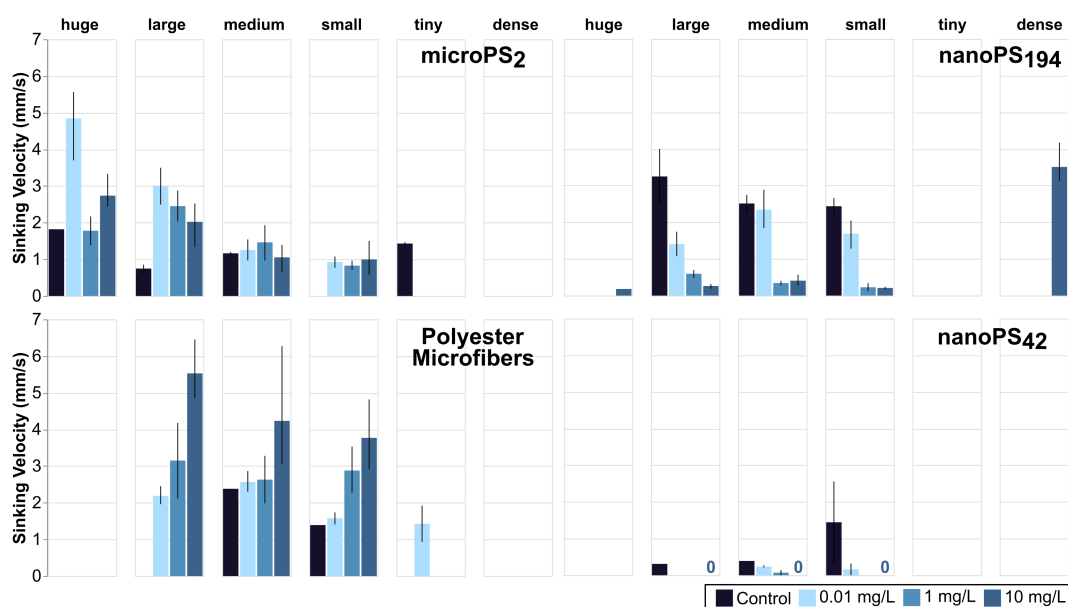
Overall, sinking velocities varied between the species and treatments. Decreasing bead size (from microPS<sub>2</sub> to nanoPS<sub>42</sub>) led to a decrease in sinking velocity to the point of neutral buoyancy in *Skeletonema grethae* (ANOVA,  $p < 0.001$ ), but not in the other two species.

Incorporation of MF also led to different results depending on the species. In *Skeletonema grethae*, sinking velocities of the pMF led to increased sinking velocities, while in *Odontella aurita* to a reduction in sinking velocities. The presence of MF increased aggregation in *Synechococcus elongatus* as the control cultures in those experiments did not aggregate well. As the MF have a higher density than water, the incorporation was expected to lead to higher sinking velocities, but

the increased aggregation was unexpected.

### *Skeletonema grethae* –

Sinking velocities were highest in the pMF experiment, with medium aggregates in the 10 mg/L treatment sinking with up to 960 meters per day (11.11 mm/s). The lowest measured sinking velocity was zero, which means that aggregates were neutrally buoyant over hours. This was observed in the 10 mg/L treatment in the nanoPS<sub>42</sub> experiment. Control aggregates in all experiments sank between 27 and 345 meters per day (0.3125 and 3.99 mm/s), depending on their size.

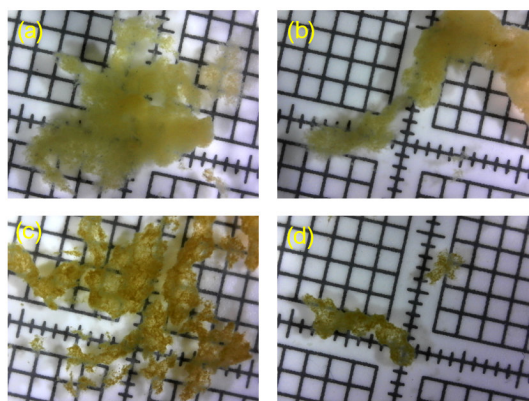


**Figure 2.22: Sinking velocities between *Skeletonema grethae* experiments.** Not all experiments displayed all size classes of aggregates, and not all aggregates could be sampled due to increased fragility (nanoPS<sub>42</sub>). Zeros in nanoPS<sub>42</sub> indicate neutral buoyancy in the treatment. Same data is displayed as in Figure 2.21, with different scaling to make the differences within the experiments more visible. The bars display confidence intervals.

In the microPS<sub>2</sub> experiment in *Skeletonema grethae*, differences between the control and the 0.01 mg/L treatment for the huge and large aggregates were significant (Kruskal-Wallis,  $p < 0.001$ ; Holm-Sidak,  $p = 0.05$ ). Sinking velocity increased in these aggregates from  $65 \pm 11$  meters per day in the control to  $100 \pm 3$  meters per day (0.0347 mm/s) in the treatment. Similarly, incorporation of oil into aggregates leads to an increase in sinking velocities as well [160]. Still, since sedimentation velocities are very heterogeneous, to begin with, depending on many factors within the plankton community, the effects are hard to determine [195]. In Long et al. [97], who also used microPS<sub>2</sub> at a similar highest concentration, changes in sinking velocities depended on the phytoplankton species. In the diatom *Chaetoceros neogracile*, sinking velocities reduced and in the cryptophyte *Rhodomonas salina* they increased [97]. The interplay between the added oil and the increased exudate (TEP) production has been observed to change the sinking behavior [99] as well. The vertical transport of  $\mu\text{P}$  within phytoplankton aggregates has been proposed as a sink of  $\mu\text{P}$ , explaining the low surface  $\mu\text{P}$  concentrations found compared to expected values (calculated and

modeled) [97, 47]. The deep sea as a  $\mu\text{P}$  sink [103] becomes more likely with the increasing sinking velocities measured in our experiment and other recent publications [97, 169].

Moving to the next smaller bead size, the aggregate size distribution of aggregates was different, and much smaller aggregates formed in the nanoPS<sub>194</sub> experiment in *Skeletonema grethae* than with the microPS<sub>2</sub> beads. For the nanoPS<sub>194</sub>, significant reductions can be seen between control and the 1 and 10 mg/L treatments (Kruskal-Wallis,  $p < 0.001$ ). This is in contrast to the microPS<sub>2</sub> experiment, and more in line with reports from the literature [97, 169]. Control aggregates sank as fast as 345 meters per day or 3.99 mm/s (mean  $280 \pm 65$  meters per day, or  $3.24 \pm 0.752$  mm/s) while aggregates of the same size in the 10 mg/L treatment only sank an average of 22 meters per day  $\pm 5$  meters per day ( $0.255 \pm 0.0579$  mm/s). Especially dense aggregates were observed in the 10 mg/L treatment of this experiment, and their sinking velocity measured as an additional class with up to 360 meters per day or 4.17 mm/s (average 303 meters per day  $\pm 40$  meters per day, or  $3.51 \pm 0.463$  mm/s). This was equal to the controls of the same size aggregates (see Figure 2.23). No such aggregates were observed in any of the other experiments or treatments.

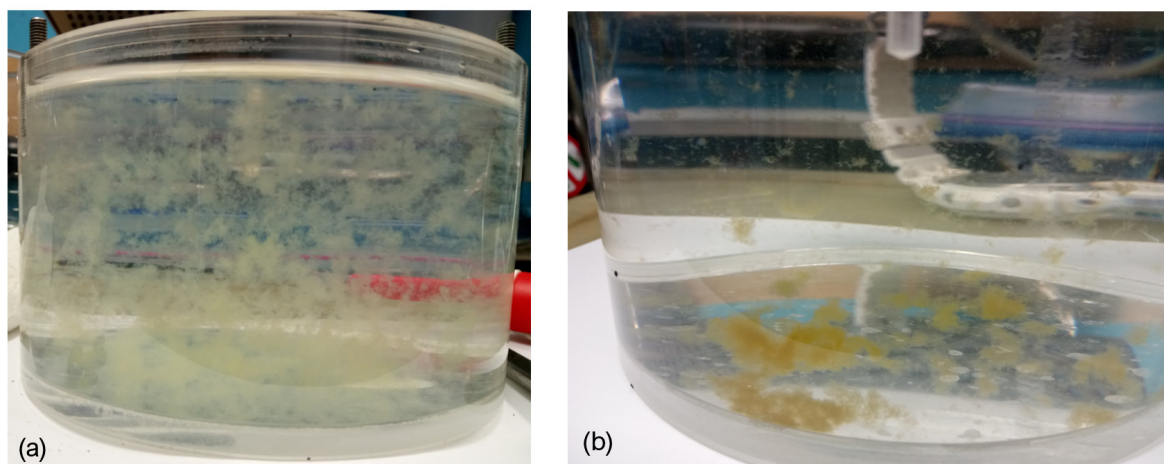


**Figure 2.23: Images showing dense aggregates** from the 10 mg/L treatment (top row, a and b) compared to control treatments (bottom row, c and d) of the same size in the NanoPS<sub>194</sub> experiments. The same sized aggregates (a/c and b/d) sunk equally fast. The large aggregates of the 10 mg/L treatment (a and b) are a very dense version with smooth edges of the controls (c and d). However, the control treatment aggregates appear darker and less uniform. While other similarly sized but less dense aggregates (not shown here) of the 10 mg/L treatment did not sink as fast, the increased density (a and b) could be explained by a change in cell packaging. One square is 5 times 5 mm. Pictures were taken with Carson eFlex microscope under experimental temperature conditions and in SSW from corresponding tanks.

Sedimentation in the nanoPS<sub>42</sub> experiment in *Skeletonema grethae* was even lower than in the previous two experiments and, for some aggregates, it was as low as zero, i.e., aggregates were neutrally buoyant without any sinking movement observed. Although all treatments had at least one aggregate of neutral buoyancy, the 10 mg/L treatment aggregates did not move at all within 3 hours (see Figure 2.24). The zeros indicate this in Figure 2.22. The 10 mg/L treatment is significantly different from the control (Kruskal-Wallis,  $p = 0.005$ ). Sinking velocities between the treatments only varied significantly for the medium-sized aggregates (Kruskal-Wallis,  $p = 0.032$ ). Sinking Velocities in all treatments and aggregate sizes of the nanoPS<sub>42</sub> varied significantly from those of microPS<sub>2</sub> (ANOVA,  $p = 0.001$ ). Decreased sinking velocities in the presence of  $\mu\text{Ps}$  have been reported for diatoms before [97]. A stronger effect is expected with decreasing particle size [175], as the particle number has increased by more than four orders of magnitude in the same treatment between the



microPS<sub>2</sub> and nanoPS<sub>42</sub>.

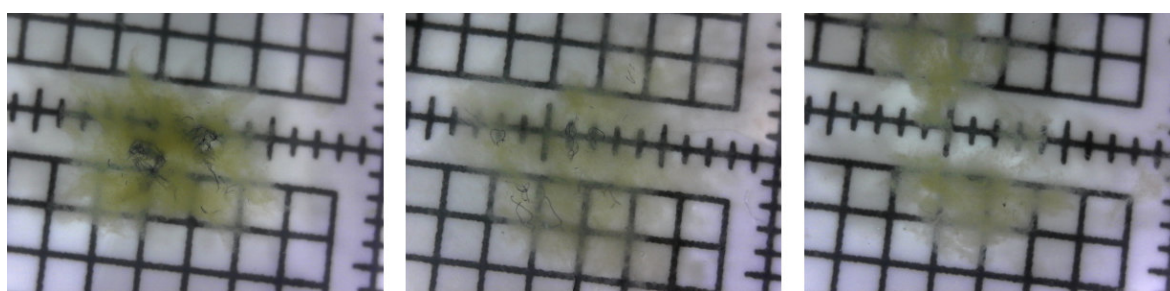


**Figure 2.24: Comparison of (a) Tank 7 (10 mg/L) to (b) Tank 3 (0.01 mg/L).** Aggregates that formed in Tank 7 did not sink over a period of 3 hours while aggregates in Tank 3 settled within 5 min. The color difference between tanks did not lead to a difference in  $F_0$  measurements (see Section 2.4.3). This indicates that chlorophyll concentration differences, not cell concentration differences are responsible.

Especially at lower plastic concentrations, where the increase in particle number between plastic sizes is small, a particularly interesting pattern with higher sinking velocities in the presences of microPS<sub>2</sub> compared controls was observed in contrast to the decreased sinking velocities under nanoPS<sub>42</sub> exposure. As these results show, there remains much to be understood about microalgae's reactions to different sized  $\mu\text{P}/\text{nP}$ . Exposure comparison of natural to synthetic particles has been proposed as important [122], especially since polymers found in the deep sea are not only plastic but also other man-made, non-plastic materials (e.g. Rayon) [103]. Koegel et al. [175] discusses the different impacts of different concentrations and sizes of  $\mu\text{P}/\text{nP}/\text{MF}$  on microalgae. It is important to understand the natural environment in which the respective microalgae occur and which particles (natural or otherwise) studied species might be exposed to. The dinoflagellates studied in Chapter 4 of this thesis are found in reef environments, which naturally has more suspended particles in the water column with which the cell can interact. The environment simulated for *Skeletonema grethae* – the open ocean and water column – does not have many naturally-occurring suspended particles of abiotic origin; hence exposure to plastic particles is a stress the algae have little pre-adaptations for. Introducing abiotic stressors in the form of  $\mu\text{P}/\text{nP}/\text{MF}$  could lead to a shift in plankton communities, favoring those species that deal better with plastic. This is mirrored in the microorganisms found in the “plastisphere” of  $\mu\text{P}$ . The attached communities are markedly different from the microorganism communities in the surrounding seawater [64]. Microorganisms, including diatoms attached via EPS [65] to the  $\mu\text{P}$ . The incorporation of  $\mu\text{P}/\text{nP}/\text{MF}$  could lead to a similar change of interacting plankton communities.

The presence of pMF in *Skeletonema grethae* had significant impact on sinking velocity at the highest plastic concentration for all aggregate sizes (Kruskal-Wallis,  $p < 0.001$ ). As the control did not aggregate well, it can be said that the presence of pMF increased aggregate formation in a diatom culture that otherwise displays poor aggregation. While control aggregates showed an average

sedimentation of  $162 \pm 42$  meters per day ( $1.88 \pm 0.486$  mm/s), those in the 10 mg/L treatment sank at to 200 meters per day (2.31 mm/s) faster in the same aggregate size classes. Small aggregates also sank faster in the 1 mg/L treatment compared to controls. Since pMF are not buoyant themselves, incorporation leads to faster sinking velocities of the aggregates, increasing sedimentation (see Figures 2.25 and D.23, D.24). Changes in aggregate size distribution were also seen in this experiment; the control cells aggregated very little (see Section 2.4.2 Figure 2.31). This hints at unfavorable aggregation conditions within the culture, demonstrating that when conditions are not optimal for forming aggregates, the presence of pMF will lead to more aggregates. Potentially, this result has a stronger impact on plankton communities, as aggregates would be formed under conditions that usually do not lead to these diatoms' aggregation.



**Figure 2.25: pMF in aggregates of different treatments.** The left aggregate is from the 10mg/L treatment, and tangled MF can be seen in the center while cells form an aggregate around them. The middle image is of the 1 mg/L treatment, much fewer MF are visible, and they are not tangled at the center. For reference, a control aggregate is displayed on the right. All MF started out disentangled and collisions in the rolling tank over time formed them into these little knots. One square is 5 times 5 mm. Pictures were taken with Carson eFlex microscope under experimental temperature conditions and in SSW from corresponding tanks.

Although all  $\mu$ P found in the deep sea study by Taylor et al. [157] were MF and with the majority of  $\mu$ P in the ocean being MF [183], no literature has been published on the transport of MF from the surface to the deep sea. These fibers were found to be ingested by organisms with different feeding mechanisms. Other expeditions have found MF at varying depths on the seafloor [196] and at a similar concentration as found in other marine habitats (between 3 to 40 MF in 50 mL of sediment from North Atlantic and Mediterranean seafloor and SW Indian ocean) [103]. As most deep-sea organisms rely on marine snow input for sustenance, either directly or indirectly, the incorporation of MF into these aggregates should be studied to evaluate the impact on marine ecosystems. Incorporation of MF yields a very different result to the incorporation of either beads in this experiment or of oil in other experiments. Both, oil and beads are spherical and, depending on the size, can directly attach to the cell surface. MF, with a markedly bigger diameter of 6  $\mu$ m and above, are more likely to have cell aggregates form around them (see Figure 2.25). The resulting aggregates sink faster, allowing for less time spent within the water column. While this ensures removal from the water column and deposition into the sediment, the bigger size combined with less time spent in the water column will also lead to less biofouling of MF, making them arrive in the deep sea largely unchanged [157]. Currently, there is a knowledge gap on the effects of MF on phytoplankton aggregates, as no study has been published to match those done with microbeads. There is a 2019 work [185] on the effects of MF on the microalgae *Isochrysis galbana*, but no aggregates were studied. As 70 to 100 % of  $\mu$ P found on the deep seafloor are MF [197,



157], the question of the fate of fragments (in these experiments represented as beads) remains. If, as seen in the nanoPS<sub>42</sub> and nanoPS<sub>194</sub> experiments, sinking velocities are reduced, it is possible that hetero-aggregates are dispersed through the water column, thereby never reaching the ocean floor. Similarly possible is the bio-fouling by the smaller nP on the way to the seafloor, resulting in chemically changed aggregates.

A first look at the changes in cell packaging was done through measurements of the 3D images aggregates. As only one aggregate per treatment has been measured so far, this is not statistically relevant, but a first look at possible explanations for sinking velocity changes though cell packaging.

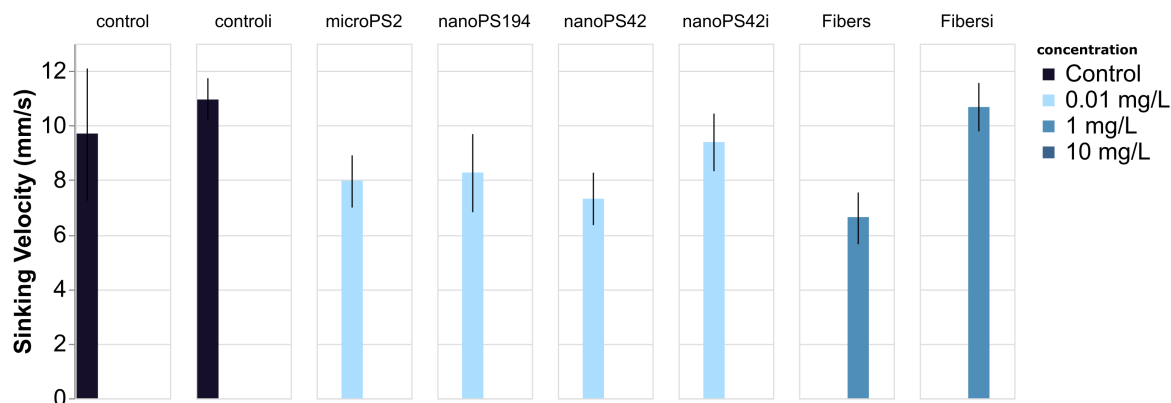
**Table 2.7: Aggregate Volume Comparison for *Skeletonema grethae*.** The total bio-volume is compared to the estimate of the aggregate volume to get the ratio. For the bio-volume we consider the cells to be spherical and of 6  $\mu\text{m}$  diameter whereas the aggregate is roughly an ellipsoid. Equivalent spherical diameter (ESD).

Treatment	Cell Count	Biovol. ( $\mu\text{m}^3$ )	Agg. Vol. ( $\mu\text{m}^3$ )	Agg. ESD	Ratio
microPS <sub>2</sub> @ Control	513	58,019	$9.76 \times 10^6$	265.18	0.594%
microPS <sub>2</sub> @ 0.01 mg/L	5538	626,333	$5.85 \times 10^8$	1037.64	0.107%
microPS <sub>2</sub> @ 1 mg/L	2600	294,053	$1.71 \times 10^8$	688.9	0.0339%
microPS <sub>2</sub> @ 10 mg/L	7469	844,724	$6.9 \times 10^8$	1096.29	0.122%
nanoPS <sub>194</sub> @ Control	10,400	$1.18 \times 10^6$	$2.22 \times 10^7$	348.6	5.3%
nanoPS <sub>194</sub> @ 0.01 mg/L	6885	778,675	$3.44 \times 10^8$	869.13	0.227%
nanoPS <sub>194</sub> @ 1 mg/L	6006	679,263	$6.39 \times 10^8$	1068.6	0.106%
nanoPS <sub>194</sub> @ 10 mg/L	356	40,263	$1.06 \times 10^6$	126.5	3.8%
nanoPS <sub>42</sub> @ Control	4540	513,462	$3.91 \times 10^8$	907.26	0.131%
nanoPS <sub>42</sub> @ 0.01 mg/L	14	1583	698,199	110.07	0.227%
nanoPS <sub>42</sub> @ 1 mg/L	14	1583	2639	17.15	60%

### *Odontella aurita* –

The sinking velocity of aggregates in this experiment was not separated into size classes. Twenty-five aggregates distributed in three sets were measured in each tank (see Figure 2.26). Sinking velocities varied between 131 meters per day (1.52 mm/s) in the aMF treatment to 1234 meters per day (14.29 mm/s) in the infected control and infected aMF treatment.

Nevertheless, statistical differences have to be viewed with care, as no biological replicas were performed. No statistical difference in the sinking velocities could be observed between the control and infected control tanks (independent t-test,  $p = 0.492$ ). This leads to the conclusion that the infection does not affect aggregation and sedimentation when the competing infection is the only stressor of the *Odontella aurita*. The average sinking velocity in controls was 957 meters per day (11.08 mm/s). The sinking velocities are comparable to reported values of aggregation experiments conducted with *Odontella aurita* in the presence of oil (average 980 meters per day) [99].



**Figure 2.26: Comparison of sinking velocities in *Odontella aurita*.** Same data is displayed as in Figure 2.21, with different scaling to make the differences within the experiments more visible. The error bars display confidence intervals.

However, the incorporation of different plastics had a significantly negative effect, resulting in decreased sinking velocity for all plastic types and concentrations in the clean treatments in comparison to the controls (Kruskal-Wallis, control vs. plastic treatments,  $p < 0.001$ ). The average sinking velocity in the clean treatments was only 653 meters per day (7.56 mm/s). In contrast, the infected treatment aggregates sank just as fast as the controls at 860 meters per day (9.96 mm/s). The incorporation of the lighter microPS<sub>2</sub>, nanoPS<sub>194</sub> and nanoPS<sub>42</sub> could explain the decrease in sinking velocities.

Incorporation of aMF led to a reduction in sinking velocities. As this fiber has a higher density than water, the incorporation was expected to lead to higher sinking velocities, as seen in *Skeletonema grethae* under pMF exposure (see Figure 2.4.1). The cell to volume ratio calculated for the 3D imaged aggregates (see Appendix D) shows that the infected aMF aggregate has a higher cell packaging density (2.12% to 5.10%, see Table 2.8), corresponding to the increased sinking velocity. More testing is needed to draw definitive conclusions.

**Table 2.8: Aggregate volume comparison in *Odontella aurita*.** Total bio-volume is compared to the estimate of the aggregate volume in the ratio. For the bio-volume we consider the cells to be ellipsoid of  $20 \mu\text{m} \times 20 \mu\text{m} \times 50 \mu\text{m}$  and the aggregate is roughly an ellipsoid. Equivalent spherical diameter (ESD).

Treatment	Cell Count	Biovol. ( $\mu\text{m}^3$ )	Agg. Vol. ( $\mu\text{m}^3$ )	Agg. ESD ( $\mu\text{m}$ )	Ratio
Control	1158	$9.7 \times 10^6$	$3.76 \times 10^8$	895.21	2.58%
Infected Control	182	$1.52 \times 10^6$	$1.06 \times 10^7$	272.96	14%
$\mu\text{PS}_2$	569	$4.77 \times 10^6$	$3.69 \times 10^7$	412.95	12.9%
nPS <sub>194</sub>	1237	$1.04 \times 10^7$	$4.63 \times 10^8$	959.63	2.24%
nPS <sub>42</sub>	445	$3.73 \times 10^6$	$1.09 \times 10^8$	593.5	3.4%
Infected nPS <sub>42</sub>	1158	$9.7 \times 10^6$	$6.08 \times 10^8$	1051.21	1.6%
aMF	674	$5.65 \times 10^6$	$2.66 \times 10^8$	798.24	2.12%
Infected aMF	432	$3.62 \times 10^6$	$7.1 \times 10^7$	513.85	5.1%

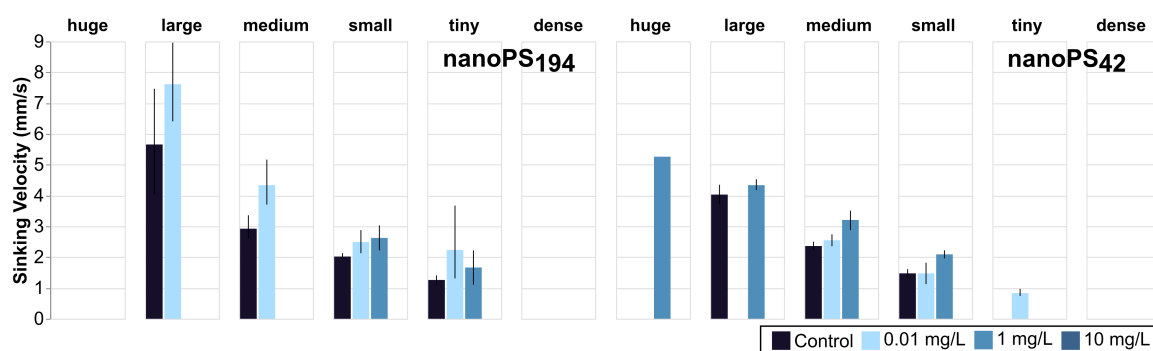
In the treatment tanks, the infection apparently played a role in changing sedimentation, as

it led to faster sinking aggregates, both in the nanoPS<sub>42</sub> treatment (independent t-test, one-tailed p-value =  $5.52 \times 10^{-3}$ ) and the aMF treatment (independent t-test,  $p < 10^{-3}$ ). This is different from the control, pointing towards an interaction between the two stressors. Especially on population levels, this interplay of stressors becomes interesting, as it could lead to changes in plankton communities. More investigations with multi-stressor experiments are needed to understand the dynamics between the plastics and plankton.

### *Synechococcus elongatus* –

Sinking velocities ranged from  $\sim 11$  mm/s in the 0.01 mg/L treatment of the nanoPS<sub>194</sub> experiment to less than  $\sim 1$  mm/s in the same treatment of the nanoPS<sub>42</sub> experiment (see Figure 2.27). No sinking velocities were measured in the pMF and aMF experiments, due to limited dust aggregation. While the controls of both experiments did not differ (t-test,  $p = 0.879$ ), the two treatments did (1 mg/L: t-test, one-tailed  $p = 0.00350$ ; 0.01 mg/L: t-test,  $p < 0.001$ ) (see Figure 2.27). This can be linked to a difference in aggregate size distribution (see Figure 2.33).

Sinking velocity and aggregate size distribution in the 0.01 mg/L treatment were higher and bigger, respectively, in the nanoPS<sub>194</sub> *Synechococcus elongatus* experiment, than in the 1 mg/L treatments, while the opposite is true for nanoPS<sub>42</sub>, where the 1 mg/L treatment showed bigger sized and faster sinking aggregates. While there is no difference in the sinking velocities of aggregates in each size class between control and treatments, the size of aggregates is affected (see Section 2.4.2 Figures 2.32 and 2.33). The 1 mg/L treatment only yielded small and tiny aggregates. While not significantly different, there is the potential for a 200 meters per day increase in sinking distance with the measured velocities, between the control and 0.01 mg/L treatment in the large aggregates.



**Figure 2.27: Comparison between sinking velocities for *Synechococcus elongatus* experiments between nanoPS<sub>194</sub> and nanoPS<sub>42</sub>.** Sinking velocity is displayed for both *Synechococcus elongatus* that yielded aggregates. Where possible, three aggregates per size class were measured. Absence of a column indicates no aggregates of that size were found in the treatments. Same data is displayed as in Figure 2.21, with different scaling for the differences within the experiments more visible. No 10 mg/L treatments were run for *Synechococcus elongatus*. The error bars display confidence intervals.

The incorporation of nanoPS<sub>42</sub> in *Synechococcus elongatus* led to significantly increased sinking velocities in *Synechococcus elongatus* in medium and small aggregates of the 1 mg/L treatment (Holm-Sidak,  $p = 0.047$ ). The 0.01 mg/L treatment produces smaller aggregates, but sinking velocities are in the same range as controls. Sinking velocities ranged from 5 mm/s in the 1 mg/L

treatment to less than one mm/s in the 0.1 mg/L treatment. Sinking velocities in the nanoPS<sub>42</sub> experiment were significantly lower than seen in the nanoPS<sub>194</sub> experiment overall and specifically different between treatments. Also, sinking velocities within this experiment differed between the control and the treatments.

Changes in sinking velocities have been reported for *Synechococcus elongatus* PCC 7002, induced by incorporation of nanoPS [169]. In our study, the 1 mg/L treatment aggregates in size classes medium and small sank significantly faster (Holm-Sidak,  $p = 0.047$ ), which could be due to higher cell packaging within these aggregates. The results in the study by de Oliveira [169] also suggests an increased effect with smaller sizes of nanoPS which was in line with our results. While the nanoPS<sub>194</sub> treatments did not show changes in sinking velocities, the ones with the smaller nanoPS<sub>42</sub> did.

Incorporation of nanoPS in marine cyanobacteria aggregates increases the speed of settling of these hetero-aggregates. The lower 0.01 mg/L treatment resulted in a reduced sinking velocity overall in this experiment but when compared by aggregate size, no difference to controls could be seen. This was the same result as was observed in the nanoPS<sub>194</sub> experiment for the 0.01 mg/L treatment, suggesting the amount of nanoPS was not high enough to induce an increase in sinking velocity. From similar experiments with oil incorporation into diatom aggregates [99], it is known that this incorporation of a similarly hydrophobic, fossil carbon derived, and less dense than seawater substance leads to an increase in sinking velocity. As both nanoPS and oil incorporation lead to higher sinking velocities compared to controls, a similar mechanism might be at play. In Passow et al. [99] higher cell packaging was proposed to explain the higher sinking velocities. This is supported by our ratios in the nanoPS<sub>42</sub> experiment but not in the nanoPS<sub>194</sub> experiment (see Table 2.9). Changes in aggregation could be aided by nutrient depletion within the *Synechococcus elongatus* culture, as nutrient depletion has been linked to changes in aggregation [189]. This nutrient depletion has been suggested by Nolte et al. [151] to be caused by  $\mu\text{P}/\text{nP}$  presence.

While not statistically relevant, the first look at changes in the cell to aggregate volume ratio is presented in Table 2.9. Just as with sinking velocities, the cell to aggregates volume ratio in the nanoPS<sub>42</sub> experiment was different between controls and treatment, while the nanoPS<sub>194</sub> was not different. The five times higher cell volume in the 10 mg/L treatment could account for higher sinking velocities, but more data needs to be collected to draw any conclusions. The ratio correspond to Figures in Appendix D: nanoPS<sub>194</sub> D.6, D.7 and D.8; nanoPS<sub>42</sub> D.9, 2.39 and D.10.

**Table 2.9: Aggregate volume comparison in *Synechococcus elongatus*.** Ratio: total bio-volume was compared to the estimate of the aggregate volume. For the bio-volume we consider the cells to be spheres of 1 $\mu$ m diameter whereas the aggregate was roughly an ellipsoid. Equivalent spherical diameter (ESD).

Treatment	Cell Count	Biovol. ( $\mu\text{m}^3$ )	Agg. Vol. ( $\mu\text{m}^3$ )	Agg. ESD ( $\mu\text{m}$ )	Ratio
nPS <sub>194</sub> @ Control	200,000	104,720	$4.25 \times 10^7$	433.059	0.246%
nPS <sub>194</sub> @ 0.01 mg/L	68,000	35,605	$2.77 \times 10^7$	375.42	0.129%
nPS <sub>194</sub> @ 1 mg/L	64,000	33,510	$1.87 \times 10^7$	329.14	0.18%
nPS <sub>42</sub> @ Control	17,000	8901	$8.26 \times 10^6$	250.81	0.108%
nPS <sub>42</sub> @ 0.01 mg/L	2333	1222	343,484	86.7	0.356%
nPS <sub>42</sub> @ 1 mg/L	80,000	41,888	$7.026 \times 10^7$	511.96	0.596%
aMF @ Control	126	66	12,425	28.74	0.531%
aMF @ 0.1 mg/L	58,700	30,735	$4.91 \times 10^7$	454.26	0.626%
aMF @ 1 mg/L	1025	536.69	366,833	88.8	0.146%

Sedimentation was affected by the incorporation of nanoPS in both sizes into *Synechococcus elongatus* aggregates, both directly via changes in sinking velocities as well as changes in the aggregate size distribution of the aggregates, which in turn leads to changes in sinking velocities, as different sized aggregates sink at different speeds.

### 2.4.2 Transparent exopolymer particles (TEP) concentration

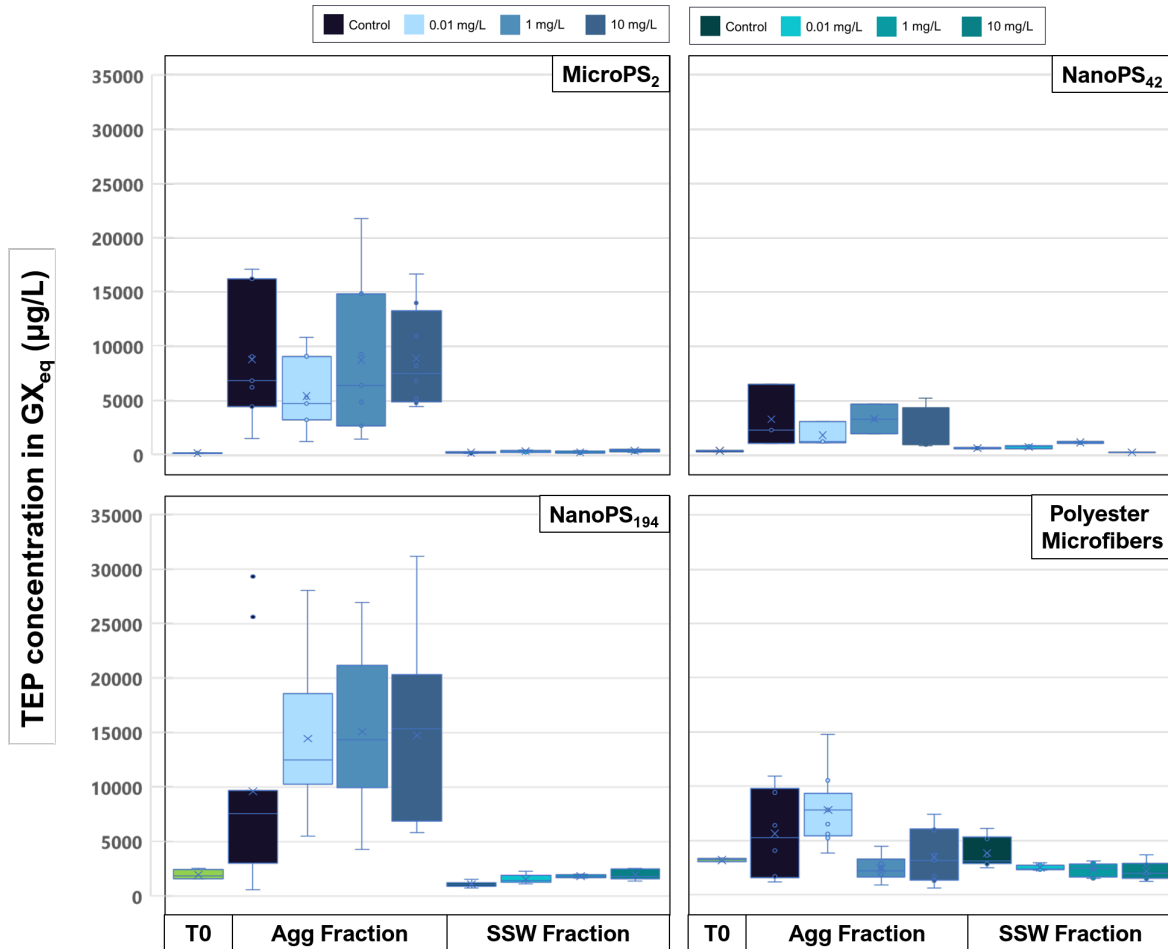
Transparent exopolymer particles (TEP) are a subgroup of extracellular polymeric substances (EPS), produced to make the microalgae environment more suitable. TEP are used as a proxy for stickiness, which plays a big part in the aggregate formation, together with collision frequency and cell concentration. TEP results are presented individually for each species below. TEP is usually not visible in either brightfield nor 3D laser imaging, but the trapped  $\mu$ P/nP/MF can be imaged and can give an idea about the spread of TEP within and around the imaged aggregates (see Section 2.4.4 and Appendix D).

#### *Skeletonema grethae* –

As cell concentrations at  $T_0$  (starting conditions, unaggregated cell culture) were always around 400,000 cells/mL and the TEP concentration was low and stable, the aggregate formation can be linked to the amount of TEP as an important variable in these experiments. TEP concentration was measured separately in the Agg fraction and SSW fraction. The values for each experiment and treatment are displayed in Figure 2.28.

The SSW fractions for all treatments and experiments did not differ significantly from each other (Kruskal-Wallis,  $p = 0.871$ ) in TEP concentrations. The Agg fractions, on the other hand, displayed a wide range of TEP concentrations between treatments and also experiments, with the nanoPS<sub>42</sub> displaying the narrowest values (mean  $2599 \pm 1759 \text{ GX}_{eq} \mu\text{g/L}$ ) and nanoPS<sub>194</sub> the widest range (mean  $13086 \pm 8033 \text{ GX}_{eq} \mu\text{g/L}$ ). These results indicate that most effects of plastic exposure on TEP production in *Skeletonema grethae* were limited to the Agg fraction. We will discuss the effects of each plastic type on the Agg fraction in the next paragraphs.

To make sure that the plastic did not interfere with the measurements, negative control tanks were analysed. The negative control tanks (data not displayed) varied significantly between each other (mean: Sea Water (SW) + 0.01 mg/L:  $53 \pm 27$   $GX_{eq}$   $\mu\text{g/L}$ , SW + 10 mg/L:  $195 \pm 126$   $GX_{eq}$   $\mu\text{g/L}$ ). Just SW (mean  $36 \pm 22$   $GX_{eq}$   $\mu\text{g/L}$ ) correlated well with the low plastic negative control (Mann-Whitney,  $p = 0.003$ ). The high plastic negative control was still one order of magnitude lower on average than the SSW fraction in all treatment experiments (Kruskal-Wallis,  $p = 0.001$ ). Therefore, the plastic is assumed to not interfere with this method.

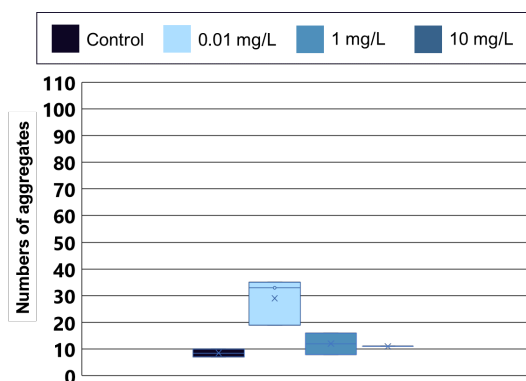


**Figure 2.28:** TEP concentration in different experiments with *Skeletonema grethae* in  $GX_{eq}$  ( $\mu\text{g/L}$ ). Different plastic types and sizes have varying effects on TEP concentration. The biggest increase in TEP concentration between fractions appears for microPS<sub>2</sub> and nanoPS<sub>194</sub> plastics while the TEP concentration in pMF is lower and the SSW fraction has a wider range than the SSW fraction of the other experiments. The TEP concentration in the Agg fraction of the nanoPS<sub>42</sub> experiment is lowest. T<sub>0</sub> is the TEP value at the time of starting the experiments.

MicroPS<sub>2</sub> exposure did not induce significant differences in TEP concentration of the treatments (ANOVA,  $p = 0.649$ ). The Agg fraction had significantly higher TEP concentrations compared to the SSW fraction and T<sub>0</sub> (t-test,  $p = 0.011$ ), while the SSW fraction and T<sub>0</sub> did not differ (t-test,  $p = 0.112$ ). Higher values in the Agg fraction are expected, as TEP helps aggregation and is thus found therein [99]. The difference to T<sub>0</sub> in the Agg Fraction can be explained by light-

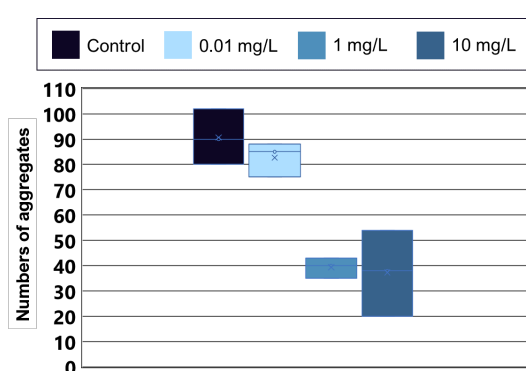


limitation stress-induced TEP production [97, 99], as controls and treatment tanks did not differ. More aggregates formed in the 0.01 mg/L treatment than in the other treatments and the control (see Figure 2.29), but increased aggregation was not due to increased TEP.



**Figure 2.29: Aggregate numbers in MicroPS<sub>2</sub> *Skeletonema grethae* experiment.** The 0.01 mg/L treatment had the highest aggregate counts with up to 35 aggregates per tank, while the control had the lowest with less than 10 aggregates per tank. Control aggregates were less solid than treatment aggregates, and fell apart when handled. Aggregates in the 10 mg/L treatment were more fluffy with a milky edge.

NanoPS<sub>194</sub> exposure significantly increased TEP concentration in the treatments' Agg fraction (ANOVA,  $p = 0.041$ ) compared to the control. The treatment fractions also differed significantly from each other (t-test,  $p = 0.004$ ), with the 0.01 mg/L treatment having lower TEP concentrations than the 1 mg/L and 10 mg/L treatments. One possible reason for increased TEP concentration compared to controls could be that nanoPS<sub>194</sub> induced nutrient limitation [151]. While not linked to plastic, nutrient limitation has been shown to increase TEP concentration [198] as well as to cause stickier TEP [199]. The increase in TEP in the 1 and 10 mg/L treatments corresponds to fewer aggregates overall (see Figure 2.30) and these also sank significantly slower (see Section 2.4.1). One possible explanation is that the increased TEP amount might have led to increased incorporation of nanoPS<sub>194</sub> into the aggregates, with both TEP (naturally more buoyant than sea water [200] and nanoPS<sub>194</sub> making them more buoyant and leading to slower sinking velocities.



**Figure 2.30: Aggregate numbers in nanoPS<sub>194</sub> *Skeletonema grethae* experiment.** The control had the most aggregates, with aggregates count decreasing with increasing plastic concentration. Control aggregates had a different color from the 1 and 10 mg/L treatments (see Figure 2.23). The edges of the control and the 0.01 mg/L treatment aggregates were sharp and distinct, while the higher plastic concentration had fluffy edges and the aggregates did not separate well.

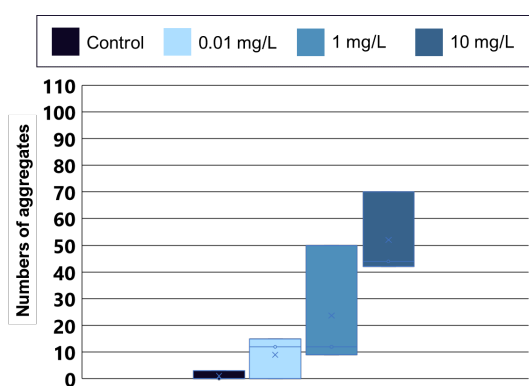
The nanoPS<sub>42</sub> had only four tanks that could be harvested, so only technical replicates of TEP were sampled rather than biological replicates. Due to the temperature variation between 15 °C and 23 °C during the experiment, stress on the microalgae was two-fold, that is increased temperature and nanoPS<sub>42</sub> exposure. Although the TEP amount is notably smaller in the SSW fraction (see Figure 2.28), due to the limited sample number (one tank of each treatment) no significance could be found. No aggregates were observed in the 10 mg/L treatment, but neutrally buoyant slurry



was present. Since there is no increase in TEP, neutral buoyancy most likely comes from nanoPS<sub>42</sub> incorporation. All tanks contained neutrally buoyant aggregates and the aggregate count decreased continuously with increasing nanoPS<sub>42</sub> concentration:

- 0 mg/L control: 25 aggregates
- 0.01 mg/L treatment: 15 aggregates
- 1 mg/L treatment: 5 aggregates
- 10 mg/L treatment: 0 aggregates

pMFs treatments show a wider range of TEP concentration within the SSW fraction. This can also be seen in the control, but not in the T<sub>0</sub> value. The higher TEP variation in the SSW fraction in this experiment might be due to cells being at a slightly earlier stage in their growth cycle and thus higher amount of unaggregated cells were seen in the SSW fraction. All treatments varied from the control (Kruskal-Wallis,  $p = 0.018$ ), with the 0.01 mg/L treatment having a significantly higher TEP concentrations than the other treatments (ANOVA,  $p = 0.002$ ) in the Agg fraction. The two highest concentrations, 1 and 10 mg/L, even show a decrease in their TEP concentration compared to the control, while the 0.01 mg/L treatment demonstrates an increase. These results mirror the F<sub>0</sub> results (see Section 2.4.3 Figure 2.37), where the 0.01 mg/L treatment had significantly higher cell concentration in the Agg fraction. As the SSW fraction in treatments had significantly decreased TEP compared to controls (Kruskal-Wallis,  $p = 0.006$ ), one hypothesis is that leachates from the pMFs might have influenced their TEP concentration. TEP has not been measured before in combination with MF exposure, so comparisons to literature are not possible. We exposed diatom *Odontella aurita* to aMF (see Section 2.4.2), but TEP values were inconclusive. Cyanobacteria *Synecococcus elongatus* were exposed to pMF, and TEP values were lower overall. Without further studies, it is not possible to conclude the effect of pMF on the TEP concentration. Overall, the cells in this experiment aggregated significantly more in the presence of higher pMF concentration (see Figure 2.31 and Section 2.4.1 Figure 2.25).



**Figure 2.31: Number of aggregates in pMF *Skeletonema grethae* experiment.** Number of aggregates increased with increasing pMF concentration. Aggregates in the control fell apart when handled. Only three could be sampled as true aggregates from the three control tanks. The 0.01 mg/L treatment also had one tank in which no aggregates could be sampled. The F<sub>0</sub> values show the increased cell concentration in the SSW fraction compared to the other experiments (see Figure 2.37, corresponding to the TEP concentration measured).

#### *Odontella aurita* –

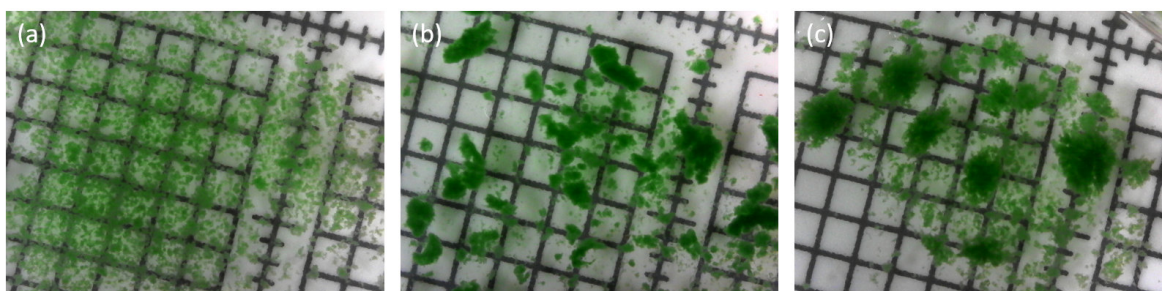
Cells in the Agg fraction produced more TEP than the SSW fraction (Mann-Whitney,  $p < 0.001$ ). Neither the Agg fraction nor the SSW fraction shows any differences between the plastic treatment and controls. Also, there was no differences between the infected and clean control

(Mann-Whitney,  $p = 0.180$ ). Further testing is needed to see if plastic exposure really does not have any effect, as with no biological replica, it is hard to give any definitive answers to this question.

### *Synechococcus elongatus* –

Transparent Exopolymer Particles were measured in the Agg and SSW fraction in the nanoPS<sub>194</sub> and nanoPS<sub>42</sub> experiments (as seen in Section 2.4.2 for *Skeletonema grethae*), while the MF experiments were separated into bottom and top fractions as described in Section 2.3, due to the lack of normal aggregation in these two experiments. Comparing the TEP content of the fractions within an experiment and between experiments can add some insight into the mechanisms as to how the aggregation and sedimentation in *Synechococcus elongatus* were affected by the plastics.

The nanoPS<sub>194</sub> experiment in *Synechococcus elongatus* showed no difference in sinking velocities, but there was a significant difference in aggregate size distribution. The aggregates in the 0.01 mg/L treatment had similar aggregate size distribution to the control and had smoother edges than the higher plastic treatment. There were no medium, large or huge aggregates found in the 1 mg/L treatment (see Figure 2.32).

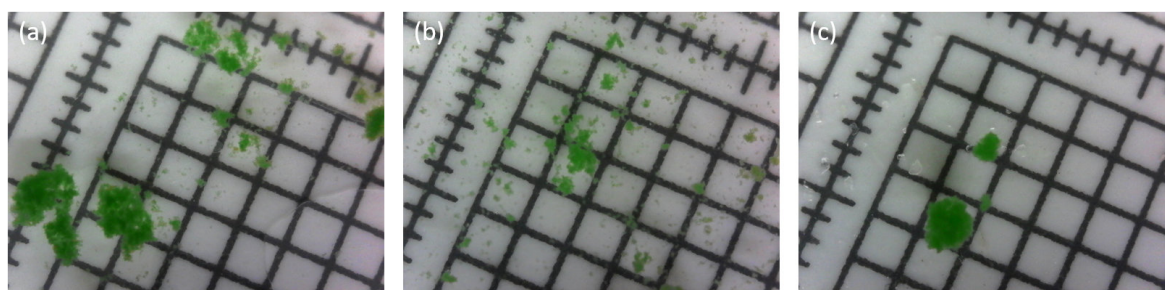


**Figure 2.32: Images showing aggregate size differences for different concentrations of nanoPS<sub>194</sub>.** While sinking velocity was not directly affected by the incorporation of nanoPS<sub>194</sub>, aggregate size is. (a) Only small and tiny aggregates are found in the 1 mg/L treatment. (b) Aggregates in the 0.01 mg/L treatment range over all size classes. (c) The aggregates in the control ranged over all size classes, like the low plastic treatment, but the aggregates were not as smooth around the edges. One square is 5 times 5 mm. Pictures were taken with Carson eFlex microscope under experimental temperature conditions and in SSW from corresponding tanks.

There was a significantly higher TEP concentration in the Agg fraction of the 1 mg/L treatment compared to controls (independent t-test, one-tailed  $p = 0.01$ ), while the 0.01 mg/L was not different from the control in terms of TEP concentration (independent t-test, one-tailed  $p = 0.0659$ ). This higher TEP concentration in the higher plastic treatment might be caused by irritation of the *Synechococcus elongatus* cells. A recent study of *Synechococcus* sp. PCC 7002 exposed to nano polyethylene (200–9900 nm) reported a significant degradation of stable RNA in these marine bacteria [201], which shows that *Synechococcus* sp. perceives nP as a stressor and synthesizing additional TEP to protect the cells against this external threat is one reasonable hypothesis. This was also found in another marine bacterium *Halomonas alkaliphila* [167] with nanoPS ( $\sim 50$  nm, different surface properties). Although TEP concentration was not measured by Lagarde et al. [149], they hypothesize that TEP concentration under  $\mu$ P/nP exposure is linked to a change in cell physiology due to nutrient depletion, which was one possible effect of  $\mu$ P/nP exposure suggested by Nolte et al. [151, 169].

The combination of increased TEP concentration (due to the presence of the nanoPS<sub>194</sub>) with the nanoPS<sub>194</sub> incorporation itself into the aggregates (see Figures D.7 and D.8), led to the formation of only small and tiny aggregates. Increased TEP has not been associated with smaller aggregates in the literature, so it is unclear why exposure to 1 mg/L caused significantly higher TEP amounts while only leading to small and tiny aggregates (see Figure 2.32). One possible hypothesis is that the nanoPS<sub>194</sub> may have been responsible via collision and mechanical stress, breaking up aggregates so bigger ones could not form.

Although sinking velocities and aggregate size distribution are different between the treatments and the control, nanoPS<sub>42</sub> exposure in *Synechococcus elongatus* did not significantly change the TEP concentration. This could be an artifact from the missing data of two treatment tanks. Since two tanks did not show any cell aggregation (see Figure 2.17), possibly due to bubble formation within the tanks and subsequent induced turbulence breaking up any aggregates forming, this experiment should be repeated to draw conclusions. Because the bigger nanoPS<sub>194</sub> plastics did induce a change in TEP concentration, smaller particles could have a more severe effect (due to more surface area to interact). Indeed, more severe effects have been reported for nanosized plastics in plankton [175] and also specifically in cyanobacteria [201]. An increased surface to volume ratio allows for more interactions with the cell membrane, which has been shown to lead to cell membrane destruction in cyanobacteria exposed to nanoPS (changed surface properties, 50 nm) [168].



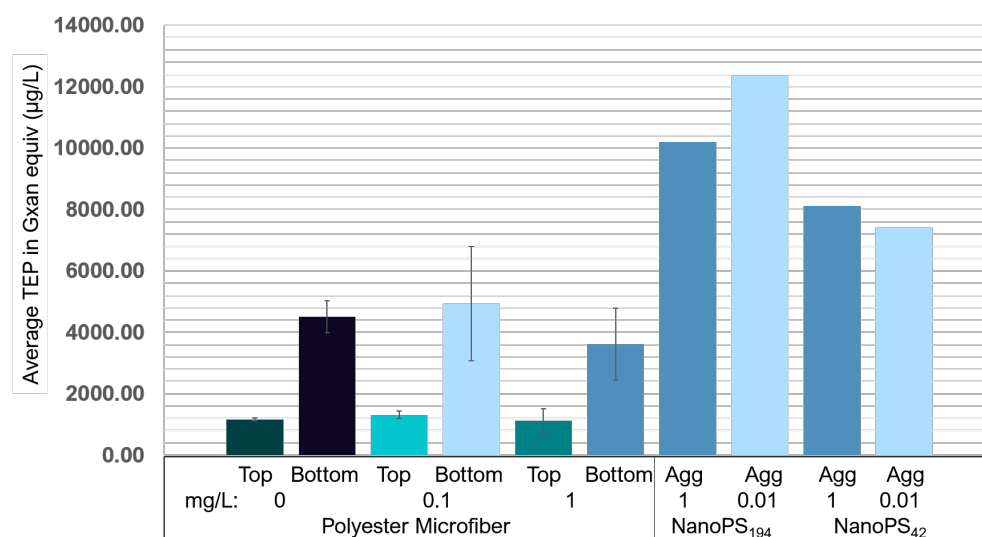
**Figure 2.33: Images showing aggregate size differences for different concentrations in nanoPS<sub>42</sub> experiment.** Aggregate size distribution was affected in addition to sinking velocities by incorporation of nanoPS<sub>42</sub>. (a) All sizes of aggregates are found in the 1 mg/L treatment, (b) while there were no big or large aggregates in the 0.01 mg/L treatment. (c) depicts the control. While the aggregates appear to be more dense and compact than in the 1 mg/L treatment of the same size, their sinking velocity was lower than those in the 1 mg/l treatment. One square is 5 times 5 mm. Pictures were taken with Carson eFlex microscope under experimental temperature conditions and in SSW from corresponding tanks.

Significant differences in TEP content were found between top and bottom fractions in treatments as well as controls (see Table 2.10) in the pMF experiment of *Synechococcus elongatus*, but there was no difference between the treatment and the controls within one fraction (see Figure 2.34).

**Table 2.10: TEP analysis in the pMF experiment.** T-tests between the fractions in each treatment in *Synechococcus elongatus*.

Plastic concentration (mg/L)	Fraction	Average TEP in Gxan equiv ( $\mu\text{g/L}$ ) and SD	t-test top vs. bottom
0	Top	$1,163 \pm 45$	$p = 0.002$
0	Bottom	$4,505 \pm 519$	
0.1	Top	$1,314 \pm 118$	$p = 0.002$
0.1	Bottom	$4,939 \pm 1861$	
1	Top	$1,125 \pm 391$	$p < 0.001$
1	Bottom	$3,621 \pm 1171$	

When comparing the TEP concentration between experiments, there was no difference between nanoPS<sub>42</sub> and pMF, which could be due to the inclusiveness of the nanoPS<sub>42</sub> experiment concerning the TEP concentration (see Figure 2.34). The Agg fraction of the nanoPS<sub>194</sub> experiment had significantly higher TEP values than the corresponding bottom fraction of the pMF experiment (t-test,  $p = 0.001$ ). Only the 1 mg/L treatment of the pMF experiment showed dust aggregation. This lack of aggregation is reflected in the lower TEP values, and could explain the lack of aggregation as the pMF experiment never reached the values seen in the nanoPS<sub>194</sub> and nanoPS<sub>42</sub> experiments (see Figure 2.34).



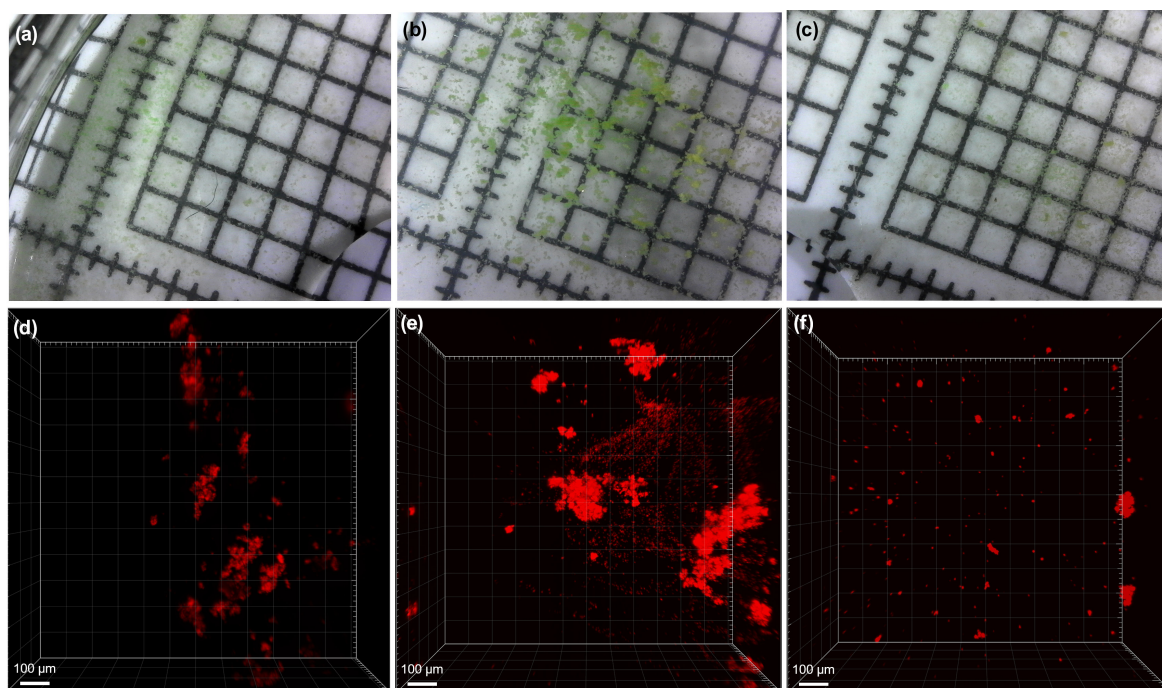
**Figure 2.34: Comparison of TEP concentrations between pMF and both nanoPS experiments.** The average for Agg fraction in the nanoPS<sub>194</sub> 1 mg/L treatment was  $10206 \pm 5752 \mu\text{g/L}$  and 0.1 mg/L treatment was  $12352 \pm 4560 \mu\text{g/L}$ . The nanoPS<sub>42</sub> 1 mg/L treatment was at  $8112 \pm 2704 \mu\text{g/L}$  and 0.1 mg/L treatment was  $7404 \mu\text{g/L}$ . The pMF experiments averages were: top fraction  $1200 \pm 81 \mu\text{g/L}$  and the bottom fraction was  $4355 \pm 548 \mu\text{g/L}$ . Error bars display standard error.

Comparing the TEP within each fraction did not show any differences, the average in the 1 mg/L treatment (which showed dust aggregation) was even slightly lower than the ones of the 0.1



mg/l treatment and the control (see Figure 2.34). Thus, the observed dust aggregation in the pMF experiment could not be explained via the TEP content.

In the aMF experiment in *Synechococcus elongatus*, as seen in the pMF experiment, the TEP concentration was significantly higher in the bottom vs. the top fraction (see Table 2.11). In addition, the 0.1 mg/L treatment showed significantly higher TEP concentration compared to controls (Holm-Sidak,  $p = 0.013$ ). The effect of the higher TEP concentration was also visible in slightly bigger dust aggregation in this treatment (see Figure 2.19).



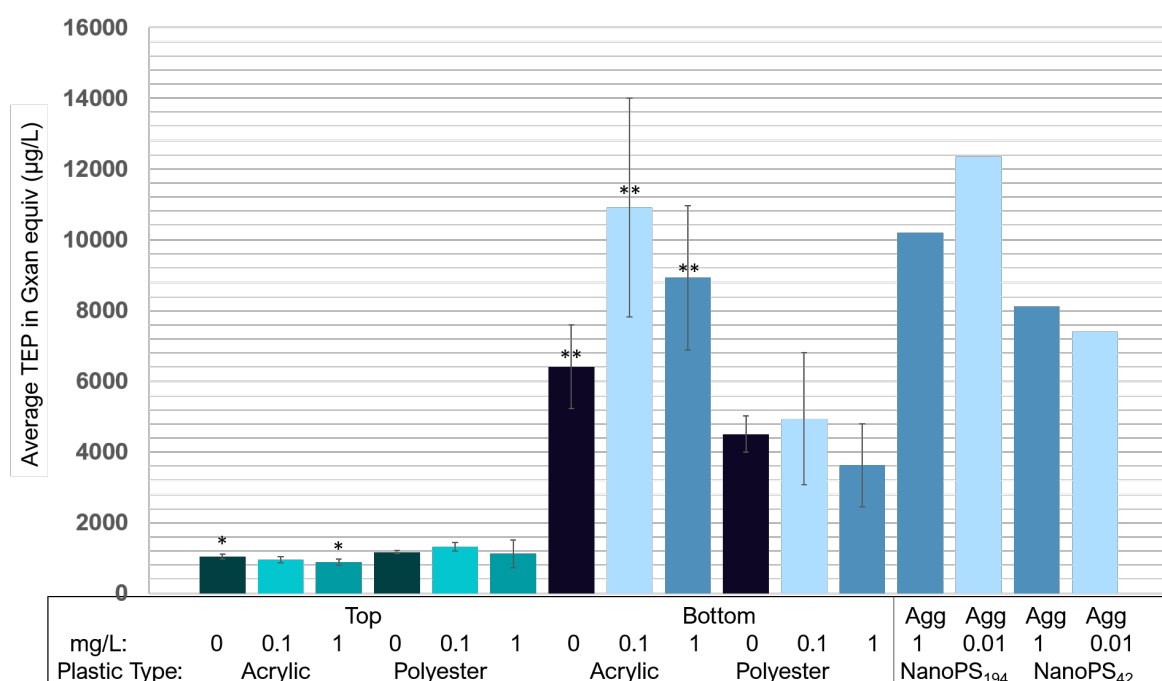
**Figure 2.35: Dust aggregation in the acrylic fiber experiment, optical images (a-c) and 3 D images (d-f) in *Synechococcus elongatus*.** (a) Dust aggregation 1 mg/L treatment with visible acrylic fiber. (b) Slightly bigger dust can be seen in the 0.01 mg/L treatment. This corresponds to significantly higher TEP concentration in the bottom fraction of this treatment compared to controls and the 1 mg/L treatment (see Table 2.11). (c) Dust aggregation in control. (d) Dust aggregation 1 mg/L treatment with about 40,900 cells. (e) Slightly bigger dust can be seen in the 0.01 mg/L treatment, with about 23,300 cells. (f) The dust aggregation in the control resembles the dust aggregation in 1 mg/L treatment visually in (a), but there are fewer cells counted in the same sized 3 D image (19,500 cells). The aggregates are smaller and less dense than the ones found in the plastic beads experiments. One square is 5 times 5 mm the optical images. Optical images were taken with Carson eFlex microscope under experimental temperature conditions and in SSW from corresponding tanks. For single aggregates, please see Figure D.11.

In the top fraction, the 1 mg/L treatment had a significantly lower TEP concentration than the control which was not visible as a difference in aggregate sizes (Holm-Sidak,  $p = 0.014$ ). There was no difference between the 1 mg/L treatment and the control, neither in TEP nor the dust aggregation sizes, while the 0.1 mg/L treatment shows slightly bigger aggregates (see Figure 2.19) and significantly higher TEP concentration in the bottom fraction.

**Table 2.11: TEP analysis in the aMF experiment.** T-tests between the fractions in each treatment in *Synechococcus elongatus*.

Plastic concentration (mg/L)	Fraction	Average TEP in Gxan equiv ( $\mu\text{g/L}$ ) and SD	t-test top vs. bottom
0	Top	$1042 \pm 73$	p = 0.002
0	Bottom	$6403 \pm 1183$	
0.1	Top	$950 \pm 86$	p = 0.002
0.1	Bottom	$10906 \pm 3094$	
1	Top	$883 \pm 80$	p = 0.002
1	Bottom	$8923 \pm 2038$	

When comparing the TEP concentrations between the two MF experiments, the top fractions are very similar, but the bottom fractions have a higher TEP content in all treatments and in the control (t-test, control: p = 0.008, 0.1 mg/L: p = 0.004, 1 mg/L: p < 0.001) (see Figure 2.36). Figure 2.36 also shows the before-mentioned higher TEP in the 0.1 mg/L treatment compared to 1 mg/L and controls (ANOVA, p = 0.013). This can be seen in the bigger dust aggregation (see Figure 2.19). As higher TEP content was associated via stickiness with more aggregation [99, 189]. It is understandable that the aMF experiment shows more dust aggregation than the pMF experiment, but it is unclear why the TEP content in this experiment was similar to the NanoPS experiments yet, but the aggregates are so different in size.



**Figure 2.36: Comparison between nanoPS and aMF TEP content.** The averages for the Agg fraction: nanoPS<sub>194</sub> 1 mg/L treatment was  $10206 \pm 5752$  and 0.1 mg/L treatment was  $12352 \pm 4560$ . The nanoPS<sub>42</sub> 1 mg/L treatment was  $8112 \pm 2704$  and the 0.1 mg/L treatment was 7404. The lack of real aggregates in this experiment cannot be explained by TEP values alone. \* indicate significance.

### 2.4.3 Photophysiology

The ecological environment simulated in these experiments was without light, as marine snow particles sink through the water column to the bottom of the ocean and photo-active sun light only reaches down to about 200 m. Cells in marine snow particles are usually not photosynthetically active after they have left that top layer. On rare occasions, through water up-welling, cells may re-enter the photic zone, but this is not simulated in the experiments. We established in trials that the cells were still photo-active, as photo-measurements were not taken from aggregates before. In subsequent experiments in Chapter 4, a different environment was simulated that did involve photo-active cells. This approach was based on the results found in this chapter (see Section 4.4.2).

The two measured photophysiology parameters (effective quantum yield  $QY_{max}$  and  $F_0$ , a proxy for cell concentration in photochemistry) are discussed separately below. For a detailed method description see Section 2.2.5.

To establish that plastics did not interfere with measurements, negative control values were compared. The negative controls had no cells added and thus contained no photosynthetically active cells. Measuring  $F_0$  in the samples show if the plastic does not ‘produces’ a signal that the Aquapen could pick up. Table 2.12 presents the measured  $F_0$  values in the negative control. There is no statistical difference between the different plastics or their concentrations. Hence, we can assume the plastic did not interfere with the measurements.

**Table 2.12: Measurements of  $F_0$  in a negative control** in relative units. Note that the bottom row, the negative control without cells or plastic shows no statistically difference to the values measured in the presence of either MF, nP or  $\mu$ P. There are no statistical differences between the plastic types (ANOVA,  $p = 0.886$ ) nor between concentrations (ANOVA,  $p = 0.514$ ). This shows that the presence of the plastic does not influence Aquapen measurements.

Plastic concentration	Fibers	nanoPS <sub>42</sub>	microPS <sub>2</sub>	mean
0.01 mg/L	62	65	80	69
10 mg/L	61	-	61	61
Seawater (no cells, no plastic)	72	72	60	68

Further analysis of the  $F_0$  data from the Aquapen measurements shows that the Agg fraction and the SSW fraction always had significantly higher  $F_0$  across all species and plastics (see Table 2.13 for statistical data). This leads to the conclusion that the Agg fraction contained significantly higher numbers of cells. This measurement refers to the fractions, not individual aggregates.

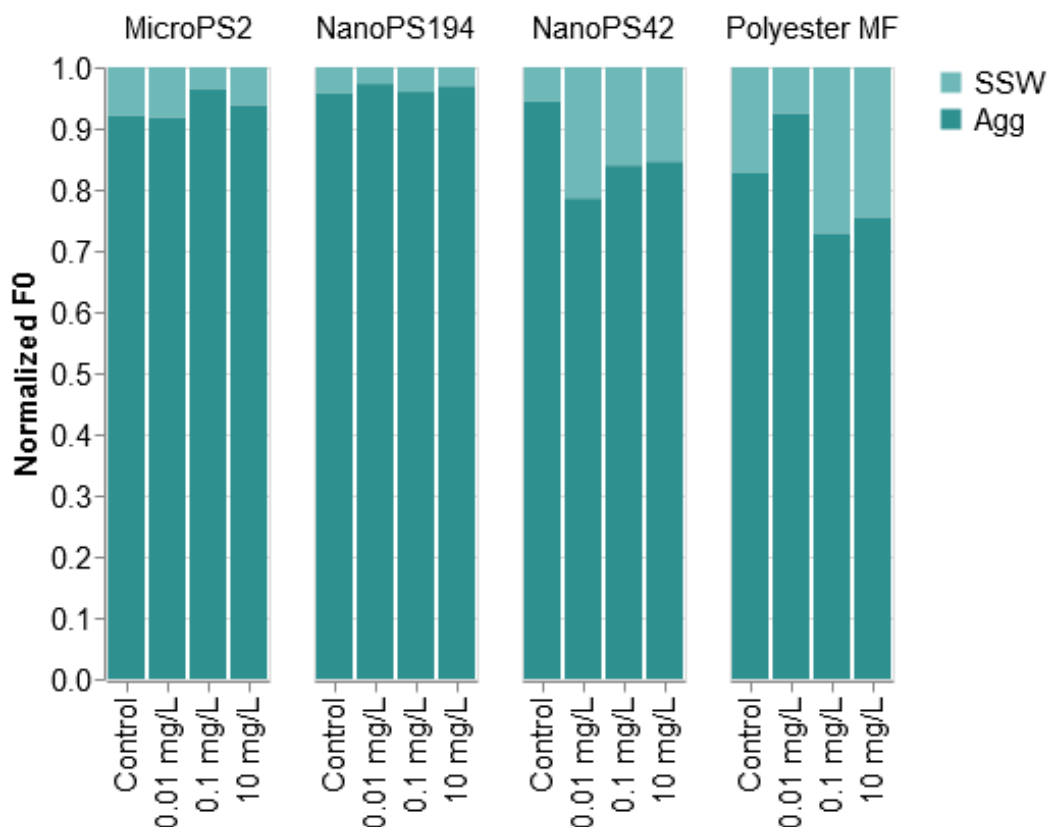
**Table 2.13: Statistical difference for  $F_0$  between fractions.**

Species	Test	p - Value
<i>Skeletonema grethae</i>	Kruskal-Wallis	$p < 0.001$
<i>Odontella aurita</i>	Mann-Whitney	$p < 0.001$
<i>Synechococcus elongatus</i>	t-test	$p = 0.001$

After establishing that, in all experiments,  $F_0$  was higher in the Agg fraction than in the SSW fraction, as expected, a more detailed comparison of the  $F_0$  between the experiments in *Skeletonema*



*grethae* is presented (see Figure 2.37).  $F_0$  in the Agg fraction varied between treatments and experiments (see Figure 2.37 for *Skeletonema grethae*) and, while great care was taken to sample aggregates of the same size, small variations could lead to differences in cell counts. Moreover, cell packaging between treatments can vary in aggregates of the same size, as seen in the sinking velocities (see Section 2.4.1) and reported from other studies on the incorporation of oil [99].

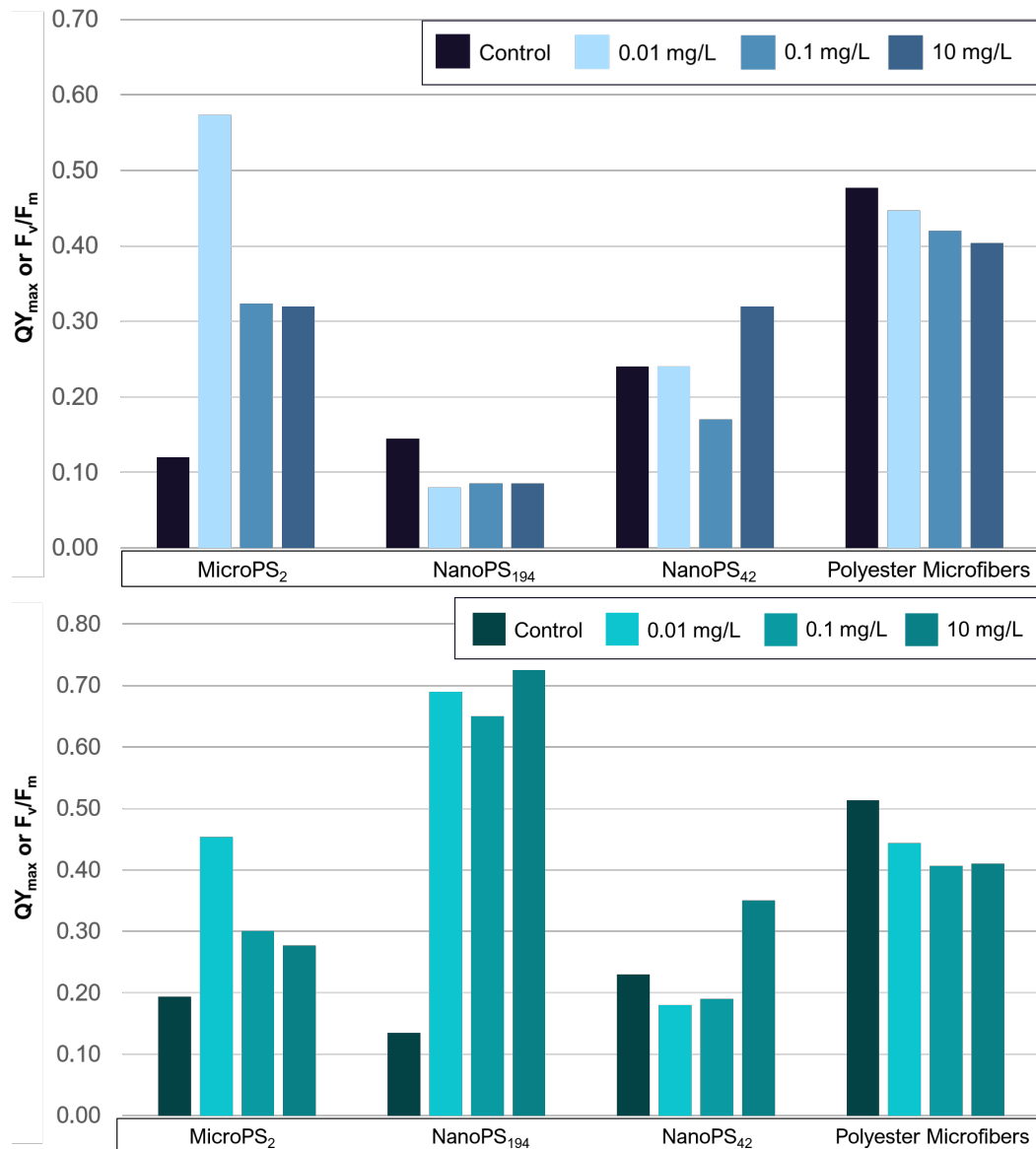


**Figure 2.37:  $F_0$  between *Skeletonema grethae* experiments.**  $F_0$  is a measure for cell concentration in photophysiology and it can be seen that the Agg fraction holds most of the cells. There is no discernible pattern between the treatments, but a higher percentage of cells remains unaggregated in the pMF experiment. There is no discernible pattern between treatments in either fraction, but it is noticeable that the pMF experiment in the SSW fraction has significantly higher  $F_0$  values than the rest of the experiments (Kruskal-Wallis,  $p = 0.004$ ). This difference to the other experiments is not reflected in the Agg fraction. As the difference is also seen in the control, it is likely a behaviour of the *Skeletonema grethae* culture. Overall, the pMF experiment showed less aggregation (see Section 2.4.1 Figure 2.25) and less TEP concentration (see Section 2.4.2 Figure 2.28). This led to more unaggregated cells and thus higher cell concentration in the SSW fraction compared to the other experiments. Dark green represents the Agg fraction, light green the SSW fraction.

The light-curve derived parameter effective quantum yield  $QY_{max}$  (or  $F_v/F_m$ ) is generally seen as an important indicator for PSII activity and health [150]. An analysis of the  $QY_{max}$  between experiments and fractions is therefore presented below, sub-sectioned by species.

**$QY_{max}$  changes in *Skeletonema grethae*** Overall, the  $QY_{max}$  is lower than for healthy diatoms ( $\sim 0.6$ ), due to the cells being at the end of the exponential growth phase to promote aggregating (see

Figure 2.38). It is also noticeable that aggregates did not display a markedly higher  $QY_{\max}$  compared to the SSW fraction. It has been reported that aggregated diatom cells have a higher photosynthesis rate due to the micro-environment they create within the aggregate [202]. The difference in this thesis to other published literature [202] could be due to the fact that the inclusion of plastics within the aggregates prevents a favorable micro-environment from being formed because of plastic-induced nutrient limitation, as suggested in [151].



**Figure 2.38:  $QY_{\max}$  between *Skeletonema grethae* experiments.** Top is Agg fraction. Bottom is SSW fraction. The  $QY_{\max}$  varied widely in the control, but was consistent between fractions of the same experiment (t-test,  $p = 0.886$ ). Detailed explanations for each experiment are found in the main text below.

MicroPS<sub>2</sub> exposure in *Skeletonema grethae* reveals a statistically significant difference in the Agg fraction between the control and the low plastic treatment (Dunn's Method,  $p = 0.029$ ), while the medium and high plastic treatments did not show any differences to controls ( $p = 0.063$  and  $p$

= 0.096, respectively). The SSW fraction did not show any significant  $QY_{\max}$  differences between treatments (Kruskal-Wallis,  $p = 0.145$ ). MicroPS exposure (1  $\mu\text{m}$  at up to 100 mg/L) has been reported to lead to a reduction in the  $QY_{\max}$  in diatoms [150]. This is thought to happen via an interplay of processes, most notably by affecting PSII. A reduction in the electron transport rate (ETR) through the PSII and a reduction of the activity of the reaction centers of PSII are proposed through effects on the cell wall. While this decrease is reported as an initial reaction to the exposure, Mao et al. [150] also find that the diatoms recover. This recovery might have led to the higher  $QY_{\max}$  seen in treatments compared to the controls. It is possible that during our microPS<sub>2</sub> experiment, only the second phase of this two-stage response was measured, the recovery, that is due to a thickening of the cell wall in combination with the increased homo-aggregation [150]. Cell wall thickening has also been observed in aluminum oxide nanoparticle exposure [203]. This limits the possibility of microPS<sub>2</sub> to interact with the cell wall and cause damage. Since the increase in  $QY_{\max}$  was observed in both the Agg fraction as well as the SSW fraction, it is likely that microPS<sub>2</sub> exposure led to a similar positive adaptation to the stress as observed in other studies [150, 203]. Other studies have also observed that the  $\mu\text{P}$  induced photosystem inhibition weakens over time, with values recovering [137].

NanoPS<sub>194</sub> exposure in *Skeletonema grethae* shows an interesting pattern of significantly higher  $QY_{\max}$  values in the SSW fraction compared to the Agg fraction (t-test,  $p < 0.001$ ). An explanation for this shift could be found in the previously described adaptation to  $\mu\text{P}$  stress of increased stability in the cell walls [150]. One other mechanism of the stress adaptation proposed in that study, is the removal of  $\mu\text{P}$  from the water column via hetero-aggregation and an increase in homo-aggregation. When the 3D images of this experiment are viewed (see Figures D.16 and D.17) it becomes clear that nanoPS<sub>194</sub> is trapped within the hetero-aggregates. The Agg fraction measurements are from cells that were trapped within these hetero-aggregates, and the increased particle number compared to the microPS<sub>2</sub> treatment could explain the reduction in  $QY_{\max}$ . The amount of nanoPS<sub>194</sub> might have led to such increased stress on the diatom cells. In contrast, the cells in the SSW were exposed to a much lower concentration, leading to the same adaption and increase in  $QY_{\max}$  as observed in the microPS<sub>2</sub> experiment.

The nanoPS<sub>42</sub> experiment in *Skeletonema grethae* shows no statistical differences between controls and treatments (see Figure 2.38). As changes in the photochemistry have been reported under changing temperature in combination with nanoparticle exposure in other microalgae [204], the change in temperature during this experiment would most likely affect the photophysiology of *Skeletonema grethae* in a similar way. As the duration and exact increase in temperature are unknown, it would be hard to distinguish any effects.

pMF exposure of *Skeletonema grethae* – led to a gradual decline in  $QY_{\max}$  values with increasing concentration of pMF (see Figure 2.38). The direct effects of the pMF in the Agg fraction were similar to those of pMF leachates in the SSW. Leachates are chemicals that leach from the fibers. Similar experiments have shown no effect in *Isochrysis galbana* [185], but the authors argued that this could be due to reduced sensitivity in the microalgae species studied. As exposure to leachates did lead to some significant effects similar to the actual exposure to MF used in that study, it is assumed that *Skeletonema grethae* is more sensitive than *Isochrysis galbana* to the leachates. Also, the pMF in the rolling tank constantly leaches into the tank, steadily increasing the chemical concentration of leachates over the duration of the experiment, whereas Rogstad [185] conducted a study with a constant, pre-prepared exposure value.

**QY<sub>max</sub> changes in *Odontella aurita*** The Agg fraction and the SSW fraction of *Odontella aurita* show significant differences in the QY<sub>max</sub> (independent t-test, one-tailed p-value =  $2.12 \times 10^{-10}$ ). This is not surprising, as chain-forming diatoms, such as *Odontella aurita*, have been reported to have higher photosynthetic activity within aggregates than their freely suspended cell counterparts [202]. As *Odontella aurita* cells create a micro-environment within the aggregate, nutrients are available in a preferred form for uptake, affecting their photosynthesis rates positively [202], both *in situ* as well as under laboratory conditions. QY<sub>max</sub> is within the range of reported values for centric diatoms (QY<sub>max</sub> from 0.36 to 0.42 [205]). Under the limited preliminary results, neither the infection nor the plastic exposure lead to photo-damage and photo-inhibition of PSII which becomes apparent in the unchanged QY<sub>max</sub> in *Odontella aurita*. Evaluating the differences caused by plastic exposure in the photochemistry poses more of a challenge due to the lack of biological replica. There are no significant differences in photochemistry based on plastic exposure. The photosystem appears to be functioning normally.

**QY<sub>max</sub> changes in *Synechococcus elongatus*** The *Synechococcus elongatus* nanoPS<sub>194</sub> experiment did not show any differences between the treatment and the control, but not all data was taken with the same Aquapen and the same settings, so this was inconclusive.

In the *Synechococcus elongatus* nanoPS<sub>42</sub> experiment, photochemistry was effected. QY<sub>max</sub> was significantly different between the Agg and the SSW fraction (t-test, p = 0.001). This is interesting, showing that the cells within the aggregates, while more numerous, also have better photochemistry indicated by the higher yield of the PS II. This has been shown to be true for marine diatoms [202], possibly due to better nutrient availability within the aggregates. As not enough tanks could be sampled, no differences could be found between the treatments and controls. Unfortunately, there is no comparison possible with the bigger nanoPS<sub>194</sub>, as there was no data from that experiment available on photochemistry. Data is not displayed.

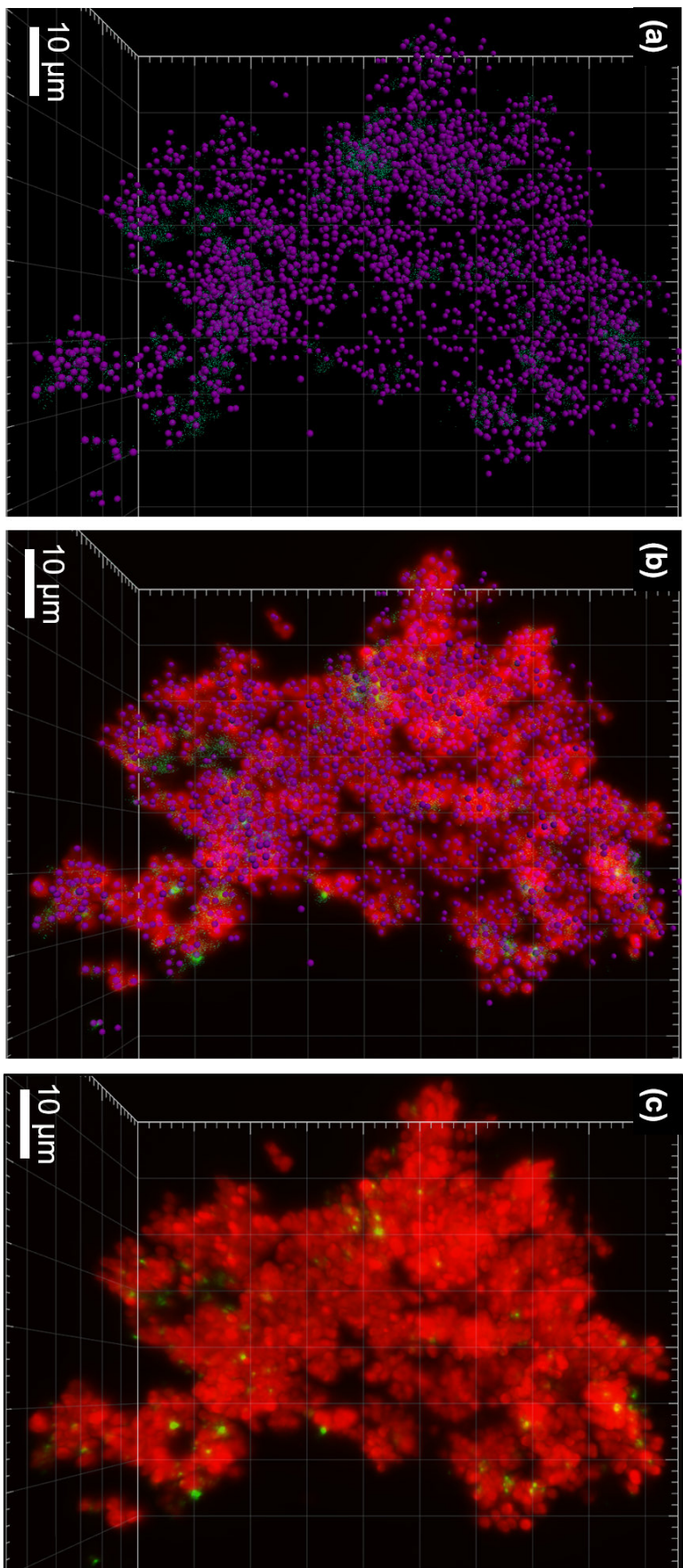
The *Synechococcus elongatus* pMF experiment compared the photochemistry between the bottom and the top fraction. Just as with the TEP concentration (see Section 2.4.2), F<sub>0</sub> was significantly different between the top and the bottom fraction (t-test, p = 0.041). This shows that the cell concentration is higher in the bottom fraction and cells did indeed settle in the dust at the bottom of the tanks (see Section 2.3 Figure 2.18). On the other hand, QY<sub>max</sub> did not differ between the fractions. So, although the cell concentration was higher in the bottom fraction, the cells did not display that increase in QY<sub>max</sub> found in the aggregates of the nanoPS<sub>42</sub> experiment. The dust aggregates could be too small to change the micro-environment that would have made more nutrients available and increased the QY<sub>max</sub> [202].

In the *Synechococcus elongatus* aMF experiment, F<sub>0</sub> differs significantly (t-test, p = 0.002) between the top and bottom fractions, as for the pMF experiment. This shows that more *Synechococcus elongatus* cells are found in the dust aggregation than in the SSW fraction. In addition, the quantum yield, QY<sub>max</sub>, also differed between the top and the bottom fraction (t-test, one-tailed p = 0.00175). The QY<sub>max</sub> values being higher in the bottom fraction compared to the top fraction could indicate that the dust aggregation created big enough aggregates to change the micro-environment and make nutrients more available in the bottom fraction [202] (see Section 2.3 Figure 2.19).

#### 2.4.4 3D images reveal internal structure of aggregates

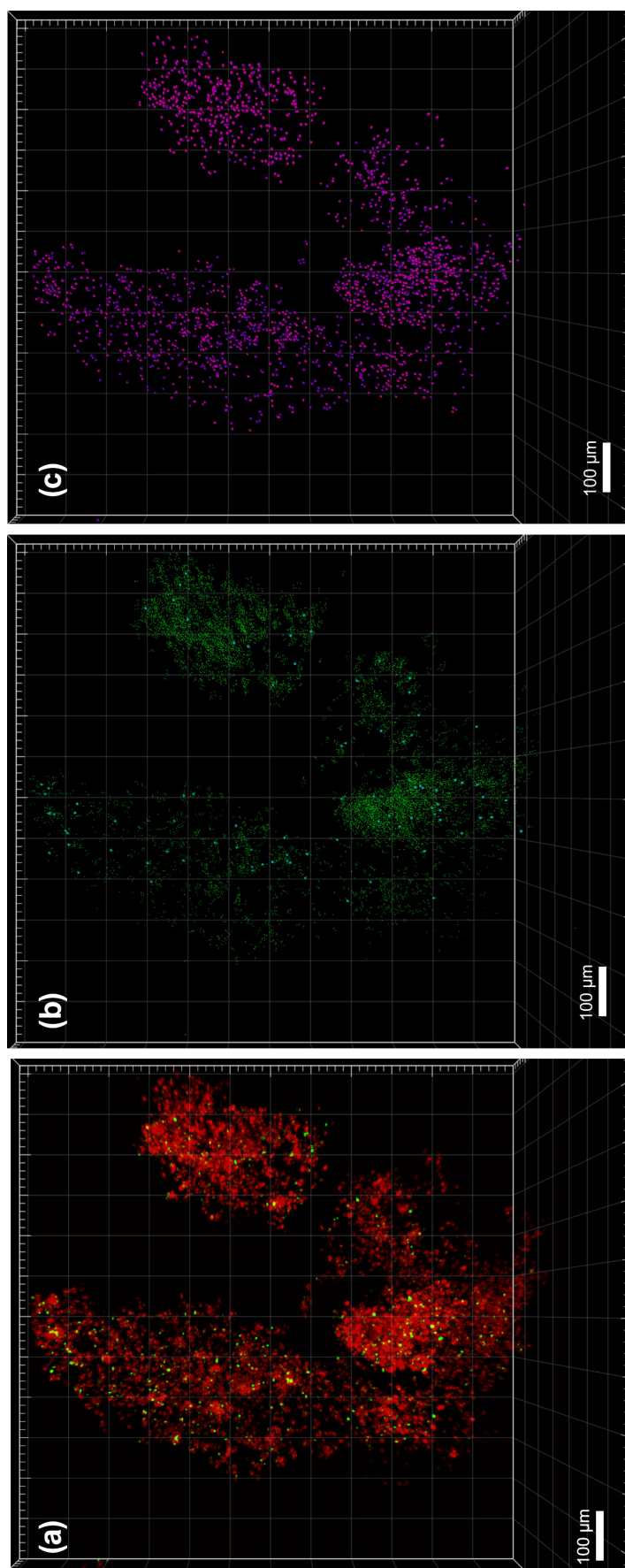
To check the distribution of plastic in the aggregates and to get some insight into the cell packaging differences at different concentrations, 3D images were obtained using Zeiss Lightsheet Z.1. (see Section 2.2.5 for detailed method). Replacing the cells in the aggregates with spots of similar size reduces the z-direction artificial stretching of the cells by the laser sheets and reveals the space between the cells. In these laser images, the plastic is green, and the cells are red. Transparent extracellular polymers (TEP) are not visible in either the brightfield or 3D images but can show up due to the trapped particles. One aggregate is displayed here, the rest can be found in Appendix D.1.



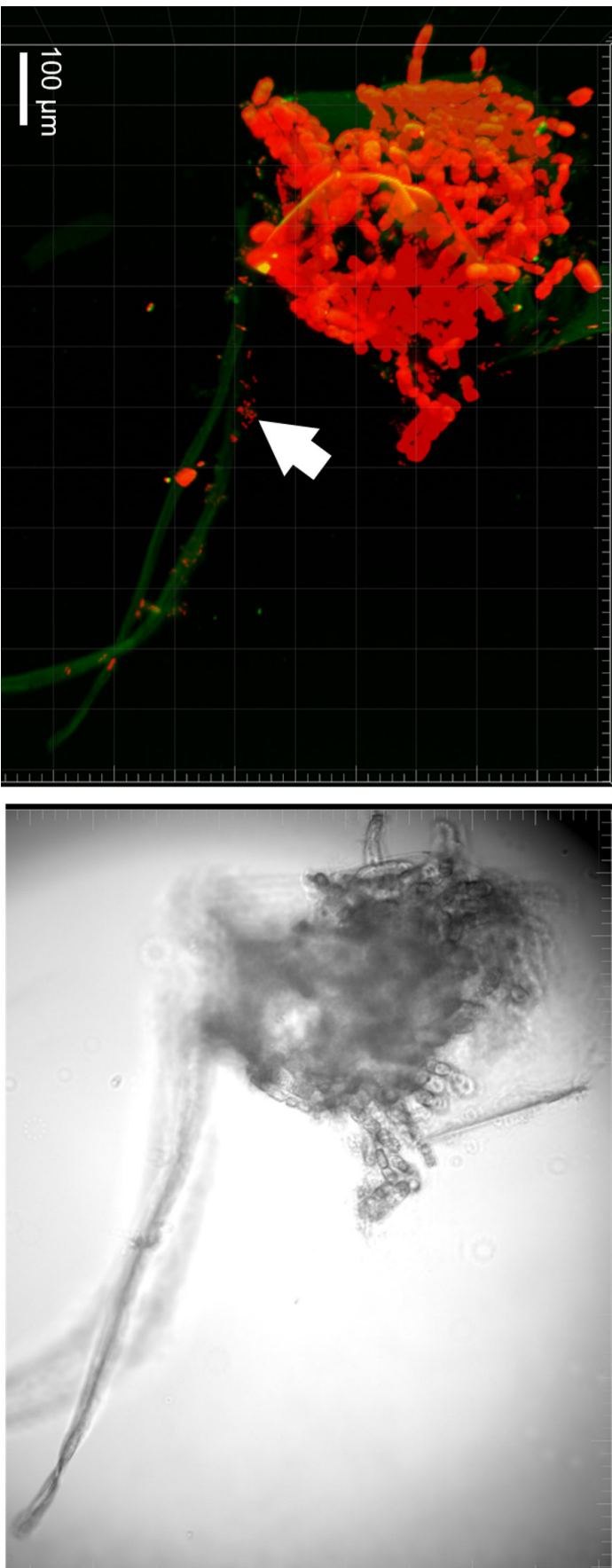


**Figure 2.39: 3D images for the nanoPS<sub>42</sub> experiments in *Synechococcus elongatus* from the 0.01 mg/L treatment.** The images display an aggregate with 103 µm height, 77.2 µm width and 82.5 µm depth (total volume of 343, 484 µm<sup>3</sup>). (a) There are about 2333 cells found in this aggregate leading to a total bio-volume of 1222 µm<sup>3</sup>. This means that the bio-volume represents only 0.356% of the total aggregate volume. Individual plastic particles could not be counted due to their small size, but there are 404 agglomerates of plastic in sizes between 0.4 µm and 1.4 µm. (b) displays the cell count with the laser overlay while (c) is just the laser. The progression of images shows that the dense wall of cells seen in the laser image (c) are actually cells held together by TEP (not visible). That is why the cells in (a) seem to be disconnected but still hold together.





**Figure 2.40: 3D images of microPS<sub>2</sub> aggregates in *Skeletonema grethae* at 1 mg/L bead concentration.** The image displays an aggregate with 962 μm height, 341, and 246 μm width for each arm, respectively, and 579 μm depth (total volume  $1.71 \times 10^8 \mu\text{m}^3$ ). There are about 2600 cells found in this aggregate leading to a total bio-volume of 294,053 μm<sup>3</sup>. This means that the bio-volume represents 0.0339% of the total aggregate volume. There are 13,700 microPS<sub>2</sub> beads in the aggregate, with 89 bigger agglomerates at six μm diameter, where the microPS<sub>2</sub> stuck together. (a) displays the laser channel of the cells with the plastic. In (b), plastic has been substituted for spheres, in cyan the agglomerates, in green the single microPS<sub>2</sub>. (c) shows just the cells, it is interesting to see the big spaces between the cells.



**Figure 2.41: Images of *Odontella aurita* infection with acrylic fiber incorporated into the aggregate.** The fiber is visible in both the bright field and the 3D image due to the overexposure in the band pass filter (Excitation: 405 nm; Emission: 505-545 nm), a green reflection is also visible on the *Odontella aurita* cells because of this. Along the fiber, the infection is visible (white arrow). The image displays an aggregate with 566 µm height, 454 µm width, and 528 µm depth (total volume of  $7.1 \times 10^7 \mu\text{m}^3$ ). There are about 432 cells found in this aggregate leading to a total bio-volume of  $3.62 \times 10^6 \mu\text{m}^3$ . This means that the bio-volume represents 5.1% of the total aggregate volume.

## 2.5 Conclusions

The overall aim of this study was to provide insights into aggregate formation of phytoplankton –  $\mu\text{P}/\text{nP}/\text{MF}$  hetero-aggregates and possible negative effects on the oceanic carbon pump. While much remains to be understood about  $\mu\text{P}/\text{nP}/\text{MF}$  and their interaction with the oceanic phytoplankton communities, my results clearly show that all types of  $\mu\text{P}/\text{nP}/\text{MF}$  have some effect on the three different species studied. The different plastics led to vastly different changes in aggregate formation, sinking velocities and TEP content.

Changes in aggregation and aggregate size distribution result in altered predator types and sizes that graze on cyanobacterium *Synechococcus elongatus* [206], having potential implications for the structure of the oceanic food web. For the photosynthetic cyanobacterium *Synechococcus elongatus* it is currently believed that it has to deal with high predator pressure and grazing rates. The different food web levels are usually separated by the predators' limitation in food size, so unaggregated *Synechococcus elongatus* will not be grazed upon by bigger zooplankton [207]. But aggregation as seen in aMF and pMF experiments changes the range of possible predators, possibly leading to structural changes within the lowest levels of the marine food web. Incidentally, changing cell size is a grazing avoidance strategy of these cyanobacteria [208, 209], which could be impaired in the presence of MF.

As in *Synechococcus elongatus*, under poor aggregation conditions pMF exposure also increased aggregation in the diatom *Skeletonema grethae* while at the same time increasing sinking velocities significantly. Although increased sinking velocity results in a swift plastic particle removal from the water column, the transport of these pollutants to the seafloor creates subsequent problems for deep-sea organisms. A decrease of this sedimentation on a large scale on the other hand would have disastrous consequences on our planet's carbon cycle at large. Neutrally buoyant aggregates, as found in experiments on *Skeletonema grethae* even at the lowest plastic particle concentration, is particularly problematic. This scenario has potentially far-reaching implications for the oceanic carbon pump, as the ultimate result of non-sinking aggregates would be a return of this organic matter into the carbon cycle of the upper ocean and thus a limitation of nutrients and carbon influx into the deep sea.

Many effects of plastics on sedimentation are hard to extrapolate from laboratory experiments, as the sinking velocity of aggregates is very heterogeneous to begin with. Mesocosm experiments are needed to discern the potential of hetero-aggregates to remove beads and fibers alike from the water column and investigate their individual fate. In my own research, presented in Chapter 3, we observed that, generally, most  $\mu\text{P}$  particles are embedded in organic matter (68.75%) while only 31.25% are free-floating in the ocean around Okinawa. A recent study found even positively buoyant  $\mu\text{PS}$  within the water column [94]. The observed interplay between infection in the *Odontella aurita* experiment and nP/MF shows the need for mesocosm experiments to understand the interactions between  $\mu\text{P}/\text{nP}/\text{MF}$  on a bigger scale with multiple factors.

While all plastic types significantly reduced sedimentation in *Odontella aurita*, the effect was reversed when an additional species was present. This may indicate complex inter-species interactions, in which  $\mu\text{P}/\text{nP}/\text{MF}$  intervene. The reduced sinking velocities – or, at the extreme, neutral buoyancy – could lead to changes in the carbon pump and carbon distribution in the ocean water column, limited carbon sequestration and nutrient input into the deep sea.

For future experiments, investigation of the impact of plastic exposure on the chain length of *Odontella aurita* should be considered. Such a reduction in chain length has been reported in other diatoms [164], and, as shorter chains are generally more buoyant, this could explain some

of the effects on sinking velocities [210]. Based on aggregation and sedimentation results from our studies,  $\mu\text{P}/\text{nP}/\text{MF}$  could lead to a shift in plankton communities, favoring those species that deal best with plastic. It has been discovered that the microorganisms found in the “plastisphere” of  $\mu\text{P}$  attached via EPS [65] are markedly different from the microorganism communities in the surrounding seawater [64]. In the same way, the incorporation of  $\mu\text{P}/\text{nP}/\text{MF}$  could lead to a shift in the interacting plankton communities.

## Chapter 3

# Micro- and Nanoplastic around Okinawa<sup>1</sup>

### 3.1 Environmental Risk Assessments of Micro- and Nanoplastic in Okinawa

Risk assessments and risk analysis are systematic procedures for predicting potential risks to humans or the environment. Although different organizations use several frameworks, there are three general steps: 1) Identify the hazard, 2) Estimate the risk it poses, and 3) Consider possible steps to mitigate that risk. In the case of marine micro- and nanoplastics ( $\mu\text{P}/\text{nP}$ ), environmental risk assessments are based, to a great extent, on laboratory analysis of the interaction between these contaminating particles and a specific component in the environment. Koelmans et al. [50] suggested a general environmental risk assessment framework for  $\mu\text{P}/\text{nP}$ , quantifying exposure and effect assessment. Effect assessment quantifies how a specific contaminant and a specific dose affect organisms and ecosystems. It is conducted using laboratory studies for the most part. In this thesis, Chapter 2 (general planktonic micro-algae species) and Chapter 4 (specific Okinawa reef micro-algae species) attempt to give some quantification to the effects of  $\mu\text{P}/\text{nP}$  on micro-algae, shedding light on the interactions at small scales. The current chapter focuses on exposure assessment, which relates to the quantification of  $\mu\text{P}/\text{nP}$  found in the environment. This can give insight into the question of how likely it is for animals, plants, and humans to actually get exposed to relevant  $\mu\text{P}/\text{nP}$  doses under normal circumstances.

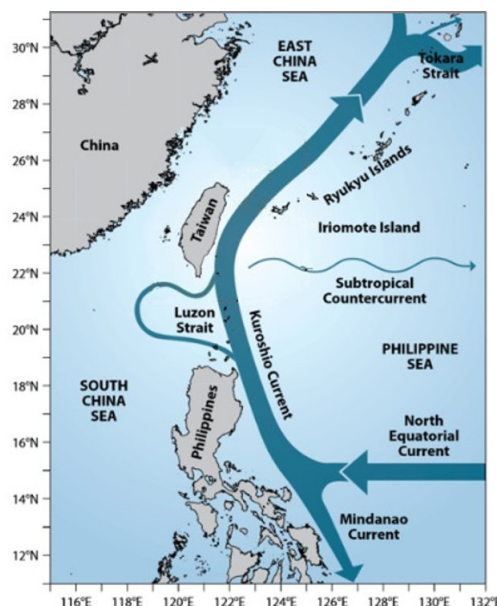
Multiple studies have been done on marine plastic pollution [211, 39, 42, 40, 41, 43] with increasing focus recently on  $\mu\text{P}/\text{nP}$  [20, 22]. Despite the first report on the emergence of small plastic particles in the oceans being 50 years ago [46] and the issue becoming globally recognized and even discussed as a planetary boundary threat [16], our understanding of this issue is still in its infancy. As our knowledge and understanding of the issue is not deep enough, many possible impacts are predicated on the mere presence of the plastic in the environment. This physical presence of plastics in the environment is indubitably undesirable for multiple reasons – aesthetic, ethical, economic, and ecological [50] – but actual risks to humans and the environment remain uncertain. Nonstandardized methods and terminology, in combination with preliminary results both on the

---

<sup>1</sup>This work is based on “In-situ analysis of small microplastics in coastal surface water samples of the subtropical island of Okinawa, Japan” by Christina Ripken, Domna G. Kotsifaki and Síle Nic Chormaic See Appendix A for manuscript and [arXiv 2008.08259](https://arxiv.org/abs/2008.08259).



effect as well as the exposure assessment, do not improve the uncertainty of the situation. A sustained interest of the general public will lead policy-makers to focus attention and money on the topic, thus enabling scientists to increase quality and quantity of exposure and effect assessment. Our study of the  $\mu\text{P}/\text{nP}$  presence around Okinawa aims to quantify the possible exposure risk of both the  $\mu\text{P}/\text{nP}$  (in abundance and polymer type) themselves as well as associated trace metals. Monitoring studies of this kind are a snapshot in space and time [50], but it is important to have this reference point to assess the increase or decrease of the  $\mu\text{P}/\text{nP}$  around Okinawa.



**Figure 3.1: Map of Okinawa (within the Ryukyu Islands) and the Kuroshio Current.** Schematic diagram of currents in the western north Pacific Ocean showing the Kuroshio. The westward-flowing North Equatorial Current runs into the Philippines and splits into the northward-flowing Kuroshio and the southward-flowing Mindanao current [212].

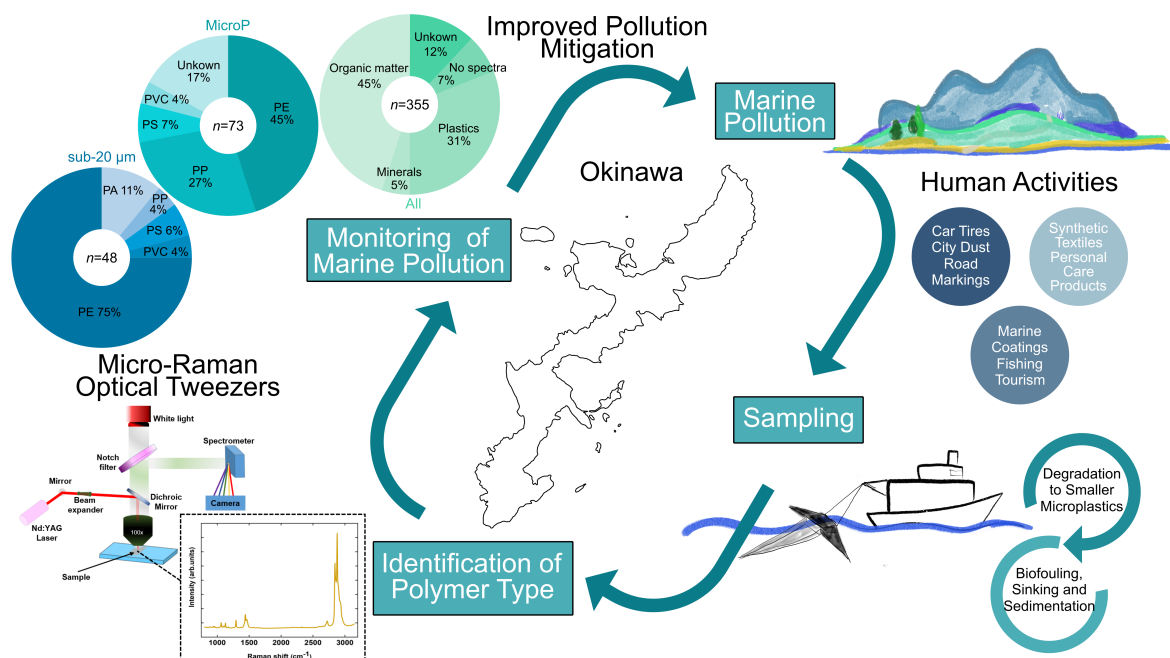
Okinawa is situated on the western edge of the continental shelf of the Eurasian Plate and the eastern edge of the Philippine Plate (see Figure 3.1).  $\mu\text{P}/\text{nP}$  found in the waters around Okinawa originate primarily from land: these small plastic particles find their way into the ocean via point sources such as river outlets, sewage outfalls, and runoff after heavy rainfall, but also via atmospheric input such as wind and rain. The other source of  $\mu\text{P}/\text{nP}$  around Okinawa is from the currents passing along the island. Notable is the Kuroshio Current that passes Okinawa on the western side through the East China Sea. Available data points to a current, wind-independent transport of  $\mu\text{P}/\text{nP}$  around the world, so  $\mu\text{P}/\text{nP}$ s found around Okinawa will be coming from the North Pacific Gyre (334 pieces/ $\text{m}^2$   $\mu\text{P}$  in the Northeast Pacific Gyre [86]), traveling with the Kuroshio Current past Taiwan to Okinawa. The Kuroshio Current tested for plastics north of Okinawa carries magnitudes lower of  $\mu\text{P}$  pollution compared to the gyre (0.0176 pieces/ $\text{m}^2$  [93]). This makes a shore deposition on the islands along the current seem more likely. Another reason for the lower plastic pollution sampled could be fragmentation and subsequent sinking of the particles to be found within the water column, not the surface waters [94] as well as fragmentation to, at present, unsampled nano sizes. As plastic pollution input into the marine environment rises [27], the mean marine plastic debris pieces sampled are getting smaller [59]. This is both due to increased primary input of smaller plastic particles –  $\mu\text{P}/\text{nP}$  can originate from medical and



cosmetic products, nanofibers from clothes and carpets, 3D printing, Styrofoam byproducts, and removal of paints from buildings and ships – as well as secondary sources due to photochemical and mechanical degradation of larger plastic debris leading to fragmentation [66, 20, 70]. Primary  $\mu\text{P}/\text{nP}$  from China are less likely to be found around Okinawa, as marine pollution from China is surface wave- and wind-driven, not current-driven [213]. The Kuroshio Current passing between Okinawa and China makes it more likely that  $\mu\text{P}/\text{nP}$  from China would be directed northwards. Wind-driven macroplastic and mesoplastic (maP/meP) pollution from China is often found on Okinawan Beaches as well as current driven maP/meP from Taiwan, both recognizable by the writing on the debris [214]. Secondary  $\mu\text{P}/\text{nP}$  found from Chinese debris, fragmented within the Okinawan coastal waters and washed onto beaches, could be found on Okinawan beaches, if the fragmentation took place after the maP travel via wind across the Kuroshio Current.

Currently, there is no standardized way of reporting  $\mu\text{P}/\text{nP}$  in environmental studies and available methods are not capable of identifying all plastics within an environmental sample [66, 50]. While large  $\mu\text{P}$  are relatively easy to spot and identify, small  $\mu\text{P}$  and especially nP pose a serious challenge.

There is a need for reliable and precise identification of  $\mu\text{P}/\text{nP}$  without separating them from the matrices in which they were collected. The current protocols for quantification and characterization of environmental  $\mu\text{P}/\text{nP}$  contamination are hampered by a lack of sensitive yet high-throughput methods. Commonly applied methods for the analysis of nPs include visual inspection or stiffness test, spectroscopy [215, 70, 158], transmission or scanning electron microscopy, and fluorescence imaging [181]. However, the chemical characterization of single nanoparticles in a liquid sample is still limited. Therefore, techniques with selectivity and precision that enable the analysis of single particles *in-situ* and in real-time are essential.



**Figure 3.2: Sampling and analysis of marine pollution found around Okinawa.** Continued monitoring can lead to improved mitigation approaches for marine plastic pollution. (The Okinawa map is under CC-BY 3.0 licence and it was modified from the one by Misakubo)

This study aims to give (1) an overview of the current  $\mu\text{P}$  pollution around Okinawa and (2) assess the risk these  $\mu\text{P}$ s pose to the Okinawan marine environment (see Figure 3.2). Including nP in the exposure assessment and risk analysis of the marine plastic pollution issue requires using new techniques [164]. The risk assessment is based on the hazard score of plastic polymers created by Lithner et al. [71] combined with the pollution load index (PLI) [116] while factoring in the heavy metals found on the plastic particles. This initial assessment of the Okinawan coastal surface waters aims to assist policy-making for the marine  $\mu\text{P}$  pollution in this region. We use the same size classification as described in the introduction:

- Microplastic ( $\mu\text{P}$ ): large (5 – 1 mm), small (1 mm – 20  $\mu\text{m}$ ), sub-20  $\mu\text{m}$  (20  $\mu\text{m}$  – 1  $\mu\text{m}$ )
- Nanoplastic (nP): large (1  $\mu\text{m}$  – 100 nm), small (100 nm – 1 nm).

Three main analysis methods are used to process the field work samples, each one being modified to suit the needs of the particle size analyzed. One method is micro-Raman, the second one is X-ray fluorescence (XRF) spectroscopy and the last is the optical tweezers micro-Raman. All three are explained below in detail.

## 3.2 Materials and Methods<sup>2</sup>

*To limit contamination of the samples from clothing or air, all samples were filtered, sorted, and prepared in a positive pressure chamber which draws its air supply through a HEPA filter (AS ONE Corporation, 3-1423-01, Pure Space 01, PS01-AD), and stored in airtight sample boxes after preparation. Only cotton clothing was worn during sampling and preparation.*

### 3.2.1 Study Region

The island of Okinawa (26.2124° N, 127.6809° E) is part of the Ryukyu Island Arc (Figure 3.3) and consists of uplifted coral reefs and, especially the northern half, igneous rock (solidified magma or lava). It is surrounded by fringing reefs, making the water intake that reaches the beaches more reliant on surface waves and wind [216]. Land-based pollution originating on Okinawa is more likely to be found in the bigger bays of the island. The six sampling regions were chosen to give an overview of the geographical distribution of pollution around Okinawa. Sites differ in population density and industry in and around the respective bays.

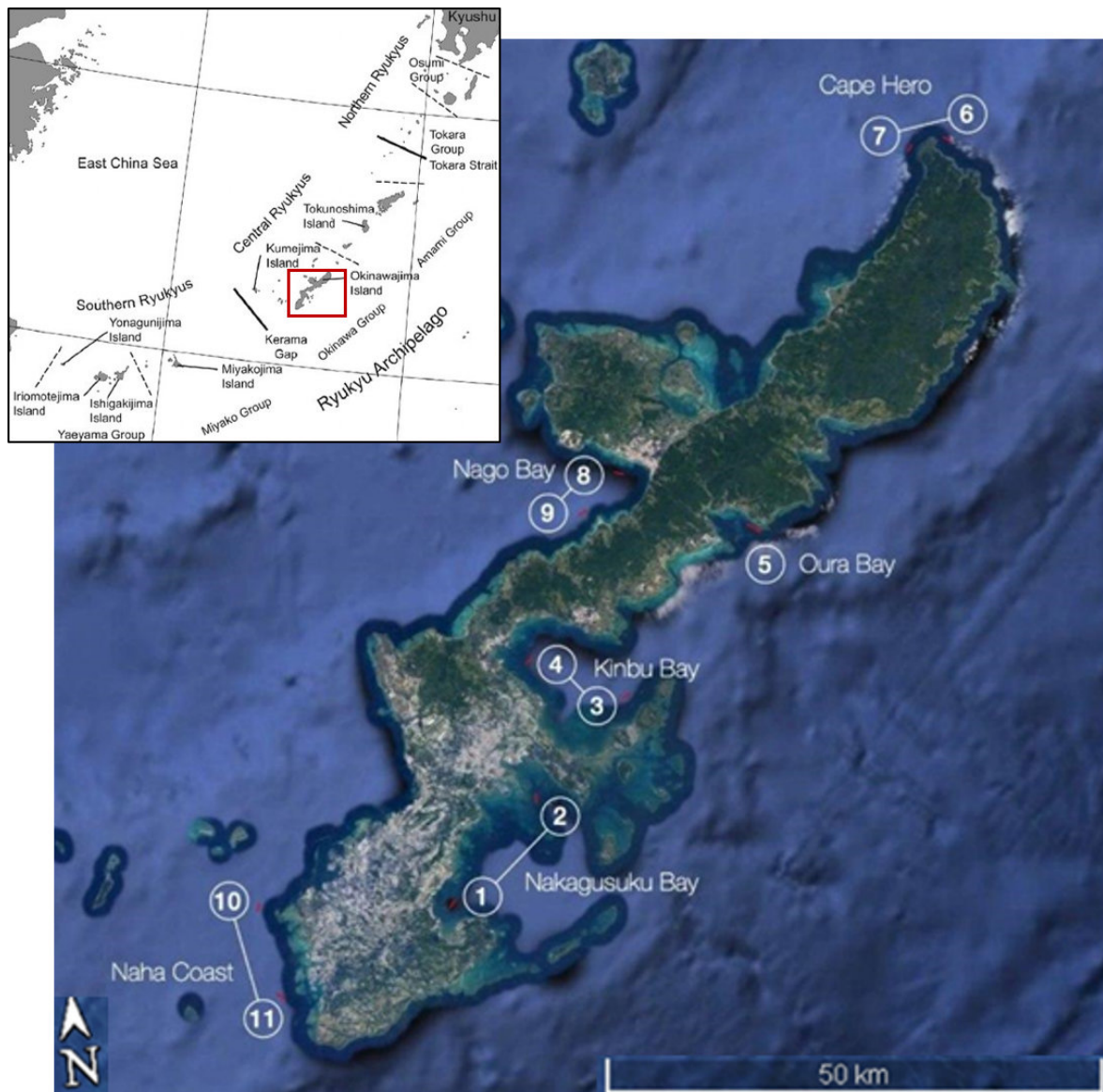
### 3.2.2 Field Sampling<sup>3</sup>

To quantify  $\mu\text{P}$ /nP abundance in the surface waters around Okinawa, water samples were collected in September of 2018. Sampling was performed within 24 h (19th - 20th September, detailed con-

---

<sup>2</sup>Some methods are explained in greater detail than traditionally done within the methods section. Especially methods that were developed, failed or could not be conducted (although they were included in the thesis proposal) are elucidated to give a better overview of the work done. The author feels this is better presented in the respective method sections than under results.

<sup>3</sup>Originally, cruises were planned monthly over the course of a year to better understand  $\mu\text{P}$ /nP abundance seasonality and weather dependence on typhoons. However, due to shifts in the main research focus of the original research unit (Marine Biophysics Unit), only the first cruise could be realized. Subsequently, the methods used for identification could be established but a meaningful risk analysis could not be realized.



**Figure 3.3: Map of field study area.** The insert shows a map of the Ryukyu Islands Arch with a red box around Okinawa [217]; Big map of Okinawa with the 11 (S1-S11) towing sites in 6 regions [218]:

South East: Nakagusuku Bay (S1, S2)	North West: Cape Hedo (S6, S7)
Center East: Kinbu Bay (S3, S4)	Center West: Nago Bay (S8, S9)
North East: Oura Bay (S5)	South West: (S10, S11)

ditions in Table 3.1) on the Okinawa Prefectural Fisheries and Ocean Research Center ship, Tonan Maru. Sampling was done using a Manta trawl (Hydro-Bios, 300  $\mu\text{m}$  net, net opening is 15 cm  $\times$  30 cm, with Hydro-Bios Mechanical Flow Meter No.: 438 110). This cruise was designed to give an overview snapshot of the  $\mu\text{P}$ / $\text{nP}$  pollution around Okinawa.

The Manta net was deployed off the starboard side of the boat and trawled for 15 min at 2–3 knots covering an average distance of 1 km, filtering an average volume of 856.8 L. After trawling, the nets were washed down twice with 0.2  $\mu\text{m}$  filtered seawater brought onto the boat, before transferring the content into 450 mL glasses. Eleven nets were trawled, two for each location – except in Oura Bay. At that location only one site could be sampled as a second site had to be given up due to the US military construction of a new base. All 11 samples were stored in a climatized environment at 15°C until processing the next day. Between each sample, the Manta net was backwashed with seawater, and the collector at the end of the Manta net was washed separately to limit cross-contamination between sampling locations.

For the collection of potential nPs, an additional water column sample was taken at each station with a Niskin bottle at 2 m below the surface. After washing the 450 mL glass jars twice with the first water out of the Niskin bottle, the jar was filled up and stored in a climatized environment at 15 ° C until processing. These samples ended up not being used, as the particle content was too low to be detected with the method used for analysis.

### 3.2.3 Laboratory Analysis

The 11 Manta trawl samples were each filtered over a 300  $\mu\text{m}$  sieve to collect the  $\mu\text{Ps}$  in the range of 300  $\mu\text{m}$  to 5 mm (note that for fibers the diameter was used rather than total length of the fiber). The filtration over 300  $\mu\text{m}$  resulted in organic and inorganic particles being collected, which were then sorted by hand. The meso- and  $\mu\text{Ps}$  contained within were picked up with forceps and prepared on carbon tape on glass slides. After that each  $\mu\text{P}$  particle was photographed and examined under an optical light microscope (Zeiss Axio Imager Z1 microscope) to determine source, type, shape, erosion and color (see Appendix C, after [66]). In order to determine the particle area, ImageJ was used with the functions: Analyze Particles (values can be found in Appendix C).

### 3.2.4 X-ray fluorescence (XRF) spectroscopy for trace metal detection

The particles were scanned for trace metal pollution using X-ray fluorescence (XRF) spectroscopy (Horiba, model XGT-7000.) This is a qualitative analytical method to determine the presence of elements above the atomic weight of Na up to Rd. The non-destructive nature of the method gives the advantage that the  $\mu\text{P}$  can be used for polymer identification afterwards. The location of the elements on the  $\mu\text{P}$  was visualized using the Horiba XGT 7000 software. Since particles were not cleaned before scanning, trace metal contamination located within the biota growing on the particles can be found as well. Distribution patterns and signal strength were compared using MATLAB image analysis. The focus was on the following elements which are considered most toxic and having the most potential impact when bio accumulated on  $\mu\text{Ps}$  [219, 37]: Arsenic (As), Mercury (Hg), Copper (Cu), Zinc (Zn), Lead (Pb), Cadmium (Cd). These elements are called “trace metals” within the thesis. As this method does not only display trace metals sorbed onto the particle, but also distributed within, as part of dyes and flame retardants (commonly using elements Cl, Br, P), the location and distribution pattern is important to examine.

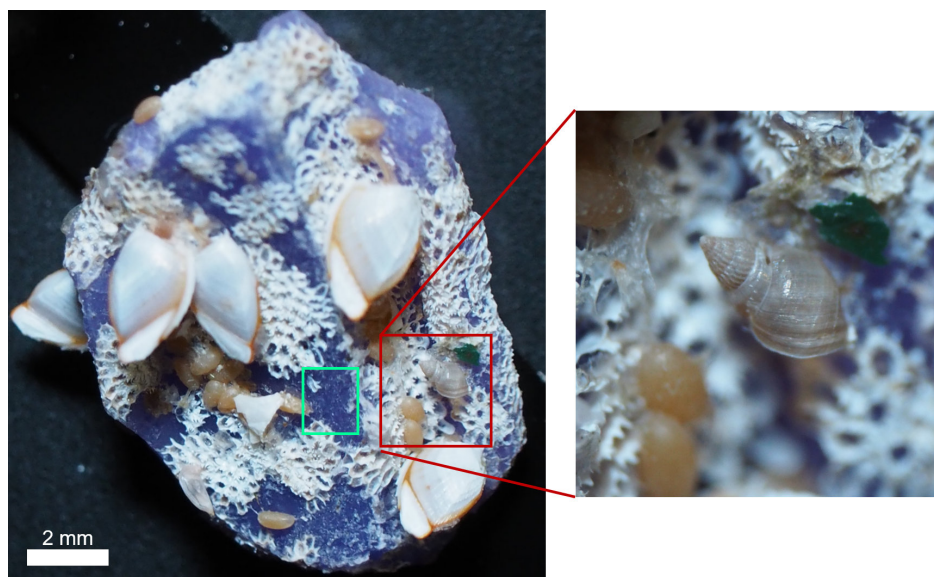
Table 3.1: Detailed trawling data, translated from log book of Tonan Maru: Start and end points, time and distance and volume filtered for every Manta net trawled.

Site	Start of Towing Net										End of Towing Net				Flow Meter					
	Date	Time (JST)	Lat (North)	Long (East)	Pressure (hPa)	Depth (m)	Wind direction	Wind speed (m/s)	Sea State	Swell direction	Swell State	Air Temp (degrees C)	Sea Temp (degrees C)	Date	Time (JST)	Lat (North)	Long (East)	Start	End	Filtered Volume (L)
Nakagusuku-1	19/09/2018	13:22	26-11.969	127-47.212	1014.8	11.2	E	5.8	1	E	1	31.9	30.4	19/09/2018	13:37	26-12.407	127-47.554	65190	68892	832.95
Nakagusuku-2	19/09/2018	14:43	26-17.471	127-52.255	1014.0	13.3	E	2.8	1	E	1	31.7	30.2	19/09/2018	14:58	26-17.471	127-52.289	68892	72692	855.00
Kin-1	19/09/2018	17:10	26-23.302	127-57.707	1013.3	42.7	ENE	2.2	1	E	1	30.7	29.6	19/09/2018	17:25	26-22.931	127-57.296	72692	76217	793.13
Kin-2	19/09/2018	18:05	26-24.839	127-51.647	1013.3	17.9	E	2.0	1	N/A	0	29.8	30.9	19/09/2018	18:20	26-25.189	127-52.047	80000	83464	779.40
Oura-1	19/09/2018	20:13	26-32.194	128-04.648	1014.3	17.6	NE	1.0	0	N/A	0	28.6	29.3	19/09/2018	20:28	26-31.771	128-05.500	83464	87203	841.28
Hedo-1	19/09/2018	23:21	26-52.285	128-16.807	1015.3	No log	SSE	3.8	1	N/A	0	27.7	29.7	19/09/2018	23:36	26-52.585	128-16.274	87203	90525	747.45
Hedo-2	19/09/2018	23:54	26-52.173	128-14.398	1014.5	144	S	2.0	1	N/A	0	28.0	29.5	20/09/2018	0:09	26-51.801	128-14.167	90525	94349	860.40
Nago-1	20/09/2018	3:37	26-34.933	127-56.869	1013.3	48.6	E	1.0	1	N/A	0	27.8	28.9	20/09/2018	3:52	26-34.817	127-57.450	94349	98592	954.68
Nago-2	20/09/2018	4:18	26-32.936	127-55.259	1012.3	83.4	ENE	2.0	1	N/A	0	27.0	28.8	20/09/2018	4:34	26-32.688	127-54.781	98592	101884	740.70
Naha-1	20/09/2018	7:22	26-12.186	127-36.052	1012.8	47.2	SE	0.6	1	N/A	0	28.4	29.0	20/09/2018	7:37	26-11.717	127-35.910	1884	6169	964.13
Naha-2	20/09/2018	8:18	26-07.439	127-37.047	1013.5	46.6	SE	3.3	1	N/A	0	29.3	29.1	20/09/2018	8:33	26-07.074	127-37.495	6169	10861	1055.70



### 3.2.5 Micro-Raman Raman Spectroscopy

To identify the polymer type of the particles contained within the field samples, Optical micro-Raman Spectroscopy (Nanofinder 30, 532 nm laser), attached to an electron-multiplying charge-coupled device (EMCCD) camera as a detector and objectives with magnifications of 20 $\times$ , 50 $\times$ , 100 $\times$  was used. Slightly different setups were used for various particle sizes. All  $\mu$ P particles above 300  $\mu$ m were measured using a 20 $\times$  or a 50 $\times$  objective. Great care was taken to avoid the illumination of the attached biota with the laser and to focus on a clear plastic area (see Figure 3.4).



**Figure 3.4:** Biota found on  $\mu$ P particle 73 at Naha station 2 (S2). The green box shows the region on the  $\mu$ P which will provide a clear Raman spectrum. The red box and insert indicates a region that should be avoided, as too much biota is on the surface.

Polymers were identified from the spectra using online databases [220], literature [24, 221] and known polymer reference samples.

Originally, for polymertype analysis of the nP, the water samples were filtered over polycarbonate (PCTE) membrane filters (pore size 20  $\mu$ m and subsequently 100 nm, Sterlitech) in a filter cascade (Vacuum Filtration system from Advantec). The filters were mounted onto glass slides. Identifying the particles on the filter was not possible, because the particles got embedded into the filter itself. So, while visible with the 50 $\times$  and 100 $\times$  magnification, the micro-Raman spectrometer could not pick up the signal.

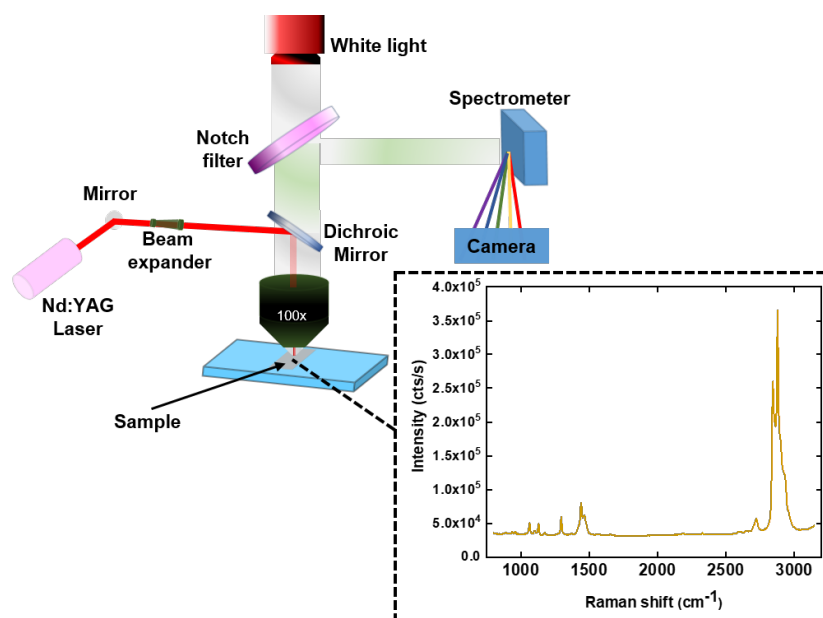
The second method we used to try to identify small  $\mu$ P/nP was optical tweezers micro-Raman spectroscopy by integrated an optical tweezers (see Figure 3.5) on the Nanofinder 30. Optical tweezers micro-Raman spectroscopy (OTRS) has recently shown promising results for *in-situ* analysis of  $\mu$ P, sub-20  $\mu$ m and nPs [24].

The optical tweezers micro-Raman spectroscopy (OTRS) used to get quantitative data on small plastic particles in the liquid environmental samples builds on the principles of the field of optical trapping. Since the first demonstration of particle optical trapping in 1986 [222], optical tweezers have emerged as a powerful tool for trapping and manipulating particles in fluids [222, 223]. They employ highly focused laser beams to trap and hold dielectric particles from 10 nm to 100  $\mu$ m in diameter. The particle has to be trapped near the focal spot because of the emergence



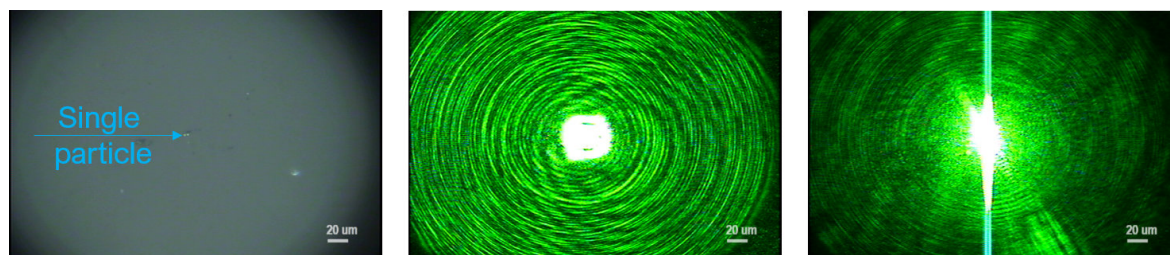
of scattering and gradient optical forces [224, 225]: the scattering forces are due to radiation pressure of the light beam along the direction of propagation of the beam, and the gradient forces pull the particle towards the high-intensity focal spot. The total optical force exerted on a particle is in the range between 100 fN to 100 pN depending on the difference between the refractive indices of the particle and the liquid medium. The ability to measure such small forces has opened the way for many new experiments in physics, chemistry, biophysics, and nanotechnology. Important examples include the development of holographic optical tweezers [226], a variety of biophysics measurements on single biomolecules [227], cell-sorting applications [228], the development of techniques for optical rotation of particles [229], optical binding of particles [230], and trapping in sub-wavelength fields created by plasmonic nanostructures [225].

As a result, the combination of optical tweezers with a range of different optical read-out techniques, for example Raman spectroscopy, has enabled various types of single-particle investigations. The first combination of micro-Raman spectroscopy and optical tweezers was presented in 1994, when Urlaub et al. [231] investigated a polymerization reaction in optically trapped emulsion particles, while Raman tweezers entered the field of biophysics in 2002 with studies of single cells and organelles [232, 233]. Recently, the OTRS technique has been used for qualitative chemical analysis of a variety of plastic particles with sizes in the sub-20  $\mu\text{m}$  regime in seawater environment [24]. The authors achieved to discriminate between plastics and mineral sediments at the single-particle level overcoming the capacities of conventional Raman spectroscopy in a liquid environment. Therefore, such a OTRS system was used for *in-situ* analysis of sub-20  $\mu\text{m}$  and nP fraction of our samples. This setup was used for all particles below 300  $\mu\text{m}$ .



**Figure 3.5:** A schematic illustration of the micro-Raman optical tweezers setup used for chemical identification of material type. The same setup was used, adjusting the lenses to lower magnification, for the chemical identification of  $\mu\text{P}$ s. Inset: A characteristic spectrum of a Polyethylene particle of 15  $\mu\text{m}$  diameter.

Our OTRS system consists of a Nd:YAG laser beam ( $\lambda = 532 \text{ nm}$  with laser power on sample plane at 17 mW) focused using a high Numerical Aperture (NA) oil Immersion Objective Lens



**Figure 3.6: Optical image of micro particle trapping process.** Single particle trapping using a laser of 532 nm. Particle is  $\sim 1 \mu\text{m}$  diameter. The left image shows the optical image of various plastics/particles in the environmental sea water sample. The middle image shows the laser turned on, focused on seawater. Under illumination conditions, the particles will be moving towards the focus of the laser due to the influence of optical forces exerted on it. The right image presents the scattering of the laser beam when a particle with arbitrary shape is trapped.

(Plan-Neofluar  $100\times$ , NA 1.30, Carl Zeiss) onto the seawater sample as shown in Figure 3.5. The trapping laser beam is integrated into a Raman spectrometer (3D Laser Raman Microspectrometer Nanofinder 30). The high NA of the lens ensures the trapping of the nanoparticles and provides the necessary laser intensity needed to maximize their Raman signal. Using adhesive microscope spacers, a microwell was formed on the glass slide, trapping the  $20 \mu\text{L}$  sample solution under a cover glass. The microwell contained particles in seawater from the sampled regions. As control, a microwell with  $10 \mu\text{L}$  milli-Q water aqua was prepared on the same microscope slide. The microscope slide was mounted and fixed on top of the translation stage. Therefore, the OTRS technique allows us to chemically identify small  $\mu\text{P}/\text{nP}$  fragments (see Figure 3.6).

### 3.2.6 Risk Assessment<sup>4</sup>

The Okinawa Prefectural Government has, in recent years, become concerned about this problem and has adopted the policy of (a) having to pay for usage of plastic bags in supermarkets and (b) the reduction of plastic trash through recycling programs. It has also funded a report concerning marine trash around Okinawa and the neighboring islands. Having additional information about the potential risks of  $\mu\text{P}/\text{nP}$  in the coastal waters can lead to more targeted policies protecting Okinawa's fringing coral reefs and mangrove habitats. The Okinawan Prefectural Government has indicated interest in this data as well as implementing more targeted policy changes fighting  $\mu\text{P}/\text{nP}$  pollution around Okinawa.

Besseling et al. [30] stress the importance of separating the different components of risk posed by  $\mu\text{P}$ , using different ecological relevant metrics for each component. Evaluating the potential risk of  $\mu\text{P}$  should take into consideration multiple factors, and in this thesis the focus was to be on:

- **concentration of  $\mu\text{P}$**  (in  $n/100\text{L}$  and per  $\text{m}^2$ , polymer risk index after [116])

<sup>4</sup>Originally a risk assessment was planned in this thesis to comprise the risk of the  $\mu\text{P}$  themselves and the trace metal sorbed onto them. Due to the reduction of the original 12 cruises to one, using the following methodology on the data is not feasible as there are not enough data points. The method is presented here to illustrate a possible further evaluation of  $\mu\text{P}$  and associated trace metal data. Individual risk as well as combinatorial risk was to be addressed, as  $\mu\text{P}$  and trace metals can interact and the risk of each is influenced (increases toxicity vs. diminished impact) by the other.

- **chemical composition** (hazard score by [71])
- **pollution load index for  $\mu\text{P}$**  (*PLI*, after [234])

For the assessment of the potential risk of the trace metal load found on the  $\mu\text{P}$ , a similar combination of multiple factors was to be used:

- **detection and abundance of trace metals on the  $\mu\text{P}$ ,**
- **pollution load index for trace metals** (*PLI*, after [234])

It is important to note that the *PLI* softens the effects and differences of each individual  $\mu\text{P}$  or trace metal at each sampling station. The benefit of using the *PLI* is that it makes comparison of different stations possible. To compensate for this smoothing of the data, individual  $\mu\text{P}$ , polymer types or trace metals can be singled out for further discussion in detail due to the high impact these might have.

As previous studies do not consistently use the same expression for risk assessment levels and no combination risk assessments are given in the literature, here Xu et al.'s [116] method is used for creating risk levels (see Table 3.2) to combine the effects together. Polymer index,  $\mu\text{P}$  pollution load index, heavy metal pollution load index and if applicable the nP pollution load index should be combined to give risk categories. As the indices have never been calculated for Okinawa, the thresholds given in Table 3.2 are preliminary and have to be adjusted to the actually found values.

**Table 3.2: Risk level Categories for microplastic, nanoplastic and trace metal pollution.**

Polymer Index	< 10	10 – 100	1000 – 1000	> 1000
$\mu\text{P}$ Pollution Load Index	< 10	10 – 20	20 – 30	> 30
nP Pollution Load Index	< 10	10 – 20	20 – 30	> 30
Heavy Metal Pollution Load Index	< 10	10 – 20	20 – 30	> 30
Risk Categories	I	II	III	IV

A meaningful analysis could not be done with the data of just one cruise. The *PLI* for Okinawa in comparison to Japan was calculated and is reported below, but this needs to be viewed with caution and does not allow any detailed risk analysis.

### Microplastic concentration and polymer risk<sup>5</sup>

Evaluating the chemical toxicity of the  $\mu\text{P}$  using the hazard score of [71] and following [116], results in the polymer risk index. This formula takes into consideration the concentration of each polymer at each respective sample station (after [116]):

$$H = \sum_n P_n S_n \quad (3.1)$$

<sup>5</sup>Both the *PLI* and the polymer risk should also be calculated for the sub-20  $\mu\text{m}$  and nP fraction of the collected particles using the equations (3.1) and (3.3). This evaluation remains to be done when more information is available from Okinawa.

- $H$  = Calculated polymer risk of  $\mu\text{P}$
- $P_n$  = percentage of a certain  $\mu\text{P}$  polymer type collected at each sampling station
- $S_n$  = hazard score taken from [71] (see Table 3.3 for reference)
- $n$  = polymer types present in the study (see Table 3.3)

### Microplastic pollution load index

To evaluate and compare different sampling stations with each other as well as with the surrounding region, the pollution load index was calculated following [234]:

$$CF_i = C_i/C_{0i} \quad (3.2)$$

$$PLI = \sqrt{C_i/C_{0i}} \quad (3.3)$$

$$PLI_{zone} = \sqrt[n]{PLI_1 PLI_2 \dots PLI_n} \quad (3.4)$$

- $C_i$  =  $\mu\text{P}$  concentration at each station
- $CF_i$  = Concentration Factor for  $\mu\text{P}$
- $C_{0i}$  = minimal average  $\mu\text{P}$  concentration

The  $PLI$  is obtained as Concentration Factor ( $CF$ ) of each  $\mu\text{P}$ . This  $CF$  is the resulting quotient of dividing the concentration of each  $\mu\text{P}$  by the minimal average concentration of  $\mu\text{P}$  assumed. Once the  $CF$  is calculated, the  $PLI$ s of the station are calculated by taking the square root [116]. With the  $PLI$  obtained from each station, the  $PLI$  for larger geographical areas (*zone*) was to be calculated by obtaining the  $n^{\text{th}}$ -root from the  $n$ - $PLI$ s [234]. The zones were to be South (S1-S4, S10, S11), North (S5-S9), East (S1-S6), West (S7-S9) and Naha (S10, S11) (see Table 3.4).

### Trace metal on microplastic pollution load index

The pollution load index for trace metals on  $\mu\text{P}$  ( $PLI_{MS}$ ) is related to the presence of each trace metal at each station. As the qualitative nature of the detection method only gives the possibility to determine presence via graphical analysis, three categories (low, medium, high) were assigned and compared to the overall presence of the trace metal. This way different stations can be compared to each other regarding their trace metal  $PLI$ :

$$CF_{Mi} = M_i/M_{0i} \quad (3.5)$$

$$PLI_{MS} = \sqrt{M_i/M_{0i}} \quad (3.6)$$

$$PLI_{Mzone} = \sqrt[n]{PLI_{M1}PLI_{M2} \cdots PLI_{Mn}} \quad (3.7)$$

- $M_i$  = Trace metal presence per station
- $M_{0i}$  = minimal trace metal presence at all stations

This pollution load index is calculated using the root of the quotient of the trace metal presence at each station ( $M_i$ ) and the minimal average trace metal presence ( $M_{0i}$ ). Once the  $CF$  is calculated, the  $PLI$ s of the stations are calculated by obtaining the  $n^{\text{th}}$  – root from the  $n - CF$ s [234]. With the  $PLI$  obtained from each station, the  $PLI$  for the zones is calculated. Zones correspond to the ones picked for the  $\mu$ P (see Table 3.4). Evaluating the inherent risk of the trace metal found on the  $\mu$ P has not been done in this fashion. Munier and Bendell [37] evaluated  $\mu$ P as a sink and source for trace metals, but their focus was on a quantitative analysis. Rochmen et al. [75] and Wang et al. [85] both also studied trace metals on  $\mu$ P but did not analyze the ecological risk using indices. This index should have been used to compare the trace metal pollution around Okinawa and is not intended to be comparable to previous studies of trace metals and their ecotoxicity in sediments or seawater.

### 3.3 Results and Discussion

#### 3.3.1 Distribution and Abundance on Microplastics

From the 11 sample sites a total of 78 particles were recovered, 73 of which were plastics. The average concentration of plastic particles per 100 L was 0.76.

**Table 3.3: Polymer types found as  $\mu$ P/nP around Okinawa:** Detailed information for polymers identified in this study, including monomer, density, and hazard score [27, 71].

Polymer	Abb	Monomer	Density (g/cm <sup>3</sup> )	Hazard score
Polyethylene	PE	Ethylene	0.91-0.96	11
Polypropylene	PP	Propylene	0.85-0.94	1
Polyvinyl chloride	PVC	Vinyl chloride	1.41	10551
Polyamide (Nylon)	PA	Adipic acid	1.14-1.15	47
Polystyrene	PS	Styrene	1.05	30
Expanded Polystyrene	ESP	Styrene	0.05	44

No previous studies of the ocean around Okinawa have looked for  $\mu$ P/nP pollution, so the reported values are a first glance at this kind of pollution in these coastal waters. Polymer types found in the study are summarized in Table 3.3. We found a significant variation in the  $\mu$ P distribution around Okinawa, when looking at the particle numbers per station. In order to determine the underlying causes for this variation, we split the sampling stations in accordance with population density (North and South, see Table 3.4, and industrial distribution (East, West, Naha, see Table 3.4).

**Table 3.4: Micro- and nanoplastic particles found around Okinawa:** Top Table displays geographic data, stations partitionings for analysis and trawling data in combination with how many particles were found in which size class. Lower Table goes into detail on the sub-20 µm particles found.

Area Name	Station Names	Population Density [n./km <sup>2</sup> ]	Station split for analysis			Mantra trawl geo information (1km, 300 m <sup>2</sup> )						Volume Filtered (L)			Microplastic data		
			Population distribution	Industry distribution	Start Lat (North)	Start Long (East)	End Lat (North)	End Long (East)	Filtered (L)	Particles per station	Particles per 100L	Particles per m <sup>2</sup>					
Nakagusku 1	S1	1433.0	Sh1	E1	26-11.969	127-47.212	26-12.407	127-47.554	833	9	1.08	0.03					
Nakagusku 2	S2	2838.0	Sh2	E2	26-17.471	127-52.255	26-17.471	127-52.289	855	8	0.94	0.03					
Kin 1	S3	1386.0	Sh3	E3	26-23.302	127-57.707	26-22.931	127-57.296	793	6	0.76	0.02					
Kin 2	S4	1386.0	Sh4	E4	26-24.839	127-51.647	26-25.189	127-52.047	779	5	0.64	0.02					
Oura	S5	110.8	N1	E5	26-32.194	128-04.648	26-31.771	128-05.500	841	2	0.24	0.01					
Cape Hedo 1	S6	110.8	N2	E6	26-52.285	128-16.807	26-52.585	128-16.274	747	4	0.54	0.01					
Cape Hedo 2	S7	110.8	N3	W1	26-52.173	128-14.398	26-51.801	128-14.167	860	0	0.00	0.00					
Nago 1	S8	295.7	N4	W2	26-34.933	127-56.869	26-34.817	127-57.450	955	2	0.21	0.01					
Nago 2	S9	295.7	N5	W3	26-32.936	127-55.259	26-32.688	127-54.781	741	6	0.81	0.02					
Naha 1	S10	8043.0	Sh5	Naha1	26-12.186	127-36.052	26-11.717	127-35.910	964	24	2.49	0.08					
Naha 2	S11	1289.0	Sh6	Naha2	26-07.439	127-37.047	26-07.074	127-37.495	1056	7	0.66	0.02					

Area Name	Station Names	total volume checked [µL]	Nanoplastic data			Raman Analysis											
			Particles found	% plastic of total Particles	% organic of total Particles	PE	PA	PP	PS	PVC	Plastics	Minerals	Cellulose	Organic Matter	unknown spectra	no spectra	
Nakagusku 1	S1	40	22	22.7	56.8	8									25	1	3
Nakagusku 2	S2	40	44				1								37		8
Kin 1	S3	not checked						1							40	4	6
Kin 2	S4	60	56	17.9	66.1	8								8		1	5
Oura	S5	not checked												38			
Cape Hedo 1	S6	60	60	13.3	66.7	3	4							8		2	6
Cape Hedo 2	S7	60	13	15.4	61.5	1	1							8		2	1
Nago 1	S8	60	58	13.8	65.5	8								4	1		5
Nago 2	S9	not checked												30			
Naha 1	S10	40	51	19.6	58.8	8				2				10	7		4
Naha 2	S11	40	25											10	7		4



One major problem for policy-makers and stake holder evaluations of the  $\mu\text{P}/\text{nP}$  pollution threat is the difference in reporting of pollution data, in addition to the uncertainty of which levels of  $\mu\text{P}/\text{nP}$  pollution are actually problematic for the different habitats. There is no consistency in the literature for normalizing  $\mu\text{P}$  pollution and no reported particle numbers for  $\text{nP}$ . Two different normalization metrics are found for  $\mu\text{P}$ :

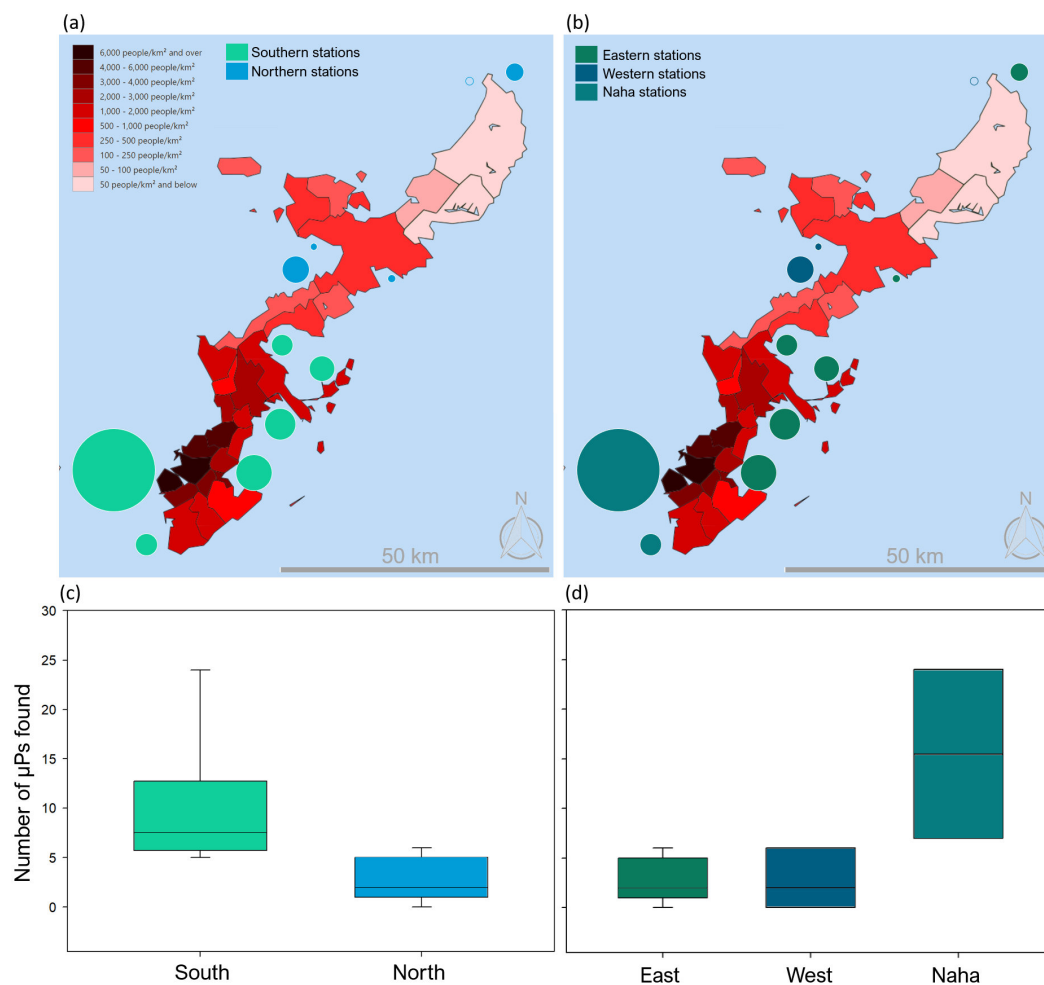
- to volume [235, 46, 236, 45, 237]
- to area [46, 49, 238, 86, 93, 66]

In this study, we provide both a normalization to area and to volume. The differences are noticeable, showing significant differences only in one case. Reporting both values helps policy-makers and other stakeholders arrive at the correct conclusion with the information provided, where hiding one would be misleading [50].

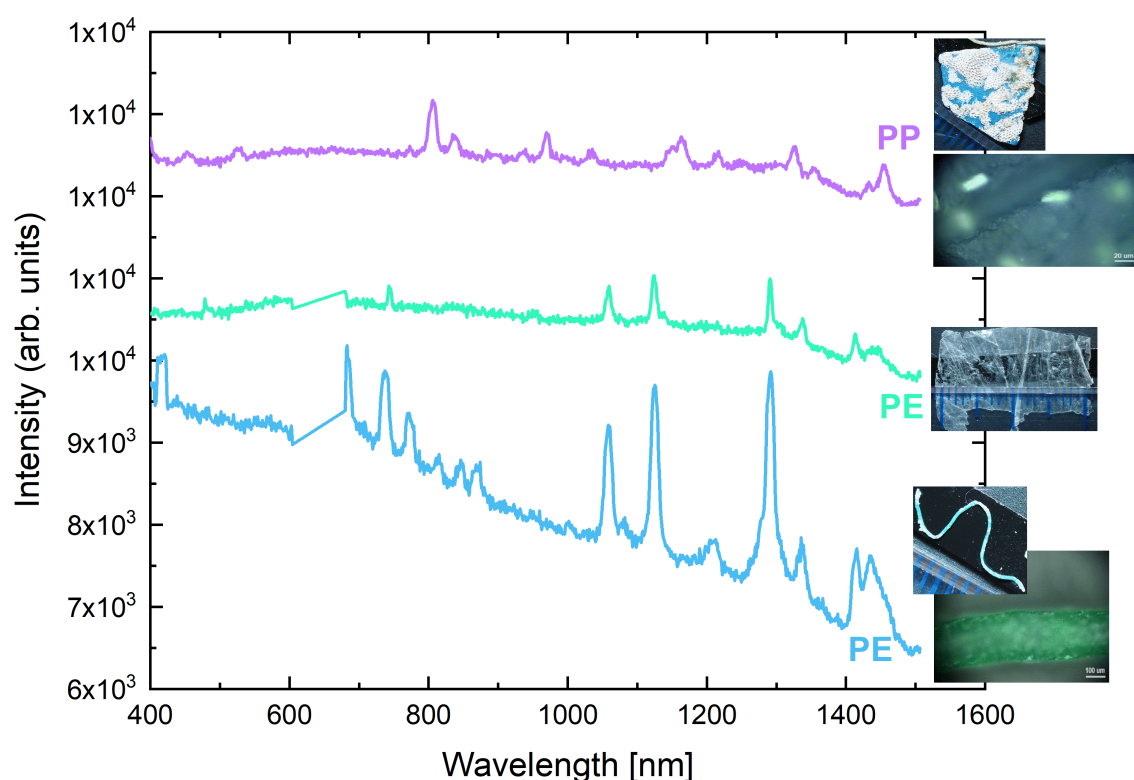
The population distribution on Okinawa follows a north-south gradient. The highest population densities are in the capital city Naha with over 8,043 people/ $\text{km}^2$  (see Figure 3.7, [239]); whilst the density falls to 50 people/ $\text{km}^2$  and below in the northern part. The  $\mu\text{P}$  distribution has been shown to follow the population density in other parts of Japan [240] and our data demonstrates the same relationship. We observe significantly lower  $\mu\text{P}$  concentrations in the north of the island compared to the south (Kruskal-Wallis, per volume:  $p = 0.030$ ; per area:  $p = 0.009$ ) (see Figure 3.7).

In contrast, the partitioning in East, West and Naha in accordance with the distribution of industry on the island does not show the concentration of  $\mu\text{P}$  following the distribution (Kruskal-Wallis, per volume:  $p = 0.262$ ; per area:  $p = 0.121$ ) (see Figure 3.7).

The east side of the island is highly industrialized, while the west side is kept largely untouched for tourism. Naha is the capital of the Okinawa Prefecture and the sample location was next to the industrial port and commercial airport. Despite being a heavily commercialized area, Naha has an estimated population of 318,270 inhabitants, representing almost 30% of the total population of Okinawa. The population density of this area is 8,043 people/ $\text{km}^2$ . On the opposite side of the capital of Okinawa sits the big bay of Nakagusku, with the cities of Nanjō (2.98% of Okinawa Population), Urasoe (7.90% of Okinawa Population), Ginowan (6.71% of Okinawa Population) and Okinawa City (9.74% of Okinawa Population). The likely reason for no significant differences in the median differences in the East West splitting is that  $\mu\text{P}$  pollution is caused primarily by human population, not the local industry [241, 242]. Point sources such as sewage outfall and run off after heavy rainfall are the cause of high  $\mu\text{P}$  pollution in the southern coastal waters around Okinawa, while the hydrodynamic processes and tidal forces around the island prevent the transport to northern sampling areas. Optical images of the some  $\mu\text{P}$  particles found are presented in Figures 3.8 and 3.9 (with matching Raman spectra (Figure 3.10) and heavy metal analysis via XRF (see Section 3.3.2). The sub-20  $\mu\text{m}$  and  $\text{nP}$  distribution follows that of the  $\mu\text{P}$  found around Okinawa along the population gradient (see Section 3.3.3).



**Figure 3.7: Map of correlating population density to  $\mu\text{P}$  distribution.** (a)(c) The correlation between the population density and the amount of  $\mu\text{P}$  found is clearly visible in the North-South partitioning, (b)(d) while the partitioning of the sampling stations into East-West-Naha along the industrial gradient does not yield any significance.  $\mu\text{P}$  abundance in particles per station (see Table 3.4). Maps from [239].



**Figure 3.8: Three  $\mu$ P found at station S10 in front of Naha, optical images with corresponding Raman spectrum.** The purple line shows a PP Raman spectrum of a blue color  $\mu$ P with biota attached. The Raman spectrum of PP is clearly observable although the laser beam is positioned between the visible attached cells. The green line shows the Raman spectrum of a PE film, although the film is thin, when focused properly on the surface of the film, a clear spectrum is displayed. The blue line shows the Raman spectrum of a PE fiber.

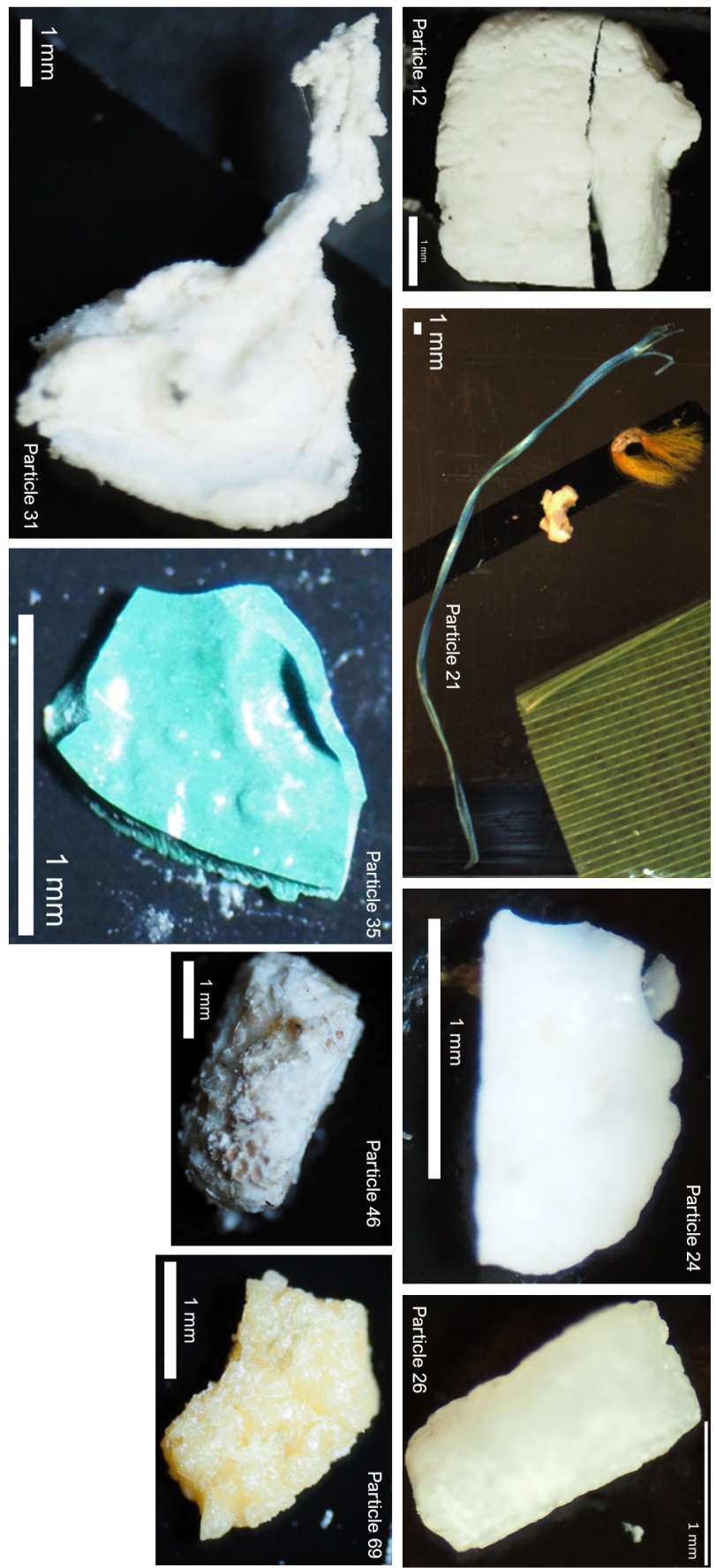
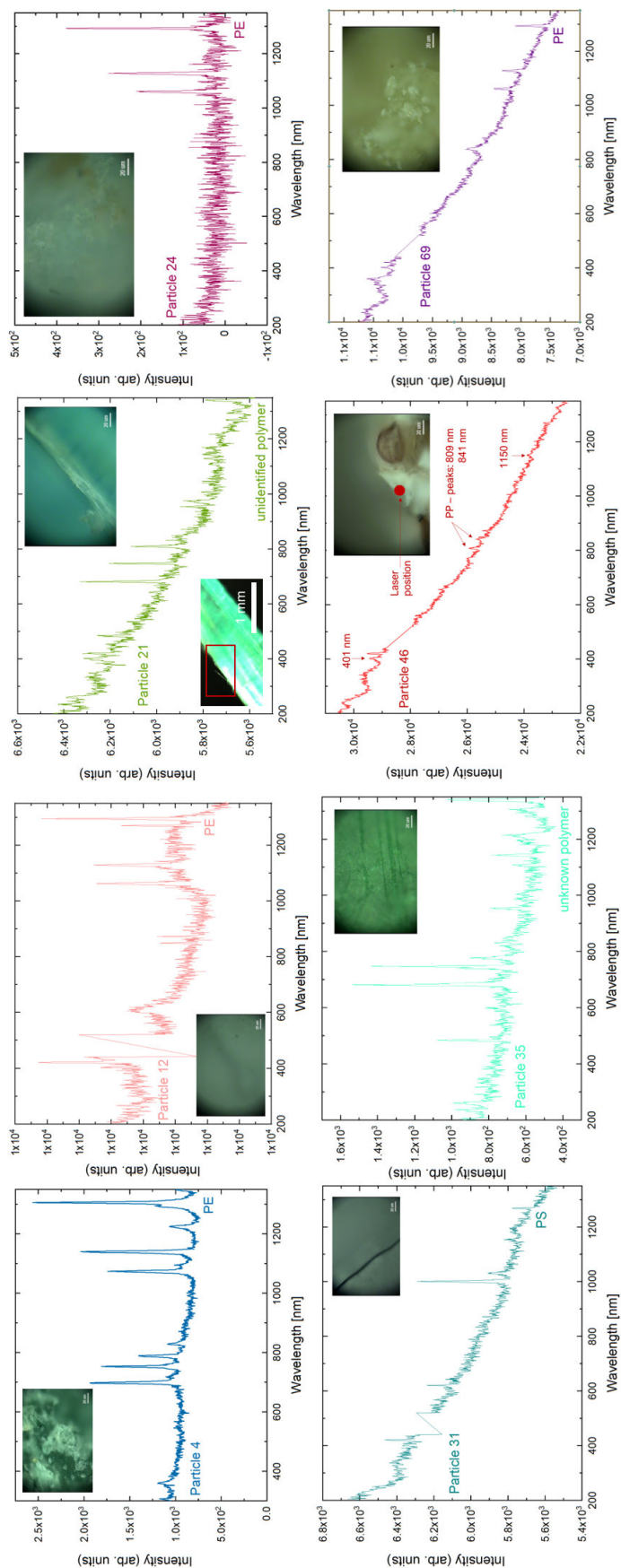


Figure 3.9: Optical images of the  $\mu$ P particles. The Raman spectra and XRF analysis are displayed in Figure 3.10.

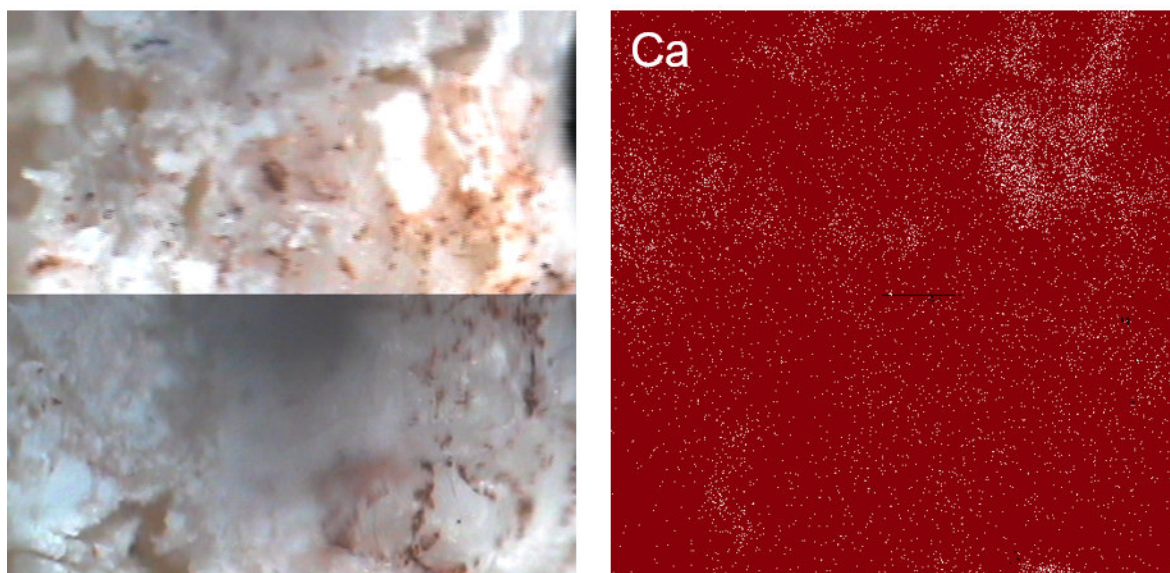


**Figure 3.10: Raman spectra of  $\mu$ Ps found at different locations around Okinawa with respective optical image.** Particle 4 was collected from Nakagusuku (S1). It is blue PE (see Figure 3.14) and has an area of  $20.54 \text{ mm}^2$ . Particle 12 was collected from the second trawling station in Nakagusuku Bay (S2), it is a white PE  $\mu$ P. Particle 21 is from the first trawling station in Kinbu Bay (S3) and a blue fiber. IN the optical image the red box shows the imminent further fragmentation into nanofibers. In the second insert (bottom) it is clearly visible how this micro-fiber is fragmenting to nP (see red box). The slope of the Raman spectrum comes from the back scattering of the material. Particle 24 was collected at the second trawling station in Kinbu Bay (S4) and is a white PS  $\mu$ P with an area of  $0.76 \text{ mm}^2$ . Particle 31 is white PS  $\mu$ P from the eastern Cape Hedo station (S6) and has an area of  $6.71 \text{ mm}^2$ . Due to the back scattering slope only the big PS peaks at  $1001 \text{ nm}$  (aromatic ring breathing mode) and  $1032 \text{ nm}$  (aromatic C-H in plane deformation) are clearly visible, with the peaks at  $622 \text{ nm}$  (aromatic C=C in plane rind deformation) and at  $1152 \text{ nm}$  (aromatic C-H in plane deformation) being less pronounced [24]. Particle 35 is from Nago Bay (S8). This green unidentified polymer is less than  $1 \text{ mm}$  in its longest dimension a small  $\mu$ P (area  $0.85 \text{ mm}^2$ ). Particle 46 is a white PP  $\mu$ P (peaks are marked). Due to the organic growth on the particle (see Figure 3.9), the position of the laser beam for the Raman spectrum measurements was marked in the optical insert image. It was collected from the first trawling station in Naha (S10). Particle 69 is from the second station in Naha (S11), a yellow PE  $\mu$ P (see Figure 3.9) with an area of  $1.39 \text{ mm}^2$ .



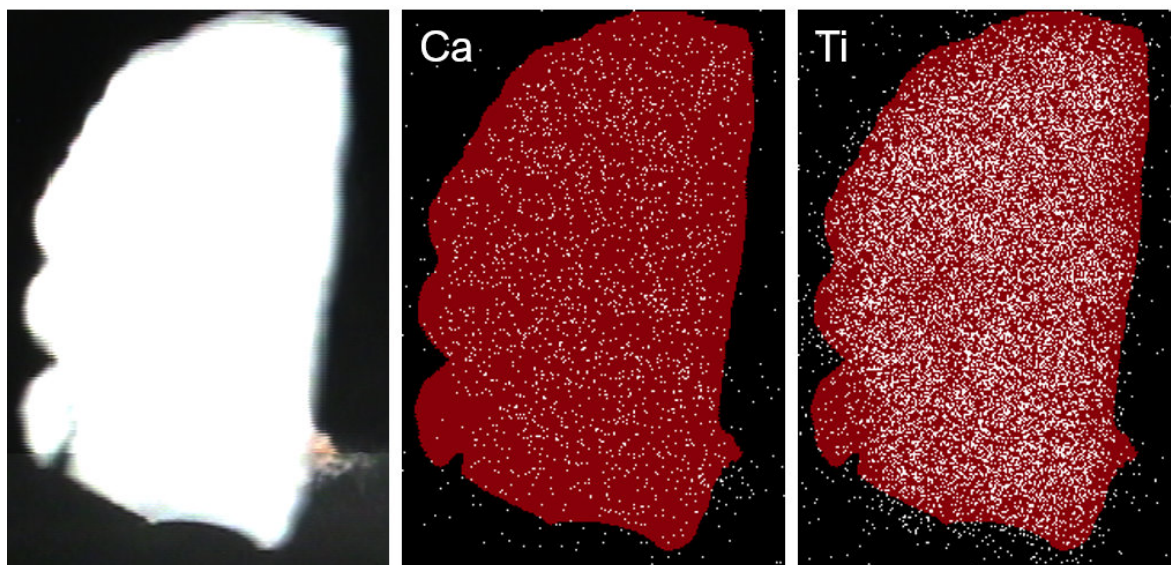
### 3.3.2 Trace Metal Distribution and Abundance on Microplastic

While the original trace metal analysis could not be realized, some particles and the distribution of trace metals on them are given and discussed below.

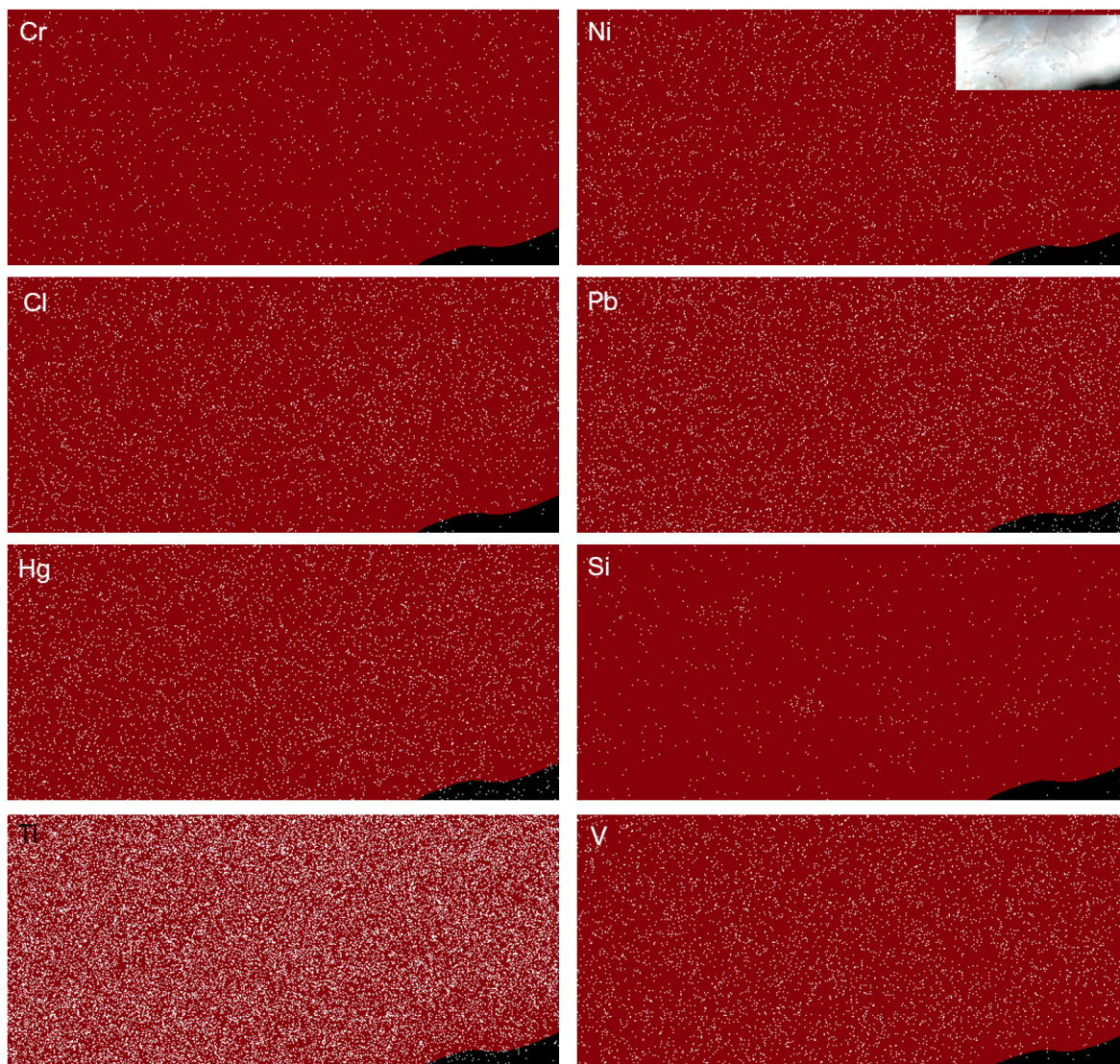


**Figure 3.11: Trace metal distribution on PP  $\mu$ P particle 46.** While this optical image and XRF image does not contain enough vacuum space for the MATLAB code to properly confirm the presence of the Ca, it is interesting to see the distribution pattern of CA on this particle, which do not follow the discoloration of the particle. It is possible that a biofilm with calcifying organisms is present that is does not produce any discoloration. This particle was collected in Naha (S10). All displayed elements were confirmed with MATLAB image analysis.

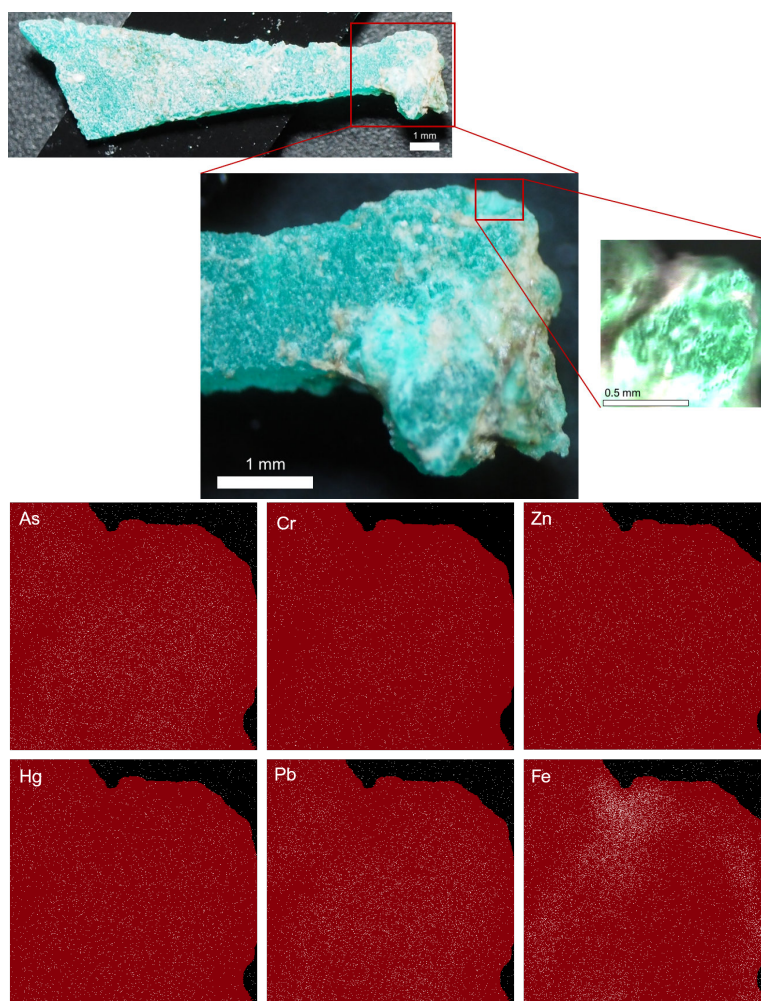




**Figure 3.12: Trace metal distribution on PE  $\mu$ P particle 24.** Calcium (Ca) and Titanium (Ti) were found in the this particle. It is clearly visible that neither element is located in the attached biota on the right side of the particle but distributed over the surface of the polymer. This particle was collected in Kin (S4). All displayed elements were confirmed with MATLAB image analysis.

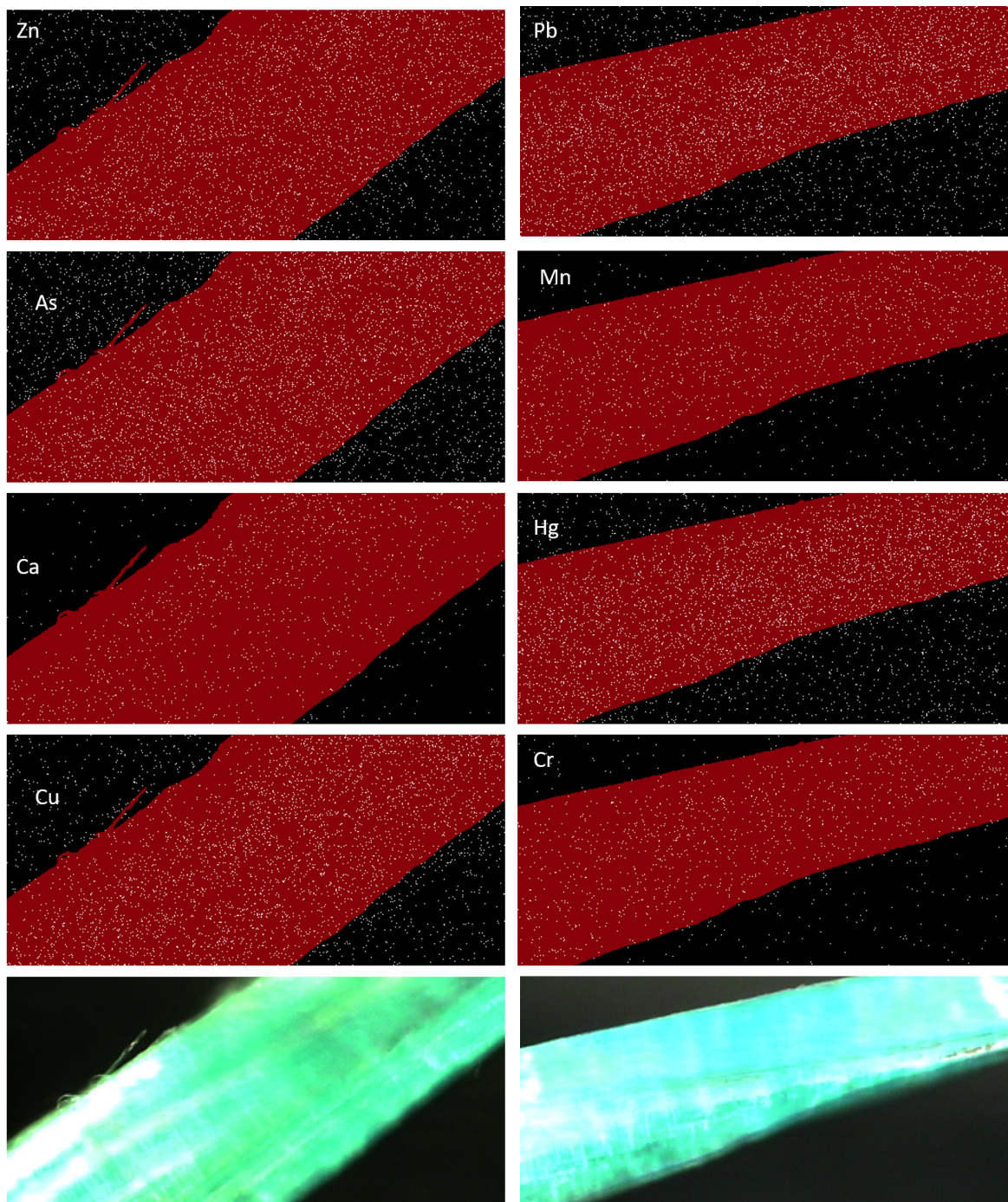


**Figure 3.13: Trace metal distribution on PE  $\mu$ P particle 12.** This white  $\mu$ P only shows a pattern for Silicon (Si) while the other elements are evenly distributed over the surface. The insert shows that the plastic itself is not as weathered as Particle 4. This particle was collected in Nakagusku (S2). All displayed elements were confirmed with MATLAB image analysis.

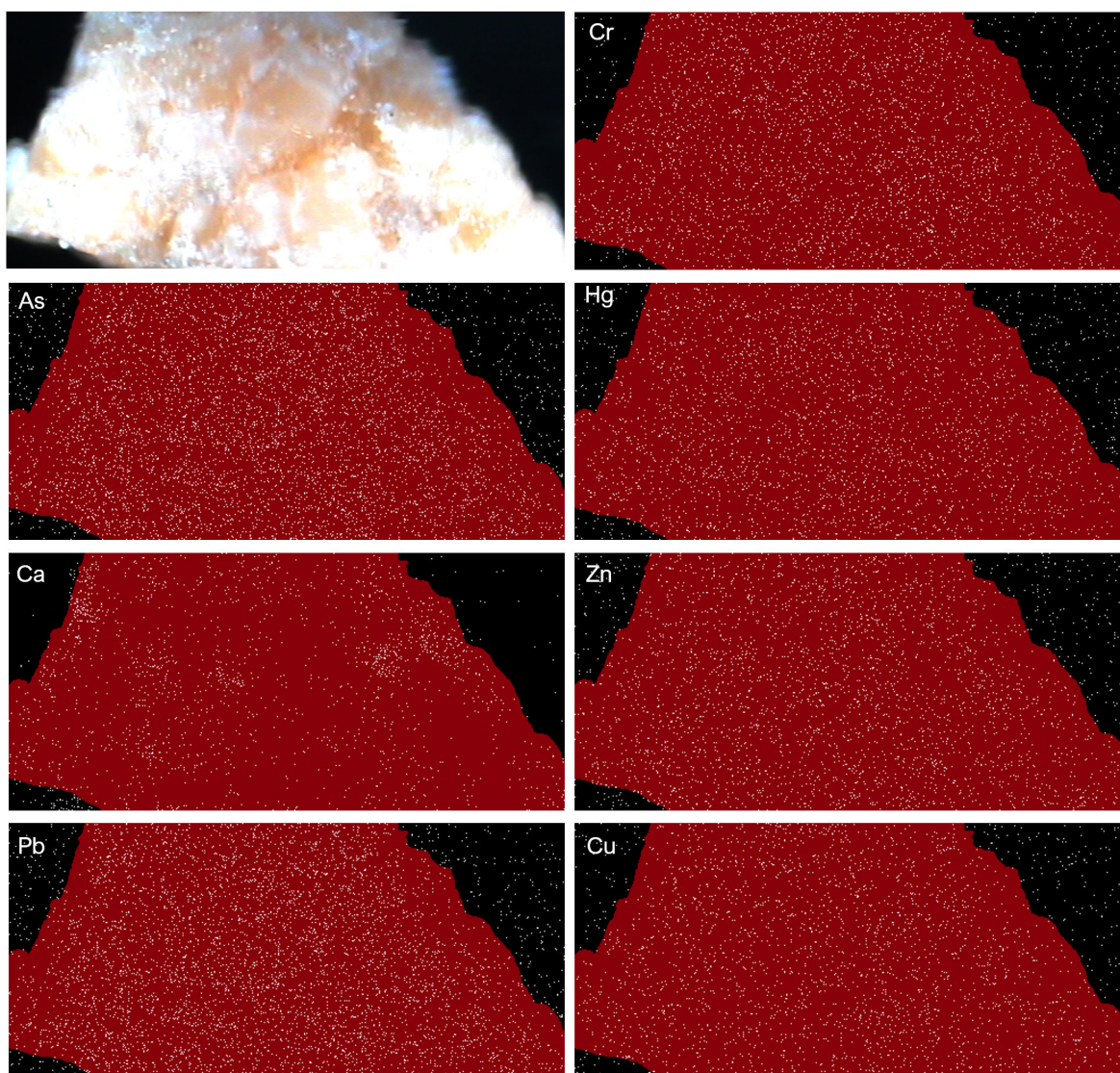


**Figure 3.14: Trace metal distribution on PE  $\mu$ P particle 4.** As can be seen in the optical image, this  $\mu$ P particle is prone to further fragmentation and the trace metal pollution shows different distribution patterns along the fragmentation cracks. While Iron (Fe) is found primarily within the crack, Chromium (Cr), Arsenic (As) and Lead (Pb) are attached to the top surface, not the visible crack. Mercury (Hg) and Zinc (Zn) seem to have no affinity for either the weather crack or the top surface, as they are more evenly distributed on the entire  $\mu$ P. This particle was collected in Nakagusku (S1). All displayed elements were confirmed with MATLAB image analysis.



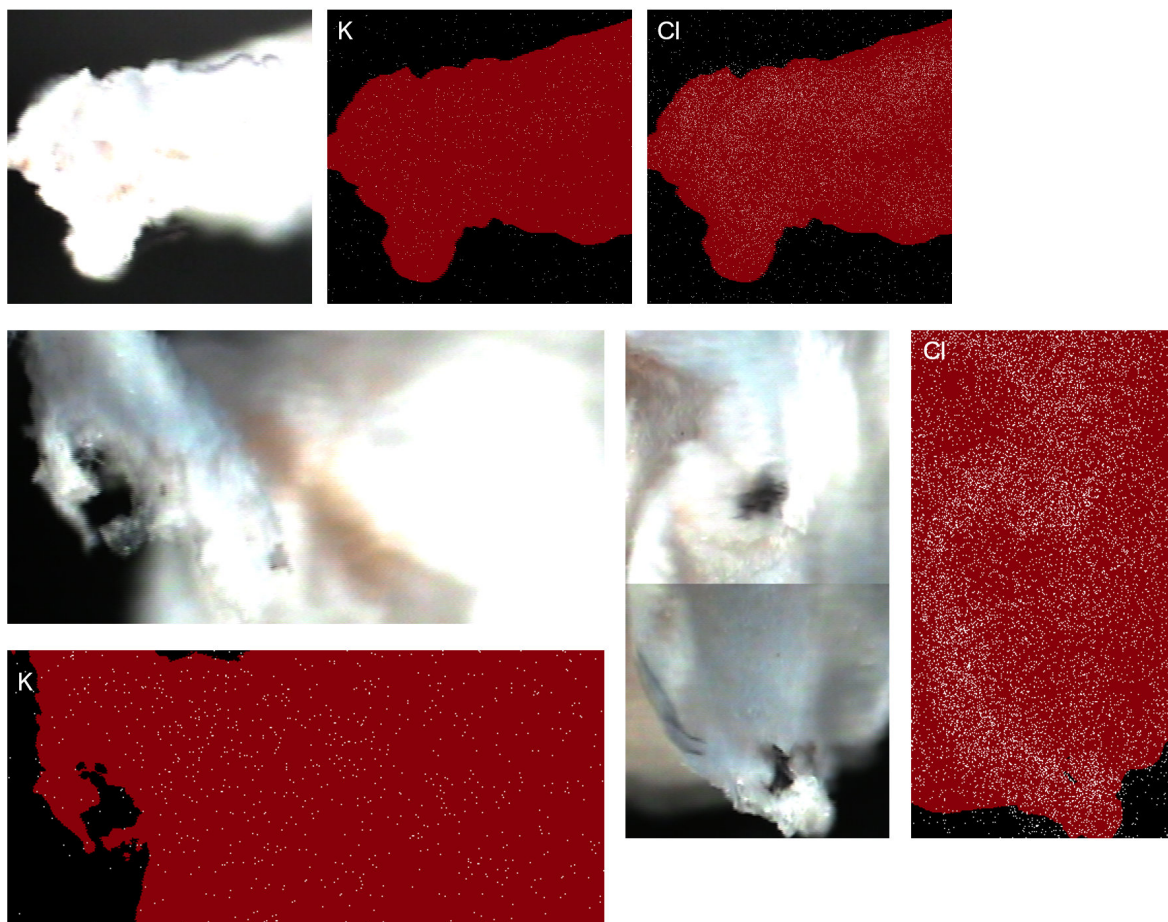


**Figure 3.15: Trace metal distribution on  $\mu\text{P}$  particle 21.** Two optical images are displayed along with the distribution of the elements on them. No pattern can be seen in any of the elements. This particle was collected in Kin (S3). All displayed elements were confirmed with MATLAB image analysis.



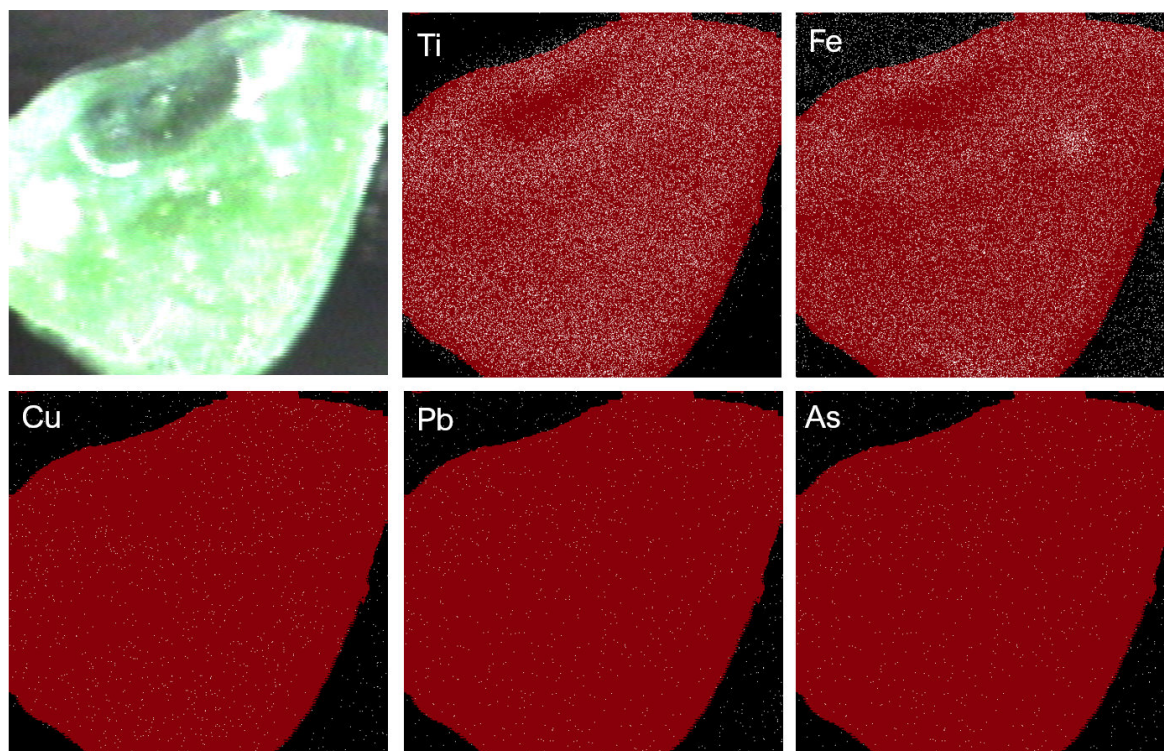
**Figure 3.16: Trace metal distribution on PE  $\mu$ P particle 69.** This yellow  $\mu$ P particle collected in Naha shows a high presence of toxic trace metals, the formerly mentioned As, Pb, Cr, Hg, Cu and Zn. When this figure is compared to the particles collected in Nago (Figure 3.18), it is clearly visible that more of these trace metals are found in this location. This can be due to different polymer affinity to trace metals, but also because the waters around Naha are potentially more contaminated due to high population and industrial presence. This particle was collected in Naha (S11). The image for the distribution of Ca was also included and the pattern aligns with the weathering grooves in the surface, indicating that there may be a bio-film with calcifying organisms. All displayed elements were confirmed with MATLAB image analysis.





**Figure 3.17: Trace metal distribution on PS  $\mu$ P particle 31.** This PS  $\mu$ P shows a distribution pattern for Chloride (Cl). The pattern does not correlate with the discoloration or the cracks seen in the optical images. In addition the distribution of Potassium (K) is displayed, this element was only found on 4 other particles. This particle was collected in Cape Hedo (S6). All displayed elements were confirmed with MATLAB image analysis.





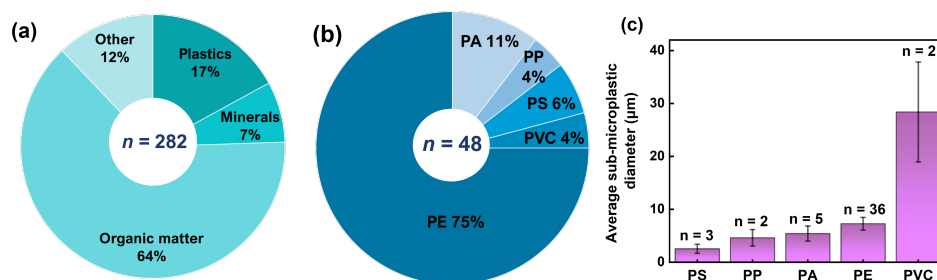
**Figure 3.18: Trace metal distribution on  $\mu$ P particle 35 of unknown polymer type.** This small green  $\mu$ P shows a distribution pattern for Ti and Fe but the trace metals Copper (Cu), Pb and As are distributed evenly across the particle. The distribution pattern follows the weathering of the particle, as the mold in the upper part of the particle does not have any Ti or Fe. This particle was collected in Nago (S8). All displayed elements were confirmed with MATLAB image analysis.

From the limited analysis above, it can be said that different particles have various distribution patterns and quantities of trace metals attached. Besides being located in the biota or bio-film attached to the particle (see Figure 3.11 for possible bio-film location), there are two possible primary sources for the metal found with the analysis. For one, as seen in Figures 3.12 and 3.13 with Ti, the trace metal can be inherently present within the polymer matrix, as modern plastics are increasingly a mix of the actual polymer (residual monomers) and different chemical additives [17], which often contain trace metals [10]. The other possibility is adsorption to the surface from the surrounding seawater [243, 37, 244, 171, 245, 246, 247, 172] (see Figure 3.14; Fe is found primarily within the crack, Cr, As and Pb on the surface). Either way,  $\mu$ P/nP can be considered a source of trace metal contamination into the water column and food web. The trace metals adsorbed onto the surface pose a greater risk to marine organisms, as they potentially detach easier than matrix locked trace metals [37, 248]. The potentially toxic effects of plastic associated trace metals are still poorly understood [15], but adsorption of trace metal ions depends mainly on the physical and chemical properties of the polymers [249]. As explained in Section 2.2.3, the plastic surface potential and with it, the possibility for adsorption of ions, is changed in seawater. Weathering and organic matter ecocorona [17] are responsible for this. Weathered  $\mu$ P adsorb up to one order of magnitude higher trace metal content than virgin  $\mu$ P pellets [250]. Also, increasing pH leads to increased adsorption of divalent cations to the negatively charged polymer surface, such as Cd, Ni, and Pb [250]. Besides direct attachment to the surface, trace metals' trapping into bio-films is also an increasingly confirmed assumption, as the adsorption of trace metals itself is not significantly

linked to polymer type [173, 64, 251]. Overall, complex processes lead to the formation of active binding sites for differently charged trace metal ions [252]. The chief anthropogenic sources of trace metals in the marine environment are ports and marinas (Naha has an industrial port and many local and private marinas are found for fishing and tourism), coatings of ships, agricultural runoff, and waste-water. A more detailed analysis of more particles is needed to see if the trace metal distribution follows the island's population and industrial distribution. The primary qualitative analysis seems to support this, as more trace metals and more toxic trace metals are found on the southern stations, see Figures 3.15 and 3.16, than in the northern stations, see Figures 3.17 and 3.18. Since  $\mu\text{P}$  and trace metals interact and the risk of each is influenced (increased vs. diminished) by the other, any risk assessment needs to address the individual risk as well as the combinatorial risk [30].

### 3.3.3 Distribution and Abundance of sub-20 $\mu\text{m}$ and Nanoplastic

Ocean surface water samples from several bays around Okinawa have been analyzed. For the sub-20  $\mu\text{m}$  and nP analysis only samples from S2, S4, S6, S7, S8 and S10 were analyzed. The chemical identification of optically trapped particles in seawater was demonstrated by employing OTRS after background subtraction. Notably, the majority of the found plastics are quasi-spherical. Analyzed plastic particles ranged from 1.38  $\mu\text{m}$  to 47.83  $\mu\text{m}$  (see Figure 3.19 (c)). As such, none can be defined as nP, only  $\mu\text{P}$  and sub-20  $\mu\text{m}$  plastic particles. In total, 329 particles were imaged, but the analysis could only be run on 282 of them, as the other data was corrupted during the saving process on the Raman system computer. Data from two stations were lost (see empty columns "Particles Plastic (%)" and "Particles Organic (%)" in Table 3.20). The composition of the 282 remaining particles is given in Figure 3.19 (a) and the partitioning of the plastics in Figure 3.19 (b).



**Figure 3.19: Plastic particle composition.** (a) Percentage composition of all particles. (b) Polymer types of sub-20  $\mu\text{m}$  plastics collected in seawater around the main Okinawa island. (c) Average diameter of sub-20  $\mu\text{m}$  plastics where  $n$  indicates the number of microplastic polymers.

Although the OTRS provides the ability to identify nP, we did not find any nP in our seawater samples. From here on out, particles will be referenced as sub-20  $\mu\text{m}$ , even though three particles were above 20  $\mu\text{m}$  and one had an unknown size due to the corruption of the optical image file.

Our analysis confirmed that 17% of particles were identified as plastic around Okinawa Island, in which PE, PP, PVC, PA and PS are among the most abundant polymer types in aquatic environments (Figure 3.19 (a) and (b)). Polyethylene (PE) was the most common plastic type, comprising 75% of all the sub-20  $\mu\text{m}$  plastics polymers analyzed (Figure 3.19 (b)). The order of numerical dominance of sub-20  $\mu\text{m}$  plastic polymers was PE > PA > PS > PP = PVC. Generally, these polymers accounted for 74% of global plastic production and are commonly used in short life-cycle

products [28]. Moreover, factors such as hydraulic conditions, salinity, temperature, wind, bio-fouling, as well as changes in surface to volume ratio may affect the distribution of sub-20  $\mu\text{m}$  plastics around Okinawa.

The source of sub-20  $\mu\text{m}$  plastics is related to anthropogenic activities on the seawater, beaches, and in the trading centers in the area around Okinawa. In the fishing communities at the fish landing beaches, woven polymer sacks are used for storage and transport of a variety of products including fishes. Over 75% of the sub-20  $\mu\text{m}$  plastics are made of polyethylene and these may originate from broken fishing nets, lines or ropes, water bottle caps, household utensils, consumer carry bags, containers/packaging, etc. Recently, a study of the abundance of microplastics in road dust samples collected from several areas in Okinawa shows a high concentration of them in urban areas in which daily vehicle traffic, industrial activity, and high population density are dominant [253]. In the road dust of Okinawa, PE was 29% of the total microplastics [253], while in seawater it is 75% of the total sub-20  $\mu\text{m}$  plastics. At the end, some of the road dust may be found in the oceans surrounding Okinawa, correlating the two findings via common high concentration areas.

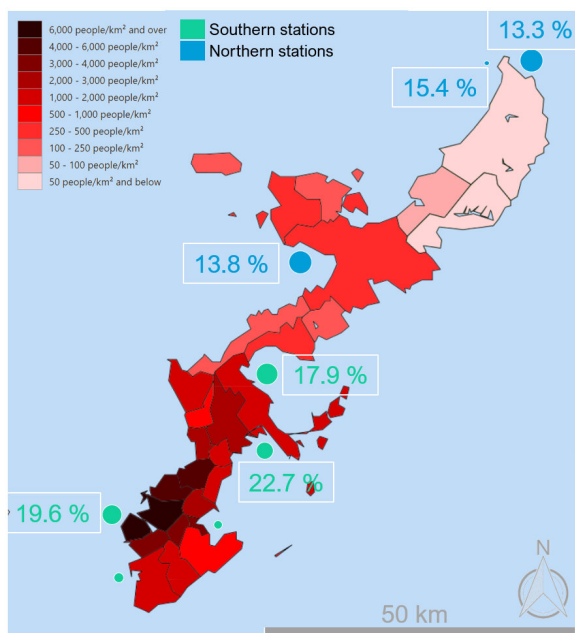
Sub-20  $\mu\text{m}$  plastics were also classified based on their size as products of degradation of large plastic materials (see optical images in Figures 3.21, 3.23 and 3.24). The average size of all collected sub-20  $\mu\text{m}$  plastics is shown in Figure 3.19 (c). The majority of sub-20  $\mu\text{m}$  plastics range from 1.4  $\mu\text{m}$  to 18.7  $\mu\text{m}$ , although we identified three microplastics with sizes of 27.2, 30.5, and 47.8  $\mu\text{m}$ . The smallest average size of  $2.53 \pm 0.85$   $\mu\text{m}$  is identified for PS polymers while the largest average size of  $28.4 \pm 9.4$   $\mu\text{m}$  is identified for PVC polymers. Likewise, the sampled sub-20  $\mu\text{m}$  plastics showed a wide range of sizes in various areas of Okinawa with the highest around Naha (S10). A shift of the Raman peaks or alteration of the bands can be expected due to their crystalline structure and level of degradation. Table 3.5 list the polymer types and abundances of sub-20  $\mu\text{m}$  plastics found and identified in seawater around Okinawa.

**Table 3.5: Nanoparticle distribution around Okinawa.** Split for population and industry around Okinawa following the respective gradients. (For more Geo-information and  $\mu\text{P}$  data, see Table 3.4)

Area Name	Station Names	Population distribution	Industry distribution	volume checked [ $\mu\text{L}$ ]	Particles	Particles plastic (%)	Particles Organic (%)
Nakagusku 1	S1	Sth1	E1	40	44	25.0	56.8
Nakagusku 2	S2	Sth2	E2	40	22		
Kin 2	S4	Sth4	E4	60	56	17.9	66.1
Cape Hedo 1	S6	N2	E6	60	60	13.3	66.7
Cape Hedo 2	S7	N3	W1	60	13	15.4	61.5
Nago 1	S8	N4	W2	60	58	13.8	65.5
Naha 1	S10	Sth5	Naha1	40	51	19.6	58.8
Naha 2	S11	Sth6	Naha2	40	25		

The plastic pollution observed for sub-20  $\mu\text{m}$  plastics follows the population gradient of the island. There is a clear distinction between the northern, less populated part of Okinawa, and the southern part with high population density. With draining rivers and waste water treatment plants into the big bays, there is a significantly higher sub-20  $\mu\text{m}$  particle % found in the southern half of the island (two tailed t-test,  $P = 0.0147$ ) (for station partitioning see Table 3.5, and 3.20).

This mirrors results from Kataoka et al. [240], who found sub-20  $\mu\text{m}$  and nP concentrations are significantly correlated with population density (and urbanization). In contrast, the partitioning of the stations in to east and west, according to industrial density, does not yield a significant difference ( $P = 0.7$ ).

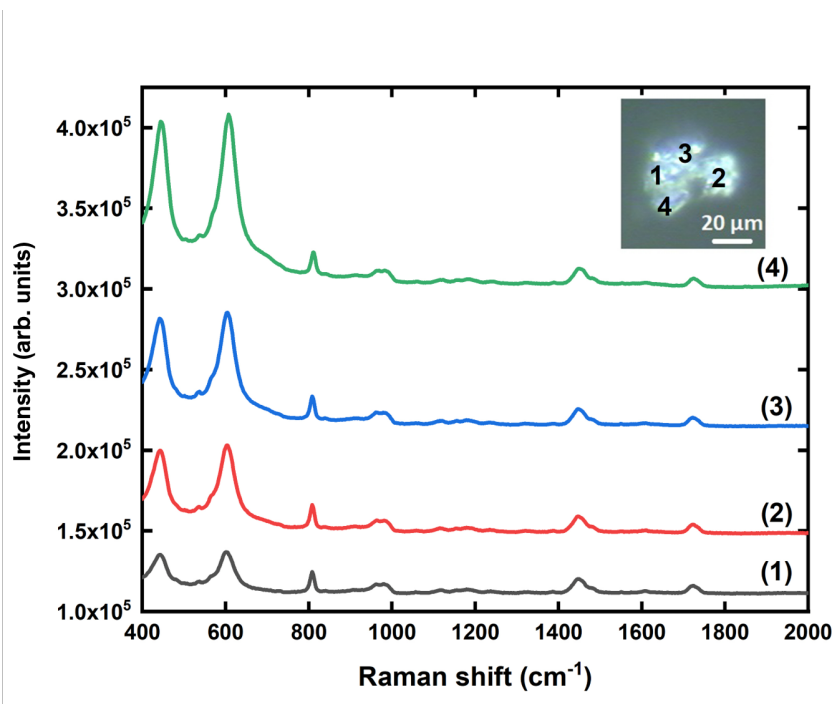


**Figure 3.20: Map correlating population density to sub-20  $\mu\text{m}$  plastics distribution.** While total number of sub-20  $\mu\text{m}$  plastics found is evenly distributed, the numbers displayed next to the stations show the percentage of plastic in these particles. These follow the indicated partitioning into North-South along the population gradient, as seen with the  $\mu\text{P}$  (see Table 3.4). Map from [239].

The abundance of sub-20  $\mu\text{m}$  plastics in each station displayed a difference between the number of plastics collected in urban and less populated areas. The heterogeneity of the plastics at the sampling stations may be caused by several factors, predominately the closeness of point sources such as sewage outfalls, river outlets and run-off after heavy rain fall. Atmospheric input of  $\mu\text{P}$ /sub-20  $\mu\text{m}$  plastic from domestic activities such as traffic should also be taken into consideration.

In Figure 3.21, we have identified the characteristic Raman peaks of polyvinyl chloride (PVC) (Table 3.6). Additionally, we investigated the Raman signal of the optically trapped microplastic for various positions on its surface. We note that the intensity of the Raman signal changes. This could be due to the difference in weathering of the material at various places. In total, 51 particles were analyzed from station S10. Out of these particles, 11 were plastic which amounts to 19.6% of the particles found. The plastics belong to two different polymer types: polyethylene, PE, ( $n=9$ ) and polyvinyl chloride, PVC, ( $n=2$ ). This is the second-highest percentage of plastics that we have found in seawater around Okinawa. This result correlates well with a recent study by Kitahara et al. [253], finding small plastics in road dust on Okinawa. Although the population density is highest in Naha and most land use is urban [254, 255], plastic particles in the road dust were lower in front of our station S10 [253]. Another reason for finding the second-highest plastic pollution at this station is the location outside of a bay. Although many rivers discharge on this side of Naha city [256], the pollution will not be trapped on this side of the island.





**Figure 3.21: Raman spectrum of a polyvinyl chloride (PVC) quasi-spherical microplastic of 47.8  $\mu\text{m}$  diameter found at station S10, near Naha.** Each spectrum relates to a different region on the trapped particle. Inset: microscope image of the plastic in which different spectral regions are labeled. The intensity of the Raman signal may indicate the difference in weathering.

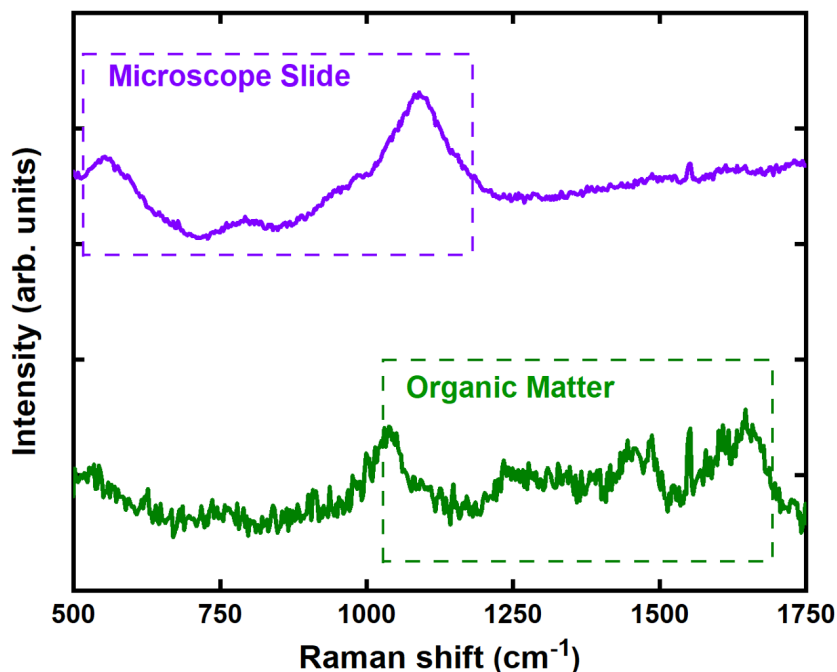
**Table 3.6: Raman modes of polyvinyl chloride (PVC).** PCV has a hazard score of 10, 551 [71], making it one of the most toxic plastics based on hazard classification of monomers. PVC is mostly used for cables, pipes & fittings, window frames, and flexible films for water proofing.

$\nu$ ( $\text{cm}^{-1}$ )	Vibration
1,724	Ester CO stretching
14,345	$\text{CH}_2$ symmetric deformation
1,325	$\text{CH}_2$ twisting
610	Crystalline C-Cl stretching

Plasticizers, dyes, and weathering can change the Raman spectrum, adding additional peaks to the spectrum of the different polymers as well as changing relative intensities and accuracy. These additives are often harmful and can leach from the polymer matrix [257]. In addition, the particles are often embedded in organic material, which can also add peaks to the actual polymer spectrum. In Figure 3.22, we show the Raman spectrum of the microscope slide that we used in our experimental process and the organic matter found in the plastics. Based on these reference spectrum we can distinguish the plastics from organic matter and identify their Raman peaks. Generally, we observed that most sub-20  $\mu\text{m}$  plastics are embedded into organic matter (68.75%) while only 31.25% are free-floating. No data is published on this ratio, as the methods for polymer identification used most often add a step of digesting the organic material in the sample first, to get a better Raman signal. This ratio is important to investigate further, as it can shed some light on the fate



of the  $\mu\text{P}$ / sub-20  $\mu\text{m}$  plastic within the water column.



**Figure 3.22: Additional Raman spectrum peaks that typically appear in the signals from the trapped particles in our samples.** Purple (upper) curve: spectrum from the microscope slide. It displays the glass solid-state structure with long-range translational symmetry – the peaks are very broad with widths up to several hundred wave numbers. Green (lower) curve: spectrum from organic matter found in the samples with CCO stretching (around  $1000\text{ cm}^{-1}$ ) and  $\text{CH}_3$  and  $\text{CH}_2$  deformations ( $1250\text{ cm}^{-1}$  to  $1750\text{ cm}^{-1}$ ) in the Raman spectrum. The individual peaks vary depending on the organic matter of the trapped particles.

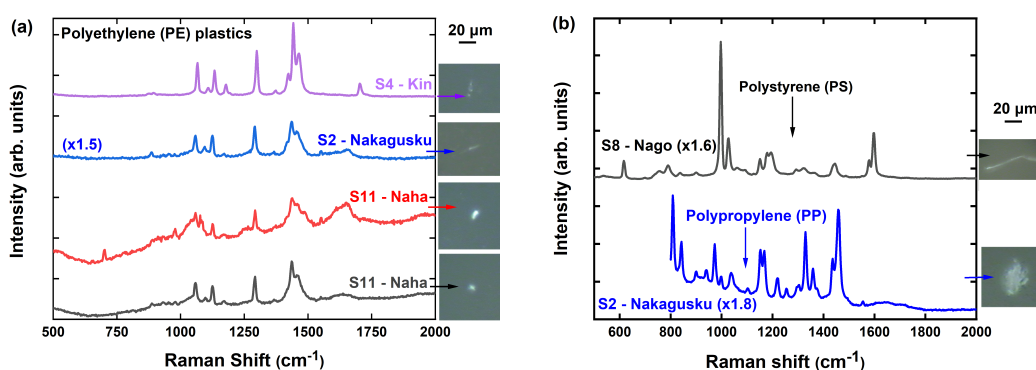
Figure 3.23(a) shows the Raman peaks of PE sub-20  $\mu\text{m}$  plastics which were found in several areas around Okinawa. In Table 3.7 we present the modes attributed to PE, all the particles have the characteristic PE peaks spanning from  $1000\text{ cm}^{-1}$  to  $1500\text{ cm}^{-1}$  [24]. Figure 3.23(b) shows the Raman spectrum for polystyrene (PS) and polypropylene (PP) particles which are not embedded in organic matter.

The most common plastic that was found in the seawater of Okinawa is PE with a percentage of 10.94% of the total particles analyzed (see Table 3.3). The reason for the high percentage of PE could be its structural characteristics and lower density compared with the other polymer types found (see Table 3.3). It has more porous structures than other plastics and, as such, it may be more easily broken down into microscopic debris by sunlight, wind, and current erosion [258]. We notice surrounding organic matter overlays the PE Raman spectrum in a microparticle of 5  $\mu\text{m}$  in diameter (red line in Figure 3.23(a)), which was collected from the Naha (S10) area. Additionally, an overlay of dyes or additives is observed in the Raman spectrum of a sub-20  $\mu\text{m}$  plastic with 5  $\mu\text{m}$  diameter (purple line in Figure 3.23(a)) which was collected from the Kin (S4) area. The characteristic peaks of polystyrene (PS) (black line in Figure 3.23(b)) and polypropylene (PP) (blue line in Figure 3.23(b)) were identified at Nago (S8) and Nakagusku (S2) areas, respectively. PS is

**Table 3.7: Raman peaks of polyethylene (PE).** the most common plastic used today. Primarily used for packaging, resulting in air trapping items such as bottles and plastic bags. Combined with its low density this leads to a majority of the PE floating at the oceans surface [23].

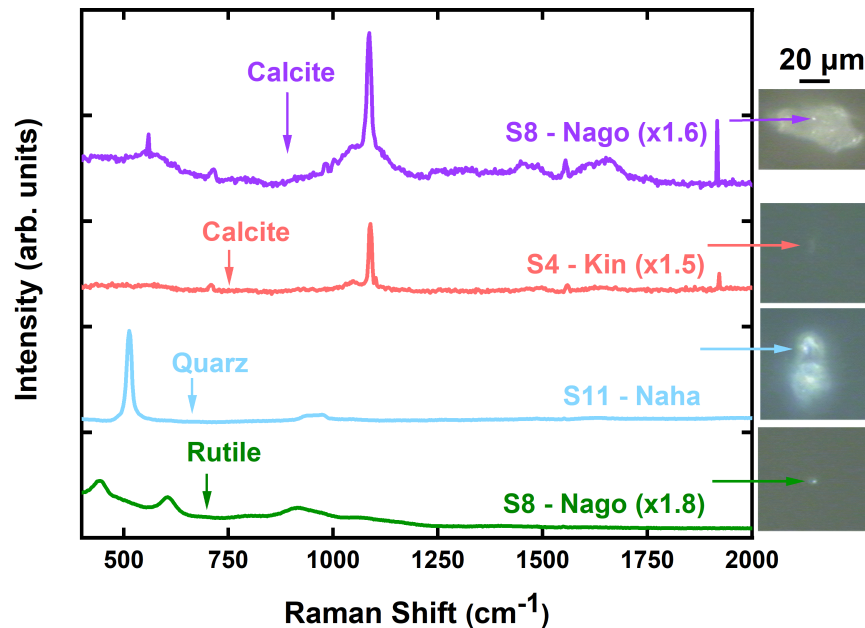
$\nu$ (cm <sup>-1</sup> )	Vibration
1058	CC symmetric stretching
11,235	CH <sub>2</sub> CC anti-sym stretching
1286	CH <sub>2</sub> twisting vibration
1408	CH <sub>2</sub> bending
1429	CH <sub>2</sub> symmetric deformation
1450	CH <sub>2</sub> scissor vibration

frequently found in the environment as a material from diverse uses such as packaging foams and disposable cups. Since it is mainly used for manufacturing single-use products, a large portion of post-consumer production ends up in oceans [259], and remains there for several hundred years due to their resistance to degradation (Table 3.3). PP is used in the manufacturing of, for example, flip-top bottles, piping systems, and food containers, amongst others.



**Figure 3.23: Raman spectra of optically trapped  $\mu$ P/nPs dispersed in seawater with their optical images.** (a) Polyethylene (PE) spectra from different particles found in different locations. The red line has an organic matter overlay, while the purple and blue lines have additional peaks most likely from dies or additives to the PE. (b) The black line indicates a Raman spectrum of Polystyrene (PS) and the blue line of Polypropylene (PP) found at Nago (S8) and Nakagusku (S2) areas, respectively.

Together with the plastics, trapped sediment micrometric and nanometric particles can also be detected (see Figure 3.24). Specifically, we note that some particles have peaks at 512 cm<sup>-1</sup> and 472 cm<sup>-1</sup> [260], indicating trapped quartz particles (blue curve-S10 in Figure 3.24). Particles of polymorphous CaCO<sub>3</sub> with one peak at 706 cm<sup>-1</sup> followed by a larger peak at 1088 cm<sup>-1</sup> indicate that they are most likely calcite and not aragonite or vaterite [261]. The origin of these particles is probably related to trace calcite-based contaminants. Finally, we find particles that display the spectral fingerprint of rutile (green curve-S8 in Figure 3.24) with microscope slide signal overlay [262]. Rutile is a mineral composed primarily of titanium dioxide (TiO<sub>2</sub>) and is the most common natural form of TiO<sub>2</sub>. These sediment-derived particles are likely found because of high river input [256].



**Figure 3.24: Raman spectra of trapped sediment particles suspended in seawater with their optical images.** In the purple line the calcite peaks are overlaid with organic matter, as observed on the optical image. The green line shows a rutile particle. The Raman spectrum is overlaid by the characteristic microscope slide Raman peaks. The integration time is 20 sec (4 acquisitions).

The plastic pollution observed for sub-20  $\mu\text{m}$  plastics follows the population gradient of the island [255, 254]. There is a clear distinction between the northern (Figure 3.3), less populated part of Okinawa, and the southern part with high population density. While the south west side with the capital Naha has the highest population density, there is no bay on that side of the island. The south east side of Okinawa, as mentioned before, is home to the big bay of Nakagusku (S2-Figure 3.3), with many population dense cities surrounding it. While only a handful of rivers drain into this bay, these rivers have been found to have the highest levels of inorganic nutrients [256] on Okinawa. We analyzed 44 particles from that bay and we calculated that 25% are plastics (8 of PE, 1 of PP, 1 of PS and 1 of PVC). We conclude that this is the area with the highest percentage of plastics due to the high population density (2,838 people/ $\text{km}^2$ ). The southern part of the island has a high proportion of urban land use [255], which, in combination with high traffic density [253], leads to high anthropogenic pressure on the coastal ecosystem [263]. This results in a significant increase of sub-20  $\mu\text{m}$  plastic percentage in the southern half of the island (t-test, two tailed  $p = 0.0147$ ). This is in reasonable agreement with studies showing microplastic abundance in areas with an increase of intensive anthropogenic activities such as: urban areas with high population density [240], tourist beaches with high density of tourists [264], areas of intensive agriculture [265], as well as fishing and shipping activities [266].

In the central part of the island, the land use shifts from urban areas to more forest cover [255, 254]. Traffic density goes down by between one third to about one half that found in the southern part of the island [253]. On the east side, we have a station at Kin (S4), while Nago (S8) is located on the west side. Kin has a surrounding population of up to 1,386 people/ $\text{km}^2$  while at Nago the population density is lower at 296 people/ $\text{km}^2$ . The anthropogenic pressure on the Kin station is predicted to be high [263]. This difference in the population density is reflected in the plastic

distribution, 17.9% (S4) and 13.8% (S8), respectively, while the percentage of organic particles is reasonably stable (66.1% (S4) and 65.5% (S8)). At Nago, we analyzed 58 particles. PE was the only plastic type found there. In Kin (S4) we characterised a similar number of particles ( $n = 56$ ) but found a wider variety of plastic polymer types (8 PE, one PS, and one PP sub-20  $\mu\text{m}$  plastics). The particles in Nago Bay ranged in size from 1.4  $\mu\text{m}$  to 27.2  $\mu\text{m}$ . According to industrial density, which is higher on the east side of the island, the partitioning of the stations into east (S2, S4, S6) and west (S10, S8, S7)) does not yield a significant difference (t-test,  $p = 0.7$ ) in sub-20  $\mu\text{m}$  plastic distribution, as most plastic is correlated with domestic activity, not industrial, on Okinawa.

Finally, in the north of Okinawa, we have Cape Hedo (Figure 3.3) with a low anthropogenic pressure prediction [263]. We collected particles from two stations (S6 and S7) located on both sides of the cape. In total, 60 particles were identified at station S6, of which 8 are plastics (3 PE, 4 polyamide (PA) and 1 PS) while at station S7 we identified 13 particles with two of them being plastics (1 PE and 1 PA). S6 is located on the east side of the cape, which has rivers draining into the ocean. Because of that, particulate organic matter content is comparable to the station located further south [267]. Polyamide is a family of polymers named Nylon. It is a ductile and strong polymer, permitting the fabrication of textile fibers and cordage. Based on Figure 3.19(b), PA is the second most common plastic identified in the sea waters of Okinawa with 1.52% of all particles analyzed.

### 3.3.4 Risk Analysis

By themselves these numbers do not say much about the  $\mu\text{P}/\text{nP}$  problem in Okinawa. The distinct pattern that can be observed shows the influence of population density on the  $\mu\text{P}/\text{nP}$  population and the implication for the marine ecosystem, but a more detailed risk evaluation is needed based on more data with seasonality to show the true impact of the problem.

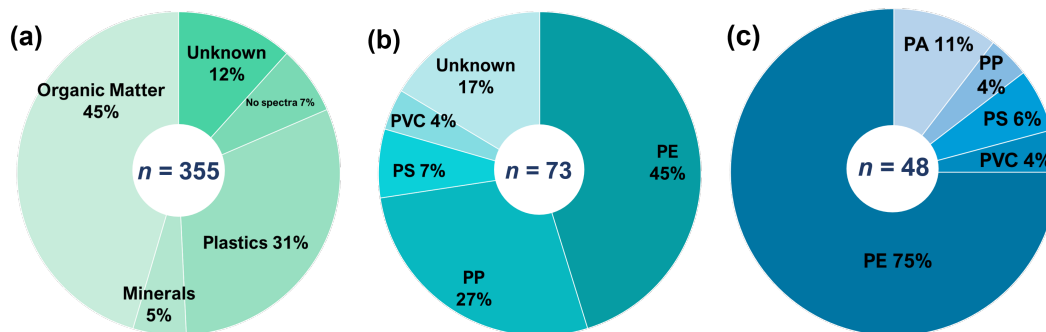
$$PLI = \sqrt{C_i/C_{0i}} \quad (3.8)$$

Using the *PLI* to smooth out any irregularities in the small data set, the  $C_{0i}$  around Okinawa itself is assumed to be  $10^{-6}$  n/100 L as S7 did not present any  $\mu\text{P}$ . Once Okinawa was compared to the greater region the  $C_{0i}$  was set to 0.05 n/100L, reflecting the  $\mu\text{P}$  concentration in the Japan Sea [268]. While using this index, the southern stations all score high (between 800 – 1500), the northern most station S6 on the east side of Cape Hedo scores almost as high with 700, while the other northern station score much lower at 400 – 500. This is due to the small data set. It can be seen that when the *PLI* of Okinawa is compared with the Japan Sea, Okinawa scores in their lowest risk category with a *PLI* of below 10 for all stations [116] see Table 3.8.

Only 73  $\mu\text{P}$  particles were found in the stations around Okinawa. This can be compared with the smaller sub-20  $\mu\text{m}$  fraction for which 48 particles were found. While not being more abundant, these were also found to be more ubiquitous, as the  $\mu\text{P}$  were not present at every station. The smaller plastics were, in addition, embedded in organic matter to a higher percentage (68.75% vs. 31.25% free-floating), making them easy to be ingested accidentally. PE is the most abundant polymer found, both in  $\mu\text{P}$  (45%) as well as in sub-20  $\mu\text{m}$  fraction (75%) (see Figure 3.25).

**Table 3.8: Pollution load index for the stations around Okinawa for  $\mu\text{P}$  in comparison to Okinawa, displaying the most polluted zones to be in the south. The PLI compared to Japan Sea shows that the overall pollution levels around Okinawa are low. PLI is based on volumes, hence this analysis could not be done for the sub-20  $\mu\text{m}$  particles.**

Town Name	Station Names	PLI Okinawa	PLI Japan Sea
Nakagusku 1	S1	980.02	4.38
Nakagusku 2	S2	1025.98	4.59
Kin 1	S3	869.77	3.89
Kin 2	S4	800.95	3.58
Oura	S5	487.58	2.18
Cape Hedo 1	S6	731.54	3.27
Cape Hedo 2	S7	0.00	0.00
Nago 1	S8	457.71	2.05
Nago 2	S9	900.02	4.03
Naha 1	S10	1577.75	7.06
Naha 2	S11	814.29	3.64



**Figure 3.25: Comparison of particles analysed.** (a) In total 355 particles were analysed from all stations around Okinawa. 121 of those were plastics, all smaller than 5 mm. Most (179) were organic matter particles smaller than 500  $\mu\text{m}$  and 27 did not yield a spectra. 46 spectra could not be identified and are listed under ‘unknown’. (b) 73  $\mu\text{P}$  were found, in 10 of the 11 stations. (c) 48 plastic particles were sub-20  $\mu\text{m}$  and were identified by the Optical tweezers micro-Raman spectroscopy.

### 3.4 Conclusion

In recent years, much progress has been made in understanding the sources, transport, fate, and biological implications of the smallest plastic pollution particles. The public interest in plastic marine pollution and its ecological impact have increased during the same time. Our results contribute to the knowledge about *in – situ* analysis and identification of microplastics and demonstrate that the seawater around Okinawa is polluted with micro and sub-20  $\mu\text{m}$  plastics. They were ubiquitously detected at all sites we tested, with the higher concentration in areas of the island characterized by human activities. All the sub-20  $\mu\text{m}$  plastics were fragments of plastic materials used by the community, with the major polymers being polyethylene and polyamide materials. Being



predominately found embedded into organic matter, the resulting interactions between marine planktonic organisms and the plastic particles are inevitable. One potential fate could be the eventual sedimentation with the rest of the organic matter particle.

As shown in previous studies of other locations across the planet [269, 270, 240], the  $\mu\text{P}$  pollution around Okinawa follows the population distribution. A total of 73  $\mu\text{P}$  particles from 11 stations were collected with one station having 0  $\mu\text{P}$  (see Figure 3.4). The abundance of sub-20  $\mu\text{m}$  (detected particles down to 1.38  $\mu\text{m}$ ) also showed the evident difference between the number of plastics found in the samples collected in the urban area and those from less populated areas. The heterogeneity of the plastics at the sampling stations may be caused by several factors, such as proximity to the wastewater treatment plant, ship traffic for tourism and fishing, research activities in the coastal area, transportation by means of ocean currents, and other human activities. While some particles might have originated and been transported over large distances, the correlation with the population densities points to land-based sources of the plastic particles found, indicating that a better treatment of wastewater and bigger penalties for littering could remove much of the plastic pollution found around the island.

The incorporation of these smaller plastics within marine aggregates also contributes to the inclusion into the food web, as well as making it likely that these particles will be deposited to the seafloor if not ingested as marine snow.

Polyolefins (i.e. polyethylene, polypropylene) are the most abundantly produced plastics [271], and along with PA, used commonly in fishing gear [272], also make up the biggest share of our plastic particles. We assume that these materials may be more prevalent in this particular coastal environment due to fishing and seaweed farming being a major source of income on the Okinawa main island as well as the surrounding islands belonging to the Okinawa Archipelago. Wave action and photo-chemical degradation as well as bio-fouling will lead to the fragment sizes we found, often integrated in organic matter particles.

Overall a relatively low pollution of  $\mu\text{P}/\text{nP}$  was found compared to other regions. This can be used as the first recorded snap shot of  $\mu\text{P}/\text{nP}$  around the island. The method used for detecting sub-20  $\mu\text{m}$  plastics in the environmental liquid samples worked, but cannot be used to calculate particles per L yet. A higher percentage of the total sample volume needs to be checked for this, preferably in ways of a through-put system. Also, if coupled with a higher magnification, nP would be easier to find within the marine snow aggregates observed. As the majority of plastic particles observed were found within marine snow aggregates, it is likely that much of the  $\mu\text{P}/\text{nP}$  are found within the water column [94].



## Chapter 4

# Nanoplastic Toxicity in Endosymbiotic Dinoflagellates<sup>1</sup>

### 4.1 Nanoplastic Pollution in Coral Reef Environments

Since the start of plastic mass production in the middle of the last century, marine plastic pollution has been steadily increasing. Due to hydrological processes and ocean currents acting as a major force for transport, plastic gets transported across ecological boundaries and entire oceans, often ending up in the coral reef environment. Coral reefs provide habitat for marine invertebrate and vertebrate species alike, sustaining the highest biodiversity among marine ecosystems [273]. Formed primarily by coralline algae and scleractinian corals, coral reefs are complex and vulnerable ecosystems. This biogenic structure can form an atoll, barrier, bank, or fringing reef (as in the case of Okinawa). Moreover, this ecosystem provides services to millions of people [274]: food provisioning (e.g., fishing), regulation (e.g., coastline protection), cultural and supporting functions [275]. Stressors, such as physical damage from human activities, weather events, ocean acidification, over-fishing, marine heatwaves, and marine pollution, interact and select for different responses within the reef-building community [274, 276]. As a result, structural complexity, and by extension, the ecosystem's capability to sustain biodiversity often declines.

Nanoplastic particles (nP) are a part of marine plastic pollution, and have been reported in ocean surface water samples [60], but have not received much attention until recently. Initially only found as secondary particles, broken down *in situ* from larger plastic objects through photochemical and mechanical degradation leading to fragmentation, there are now primary sources of plastic nanoparticles (medical and cosmetic applications, nanofibers from clothes and carpets, 3D printing and styrofoaming by-products). Although an estimate about the numbers of nP in the different marine ecosystems is currently not available, yearly microplastic ( $\mu$ P) input into the marine ecosystem is estimated to have reached over 200,000 tons. As both primary and secondary  $\mu$ Ps are found in the coral reef environment [92], it stands to reason that both primary and secondary nP particles can be found in this ecosystem. They may find their way there via point sources such

---

<sup>1</sup>This work presented in this chapter is based on “Response of coral reef dinoflagellates to nanoplastics under experimental conditions” by Christina Ripken, Eiichi Shoguchi and Konstantin Khalturin. See Appendix A for manuscript. C.R. designed the study and performed the experiment, contributed to RNAseq mapping and cluster analyses, and drafted the text.

as river outlets, sewage outfalls, and runoff after heavy rainfall, as well as via atmospheric input. In addition, plastic particles of all sizes pose an increased risk of chemical contamination exposure, as the latter is found at raised levels attached to the hydrophobic surface of the particles [277, 26].

Recently, the investigation into the effects of  $\mu$ P on different inhabitants of coral reef ecosystems has become of great interest, especially as small plastic particles ( $< 1$  mm, including  $\mu$ P) have been reported from coral islands at densities of more than 1000 items/m<sup>2</sup> [278]. More recently, studies have been conducted to compare different coral reef habitats (fringing reefs vs. atoll islands) [279]. Abundance was dependent on the water exchange rate in these uninhabited islands, leading to the conclusion that in addition to the land-based sources of  $\mu$ P pollution of coral reef habitats long-range transport can also be counted, entering the reef with the water [280].  $\mu$ P have been detected in seawater samples of the outer reef slopes, the reef flats and the lagoons with increasing abundance of up to 45 items/L [281], leading to the conclusion that the plastic entering the coral reef will accumulate and be deposited out of the open ocean ecosystem [280]. This correlates with the hypothesis that coral reef habitats are a potential sink for  $\mu$ P pollution [282]. While the plastics reported from the coral islands and reef environments have a higher percentage of the smaller  $\mu$ P [281], no studies have been conducted on nPs. Due to the wave action on the outer reef, there likely will be further fragmentation to nPs within the reef environment.

$\mu$ P have also been detected inside and attached to the corals sampled from the reef environment [281, 282]. However,  $\mu$ P effect studies in corals have focused firstly on the uptake by and effects of  $\mu$ P on adult individuals and secondly on the symbiont-host relationship in the lab; not on the effects of  $\mu$ P/nPs on the isolated symbiont itself.  $\mu$ P leads to stress responses in scleractinian corals as well as suppressed detoxification and immune capacity [283]. These corals have been shown to ingest  $\mu$ P of various sizes [114], and the presence of micro-sized plastic particles has been shown to disrupt the anthozoan-algae symbiotic relationship [284]. Moreover,  $\mu$ P have also been linked to potential adverse effects on calcification [285]. However, the exact process of *Symbiodinium* spp. infection in anthozoans is unknown, and the reported experiments show that the presence of plastic microspheres in the corresponding size leads to a reduction of *Symbiodinium* spp. infection. One other study shows that corallimorpha ingest  $\mu$ P as well [92]. The study of Reichert et al. [115] showed that corals exhibit different responses to  $\mu$ P exposure: attachment of  $\mu$ P particles to tentacles or mesenterial filaments, ingestion of  $\mu$ P particles, mucus production, and overgrowth. In a 2020 study, Su et al. [166] exposed just the coral symbiont *Cladocopium goreaui* to 1  $\mu$ m polystyrene spheres, leading to a declined detoxification activity, nutrient uptake, and photosynthesis decrease as well as raised oxidative stress, apoptosis levels, and ion transport.

The aforementioned studies clearly show that  $\mu$ P have negative impacts on the fundamental relationship between corals and their symbionts and with this on the entire coral reef ecosystem. Increasing the insight we have into the effects of nPs on symbiotic dinoflagellates before entering a symbiont-host relationship will complete the emerging picture of this environmental pollutant as a problem in this ecosystem. From other studies, we know that small plastic particles have a negative effect on different algae groups, symbiotic dinoflagellates of the Clade C (*Cladocopium goreaui*) among them [154].

In order to understand the effects of nPs, Bellingeri et al. [164] studied the effects of polystyrene nP particles on the planktonic microalgae *Skeletonema marinoi*. They found that these nP particles increase intra- and extracellular oxidative stress and reduce the length of the microalgae *Skeletonema marinoi* chains from 8-cell chains to 2-cell chains, by adhering to their cell surfaces. This shows that plastic nanoparticles seem to impact symbiotic relationships between corals and their microalgae negatively, thereby degrading the entire coral reef ecosystem, but this has not been systematically

investigated.

## 4.2 Coral Reef Environments - Not Just Corals

The foundation of the trophic and structural integrity of this nutrient-deficient ecosystem is the photosymbiotic association between photosynthetic microalgae and heterotrophic animal hosts [286, 287]. Providing photosynthetic products to their various hosts, microalgae obtain shelter and inorganic nutrients - enabling both partners to thrive in these oligotrophic waters. This symbiosis has evolved separately in a high number of marine lineages, most notably Foraminifera (planktonic, same as Radiolaria, but in reef, they are benthic and often have a very heat resistant photosymbiosis), Porifera (sea sponges, often the ones in intertidal zones [288]), Cnidaria (Scleractinian corals, main reef components due to their bioconstructing abilities, and sea anemones as well), and Mollusca. Obligate association is only found in two mixotrophic marine bivalve sub-families, Tridacninae (giant clams) and Fraginae (heart cockles) [177].

While the symbiosis with photosynthetic dinoflagellates, zooxanthellae belonging to the family Symbiodiniaceae [289], has been known in Tridacna since 1888 [290] it has only been confirmed in 1983 for *Fragum* [291]. The majority of host animals obtain their indispensable symbiotic dinoflagellates from coral reef sand and the water column [292, 293, 294], where *Symbiodinium* spp. is found there in their free-living vegetative cell state [295]. Different lineages of *Symbiodinium* spp. may vary extremely in their geographical distributions [296, 297], physiological tolerance [298], and host specificity [299, 300, 301]. There are generalistic lineages (e.g., Clades A and C) with a diverse array of hosts from different phyla and relatively host-specific lineages (e.g., Clade H) [300].

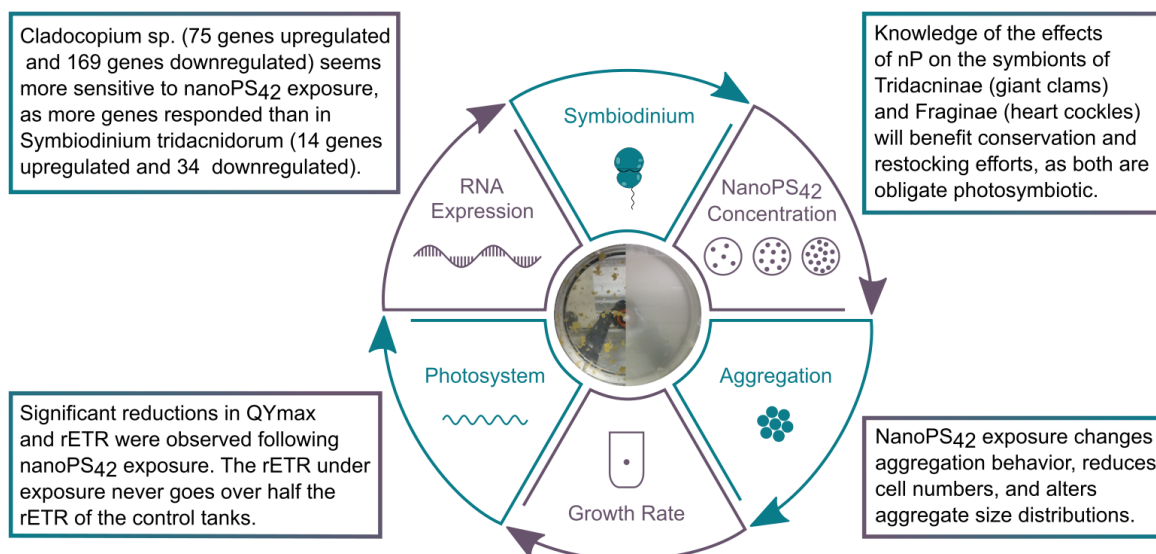
Tridacninae have been part of the coral reef ecosystem since the late Eocene [302]. Secondary production in tridacninae strongly relies on the uptake rate of ambient dissolved carbon [303]. This combination of filter-feeding with photosymbiosis allows the tridacnids to grow to be the largest living bivalves [304]. Somewhat surprisingly, tridacnids have considerable mobility - larvae swim and glide while juveniles and adults can crawl [305]. They are ecologically important in the coral reef ecosystem. Aiding in the creation of the calcium carbonate reef structure and acting as substrates for epibionts (barnacles, polychaetes, and sponges), they contribute to the overall reef productivity. Net primary production of giant clams can exceed that of corals by two thirds [303]. Their presence (big shells) acts as fish nurseries, changing the coral reef topography in such a way that fish communities are replenished [306]. They act as natural biofilters for dissolved nutrients, as well as providing expelled organic material (gametes faeces and pseudofaeces) to opportunistic feeders [307] and biomass for predators and scavengers. Ecosystem services from giant clams include food and materials [308]. They are also flagship taxa, drawing attention to coral reef habitat degradation. These iconic invertebrates are prominent inhabitants of coral reefs, being very visible with the intricately patterned and pigmented mantel tissue, visible often from the water surface. Zooxanthellae are not inherited, and symbiosis is only permanently established after metamorphosis to juvenile [290], while larvae still benefit from the association with zooxanthellae [292]. Filter feeding is present in all life stages. Within two weeks of spawning, they settle as early juveniles [309]. Their hypertrophied dorsal siphonal mantel is directed upwards. This adaptation exposes the zooxanthellae contained within tubular networks to the sunlight and orients the byssus downwards for attaching to the hard coral reef substrate [310]. Tridacnid-associated zooxanthellae symbionts are relatively well-studied, being placed into *Symbiodinium* spp. Clade A, C, and occasionally D [311]



and more than 42% of individuals had multiple symbiont lineages [312].

*Fragum*, on the other hand, is far less well understood and, at the same time, the most species-rich group of photosymbiotic fragines [313]. They create and modify coral reef ecosystems for other organisms across vast spatial and temporal scales, dating back to the late Triassic [314]. Collectively, *Fragum* aggregations can affect the ecosystem via their influence on hydrodynamics, light penetration/availability, physical stability, and C/nutrient fluxes. Individuals host biofilms and invertebrates on their shell surface, and shell accumulations can affect secondary production [315]. Compared to the Tridacnids, much less is known about *Fragum*'s roll in the coral reef ecosystem, but using bivalves for ecotoxicological purposes has long been done and could prove advantageous in this context. Assessing stress and immune responses via hemolymph is a nonlethal way to monitor biomarkers such as heat shock proteins, antioxidant enzymes, and stress hormones [316]. Just as the Tridacnids, *Fragum* shelters extracellular symbionts within the lumen of their tertiary tubular network, which originates from the digestive system and extends into the mantle and differently from Tridacnids, also into the gill tissues [317]. As with their ecology, the diversity of Fraginae-associated symbiont communities are under-explored [311]. Existing literature on zooxanthellae is most comprehensive for coral-associated photosymbioses. Most freshly isolated symbionts are from *Symbiodinium* Clade C while culturing from host tissues leads to Clade A [318]. This divergence may arise from the fact that certain *Symbiodinium* spp. strains grow better in culture medium, although they are not the dominant strains within the host [319]. Hence, freshly isolated symbionts reflect more accurately the symbiont diversity in Fraginae.

Should growth rates be affected by exposure to  $\mu\text{P}$ , as is the case in other algae groups, this will enhance the effects of the reported disruption of symbiotic relationship, as in addition to being expelled at a higher rate ([284], *Symbiodinium* spp.) will also be available in fewer numbers in the reef environment. Effects on the photosynthetic activity should be of utmost importance, especially since it is possible that subsequent generations grown in clean media will also be affected. This could lead to hosts being affected through a decreased photosynthetic activity of *Symbiodinium* spp.. The last remaining question would be if the  $\mu\text{P}$  changes gene expression patterns in *Symbiodinium* spp. It was not investigated if the unsuccessful infection of *Symbiodinium* spp. was due to a change within the gene expression of *Symbiodinium* spp. or just the previous over-infection with  $\mu\text{P}$ , so shedding light on this aspect would complete the picture.



**Figure 4.1: Endosymbiotic dinoflagellates species and experimental set up.** Understanding the reaction of photosymbionts to nano-sized plastic pollution can help efforts to protect the reef. QY<sub>max</sub> is the effective quantum yield, rETR is relative Electron Transport Rate.

In this study, we focused on the symbionts of a different group of invertebrates, Mollusca, inhabitants of the fringing coral reefs of Okinawa. Three main questions addressed in the experiments shed light on effects of nP (42 nm polystyrene spheres) on the growth rate and cell aggregation, photosynthetic activity and the gene expression changes of the symbionts of Tridacninae (giant clams) and Fraginae (heart cockles), *Cladocopium* sp. (formally, *Symbiodinium* clade C) and *Symbiodinium tridacnidorum* (formally, *Symbiodinium* clade A 3) respectively. Knowledge of the effects of nP on the symbionts of Tridacninae (giant clams) and Fraginae (heart cockles) will benefit conservation and restocking efforts, as both are obligate photosymbiotic. Previous studies have been conducted on the effects of micro- and nP on the members of the mollusc family [320, 321, 322, 323], specifically focusing on the giant clam *Tridacna maxima* for active retention inside the animal and passive adherence to the shell [324]. These studies found diverse adverse effects of the plastic pollution on the bivalves. In combination, these potentially adverse effects for the obligatory photosymbiotic members of the Mollusca, in terms of direct effects [324] but also indirectly via the endosymbionts, should be critically investigated to understand the potential risks to the coral reef ecosystem.

### 4.3 Materials and Methods<sup>2</sup>

15 roller tanks were used to investigate how nP incorporation into *Symbiodinium tridacnidorum* and *Cladocopium* sp. aggregates. Changes in gene expression patterns and growth rates, sinking

<sup>2</sup>Some methods are explained in greater detail than traditionally done within the methods section. Especially methods that were developed, failed or could not be conducted (although they were included in the thesis proposal) are elucidated to give a better overview of the work done. The author feels this is better presented in the respective method sections than under results.

velocity of aggregates, and photosystem activity were measured. Three different treatments of 42 nm polystyrene nP (nanoPS<sub>42</sub>) were used in triplicates with the exposure lasting for ten days.

### 4.3.1 Roller tanks<sup>3</sup>

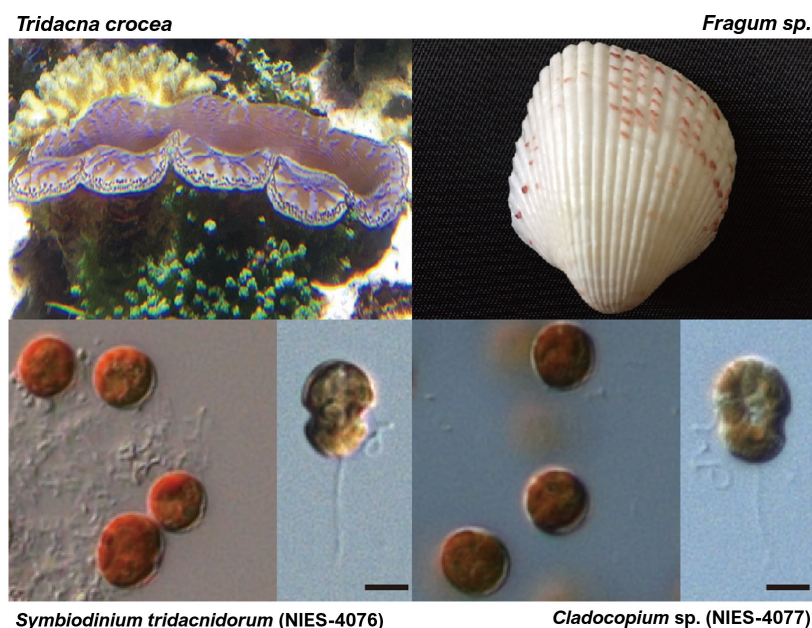
15 roller tanks were employed. Roller tanks and tables were used to simulate the natural environment of the dinoflagellate vegetative cells in their free-living state [159, 295], as the majority of host animals obtain their indispensable symbiotic dinoflagellates from coral reef sand and the water column [292, 293]. This method consequently ensured that microalgae are exposed to the nanoPS<sub>42</sub> in a way that mimics their natural habitat and that exposure levels remained constant throughout the experiment [161]. Once rotation commenced, continuous aggregate formation and suspension were ensured [99] as well as continuous exposure to nanoPS<sub>42</sub>. Rolling tanks have commonly been used to promote aggregation since the late 1980s [159, 97]. The tanks are closed for the entire duration of the experiment so that exposure levels of the nanoPS<sub>42</sub> remain constant throughout. Moreover, the tanks were closed without bubbles so as not to disturb the aggregation process with turbulence. The rotation was set to 6 rounds per min, leading to a continuous aggregate suspension and collision of particles with different sinking rates [160].

### 4.3.2 Biological materials

Both dinoflagellate cultures used in this experiment were isolated in Okinawa, Japan. Using sterilized seawater and micropipettes, isolation of these Symbiodiniaceae was first performed by Prof. Terufumi Yamasu in the 1980s at the University of the Ryukyus [325]. Since then, they have been maintained in the laboratory of Prof. Michio Hidaka, at the University of the Ryukyus. In that laboratory, *Symbiodinium tridacnidorum* (Clade A3 strain, ID: NIES-4076) and *Cladocopium* sp. (Clade C strain, ID: NIES-4077) are labeled as strains “Y106” and “Y103,” respectively. *Symbiodinium tridacnidorum* and *Cladocopium* sp. are endosymbionts of *Tridacna crocea* and *Fragum* sp., respectively [326] (see Figure 4.2). In regard to host habitats, *Tridacna crocea* is epifaunal and *Fragum* sp. is infaunal [313]. In 2009, isoclonal lines were established for each culture at the Marine Genomics Unit of Okinawa Institute of Science and Technology Graduate University. This was achieved by isolating single cells under a microscope using a glass micropipette [327]. From then on, repetitive subculture in 250-mL flasks has continued for eight years [327].

---

<sup>3</sup>The roller tanks used in this experiment were made in Okinawa, fashioned after the design of the tanks used at the University of California, Santa Barbara. The volume ( $V = \pi r^2 h = \pi 6.7^2 7.5 \approx 1057$  mL) was matched, and the opening mechanism is the same for comparability. The rolling tanks are made of acrylic and were incubated in seawater (sand filtered, 25  $\mu$ m filter, plus UV sterilization; changed every seven days) for a month before use to minimize any leaching of additives and outgassing during the experiment—manufacturing company: HOKUCHO KOGYO CO., LTD.



**Figure 4.2:** Pictures of host animal *Tridacna crocea*, *Fragum* sp., symbionts *Symbiodinium tridacnidorum* and *Cladocopium* sp., from left to right and top to bottom. Scale bar is 10  $\mu\text{m}$ . Pictures by E. Shoguchi. Images were taken with Zeiss Axio Imager Z1 microscope.

Cultures were maintained at 25 °C on a 12 h-light/12 h-dark cycle at about 20  $\mu\text{mol}/(\text{m}^2 \text{ s})$  illumination with white fluorescent lamps (incubator: CLE-303, TOMY). Artificial seawater (ASW) containing 1x Guillard's (F/2) marine-water enrichment solution (Sigma-Aldrich) in combination with three antibiotics, ampicillin (100  $\mu\text{g}/\text{mL}$ ), kanamycin (50  $\mu\text{g}/\text{mL}$ ), and streptomycin (50  $\mu\text{g}/\text{mL}$ ) was used as a culture solution [327, 326]. In the Marine Genomics Unit similar growth rates are reported for the same culturing conditions in *Symbiodinium tridacnidorum* and *Cladocopium* sp. [326], although culturing difficulties for some *Cladocopium* sp. have been reported [328]. Both cultures were transferred to glass flasks seven months prior to the start of the experiment. In the experiment itself, no antibiotics were used.

### 4.3.3 Exposure

As particles, 42 nm pristine fluorescent polystyrene beads (density 1.05 mg/L in 0.1% Tween 20 solution) from Bang Labs (catalogue number FSDG001) were used (see Figure 2.5 for optical image). Fluorescent "Dragon Green" color was selected to give a contrast in 3D imaging. Three densities (10 mg/L, 0.1 mg/L, 0.01 mg/L, see Table 2.2) were used. See Chapter 2.2.3 for more details on the nanoPS<sub>42</sub> beads.

Treatment tanks as well as control tanks (no nanoPS<sub>42</sub>) were established in triplicate. Two different controls were run with the treatment tanks:

- **positive controls**, non-exposed microalgae - tanks without addition of nanoPS<sub>42</sub>,
- **negative controls**, nanoPS<sub>42</sub> in clean medium without any algae, at 10 mg/L, 0.01 mg/L and 0 mg/L.

Every treatment tank was filled with

- 500 mL culture (680,000 cells/mL, stationary growth phase),
- 100 mL F/2 (Sigma-Aldrich) (to avoid any nutrient deficiency effects in RNA expression patterns) and
- 400 mL ASW.

NanoPS<sub>42</sub> inoculation was done after half the tank was filled to promote mixing before the tank was closed. All tanks were rotated under the same light cycle and temperature conditions as the culturing conditions (25 °C on a 12 h-light/12-dark cycle).

#### 4.3.4 Aggregate characterization: sampling and analysis

Tanks were sampled as biological replicates on three consecutive days (day 9, 10 and 11; see Table 4.1).

**Table 4.1: Sampling schedule for all tanks.** Tanks of same treatment were sampled at the same time, creating biological replicas.

	Bio. Replica 9 days	Bio. Replica 10 days	Bio. Replica 11 days
Pos. Control	12	11	10
0.01 mg/L	1	2	3
0.1 mg/L	4	6	5
10 mg/L	7	8	9
Neg. Control	13	14	15

Tanks of the same treatment were always sampled at the same time of day; controls were sampled first, then in increasing nanoPS<sub>42</sub> treatment order. As cell division takes 24 h [329], these are three subsequent generations that are sampled. In order to have a full overview of how nanoPS<sub>42</sub> affects aggregate formation, different parameters were measured at the end of the experiment.

The harvest included separate sampling of the aggregate fraction (aggregates > 0.5 mm, Agg), and the surrounding seawater fraction (aggregates < 0.5 mm and unaggregated cells, SSW) [99]. Tanks were imaged before sampling. Material was collected for:

- Total aggregate count: enumerate the total number of aggregates, counted clockwise.
- Collection of 1/2 of all aggregates for RNA analysis. 2 min spin down at 12,000 rpm and discarding the supernatant, freezing in liquid nitrogen and storage at -80°C.
- Samples for photosystem efficiency measurements.
- Aggregate sample 3D imaging.
- Cell counts.
- Aggregate size measurements.
- Aggregate sinking velocity measurements.



- Collection of remaining aggregates for RNA analysis, 2 min spin down at 12,000 rpm and discarding the supernatant, freezing in liquid nitrogen and storage at  $-80^{\circ}\text{C}$ .

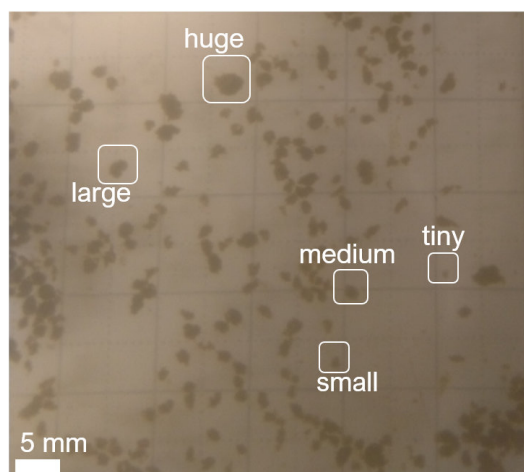
A detailed description of the methods used can be found below.

**Total aggregate count** See Section 2.2.5.

**Sinking velocity** Sinking rates of three aggregates per size class (huge, large, medium, small, tiny). Measured in a 100 mL glass graduated cylinder (water to fill the cylinder came from the same ASW batch that was used to fill the tanks and was stored in the same conditions as the rolling tanks). The time was measured for the aggregate to sink 11.5 cm.

For more detailed description, see Section 2.2.5.

**Size** Aggregates were categorized into five size classes: huge:  $> 3.5$  mm; large:  $2.5 - 3.5$  mm; medium:  $1 - 2.5$  mm; small:  $0.5 - 1$  mm; and tiny:  $< 0.5$  mm in the longest dimension (see Figure 4.3).



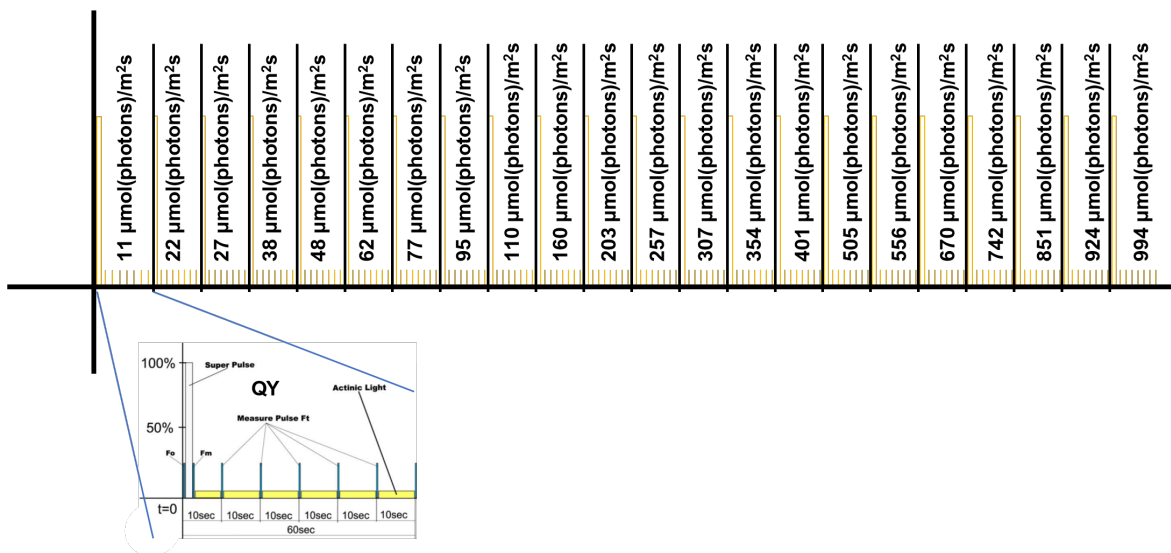
**Figure 4.3: Size classes in control Tank 12.** Picture of Control Tank 12 after 9 days of exposure. Due to different collision rates over the time of the experiment, aggregates vary in size and shape. Five size classes - huge:  $> 3.5$  mm; large:  $2.5 - 3.5$  mm; medium:  $1 - 2.5$  mm; small:  $0.5 - 1$  mm; and tiny:  $< 0.5$  mm - were used to reflect these differences.

**Cell counts** Cells were originally counted with via Flow Cytometer Accuri C6 4523. The machine had problems counting the cells correctly, due to aggregation. The same problem was observed before for the microalgae from Section 2.2.5. Cells were then counted by hand with a hemocytometer (C-Chip DHC-N01) on a Zeiss Axio Imager Z1 microscope (Zeiss, Jena, Germany). At least two subsamples and 200 cells were counted per sample.

**Internal structure through 3D fluorescent microscopy** One aggregate in 1% agarose in a 1 mL syringe for 3D imaging (z-stacks in the Zeiss Lightsheet Z.1 (stored at  $4^{\circ}\text{C}$ ). To show if the plastics were directly attached to the algae and where they were located within the aggregates, microscope observations were conducted with the Zeiss Lightsheet Z.1. Fluorescent polystyrene beads were observed with BP filter (Excitation: 405 nm; Emission: 505-545 nm), and chloroplasts were visible using a long pass red filter (Excitation: 488 nm, Emission: 660 nm). Z-stacks were analyzed using Imaris software to determine the location of the plastics and cells within each aggregate.

For more detailed description, see Section 2.2.5.

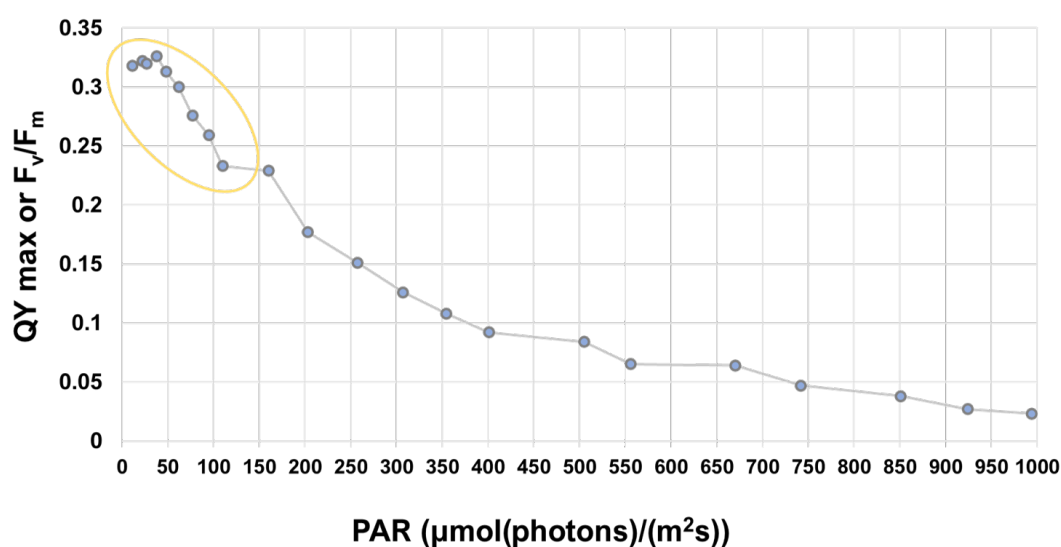
**Photophysiology** A Pulse Amplitude Modulated fluorometer (PAM, PHYTO-PAM-II, Heinz Walz GmbH, Effeltrich, Germany) was used to measure indicators of changes in the efficiency of the photosystem. These included  $QY_{\max}$ ,  $F_0$  and relative Electron Transport Rate (rETR). Measuring the light energy emitted from light-harvesting pigments associated with the process of photosynthesis [330], this non-invasive technique tests the operating efficiency of the photosystem II (PSII) in the dark-adapted state [331].  $QY_{\max}$  and rETR were derived from measuring a light curve (LC) (see Figure 4.4). The  $QY_{\max}$  also referred to as  $F_v/F_m$ , is the maximum quantum yield of PSII in the dark-adapted state. Together with the rETR, the functionality of the photosystem can be tested. The  $F_0$  is the in-vivo chlorophyll autofluorescence, a proxy for cell density in photophysiology. Understanding the damage done by the exposure to nanoPS<sub>42</sub> to the photosystem, especially in combination with RNA expression data, can give a clearer picture of the reasons for the reported reduction in chlorophyll a and growth rate [51].



**Figure 4.4:** Light Curve (LC) protocol created via the PHYTO-PAM-II software to measure  $QY_{\max}$  and  $F_0$ . The LC3 protocol has 20 phases, with each phase lasting 60s. The actinic illumination (Actinic Light Intensity or A-pulse) intensities [in  $\mu\text{mol photons}/(\text{m}^2\text{s})$ ] increase in the following steps: 11, 22, 27, 38, 48, 62, 77, 95, 110, 160, 203, 257, 307, 354, 401, 505, 556, 670, 742, 851, 924 and 994. Saturation pulses (F-pulses) of  $2000 \mu\text{mol photons}/(\text{m}^2\text{s})$  were given at the end of each illumination step. This method is based on the successive measurement of the sample exposed to a stepwise increase of light intensity and can relate the rate of photosynthesis to photon flux density. Displayed is the protocol created using the PHYTO-PAM-II software, extending the LC 3 used in Chapter 1.

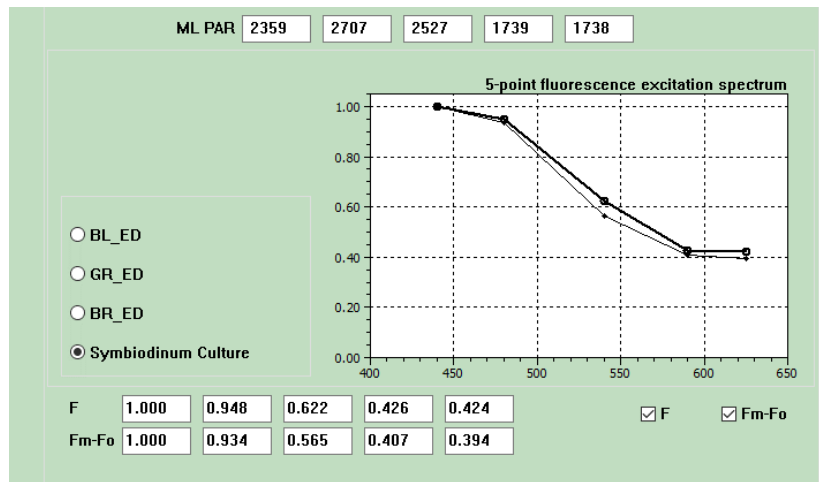
The PHYTO-PAM-II software allows for the creation of a custom rapid-response light curve, used to derive these measurements (see Figure 4.4). These settings were picked so as to enable determination of  $QY_{\max}$ ,  $F_0$ , and rETR. Samples were measured after 30 min of dark adaptation at the same temperatures as experiments were run. The created LC measured instantaneous ( $F_t$ ) and maximal ( $F_m$ ) fluorescence over 20 60-seconds phases between 11 and  $994 \mu\text{mol photons}/(\text{m}^2\text{s})$ . As can be seen from Figure 4.5 the steps are closer together at the beginning of the light curve to give a more detailed picture of increasing phase (initial slope of the corresponding photosynthesis efficiency curve) and the steps become wider at the end in the photodamage phase of the light curve.

This distribution of steps was chosen because we are interested in seeing if the plastic exposure changes the ability to ramp up initial photosynthesis rates and, at which point the photodamage becomes apparent, not the behavior of the photosystem under photo damaging conditions. In that case, an even distribution of the steps would have been better suited.



**Figure 4.5:  $QY_{\max}$  curve created with the 20 step measurement protocol seen in Figure 4.4.** It is visible from the spacing of the measuring point that the focus is on initial reactions of the photosystem seen in the yellow ellipse. For this example a  $QY_{\max}$  curve of unstressed culture is displayed.

The PHYTO-PAM-II software also allows for the creation of custom reference excitation spectra (see Figure 4.6), set up in correspondence to the light intensity list with 20 steps, termed "PAR list" (see Figure 4.4 for 20 steps and sequence of the intensity increases). The PAR list was used in combination with the software's function of creating a custom script to produce measurements that are comparable to the LC3 light curve, which was measured via the AquaPen in the experiments of Chapter 2.



**Figure 4.6:** Image of 5-point fluorescence excitation spectrum created as reference for this specific *Symbiodinium* culture. F and  $F_m - F_0$  values of unstressed cultures are recorded in this software as a reference when measuring the experimental samples.

The  $QY_{max}$ ,  $F_0$ , and rETR were measured after 30 min dark adaptation for every tank for the SSW and AGG fraction separately. All three values were plotted against the PAR and compared between exposure length and treatments.  $QY_{max}$  and rETR were compared to complete the picture.

**RNA extraction, library construction, and sequencing** Frozen cells were broken mechanically using a polytron (KINEMATICA Inc.) in tubes chilled with liquid nitrogen. RNAs were extracted using Trizol reagent (Invitrogen) according to the manufacturer's protocol. The quantity and quality of total RNA were checked using a Qubit fluorometer (ThermoFisher) and a TapeStation (Agilent), respectively. Libraries for RNA-seq were constructed using the NEBNext Ultra II Directional RNA Library Prep Kit for Illumina (#E7760, NEB). Sequencing was performed on a NovaSeq6000 SP platform. RNA from frozen cells (Electronic Supplementary Material, Table S2) was extracted using Trizol reagent (Invitrogen) according to the manufacturer's protocol. Libraries for RNA-seq were constructed using NEBNext Ultra II Directional RNA Library Prep Kits for Illumina (#E7760, NEB). Sequencing was performed on a NovaSeq6000 SP (Illumina) platform.

**Gene annotations** – Annotations were performed using BLAST2GO and Pfam databases [327] and are available at the genome browser site (<https://marinegenomics.oist.jp>). The best hits to proteins encoded by differentially expressed genes were searched against the database at NCBI (<https://blast.ncbi.nlm.nih.gov/Blast.cgi>) using Blastp. The majority comprised hypothetical proteins of *Symbiodinium microadriaticum*.

**RNA-seq data mapping and clustering analysis** – Raw sequencing data obtained from the NovaSeq6000 were quality trimmed with Trimmomatic (v0.32) in order to remove adapter sequences and low-quality reads. Paired reads that survived the trimming step (on average 92%) were mapped against reference transcripts of *Symbiodinium*, Clades A3 and C. For each gene in the genomes of Clade A3 or C a \*.t1 transcript form was used as a reference sequence. Mapping was performed using RSEM (Li and Dewet, 2011) with bowtie (v1.1.2) as an alignment tool. Expression values across all samples were normalized by the TMM method (see perl script abundance\_estimates\_to\_matrix.pl in Trinity-v2.3.2 /util folder) [332]. Genes with differential expression (2-fold or 4-fold different)

were identified with edgeR Bioconductor, based on the matrix of TMM normalized TPM values. Experimental samples were clustered according to their gene expression characteristics using edgeR.

## 4.4 Results and Discussion

In this study, we focused on the microalgal symbionts of mollusks that inhabit fringing coral reefs of Okinawa. Knowledge of the effects of nP on the symbionts of Tridacninae (giant clams) and Fraginae (heart cockles) will benefit conservation and restocking efforts, as both are obligatory photo-symbionts and important contributors to coral reef ecosystems. No previous studies have been conducted on these specific parts of the host-symbiont relationship and the influence of nP on it. This study specifically investigated effects of nP (nanoPS<sub>42</sub>) on the growth rates, aggregations, and gene expression changes in *Symbiodinium tridacnidorum* (symbionts of the *Tridacna crocea*) and *Cladocodium* sp. (symbionts of the *Fragum* sp.).

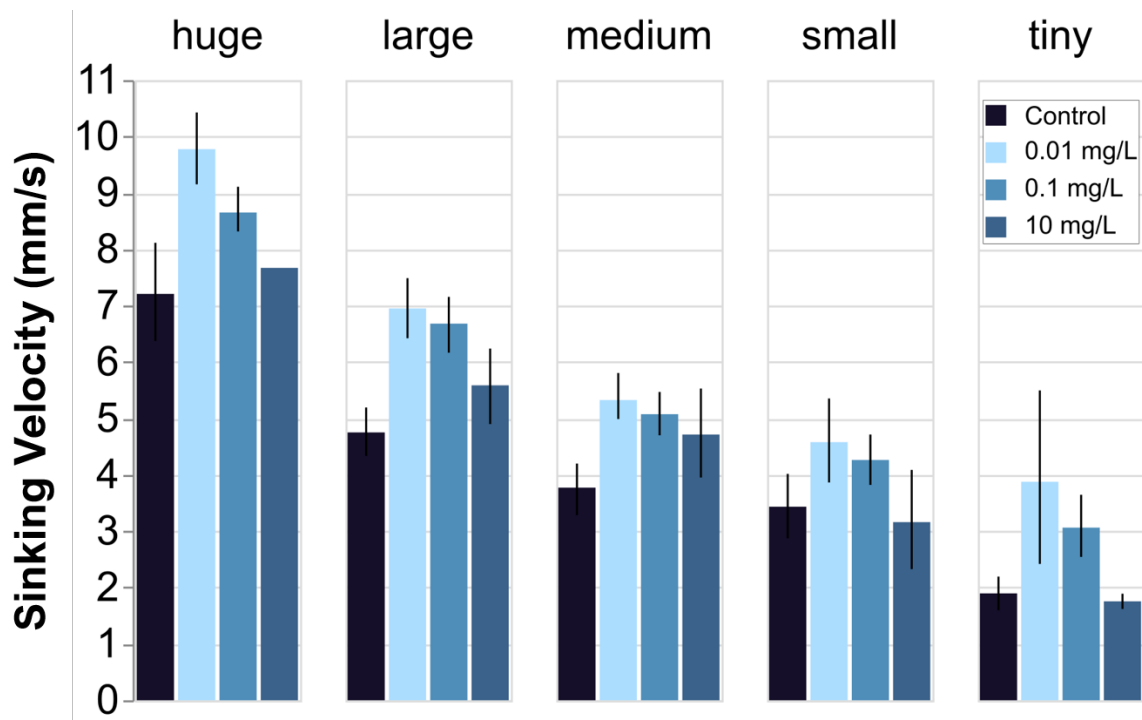
### Sinking velocity of aggregates changes with nanoPS<sub>42</sub> exposure

Sinking velocities of five size classes of aggregates were evaluated in every treatment. NanoPS<sub>42</sub> impacted sinking velocities of aggregates when treatments were compared. The sinking velocity ranged from just below 10 mm/s in the 0.01 mg/L treatment to less than 2 mm/s in the 10 mg/L treatment.

Significant differences in sinking velocities are evident between control and the nanoPS<sub>42</sub> plastic treatments (Mann-Whitney,  $p = 0.010$  and  $p = 0.041$ , respectively). Aggregates under low and intermediate nanoPS<sub>42</sub> exposure had significantly increased sinking velocities, by 34% and 19% respectively, when compared to controls (see Figure 4.7). These changes are most likely due to hetero-aggregates of algae and nanoPS<sub>42</sub> (see Figure 4.8) similarly to what has been previously reported in microalgae *Chaetoceros neogracile* and *Rhodomonas salina* [97] under  $\mu\text{P}$  exposure. In the diatom *Chaetoceros neogracile* sinking velocities reduced and increased in the cryptophyte *Rhodomonas salina* [97]. Lagarde et al. [149] notice different aggregate formation under different plastic treatment and sizes, corresponding to our results.

Changes in aggregation and resulting sedimentation were observed under nanoPS<sub>42</sub> exposure. It is interesting to see that the biggest changes in sinking velocity correspond to increases in aggregation and are observed in the lowest plastic treatment at 0.01 mg/L. On the other hand, the 10 mg/L treatment did not have any significant effect on the sinking rates but did affect sedimentation indirectly through changes in the aggregate size distribution (see Figure 4.9). These changes, both sinking velocities and aggregate size distribution, are most likely due to hetero-aggregation between algae and nanoPS<sub>42</sub> (see Figure 4.8). Under different treatments, the size distribution of aggregates was significantly different (see Figure 4.9). In combination, it is likely that the same effect that led to that difference in aggregation is also responsible for the difference in sinking velocities. Changes in extracellular polymeric substances (EPS) (a subgroup of EPS, transparent exopolymer particles (TEP) were used to characterize nanoPS-hetero-aggregates in Chapter 2, see Section 2.2.5) production and stickiness will lead to different cell packaging within the aggregates, possibly creating tighter packed aggregates in the lowest and intermediate treatment. This effect might be counteracted under the highest nanoPS<sub>42</sub> exposure, by the sheer volume of EPS, which is lighter than seawater [333]. The nP itself trapped in these could also add to the sinking velocity returning back



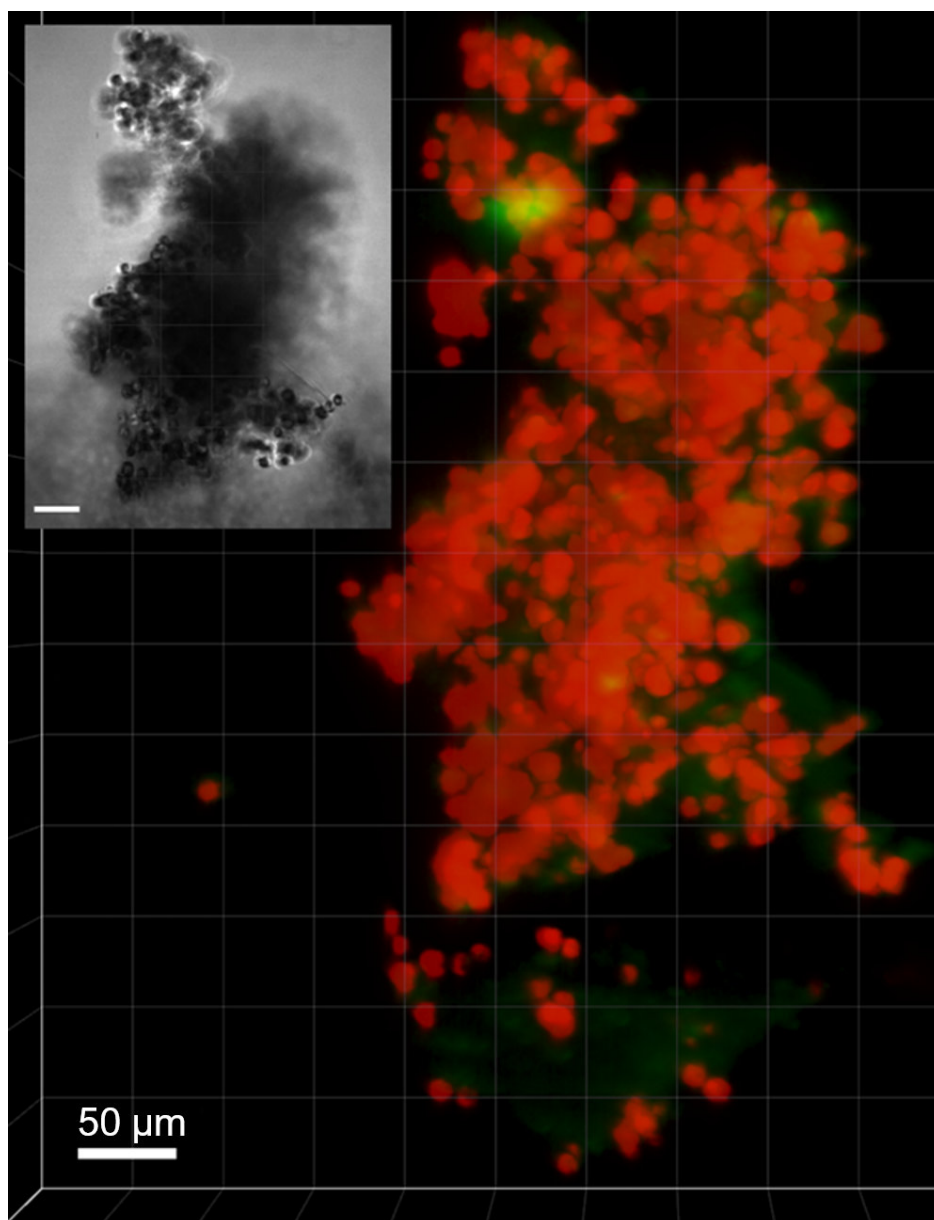


**Figure 4.7: Sinking velocity change with nanoPS<sub>42</sub> exposure.** Sinking velocities decrease with aggregate size, from more than 7 mm/s (huge) to less than 2 mm/s (tiny). In all size classes, the control (black blue) was similar in sinking velocity to the highest nanoPS<sub>42</sub> treatment (dark blue, 10 mg/L). The low nanoPS<sub>42</sub> treatment (light blue, 0.01 mg/L) differed significantly from both controls (t-test, two-tailed  $p = 5.56 \times 10^{-4}$ ) and the highest nanoPS<sub>42</sub> treatment (t-test, two-tailed  $p = 9.03 \times 10^{-4}$ ). This was also true for the intermediate nanoPS<sub>42</sub> treatment (darker blue, 0.1 mg/L). Error bars are 95% confidence intervals. Only one huge aggregate was measured in the highest nanoPS<sub>42</sub> treatment. No differences in sinking velocity were observed in relation to exposure length.

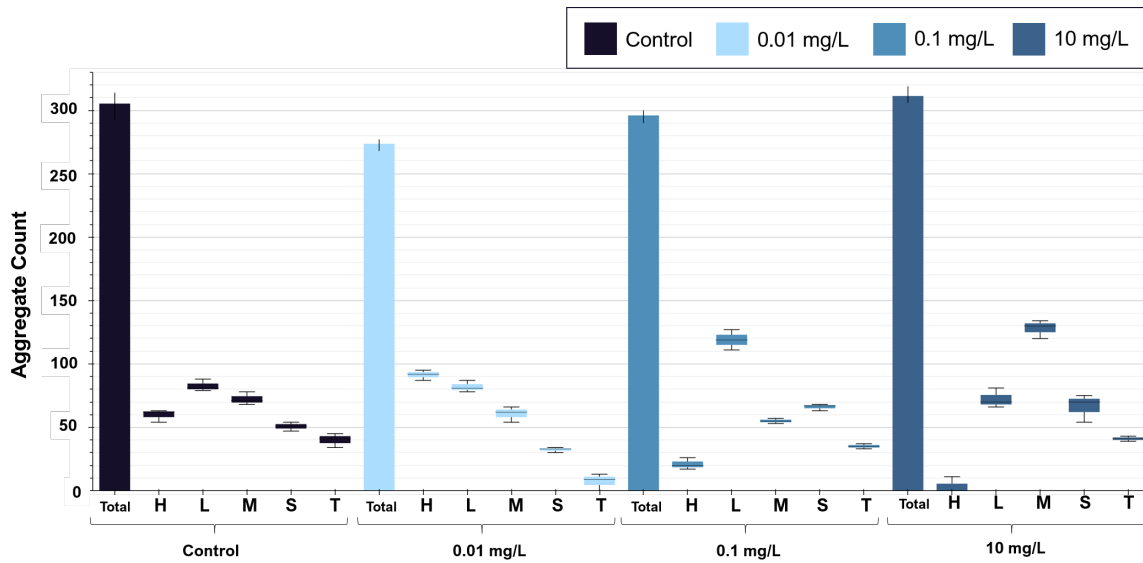
to control levels in the high plastic treatments (see Figure 4.8 for nanoPS<sub>42</sub> trapped in EPS). As these symbionts are paired with the mobile larvae of the host animals, a higher sinking velocity could remove the potential symbiont from the pelagic area and reduce the chance of a match.

#### 4.4.1 NanoPS<sub>42</sub> exposure influences the size and number of cell aggregates

To understand the impact of nanoPS<sub>42</sub> on aggregation in these two Symbiodiniaceae cultures, the total number of algal aggregates per tank and in five aggregate size classes was recorded (see Figure 4.9). All tanks showed aggregation, which was expected, as self-aggregation of Symbiodiniaceae has been observed previously [166].



**Figure 4.8: 3D images of aggregates under high nanoPS exposure (10 mg/L).** Algal cells are shown in red (long pass red filter; excitation: 488 nm, emission: 660 nm), while nanoPS<sub>42</sub> is green (BP filter; excitation: 405 nm; emission: 505-545 nm). Individual nanoPS<sub>42</sub> cannot be seen, due to their small size. EPS, usually not visible with this technique, is seen here because nanoPS<sub>42</sub> is trapped inside. Cells were counted with Imaris software, there are approximately 663 cells. The aggregate has a diameter of 353.8  $\mu\text{m}$  and a volume of 0.00277  $\text{mm}^3$ .

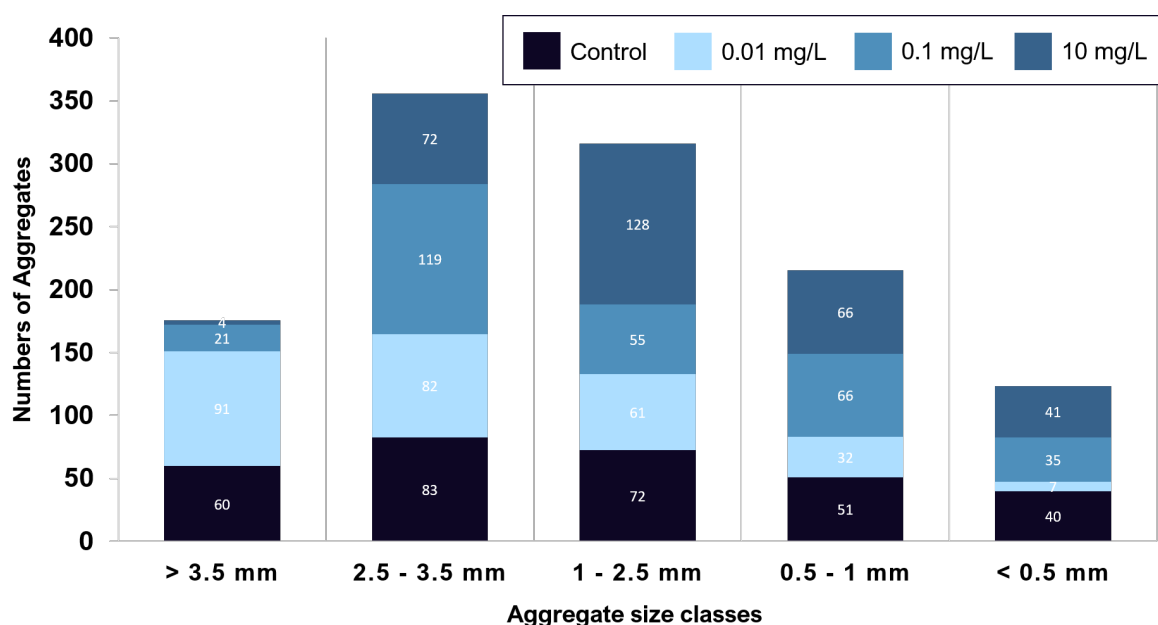


**Figure 4.9: NanoPS<sub>42</sub> exposure changes aggregation behavior, reduces cell numbers, and alters aggregate size distributions.** The figure shows the total aggregate count (Total) and how the aggregates are distributed in size (see Figure 4.3 for size classes): H for Huge; L for Large; M for Medium; S for Small; T for Tiny. The lowest nanoPS<sub>42</sub> treatment (light blue, 0.01 mg/L) show a significant 10% reduction in the total aggregate count (Holm-Sidak,  $p = 0.002$ ). While there was also a reduction of 3% in the intermediate nanoPS<sub>42</sub> treatment (darker blue, 0.1 mg/L), this was not significant (t-test,  $p = 0.496$ ). The highest treatment shows an increase in total aggregate count. However, this was not significant (Holm-Sidak,  $p = 0.367$ ). The observed changes in aggregation patterns could be due to higher production of extracellular polymeric substances (EPS) with sticky properties, trapping more cells in each aggregate, and keeping aggregates closer together. Nutrient depletion, which has been linked to the presence of  $\mu\text{P}$  in algae cultures [137], is associated with increased stickiness of the EPS [199]. Differences in EPS production and its stickiness due to the presence of nP likely contribute to the observed differences in aggregation. In addition, in *Symbiodinium tridacnidorum*, genes encoding a protein with a TIG domain were upregulated. As this protein is found in surface cell receptors, it may influence changes in hetero-aggregation. No differences are observed when the exposure length is compared. Error bars show standard deviations.

The majority of aggregates exhibited an ovoid form. A significant difference can be observed when aggregate numbers are compared over all size classes and all treatments, showing that the nanoPS<sub>42</sub> influences the aggregation process. The lowest nanoPS<sub>42</sub> treatments (0.01 mg/L) shows significant reduction in the total aggregates count by 10% (Holm-Sidak,  $p = 0.003$ ). While there is also a reduction of 3% in the intermediate nanoPS<sub>42</sub> treatment (0.1 mg/L), this is not significant. The different aggregate sizes classes show significantly different distributions in all three treatments and the control (ANOVA,  $p < 0.001$ ) (see Figure 4.9). In the control, the self-aggregation led to a specific distribution pattern of aggregate sizes, which was not repeated in the treatments. Self-aggregation was also observed in the  $\mu\text{P}$  experiments of Su et al. [166]. The fact that the presence of nanoPS<sub>42</sub> changes the aggregation between the cells and leads to more aggregates in the bigger size classes is possibly due to the higher production of EPS with sticky properties, trapping more cells in one aggregate and keeping aggregates closer together. Such self-aggregation also leads to biofilms, which have been reported in Symbiodiniaceae [334]. Nutrient depletion, which has been

linked to the presence of  $\mu\text{P}$  in algae cultures [137], is associated with increased stickiness of the EPS [199, 198, 335]. Differences in EPS production due to the presence of nanoPS<sub>42</sub> is a likely factor contributing to the differences in aggregation seen in the study. EPS production was not measured, so further studies are needed to confirm this hypothesis linking the aggregation process and EPS production in Symbiodiniaceae under nP influence. Lagarde et al. [149] notice different aggregate formation under different plastic treatment and sizes, which matches with our results.

Significant differences are evident when aggregate numbers are compared over size classes and treatments, showing that nanoPS<sub>42</sub> influences aggregation. Aggregate size classes show significantly different distributions in all three treatments vs. controls (ANOVA,  $p < 0.001$ ) (see Figure 4.10). These differences in aggregation could be due to changes of the cell surface receptors, as nanoPS<sub>42</sub> increases genes related to those two-fold (see Section 4.4.5).



**Figure 4.10: NanoPS<sub>42</sub> exposure leads to change in aggregation.** Aggregates sorted by size class show a significant change in distribution pattern under nanoPS<sub>42</sub> exposure (Holm-Sidak,  $p = 0.05$ ). The number of aggregates is reduced by 10% in the 0.01 mg/L treatment (Holm-Sidak,  $p=0.003$ ), but aggregation was enhanced overall in that treatment to have a higher percentage of huge aggregates than in the control treatment (Holm-Sidak,  $p = 0.001$ ). In the higher plastic treatment at 10 mg/L this is reversed, leading to more aggregates overall and more of those being of smaller sizes. No differences are observed when the exposure length is compared.

Due to nanoPS<sub>42</sub> exposure, aggregation and sinking velocities are impacted, which in turn leads to change in sedimentation. As the majority of the host animals obtain their symbiotic dinoflagellates from the sand and water column [293], these changes in dinoflagellate sedimentation might lead to problems in the acquisition of symbionts for the host animals. The lowest plastic treatment used, which is environmentally possible, already induces changes to the sedimentation. This lowest treatment led to bigger aggregates, which at the same time sank faster, possibly removing the symbionts from the water column faster than required from the host animals and reducing changes of encountering symbionts before settling.

#### 4.4.2 Photophysiology

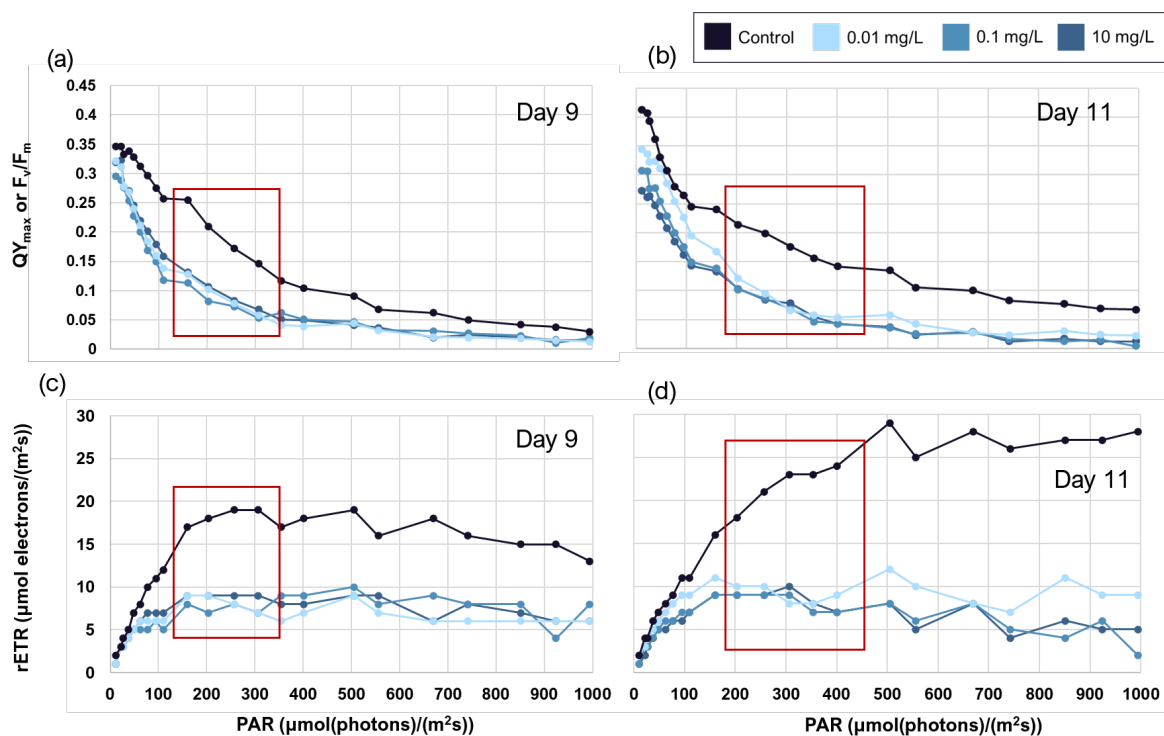
In addition to seeing how sedimentation is affected, it is vital to know about changes in the photosystem of *Symbiodinium tridacnidorum* and *Cladocopium* sp., as they are symbionts of host animals that are obligatory photosymbiotic.

In Chapter 2, ecologically photo-inactive plankton cells were exposed to  $\mu\text{P/nP}$ . While the experiments simulated an environment that does not include the plankton photosynthesising, we took the opportunity after harvesting to see if these cells were still photo active. After establishing this during preliminary trails, these measurements were included into the experimental setup. They yielded different results in the different species used, but overall it was clear that the  $\mu\text{P/nP}$  used did affect the photophysiology of the cell as controls and exposed cells reacted differently to the light stimulus. For further explanation about the different species response, see Sections 2.4.3, 2.4.3 and 2.4.3.

In this chapter, the simulated environment is flooded with light during the day and the species used are photosymbionts, to determine if exposure to NanoPS<sub>42</sub> will lead to a change in any part of the photophysiology.

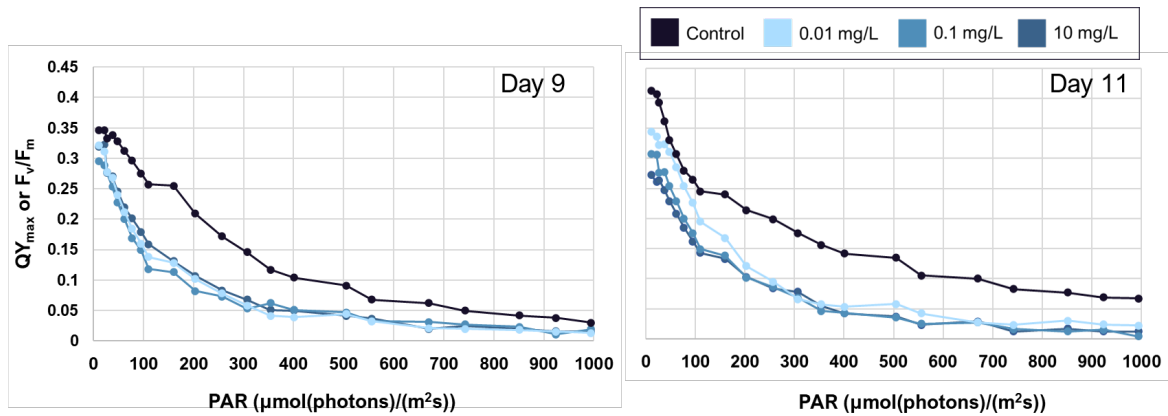
After 30 min of dark adaptation, photosystem efficiency changes were measured in terms of changes in the effective quantum yield ( $\text{QY}_{\text{max}}$  or  $F_v/F_m$ ) and the relative Electron Transport Rate (rETR). NanoPS<sub>42</sub> exposure already had a negative effect on the microalgae (see Figure 4.11) at the lowest treatment dose. Only day 9 and day 11 are discussed, as there was a measurement error in Tank 11 on day 10, and as these are relative measurements without a control, the values cannot be used without a control as reference. The results presented here are only from the seawater fraction. The Agg fraction results cannot be compared to each other due to a variation in the gain settings of the PHYTO-PAM-II instrument used. When cell levels are too high, the instrument does not record accurately. In future experiments, the cell concentration has to be lowered within the Agg fraction through dilution before dark incubation to avoid this problem. At low light levels,  $\text{QY}_{\text{max}}$  in treatment tanks did not differ significantly from controls. However, a two-fold difference was seen as light exposure increased to about  $150 \mu\text{mol}(\text{photons})/(\text{m}^2\text{s})$ . As light exposure increased further to about  $500 \mu\text{mol}(\text{photons})/(\text{m}^2\text{s})$ , the difference between the treatments and controls decreased, with the treatments consistently showing lower  $\text{QY}_{\text{max}}$  values. Significant reductions in  $\text{QY}_{\text{max}}$  and the rETR were observed following 11 days of nanoPS<sub>42</sub> exposure (see Figure 4.12 and Figure 4.13). With increasing light intensity past  $500 \mu\text{mol}/(\text{m}^2\text{s})$ , photo-damage and photo-inhibition of PSII becomes apparent in significantly lower  $\text{QY}_{\text{max}}$  and rETR values in all treatment tanks. Between  $150 \mu\text{mol}(\text{photons})/(\text{m}^2\text{s})$  -  $350 \mu\text{mol}(\text{photons})/(\text{m}^2\text{s})$ , the range in which the PSII is working efficiently, the rETR of the control tanks ramps up while the treatment tanks never go over half the rETR of the control tanks. These results show that nanoPS<sub>42</sub> impairs PSII and the rETR, leading to the overall photosystem efficiency going down compared to controls.



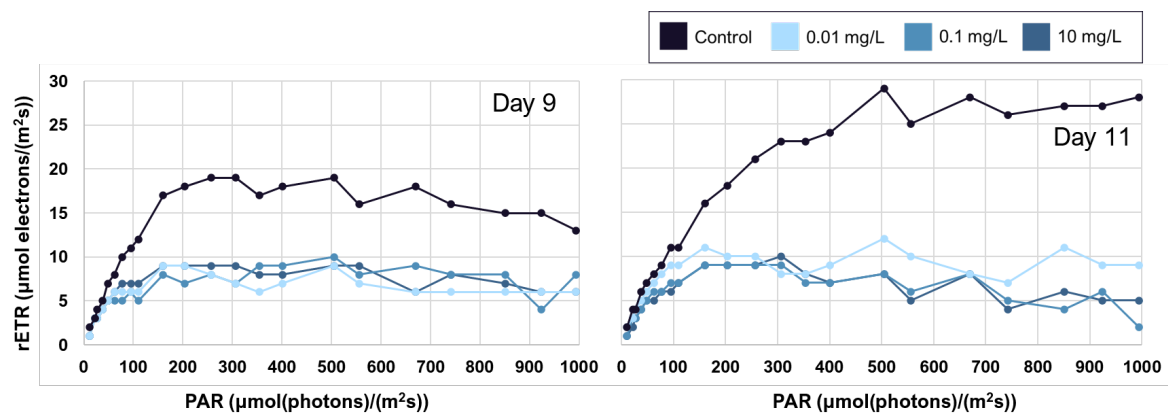


**Figure 4.11: The direct comparison of the rETR to the  $QY_{max}$  reveals the effects of nanoPS<sub>42</sub> exposure on the PSII.** At low light levels,  $QY_{max}$  in the treatment tanks did not differ significantly from controls. However, a two-fold decrease was seen as light exposure increased to  $\sim 150$   $\mu\text{mol}(\text{photons})/(\text{m}^2\text{s})$  in the treatment tanks (see red box). As the light intensity increased further to about  $500$   $\mu\text{mol}(\text{photons})/(\text{m}^2\text{s})$ , the difference between the treatments and controls decreased, even though the treatments consistently showed lower  $QY_{max}$  values. The red box indicates the Photosynthetic Active Radiation (PAR) range at which the photosystem is working optimally (see control values of  $QY_{max}$ , (a) and (b)) and the rETR is peaking in the controls (see (c) and (d)), but all treatment tanks show lower  $QY_{max}$  and rETR. With increasing light intensity, photo-damage and photo-inhibition of PSII becomes apparent in lower  $QY_{max}$  and rETR in all treatment tanks. No treatment-dependent differences among the treatment tanks were observed.

Interestingly, no treatment-dependent differences among the treatment tanks were observed. There have been no reports of rETR measured under nanoPS<sub>42</sub> exposure, so we cannot compare our results with those of other studies. A study by Mao et al. [150] theorizes that the reduction in the photosystem efficiency under plastic exposure is caused by an interplay of processes, most notably the reduction of the ETR, corresponding to our findings. It would be interesting to investigate the effects of even lower concentrations to see what is the minimal nanoPS<sub>42</sub> level required to start disrupting the photosystem.



**Figure 4.12: NanoPS<sub>42</sub> impairs PSII, seen as reduction in the effective quantum yield ( $QY_{\max}$  or  $F_v/F_m$ ).** In the presence of nanoPS<sub>42</sub> there is an observable difference in  $QY_{\max}$  over all light intensities between control and treatment tanks. (A) This trend is seen at 9 days (Kruskal-Wallis,  $p = 0.075$ ) and (B) becomes significant at 11 days (Kruskal-Wallis,  $p = 0.018$ ). Already at low light intensities, the photosystem of the control has a higher  $QY_{\max}$  (Holm-Sidak: day 9,  $p = 0.05$ ; day 11,  $p < 0.001$ ) than the treatment tanks and an increase in this difference can be seen over time. The reduction of the  $QY_{\max}$  with increasing light intensity follows the same pattern in control and treatment tanks.



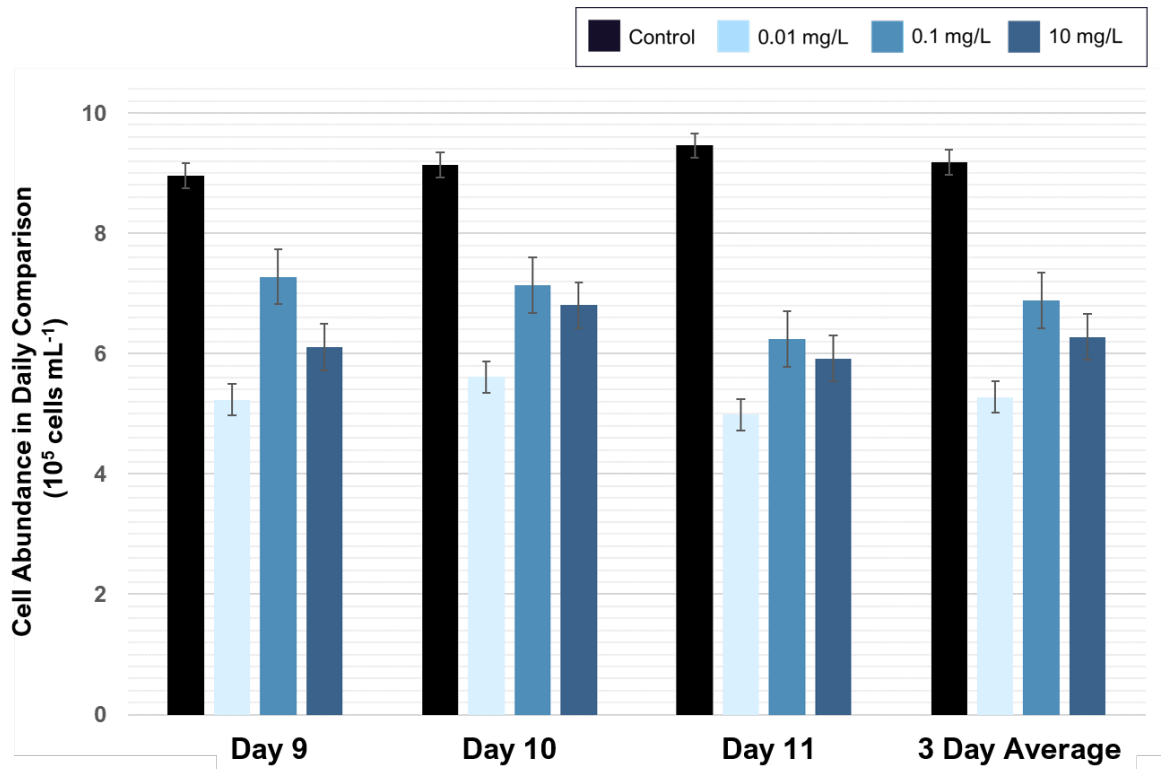
**Figure 4.13: nanoPS<sub>42</sub> exposure lowers photosynthetic activity of coral reef dinoflagellates under experimental conditions.** The increase of the rETR with increasing light intensity results in significantly higher values in the control (ANOVA,  $p < 0.001$ ) over the treatment tanks in the seawater fraction. In contrast to the  $QY_{\max}$ , which was only significantly impacted after 11 days of exposure, the rETR presented in this graph was also significantly reduced after 9 days of exposure (ANOVA,  $p = 0.001$ ). While under low light intensities there is no observable difference in the rETR of the control and treatment tanks, the rETR of the control quickly rises above that of the treatment tanks.

The combination of  $QY_{\max}$  and rETR values serves as an overall indicator of the health of PSII, photosynthetic performance, and light saturation in these cultures, leading to the conclusion that nanoPS<sub>42</sub> negatively influences the photosynthetic capacity of the microalgae studied. Photoinhibition has been reported in the presence of nanoPS<sub>42</sub> (<70 nm) for freshwater algae, *Scenedesmus*

sp. at 1 g/L [51] and *Chlorella* sp. at 1.8 mg/L [153] and for  $\mu\text{P}$  in Symbiodiniaceae *Cladocopium goreau* [166]. This PSII inhibition might be due to interactions between the nanoPS<sub>42</sub> and the cell membrane, inducing shading, and blocking of the gas exchange [153]. A molecular simulation study [336] predicted a permeation of the lipid membranes by polystyrene nanoparticles. If this holds true, the activity of membrane proteins could be affected by the nanoPS<sub>42</sub> particles, which could lead to the seen inhibitions of the photosystem, growth rates, and changes in aggregation. As photosymbionts, both *Symbiodinium tridacnidorum* and *Cladocopium* sp. photosystem' s inhibition in the presence of even low, environmentally possible concentrations on nanoPS<sub>42</sub> would have a significant impact on the overall health of the reef community. Further studies are necessary to show the correct relationship between the inhibition and the presence of nanoPS<sub>42</sub>. As there are changes to multiple genes in the RNA expression patterns of the photosystem related genes in *Cladocopium* sp. but only one gene is affected in *Symbiodinium tridacnidorum*, it becomes clear that nanoPS<sub>42</sub> affects the photosynthetic ability on a genetic level (see Section 4.4.5, Figures 4.21 and 4.20). *Cladocopium* sp. seems to be more susceptible to nanoPS<sub>42</sub> than *Symbiodinium tridacnidorum* which is seen in more affected genes (see Section 4.4.5, Tables B.3 and B.4). One remaining question for future experiments is, if the observed change in the photophysiology of the symbionts is reversibly after the nP is removed as well as if an adaption can be observed to this stress, as in [150].

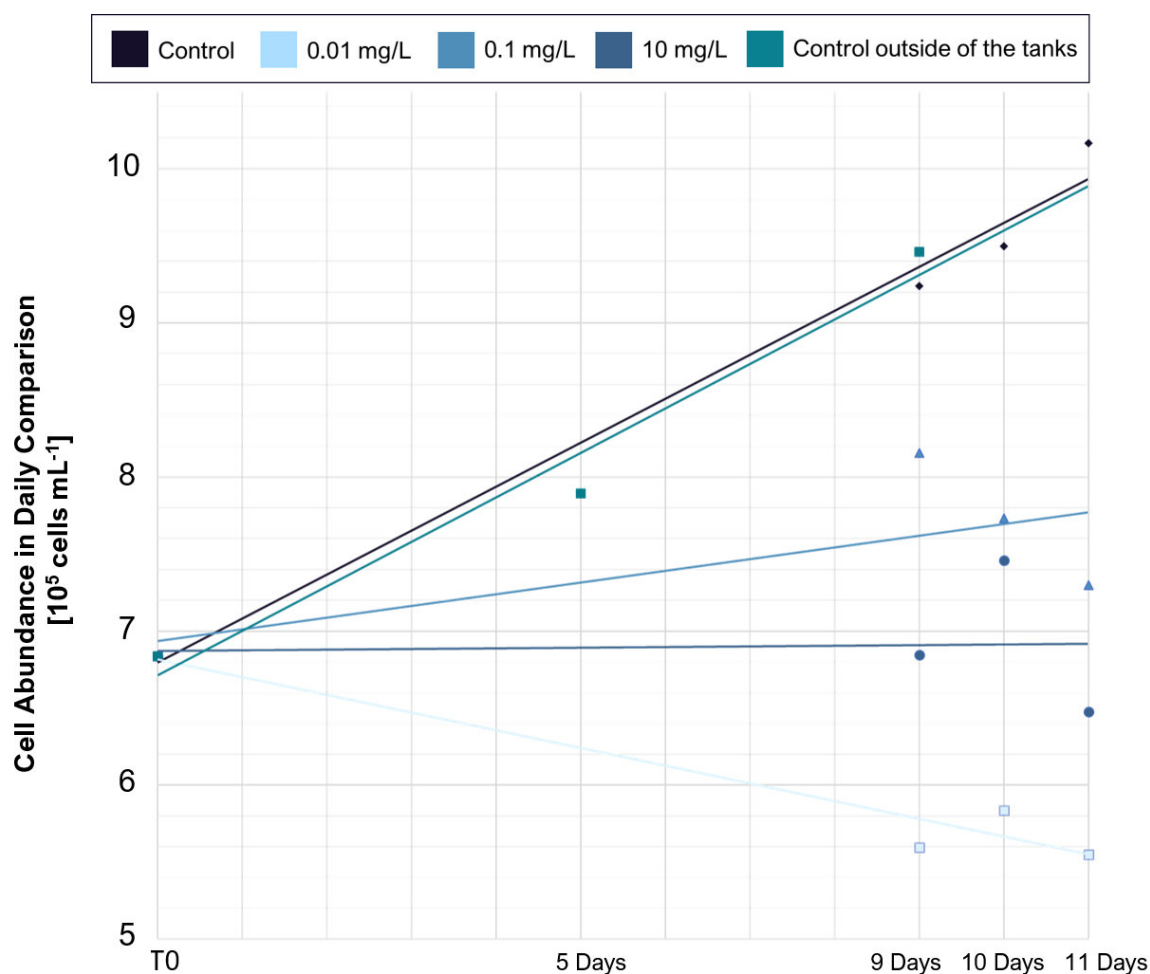
#### 4.4.3 Suppression of Algal Growth under nanoPS<sub>42</sub> Exposure

Exposure to nanoPS<sub>42</sub> decreases the mean growth rate of photosymbiotic algae (see Figure 4.14 and Figure 4.15). The greatest reduction in growth rate was seen at the lowest nanoPS<sub>42</sub> treatment (0.01 mg/L), with cell densities reduced from starting values by  $-0.062 \pm 0.02$  (Holm-Sidak,  $p = 0.002$ ); followed by the highest nanoPS<sub>42</sub> treatment (10 mg/L) with  $-0.013 \pm 0.05$  (Holm-Sidak,  $p=0.026$ ). In the 0.1 mg/L treatment, cell densities increased slightly by  $0.028 \pm 0.04$ . Thus, nanoPS<sub>42</sub> either inhibited algal growth in a non-linear manner or had a limited effect [145]. Reductions in growth rates have also been reported in the  $\mu\text{P}$  study of [166] in *Cladocopium goreau* and in other microalgae exposed to  $\mu\text{P}$  (*Chlamydomonas reinhardtii*, [149] and *Skeletonema costatum* [137]).



**Figure 4.14: Cell abundance in treatment and control tanks.** Treatment and control tanks were sampled after 9, 10, and 11 days. Experiments started with 680,000 cells/mL in all tanks. There are differences between the growth rate in the different treatments, but the ratio stays the same over all three sampling days. Bars display confidence interval.

In addition, Su et al. [166] reported a reduction in cell size in *Cladocopium* sp., further investigations are needed to see if this is the case under nP exposure. Interesting to note is that the biggest growth rate reduction observed was at 0.01 mg/L nanoPS<sub>42</sub>, far below the 5 mg/L used by Su et al. [166]. They propose “apoptosis promoting or proliferation and nutrient uptake inhibiting effects of  $\mu$ Ps” for their observation, stating that this “is consistent with the results of our transcriptomic analysis”. The nutrient deficiency is also a reason discussed in [136] which could explain the larger effects on growth rates at lower concentrations. The reason for nutrient limitation induced by plastic is proposed to be interactions of the nutrients with the surface of the plastics [151]. NanoPS<sub>42</sub> self aggregation could account for the higher nanoPS<sub>42</sub> treatments having less effect on the growth rates.



**Figure 4.15: Cell abundance in treatment and control tanks, and outside controls.** Treatment and control tanks were sampled after 9, 10, and 11 days. Experiments started with  $680,000$  cells/mL in all tanks. To control for the effect of the rolling tanks, an outside control (in a glass cylinder in the incubator under the same growth conditions as the cultures were raised) was also measured. The outside control and control tanks did not differ significantly, with growth rates of 12.45% and 15.01%, respectively (Holm-Sidak,  $p = 0.244$ ). The higher growth rate in the control tank compared to the outside control may be an artefact from counting in the hemocytometer, as the cells clump in aggregates. It was not possible to break the aggregates for counting in the cell counter. The cell density in the control was  $9.83 \pm 0.39 \times 10^5$  cells per mL, while treatment tanks were significantly lower: 0.01 mg/mL:  $5.69 \pm 0.12 \times 10^5$  cells per mL; 0.1 mg/mL:  $7.51 \pm 0.34 \times 10^5$  cells per mL; 10 mg/mL:  $6.96 \pm 0.40 \times 10^5$  cells per mL. Dotted lines show a linear regression trendline.

#### 4.4.4 Composition, 3D imaging for Internal Structure

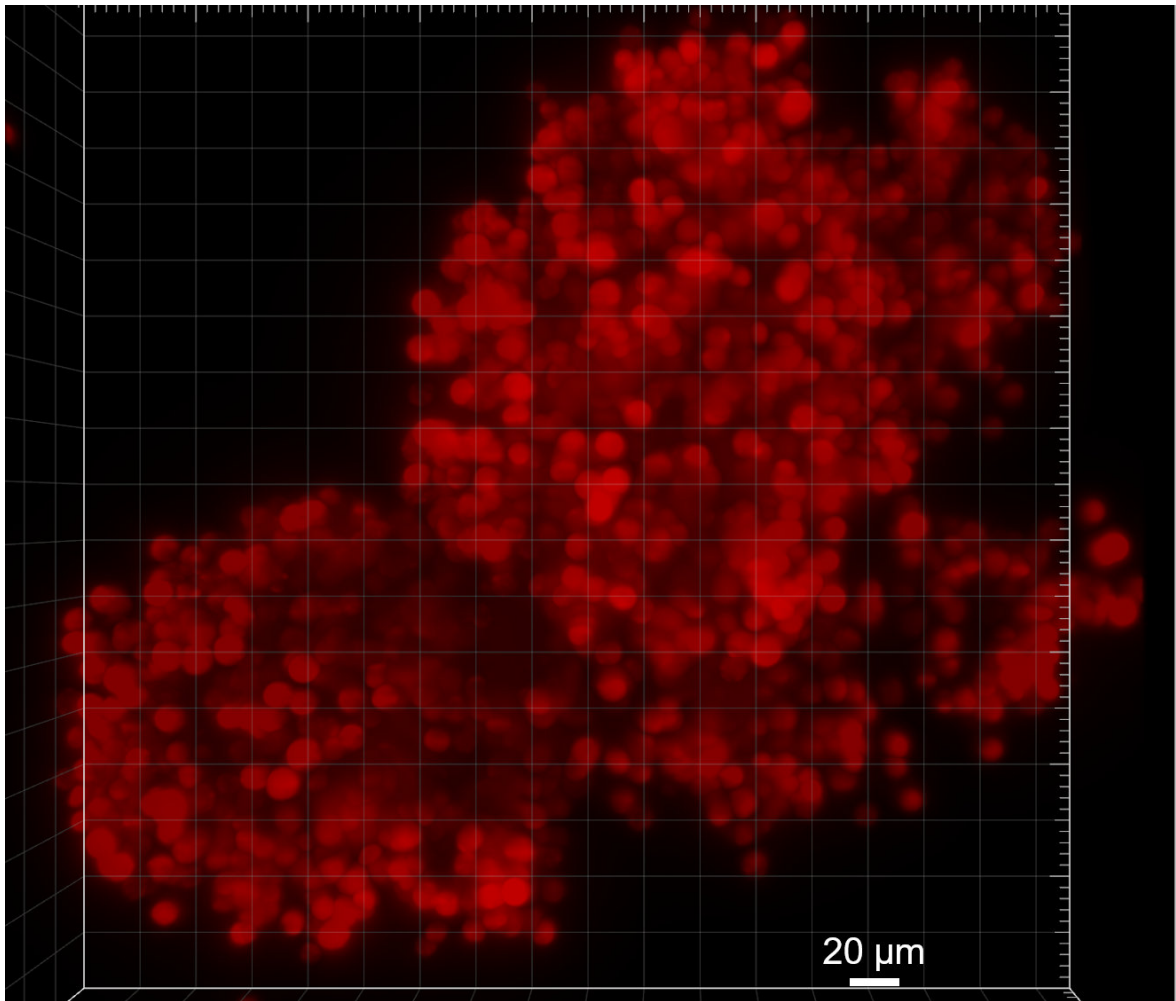
To check the distribution of plastic in the aggregates and to get some insight into the cell packaging differences at different treatments, 3D images were obtained using Zeiss Lightsheet Z.1. The nanoPS<sub>42</sub> was observed with a band-pass filter (excitation: 405 nm; emission: 505-545 nm) and chloroplasts were visible using a long-pass red filter (excitation: 488 nm, emission: 660 nm). In

these laser images, the plastic is green, and the cells are red. Individual nanoPS<sub>42</sub> cannot be seen, due to their small size, but clusters are visible. EPS, usually not visible with this technique can be seen because of the nanoPS<sub>42</sub> trapped inside. The bright green clusters of nanoPS<sub>42</sub> were observed only at the highest treatment. In the captions of the aggregates, the aggregate volume and bio-volume are given and compared. The bio-volume of an aggregate is the part of the aggregate volume that is taken by live cells. Most of the volume of aggregates is made up of water and EPS. This volume is calculated by counting the cells with the spot tool in Imaris. Table 4.2 gives a comparison of these measures over all treatments. The aggregates measured are smaller than the lowest size class measured for sinking velocities and thus cannot be compared to results of the sinking velocity.

**Table 4.2: Composition comparison in aggregates of all treatments.** The total estimated bio-volume is compared to the estimated aggregate volume and a ratio is presented. The total number of cells in the aggregate is given. For the bio-volume we consider the cells to be spherical with 10  $\mu\text{m}$  in diameter whereas the aggregate is roughly an ellipsoid. The equivalent spherical diameter (ESD) of the aggregate is also calculated. All of these aggregates are smaller than the tiny size class.

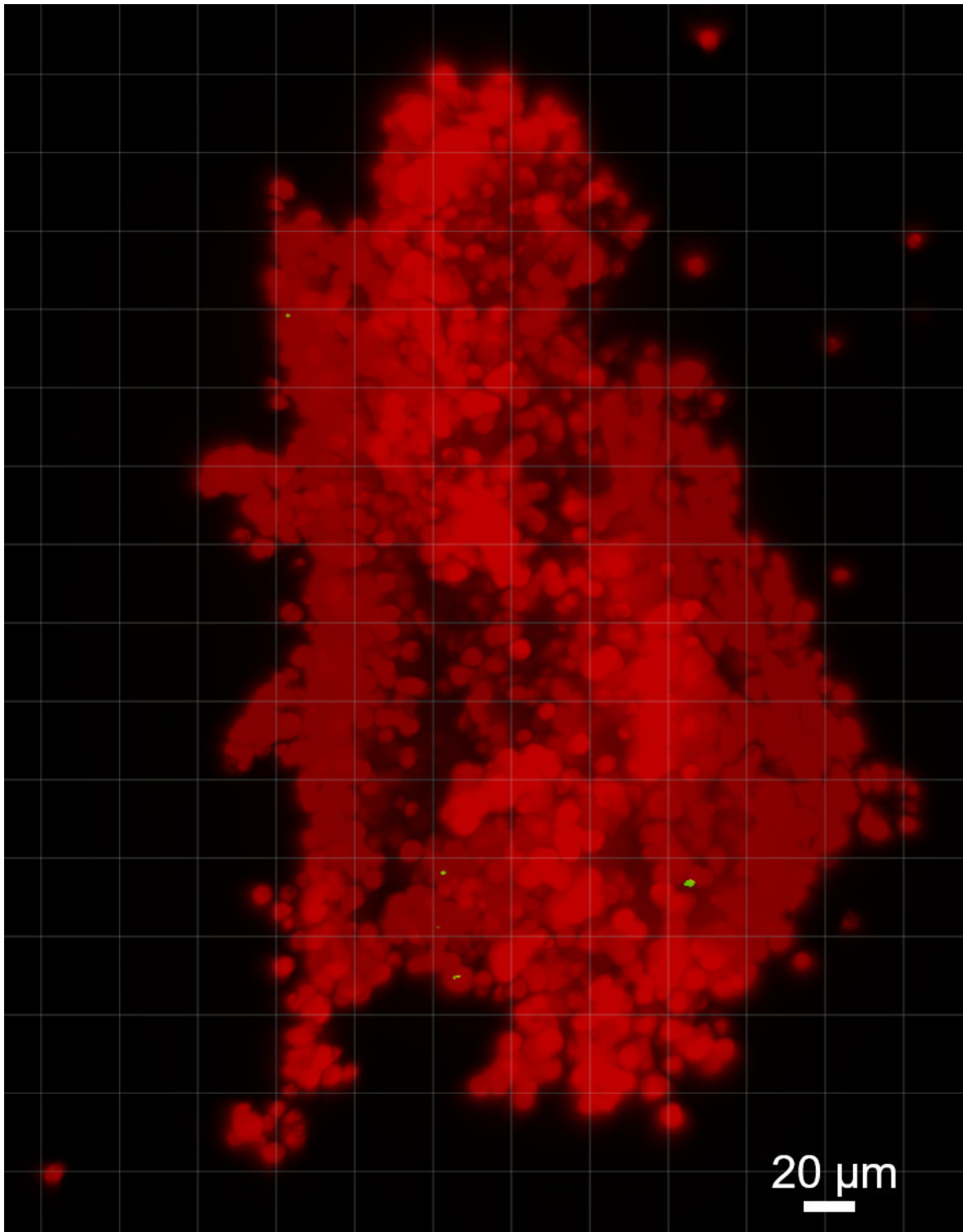
Treatment	Cells	Biovol. ( $\mu\text{m}^3$ )	Agg. Vol. ( $\mu\text{m}^3$ )	Agg. ESD ( $\mu\text{m}$ )	Ratio
nPS <sub>42</sub> @ control	611	319, 919	$3.39 \times 10^6$	186.31	9.45%
nPS <sub>42</sub> @ 0.01 mg/L	1439	753, 459	$1.14 \times 10^7$	279	6.62%
nPS <sub>42</sub> @ 0.1 mg/L	510	267, 035	$5 \times 10^6$	212	5.34%
nPS <sub>42</sub> @ 10 mg/L	663	347, 146	$2.77 \times 10^6$	174.3	12.5%





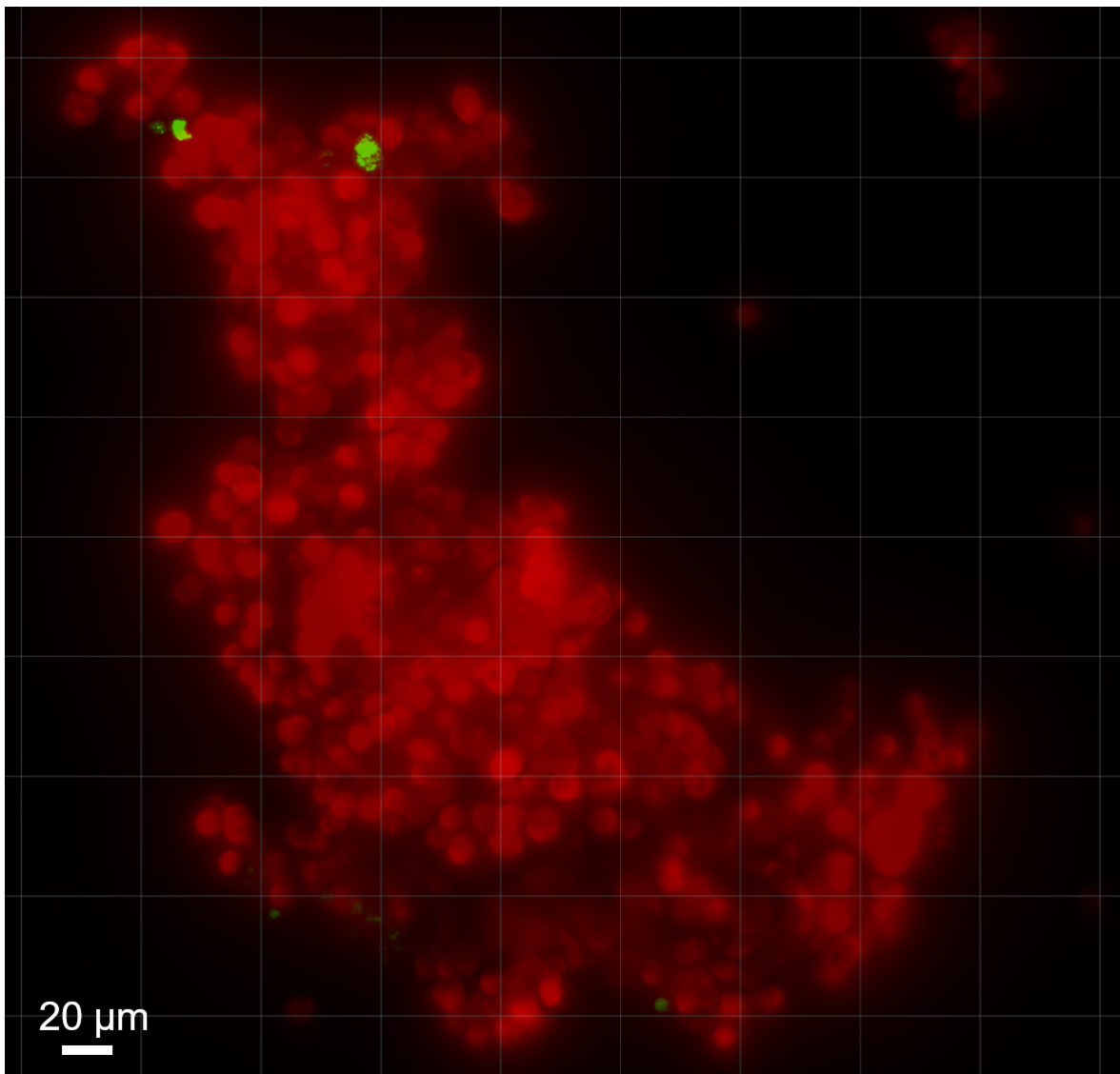
**Figure 4.16: 3D images of aggregate in the control.** Algal cells are shown in red. The aggregate is 249  $\mu\text{m}$  in height, 302  $\mu\text{m}$  in width and 86  $\mu\text{m}$  in depth. There are about 611 cells found in this aggregate and it has a volume of  $3.39 \times 10^6 \mu\text{m}^3$ . The bio-volume is  $3.2 \times 10^5 \mu\text{m}^3$ .

The control aggregate in Figure 4.16 displays a tiny aggregate with a diameter of 302  $\mu\text{m}$  in its longest dimension. The cell volume is  $3.2 \times 10^5 \mu\text{m}^3$  while the aggregate volume is  $3.39 \times 10^6 \mu\text{m}^3$ . This indicates that large parts of the aggregate are made up of water or EPS, which is the same as for previously described aggregates of other micro-algae species [189, 335] and corresponds to our results found in Chapter 3. Although the aggregate displayed here for the 0.01 mg/L treatment is slightly bigger than the control aggregate (see Figure 4.17), it still  $< 0.5 \text{ mm}$  in its longest dimension, placing it below the tiny size class. Disproportionately more cells are found in this aggregate (see Table 4.2).



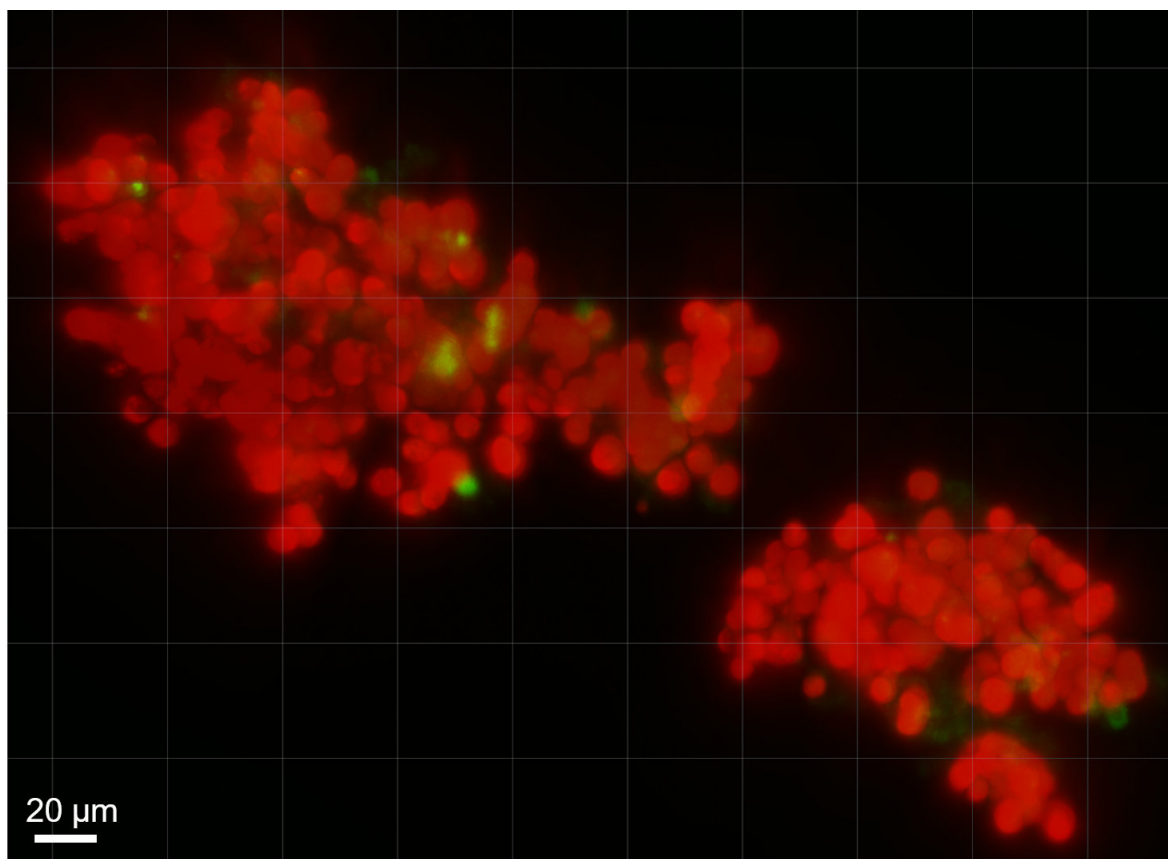
**Figure 4.17: 3D images of aggregates under low nanoPS<sub>42</sub> exposure.** Algal cells are shown in red, while nanoPS<sub>42</sub> is green. The aggregate is 457  $\mu\text{m}$  in height, 299  $\mu\text{m}$  in width, and 159  $\mu\text{m}$  in depth. There are about 1439 cells found in this aggregate. Only four small patches of nanoPS<sub>42</sub> are observed in the aggregate, but more could be located within, too small to be visible with this magnification. The total aggregate volume is  $1.14 \times 10^7 \mu\text{m}^3$  with a bio-volume of  $7.53 \times 10^5 \mu\text{m}^3$ .

With 1439 cells in an aggregate volume of  $1.14 \times 10^7 \mu\text{m}^3$ , it is not denser in cells than the aggregate found in the control treatment. As the aggregates measured do not belong to the size classes measured for sinking velocity, the theory of higher sinking velocities through higher cell packaging could still explain the observations. An increase in gene expression of genes related to various cell surface receptors (see Section 4.4.5, Figures 4.21 and 4.20) could be responsible for increased cell packaging. Increased amounts of the sticky fraction (TEP) of the EPS, and increased stickiness of that fraction [199] have been linked to nutrient deficiency, which in turn has been linked to  $\mu\text{P}$  exposure [151, 51]. This effect could be enhanced even more through the nanoPS<sub>42</sub>, which has a much higher surface area to cause these nutrient deficiencies.



**Figure 4.18:** 3D images of aggregate under medium nanoPS<sub>42</sub> exposure. Algal cells are shown in red, while nanoPS<sub>42</sub> is green. The clouds of nanoPS<sub>42</sub> are visible at the top of the aggregate, and at the bottom. The aggregate is 357  $\mu\text{m}$  in height, 250  $\mu\text{m}$  in width, and 107  $\mu\text{m}$  in depth. There are about 510 cells found in this aggregate. This aggregate has a total volume of  $5 \times 10^6 \mu\text{m}^3$  with a bio-volume of  $2.67 \times 10^5 \mu\text{m}^3$ .

The 0.1 mg/L nanoPS<sub>42</sub> exposure also led to faster sinking aggregates than the control (see Figure 4.18), while cell volume ( $2.67 \times 10^5 \mu\text{m}^3$ ) to aggregate volume ( $5 \times 10^6 \mu\text{m}^3$ ) ratio is not as dense as the lower plastic treatment. The aggregates of the highest nanoPS<sub>42</sub> treatment showed no changes in cell volume or aggregate volume to controls (see Figure 4.19).



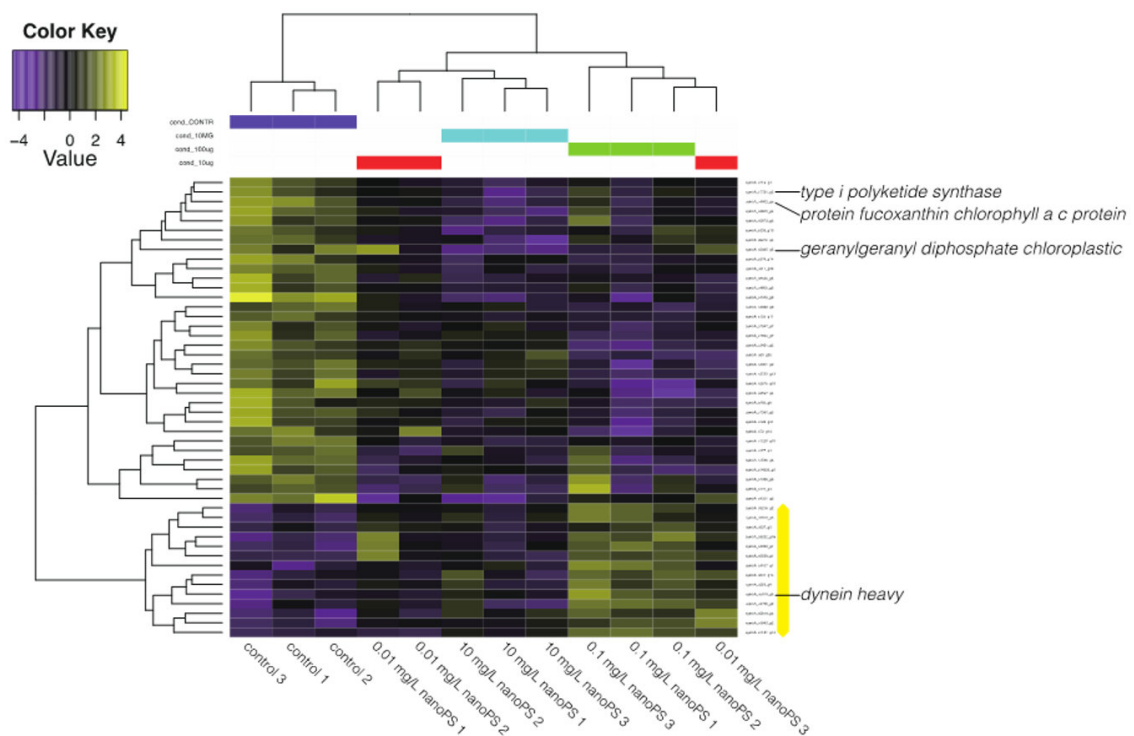
**Figure 4.19: 3D images of aggregates under high nanoPS<sub>42</sub> exposure.** Algal cells are shown in red, Clouds of nanoPS<sub>42</sub> can be seen brightly in the left aggregate, while the right one has much less nanoPS<sub>42</sub>. The left aggregate is 232  $\mu\text{m}$  in height, 123  $\mu\text{m}$  in width, and 32  $\mu\text{m}$  in depth. There are about 223 cells found in this aggregate. The bio-volume of this aggregate is  $1.17 \times 10^5 \mu\text{m}^3$ , while the total volume amounts to  $4.78 \times 10^5 \mu\text{m}^3$ . The right one is smaller, 137  $\mu\text{m}$  in height, 115  $\mu\text{m}$  in width, and 38  $\mu\text{m}$  in depth, with fewer cells,  $\sim 110$  cells. This aggregate is smaller, having a total volume of  $3.13 \times 10^5 \mu\text{m}^3$  with a bio-volume of  $84.28 \mu\text{m}^3$ .

Many differences have been observed between the treatment and the controls, in aggregation, sedimentation and photosystem efficiency. These can be linked to changes in the RNA expression patterns, discussed below.

#### 4.4.5 NanoPS<sub>42</sub> Effects on Gene Expression

Nine mRNA-seq libraries from nanoPS<sub>42</sub>-exposed photosymbiotic algae were sequenced (3 treatments  $\times$  3 exposure times) plus three controls. Using edgeR analysis, we identified differentially expressed genes (DEGs) between nanoPS<sub>42</sub>-exposed cells and controls. In *Symbiodinium tridacnidorum* algae, 14 genes were upregulated, and 34 were downregulated relative to controls (see

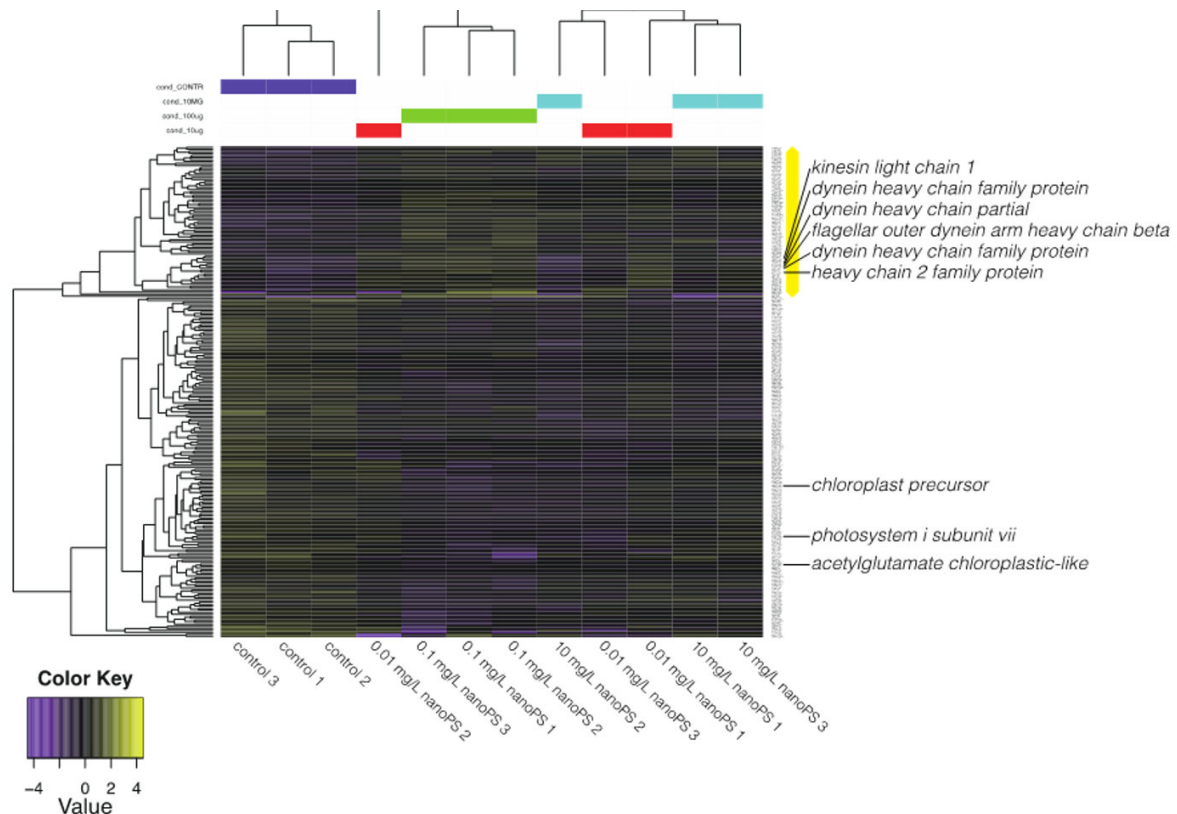
Figure 4.20).



**Figure 4.20: Heatmap and clustering of differentially expressed genes (2-fold changes) between dinoflagellates exposed to nPs and controls manifest cell responses in gene regulation level. DEGs in *Symbiodinium tridacnidorum*.** Values indicate the relative gene expression level, with purple and yellow showing downregulation and upregulation, respectively. The yellow bar shows a cluster of upregulated genes. Annotations by Blast2GO show the presence of microtubule- or photosynthesis-related genes among DEGs.

In *Cladocopium* sp., 75 genes were upregulated, and 169 genes were downregulated (see Figure 4.21). *Cladocopium* sp. seems more sensitive to nanoPS<sub>42</sub> exposure, as more genes responded than in *Symbiodinium tridacnidorum*.





**Figure 4.21: Heatmap and clustering of differentially expressed genes (two-fold changes) between dinoflagellates exposed to nPs and controls manifest cell responses in gene regulation level.** DEGs in *Cladocopium* sp.. Values indicate the relative gene expression level, with purple and yellow showing downregulation and upregulation, respectively. The yellow bar shows a cluster of upregulated genes. Annotations by Blast2GO show the presence of microtubule- or photosynthesis-related genes among DEGs.

DEGs were annotated using the Pfam database, a large collection of protein families [337], and BLAST2GO [338]. Since Pfam analysis had more annotations than BLAST2GO in DEGs of *Cladocopium* sp., we list the major domains encoded by the DEGs of *Cladocopium* sp. (see Appendix B.2 and Appendix B.4).

The largest group of upregulated genes was a subfamily of dynein-related proteins having an AAA\_5 domain (see Table 4.3). Dynein is a microtubule-associated motor protein [339]. Ten genes for dynein-related proteins with AAA (ATPase family associated with various cellular activities) and/or DHC (Dynein heavy chain) were upregulated in *Cladocopium* sp. by nanoPS<sub>42</sub> exposure (see Figure 4.3 and Appendix B.2). It has been shown that  $\mu$ P exposure induces production of reactive oxygen species (ROS) in microalgae [166, 145] and dynein upregulation, therefore, it might be needed to balance cytoskeletal dynamics as microtubule polymerization is impaired by oxidative stress [340]. Interestingly, dynein light chain genes were also shown to be upregulated in gill cells of zebra mussels exposed to polystyrene  $\mu$ P [341].



**Table 4.3: Domains encoded by more than three upregulated genes in *Cladocopium* sp.**

Domain name	Summary from Pfam database	Gene number
AAA_5	AAA domain (dynein-related subfamily)	6
DHC_N2	Dynein heavy chain, N-terminal region 2	5
AAA	ATPase family associated with various cellular activities	4
AAA_6	Hydrolytic ATP binding site of dynein motor region	4
TIG	IPT/TIG domain	4

Additionally, only one gene (symbA\_s5819\_g6) for dynein heavy chain was upregulated in *Symbiodinium tridacnidorum* (Appendix B.1 and Appendix B.3), which seems to indicate lower sensitivity to nanoPS<sub>42</sub> exposure. It also suggests that nanoPS<sub>42</sub> exposure in the Symbiodiniaceae has a similar effect to upregulation of dynein light chain in gill cells of zebra mussels by polystyrene  $\mu$ P exposures [341]. As dynein is also a flagellum-associated protein in dinoflagellates [342], examining the effect of nanoPS<sub>42</sub> on motile activity will be the subject of a future study.

Four upregulated genes in *Cladocopium* sp. (see Figure 4.3 and Appendix B.4) encoded proteins with TIG domains that have an immunoglobulin-like fold and are found in cell surface receptors that control cell dissociation [343, 344]. In *Symbiodinium tridacnidorum*, only one gene (symbA\_5216\_g2) for TIG was upregulated. This might contribute to adhesion between neighboring cells and to extracellular matrix composition, and explain some of the changes observed in cell aggregations.

There were more downregulated genes than upregulated ones in both *Symbiodinium tridacnidorum* and *Cladocopium* sp. (see Appendix B.1 and Appendix B.2). Expression of Ankyrin (ANK) repeat domain-containing protein was downregulated (see Figure 4.4) and is likely to result in reduced protein-protein interactions [345]. It is known that PPR (pentatricopeptide repeat) protein is involved in RNA editing [346] and extensive RNA editing has been reported in organelles of symbiotic dinoflagellates [347, 348]. The chloroplast precursor (s250\_g32) that is likely involved in the photosynthetic electron transport chain (GO:0009767) and PSI subunit VII (s2581\_g5) were downregulated in *Cladocopium* sp.. The gene (symbA\_s4902\_g5) for chlorophyll A-B-binding protein was also downregulated in *Symbiodinium tridacnidorum* (see Appendix B.1). These changes may explain our observed reductions in photosystem efficiency, as observed in *Cladocopium goreau* [166].

**Table 4.4: Domains encoded by more than three downregulated genes in *Cladocopium* sp.**

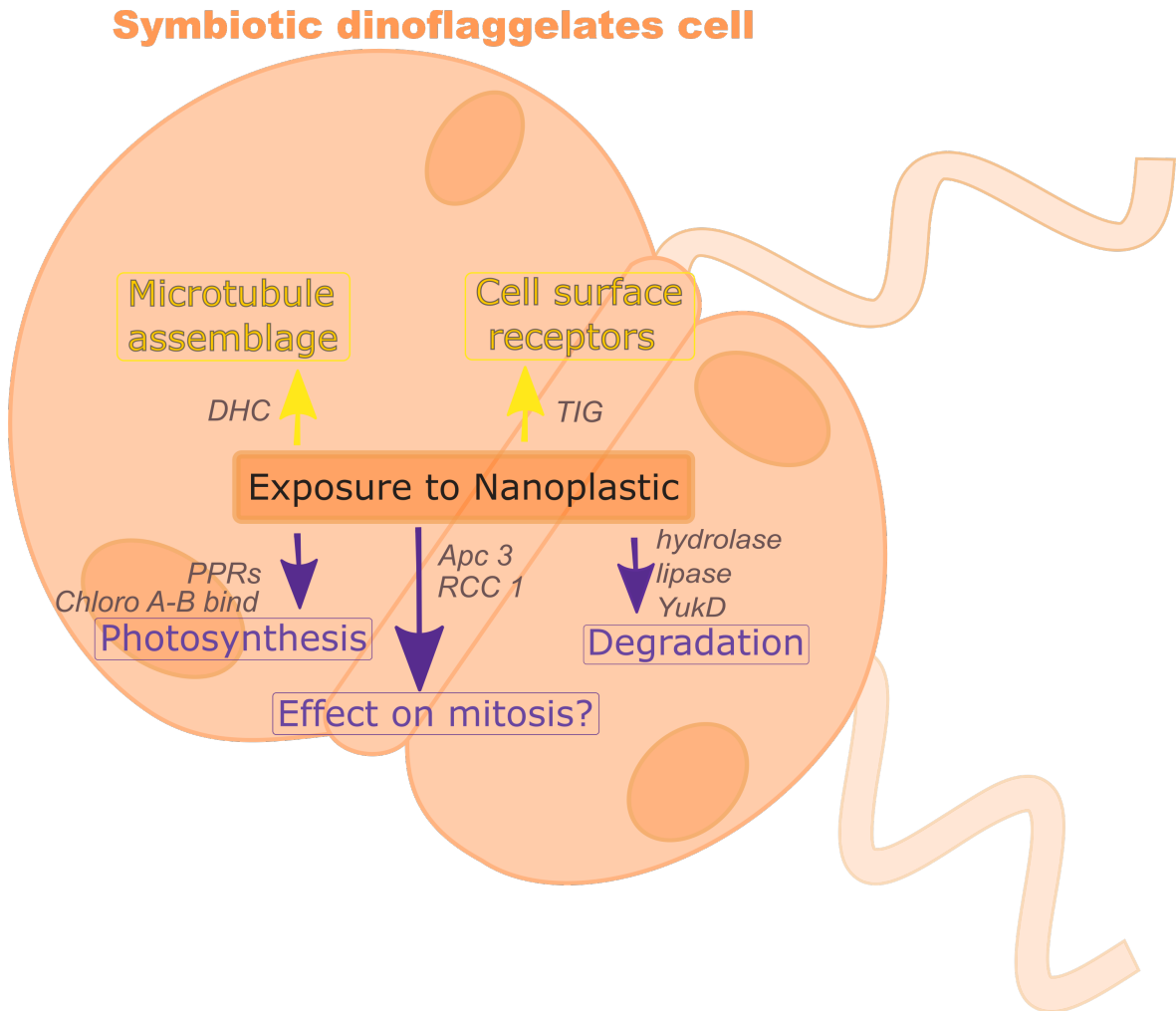
Domain name	Summary from Pfam database	Gene number
Ank	Ankyrin repeat	10
Ank_2	Ankyrin repeats (3 copies)	10
Ank_3	Ankyrin repeat	10
Ank_4	Ankyrin repeats (many copies)	10
Ank_5	Ankyrin repeats (many copies)	10
PPR_2	PPR repeat family	6
RCC1_2	Regulator of chromosome condensation (RCC1) repeat	6
ANAPC3 (Apc3)	Anaphase-promoting complex, cyclosome, subunit 3	5
Pkinase	Protein kinase domain	5
PPR	PPR repeat	5
PPR_3	Pentatricopeptide repeat domain	5
Abhydrolase_5	Alpha/beta hydrolase family	4
Abhydrolase_6	Alpha/beta hydrolase family	4
Lipase_3	Lipase (class 3)	4
PPR_1	PPR repeat	4
TPR_14	Tetratricopeptide repeat	4
YukD	WXG100 protein secretion system (Wss), protein YukD	4

Other downregulated gene groups were related to intracellular degradation processes, including hydrolase and lipase, and to subunit 3 of the anaphase-promoting complex/cyclosome [349]. When the gene, *s576\_g21*, for cell division control protein 2 is also downregulated, mitosis may be reduced in *Cladocopium* sp.. downregulation of six genes with RCC1 (regulator of chromosome condensation) and three genes with CDC (cell division control) domains also support that possibility. The downregulated gene (*s3282\_g2*) with abhydrolase and chlorophyllase domains is likely related to chlorophyll degradation [350].

In summary, several possible negative effects on symbiotic dinoflagellates by nanoPS are documented and negative consequences are suggested by DEGs (see Figure 4.22). The major gene groups that are modulated by nanoPS<sub>42</sub> exposure are dynein-related genes, photosynthesis-related genes, and mitosis-related genes with likely consequences for motility, aggregation, metabolism, and reproduction of algal symbionts.

## 4.5 Conclusion

Previous studies have shown that nP leads to adverse effects in different algae groups [51, 151, 164], and a recent study shows that  $\mu$ P has a similar effect on an endosymbiotic dinoflagellate *Cladocopium goreau* [166]. No previous studies have been conducted on nP effects on Symbiodiniaceae. We found significant changes in aggregation, sinking velocity, and photosystem efficiency of *Symbiodinium tridacnidorum* and *Cladocopium* sp., coupled with variations in gene expression patterns after exposure to nanoPS<sub>42</sub> (see Figure 4.22). This suggests that nP in coral reef ecosystems have the potential to influence the acquisition of symbionts by mollusks and corals, likely damaging these symbiotic relationships. Since both are the architects of reef structure, nanoPS<sub>42</sub> pollution has the potential to lead to structural changes in reef ecosystem dynamics.



**Figure 4.22:** Exposure to nanoPS<sub>42</sub> changes gene expression levels in symbiotic dinoflagellates. Yellow and purple arrows show upregulation and downregulation of gene expression, respectively.

In *Symbiodinium tridacnidorum*, 14 genes were upregulated, and 34 were downregulated relative to controls. In *Cladocopium* sp., 75 genes were upregulated, and 169 genes were downregulated. *Cladocopium* sp. seems more sensitive to nanoPS<sub>42</sub> exposure, as more genes responded than in *Symbiodinium tridacnidorum*.



# Chapter 5

## Conclusion and Outlook

In isolation,  $\mu\text{P}/\text{nP}/\text{MF}$  are certainly not the most toxic - neither lethal nor sublethal - environmental pollutants. Nevertheless,  $\mu\text{P}/\text{nP}/\text{MF}$  are now near-permanent constituents of natural marine environments globally. The continuous addition of new plastics and subsequent fragmentation will ensure  $\mu\text{P}/\text{nP}/\text{MF}$  will remain a long-term problem. As even the smallest plastics ( $<1\ \mu\text{m}$ ) have been found in the surface waters of the oceans [351] and  $\mu\text{P}$  in and throughout the water column [94] with MF in the deep sea [157], the potential for exposure of open ocean plankton communities has been established.

### 5.1 Open Ocean - Plankton Communities Under Change

Net primary production by plankton communities in the oligotrophic open oceans is comparable to terrestrial rain forests [352], making these communities responsible for extracting and converting vast amounts of atmospheric carbon into biomass.

The results of Chapter 2 of this thesis work detail how  $\mu\text{P}/\text{nP}/\text{MF}$  affect aggregation and sedimentation along with TEP production and photosynthesis of different fractions of plankton communities. Aggregation of otherwise spread out phytoplankton cells makes them available for different predators [206] (see Figure 2.1) which has potential implications for the marine food web as it would shift the plankton community to bigger grazers. Sedimentation affects the carbon cycle and the length of time that  $\mu\text{P}/\text{nP}/\text{MF}$  are retained within the water column, with potential disruptions of the deep-sea food web. Moreover, TEP production in the different species in this study was affected, often resulting in changes in aggregation and sedimentation. Last but not least, reduction of the photosynthesis process has negative implications for the yearly  $\text{O}_2$  production and carbon fixation, but research on this topic is still in its early phase.

Based on widely varying responses by the diatoms *Skeletonema grethae* and *Odontella aurita*, and the cyanobacterium *Synechococcus elongatus* to different  $\mu\text{P}/\text{nP}/\text{MF}$ , a shift in plankton communities favoring those species that deal best with plastic is possible. A similar shift has been found in the community members on the plastisphere, which differs from surrounding seawater communities [64]. In the same way, the incorporation of  $\mu\text{P}/\text{nP}/\text{MF}$  could lead to a shift in the interacting plankton communities.

To understand the intricacies and interactions of  $\mu\text{P}/\text{nP}/\text{MF}$  with the plankton communities, effect studies on a large scale in mesocosms are needed. These should include environmentally relevant and future projected  $\mu\text{P}/\text{nP}/\text{MF}$  concentrations [353] but also naturally occurring particles

as controls [122].

Physical effects on the planktonic species used were found, thereby answering the first question posed in the Introduction. Differing from species to species and between plastic types and concentrations, effects were measured in aggregation and TEP production, leading to different sedimentation. Photophysiology was affected too, but those results need to be viewed with care, as their ecological transferability is uncertain. The second question about the carbon pump's infiltration via aggregation with phytoplankton should be answered with yes, especially the gravitational settling of biomass will be affected with the growing abundance of these tiny pollutants.

## 5.2 Coastal Waters - Plastics around Okinawa

Since, for logistic reasons, it was not possible to perform a long-term / repeated inventory of microplastics in Okinawan coastal waters, this project remains a snapshot on temporal and spatial scales. Integrating typhoons and rainy seasons into a more comprehensive study would vastly contribute to the understanding of  $\mu\text{P}/\text{nP}/\text{MF}$  pollution under different weather conditions. Increasing the spatial aspect by sampling different depths of the water column would allow for more informed conclusions about the fate and distribution of microplastics around Okinawa.

Chapter 3 presents a snapshot of marine  $\mu\text{P}$  pollution around Okinawa. It follows the human population density, with the most abundant polymer type being PE (45%). Our study is consistent with Japanese [253, 240] and global [264, 265, 266] studies.  $\mu\text{P}$  were found at 10 out of 11 stations, while smaller sub-20  $\mu\text{m}$  particles were found to be ubiquitous. In addition, the smaller plastics were embedded in organic matter at a higher percentage (68.75% vs. 31.25% free-floating), making them easy to be ingested accidentally. The incorporation of these smaller plastics within marine aggregates also contributes to their inclusion into the food web, as well as making it more likely that these particles will be deposited on the seafloor if not ingested as marine snow. This connection to the infiltration of the carbon pump introduced Chapter 2.

Trace metals have been found on many of the analysed  $\mu\text{P}$ , including toxic ones such as Chromium (Cr), Arsenic (As) and Lead (Pb) following weathering patterns on the grooves of  $\mu\text{P}$  and Mercury (Hg) and Zinc (Zn) evenly distributed. These  $\mu\text{P}$  and MF embedded into organic matter and contaminated with trace metals from the near-shore coastal waters poses clearly pose a risk to neighboring ecosystems. As marine ecosystems are interconnected through wind and currents, characterizing one system will contribute to the knowledge of the surrounding systems – in this case subtropical reefs, stressed by tourism, fishery, and climate change.

## 5.3 Inside the Reef - Impacts on Endosymbionts

Coral reef environments have been shown to carry high loads of  $\mu\text{P}/\text{nP}/\text{MF}$  at various locations within the reef [280, 92, 279, 278].

Laboratory experiments presented in Chapter 4 show that nanoPS<sub>42</sub> exposure of the endosymbiotic dinoflagellates *Symbiodinium tridacnidorum* and *Cladocopium* sp. leads to differentially expressed genes which could be causing the observed changes in growth rates, photosynthesis, aggregation, and subsequent sedimentation. The major gene groups that are modulated by nanoPS<sub>42</sub> exposure are dynein-related genes, photosynthesis-related genes, and mitosis-related genes with likely consequences for motility, aggregation, metabolism, and reproduction of algal symbionts. This



correspondence between the results of the RNA analysis with the outcomes of the photophysiology measurements, growth rates and aggregation leads to the conclusion that nanoPS<sub>42</sub> affects the endosymbionts on a genetic level.

In the literature, similar negative results have been reported. Exposure of corals to  $\mu\text{P}$  of similar size to endosymbionts has led to endosymbionts being expelled from the coral [284], and various reef inhabitants have been shown to ingest  $\mu\text{P}$  [92, 114, 324]. Although the exact process of *Symbiodinium* spp. infection is unknown, affecting the endosymbiont before infections and reducing the accessibility by increased sedimentation can well prove detrimental to an already gravely stressed ecosystem.

In light of these results, more studies on the effects of nanoplastics on the reef environment and the endosymbiont that fuels this oligotrophic environment are needed. Multi-stressor experiments, combining increased temperature and ocean acidification with nanoplastic exposure and allowing for control particles such as silt and sand, would be ideal for increasing insight into these complex interactions.

In summary, several possible negative effects on symbiotic dinoflagellates by nanoPS are documented and negative consequences are suggested by DEGs (see Figure 4.22).



# Bibliography

- [1] DeBono, H., Goren-Inbar, N. “Note on a link between Acheulian handaxes and the Levallois method”. In: *Journal of the Israel Prehistoric Society* 31.9 (2001), p. 23.
- [2] Ran Barkai. “Resharpener and Recycling of Flint Bifacial Tools from the Southern Levant Neolithic and Chalcolithic”. In: *Proceedings of the Prehistoric Society* 65 (1999), pp. 303–318. ISSN: 0079-497X. DOI: [10.1017/s0079497x00002036](https://doi.org/10.1017/s0079497x00002036).
- [3] Ron Shimelmitz and Sharon Zuckerman. *Flint knapping in the late bronze age: A dying technology? a perspective from the lower city of hazor*. 2014. DOI: [10.1179/0075891413Z.00000000035](https://doi.org/10.1179/0075891413Z.00000000035).
- [4] H. Martin. “Silex a double patine”. In: *Bulletin de la Société Préhistorique de France* 3 (1906), pp. 273–274.
- [5] Jean Louis Martin, Virginie Maris, and Daniel S. Simberloff. “The need to respect nature and its limits challenges society and conservation science”. In: *Proceedings of the National Academy of Sciences of the United States of America* 113.22 (2016), pp. 6105–6112. ISSN: 10916490. DOI: [10.1073/pnas.1525003113](https://doi.org/10.1073/pnas.1525003113).
- [6] Daniel S. Amick. “Reflection on the origins of recycling: A paleolithic perspective”. In: *Lithic Technology* 39.1 (2014), pp. 64–69. ISSN: 01977261. DOI: [10.1179/0197726113Z.00000000025](https://doi.org/10.1179/0197726113Z.00000000025).
- [7] Sheeana Gangadoo et al. “Nano-plastics and their analytical characterisation and fate in the marine environment: From source to sea”. In: *Science of the Total Environment* 732 (2020), p. 138792. ISSN: 18791026. DOI: [10.1016/j.scitotenv.2020.138792](https://doi.org/10.1016/j.scitotenv.2020.138792). URL: <https://doi.org/10.1016/j.scitotenv.2020.138792>.
- [8] Imre Szeman. “System failure: Oil, futurity, and the anticipation of disaster”. In: *South Atlantic Quarterly* 106.4 (2007), pp. 805–823. ISSN: 00382876. DOI: [10.1215/00382876-2007-047](https://doi.org/10.1215/00382876-2007-047).
- [9] Yoshito Ohtake et al. “Studies on biodegradation of LDPE - Observation of LDPE films scattered in agricultural fields or in garden soil”. In: *Polymer Degradation and Stability* 60.1 (1998), pp. 79–84. ISSN: 01413910. DOI: [10.1016/S0141-3910\(97\)00032-3](https://doi.org/10.1016/S0141-3910(97)00032-3).
- [10] John N. Hahladakis et al. “An overview of chemical additives present in plastics: Migration, release, fate and environmental impact during their use, disposal and recycling”. In: *Journal of Hazardous Materials* 344 (Feb. 2018), pp. 179–199. ISSN: 18733336. DOI: [10.1016/j.jhazmat.2017.10.014](https://doi.org/10.1016/j.jhazmat.2017.10.014). URL: <http://dx.doi.org/10.1016/j.jhazmat.2017.10.014>.





- [33] Kay Critchell and Jonathan Lambrechts. “Modelling accumulation of marine plastics in the coastal zone; what are the dominant physical processes?” In: *Estuarine, Coastal and Shelf Science* 171 (2016), pp. 111–122. ISSN: 02727714. DOI: [10.1016/j.ecss.2016.01.036](https://doi.org/10.1016/j.ecss.2016.01.036). URL: <http://dx.doi.org/10.1016/j.ecss.2016.01.036>.
- [34] C. Anela Choy et al. “The vertical distribution and biological transport of marine microplastics across the epipelagic and mesopelagic water column”. In: *Scientific Reports* 9.1 (2019), pp. 1–9. ISSN: 20452322. DOI: [10.1038/s41598-019-44117-2](https://doi.org/10.1038/s41598-019-44117-2).
- [35] Shahidul Md. Islam and Masaru Tanaka. “Impacts of pollution on coastal and marine ecosystems including coastal and marine fisheries and approach for management: a review and synthesis”. In: *Marine Pollution Bulletin* 48.7-8 (2004), pp. 624–649. ISSN: 0025326X. DOI: [10.1016/j.marpolbul.2003.12.004](https://doi.org/10.1016/j.marpolbul.2003.12.004).
- [36] D. K.A. Barnes and P. Milner. *Drifting plastic and its consequences for sessile organism dispersal in the Atlantic Ocean*. Mar. 2005. DOI: [10.1007/s00227-004-1474-8](https://doi.org/10.1007/s00227-004-1474-8).
- [37] B. Munier and L. I. Bendell. “Macro and micro plastics sorb and desorb metals and act as a point source of trace metals to coastal ecosystems”. In: *PLOS ONE* 13.2 (Feb. 2018). Ed. by Amitava Mukherjee, e0191759. ISSN: 1932-6203. DOI: [10.1371/journal.pone.0191759](https://doi.org/10.1371/journal.pone.0191759). URL: <https://dx.plos.org/10.1371/journal.pone.0191759>.
- [38] David K A Barnes et al. “Accumulation and fragmentation of plastic debris in global environments”. In: *Philosophical Transactions of the Royal Society B: Biological Sciences* 364.1526 (June 2009), pp. 1985–1998. ISSN: 0962-8436. DOI: [10.1098/rstb.2008.0205](https://doi.org/10.1098/rstb.2008.0205). URL: <http://rstb.royalsocietypublishing.org/content/364/1526/1985.abstract> <http://dx.doi.org/10.1098/rstb.2008.0205> <http://www.ncbi.nlm.nih.gov/pubmed/19528051> <http://www.ncbi.nlm.nih.gov/pmc/articles/PMC2873009> <http://rstb.royalsocietypublishing.org/cgi/pmidl>.
- [39] Murray R Gregory. “Environmental implications of plastic debris in marine settings—entanglement, ingestion, smothering, hangers-on, hitch-hiking and alien invasions”. In: *Philosophical Transactions of the Royal Society B: Biological Sciences* 364.1526 (June 2009), 2013 LP–2025. DOI: [10.1098/rstb.2008.0265](https://doi.org/10.1098/rstb.2008.0265). URL: <http://rstb.royalsocietypublishing.org/content/364/1526/2013.abstract>.
- [40] Judith E. Winston. “Drift plastic—An expanding niche for a marine invertebrate?” In: *Marine Pollution Bulletin* 13.10 (Oct. 1982), pp. 348–351. ISSN: 0025326X. DOI: [10.1016/0025-326X\(82\)90038-8](https://doi.org/10.1016/0025-326X(82)90038-8). URL: <http://linkinghub.elsevier.com/retrieve/pii/0025326X82900388>.
- [41] Alex Sivan. “New perspectives in plastic biodegradation”. In: *Current Opinion in Biotechnology* 22.3 (2011), pp. 422–426. ISSN: 09581669. DOI: [10.1016/j.copbio.2011.01.013](https://doi.org/10.1016/j.copbio.2011.01.013).
- [42] Charles James Moore. “Synthetic polymers in the marine environment: a rapidly increasing, long-term threat”. In: *Environ. Res.* 108.2 (2008), pp. 131–139. ISSN: 0013-9351. DOI: [10.1016/j.envres.2008.07.025](https://doi.org/10.1016/j.envres.2008.07.025). URL: <http://www.ncbi.nlm.nih.gov/pubmed/18949831> <http://dx.doi.org/10.1016/j.envres.2008.07.025> [http://All%20Papers/M/Moore%202008%20-%20Synthetic%20polymers%](http://All%20Papers/M/Moore%202008%20-%20Synthetic%20polymers%20)



- 20in%20the%20marine%20environment%20-%20a%20rapidly%20increasing,  
%20long-term%20threat.pdf.
- [43] Rebeca Lozano Lopez and John Mouat. *Marine litter in the North-East Atlantic Region*. 2009, pp. 1–136.
- [44] *The Ocean Cleanup*. URL: <https://theoceancleanup.com/> (visited on 02/21/2020).
- [45] Richard C. Thompson et al. “Lost at Sea: Where Is All the Plastic?” In: *Science* 304.5672 (May 2004), 838 LP –838. ISSN: 0036-8075. DOI: 10.1126/science.1094559. URL: <http://science.sciencemag.org/content/304/5672/838.abstract%20All%20Papers/T/Thompson%20et%20al.%202004%20-%20Lost%20at%20Sea%20-%20Where%20Is%20All%20the%20Plastic.pdf>.
- [46] Edward J. Carpenter and K L Smith. “Plastics on the Sargasso Sea Surface”. In: *Science (New York, N.Y.)* 175.4027 (1972), pp. 1240–1241. DOI: 10.1126/science.175.4027.1240.
- [47] Andrés Cózar et al. “Plastic debris in the open ocean.” In: *Proc. Natl. Acad. Sci. U. S. A.* 111.28 (July 2014), pp. 10239–10244. ISSN: 1091-6490. DOI: 10.1073/pnas.1314705111. URL: <http://www.pnas.org/cgi/content/short/111/28/10239%20http://dx.doi.org/10.1073/pnas.1314705111%20http://www.ncbi.nlm.nih.gov/pubmed/24982135%20http://www.ncbi.nlm.nih.gov/pmc/articles/PMC4104848%20http://www.pnas.org/cgi/pmidlookup?view=long%7B%5C%7Dpmid=24982135%20All%20Pap>.
- [48] V Hidalgo-Ruz, M Thiel - Marine environmental Research, and undefined 2013. “Distribution and abundance of small plastic debris on beaches in the SE Pacific (Chile): a study supported by a citizen science project”. In: *Elsevier* (). DOI: 10.1016/j.marenvres.2013.02.015. URL: <https://www.sciencedirect.com/science/article/pii/S0141113613000445>.
- [49] R. Jude Wilber. *Plastic in the North Atlantic*. 1987.
- [50] Albert A. Koelmans et al. “Risks of Plastic Debris: Unravelling Fact, Opinion, Perception, and Belief”. In: *Environmental Science and Technology* 51.20 (Oct. 2017), pp. 11513–11519. ISSN: 15205851. DOI: 10.1021/acs.est.7b02219.
- [51] Ellen Besseling et al. “Nanoplastic affects growth of *S. obliquus* and reproduction of *D. magna*”. In: *Environmental Science and Technology* 48.20 (2014), pp. 12336–12343. ISSN: 1520-5851. DOI: 10.1021/es503001d. URL: <http://dx.doi.org/10.1021/es503001d%20http://www.ncbi.nlm.nih.gov/pubmed/25268330%20http://pubs.acs.org/doi/pdf/10.1021/es503001d%20All%20Papers/B/Besseling%20et%20al.%202014%20-%20Nanoplastic%20affects%20growth%20of%20S.%20obliquus%20and%20reproduction%20of%20D.%20magna.pdf>.
- [52] Kara Law and Richard C. Thompson. “Microplastics in the seas - Concern is rising about widespread contamination of the marine environment by microplastics”. In: *Science* 345.6193 (2014), pp. 144–145. ISSN: 00218790. DOI: 10.1002/2014EF000240/polymer.
- [53] European Environment Agency. *Marine Strategy Framework Directive* —. URL: <https://www.eea.europa.eu/policy-documents/2008-56-ec>.

- [54] Christiane Zarfl et al. “Microplastics in oceans”. In: *Marine Pollution Bulletin* 62.8 (2011), pp. 1589–1591. ISSN: 0025326X. DOI: [10.1016/j.marpolbul.2011.02.040](https://doi.org/10.1016/j.marpolbul.2011.02.040).
- [55] Makoto Ōmori and Tsutomu Ikeda. *Methods in marine zooplankton ecology*. Malabar Fla.: Krieger, 1992, p. 332.
- [56] C. Arthur, J. Baker, and H. Bamford. “Effects and Fate of Microplastic Marine Debris”. In: *Proceedings of the International Research Workshop on the Occurrence, Effects and Fate of Microplastic Marine Debris*. 2009.
- [57] Martin Wagner et al. “Microplastics in freshwater ecosystems : what we know and what we need to know”. In: *Environmental Sciences Europe* (2014), pp. 1–9. DOI: [10.1186/s12302-014-0012-7](https://doi.org/10.1186/s12302-014-0012-7).
- [58] Albert A. Koelmans, Ellen Besseling, and Won J Shim. *Marine Anthropogenic Litter (Chapter 12)*. Ed. by Melanie Bergmann, Lars Gutow, and Michael Klages. 2015.
- [59] Skye Morét-Ferguson et al. “The size, mass, and composition of plastic debris in the western North Atlantic Ocean”. In: *Marine Pollution Bulletin* 60.10 (2010), pp. 1873–1878. ISSN: 0025326X. DOI: [10.1016/j.marpolbul.2010.07.020](https://doi.org/10.1016/j.marpolbul.2010.07.020).
- [60] Alexandra Ter Halle et al. “Nanoplastic in the North Atlantic Subtropical Gyre”. In: *Environmental Science and Technology* 51.23 (2017), pp. 13689–13697. ISSN: 15205851. DOI: [10.1021/acs.est.7b03667](https://doi.org/10.1021/acs.est.7b03667).
- [61] Anthony L. Andrady. “Weathering of polyethylene (LDPE) and enhanced photodegradable polyethylene in the marine environment”. In: *Journal of Applied Polymer Science* 39.2 (1990), pp. 363–370. ISSN: 10974628. DOI: [10.1002/app.1990.070390213](https://doi.org/10.1002/app.1990.070390213).
- [62] G. Geuskens. “Chapter 3 Photodegradation of Polymers”. In: *Comprehensive Chemical Kinetics* 14.C (1975), pp. 333–424. ISSN: 00698040. DOI: [10.1016/S0069-8040\(08\)70335-2](https://doi.org/10.1016/S0069-8040(08)70335-2).
- [63] I C McNeill. “Thermal degradation [of polymers]”. In: *Comprehensive Polymer Science* 6 (1989), p. 451.
- [64] Erik R. Zettler, Tracy J. Mincer, and Linda A. Amaral-Zettler. “Life in the ”plastisphere”: Microbial communities on plastic marine debris”. In: *Environmental Science and Technology* 47.13 (July 2013), pp. 7137–7146. ISSN: 0013936X. DOI: [10.1021/es401288x](https://doi.org/10.1021/es401288x).
- [65] Inga Vanessa Kirstein et al. “The plastisphere - Uncovering tightly attached plastic “specific” microorganisms”. In: *PLoS ONE* 14.4 (2019), pp. 1–17. ISSN: 19326203. DOI: [10.1371/journal.pone.0215859](https://doi.org/10.1371/journal.pone.0215859).
- [66] Valeria Hidalgo-Ruz et al. “Microplastics in the marine environment: a review of the methods used for identification and quantification”. In: *... Science & Technology* 46.6 (2012), pp. 3060–3075. ISSN: 0013-936X. DOI: [10.1021/es2031505](https://doi.org/10.1021/es2031505). URL: <http://dx.doi.org/10.1021/es2031505%20http://www.ncbi.nlm.nih.gov/pubmed/22321064%20All%20Papers/H/Hidalgo-Ruz%20et%20al.%202012%20-%20Microplastics%20in%20the%20Marine%20Environment%20A%20Review%20of%20the%20Methods.pdf%20All%20Papers/H/Hidalgo-Ruz%20et%20al.%202012%20-%20Microplastics%20in%20the%20marine%20e>.

- [67] Paul Kay et al. “Wastewater treatment plants as a source of microplastics in river catchments”. In: *Environmental Science and Pollution Research* 25.20 (2018), pp. 20264–20267. ISSN: 16147499. DOI: [10.1007/s11356-018-2070-7](https://doi.org/10.1007/s11356-018-2070-7).
- [68] Brent Stephens et al. “Ultrafine particle emissions from desktop 3D printers”. In: *Atmospheric Environment* 79 (2013), pp. 334–339. ISSN: 13522310. DOI: [10.1016/j.atmosenv.2013.06.050](https://doi.org/10.1016/j.atmosenv.2013.06.050). URL: <http://dx.doi.org/10.1016/j.atmosenv.2013.06.050>.
- [69] Therese M. Karlsson et al. “The unaccountability case of plastic pellet pollution”. In: *Marine Pollution Bulletin* 129.1 (2018), pp. 52–60. ISSN: 18793363. DOI: [10.1016/j.marpolbul.2018.01.041](https://doi.org/10.1016/j.marpolbul.2018.01.041). URL: <https://doi.org/10.1016/j.marpolbul.2018.01.041>.
- [70] L Frère et al. “A semi-automated Raman micro-spectroscopy method for morphological and chemical characterizations of microplastic litter”. In: *Marine Pollution Bulletin* 113.1 (2016), pp. 461–468. DOI: [10.1016/j.marpolbul.2016.10.051](https://doi.org/10.1016/j.marpolbul.2016.10.051).
- [71] Delilah Lithner, Ake Larsson, and Göran Dave. “Environmental and health hazard ranking and assessment of plastic polymers based on chemical composition”. In: *Science of the Total Environment* 409.18 (Aug. 2011), pp. 3309–3324. ISSN: 00489697. DOI: [10.1016/j.scitotenv.2011.04.038](https://doi.org/10.1016/j.scitotenv.2011.04.038).
- [72] Thomas Roy Crompton. *Additive Migration from Plastics Into Foods: A Guide for Analytical Chemists* -. URL: <https://books.google.co.jp/books?hl=en%7B%5C%7Dlr=%7B%5C%7Ddid=xnPcJiKd6PwC%7B%5C%7Ddoi=fnd%7B%5C%7Dpg=PA1%7B%5C%7Ddq=Crompton,+2007+plastic%7B%5C%7Ddots=Cc2PPwPtDN%7B%5C%7Dsig=BYul1-PU6DGV9GfpIsu3zmR4Vz0%7B%5C%7Dredir%7B%5C%7Ddesc=y%7B%5C%7Dv=onepage%7B%5C%7Dq=Crompton%7B%5C%7D2c%202007%20plastic%7B%5C%7Df=false> (visited on 02/21/2020).
- [73] Shannon K. Lee and D. N.Rao Veeramachaneni. “Subchronic exposure to low concentrations of di-n-butyl phthalate disrupts spermatogenesis in *Xenopus laevis* frogs”. In: *Toxicological Sciences* 84.2 (2005), pp. 394–407. ISSN: 10966080. DOI: [10.1093/toxsci/kfi087](https://doi.org/10.1093/toxsci/kfi087).
- [74] Pengfei Wu et al. “Adsorption mechanisms of five bisphenol analogues on PVC microplastics”. In: *Science of the Total Environment* 650 (2019), pp. 671–678. ISSN: 18791026. DOI: [10.1016/j.scitotenv.2018.09.049](https://doi.org/10.1016/j.scitotenv.2018.09.049). URL: <https://doi.org/10.1016/j.scitotenv.2018.09.049>.
- [75] Chelsea M Rochman et al. “Ingested plastic transfers hazardous chemicals to fish and induces hepatic stress.” In: *Scientific reports* 3 (2013), p. 3263. ISSN: 2045-2322. DOI: [10.1038/srep03263](https://doi.org/10.1038/srep03263). URL: <http://www.pubmedcentral.nih.gov/articlerender.fcgi?artid=3836290%7B%5C%7Dtool=pmcentrez%7B%5C%7Drendertype=abstract>.
- [76] Anthony L. Andrady. *The plastic in microplastics: A review*. June 2017. DOI: [10.1016/j.marpolbul.2017.01.082](https://doi.org/10.1016/j.marpolbul.2017.01.082).
- [77] Lorena M. Rios Mendoza and Patrick R. Jones. “Characterisation of microplastics and toxic chemicals extracted from microplastic samples from the North Pacific Gyre”. In: *Environmental Chemistry* 12 (2015), pp. 611–617. DOI: [10.1071/en14236](https://doi.org/10.1071/en14236).

- [78] Albert A. Koelmans et al. “Plastic as a carrier of POPs to aquatic organisms: a model analysis”. In: *Environ. Sci. Technol.* 47.14 (2013), pp. 7812–7820. ISSN: 0013-936X. DOI: 10.1021/es401169n. URL: <http://dx.doi.org/10.1021/es401169n%20http://www.ncbi.nlm.nih.gov/pubmed/23758580%20All%20Papers/K/Koelmans%20et%20al.%202013%20-%20Plastic%20as%20a%20Carrier%20of%20POPs%20to%20Aquatic%20Organisms%20A%20Model%20Analysis.pdf%20All%20Papers/K/Koelmans%20et%20al.%202013%20-%20Supporting%20Information%20for%20plast>.
- [79] Kalliopi N. Fotopoulou and Hrissi K. Karapanagioti. “Surface properties of beached plastic pellets”. In: *Marine Environmental Research* 81. August 2012 (2012), pp. 70–77. ISSN: 01411136. DOI: 10.1016/j.marenvres.2012.08.010. URL: <http://dx.doi.org/10.1016/j.marenvres.2012.08.010>.
- [80] A. L. Lusher, M. McHugh, and Richard C. Thompson. “Occurrence of microplastics in the gastrointestinal tract of pelagic and demersal fish from the English Channel”. In: *Marine Pollution Bulletin* 67.1-2 (2013), pp. 94–99. ISSN: 0025326X. DOI: 10.1016/j.marpolbul.2012.11.028. URL: <http://dx.doi.org/10.1016/j.marpolbul.2012.11.028>.
- [81] Jiana Li et al. “Microplastics in commercial bivalves from China”. In: *Environmental Pollution* 207 (Dec. 2015), pp. 190–195. ISSN: 18736424. DOI: 10.1016/j.envpol.2015.09.018.
- [82] Khalida Jabeen et al. “Microplastics and mesoplastics in fish from coastal and fresh waters of China”. In: *Environmental Pollution* 221 (Feb. 2017), pp. 141–149. ISSN: 18736424. DOI: 10.1016/j.envpol.2016.11.055.
- [83] Carlo Giacomo Avio, Stefania Gorbi, and Francesco Regoli. “Plastics and microplastics in the oceans: From emerging pollutants to emerged threat”. In: *Marine Environmental Research* 128 (July 2017), pp. 2–11. ISSN: 18790291. DOI: 10.1016/j.marenvres.2016.05.012.
- [84] Paul Farrell and Kathryn Nelson. “Trophic level transfer of microplastic: *Mytilus edulis* (L.) to *Carcinus maenas* (L.)” 2013.
- [85] Jundong Wang et al. “Microplastics in the surface sediments from the Beijiang River littoral zone: Composition, abundance, surface textures and interaction with heavy metals”. In: *Chemosphere* 171 (Mar. 2017), pp. 248–258. ISSN: 18791298. DOI: 10.1016/j.chemosphere.2016.12.074.
- [86] Charles James Moore et al. “A Comparison of Plastic and Plankton in the North Pacific Central Gyre”. In: *Mar. Pollut. Bull.* 42.12 (2001), pp. 1297–1300. ISSN: 0025-326X. DOI: 10.1016/S0025-326X(01)00114-X. URL: <https://www.ncbi.nlm.nih.gov/pubmed/11827116%20http://www.sciencedirect.com/science/article/pii/S0025326X0100114X%20http://www.vliz.be/imisdocs/publications/135813.pdf%20All%20Papers/M/Moore%20et%20al.%202001%20-%20A%20comparison%20of%20plastic%20and%20plankton%20in%20the%20north%20Pacific>.





- [98] Roman Netzer et al. “Petroleum hydrocarbon and microbial community structure successions in marine oil-related aggregates associated with diatoms relevant for Arctic conditions”. In: *Marine Pollution Bulletin* 135. August (2018), pp. 759–768. ISSN: 18793363. DOI: [10.1016/j.marpolbul.2018.07.074](https://doi.org/10.1016/j.marpolbul.2018.07.074). URL: <https://doi.org/10.1016/j.marpolbul.2018.07.074>.
- [99] U Passow et al. “Incorporation of oil into diatom aggregates”. In: *Marine Ecology Progress Series* 612 (Mar. 2019), pp. 65–86. ISSN: 0171-8630. DOI: [10.3354/meps12881](https://doi.org/10.3354/meps12881). URL: <http://www.int-res.com/abstracts/meps/v612/p65-86/>.
- [100] Shiye Zhao et al. “An approach for extraction, characterization and quantitation of microplastic in natural marine snow using Raman microscopy”. In: *Analytical Methods* 9.9 (2017), pp. 1470–1478. ISSN: 17599679. DOI: [10.1039/c6ay02302a](https://doi.org/10.1039/c6ay02302a).
- [101] Richard T. Barber. “Picoplankton Do Some Heavy Lifting”. In: *Science* 315.5813 (2007), pp. 776–777. ISSN: 0036-8075. URL: [All%20Papers/B/Barber%202007%20-%20Picoplankton%20Do%20Some%20Heavy%20Lifting.pdf%20All%20Papers/B/Barber%202007%20-%20Barber%202007.pdf](https://www.sciencemag.org/papers/2007/07/20Picoplankton%20Do%20Some%20Heavy%20Lifting.pdf).
- [102] Ben A Ward and Michael J Follows. “Marine mixotrophy increases trophic transfer efficiency, mean organism size, and vertical carbon flux.” In: *Proceedings of the National Academy of Sciences of the United States of America* 113.11 (2016), pp. 2958–2963. ISSN: 1091-6490. DOI: [10.1073/pnas.1517118113](https://doi.org/10.1073/pnas.1517118113). URL: <http://www.scopus.com/inward/record.url?eid=2-s2.0-84961829806%7B%5C%7DpartnerID=tZ0tx3y1>.
- [103] Lucy C Woodall et al. “The deep sea is a major sink for microplastic debris”. In: *Royal Society Open Science* (2014). DOI: [10.1098/rsos.140317](https://doi.org/10.1098/rsos.140317).
- [104] S. D. Ling et al. “Ubiquity of microplastics in coastal seafloor sediments”. In: *Marine Pollution Bulletin* 121.1-2 (Aug. 2017), pp. 104–110. ISSN: 18793363. DOI: [10.1016/j.marpolbul.2017.05.038](https://doi.org/10.1016/j.marpolbul.2017.05.038).
- [105] Peter J. Mumby et al. “High resilience masks underlying sensitivity to algal phase shifts of Pacific coral reefs”. In: *Oikos* 125.5 (May 2016), pp. 644–655. ISSN: 16000706. DOI: [10.1111/oik.02673](https://doi.org/10.1111/oik.02673). URL: <http://doi.wiley.com/10.1111/oik.02673>.
- [106] Mélanie L. Trapon, Morgan S. Pratchett, and Lucie Penin. “Comparative Effects of Different Disturbances in Coral Reef Habitats in Moorea, French Polynesia”. In: *Journal of Marine Biology* 2011 (2011), pp. 1–11. ISSN: 1687-9481. DOI: [10.1155/2011/807625](https://doi.org/10.1155/2011/807625).
- [107] Marjorie L. Reaka-Kudla. “The Global Biodiversity of Coral Reefs: A Comparison with Rain Forests”. In: *Biodiversity II: Understanding and Protecting Our Biological Resources*. Ed. by Marjorie L. Reaka-Kudla. 1997. URL: <https://books.google.co.jp/books?hl=en%7B%5C%7Dlr=%7B%5C%7Ddid=-X50AgAAQBAJ%7B%5C%7Ddoi=fnd%7B%5C%7Dpg=PA83%7B%5C%7Ddots=f2XjmFZ16n%7B%5C%7Dsig=1D2Hs5rwehGN4RYyKy0TAb0ADFA%7B%5C%7Dredir%7B%5C%7Ddesc=y%7B%5C%7Ddv=onepage%7B%5C%7Dq%7B%5C%7Ddf=false>.
- [108] Robert Costanza et al. “The value of the world’s ecosystem services and natural capital”. In: *Nature* 387.6630 (May 1997), pp. 253–260. ISSN: 00280836. DOI: [10.1038/387253a0](https://doi.org/10.1038/387253a0).
- [109] Clive R. Wilkinson. *Global and local threats to coral reef functioning and existence: Review and predictions*. 1999. DOI: [10.1071/MF99121](https://doi.org/10.1071/MF99121).



- [110] O. Hoegh-Guldberg et al. *Coral reefs under rapid climate change and ocean acidification*. Dec. 2007. DOI: [10.1126/science.1152509](https://doi.org/10.1126/science.1152509).
- [111] Kenneth R.N. Anthony. “Coral Reefs Under Climate Change and Ocean Acidification: Challenges and Opportunities for Management and Policy”. In: *Annual Review of Environment and Resources* 41.1 (Nov. 2016), pp. 59–81. ISSN: 1543-5938. DOI: [10.1146/annurev-environ-110615-085610](https://doi.org/10.1146/annurev-environ-110615-085610). URL: <http://www.annualreviews.org/doi/10.1146/annurev-environ-110615-085610>.
- [112] Mary J. Donohue et al. “Derelict fishing gear in the Northwestern Hawaiian Islands: Diving surveys and debris removal in 1999 confirm threat to Coral Reef ecosystems”. In: *Marine Pollution Bulletin* 42.12 (Dec. 2001), pp. 1301–1312. ISSN: 0025326X. DOI: [10.1016/S0025-326X\(01\)00139-4](https://doi.org/10.1016/S0025-326X(01)00139-4).
- [113] Julia Reisser et al. “Marine Plastic Pollution in Waters around Australia: Characteristics, Concentrations, and Pathways”. In: *PLoS ONE* 8.11 (Nov. 2013). Ed. by Graeme Clive Hays, e80466. ISSN: 1932-6203. DOI: [10.1371/journal.pone.0080466](https://doi.org/10.1371/journal.pone.0080466). URL: <https://dx.plos.org/10.1371/journal.pone.0080466>.
- [114] N. M. Hall et al. “Microplastic ingestion by scleractinian corals”. In: *Marine Biology* 162.3 (Feb. 2015), pp. 725–732. ISSN: 00253162. DOI: [10.1007/s00227-015-2619-7](https://doi.org/10.1007/s00227-015-2619-7).
- [115] Jessica Reichert et al. “Responses of reef building corals to microplastic exposure”. In: *Environmental Pollution* 237 (June 2018), pp. 955–960. ISSN: 18736424. DOI: [10.1016/j.envpol.2017.11.006](https://doi.org/10.1016/j.envpol.2017.11.006).
- [116] Pei Xu et al. “Microplastic risk assessment in surface waters: A case study in the Changjiang Estuary, China”. In: *Marine Pollution Bulletin* 133 (Aug. 2018), pp. 647–654. ISSN: 18793363. DOI: [10.1016/j.marpolbul.2018.06.020](https://doi.org/10.1016/j.marpolbul.2018.06.020).
- [117] Carl Folke et al. “Regime Shifts, Resilience, and Biodiversity in Ecosystem Management”. In: *Annual Review of Ecology, Evolution, and Systematics* 35.1 (Dec. 2004), pp. 557–581. ISSN: 1543-592X. DOI: [10.1146/annurev.ecolsys.35.021103.105711](https://doi.org/10.1146/annurev.ecolsys.35.021103.105711). URL: <http://www.annualreviews.org/doi/10.1146/annurev.ecolsys.35.021103.105711>.
- [118] Garry Peterson, Craig R. Allen, and C. S. Holling. “Ecological resilience, biodiversity, and scale”. In: *Ecosystems* 1.1 (1998), pp. 6–18. ISSN: 14329840. DOI: [10.2307/3658701](https://doi.org/10.2307/3658701).
- [119] Gilberto C. Gallopín. “Linkages between vulnerability, resilience, and adaptive capacity”. In: *Global Environmental Change* 16.3 (Aug. 2006), pp. 293–303. ISSN: 09593780. DOI: [10.1016/j.gloenvcha.2006.02.004](https://doi.org/10.1016/j.gloenvcha.2006.02.004).
- [120] C. S. Holling and L. H. Gunderson. “Resilience and adaptive cycles”. In: (2002). URL: <http://hdl.handle.net/10919/67621>.
- [121] C S Holling. “Resilience and Stability of Ecological Systems”. In: *Annual Review of Ecology and Systematics* 4.1 (Nov. 1973), pp. 1–23. ISSN: 0066-4162. DOI: [10.1146/annurev.es.04.110173.000245](https://doi.org/10.1146/annurev.es.04.110173.000245). URL: <http://www.annualreviews.org/doi/10.1146/annurev.es.04.110173.000245>.

- [122] Martin Ogonowski, Zandra Gerdes, and Elena Gorokhova. “What we know and what we think we know about microplastic effects - A critical perspective”. In: *Current Opinion in Environmental Science and Health* 1 (2018), pp. 41–46. ISSN: 24685844. DOI: [10.1016/j.coesh.2017.09.001](https://doi.org/10.1016/j.coesh.2017.09.001). URL: <https://doi.org/10.1016/j.coesh.2017.09.001>.
- [123] Gwen Lattin et al. “A comparison of neustonic plastic and zooplankton at different depths near the southern California shore”. In: *Marine Pollution Bulletin* 49.4 (2004), pp. 291–294. ISSN: 0025326X. DOI: [10.1016/j.marpolbul.2004.01.020](https://doi.org/10.1016/j.marpolbul.2004.01.020).
- [124] Juliana A. Ivar do Sul, Ângela Spengler, and Monica F. Costa. “Here, there and everywhere. Small plastic fragments and pellets on beaches of Fernando de Noronha (Equatorial Western Atlantic)”. In: *Marine Pollution Bulletin* 58.8 (Aug. 2009), pp. 1236–1238. ISSN: 0025326X. DOI: [10.1016/j.marpolbul.2009.05.004](https://doi.org/10.1016/j.marpolbul.2009.05.004).
- [125] Nishihira M. “Natural and human interference with the coral reef and coastal environments in Okinawa”. In: *Galaxea. Nishihara* 6.1 (1987), pp. 311–321. URL: <https://ci.nii.ac.jp/naid/10008277895/en/>.
- [126] Makoto Omori. “Degradation and restoration of coral reefs: Experience in Okinawa, Japan”. In: *Marine Biology Research* 7.1 (2011), pp. 3–12. ISSN: 17451000. DOI: [10.1080/17451001003642317](https://doi.org/10.1080/17451001003642317).
- [127] Nobuyuki Yagi et al. “Marine protected areas in Japan: Institutional background and management framework”. In: *Marine Policy* 34.6 (2010), pp. 1300–1306. ISSN: 0308597X. DOI: [10.1016/j.marpol.2010.06.001](https://doi.org/10.1016/j.marpol.2010.06.001). URL: <http://dx.doi.org/10.1016/j.marpol.2010.06.001>.
- [128] Luciana Porter-Bolland et al. “Community managed forests and forest protected areas: An assessment of their conservation effectiveness across the tropics”. In: *Forest Ecology and Management* 268 (2012), pp. 6–17. ISSN: 03781127. DOI: [10.1016/j.foreco.2011.05.034](https://doi.org/10.1016/j.foreco.2011.05.034). URL: <http://dx.doi.org/10.1016/j.foreco.2011.05.034>.
- [129] Richard T. Carson and Jordan J. Louviere. “A Common Nomenclature for Stated Preference Elicitation Approaches”. In: *Environmental and Resource Economics* 49.4 (2011), pp. 539–559. ISSN: 09246460. DOI: [10.1007/s10640-010-9450-x](https://doi.org/10.1007/s10640-010-9450-x).
- [130] Samuel Cameron. *Handbook on the economics of leisure*. 2011. DOI: [10.4337/9780857930569](https://doi.org/10.4337/9780857930569).
- [131] A B Barbosa. “Dynamics of living phytoplankton: Implications for paleoenvironmental reconstructions”. In: *IOP Conference Series: Earth and Environmental Science* 5 (2009), p. 012001. DOI: [10.1088/1755-1307/5/1/012001](https://doi.org/10.1088/1755-1307/5/1/012001).
- [132] R. Abernethy et al. “State of the climate in 2017”. In: *Bulletin of the American Meteorological Society* 99.8 (2018), Si–S310. ISSN: 00030007. DOI: [10.1175/2018bamsstateofthecclimate.1](https://doi.org/10.1175/2018bamsstateofthecclimate.1).
- [133] Thomas F. Stocker et al. “Climate change 2013 the physical science basis: Working Group I contribution to the fifth assessment report of the intergovernmental panel on climate change”. In: *Climate Change 2013 the Physical Science Basis: Working Group I Contribution to the Fifth Assessment Report of the Intergovernmental Panel on Climate Change* 9781107057 (2013), pp. 1–1535. DOI: [10.1017/CB09781107415324](https://doi.org/10.1017/CB09781107415324).

- [134] URL: <https://www.acs.org/content/acs/en/climatescience/greenhousegases/industrialrevolution.html>.
- [135] George A. Jackson. “Effect of coagulation on a model planktonic food web”. In: *Deep-Sea Research Part I: Oceanographic Research Papers* 48.1 (Jan. 2001), pp. 95–123. ISSN: 09670637. DOI: [10.1016/S0967-0637\(00\)00040-6](https://doi.org/10.1016/S0967-0637(00)00040-6).
- [136] Marc Long et al. “Interactions between polystyrene microplastics and marine phytoplankton lead to species-specific hetero-aggregation”. In: *Environmental Pollution* 228 (Sept. 2017), pp. 454–463. ISSN: 18736424. DOI: [10.1016/j.envpol.2017.05.047](https://doi.org/10.1016/j.envpol.2017.05.047).
- [137] Cai Zhang et al. “Toxic effects of microplastic on marine microalgae *Skeletonema costatum*: Interactions between microplastic and algae”. In: *Environmental Pollution* 220 (Jan. 2017), pp. 1282–1288. ISSN: 18736424. DOI: [10.1016/j.envpol.2016.11.005](https://doi.org/10.1016/j.envpol.2016.11.005).
- [138] Ana Markic et al. “Plastic ingestion by marine fish in the wild”. In: *Critical Reviews in Environmental Science and Technology* 50.7 (2020), pp. 657–697. ISSN: 15476537. DOI: [10.1080/10643389.2019.1631990](https://doi.org/10.1080/10643389.2019.1631990). URL: <https://doi.org/10.1080/10643389.2019.1631990>.
- [139] Cheryl Qian Ying Yong, Suresh Valiyaveetil, and Bor Luen Tang. “Toxicity of microplastics and nanoplastics in Mammalian systems”. In: *International Journal of Environmental Research and Public Health* 17.5 (2020). ISSN: 16604601. DOI: [10.3390/ijerph17051509](https://doi.org/10.3390/ijerph17051509).
- [140] Martin Thiel et al. “Impacts of marine plastic pollution from continental coasts to subtropical gyres-fish, seabirds, and other vertebrates in the SE Pacific”. In: *Frontiers in Marine Science* 5, July (2018), pp. 1–16. ISSN: 22967745. DOI: [10.3389/fmars.2018.00238](https://doi.org/10.3389/fmars.2018.00238).
- [141] Neil S. Banas. “Adding complex trophic interactions to a size-spectral plankton model: Emergent diversity patterns and limits on predictability”. In: *Ecological Modelling* 222.15 (Aug. 2011), pp. 2663–2675. ISSN: 03043800. DOI: [10.1016/j.ecolmodel.2011.05.018](https://doi.org/10.1016/j.ecolmodel.2011.05.018).
- [142] Susie M. Grant et al. “Ecosystem services of the Southern Ocean: Trade-offs in decision-making”. In: *Antarctic Science* 25.5 (2013), pp. 603–617. ISSN: 09541020. DOI: [10.1017/S0954102013000308](https://doi.org/10.1017/S0954102013000308).
- [143] T. W. Dahl et al. “Reorganisation of earth’s biogeochemical cycles briefly oxygenated the oceans 520 myr ago”. In: *Geochemical Perspectives Letters* 10 (2019), pp. 210–220. ISSN: 24103403. DOI: [10.7185/geochemlet.1724](https://doi.org/10.7185/geochemlet.1724).
- [144] Ove Hoegh-Guldberg et al. *The Coral Triangle and climate change: ecosystems, people and societies at risk*. 2009.
- [145] Joana C. Prata et al. “Influence of microplastics on the toxicity of the pharmaceuticals procainamide and doxycycline on the marine microalgae *Tetraselmis chuii*”. In: *Aquatic Toxicology* 197 (Apr. 2018), pp. 143–152. ISSN: 18791514. DOI: [10.1016/j.aquatox.2018.02.015](https://doi.org/10.1016/j.aquatox.2018.02.015).
- [146] L. Manfra et al. “Comparative ecotoxicity of polystyrene nanoparticles in natural seawater and reconstituted seawater using the rotifer *Brachionus plicatilis*”. In: *Ecotoxicology and Environmental Safety* 145 (Nov. 2017), pp. 557–563. ISSN: 10902414. DOI: [10.1016/j.ecoenv.2017.07.068](https://doi.org/10.1016/j.ecoenv.2017.07.068).

- [147] Patrick M. Canniff and Tham C. Hoang. “Microplastic ingestion by *Daphnia magna* and its enhancement on algal growth”. In: *Science of the Total Environment* 633 (Aug. 2018), pp. 500–507. ISSN: 18791026. DOI: [10.1016/j.scitotenv.2018.03.176](https://doi.org/10.1016/j.scitotenv.2018.03.176).
- [148] Maria P. Casado, Ailbhe Macken, and Hugh J. Byrne. “Ecotoxicological assessment of silica and polystyrene nanoparticles assessed by a multitrophic test battery”. In: *Environment International* 51 (Jan. 2013), pp. 97–105. ISSN: 18736750. DOI: [10.1016/j.envint.2012.11.001](https://doi.org/10.1016/j.envint.2012.11.001).
- [149] Fabienne Lagarde et al. “Microplastic interactions with freshwater microalgae: Hetero-aggregation and changes in plastic density appear strongly dependent on polymer type”. In: *Environmental Pollution* 215 (Aug. 2016), pp. 331–339. ISSN: 02697491. DOI: [10.1016/j.envpol.2016.05.006](https://doi.org/10.1016/j.envpol.2016.05.006).
- [150] Yufeng Mao et al. “Phytoplankton response to polystyrene microplastics: Perspective from an entire growth period”. In: *Chemosphere* 208 (Oct. 2018), pp. 59–68. ISSN: 18791298. DOI: [10.1016/j.chemosphere.2018.05.170](https://doi.org/10.1016/j.chemosphere.2018.05.170).
- [151] Tom M. Nolte et al. “The toxicity of plastic nanoparticles to green algae as influenced by surface modification, medium hardness and cellular adsorption”. In: *Aquatic Toxicology* 183 (2017), pp. 11–20. ISSN: 0166445X. DOI: [10.1016/j.aquatox.2016.12.005](https://doi.org/10.1016/j.aquatox.2016.12.005). URL: <http://dx.doi.org/10.1016/j.aquatox.2016.12.005>.
- [152] Sascha B. Sjollem et al. “Do plastic particles affect microalgal photosynthesis and growth?” In: *Aquatic Toxicology* 170 (Jan. 2016), pp. 259–261. ISSN: 18791514. DOI: [10.1016/j.aquatox.2015.12.002](https://doi.org/10.1016/j.aquatox.2015.12.002).
- [153] Priyanka Bhattacharya et al. “Physical adsorption of charged plastic nanoparticles affects algal photosynthesis”. In: *Journal of Physical Chemistry C* 114.39 (Oct. 2010), pp. 16556–16561. ISSN: 19327447. DOI: [10.1021/jp1054759](https://doi.org/10.1021/jp1054759).
- [154] Lei Su et al. “Microplastics biomonitoring in Australian urban wetlands using a common noxious fish (*Gambusia holbrooki*)”. In: *Chemosphere* 228 (Aug. 2019), pp. 65–74. ISSN: 18791298. DOI: [10.1016/j.chemosphere.2019.04.114](https://doi.org/10.1016/j.chemosphere.2019.04.114).
- [155] *Plastic atlas 2019: Facts and figures about the world of synthetic polymers*. Heinrich Böll foundation, 2019.
- [156] Erik van Sebille et al. “A global inventory of small floating plastic debris”. In: *Environmental Research Letters* 10.12 (2015), p. 124006.
- [157] M. L. Taylor et al. “Plastic microfibre ingestion by deep-sea organisms”. In: *Scientific Reports* 6.1 (Sept. 2016), pp. 1–9. ISSN: 20452322. DOI: [10.1038/srep33997](https://doi.org/10.1038/srep33997).
- [158] Julien Gigault et al. “Current opinion: What is a nanoplastic?” In: *Environmental Pollution* 235 (2018), pp. 1030–1034. ISSN: 18736424. DOI: [10.1016/j.envpol.2018.01.024](https://doi.org/10.1016/j.envpol.2018.01.024).
- [159] A. L. Shanks and E. W. Edmondson. “Laboratory-made artificial marine snow: a biological model of the real thing”. In: *Marine Biology* 101.4 (1989), pp. 463–470. ISSN: 00253162. DOI: [10.1007/BF00541648](https://doi.org/10.1007/BF00541648).

- [160] U Passow and CA Carlson. “The biological pump in a high CO<sub>2</sub> world”. In: *Marine Ecology Progress Series* 470 (Dec. 2012), pp. 249–271. ISSN: 0171-8630. DOI: [10.3354/meps09985](https://doi.org/10.3354/meps09985). URL: <http://www.int-res.com/abstracts/meps/v470/p249-271/>.
- [161] Lukas Roß. “Verteilungsmuster von Mikropartikeln in komplexen dynamischen Systemen”. PhD thesis. 2017.
- [162] Sourav Bhattacharjee. “DLS and zeta potential - What they are and what they are not?” In: *Journal of Controlled Release* 235 (2016), pp. 337–351. ISSN: 18734995. DOI: [10.1016/j.jconrel.2016.06.017](https://doi.org/10.1016/j.jconrel.2016.06.017). URL: <http://dx.doi.org/10.1016/j.jconrel.2016.06.017>.
- [163] E. Bergami et al. “Long-term toxicity of surface-charged polystyrene nanoplastics to marine planktonic species *Dunaliella tertiolecta* and *Artemia franciscana*”. In: *Aquatic Toxicology* 189.March (2017), pp. 159–169. ISSN: 18791514. DOI: [10.1016/j.aquatox.2017.06.008](https://doi.org/10.1016/j.aquatox.2017.06.008). URL: <http://dx.doi.org/10.1016/j.aquatox.2017.06.008>.
- [164] Arianna Bellingeri et al. “Impact of polystyrene nanoparticles on marine diatom *Skeletonema marinoi* chain assemblages and consequences on their ecological role in marine ecosystems”. In: *Environmental Pollution* 262 (2020), p. 114268. ISSN: 18736424. DOI: [10.1016/j.envpol.2020.114268](https://doi.org/10.1016/j.envpol.2020.114268). URL: <https://doi.org/10.1016/j.envpol.2020.114268>.
- [165] Giacomo Grassi et al. “Interplay between extracellular polymeric substances (EPS) from a marine diatom and model nanoplastic through eco-corona formation”. In: *Science of the Total Environment* 725 (2020), p. 138457. ISSN: 18791026. DOI: [10.1016/j.scitotenv.2020.138457](https://doi.org/10.1016/j.scitotenv.2020.138457). URL: <https://doi.org/10.1016/j.scitotenv.2020.138457>.
- [166] Yilu Su et al. “Microplastic exposure represses the growth of endosymbiotic dinoflagellate *Cladocopium goreau* in culture through affecting its apoptosis and metabolism”. In: *Chemosphere* 244 (Apr. 2020), p. 125485. ISSN: 18791298. DOI: [10.1016/j.chemosphere.2019.125485](https://doi.org/10.1016/j.chemosphere.2019.125485).
- [167] Xuemei Sun et al. “Toxicities of polystyrene nano- and microplastics toward marine bacterium *Halomonas alkaliphila*”. In: *Science of the Total Environment* 642 (2018), pp. 1378–1385. ISSN: 18791026. DOI: [10.1016/j.scitotenv.2018.06.141](https://doi.org/10.1016/j.scitotenv.2018.06.141). URL: <https://doi.org/10.1016/j.scitotenv.2018.06.141>.
- [168] Li Juan Feng et al. “Short-term exposure to positively charged polystyrene nanoparticles causes oxidative stress and membrane destruction in cyanobacteria”. In: *Environmental Science: Nano* 6.10 (2019), pp. 3072–3079. ISSN: 20518161. DOI: [10.1039/c9en00807a](https://doi.org/10.1039/c9en00807a).
- [169] Tania Thalyta Silva De Oliveira et al. “Interaction of Cyanobacteria with Nanometer and Micron Sized Polystyrene Particles in Marine and Fresh Water”. In: *Langmuir* 36.14 (2020), pp. 3963–3969. ISSN: 15205827. DOI: [10.1021/acs.langmuir.9b03644](https://doi.org/10.1021/acs.langmuir.9b03644).
- [170] Zhi lin Zhu et al. “Joint toxicity of microplastics with triclosan to marine microalgae *Skeletonema costatum*”. In: *Environmental Pollution* 246 (2019), pp. 509–517. ISSN: 18736424. DOI: [10.1016/j.envpol.2018.12.044](https://doi.org/10.1016/j.envpol.2018.12.044). URL: <https://doi.org/10.1016/j.envpol.2018.12.044>.



- [171] Karen Ashton, Luke Holmes, and Andrew Turner. “Association of metals with plastic production pellets in the marine environment”. In: *Marine Pollution Bulletin* 60.11 (2010), pp. 2050–2055. ISSN: 0025326X. DOI: [10.1016/j.marpolbul.2010.07.014](https://doi.org/10.1016/j.marpolbul.2010.07.014). URL: <http://dx.doi.org/10.1016/j.marpolbul.2010.07.014>.
- [172] Luke A. Holmes, Andrew Turner, and Richard C. Thompson. “Adsorption of trace metals to plastic resin pellets in the marine environment”. In: *Environmental Pollution* 160.1 (2012), pp. 42–48. ISSN: 02697491. DOI: [10.1016/j.envpol.2011.08.052](https://doi.org/10.1016/j.envpol.2011.08.052). URL: <http://dx.doi.org/10.1016/j.envpol.2011.08.052>.
- [173] Chelsea M. Rochman, Brian T. Hentschel, and Swee J. The. “Long-term sorption of metals is similar among plastic types: Implications for plastic debris in aquatic environments”. In: *PLoS ONE* 9.1 (2014). ISSN: 19326203. DOI: [10.1371/journal.pone.0085433](https://doi.org/10.1371/journal.pone.0085433).
- [174] Andrew Turner. “Heavy metals, metalloids and other hazardous elements in marine plastic litter”. In: *Marine Pollution Bulletin* 111.1-2 (2016), pp. 136–142. ISSN: 18793363. DOI: [10.1016/j.marpolbul.2016.07.020](https://doi.org/10.1016/j.marpolbul.2016.07.020). URL: <http://dx.doi.org/10.1016/j.marpolbul.2016.07.020>.
- [175] Tanja Kögel et al. “Micro- and nanoplastic toxicity on aquatic life: Determining factors”. In: *Science of the Total Environment* 709.5817 (2020). ISSN: 18791026. DOI: [10.1016/j.scitotenv.2019.136050](https://doi.org/10.1016/j.scitotenv.2019.136050).
- [176] Marco Mühlenbruch et al. “Mini-review: Phytoplankton-derived polysaccharides in the marine environment and their interactions with heterotrophic bacteria”. In: *Environmental Microbiology* 20.8 (2018), pp. 2671–2685. ISSN: 14622920. DOI: [10.1111/1462-2920.14302](https://doi.org/10.1111/1462-2920.14302).
- [177] Shuocong Li et al. “Aggregation kinetics of microplastics in aquatic environment: Complex roles of electrolytes, pH, and natural organic matter”. In: *Environmental Pollution* 237 (2018), pp. 126–132. ISSN: 18736424. DOI: [10.1016/j.envpol.2018.02.042](https://doi.org/10.1016/j.envpol.2018.02.042). URL: <https://doi.org/10.1016/j.envpol.2018.02.042>.
- [178] Hui Xu and Leah B. Casabianca. “Probing driving forces for binding between nanoparticles and amino acids by saturation-transfer difference NMR”. In: *Scientific Reports* 10.1 (2020), pp. 1–8. DOI: [10.1038/s41598-020-69185-7](https://doi.org/10.1038/s41598-020-69185-7). URL: <https://doi.org/10.1038/s41598-020-69185-7>.
- [179] Stephen Summers, Theodore Henry, and Tony Gutierrez. “Agglomeration of nano- and microplastic particles in seawater by autochthonous and de novo-produced sources of expolymeric substances”. In: *Marine Pollution Bulletin* 130. February (2018), pp. 258–267. ISSN: 18793363. DOI: [10.1016/j.marpolbul.2018.03.039](https://doi.org/10.1016/j.marpolbul.2018.03.039). URL: <https://doi.org/10.1016/j.marpolbul.2018.03.039>.
- [180] Matthew Cole. “A novel method for preparing microplastic fibers”. In: *Scientific Reports* 6. October (2016), pp. 1–7. ISSN: 20452322. DOI: [10.1038/srep34519](https://doi.org/10.1038/srep34519).
- [181] Matthew Cole and Tamara S Galloway. “Ingestion of Nanoplastics and Microplastics by Pacific Oyster Larvae”. In: *Environmental Science & Technology* 49.24 (2015), pp. 14625–14632. DOI: [10.1021/acs.est.5b04099](https://doi.org/10.1021/acs.est.5b04099).
- [182] Jung Hoon Kang et al. “Marine neustonic microplastics around the southeastern coast of Korea”. In: *Marine Pollution Bulletin* 96.1-2 (2015), pp. 304–312. ISSN: 18793363. DOI: [10.1016/j.marpolbul.2015.04.054](https://doi.org/10.1016/j.marpolbul.2015.04.054).





- [194] Song Xia et al. “Effects of nutrients and light intensity on the growth and biochemical composition of a marine microalga *Odontella aurita*”. In: *Chinese Journal of Oceanology and Limnology* 31.6 (2013), pp. 1163–1173. ISSN: 02544059. DOI: [10.1007/s00343-013-2092-4](https://doi.org/10.1007/s00343-013-2092-4).
- [195] Adrian B. Burd et al. “The science behind marine-oil snow and MOSSFA: Past, present, and future”. In: *Progress in Oceanography* 187.July (2020). ISSN: 00796611. DOI: [10.1016/j.pocean.2020.102398](https://doi.org/10.1016/j.pocean.2020.102398).
- [196] Viola Fischer et al. “Plastic pollution of the kuril-kamchatka trench area (NW pacific)”. In: *Deep-Sea Research Part II: Topical Studies in Oceanography* 111 (2015), pp. 399–405. ISSN: 09670645. DOI: [10.1016/j.dsr2.2014.08.012](https://doi.org/10.1016/j.dsr2.2014.08.012). URL: <http://dx.doi.org/10.1016/j.dsr2.2014.08.012>.
- [197] Ian A. Kane et al. “Seafloor microplastic hotspots controlled by deep-sea circulation”. In: *Science* 368.6495 (2020), pp. 1140–1145. ISSN: 10959203. DOI: [10.1126/science.aba5899](https://doi.org/10.1126/science.aba5899).
- [198] T. Kiørboe, K. P. Andersen, and H. G. Dam. “Coagulation efficiency and aggregate formation in marine phytoplankton”. In: *Marine Biology* 107.2 (1990), pp. 235–245. ISSN: 00253162. DOI: [10.1007/BF01319822](https://doi.org/10.1007/BF01319822).
- [199] C. Joiris, F Metz, and H J Callot. “A budget of carbon cycling in the Belgian coastal zone: relative roles of zooplankton, bacterioplankton and benthos in the utilization of primary production”. In: *Tetrahedron Lett.* 23.42 (1982), pp. 4321–4324. DOI: [10.1016/0077-7579\(82\)90035-7](https://doi.org/10.1016/0077-7579(82)90035-7).
- [200] Xavier Mari et al. “Transparent exopolymer particles: Effects on carbon cycling in the ocean”. In: *Progress in Oceanography* 151 (2017), pp. 13–37. ISSN: 0079-6611. DOI: <https://doi.org/10.1016/j.pocean.2016.11.002>. URL: <http://www.sciencedirect.com/science/article/pii/S0079661116300696>.
- [201] Mary C. Machado et al. “The response of *Synechococcus* sp. PCC 7002 to micro-/nano polyethylene particles - Investigation of a key anthropogenic stressor”. In: *PloS one* 15.7 (2020), e0232745. ISSN: 19326203. DOI: [10.1371/journal.pone.0232745](https://doi.org/10.1371/journal.pone.0232745). URL: <http://dx.doi.org/10.1371/journal.pone.0232745>.
- [202] C. C. Gotschalk and A. L. Alldredge. “Enhanced primary production and nutrient regeneration within aggregated marine diatoms”. In: *Marine Biology* 103.1 (1989), pp. 119–129. ISSN: 00253162. DOI: [10.1007/BF00391070](https://doi.org/10.1007/BF00391070).
- [203] Sunandan Pakrashi et al. “Cytotoxicity of aluminium oxide nanoparticles towards fresh water algal isolate at low exposure concentrations”. In: *Aquatic Toxicology* 132-133 (2013), pp. 34–45. ISSN: 0166445X. DOI: [10.1016/j.aquatox.2013.01.018](https://doi.org/10.1016/j.aquatox.2013.01.018). URL: <http://dx.doi.org/10.1016/j.aquatox.2013.01.018>.
- [204] Abdallah Oukarroum et al. “Temperature influence on silver nanoparticles inhibitory effect on photosystem II photochemistry in two green algae, *Chlorella vulgaris* and *Dunaliella tertiolecta*”. In: *Environmental Science and Pollution Research* 19.5 (2012), pp. 1755–1762. ISSN: 09441344. DOI: [10.1007/s11356-011-0689-8](https://doi.org/10.1007/s11356-011-0689-8).
- [205] A. McMinn et al. “Preliminary investigation of Okhotsk Sea ice algae; taxonomic composition and photosynthetic activity”. In: *Polar Biology* 31.8 (2008), pp. 1011–1015. ISSN: 07224060. DOI: [10.1007/s00300-008-0433-0](https://doi.org/10.1007/s00300-008-0433-0).

- [206] Jakob Pernthaler. “Predation on prokaryotes in the water column and its ecological implications”. In: *Nature Reviews Microbiology* 3.7 (2005), pp. 537–546. ISSN: 17401526. DOI: [10.1038/nrmicro1180](https://doi.org/10.1038/nrmicro1180).
- [207] Klaus Jürgens et al. “Feeding rates of macro- and microzooplankton on heterotrophic nanoflagellates”. In: *Limnology and Oceanography* 41.8 (1996), pp. 1833–1839. ISSN: 00243590. DOI: [10.4319/lo.1996.41.8.1833](https://doi.org/10.4319/lo.1996.41.8.1833).
- [208] Klaus Jürgens et al. “Morphological and compositional changes in a planktonic bacterial community in response to enhanced protozoan grazing”. In: *Applied and Environmental Microbiology* 65.3 (1999), pp. 1241–1250. ISSN: 00992240. DOI: [10.1128/aem.65.3.1241-1250.1999](https://doi.org/10.1128/aem.65.3.1241-1250.1999).
- [209] Miroslav Macek et al. “Ciliate-Vibrio cholerae interactions within a microbial loop: An experimental study”. In: *Aquatic Microbial Ecology* 13.3 (1997), pp. 257–266. ISSN: 09483055. DOI: [10.3354/ame013257](https://doi.org/10.3354/ame013257).
- [210] Theodore J. Smayda and Brenda J. Boleyn. “Experimental Observations on the Flotation of Marine Diatoms. I. Thalassiosira Cf. Nana, Thalassiosira Rotula and Nitzschia Seriata”. In: *Limnology and Oceanography* 10.4 (1965), pp. 499–509. ISSN: 19395590. DOI: [10.4319/lo.1965.10.4.0499](https://doi.org/10.4319/lo.1965.10.4.0499).
- [211] David K. A. Barnes et al. “Accumulation and fragmentation of plastic debris in global environments”. In: *Philosophical Transactions of the Royal Society B: Biological Sciences* 364.1526 (2009), pp. 1985–1998.
- [212] Ganesh Gopalakrishnan et al. “Structure and evolution of the cold dome off northeastern Taiwan: A numerical study”. In: *Oceanography* 26.1 (2013), pp. 66–79. ISSN: 10428275. DOI: [10.5670/oceanog.2013.06](https://doi.org/10.5670/oceanog.2013.06).
- [213] Hiroshi Ichikawa and Beardsley Robert C. *Ichikawa and Beardsley.Pdf*. DOI: [10.1023/A:1015876701363](https://doi.org/10.1023/A:1015876701363).
- [214] Environmental Waste Management Division Okinawa Prefectural Government. 1. 2016, pp. 1–750.
- [215] Andrea K ppler et al. “Analysis of environmental microplastics by vibrational microspectroscopy: FTIR, Raman or both?” In: *Analytical and Bioanalytical Chemistry* 408.29 (2016), pp. 8377–8391. DOI: [10.1007/s00216-016-9956-3](https://doi.org/10.1007/s00216-016-9956-3).
- [216] James L. Hench, James J. Leichter, and Stephen G. Monismith. “Episodic circulation and exchange in a wave-driven coral reef and lagoon system”. In: *Limnology and Oceanography* 53.6 (2008), pp. 2681–2694. ISSN: 00243590. DOI: [10.4319/lo.2008.53.6.2681](https://doi.org/10.4319/lo.2008.53.6.2681). URL: <http://www.jstor.org/stable/40058355?Search=yes%7B%5C%7DresultItemClick=true%7B%5C%7DsearchText=connectivity%7B%5C%7DsearchText=reef%7B%5C%7DsearchText=estuary%7B%5C%7DsearchUri=/action/doBasicSearch?Query=connectivity+reef+estuary%7B%5C%7Dacc=on%7B%5C%7Dwc=on%7B%5C%7Dfc=off%7B%5C%7D252>.
- [217] Fes a De Scally. “Historical Tropical Cyclone Activity and Impacts in the Cook Islands 1”. In: *Pacific Science* 62.4 (2004), pp. 443–459. ISSN: 1534-6188. DOI: [10.2984/1534-6188\(2008\)62](https://doi.org/10.2984/1534-6188(2008)62). URL: <http://scholarspace.manoa.hawaii.edu/bitstream/handle/10125/22721/vol162n4-443-460.pdf?sequence=1>.

- [218] Google Earth. “Okinawa Island 26.2124°N, 127.6809°E, viewed June 2020”. Version 7.3.3.7699 (64-bit), OpenGL Microsoft Windows (6.2.9200.0) NVIDIA Corporation (00026.00021.00014.03086). In: ().
- [219] T M Ansari, I L Marr, and N Tariq. “Heavy Metals in Marine Pollution Perspective-A Mini Review”. In: *Journal of Applied Sciences* 4.1 (2004), pp. 1–20. DOI: [10.3923/jas.2004.1.20](https://scialert.net/abstract/?doi=jas.2004.1.20). URL: <https://scialert.net/abstract/?doi=jas.2004.1.20>.
- [220] IRUG. URL: [http://www.irug.org/search-spectral-database/spectra-index?sortHeader=data\\_type\\_raman](http://www.irug.org/search-spectral-database/spectra-index?sortHeader=data_type_raman).
- [221] Paulo Ribeiro-Claro, Mariela M. Nolasco, and Catarina Araújo. “Characterization of Microplastics by Raman Spectroscopy”. In: *Comprehensive Analytical Chemistry* 75 (2017), pp. 119–151. ISSN: 0166526X. DOI: [10.1016/bs.coac.2016.10.001](https://doi.org/10.1016/bs.coac.2016.10.001).
- [222] A Ashkin et al. “Observation of a single-beam gradient force optical trap for dielectric particles”. In: *Optics Letters* 11.5 (1986), pp. 288–290. DOI: [10.1364/ol.11.000288](https://doi.org/10.1364/ol.11.000288).
- [223] A Ashkin. “Acceleration and Trapping of Particles by Radiation Pressure”. In: *Physical Review Letters* 24.4 (1970), pp. 156–159. DOI: [10.1103/physrevlett.24.156](https://doi.org/10.1103/physrevlett.24.156).
- [224] A Ashkin. “Optical trapping and manipulation of neutral particles using lasers”. In: *Proceedings of the National Academy of Sciences* 94.10 (1997), pp. 4853–4860. DOI: [10.1142/4208](https://doi.org/10.1142/4208).
- [225] Domna G Kotsifaki and Síle Nic Chormaic. “Plasmonic optical tweezers based on nanostructures: fundamentals, advances and prospects”. In: *Nanophotonics* 8.7 (2019), pp. 1227–1245. DOI: [10.1515/nanoph-2019-0151](https://doi.org/10.1515/nanoph-2019-0151).
- [226] David G. Grier and Yael Roichman. “Holographic optical trapping”. In: *Appl. Opt.* 45.5 (2006), pp. 880–887.
- [227] Claudia Arbore et al. “Probing force in living cells with optical tweezers: from single-molecule mechanics to cell mechanotransduction”. In: *Biophysical Reviews* 11.5 (2019), pp. 765–782. DOI: [10.1007/s12551-019-00599-y](https://doi.org/10.1007/s12551-019-00599-y).
- [228] Robert W Applegate et al. “Optical trapping, manipulation, and sorting of cells and colloids in microfluidic systems with diode laser bars”. In: *Opt. Express* 12.19 (Sept. 2004), pp. 4390–4398. DOI: [10.1364/opex.12.004390](https://doi.org/10.1364/opex.12.004390).
- [229] Péter Galajda and Pál Ormos. “Orientation of flat particles in optical tweezers by linearly polarized light”. In: *Opt. Express* 11.5 (Mar. 2003), pp. 446–451.
- [230] Richard W Bowman and Miles J Padgett. “Optical trapping and binding”. In: *Reports on Progress in Physics* 76.2 (Jan. 2013), p. 26401. DOI: [10.1088/0034-4885/76/2/026401](https://doi.org/10.1088/0034-4885/76/2/026401).
- [231] Eva Urlaub et al. “Raman investigation of styrene polymerization in single optically trapped emulsion particles”. In: *Chemical Physics Letters* 231.4 (1994), pp. 511–514.
- [232] Katsuhiko Ajito and Keiichi Torimitsu. “Single Nanoparticle Trapping Using a Raman Tweezers Microscope”. In: *Applied Spectroscopy, Vol. 56, Issue 4, pp. 541-544* 56.4 (Apr. 2002), pp. 541–544. DOI: [10.1366/0003702021955015](https://doi.org/10.1366/0003702021955015).
- [233] Changan Xie, Mumtaz A. Dinno, and Yong-Qing Li. “Near-infrared Raman spectroscopy of single optically trapped biological cells”. In: *Opt. Lett.* 27.4 (2002), pp. 249–251.

- [234] D. L. Tomlinson et al. “Problems in the assessment of heavy-metal levels in estuaries and the formation of a pollution index”. In: *Helgoländer Meeresuntersuchungen* 33.1-4 (Mar. 1980), pp. 566–575. ISSN: 00179957. DOI: [10.1007/BF02414780](https://doi.org/10.1007/BF02414780). URL: <http://link.springer.com/10.1007/BF02414780>.
- [235] JB Buchanan, JM Kain - for the study ..., and undefined 1971. “Measurement of the physical and chemical environment”. In: *Blackwell Scientific Publications ...* ().
- [236] C. J. Moore et al. “A comparison of neustonic plastic and zooplankton abundance in southern California’s coastal waters”. In: *Marine Pollution Bulletin* 44.10 (Oct. 2002), pp. 1035–1038. ISSN: 0025326X. DOI: [10.1016/S0025-326X\(02\)00150-9](https://doi.org/10.1016/S0025-326X(02)00150-9).
- [237] Juliana A. Ivar Do Sul and Monica F. Costa. *The present and future of microplastic pollution in the marine environment*. Feb. 2014. DOI: [10.1016/j.envpol.2013.10.036](https://doi.org/10.1016/j.envpol.2013.10.036).
- [238] P. G. Ryan. “Effects of ingested plastic on seabird feeding: Evidence from chickens”. In: *Marine Pollution Bulletin* 19.3 (Mar. 1988), pp. 125–128. ISSN: 0025326X. DOI: [10.1016/0025-326X\(88\)90708-4](https://doi.org/10.1016/0025-326X(88)90708-4).
- [239] OkinawajapaneseWiki. 沖縄県に属する地方自治体の人口密度分布図. URL: [https://ja.m.wikipedia.org/wiki/%E3%83%95%E3%82%A1%E3%82%A4%E3%83%AB:Population\\_density\\_map\\_of\\_the\\_municipalities\\_of\\_Okinawa\\_prefecture,\\_Japan.svg](https://ja.m.wikipedia.org/wiki/%E3%83%95%E3%82%A1%E3%82%A4%E3%83%AB:Population_density_map_of_the_municipalities_of_Okinawa_prefecture,_Japan.svg).
- [240] Tomoya Kataoka et al. “Assessment of the sources and inflow processes of microplastics in the river environments of Japan”. In: *Environmental Pollution* 244 (2019), pp. 958–965. ISSN: 18736424. DOI: [10.1016/j.envpol.2018.10.111](https://doi.org/10.1016/j.envpol.2018.10.111). URL: <https://doi.org/10.1016/j.envpol.2018.10.111>.
- [241] Teresa Romeo et al. *First record of plastic debris in the stomach of Mediterranean lanternfishes*. Tech. rep. 1. 2016, pp. 115–124. URL: <https://pdfs.semanticscholar.org/3c49/4c3d751d4017047765dd1037050ef1e8d1b8.pdf>.
- [242] Holly A. Nel, Tatenda Dalu, and Ryan J. Wasserman. “Sinks and sources: Assessing microplastic abundance in river sediment and deposit feeders in an Austral temperate urban river system”. In: *Science of the Total Environment* 612 (Jan. 2018), pp. 950–956. ISSN: 18791026. DOI: [10.1016/j.scitotenv.2017.08.298](https://doi.org/10.1016/j.scitotenv.2017.08.298).
- [243] Ksenia J. Groh et al. “Overview of known plastic packaging-associated chemicals and their hazards”. In: *Science of the Total Environment* 651 (2019), pp. 3253–3268. ISSN: 18791026. DOI: [10.1016/j.scitotenv.2018.10.015](https://doi.org/10.1016/j.scitotenv.2018.10.015).
- [244] Jasna Maršić-Lučić et al. “Levels of trace metals on microplastic particles in beach sediments of the island of Vis, Adriatic Sea, Croatia”. In: *Marine Pollution Bulletin* 137. July (2018), pp. 231–236. ISSN: 18793363. DOI: [10.1016/j.marpolbul.2018.10.027](https://doi.org/10.1016/j.marpolbul.2018.10.027).
- [245] Juan Santos-Echeandía et al. “Interaction of mercury with beached plastics with special attention to zonation, degradation status and polymer type”. In: *Marine Chemistry* 222. March (2020), p. 103788. ISSN: 03044203. DOI: [10.1016/j.marchem.2020.103788](https://doi.org/10.1016/j.marchem.2020.103788). URL: <https://doi.org/10.1016/j.marchem.2020.103788>.
- [246] Etsuko Nakashima et al. “Quantification of toxic metals derived from macroplastic litter on Ookushi Beach, Japan”. In: *Environmental Science and Technology* 46.18 (2012), pp. 10099–10105. ISSN: 0013936X. DOI: [10.1021/es301362g](https://doi.org/10.1021/es301362g).



- [247] Yukie Mato et al. “Plastic resin pellets as a transport medium for toxic chemicals in the marine environment”. In: *Environmental Science and Technology* 35.2 (2001), pp. 318–324. ISSN: 0013936X. DOI: [10.1021/es0010498](https://doi.org/10.1021/es0010498).
- [248] Chelsea M. Rochman et al. “Anthropogenic debris in seafood: Plastic debris and fibers from textiles in fish and bivalves sold for human consumption”. In: *Scientific Reports* 5.1 (Nov. 2015), p. 14340. ISSN: 2045-2322. DOI: [10.1038/srep14340](https://doi.org/10.1038/srep14340). URL: <http://www.nature.com/articles/srep14340>.
- [249] Emma L. Teuten et al. “Potential for plastics to transport hydrophobic contaminants”. In: *Environmental Science and Technology* 41.22 (2007), pp. 7759–7764. ISSN: 0013936X. DOI: [10.1021/es071737s](https://doi.org/10.1021/es071737s).
- [250] Luke A. Holmes, Andrew Turner, and Richard C. Thompson. “Interactions between trace metals and plastic production pellets under estuarine conditions”. In: *Marine Chemistry* 167 (2014), pp. 25–32. ISSN: 03044203. DOI: [10.1016/j.marchem.2014.06.001](https://doi.org/10.1016/j.marchem.2014.06.001). URL: <http://dx.doi.org/10.1016/j.marchem.2014.06.001>.
- [251] Song Ye and Anthony L. Andrady. “Fouling of floating plastic debris under Biscayne Bay exposure conditions”. In: *Marine Pollution Bulletin* 22.12 (1991), pp. 608–613. ISSN: 0025326X. DOI: [10.1016/0025-326X\(91\)90249-R](https://doi.org/10.1016/0025-326X(91)90249-R).
- [252] Dennis Brennecke et al. “Microplastics as vector for heavy metal contamination from the marine environment”. In: *Estuarine, Coastal and Shelf Science* 178 (2016), pp. 189–195. ISSN: 02727714. DOI: [10.1016/j.ecss.2015.12.003](https://doi.org/10.1016/j.ecss.2015.12.003).
- [253] Ken Ichi Kitahara and Haruhiko Nakata. “Plastic additives as tracers of microplastic sources in Japanese road dusts”. In: *Science of the Total Environment* 736 (2020), p. 139694. ISSN: 18791026. DOI: [10.1016/j.scitotenv.2020.139694](https://doi.org/10.1016/j.scitotenv.2020.139694). URL: <https://doi.org/10.1016/j.scitotenv.2020.139694>.
- [254] Kwanchai Pakoksung et al. “Estimating tsunami economic losses of okinawa island with multi-regional-input-output modeling”. In: *Geosciences (Switzerland)* 9.8 (2019), pp. 1–21. ISSN: 20763263. DOI: [10.3390/geosciences9080349](https://doi.org/10.3390/geosciences9080349).
- [255] Samuel R.P.J. Ross et al. “Listening to ecosystems: data-rich acoustic monitoring through landscape-scale sensor networks”. In: *Ecological Research* 33.1 (2018), pp. 135–147. ISSN: 14401703. DOI: [10.1007/s11284-017-1509-5](https://doi.org/10.1007/s11284-017-1509-5).
- [256] Dativa J. SHILLA et al. “Preliminary survey of the nutrient discharge characteristics of Okinawa Rivers, and their potential effects on inshore coral reefs”. In: *Galaxea, Journal of Coral Reef Studies* 15.Supplement (2013), pp. 172–181. ISSN: 1883-0838. DOI: [10.3755/galaxea.15.172](https://doi.org/10.3755/galaxea.15.172).
- [257] Swetlana Wagner and Martin Schlummer. “Legacy additives in a circular economy of plastics: Current dilemma, policy analysis, and emerging countermeasures”. In: *Resources, Conservation and Recycling* 158 (2020), p. 104800.
- [258] Young Kyoung Song et al. “Combined Effects of UV Exposure Duration and Mechanical Abrasion on Microplastic Fragmentation by Polymer Type”. In: *Environmental Science & Technology* 51.8 (2017), pp. 4368–4376.
- [259] Marcus Eriksen et al. “Plastic Pollution in the World’s Oceans: More than 5 Trillion Plastic Pieces Weighing over 250,000 Tons Afloat at Sea”. In: *PLoS One* 9.12 (2014), e111913.





- [273] Michael L. McKinney. “Is Marine Biodiversity at Less Risk ? Evidence and Implications”. Author(s): Michael L. McKinney Published by : Wiley Stable URL : <http://www.jstor.org/stable/2999807> Accessed : 12-04-2016 02 : 10 UTC Your use of the JSTOR archive indicates your acceptance”. In: 4.1 (1998), pp. 3–8.
- [274] Anna J. Woodhead et al. “Coral reef ecosystem services in the Anthropocene”. In: *Functional Ecology* 33.6 (2019), pp. 1023–1034. ISSN: 13652435. DOI: [10.1111/1365-2435.13331](https://doi.org/10.1111/1365-2435.13331).
- [275] MEA. *Overview of the millennium ecosystem assessment*. 2005.
- [276] Terry P. Hughes et al. “Spatial and temporal patterns of mass bleaching of corals in the Anthropocene”. In: *Science* 359.6371 (Jan. 2018), pp. 80–83. ISSN: 10959203. DOI: [10.1126/science.aan8048](https://doi.org/10.1126/science.aan8048).
- [277] Kelsey L. Rogers et al. “Micro-by-micro interactions: How microorganisms influence the fate of marine microplastics”. In: *Limnology and Oceanography Letters* 5.1 (Feb. 2020), pp. 18–36. ISSN: 2378-2242. DOI: [10.1002/lol2.10136](https://doi.org/10.1002/lol2.10136).
- [278] Hannes K. Imhof et al. “Spatial and temporal variation of macro-, meso- and microplastic abundance on a remote coral island of the Maldives, Indian Ocean”. In: *Marine Pollution Bulletin* 116.1-2 (Mar. 2017), pp. 340–347. ISSN: 18793363. DOI: [10.1016/j.marpolbul.2017.01.010](https://doi.org/10.1016/j.marpolbul.2017.01.010). URL: <http://dx.doi.org/10.1016/j.marpolbul.2017.01.010>.
- [279] Linlin Zhang et al. “The spatial distribution of microplastic in the sands of a coral reef island in the South China Sea: Comparisons of the fringing reef and atoll”. In: *Science of the Total Environment* 688 (2019), pp. 780–786. ISSN: 18791026. DOI: [10.1016/j.scitotenv.2019.06.178](https://doi.org/10.1016/j.scitotenv.2019.06.178). URL: <https://doi.org/10.1016/j.scitotenv.2019.06.178>.
- [280] Fei Tan et al. “Microplastic pollution around remote uninhabited coral reefs of Nansha Islands, South China Sea”. In: *Science of the Total Environment* 725 (2020), p. 138383. ISSN: 18791026. DOI: [10.1016/j.scitotenv.2020.138383](https://doi.org/10.1016/j.scitotenv.2020.138383). URL: <https://doi.org/10.1016/j.scitotenv.2020.138383>.
- [281] Jinfeng Ding et al. “Microplastics in the coral reef systems from Xisha Islands of South China Sea”. In: *Environmental Science and Technology* 53.14 (2019), pp. 8036–8046. ISSN: 15205851. DOI: [10.1021/acs.est.9b01452](https://doi.org/10.1021/acs.est.9b01452).
- [282] Cecilia Martin et al. “Adhesion to coral surface as a potential sink for marine microplastics”. In: *Environmental Pollution* 255 (2019), p. 113281. ISSN: 18736424. DOI: [10.1016/j.envpol.2019.113281](https://doi.org/10.1016/j.envpol.2019.113281). URL: <https://doi.org/10.1016/j.envpol.2019.113281>.
- [283] Jia Tang et al. “Acute microplastic exposure raises stress response and suppresses detoxification and immune capacities in the scleractinian coral *Pocillopora damicornis*”. In: *Environmental Pollution* 243 (Dec. 2018), pp. 66–74. ISSN: 18736424. DOI: [10.1016/j.envpol.2018.08.045](https://doi.org/10.1016/j.envpol.2018.08.045).
- [284] Nami Okubo, Shunichi Takahashi, and Yoshikatsu Nakano. “Microplastics disturb the anthozoan-algae symbiotic relationship”. In: *Marine Pollution Bulletin* 135 (Oct. 2018), pp. 83–89. ISSN: 18793363. DOI: [10.1016/j.marpolbul.2018.07.016](https://doi.org/10.1016/j.marpolbul.2018.07.016).

- [285] Cheryl Hankins, Allyn Duffy, and Kathryn Drisco. “Scleractinian coral microplastic ingestion: Potential calcification effects, size limits, and retention”. In: *Marine Pollution Bulletin* 135 (Oct. 2018), pp. 587–593. ISSN: 18793363. DOI: [10.1016/j.marpolbul.2018.07.067](https://doi.org/10.1016/j.marpolbul.2018.07.067).
- [286] Richard Cowen. “The Role of Algal Symbiosis in Reefs through Time”. In: *PALAIOS* 3.2 (Apr. 1988), p. 221. ISSN: 08831351. DOI: [10.2307/3514532](https://doi.org/10.2307/3514532).
- [287] George D. Stanley and Jere H. Lipps. “Photosymbiosis: The Driving Force for Reef Success and Failure”. In: *The Paleontological Society Papers* 17 (Oct. 2011), pp. 33–59. ISSN: 1089-3326. DOI: [10.1017/s1089332600002436](https://doi.org/10.1017/s1089332600002436).
- [288] L Steindler, S Beer, and M Ilan. *Photosymbiosis in Intertidal and Subtidal Tropical Sponges*. Tech. rep. 2002. URL: <https://new.tau.ac.il/lifesci/departments/zology/members/ilan/documents/Symbiosis.pdf>.
- [289] Todd C. LaJeunesse et al. “Systematic Revision of Symbiodiniaceae Highlights the Antiquity and Diversity of Coral Endosymbionts”. In: *Current Biology* 28.16 (2018), 2570–2580.e6. ISSN: 09609822. DOI: [10.1016/j.cub.2018.07.008](https://doi.org/10.1016/j.cub.2018.07.008). URL: <https://doi.org/10.1016/j.cub.2018.07.008>.
- [290] WILLIAM K. FITT and ROBERT K. TRENCH. “ SPAWNING, DEVELOPMENT, AND ACQUISITION OF ZOOXANTHELLAE BY TRIDACNA SQUAMOSA (MOLLUSCA, BIVALVIA) ”. In: *The Biological Bulletin* 161.2 (Oct. 1981), pp. 213–235. ISSN: 0006-3185. DOI: [10.2307/1540800](https://doi.org/10.2307/1540800).
- [291] Siro KAWAGUTI. “The Third Record of Association between Bivalve Mollusks and Zooxanthellae”. In: *Proceedings of the Japan Academy. Ser. B: Physical and Biological Sciences* 59.2 (1983), pp. 17–20. ISSN: 0386-2208. DOI: [10.2183/pjab.59.17](https://doi.org/10.2183/pjab.59.17). URL: <http://joi.jlc.jst.go.jp/JST.Journalarchive/pjab1977/59.17?from=CrossRef>.
- [292] Miguel Mies. *Evolution, diversity, distribution and the endangered future of the giant clam-Symbiodiniaceae association*. Dec. 2019. DOI: [10.1007/s00338-019-01857-x](https://doi.org/10.1007/s00338-019-01857-x).
- [293] Mamiko Hirose et al. “Phylogenetic analyses of potentially free-living Symbiodinium spp. isolated from coral reef sand in Okinawa, Japan”. In: *Marine Biology* 155.1 (2008), pp. 105–112. ISSN: 00253162. DOI: [10.1007/s00227-008-1011-2](https://doi.org/10.1007/s00227-008-1011-2).
- [294] Hiroshi Yamashita and Kazuhiko Koike. “Genetic identity of free-living Symbiodinium obtained over a broad latitudinal range in the Japanese coast”. In: *Phycological Research* 61.1 (2013), pp. 68–80. ISSN: 14401835. DOI: [10.1111/pre.12004](https://doi.org/10.1111/pre.12004).
- [295] D. A. Schoenberg and R. K. Trench. “Genetic variation in Symbiodinium (=Gymnodinium) microadriaticum Freudenthal, and specificity in its symbiosis with marine invertebrates. I. Isoenzyme and soluble protein patterns of axenic cultures of Symbiodinium microadriaticum”. In: *Proceedings of the Royal Society of London - Biological Sciences* 207.1169 (1980), pp. 405–427. ISSN: 09628452. DOI: [10.1098/rspb.1980.0031](https://doi.org/10.1098/rspb.1980.0031).
- [296] J. Christine Finney et al. “The relative significance of host-habitat, depth, and geography on the ecology, endemism, and speciation of coral endosymbionts in the genus Symbiodinium”. In: *Microbial Ecology* 60.1 (May 2010), pp. 250–263. ISSN: 00953628. DOI: [10.1007/s00248-010-9681-y](https://doi.org/10.1007/s00248-010-9681-y).

- [297] Todd C. LaJeunesse et al. “Long-standing environmental conditions, geographic isolation and host-symbiont specificity influence the relative ecological dominance and genetic diversification of coral endosymbionts in the genus *Symbiodinium*”. In: *Journal of Biogeography* 37.5 (May 2010), pp. 785–800. ISSN: 03050270. DOI: [10.1111/j.1365-2699.2010.02273.x](https://doi.org/10.1111/j.1365-2699.2010.02273.x). URL: <http://doi.wiley.com/10.1111/j.1365-2699.2010.02273.x>.
- [298] Yi T. Lien et al. “Occurrence of the putatively heat-tolerant *Symbiodinium* phylotype D in high-latitude outlying coral communities”. In: *Coral Reefs* 26.1 (Mar. 2007), pp. 35–44. ISSN: 07224028. DOI: [10.1007/s00338-006-0185-7](https://doi.org/10.1007/s00338-006-0185-7).
- [299] Andrew C. Baker. “Flexibility and Specificity in Coral-Algal Symbiosis: Diversity, Ecology, and Biogeography of *Symbiodinium*”. In: *Annual Review of Ecology, Evolution, and Systematics* 34.1 (Nov. 2003), pp. 661–689. ISSN: 1543-592X. DOI: [10.1146/annurev.ecolsys.34.011802.132417](https://doi.org/10.1146/annurev.ecolsys.34.011802.132417). URL: <http://www.annualreviews.org/doi/10.1146/annurev.ecolsys.34.011802.132417>.
- [300] Xavier Pochon et al. “Molecular phylogeny, evolutionary rates, and divergence timing of the symbiotic dinoflagellate genus *Symbiodinium*”. In: *Molecular Phylogenetics and Evolution* 38.1 (Jan. 2006), pp. 20–30. ISSN: 10557903. DOI: [10.1016/j.ympev.2005.04.028](https://doi.org/10.1016/j.ympev.2005.04.028).
- [301] M Yorifuji et al. “Comparison of *Symbiodinium* dinoflagellate flora in sea slug populations of the *Pteraeolia ianthina* complex”. In: *Marine Ecology Progress Series* 521 (Feb. 2015), pp. 91–104. ISSN: 0171-8630. DOI: [10.3354/meps11155](https://doi.org/10.3354/meps11155). URL: <http://www.int-res.com/abstracts/meps/v521/p91-104/>.
- [302] Mathias Harzhauser et al. “Tracing back the origin of the Indo-Pacific mollusc fauna: Basal tridacninae from the Oligocene and Miocene of the Sultanate of Oman”. In: *Palaeontology* 51.1 (Jan. 2008), pp. 199–213. ISSN: 00310239. DOI: [10.1111/j.1475-4983.2007.00742.x](https://doi.org/10.1111/j.1475-4983.2007.00742.x). URL: <http://doi.wiley.com/10.1111/j.1475-4983.2007.00742.x>.
- [303] Mei Lin Neo et al. *The ecological significance of giant clams in coral reef ecosystems*. Jan. 2015. DOI: [10.1016/j.biocon.2014.11.004](https://doi.org/10.1016/j.biocon.2014.11.004).
- [304] C M Yonge and C M Yonge. “MODE OF LIFE, FEEDING, DIGESTION AND SYMBIOSIS WITH ZOOXANTHELLAE IN THE TRIDACNIDAE”. In: *Scientific Reports / Great Barrier Reef Expedition 1928-29*. 1 (Feb. 1936), pp. 283–321. URL: <https://www.biodiversitylibrary.org/part/183507>.
- [305] Pamela Soo and Peter A. Todd. *The behaviour of giant clams (Bivalvia: Cardiidae: Tridacninae)*. Nov. 2014. DOI: [10.1007/s00227-014-2545-0](https://doi.org/10.1007/s00227-014-2545-0).
- [306] Patrick C. Cabaitan, Edgardo D. Gomez, and Porfirio M. Aliño. “Effects of coral transplantation and giant clam restocking on the structure of fish communities on degraded patch reefs”. In: *Journal of Experimental Marine Biology and Ecology* 357.1 (Mar. 2008), pp. 85–98. ISSN: 00220981. DOI: [10.1016/j.jembe.2008.01.001](https://doi.org/10.1016/j.jembe.2008.01.001).
- [307] John S. Lucas. “The Biology, Exploitation, and Mariculture of Giant Clams (Tridacnidae)”. In: *Reviews in Fisheries Science* 2.3 (1994), pp. 181–223. ISSN: 10641262. DOI: [10.1080/10641269409388557](https://doi.org/10.1080/10641269409388557).

- [308] E Hviding. *The rural context of giant clam mariculture in Solomon Islands: an anthropological study*. 1993. URL: <https://books.google.com/books?hl=en%7B%5C%7Dlr=%7B%5C%7Ddid=0ZrW5Z84iMcC%7B%5C%7Ddoi=fnd%7B%5C%7Dpg=PR8%7B%5C%7Ddots=o-mMYCLkUa%7B%5C%7Dsig=PpuwG0ykstSMh3EwwQ1a4g0AGD0>.
- [309] E. Blidberg. “Effects of copper and decreased salinity on survival rate and development of *Tridacna gigas* larvae”. In: *Marine Environmental Research*. Vol. 58. 2-5. Elsevier, Aug. 2004, pp. 793–797. DOI: [10.1016/j.marenvres.2004.03.095](https://doi.org/10.1016/j.marenvres.2004.03.095).
- [310] John Norton and Gareth Jones. *The Giant Clam - an anatomical and histological atlas*. Tech. rep. Canberra: Australian Centre for International Agricultural Research, 1992.
- [311] Lisa Kirkendale and Gustav Paulay. “Treatise Online no 89: Part N, Revised, Volume 1, Chapter 9: Photosymbiosis in Bivalvia”. In: *Treatise Online* (Feb. 2017). ISSN: 2153-4012. DOI: [10.17161/to.v0i0.6554](https://doi.org/10.17161/to.v0i0.6554).
- [312] TS DeBoer et al. “Patterns of Symbiodinium distribution in three giant clam species across the biodiverse Bird’s Head region of Indonesia”. In: *Marine Ecology Progress Series* 444 (Jan. 2012), pp. 117–132. ISSN: 0171-8630. DOI: [10.3354/meps09413](https://doi.org/10.3354/meps09413). URL: <http://www.int-res.com/abstracts/meps/v444/p117-132/>.
- [313] Terufumi Ohno, Tetzuya Katoh, and Terufumi Yamasu. “The origin of algal-bivalve photosymbiosis”. In: *Palaeontology* 38.1 (1995), pp. 1–21. URL: <https://www.palass.org/publications/palaeontology-journal/archive/38/1/article%7B%5C%7Dpp1-21>.
- [314] A Myra Keen. *THE PELECYPOD FAMILY CARDIIDAE: A TAXONOMIC SUMMARY*. Tech. rep. 1. 1980.
- [315] Caryn C. Vaughn and Timothy J. Hoellein. “Bivalve Impacts in Freshwater and Marine Ecosystems”. In: *Annual Review of Ecology, Evolution, and Systematics* 49.1 (Nov. 2018), pp. 183–208. ISSN: 1543-592X. DOI: [10.1146/annurev-ecolsys-110617-062703](https://doi.org/10.1146/annurev-ecolsys-110617-062703). URL: <https://www.annualreviews.org/doi/10.1146/annurev-ecolsys-110617-062703>.
- [316] Andrea K. Fritts et al. “Nonlethal assessment of freshwater mussel physiological response to changes in environmental factors”. In: *Canadian Journal of Fisheries and Aquatic Sciences* 72.10 (Oct. 2015). Ed. by Deborah MacLachy, pp. 1460–1468. ISSN: 0706-652X. DOI: [10.1139/cjfas-2014-0565](https://doi.org/10.1139/cjfas-2014-0565). URL: <http://www.nrcresearchpress.com/doi/10.1139/cjfas-2014-0565>.
- [317] Jan Johan ter Poorten. *The Cardiidae of the Panglao Marine Biodiversity Project 2004 and the Panglao 2005 Deep-Sea Cruise with descriptions of four new species (Bivalvia) ter*. Tech. rep. 2009, pp. 9–96. URL: <https://hdl.handle.net/11245/1.310282>.
- [318] Alvin A. Carlos et al. “Phylogenetic position of Symbiodinium (Dinophyceae) isolates from tridacnids (Bivalvia), cardiids (Bivalvia), a sponge (Porifera), a soft coral (Anthozoa), and a free-living strain”. In: *Journal of Phycology* 35.5 (Oct. 1999), pp. 1054–1062. ISSN: 00223646. DOI: [10.1046/j.1529-8817.1999.3551054.x](https://doi.org/10.1046/j.1529-8817.1999.3551054.x). URL: <http://doi.wiley.com/10.1046/j.1529-8817.1999.3551054.x>.
- [319] Rob Rowan. *Diversity and ecology of zooxanthellae on coral reefs*. June 1998. DOI: [10.1046/j.1529-8817.1998.340407.x](https://doi.org/10.1046/j.1529-8817.1998.340407.x). URL: <http://doi.wiley.com/10.1046/j.1529-8817.1998.340407.x>.



- [320] Agathe Bour et al. “Environmentally relevant microplastic exposure affects sediment-dwelling bivalves”. In: *Environmental Pollution* 236 (2018), pp. 652–660. ISSN: 18736424. DOI: [10.1016/j.envpol.2018.02.006](https://doi.org/10.1016/j.envpol.2018.02.006). URL: <https://doi.org/10.1016/j.envpol.2018.02.006>.
- [321] Carlo Giacomo Avio et al. “Pollutants bioavailability and toxicological risk from microplastics to marine mussels”. In: *Environmental Pollution* 198 (2015), pp. 211–222. ISSN: 18736424. DOI: [10.1016/j.envpol.2014.12.021](https://doi.org/10.1016/j.envpol.2014.12.021). URL: <http://dx.doi.org/10.1016/j.envpol.2014.12.021>.
- [322] Francisca Ribeiro et al. “Microplastics effects in *Scrobicularia plana*”. In: *Marine Pollution Bulletin* 122.1-2 (2017), pp. 379–391. ISSN: 18793363. DOI: [10.1016/j.marpolbul.2017.06.078](https://doi.org/10.1016/j.marpolbul.2017.06.078).
- [323] Nadia Von Moos, Patricia Burkhardt-Holm, and Angela Köhler. “Uptake and effects of microplastics on cells and tissue of the blue mussel *Mytilus edulis* L. after an experimental exposure”. In: *Environmental Science and Technology* 46.20 (2012), pp. 11327–11335. ISSN: 0013936X. DOI: [10.1021/es302332w](https://doi.org/10.1021/es302332w).
- [324] Silvia Arossa et al. “Microplastic removal by Red Sea giant clam (*Tridacna maxima*)”. In: *Environmental Pollution* 252 (Sept. 2019), pp. 1257–1266. ISSN: 18736424. DOI: [10.1016/j.envpol.2019.05.149](https://doi.org/10.1016/j.envpol.2019.05.149).
- [325] Jun’ichi Kobayashi et al. “Amphidinolide C: The first 25-membered macrocyclic lactone with potent antineoplastic activity from the cultured dinoflagellate amphidinium sp”. In: *Journal of the American Chemical Society* 110.2 (1988), pp. 490–494. ISSN: 15205126. DOI: [10.1021/ja00210a029](https://doi.org/10.1021/ja00210a029).
- [326] Girish Beedessee et al. “Diversified secondary metabolite biosynthesis gene repertoire revealed in symbiotic dinoflagellates”. In: *Scientific Reports* 9.1 (2019), pp. 1–12. ISSN: 20452322. DOI: [10.1038/s41598-018-37792-0](https://doi.org/10.1038/s41598-018-37792-0). URL: <http://dx.doi.org/10.1038/s41598-018-37792-0>.
- [327] Eiichi Shoguchi et al. “Two divergent Symbiodinium genomes reveal conservation of a gene cluster for sunscreen biosynthesis and recently lost genes”. In: *BMC Genomics* 19.1 (2018), pp. 1–11. ISSN: 14712164. DOI: [10.1186/s12864-018-4857-9](https://doi.org/10.1186/s12864-018-4857-9).
- [328] Thomas Krueger and Ruth D. Gates. “Cultivating endosymbionts - Host environmental mimics support the survival of Symbiodinium C15 ex hospite”. In: *Journal of Experimental Marine Biology and Ecology* 413. February (2012), pp. 169–176. ISSN: 00220981. DOI: [10.1016/j.jembe.2011.12.002](https://doi.org/10.1016/j.jembe.2011.12.002). URL: <http://dx.doi.org/10.1016/j.jembe.2011.12.002>.
- [329] Anke Klueter et al. “Comparative growth rates of cultured marine dinoflagellates in the genus Symbiodinium and the effects of temperature and light”. In: *PLoS ONE* 12.11 (2017). ISSN: 19326203. DOI: [10.1371/journal.pone.0187707](https://doi.org/10.1371/journal.pone.0187707).
- [330] Mireille Consalvey et al. “Pam fluorescence: A beginners guide for benthic diatomists”. In: *Diatom Research* 20.1 (2005), pp. 1–22. ISSN: 21598347. DOI: [10.1080/0269249X.2005.9705619](https://doi.org/10.1080/0269249X.2005.9705619).
- [331] Daniel Wangpraseurt et al. “Spectral effects on Symbiodinium photobiology studied with a programmable light engine”. In: *PLoS ONE* 9.11 (2014). ISSN: 19326203. DOI: [10.1371/journal.pone.0112809](https://doi.org/10.1371/journal.pone.0112809).



- [332] Mark D. Robinson and Alicia Oshlack. “A scaling normalization method for differential expression analysis of RNA-seq data”. In: *Genome Biology* 11.3 (2010). ISSN: 14747596. DOI: [10.1186/gb-2010-11-3-r25](https://doi.org/10.1186/gb-2010-11-3-r25).
- [333] Xavier Mari et al. “Transparent exopolymer particles: Effects on carbon cycling in the ocean”. In: *Progress in Oceanography* 151.November (2017), pp. 13–37. ISSN: 00796611. DOI: [10.1016/j.pocean.2016.11.002](https://doi.org/10.1016/j.pocean.2016.11.002). URL: <http://dx.doi.org/10.1016/j.pocean.2016.11.002>.
- [334] Jörg C. Frommlet et al. “Symbiodinium-induced formation of microbialites: Mechanistic insights from in Vitro experiments and the prospect of its occurrence in nature”. In: *Frontiers in Microbiology* 9.MAY (2018), pp. 1–18. ISSN: 1664302X. DOI: [10.3389/fmicb.2018.00998](https://doi.org/10.3389/fmicb.2018.00998).
- [335] B. E. Logan and A. L. Alldredge. “Potential for increased nutrient uptake by flocculating diatoms”. In: *Marine Biology* 101.4 (1989), pp. 443–450. ISSN: 00253162. DOI: [10.1007/BF00541645](https://doi.org/10.1007/BF00541645).
- [336] Giulia Rossi and Luca Monticelli. “Modeling the effect of nano-sized polymer particles on the properties of lipid membranes”. In: *Journal of Physics Condensed Matter* 26.50 (2014). ISSN: 1361648X. DOI: [10.1088/0953-8984/26/50/503101](https://doi.org/10.1088/0953-8984/26/50/503101).
- [337] Robert D. Finn et al. “The Pfam protein families database”. In: *Nucleic Acids Research* 38.SUPPL.1 (2009), pp. 211–222. ISSN: 03051048. DOI: [10.1093/nar/gkp985](https://doi.org/10.1093/nar/gkp985).
- [338] Ana Conesa et al. “Blast2GO: A universal tool for annotation, visualization and analysis in functional genomics research”. In: *Bioinformatics* 21.18 (2005), pp. 3674–3676. ISSN: 13674803. DOI: [10.1093/bioinformatics/bti610](https://doi.org/10.1093/bioinformatics/bti610).
- [339] Bill Wickstead and Keith Gull. “Dyneins across eukaryotes: A comparative genomic analysis”. In: *Traffic* 8.12 (2007), pp. 1708–1721. ISSN: 13989219. DOI: [10.1111/j.1600-0854.2007.00646.x](https://doi.org/10.1111/j.1600-0854.2007.00646.x).
- [340] Carlos Wilson and Christian González-Billault. “Regulation of cytoskeletal dynamics by redox signaling and oxidative stress: Implications for neuronal development and trafficking”. In: *Frontiers in Cellular Neuroscience* 9.SEPTEMBER (2015), pp. 1–10. ISSN: 16625102. DOI: [10.3389/fncel.2015.00381](https://doi.org/10.3389/fncel.2015.00381).
- [341] S. Magni et al. “First evidence of protein modulation by polystyrene microplastics in a freshwater biological model”. In: *Environmental Pollution* 250 (2019), pp. 407–415. ISSN: 18736424. DOI: [10.1016/j.envpol.2019.04.088](https://doi.org/10.1016/j.envpol.2019.04.088). URL: <https://doi.org/10.1016/j.envpol.2019.04.088>.
- [342] Se Hyeon Jang et al. “De novo assembly and characterization of the transcriptome of the newly described dinoflagellate *Ansanella granifera*: Spotlight on flagellum-associated genes”. In: *Marine genomics* 33 (June 2017), pp. 47–55. ISSN: 1874-7787. DOI: [10.1016/j.margen.2017.01.003](https://doi.org/10.1016/j.margen.2017.01.003). URL: <https://doi.org/10.1016/j.margen.2017.01.003>.
- [343] P Bork et al. “Domains in plexins: links to integrins and transcription factors.” eng. In: *Trends in biochemical sciences* 24.7 (July 1999), pp. 261–263. ISSN: 0968-0004 (Print). DOI: [10.1016/s0968-0004\(99\)01416-4](https://doi.org/10.1016/s0968-0004(99)01416-4).

- [344] C Collesi et al. “A splicing variant of the RON transcript induces constitutive tyrosine kinase activity and an invasive phenotype.” In: *Molecular and Cellular Biology* 16.10 (1996), pp. 5518–5526. ISSN: 0270-7306. DOI: [10.1128/mcb.16.10.5518](https://doi.org/10.1128/mcb.16.10.5518).
- [345] P Michaely and V Bennett. “The ANK repeat: a ubiquitous motif involved in macromolecular recognition.” eng. In: *Trends in cell biology* 2.5 (May 1992), pp. 127–129. ISSN: 0962-8924 (Print). DOI: [10.1016/0962-8924\(92\)90084-z](https://doi.org/10.1016/0962-8924(92)90084-z).
- [346] A. Barkan et al. “A nuclear mutation in maize blocks the processing and translation of several chloroplast mRNAs and provides evidence for the differential translation of alternative mRNA forms”. In: *EMBO Journal* 13.13 (1994), pp. 3170–3181. ISSN: 02614189. DOI: [10.1002/j.1460-2075.1994.tb06616.x](https://doi.org/10.1002/j.1460-2075.1994.tb06616.x).
- [347] Sutada Mungpakdee et al. “Massive gene transfer and extensive RNA editing of a symbiotic dinoflagellate plastid genome”. In: *Genome Biology and Evolution* 6.6 (2014), pp. 1408–1422. ISSN: 17596653. DOI: [10.1093/gbe/evu109](https://doi.org/10.1093/gbe/evu109).
- [348] Eiichi Shoguchi et al. “The large mitochondrial genome of symbiodinium minutum reveals conserved noncoding Sequences between dinoflagellates and apicomplexans”. In: *Genome Biology and Evolution* 7.8 (2015), pp. 2237–2244. ISSN: 17596653. DOI: [10.1093/gbe/evv137](https://doi.org/10.1093/gbe/evv137).
- [349] Jan-Michael Peters. “The anaphase promoting complex/cyclosome: a machine designed to destroy.” eng. In: *Nature reviews. Molecular cell biology* 7.9 (Sept. 2006), pp. 644–656. ISSN: 1471-0072 (Print). DOI: [10.1038/nrm1988](https://doi.org/10.1038/nrm1988).
- [350] Tohru Tsuchiya et al. “Cloning of chlorophyllase, the key enzyme in chlorophyll degradation: Finding of a lipase motif and the induction by methyl jasmonate”. In: *Proceedings of the National Academy of Sciences of the United States of America* 96.26 (1999), pp. 15362–15367. ISSN: 00278424. DOI: [10.1073/pnas.96.26.15362](https://doi.org/10.1073/pnas.96.26.15362).
- [351] Alexandra Ter Halle et al. “Understanding the Fragmentation Pattern of Marine Plastic Debris”. In: *Environmental Science and Technology* 50.11 (2016), pp. 5668–5675. ISSN: 15205851. DOI: [10.1021/acs.est.6b00594](https://doi.org/10.1021/acs.est.6b00594).
- [352] Christopher B. Field et al. “Primary production of the biosphere: Integrating terrestrial and oceanic components”. In: *Science* 281.5374 (1998), pp. 237–240. ISSN: 00368075. DOI: [10.1126/science.281.5374.237](https://doi.org/10.1126/science.281.5374.237).
- [353] Britta D. Hardesty et al. “Using Numerical Model Simulations to Improve the Understanding of Micro-plastic Distribution and Pathways in the Marine Environment”. In: *Frontiers in Marine Science* 4.MAR (Mar. 2017), p. 30. ISSN: 2296-7745. DOI: [10.3389/fmars.2017.00030](https://doi.org/10.3389/fmars.2017.00030). URL: <http://journal.frontiersin.org/article/10.3389/fmars.2017.00030/full>.

# **Appendix A**

## **Articles under review**



Communication

# Response of Coral Reef Dinoflagellates to Nanoplastics under Experimental Conditions Suggests Downregulation of Cellular Metabolism

Christina Ripken <sup>1,2,\*</sup>, Konstantin Khalturin <sup>2</sup> and Eiichi Shoguchi <sup>2</sup>

<sup>1</sup> Light-Matter Interactions for Quantum Technologies Unit, Okinawa Institute of Science and Technology Graduate University, Onna, Okinawa 904-0495, Japan

<sup>2</sup> Marine Genomics Unit, Okinawa Institute of Science and Technology Graduate University, Onna, Okinawa 904-0495, Japan; konstantin.khalturin@oist.jp (K.K.); eiichi@oist.jp (E.S.)

\* Correspondence: christina.ripken@oist.jp

Received: 25 September 2020; Accepted: 5 November 2020; Published: date

**Abstract:** Plastic products contribute heavily to anthropogenic pollution of the oceans. Small plastic particles in the microscale and nanoscale ranges have been found in all marine ecosystems, but little is known about their effects upon marine organisms. In this study, we examine changes in cell growth, aggregation, and gene expression of two symbiotic dinoflagellates of the family Symbiodiniaceae, *Symbiodinium tridacnidorum* (clade A3), and *Cladocopium* sp. (clade C) under exposure to 42-nm polystyrene beads. In laboratory experiments, the cell number and aggregation were reduced after 10 days of nanoplastic exposure at 0.01, 0.1, and 10 mg/L concentrations, but no clear correlation with plastic concentration was observed. Genes involved in dynein motor function were upregulated when compared to control conditions, while genes related to photosynthesis, mitosis, and intracellular degradation were downregulated. Overall, nanoplastic exposure led to more genes being downregulated than upregulated and the number of genes with altered expression was larger in *Cladocopium* sp. than in *S. tridacnidorum*, suggesting different sensitivity to nano-plastics between species. Our data show that nano-plastic inhibits growth and alters aggregation properties of microalgae, which may negatively affect the uptake of these indispensable symbionts by coral reef organisms.

**Keywords:** nanoplastics; dinoflagellate; coral reef; *Symbiodinium*; *Cladocopium*; gene expression

## 1. Introduction

Coral reefs provide a habitat for marine invertebrate and vertebrate species alike, sustaining the highest biodiversity among marine ecosystems [1]. Formed primarily by scleractinian corals and coralline algae, coral reefs are complex and vulnerable ecosystems. Structural complexity of coral reefs, and, by extension, the capability to sustain biodiversity often declines due to natural and human-related stressors [2,3].

One important stressor for coral reef ecosystems is plastic pollution. Small plastic particles (>1 mm) have been reported from coral islands at more than 1000 items/m<sup>2</sup> [4]. Further fragmentation of these particles leads to nano-plastics (<1 μm) [5]. Microplastic particles induce stress responses in scleractinian corals, and suppress their immune systems and capacity to cope with environmental toxins [6]. When ingested by corals [7–9], microplastics disrupt the anthozoan-algal symbiotic relationship [10]. They are also linked to potential adverse effects on calcification [11] with exposure resulting in attachment of microplastic particles to tentacles or mesenterial filaments, ingestion of microplastic particles, and increased mucus production [12]. Su et al. [13] exposed the coral symbiont,

*Cladocopium goreauii*, to 1- $\mu\text{m}$  polystyrene spheres, leading to diminished detoxification activity, nutrient uptake, and photosynthesis as well as increased oxidative stress, apoptosis levels, and ion transport. Plastic particles seem to negatively impact symbiotic relationships between corals and their microalgae, thereby degrading the entire coral reef ecosystem. However, this has not been systematically investigated.

Nano-plastics can originate by fragmentation of larger plastic objects through photochemical and mechanical degradation. There are also primary sources of nano-plastics. Medical and cosmetic products, nanofibers from clothes and carpets, 3D printing, and Styrofoam byproducts find their way into coral reef ecosystems via river drainages, sewage outfalls, and runoff after heavy rainfall, as well as via atmospheric input and ocean currents. Nano-plastics have recently been reported in ocean surface water samples [14]. Since the nanoplastic research is still in its infancy, many unanswered questions remain, starting with the environmental concentrations in various ecosystems [15,16]. Since detecting nano-plastics' concentrations directly is still not possible [17], a better understanding of the potential impacts is necessary to encompass a range of different concentrations. The miniature size of these particles leads to higher surface area to volume ratios and enhanced reactivity of smaller particles coupled with the ability to pass across biological barriers and enter cells [18] when compared to micro-plastics.

In this study, we focused on the microalgal symbionts of mollusks that inhabit fringing coral reefs of Okinawa. Knowledge of the effects of nano-plastics on the symbionts of Tridacninae (giant clams) and Fraginiae (heart cockles) will benefit conservation and restocking efforts, since both are obligatory photo-symbionts and important contributors to coral reef ecosystems. Approximately 30 Symbiodiniaceae phylotypes are economically important for fisheries [19]. This study specifically investigated effects of nano-plastics (42-nm polystyrene spheres) on the growth rates, aggregations, and gene expression changes in *Symbiodinium tridacnidorum* (symbionts of the Tridacninae) and *Cladocopium* sp. (symbionts of the Fraginiae).

## 2. Materials and Methods

### 2.1. Exposure to Nano-Plastics Using Roller Tanks

The majority of host animals obtain their indispensable symbiotic dinoflagellates from coral reef sand and the water column [20,21]. Roller tanks and tables were used to simulate the natural environment of the dinoflagellate vegetative cells in their free-living state [22,23]. Roller tanks have commonly been used to promote aggregation since Shanks and Edmondson [23,24]. Fifteen roller tanks of 13.4 cm in diameter and 7.5 cm in height with a capacity of 1057 mL were employed. In tanks, aggregation can occur [23], ensuring that microalgae are exposed to the polystyrene nano-plastics (nanoPS) in a way that mimics their natural habitat. Once rotation commenced, continuous aggregate formation and suspension were ensured [24] as well as continuous exposure to nanoPS. Roller tanks are closed for the entire duration of the experiment, so that exposure levels of the nanoPS remain constant throughout. Tanks were closed without bubbles so as not to disturb the aggregation process with turbulence. To compare differences between species, two dinoflagellates, *Symbiodinium tridacnidorum* (clade A3 strain, ID: NIES-4076) and *Cladocopium* sp. (clade C strain, ID: NIES-4077) were cultured in artificial seawater containing 0.2x Guillard's (F/2) marine-water enrichment solution (Sigma-Aldrich) in roller tanks [25,26]. *S. tridacnidorum* and *Cladocopium* sp. were isolated from *Tridacna crocea* and *Fragum* sp. in Okinawa, Japan [25]. Using glass flasks, precultures for the stress experiment were established, as previously described [26].

Microplastics (>1 mm) from a coral reef and the ingestion (53 to 500  $\mu\text{m}$ ) by coral reef clams have been reported and microplastic removal by giant clams has been proposed [4,27]. To simulate nano-plastic accumulation in coral reefs and in the host organisms, three different concentrations (0.01 mg/L, 0.1 mg/L, and 10 mg/L) of nano-plastic (42-nm pristine polystyrene beads, nanoPS<sub>42</sub>, from Bangs Laboratories Inc., catalog number FSDG001, polystyrene density 1.05 g/cm<sup>3</sup>, nanoPS) were added to the treatment tanks (Table S1). Preliminary tests were run to confirm no leaching of the fluorescent dye (data not shown). Concentrations were chosen to span a range of possible

environmental concentrations, starting at 0.01 mg/L with a surface area of  $1.36 \times 10^6 \mu\text{m}^2/\text{L}$  and  $2.46 \times 10^8$  particles per L. The next highest concentration is just one magnitude higher (0.1 mg/L, surface area  $1.36 \times 10^7 \mu\text{m}^2/\text{L}$  and  $2.46 \times 10^9$  particles per L). This middle range concentration corresponds to actually observed lower concentrations of microplastic particles [28]. Just as microplastic concentrations are highly variable, nanoplastic concentrations are assumed to change depending on the proximity to human activity. To account for these variables, but not at the highest measured microplastic concentration, we placed our highest concentration at 10 mg/L with a surface area of  $1.36 \times 10^9 \mu\text{m}^2/\text{L}$  and  $2.46 \times 10^{11}$  particles per L (Table S1). Treatment tanks as well as control tanks (no nanoPS) were established in triplicate. Three tanks without algae were prepared as negative controls (at 10 mg/L, 0.01 mg/L, and 0 mg/L nano-plastic). In each culture tank, the final cell density of the two strains was adjusted to  $\sim 7 \times 10^5$  cells/mL. Tanks were harvested after 9–11 days for logistical reasons, making replicates a day apart (Table S2).

## 2.2. Measurements of Cell Density and Aggregation

Cells for growth rates were counted using hemocytometers (C-Chip DHC-N01) under a Zeiss Axio Imager Z1 microscope (Jena, Germany). At least two subsamples and 200 cells were counted per sample.

Aggregates were imaged and counted in each tank and for five size classes, as follows: 0.2–0.5 mm, 0.5–1 mm, 1–2.5 mm, 2.5–3.5 mm, and >3.5 mm in the longest dimension. Tanks of the same concentration were sampled at the same time of day. Controls were sampled first and then in order of increasing nanoPS<sub>2</sub> concentration to avoid nano-plastic carry over from higher concentrations to lower. In order to examine how nanoPS<sub>2</sub> affects aggregate formation, aggregates were collected for different measurements after the approximate total number of aggregates in each tank had been determined. Aggregation of algae and plastic was confirmed with 3D imaging using a Zeiss Lightsheet Z.1 and Imaris software. NanoPS<sub>2</sub> was observed with a BP (Band path) filter (excitation: 405 nm, emission: 505–545 nm) and chloroplasts were visualized using a long-pass red filter (excitation: 488 nm, emission: 660 nm).

One fourth of all aggregates were collected for RNA analysis (2 min spin down at 12,000 rpm and discarding the supernatant, freezing in liquid nitrogen, and storage at  $-80^\circ\text{C}$ ). For all other measured factors, harvest included separate sampling of the aggregate fraction (aggregates >0.5 mm, Agg) and the surrounding sea water fraction (aggregates <0.5 mm and un-aggregated cells, ~~SSW~~) [29]. Aggregates for sinking velocity (three aggregates per size class for 11.5 cm in a 100-mL glass graduated glassware cylinder) was collected in artificial seawater at the same temperature as experiments were conducted.

## 2.3. RNA Extraction, Library Construction, and Sequencing

Frozen cells were broken mechanically using a polytron (KINEMATICA Inc., Luzern, Switzerland) in tubes chilled with liquid nitrogen. RNAs were extracted using Trizol reagent (Invitrogen) according to the manufacturer's protocol. The quantity and quality of total RNA were checked using a Qubit fluorometer (ThermoFisher, Waltham, MA) and a TapeStation (Agilent, Santa Clara, CA), respectively. Libraries for RNA-seq were constructed using the NEBNext Ultra II Directional RNA Library Prep Kit for Illumina (#E7760, NEB). Sequencing was performed on a NovaSeq6000 SP platform. Nine mRNA-seq libraries from nanoPS-exposed photosymbiotic algae were sequenced (3 concentrations  $\times$  3 exposure times) plus three controls (Table S2).

## 2.4. RNA-Seq Data Mapping and Clustering Analysis

Raw sequencing data obtained from the NovaSeq6000 were quality trimmed with Trimmomatic (v. 0.32) in order to remove adapter sequences and low-quality reads. Paired reads that survived the trimming step (on average 92%) were mapped against reference transcripts of *Symbiodinium* and *Cladocopium* sp. For each gene in the genomes of *Symbiodinium* and *Cladocopium* sp. a \*.t1 transcript form was used as a reference sequence. Mapping was performed using RSEM (RNA-Seq by

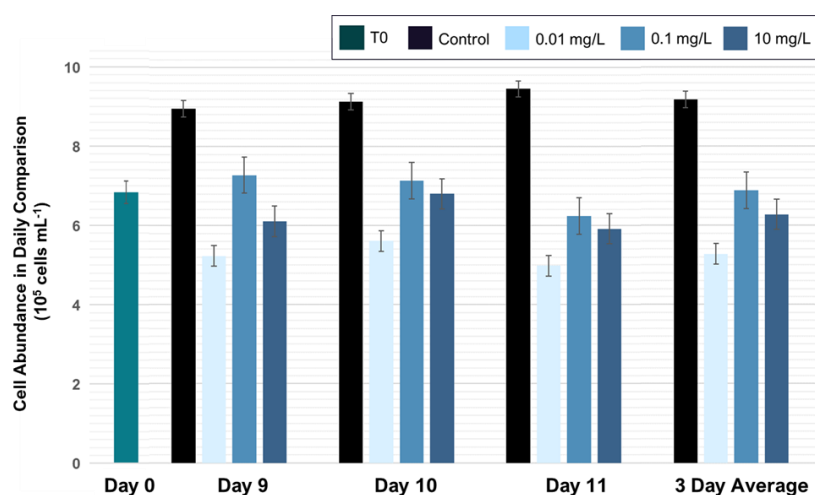


Expectation-Maximization) [30] with the bowtie (v. 1.1.2) as an alignment tool. Expression values across all samples were normalized by the TMM (Trimmed Mean of M-values) method [31]. Genes with differential expression (two-fold difference and  $p < 0.001$ ) were identified with edgeR Bioconductor, based on the matrix of TMM normalized TPM Transcripts Per Kilobase values. Experimental samples were clustered according to their gene expression characteristics using edgeR. Annotations were performed using BLAST2GO and Pfam databases [25] and are available at the genome browser site (<https://marinegenomics.oist.jp>).

### 3. Results and Discussion

#### 3.1. Suppression of Algal Growth by Nano-Plastic Exposure

Exposure to nanoPS<sub>42</sub> decreased the mean growth rate of photosymbiotic algae (Figure 1 and Figure S1). The greatest reduction in growth rate was seen at the lowest nanoPS<sub>42</sub> treatment (0.01 mg/L) with cell densities reduced from starting values by  $-0.062 \pm 0.02$  (Holm-Sidak,  $p = 0.002$ ), which was followed by the highest nanoPS<sub>42</sub> treatment (10 mg/L) with  $-0.013 \pm 0.05$  (Holm-Sidak,  $p = 0.026$ ). In the 0.1 mg/L treatment, cell densities increased slightly by  $0.028 \pm 0.04$ . Thus, nanoPS<sub>42</sub> either inhibited algal growth in a non-linear manner or had a limited effect [32]. Reductions in growth rates have also been reported in the micro-plastic study of Reference [13] in *Cladocopium goreau* and in other microalgae exposed to micro-plastics (*Chlamydomonas reinhardtii* [33] and *Skeletonema costatum* [34]).



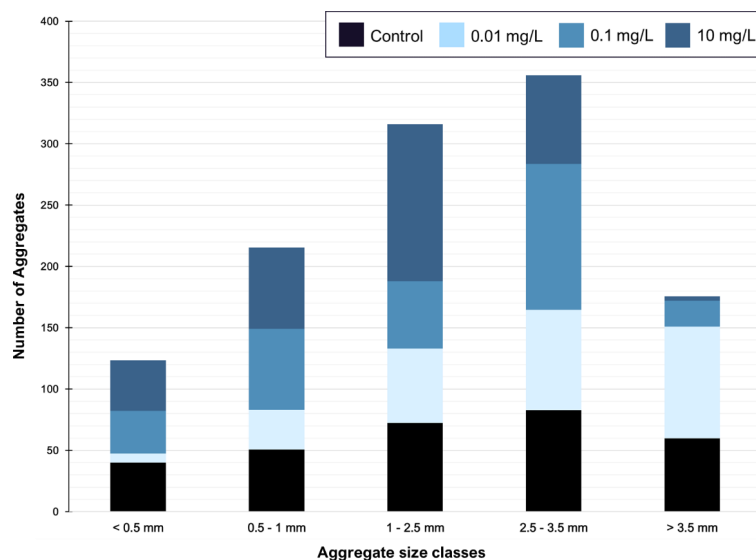
**Figure 1.** Treatment and control tanks were sampled after 9, 10, and 11 days. Experiments started with  $\sim 680,000$  cells/mL in all tanks. There are differences between the growth rate in the different treatments, but the ratio stays the same over all three sampling days. The cell density in the control was  $9.83 \pm 0.39 \times 10^5$  cells per mL, while treatment tanks were significantly lower: 0.01 mg/mL:  $5.69 \pm 0.12 \times 10^5$  cells per mL, 0.1 mg/mL:  $7.51 \pm 0.34 \times 10^5$  cells per mL, and 10 mg/mL:  $6.96 \pm 0.40 \times 10^5$  cells per mL. Bars display a confidence interval.

In addition, Su et al. [13] reported a reduction in cell size in *Cladocopium goreau*. Further investigations are needed to see if this is the case under nano-plastic exposure. The biggest growth rate reduction observed was at 0.01 mg/L nanoPS<sub>42</sub>, which is far below the 5 mg/L used by Su et al. [13]. The nutrient deficiency is also a reason discussed in Reference [23], which could explain the larger effects on growth rates at lower concentrations. The reason for nutrient limitation induced by plastic is proposed to be interactions of the nutrients with the surface of the plastics [35]. NanoPS<sub>42</sub>

self-aggregation could account for the higher nanoPS<sub>42</sub> treatments having less of an effect on the growth rates.

### 3.2. Nano-Plastic Exposure Influences the Number and Sinking Velocity of Cell Aggregates

To understand the impact of nanoPS<sub>42</sub> on aggregation in these two Symbiodiniaceae cultures, the total number of algal aggregates per tank and in five aggregate class sizes was recorded (Figure 2 and Figure S2). All tanks showed aggregation, which was expected, as self-aggregation of Symbiodiniaceae has been observed previously [13].



**Figure 2.** NanoPS exposure leads to a change in aggregation. Aggregates sorted by class size show a significant change in the distribution pattern under nanoPS<sub>42</sub> exposure (Holm-Sidak,  $p = 0.05$ ). No differences are observed when exposure length is compared.

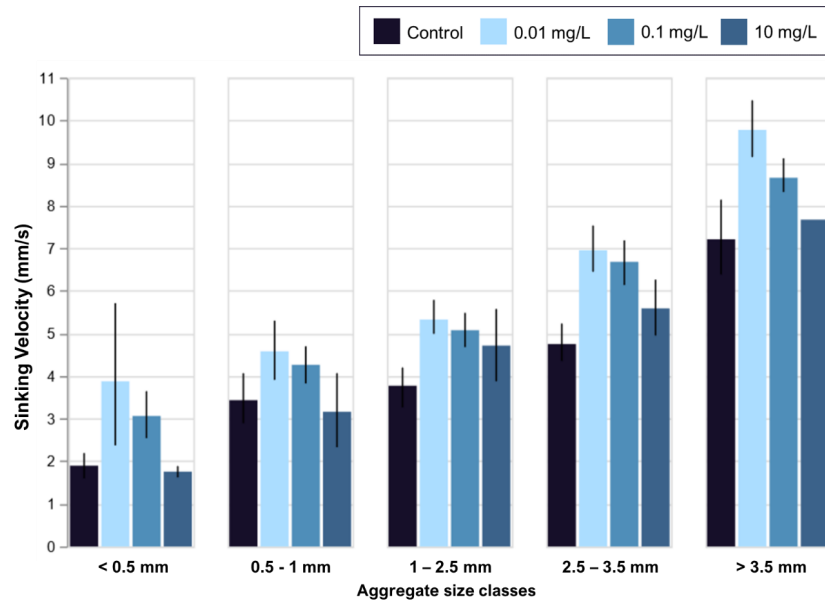
The majority of aggregates exhibited an ovoid form. A significant difference can be observed when aggregate numbers are compared over all class sizes and all treatments, showing that the nanoPS has an influence on the aggregation process. The lowest nanoPS<sub>42</sub> treatments (0.01 mg/L) shows significant reduction in the total aggregates count by 10% (Holm-Sidak,  $p = 0.003$ ), but aggregation was enhanced overall in that treatment to have a higher percentage of huge aggregates than in the control treatment (Holm-Sidak,  $p = 0.001$ ). While there is also a reduction of 3% in the intermediate nanoPS<sub>42</sub> treatment (0.1 mg/L), this is not significant (Holm-Sidak,  $p = 0.319$ ). In the highest plastic treatment at 10 mg/L, this is reversed, leading to more aggregates overall, and more of those being of smaller sizes. The different aggregate class sizes show significantly different distributions in all three treatments and the control (ANOVA,  $p < 0.001$ ) (Figure S2). In the control, the self-aggregation led to a specific distribution pattern of aggregate sizes, which was not repeated in the treatments. Self-aggregation was also observed in the microplastic experiments of Su et al. [13]. The fact that the presence of nanoPS changes the aggregation between the cells and leads to more aggregates in the bigger size classes is possible due to higher production of extracellular polymeric substances (EPS) with sticky properties, trapping more cells in one aggregate and keeping aggregates closer together. Nutrient depletion, which has been linked to the presence of micro-plastics in algae cultures [35], is associated with increased stickiness of the EPS [36,37]. Differences in the EPS production due to the presence of nanoPS is a likely factor contributing to the differences in

aggregation seen in the study. EPS production was not measured, so further studies are needed to confirm this hypothesis linking the aggregation process and EPS production in Symbiodiniaceae under nanoPS influence. Lagarde et al. [33] notices different aggregate formation under different plastic treatment and sizes, which matches with our results. In addition, in *Symbiodinium tridacnidorum*, genes encoding a protein with a TIG (Transcription factor immunoglobulin) domain were upregulated. Since this protein is found in surface cell receptors, it may influence changes in hetero aggregation.

Significant differences are evident when aggregate numbers are compared over size classes and treatments, showing that nanoPS influences aggregation. Aggregate size classes show significantly different distributions in all three treatments vs. controls (ANOVA,  $p < 0.001$ ) (see Figure 2). These differences in aggregation could be due to changes of the cell surface receptors, as nanoPS increases genes related to those two-fold (see Section 3.3. NanoPS effects on gene expression).

Due to nanoPS exposure, aggregation and sinking velocities are impacted, which, in turn, leads to change in sedimentation. Since the majority of the host animals obtain their symbiotic dinoflagellates from the sand and water column [20], these changes in dinoflagellate sedimentation might lead to problems in acquisition of symbionts for the host animals. The lowest plastic treatment used, which is environmentally possible, already induces changes to the sedimentation. This lowest treatment led to bigger aggregates, which, at the same time, sank faster, possibly removing the symbionts from the water column faster than required from the host animals and reducing chances of encountering symbionts.

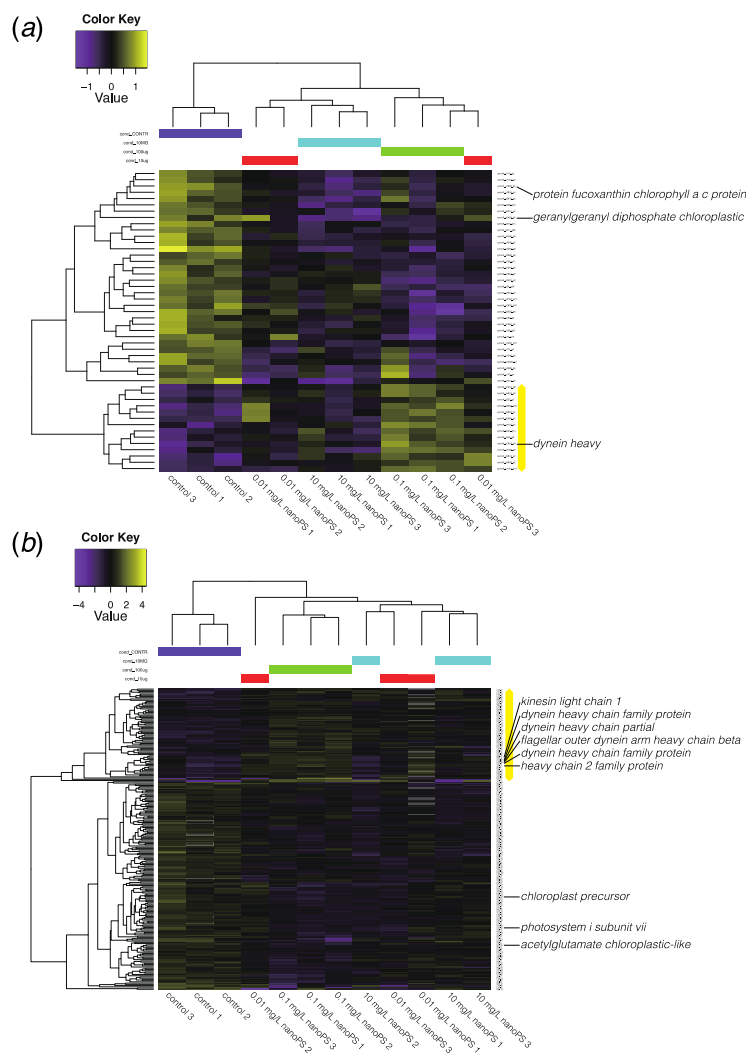
Changes in aggregation and resulting sedimentation were observed under nanoPS exposure (Figure 3). The biggest changes in sinking velocity correspond to increases in aggregation and are observed in the lowest plastic treatment at 0.01 mg/L. On the other hand, the 10 mg/L treatment did not have any significant effect on the sinking rates but did affect sedimentation indirectly through changes in the aggregate size distribution (Figure 3). These changes, including both sinking velocities and aggregate size distribution, are most likely due to hetero-aggregation between algae and nanoPS. Under different treatments, the size distribution of aggregates was significantly different (Figure 2). In combination, it is likely that the same effect that led to that difference in aggregation is also responsible for the difference in sinking velocities. Changes in EPS production and stickiness will lead to different cell packaging within the aggregates, possibly creating tighter packed aggregates in the lowest and intermediate treatment. This effect might be counteracted under the highest nanoPS exposure by the sheer volume of EPS, which is lighter than seawater. The nano-plastic itself trapped in these could also add to the sinking velocity returning back to control levels in the high plastic treatments. Since these symbionts are paired with the mobile larvae of the host animals, a higher sinking velocity would remove the potential symbiont from the pelagic area and reduce the chance of a match.



**Figure 3.** Sinking velocity change with nanoPS exposure. Sinking velocities decrease with aggregate size from more than 7 mm/s (>3.5 mm) to less than 2 mm/s (<0.5 mm). In all class sizes, the control was similar in sinking velocity to the highest nanoPS treatment (10 mg/L). The low nanoPS treatment (0.01 mg/L) differed significantly from both controls ( $t$ -test, two-tailed  $p = 5.56 \times 10^{-4}$ ) and the highest nanoPS treatment ( $t$ -test, two-tailed  $p = 9.03 \times 10^{-4}$ ). This was also true for the intermediate nanoPS treatment (darker blue, 0.1 mg/L). Error bars are 95% confidence intervals. Only one huge aggregate was measured in the highest nanoPS treatment. No differences in sinking velocity were observed in relation to exposure length.

### 3.3. NanoPS Effects on Gene Expression

Analysis of differential gene expression showed that, in *Symbiodinium*, 14 genes were upregulated after nanoPS<sub>42</sub> exposure, and 34 were downregulated relative to controls (Figure 4a). In *Cladocodium*, 75 genes were upregulated, and 169 genes were downregulated (Figure 4b). *Cladocodium* seems more sensitive to nanoPS<sub>42</sub> exposure, as overall more genes responded than in *Symbiodinium*. Since Pfam analysis had more annotations than BLAST2GO in DEGs of *Cladocodium*, we list the major domains encoded by the differentially expressed genes (DEGs) of *Cladocodium* (Tables S3–S6).



**Figure 4.** Heatmap and clustering of differentially expressed genes (2-fold changes,  $p < 0.001$ ) between dinoflagellates exposed to nano-plastics and controls. (a) DEGs in *Symbiodinium tridacnidorum*. (b) DEGs in *Cladocopium* sp. Values indicate the relative gene expression level with purple and yellow showing downregulation and upregulation, respectively. The yellow bar shows a cluster of upregulated genes. Annotations by Blast2GO show the presence of microtubule-related or photosynthesis-related genes among DEGs.

The largest group of upregulated genes was a subfamily of dynein-related proteins having an AAA<sub>5</sub> domain (Table 1). Dynein is a microtubule-associated motor protein. Ten genes for dynein-related proteins with AAA and/or DHC (Dynein heavy chain) were upregulated in *Cladocopium* sp. by nanoPS<sub>42</sub> (Table 1 and Table S4). It has been shown that microplastic exposure induces production of reactive oxygen species (ROS) in microalgae [13,33] and dynein upregulation. Therefore, it might

be needed to balance cytoskeletal dynamics as microtubule polymerization is impaired by oxidative stress [38]. Dynein light chain genes were also shown to be upregulated in gill cells of zebra mussels exposed to polystyrene micro-plastic [39].

**Table 1.** Domains encoded by more than three up-regulated genes in *Cladocopium* sp.

Domain Name	Summary from Pfam Database	Gene Number
AAA_5	AAA domain (dynein-related subfamily)	6
DHC_N2	Dynein heavy chain, N-terminal region 2	5
AAA	ATPase family associated with various cellular activities	4
AAA_6	Hydrolytic ATP binding site of dynein motor region	4
TIG	IPT/TIG domain	4

Four upregulated genes in *Cladocopium* (Table 1) encoded proteins with TIG domains that have an immunoglobulin-like fold and are found in cell surface receptors that control cell dissociation [40,41]. This might contribute to adhesion between neighboring cells and to the extracellular matrix composition and explain some of the changes observed in cell aggregations.

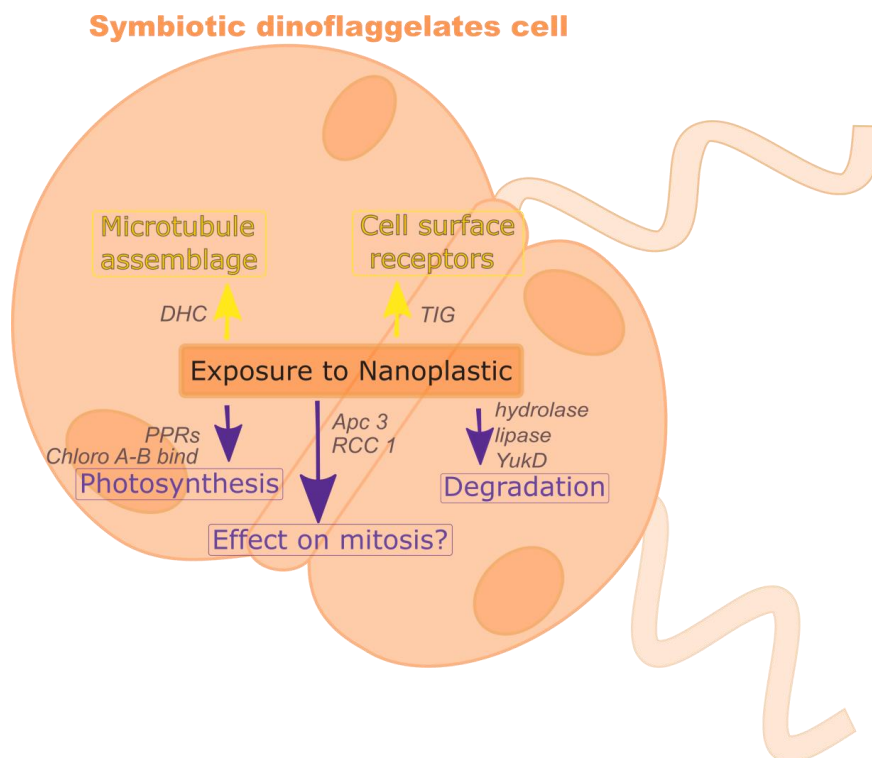
There were more downregulated genes than upregulated genes in both *Symbiodinium* and *Cladocopium* (Figure 4). PPR (pentatricopeptide repeat) protein (Table 2) is involved in RNA editing [42] and extensive RNA editing has been reported in organelles of Symbiodiniaceae [43,44]. Five genes for photosynthesis were downregulated (Figure 4). These changes may explain observed reductions in photosystem efficiency in *C. goreau* [13].

**Table 2.** Domains encoded by more than three down-regulated genes in *Cladocopium* sp.

Domain Name	Summary from Pfam Database	Gene Number
Ank	Ankyrin repeat	10
Ank_2	Ankyrin repeats (3 copies)	10
Ank_3	Ankyrin repeat	10
Ank_4	Ankyrin repeats (many copies)	10
Ank_5	Ankyrin repeats (many copies)	10
PPR_2	PPR repeat family	6
RCC1_2	Regulator of chromosome condensation (RCC1) repeat	6
ANAPC3 (Apc3)	Anaphase-promoting complex, cyclosome, subunit 3	5
Pkinase	Protein kinase domain	5
PPR	PPR repeat	5
PPR_3	Pentatricopeptide repeat domain	5
Abhydrolase_5	Alpha/beta hydrolase family	4
Abhydrolase_6	Alpha/beta hydrolase family	4
Lipase_3	Lipase (class 3)	4
PPR_1	PPR repeat	4
TPR_14	Tetratricopeptide repeat	4
YukD	WXG100 protein secretion system (Wss), protein YukD	4

Other downregulated gene groups were related to intracellular degradation processes, including hydrolase and lipase, and to subunit 3 of the anaphase-promoting complex/cyclosome [45]. The downregulated gene (s3282\_g2) with abhydrolase and chlorophyllase domains is likely related to chlorophyll degradation [46]. The gene, s576\_g21, for cell division control (CDC) protein 2 is downregulated in *Cladocopium*. Downregulation of six genes with RCC1 (regulator of chromosome condensation) and three genes with CDC domains suggest some effect on cell division. Thus, several negative consequences of nanoPS<sub>42</sub> exposure are suggested by DEGs (summarized in Figure 5).





**Figure 5.** Exposure to nanoPS<sub>42</sub> changes gene expression levels in symbiotic dinoflagellates. Yellow and purple arrows show up-regulation and down-regulation of gene expression, respectively.

#### 4. Conclusions

Previous studies have shown that nano-plastics have adverse effects on different algae groups [32,34,35,47,48], and a recent study shows that micro-plastics have similarly negative effects on an endosymbiotic dinoflagellate *Cladocopium goreauii* [13]. No previous studies have been conducted on nanoPS<sub>42</sub> effects on Symbiodiniaceae. We found significant changes in aggregation, photosystem efficiency, and aggregate sinking velocity of symbiotic dinoflagellates, which is coupled with variations in gene expression patterns after exposure to nanoPS<sub>42</sub>. The reduction in photosystem efficiency and photosystem gene expression patterns could have led to the observed reduced growth rates and are especially problematic given the obligate photosymbiotic nature of the host animals of the dinoflagellates.

**Supplementary Materials:** The following are available online at [www.mdpi.com/xxx/s1](http://www.mdpi.com/xxx/s1). Figure S1: Cell abundance in treatment tanks, control tanks, and outside controls. Figure S2: NanoPS exposure changes aggregation behaviour, reduces cell numbers, and alters size class distributions. Table S1: Relationship between nanoPS<sub>42</sub> concentration and particles per tank. Table S2: Sampling days of each tank. Table S3: Genes that responded to nano-plastic exposure in *Symbiodinium tridacnidorum*. Table S4: Genes that responded to nano-plastic exposure in *Cladocopium* sp. Table S5: Differentially expressed genes with a two-fold difference between the controls and nano-plastic exposure (*Symbiodinium tridacnidorum* cladeA, TMM FPKM values,  $p < 0.001$ ). Table S6: Differentially expressed genes with a two-fold difference between the controls and nano-plastic exposure (*Cladocopium* sp. cladeC, TMM FPKM values,  $p < 0.001$ ).

**Author Contributions:** C.R. designed the study and performed the experiment. E.S. carried out RNA analyses. K.K. and C.R. performed RNA-seq mapping and cluster analyses. All authors wrote the manuscript. All authors have read and agreed to the published version of the manuscript.

**Funding:** This research received no external funding. This research was funded by OIST support for the Light-Matter Interactions for Quantum Technologies (SNC) and the Marine Genomics Unit (NS).

**Acknowledgments:** We are grateful to the DNA sequencing section of OIST for RNA preparation and sequencing and to the OIST imaging section for 3D image support. We thank members of the MGU, especially Haruhi Narisoko for cell culturing and Kanako Hisata for IT support. We are grateful for the help and support provided by K. Deasy from the Engineering Support Section of Research Support Division at OIST. We gratefully acknowledge Sile Nic Chormaic and Noriyuki Satoh for their continuing personal and material support and kind encouragement throughout the project.

**Conflicts of Interest:** The authors declare no conflict of interest.

**Availability of Data:** Data are available in the electronic supplementary material. Raw sequence data are available from PRJNA627564 in NCBI database. Symbiodinium (currently the family Symbiodiniaceae) clade A3 and C genomes: clade A3 ([https://marinegenomics.oist.jp/symb/viewer/info?project\\_id=37](https://marinegenomics.oist.jp/symb/viewer/info?project_id=37)) and clade C ([https://marinegenomics.oist.jp/symb/viewer/info?project\\_id=40](https://marinegenomics.oist.jp/symb/viewer/info?project_id=40)). Transcript models of Symbiodinium clades A3 and C: [https://marinegenomics.oist.jp/symb/download/syma\\_transcriptome\\_37.fasta.gz](https://marinegenomics.oist.jp/symb/download/syma_transcriptome_37.fasta.gz) and [https://marinegenomics.oist.jp/symb/download/symC\\_aug\\_40.fa.gz](https://marinegenomics.oist.jp/symb/download/symC_aug_40.fa.gz).

## References

- McKinney, M.L. Is Marine Biodiversity at Less Risk? Evidence and Implications. *Divers. Distrib.* **1998**, *4*, 3–8.
- Hughes, T.P.; Anderson, K.D.; Connolly, S.R.; Heron, S.F.; Kerry, J.T.; Lough, J.M.; Baird, A.H.; Baum, J.K.; Berumen, M.L.; Bridge, T.C.; et al. Spatial and temporal patterns of mass bleaching of corals in the Anthropocene. *Science* **2018**, *359*, 80–83, doi:10.1126/science.aan8048.
- Woodhead, A.J.; Hicks, C.C.; Norström, A.V.; Williams, G.J.; Graham, N.A.J. Coral reef ecosystem services in the Anthropocene. *Funct. Ecol.* **2019**, 1023–1034, doi:10.1111/1365-2435.13331.
- Imhof, H.K.; Sigl, R.; Brauer, E.; Feyl, S.; Gieseemann, P.; Klink, S.; Leupolz, K.; Löder, M.G.; Löschel, L.A.; Missun, J.; et al. Spatial and temporal variation of macro-, meso- and microplastic abundance on a remote coral island of the Maldives, Indian Ocean. *Mar. Pollut. Bull.* **2017**, *116*, 340–347, doi:10.1016/j.marpolbul.2017.01.010.
- Gillibert, R.; Balakrishnan, G.; Deshoules, Q.; Tardivel, M.; Magazzù, A.; Donato, M.G.; Maragò, O.M.; De La Chapelle, M.L.; Colas, F.J.; Lagarde, F.; et al. Raman Tweezers for Small Microplastics and Nanoplastics Identification in Seawater. *Environ. Sci. Technol.* **2019**, *53*, 9003–9013, doi:10.1021/acs.est.9b03105.
- Tang, J.; Ni, X.; Zhou, Z.; Wang, L.; Lin, S. Acute microplastic exposure raises stress response and suppresses detoxification and immune capacities in the scleractinian coral *Pocillopora damicornis*. *Environ. Pollut.* **2018**, *243*, 66–74, doi:10.1016/j.envpol.2018.08.045.
- Hall, N.M.; Berry, K.L.E.; Rintoul, L.; Hoogenboom, M.O. Microplastic ingestion by scleractinian corals. *Mar. Biol.* **2015**, *162*, 725–732, doi:10.1007/s00227-015-2619-7.
- Connors, E.J. Distribution and biological implications of plastic pollution on the fringing reef of Mo'orea, French Polynesia. *PeerJ* **2017**, *5*, e3733, doi:10.7717/peerj.3733.
- Axworthy, J.B.; Padilla-Gamiño, J.L. Microplastics ingestion and heterotrophy in thermally stressed corals. *Sci. Rep.* **2019**, *9*, 1–8, doi:10.1038/s41598-019-54698-7.
- Okubo, N.; Takahashi, S.; Nakano, Y. Microplastics disturb the anthozoan-algae symbiotic relationship. *Mar. Pollut. Bull.* **2018**, *135*, 83–89, doi:10.1016/j.marpolbul.2018.07.016.
- Hankins, C.; Duffy, A.; Drisco, K. Scleractinian coral microplastic ingestion: Potential calcification effects, size limits, and retention. *Mar. Pollut. Bull.* **2018**, *135*, 587–593, doi:10.1016/j.marpolbul.2018.07.067.
- Reichert, J.; Schellenberg, J.; Schubert, P.; Wilke, T. Responses of reef building corals to microplastic exposure. *Environ. Pollut.* **2018**, *237*, 955–960, doi:10.1016/j.envpol.2017.11.006.
- Su, Y.; Zhang, K.; Zhou, Z.; Wang, J.; Yang, X.; Tang, J.; Li, H.; Lin, S. Microplastic exposure represses the growth of endosymbiotic dinoflagellate *Cladocodium goreau* in culture through affecting its apoptosis and metabolism. *Chemosphere* **2020**, *244*, 125485, doi:10.1016/j.chemosphere.2019.125485.

14. Ter Halle, A.; Jeanneau, L.; Martignac, M.; Jardé, E.; Pedrono, B.; Brach, L.; Gigault, J. Nanoplastic in the North Atlantic Subtropical Gyre. *Environ. Sci. Technol.* **2017**, *51*, 13689–13697, doi:10.1021/acs.est.7b03667.
15. Nanoplastic should be better understood. *Nat. Nanotechnol.* **2019**, *14*, 299, doi:10.1038/s41565-019-0437-7.
16. Gago, J.; Carretero, O.; Filgueiras, A.; Viñas, L. Synthetic microfibers in the marine environment: A review on their occurrence in seawater and sediments. *Mar. Pollut. Bull.* **2018**, *127*, 365–376, doi:10.1016/j.marpolbul.2017.11.070.
17. Koelmans, A.A.; Besseling, E.; Foekema, E.; Kooi, M.; Mintenig, S.; Ossendorp, B.C.; Redondo-Hasselerharm, P.E.; Verschoor, A.; Van Wezel, A.P.; Scheffer, M. Risks of Plastic Debris: Unravelling Fact, Opinion, Perception, and Belief. *Environ. Sci. Technol.* **2017**, *51*, 11513–11519, doi:10.1021/acs.est.7b02219.
18. Galloway, T.S.; Cole, M.; Lewis, C. Interactions of microplastic debris throughout the marine ecosystem. *Nat. Ecol. Evol.* **2017**, *1*, 116, doi:10.1038/s41559-017-0116.
19. Mies, M.; Braga, F.; Scozzafave, M.S.; De Lemos, D.E.L.; Sumida, P.Y.G. Early development, survival and growth rates of the giant clam *Tridacna crocea* (Bivalvia: Tridacnidae). *Braz. J. Oceanogr.* **2012**, *60*, 127–133, doi:10.1590/s1679-87592012000200003.
20. Hirose, M.; Reimer, J.D.; Hidaka, M.; Suda, S. Phylogenetic analyses of potentially free-living *Symbiodinium* spp. isolated from coral reef sand in Okinawa, Japan. *Mar. Biol.* **2008**, *155*, 105–112, doi:10.1007/s00227-008-1011-2.
21. Yamashita, H.; Koike, K. Genetic identity of free-living *Symbiodinium* obtained over a broad latitudinal range in the Japanese coast: Phylogeny of free-living *Symbiodinium*. *Phycol. Res.* **2013**, *61*, 68–80.
22. Schoenberg, D.A.; Trench, R.K. Genetic variation in *Symbiodinium* (=Gymnodinium) microadriaticum Freudenthal, and specificity in its symbiosis with marine invertebrates. I. Isoenzyme and soluble protein patterns of axenic cultures of *Symbiodinium* microadriaticum. In Proceedings of the Royal Society of London. Series B. Biological Sciences; The Royal Society: London, UK, 1980; Volume 207, pp. 405–427.
23. Long, M.; Moriceau, B.; Gallinari, M.; Lambert, C.; Huvet, A.; Raffray, J.; Soudant, P. Interactions between microplastics and phytoplankton aggregates: Impact on their respective fates. *Mar. Chem.* **2015**, *175*, 39–46, doi:10.1016/j.marchem.2015.04.003.
24. Shanks, A.L.; Edmondson, E.W. Laboratory-made artificial marine snow: A biological model of the real thing. *Mar. Biol.* **1989**, *101*, 463–470, doi:10.1007/bf00541648.
25. Shoguchi, E.; Beedessee, G.; Tada, I.; Hisata, K.; Kawashima, T.; Takeuchi, T.; Arakaki, N.; Fujie, M.; Koyanagi, R.; Roy, M.C.; et al. Two divergent *Symbiodinium* genomes reveal conservation of a gene cluster for sunscreen biosynthesis and recently lost genes. *BMC Genom.* **2018**, *19*, 1–11, doi:10.1186/s12864-018-4857-9.
26. Beedessee, G.; Hisata, K.; Roy, M.C.; Van Dolah, F.M.; Satoh, N.; Shoguchi, E. Diversified secondary metabolite biosynthesis gene repertoire revealed in symbiotic dinoflagellates. *Sci. Rep.* **2019**, *9*, 1–12, doi:10.1038/s41598-018-37792-0.
27. Arossa, S.; Martin, C.; Rossbach, S.; Duarte, C.M. Microplastic removal by Red Sea giant clam (*Tridacna maxima*). *Environ. Pollut.* **2019**, *252*, 1257–1266, doi:10.1016/j.envpol.2019.05.149.
28. Cole, M.; Lindeque, P.; Halsband, C.; Galloway, T.S. Microplastics as contaminants in the marine environment: A review. *Mar. Pollut. Bull.* **2011**, *62*, 2588–2597, doi:10.1016/j.marpolbul.2011.09.025.
29. Passow, U.; Sweet, J.; Francis, S.; Xu, C.; Dissanayake, A.; Lin, Y.; Santschi, P.; Quigg, A. Incorporation of oil into diatom aggregates. *Mar. Ecol. Prog. Ser.* **2019**, *612*, 65–86, doi:10.3354/meps12881.
30. Li, B.; Dewey, C.N. RSEM: Accurate transcript quantification from RNA-Seq data with or without a reference genome. *BMC Bioinform.* **2011**, *12*, 323, doi:10.1186/1471-2105-12-323.
31. Robinson, M.D.; Oshlack, A. A scaling normalization method for differential expression analysis of RNA-seq data. *Genome Biol.* **2010**, *11*, R25.
32. Prata, J.C.; Lavorante, B.R.; Montenegro, M.D.C.B.; Guilhermino, L. Influence of microplastics on the toxicity of the pharmaceuticals procainamide and doxycycline on the marine microalgae *Tetraselmis chuii*. *Aquat. Toxicol.* **2018**, *197*, 143–152, doi:10.1016/j.aquatox.2018.02.015.
33. Lagarde, F.; Olivier, O.; Zanella, M.; Daniel, P.; Hiard, S.; Caruso, A. Microplastic interactions with freshwater microalgae: Hetero-aggregation and changes in plastic density appear strongly dependent on polymer type. *Environ. Pollut.* **2016**, *215*, 331–339, doi:10.1016/j.envpol.2016.05.006.
34. Zhang, C.; Chen, X.; Wang, J.; Tan, L. Toxic effects of microplastic on marine microalgae *Skeletonema costatum*: Interactions between microplastic and algae. *Environ. Pollut.* **2017**, *220*, 1282–1288, doi:10.1016/j.envpol.2016.11.005.

35. Nolte, T.M.; Hartmann, N.B.; Kleijn, J.M.; Garnæs, J.; Van De Meent, D.; Hendriks, A.J.; Baun, A. The toxicity of plastic nanoparticles to green algae as influenced by surface modification, medium hardness and cellular adsorption. *Aquat. Toxicol.* **2017**, *183*, 11–20, doi:10.1016/j.aquatox.2016.12.005.
36. Logan, B.E.; Alldredge, A.L. Potential for increased nutrient uptake by flocculating diatoms. *Mar. Biol.* **1989**, *101*, 443–450, doi:10.1007/bf00541645.
37. Andersen, K.P.; Dam, H.G. Coagulation efficiency and aggregate formation in marine phytoplankton. *Mar. Biol.* **1990**, *107*, 235–245, doi:10.1007/bf01319822.
38. Ewilson, C.; González-Billault, C. Regulation of cytoskeletal dynamics by redox signaling and oxidative stress: Implications for neuronal development and trafficking. *Front. Cell. Neurosci.* **2015**, *9*, 381, doi:10.3389/fncel.2015.00381.
39. Magni, S.; Della Torre, C.; Garrone, G.; D'Amato, A.; Parenti, C.; Binelli, A. First evidence of protein modulation by polystyrene microplastics in a freshwater biological model. *Environ. Pollut.* **2019**, *250*, 407–415, doi:10.1016/j.envpol.2019.04.088.
40. Collesi, C.; Santoro, M.M.; Gaudino, G.; Comoglio, P.M. A splicing variant of the RON transcript induces constitutive tyrosine kinase activity and an invasive phenotype. *Mol. Cell. Biol.* **1996**, *16*, 5518–5526, doi:10.1128/mcb.16.10.5518.
41. Bork, P.; Doerks, T.; Springer, T.A.; Snel, B. Domains in plexins: Links to integrins and transcription factors. *Trends Biochem. Sci.* **1999**, *24*, 261–263, doi:10.1016/s0968-0004(99)01416-4.
42. Barkan, A.; Walker, M.; Nolasco, M.; Johnson, D. A nuclear mutation in maize blocks the processing and translation of several chloroplast mRNAs and provides evidence for the differential translation of alternative mRNA forms. *EMBO J.* **1994**, *13*, 3170–3181, doi:10.1002/j.1460-2075.1994.tb06616.x.
43. Mungpakdee, S.; Shinzato, C.; Takeuchi, T.; Kawashima, T.; Koyanagi, R.; Hisata, K.; Tanaka, M.; Goto, H.; Fujie, M.; Lin, S.; et al. Massive Gene Transfer and Extensive RNA Editing of a Symbiotic Dinoflagellate Plastid Genome. *Genome Biol. Evol.* **2014**, *6*, 1408–1422, doi:10.1093/gbe/evu109.
44. Shoguchi, E.; Shinzato, C.; Hisata, K.; Satoh, N.; Mungpakdee, S. The Large Mitochondrial Genome of *Symbiodinium minutum* Reveals Conserved Noncoding Sequences between Dinoflagellates and Apicomplexans. *Genome Biol. Evol.* **2015**, *7*, 2237–2244, doi:10.1093/gbe/evv137.
45. Peters, J.-M. The anaphase promoting complex/cyclosome: A machine designed to destroy. *Nat. Rev. Mol. Cell Biol.* **2006**, *7*, 644–656, doi:10.1038/nrm1988.
46. Tsuchiya, T.; Ohta, H.; Okawa, K.; Iwamatsu, A.; Shimada, H.; Masuda, T.; Takamiya, K.-I. Cloning of chlorophyllase, the key enzyme in chlorophyll degradation: Finding of a lipase motif and the induction by methyl jasmonate. *Proc. Natl. Acad. Sci. USA* **1999**, *96*, 15362–15367, doi:10.1073/pnas.96.26.15362.
47. Besseling, E.; Wang, B.; Lürling, M.; Koelmans, A.A. Nanoplastic Affects Growth of *S. obliquus* and Reproduction of *D. magna*. *Environ. Sci. Technol.* **2014**, *48*, 12336–12343, doi:10.1021/es503001d.
48. Bellingeri, A.; Casabianca, S.; Capellacci, S.; Faleri, C.; Paccagnini, E.; Lupetti, P.; Koelmans, A.A.; Penna, A.; Corsi, I. Impact of polystyrene nanoparticles on marine diatom *Skeletonema marinoi* chain assemblages and consequences on their ecological role in marine ecosystems. *Environ. Pollut.* **2020**, *262*, 114268, doi:10.1016/j.envpol.2020.114268.

**Publisher's Note:** MDPI stays neutral with regard to jurisdictional claims in published maps and institutional affiliations.



© 2020 by the authors. Submitted for possible open access publication under the terms and conditions of the Creative Commons Attribution (CC BY) license (<http://creativecommons.org/licenses/by/4.0/>).

## Graphical Abstract

1

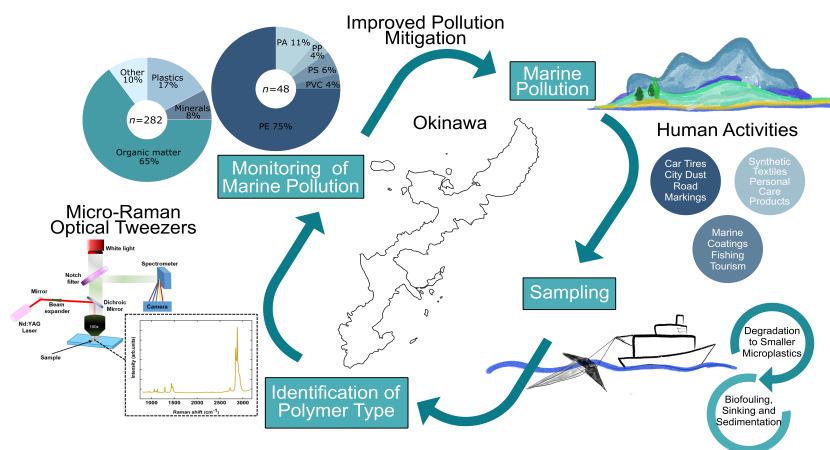
**Analysis of small microplastics in coastal surface water samples of the subtropical island of Okinawa, Japan**

2

3

Christina Ripken, Domna G. Kotsifaki, Síle Nic Chormaic

4



5 Highlights

6 **Analysis of small microplastics in coastal surface water samples of the subtropical island of Oki-**  
7 **nawa, Japan**

8 Christina Ripken, Domna G. Kotsifaki, Síle Nic Chormaic

- 9
- A method to detect and chemically identify single small microplastics in seawater was demonstrated.
- 10
- The occurrence of small microplastics was investigated in the surface waters around Okinawa, which belongs to a "blue
- 11 zone" region.
- 12
- Effective identification of different types of particles.
- 13
- Polyethylene was the most abundant polymer type found around Okinawa.
- 14
- The abundance of small microplastics was highest in areas associated with more intense human activities.



# Analysis of small microplastics in coastal surface water samples of the subtropical island of Okinawa, Japan

Christina Ripken<sup>a,b</sup>, Domna G. Kotsifaki<sup>a</sup> and Síle Nic Chormaic<sup>a</sup>

<sup>a</sup>Light-Matter Interactions for Quantum Technologies Unit, Okinawa Institute of Science and Technology, 1919-1 Tancha, 904-0495 Onna, Okinawa, Japan

<sup>b</sup>Marine Genomics Unit, Okinawa Institute of Science and Technology, 1919-1 Tancha, 904-0495 Onna, Okinawa, Japan

## ARTICLE INFO

### Keywords:

Microplastics  
Surface water  
Micro-Raman Optical Tweezers  
Environmental pollution  
Nanoparticles  
Okinawa-Japan

## ABSTRACT

Marine plastic debris is widely recognized as a global environmental issue. Small microplastic particles, with an upper size limit of 20  $\mu\text{m}$ , have been identified as having the highest potential for causing damage to marine ecosystems. Having accurate methods for quantifying the abundance of such particles in a natural environment is essential for defining the extent of the problem they pose. Using an optical micro-Raman tweezers setup, we have identified the composition of particles trapped in marine aggregates collected from the coastal surface waters around the subtropical island of Okinawa. Chemical composition analysis at the single-particle level indicates dominance by low-density polyethylene, which accounted for 75% of the small microplastics analysed. The smallest microplastics identified were  $(2.53 \pm 0.85) \mu\text{m}$  polystyrene. Our results show the occurrence of plastics at all test sites, with the highest concentration in areas with high human activities. We also observed additional Raman peaks on the plastics spectrum with decreasing debris size which could be related to structural modification due to weathering or embedding in organic matter. By identifying small microplastics at the single-particle level, we obtain some indication on their dispersion in the ocean which could be useful for future studies on their potential impact on marine biodiversity.

## 1. Introduction

Plastic polymers are a versatile, widely used material fully integrated in our daily lives. In the environment, plastics accumulate because of their recalcitrant nature [1]. Once plastic items are discarded in the environment, they often end up in waterways and are ultimately transported to the ocean [2]. The first report on the emergence of small plastic particles in the oceans drew worldwide concern [3]. Because most plastics undergo very slow chemical or biological degradation in the environment, the debris can remain in the ocean for years, decades, or even longer [4]. Moreover, plastic debris can entrap marine fauna [5] and be ingested by a wide variety of animals, ranging in size from plankton

to mammals [6]. Ingestion of marine plastic fragments and fibres into the trophic chain may cause human health problems. Furthermore, field observations and oceanographic models show that five subtropical ocean gyres are hotspots for plastic debris accumulation [7]. Supporting this, it has been reported that the global microplastic distribution across the oceans is estimated to be 236 thousand metric tons [8]. However, a discrepancy of orders of magnitude exists between these observations and the expected mass of microplastic in oceans, suggesting complicated export dynamics are at play.

While mesoplastic (5 mm – 2.5 cm) and macroplastic (> 2.5 cm) marine pollution has been extensively studied for many oceanic regions and across different ecosystems [9, 10], small microplastic pollution has been less of a focus [1,

\*Corresponding author: Domna G. Kotsifaki: domna.kotsifaki@oist.jp

## Small microplastics Okinawa

6]. As proposed by the National Oceanic and Atmospheric Administration (NOAA), the term microplastics refers to very small, ubiquitous plastic particles < 5 mm in diameter [11]. They have been separated into different fractions, large (1–5 mm) or small (1  $\mu\text{m}$  – 1 mm) microplastics [12] and the sub-20- $\mu\text{m}$  fraction (20  $\mu\text{m}$  – 1  $\mu\text{m}$ ). Like large microplastics, small microplastics can adsorb and carry hydrophobic chemicals that have a potential biological and toxicological impact on the environment [13]. Therefore, a clear understanding of the interaction of small microplastics with the environment, especially with living organisms, is essential to assess possible health hazards.

Currently, there is a need for reliable and precise identification of plastics without separating them from the matrices in which they are collected. The current protocols for quantification and characterisation of environmental plastic contamination is hampered by a lack of sensitive yet high-throughput methods. Commonly applied techniques for the analysis of plastics include a visual inspection or stiffness test [14], spectroscopy [15], transmission or scanning electron microscopy [16], and fluorescence imaging [17]. Very recently, surface-enhanced Raman spectroscopy was used to chemically identify commercial, standardised micro- and nano-particles suspended in a NaCl liquid environment, as a model system for plastics in seawater [18]. However, the chemical characterisation of single, plastic particles in a liquid environment is still limited. Therefore, techniques with selectivity and precision that enable the analysis of single particles *in situ* in any collected seawater sample and in real-time are necessary.

Since the first demonstration of single microparticle optical trapping in 1986 [19], optical tweezers have emerged as a powerful tool for controlling particles in fluids [19]. Optical tweezers use a highly focussed laser beam to trap and manipulate (typically) dielectric particles from 10 nm to 100  $\mu\text{m}$  in diameter. The particle is trapped near the focal spot due to scattering and gradient optical forces [20, 21]; the scattering force is from radiation pressure of the light beam along its direction of propagation and the gradient force pulls the particle towards the high-intensity focal point. The total optical force exerted on a particle is in the range of 100 fN to 100 pN depending on the difference between the refractive indices of the particle and the liquid medium, and the intensity of the laser beam. The ability to measure such small forces has opened the way for many new experiments in physics, chemistry, biophysics, and nanotechnology. Important examples include the development of multiple particle trapping [22], a variety of biophysics measurements on single biomolecules [23], and trapping in subwavelength fields created by plasmonic nanostructures [21].

The combination of optical tweezers with a range of different optical read-out techniques has enabled various single-particle investigations to be performed. With regard to *in situ* small microplastic analysis, optical tweezers micro-Raman spectroscopy (OTRS) is a viable option. Raman spectroscopy has already been used to analyse single cells and biomolecules suspended in an aqueous environment. Recently, the combined OTRS technique has been used for chemical qualita-

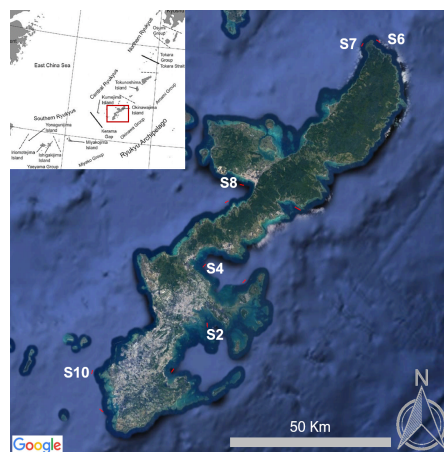
## Small microplastics Okinawa

101 tive analysis of different plastic particles with sizes in the  
 102 sub-20  $\mu\text{m}$  regime in a seawater environment [24]. The au-  
 103 thors successfully discriminated between plastics and min-  
 104 eral sediments at the single-particle level, overcoming the  
 105 limitations of conventional Raman spectroscopy in a liquid  
 106 environment [24].

107 Compared to the rest of the world, there is limited infor-  
 108 mation on plastic pollution of seawater in a "blue zone" area,  
 109 regions of the world in which exceptional longevity has been  
 110 recorded [25]. In this work, we have collected environmen-  
 111 tal samples around the subtropical island of Okinawa and  
 112 analysed them using an OTRS technique, to determine the  
 113 occurrence, the average size and the polymer type of small  
 114 microplastic particles. Crucially, OTRS has the ability to un-  
 115 ambiguously chemically identify different microplastics in  
 116 real-time. This study improves our knowledge on the extent  
 117 and magnitude of small microplastics pollution in the ocean  
 118 around a blue zone region. It also gives an estimate on the  
 119 current state of pollution, as well as how the pollution cor-  
 120 relates with population and industrial densities on the island  
 121 of Okinawa.

## 122 2. Materials and Methods

123 The main island of Okinawa (26.2124° N, 127.6809° E)  
 124 is part of the Ryukyu Island Arc (inset in Figure 1) and con-  
 125 sists of uplifted coral reefs and, particularly in the north-  
 126 ern half, igneous rock (solidified magma or lava). It is sur-  
 127 rounded by fringing reefs, making the water intake that reaches  
 128 the beaches more reliant on surface waves and wind [26].



129 **Figure 1:** Map of field study area in Okinawa with the locations  
 130 of the six towing stations from which particles were collected  
 131 and analysed [28]. Inset: Geographical location of Okinawa in  
 132 the Ryukyu Island Arc [29].

133 Land-based pollution originating on Okinawa is more likely  
 134 to be found in the bigger bays of the island. The six sam-  
 135 pling sites were chosen to provide a road map of the pol-  
 136 lution distribution of Okinawa (Figure 1). Sites differ in  
 137 population density and industry in and around the respec-  
 138 tive bay regions. Additionally, Okinawa has been previously  
 139 deemed as a "blue zone" [27]. Therefore, it is crucial to mon-  
 140 itor ocean pollution as it may adversely affect the residents'  
 141 longevity in such a region.

### 138 2.1. Study Region

139 To quantify small microplastic abundance in the surface  
 140 waters around Okinawa, the water samples were collected  
 141 over 24 hours in September 2018 with the Okinawa Pre-  
 142 fectural Fisheries (OPF) and Ocean Research Center (ORC)

## Small microplastics Okinawa

143 ship, Tonan Maru. The cruise was designed to obtain an  
144 overview of the small microplastic pollution around Oki-  
145 nawa.

## 146 2.2. Field Sampling

147 The sampling was performed using a manta trawl (Hydro-  
148 Bios Manta, 300  $\mu\text{m}$  net, net opening of 15 cm  $\times$  30 cm, with  
149 a Hydro-Bios Mechanical Flow Meter No.: 438 110). The  
150 manta net was deployed off the starboard side of the boat to  
151 the surface and trawled for 15 min at 2 - 3 knots covering an  
152 average distance of 1 km and filtering an average volume of  
153 856.8 L. It is worth noting that, during the collection process,  
154 we did not observe any seaweed or woody debris floating in  
155 the seawater which may have been scooped up in the manta  
156 trawl. After trawling, the nets were washed down twice be-  
157 fore transferring the contents into 450 mL glasses. All sam-  
158 ples were stored in a climatized environment until processing  
159 the next day. Between each sample, the Manta net was back-  
160 washed with seawater and the collector at the end of the net  
161 was washed separately to limit cross-contamination between  
162 sampling locations.

## 163 2.3. Laboratory Analysis

164 Each of the stored sample solutions was filtered over a  
165 300  $\mu\text{m}$  sieve to remove large agglomerates and microplas-  
166 tics. No additional digestion steps were added to remove the  
167 organic matter. The remaining seawater solutions after the  
168 filtering process were stored in new, clean glasses bottles.  
169 After one hour, we collected a small volume of liquid from  
170 the top of each of these remaining seawater solutions and

we carefully examined them using an optical microscope. 171  
It was evident that small microplastics (less than 300  $\mu\text{m}$ ) 172  
were contained in this small volume and these samples were 173  
used for the studies reported herein. Therefore, the small 174  
microplastics are analysed within the agglomerate matrix in 175  
which they were trapped in this study. 176

To limit contamination of the samples via clothing or air, 177  
all samples were filtered, sorted, and prepared onto the mi- 178  
croscope slides in a positive pressure chamber. Only cotton 179  
clothing was worn during sampling and preparation. For the 180  
experiments, a blank control sample of Milli-Q water was 181  
prepared simultaneously in order to detect any possible con- 182  
tamination during sample processing in the laboratory envi- 183  
ronment. 184

## 2.4. Optical micro-Raman Tweezers Spectroscopy 185

The OTRS system we used consists of a Nd:YAG laser 186  
beam ( $\lambda = 532$  nm with 17 mW of power at the sample plane) 187  
focussed using a high numerical aperture (NA = 1.3) oil 188  
immersion objective lens (Plan-Neofluar 100 $\times$ , Carl Zeiss) 189  
onto the seawater sample, as shown in Figure 2. We use a 190  
trapping laser at 532 nm which provides better Raman effi- 191  
ciency compared to longer wavelengths. The trapping laser 192  
beam is integrated into a Raman spectrometer (3D Laser Ra- 193  
man Microspectrometer Nanofinder 30). The high NA of the 194  
lens ensures trapping of the small microparticle and provides 195  
the necessary laser intensity needed to maximise its Raman 196  
signal. Using adhesive microscope spacers, a microwell was 197  
formed on the microscope glass slide, and trapping occurs 198

199 in the 20  $\mu\text{L}$  sample solution under a glass cover slide. The  
 200 sample of water in the microwell was taken from the small  
 201 volumes collected from the top of the seawater solutions, as  
 202 mentioned in Section 2.3. Therefore, the microwell contains  
 203 small microplastics and nanoparticles in seawater from the  
 204 sampled regions around Okinawa. As a control, a microwell  
 205 with 10  $\mu\text{l}$  milli-Q water aqua was prepared on the same  
 206 microscope slide. The microscope slide was mounted and  
 207 fixed on top of a translation stage. A CCD camera is used  
 208 to image the trapped microplastic during the trapping pro-  
 209 cess. The optical images are analysed using ImageJ software  
 210 to identify the shape and the size of the trapped microplas-  
 211 tic as well as to confirm that the analysis is performed on a  
 212 newly trapped particle in the same sample solution. Using  
 213 this setup, the OTRS technique allows us to identify small  
 214 microplastic fragments trapped by the laser.

### 3. Results and Discussion

215 Ocean surface water samples from several bays around 216  
 217 Okinawa have been collected (see Figure 1) and analysed,  
 218 as shown in Figure 2. The chemical identification of opti-  
 219 cally trapped particles within the seawater sample was ac-  
 220 complished by employing OTRS after background subtrac-  
 221 tion. Notably, the majority of the small microplastics are  
 222 quasispherical. A shift of the Raman peaks or alteration of  
 223 the bands can be expected due to their crystalline structure  
 224 and level of degradation.

225 Table 1 lists the most dominant types of plastics which  
 226 we have identified in our samples that contain seawater col-  
 227 lected around Okinawa. Moreover, we include their hazard  
 228 score [30] in order to indicate their potential impact on the  
 229 environment and human health.

230 Figure 3(a) shows Raman spectra for a quasispherical,  
 231 optically trapped microplastic diluted in seawater from a sam-  
 232 ple collected near the Naha region (S10 in Figure 1). Naha  
 233 is the capital of the Okinawa Prefecture and the sample loca-  
 234 tion was next to the industrial port and commercial airport.  
 235 Despite being a heavily commercialised area, Naha has an  
 236 estimated population of 318,270 inhabitants, representing  
 237 almost 30% of the total population of Okinawa island and a  
 238 population density of 8,043 people/ $\text{km}^2$ . In Figure 3(a), we  
 239 have identified the characteristic Raman peaks of polyvinyl  
 240 chloride (PVC) (Table 2-left). Additionally, we investigated  
 241 the Raman signal of the optically trapped microplastic for  
 242 various positions on its surface. We note that the intensity  
 243 of the Raman signal changes. This could be due to the dif-

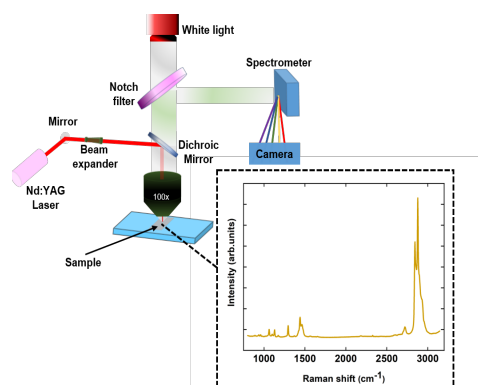


Figure 2: A schematic illustration of the optical tweezers micro-Raman setup used in our experiments. Inset: characteristic spectrum of a polyethylene (PE) particle of 15  $\mu\text{m}$  diameter in a seawater environment.

## Small microplastics Okinawa

**Table 1**

**Polymer types found as nanoplastics around Okinawa:** Detailed information for polymers identified in this study, including monomer, hazard score [30], and plastic size range for each polymer type.

Polymer	Abb	Monomer	Hazard score	% of total particles analysed	plastic size range ( $\mu\text{m}$ )
Polyethylene	PE	Ethylene	11	10.94	1.40-30.5
Polypropylene	PP	Propylene	1	0.61	3.07-6.15
Polyvinyl chloride	PVC	Vinyl chloride	10551	0.61	8.97-47.8
Polyamide (Nylon)	PA	Adipic acid	47	1.52	2.06-10.5
Polystyrene	PS	Styrene	30	0.91	1.38-4.18

244 ference in weathering of the material at various places. In  
 245 total, 51 particles were analysed from station S10, with ap-  
 246 proximately 19.6% being plastic such as polyethylene (PE)  
 247 or polyvinyl chloride (PVC). This is the second highest per-  
 248 centage of plastics that we have found contained within the  
 249 samples taken from seawater around Okinawa. This result  
 250 correlates well with a recent study by Kitahara et al. [31],  
 251 finding small plastics in road dust on Okinawa. Although  
 252 the population density is highest in Naha and most land use  
 253 is urban [32], plastic particles in the road dust were lower in  
 254 front of our station S10 [31]. One possible reason for find-  
 255 ing many small microplastics within the sampled volume,  
 256 although it was not the highest percentage measured, could  
 257 be due to its location outside of a bay. Although many rivers  
 258 discharge on this side of Naha city [33], pollution is not eas-  
 259 ily trapped this side of the island.

260 Plasticisers, dyes, and weathering can change the Ra-

261 man spectra, adding additional peaks to the spectra of the  
 262 different polymers as well as changing relative intensities  
 263 and accuracy. These additives are often harmful and can  
 264 leach from the polymer matrix [34]. In addition, the parti-  
 265 cles are often embedded in organic material, which can also  
 266 add peaks to the actual polymer spectra. In Figure 3(b), we  
 267 show the Raman spectra of the microscope slide that we used  
 268 in our experimental process and the organic matter found in  
 269 the plastics. Based on these reference spectra we can dis-  
 270 tinguish the plastics from organic matter and identify their  
 271 Raman peaks. Generally, we observed that most small mi-  
 272 croplastics are embedded in organic matter (68.75%) while  
 273 only 31.25% are free-floating. No data is published on this  
 274 ratio, as the methods for polymer identification used most of-  
 275 ten add a step of digesting the organic material in the sample  
 276 first, so as to get a better Raman signal. This ratio is impor-  
 277 tant to investigate further, as it could shed some light on the



## Small microplastics Okinawa

Table 2

**Raman peaks of: (Left):** Polyvinyl chloride (PCV) has a hazard score of 10551 [30], making it one of the most toxic plastics based on hazard classification of monomers. PVC is mostly used for cables, pipes & fittings, window frames, and flexible films for water proofing. **(Right):** Polyethylene (PE) is the most common plastic used in daily life. Primarily used for packaging, resulting in air trapping items such as bottles and plastic bags. Combined with its low density this leads to a majority of the PE floating at the ocean's surface [24].

PVC : $\nu$ ( $\text{cm}^{-1}$ )	Vibration	PE : $\nu$ ( $\text{cm}^{-1}$ )	Vibration
1724	Ester CO stretching	1058	CC symmetric stretching
1434	$\text{CH}_2$ symmetric deformation	1123	CC anti-sym stretching
1325	$\text{CH}_2$ twisting	1286	$\text{CH}_2$ twisting vibration
610	Crystalline C-Cl stretching	1408	$\text{CH}_2$ bending
		1429	$\text{CH}_2$ symmetric deformation
		1450	$\text{CH}_2$ scissor vibration

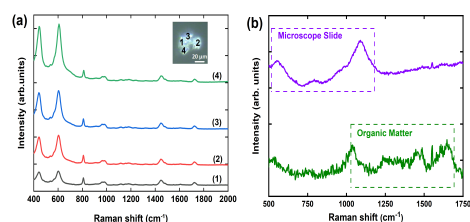
278 fate of the (small) microplastics within the water column.

279 Figure 4(a) shows the Raman peaks of PE small microplas-  
 280 tics which were found in several areas around Okinawa, while  
 281 in Table 2 (right) we present the modes attributed to PE. We  
 282 note that all the particles have the characteristic PE peaks  
 283 spanning from  $1000 \text{ cm}^{-1}$  to  $1500 \text{ cm}^{-1}$  [24]. Figure 4(b)  
 284 shows the Raman spectra for polystyrene (PS) and polypropy-  
 285 lene (PP) particles which were not embedded in organic mat-  
 286 ter.

287 The most common plastic that was found in the samples  
 288 taken from seawater of Okinawa is PE with a percentage of  
 289 10.94% of the total particles analysed (see Table 1). The rea-  
 290 son for the high percentage of PE within the sampled volume  
 291 could be its structural characteristics and lower density com-

pared with the other polymer types found (see Table 1). It  
 has more porous structures than other plastics and, as such,  
 it may be more easily broken down into microscopic debris  
 by sunlight, wind, and current erosion [35]. We notice sur-  
 rounding organic matter overlays the PE Raman spectra in  
 a microparticle of  $5 \mu\text{m}$  diameter (red line in Figure 4(a)),  
 which was collected from the Naha (S10) area. Additionally,  
 an overlay of dyes or additives is observed in Raman spec-  
 tra of small microplastic with  $5 \mu\text{m}$  diameter (purple line in  
 Figure 4(a)) which was collect from the Kin (S4) area. The  
 characteristic peaks of polystyrene (PS) (black line in Fig-  
 ure 4(b)) and polypropylene (PP) (blue line in Figure 4(b))  
 were identified at Nago (S8) and Nakagusku (S2) areas, re-  
 spectively. PS is frequently found in the environment as a

## Small microplastics Okinawa



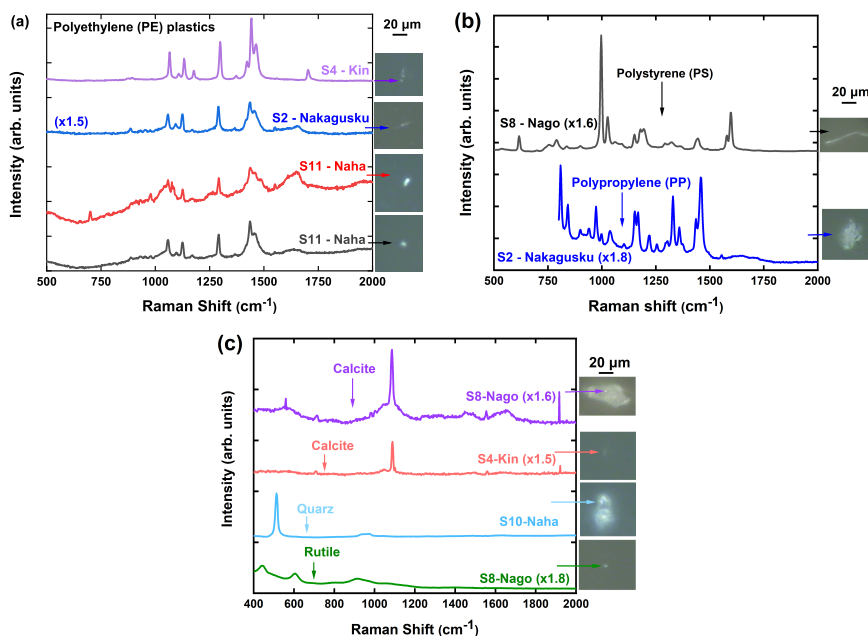
**Figure 3:** (a) Raman spectra of a polyvinyl chloride (PVC) quasispherical microplastic of 47.8  $\mu\text{m}$  diameter found at station S10, near Naha. Each spectrum relates to a different region on the trapped particle. Inset: microscope image of the plastic in which different spectral regions are labelled. The intensity of the Raman signal may indicate the difference in weathering. (b) Additional Raman spectra peaks that typically appear in the signals from the trapped particles in our samples. Purple (upper) curve: spectrum from the microscope slide. It displays the glass solid-state structure with no long range translational symmetry manifesting – the peaks are very broad with widths up to several hundred wavenumbers. Green (lower) curve: spectrum from organic matter found in the samples with CCO stretching (around  $1000\text{ cm}^{-1}$ ) and  $\text{CH}_3$  and  $\text{CH}_2$  deformations ( $1250\text{ cm}^{-1}$  to  $1750\text{ cm}^{-1}$ ) in the Raman spectrum. The individual peaks vary depending on the organic matter of the trapped particles.

306 material from diverse uses such as packaging foams and dis-  
 307 posable cups. Since it is mainly used for manufacturing of  
 308 single-use products, a large portion of post-consumer pro-  
 309 duction ends up into oceans [2], and remains there for sev-  
 310 eral hundred years due to their resistance to degradation (Ta-  
 311 ble 1). PP is used in the manufacturing of, for example, flip-  
 312 top bottles, piping systems, and food containers, amongst  
 313 others.

Together with the plastics, trapped sediment micromet- 314  
 ric and nanometric particles can also be detected (see Fig- 315  
 ure 4(c)). Specifically, we note that some particles have peaks 316  
 at  $512\text{ cm}^{-1}$  and  $472\text{ cm}^{-1}$  [36], indicating trapped quartz 317  
 particles (blue curve-S10 in Figure 4(c)). Particles of poly- 318  
 morphous  $\text{CaCO}_3$  with one peak at  $706\text{ cm}^{-1}$  followed by a 319  
 larger peak at  $1088\text{ cm}^{-1}$  indicate that they are most likely 320  
 calcite and not aragonite or vaterite [37]. The origin of these 321  
 particles is probably related to trace calcite-based contam- 322  
 inants. Finally, we find particles that display the spectral 323  
 fingerprint of rutile (green curve-S8 in Figure 4(c)) with mi- 324  
 croscope slide signal overlay [38]. Rutile is a mineral com- 325  
 posed primarily of titanium dioxide ( $\text{TiO}_2$ ) and is the most 326  
 common natural form of  $\text{TiO}_2$ . These sediment-derived par- 327  
 ticles are likely found because of high river input [33]. 328

The abundance of small microplastics in the sampled 329  
 volume taken from each station displayed a difference be- 330  
 tween those collected in urban and less populated areas. The 331  
 heterogeneity of the small microplastics in the volume at the 332  
 sampling stations may be caused by several factors, predomi- 333  
 nately the closeness of point sources such as sewage outfalls, 334  
 river outlets and run-off after heavy rain fall. Atmospheric 335  
 input of micro- and small microplastic from domestic ac- 336  
 tivities such as traffic should also be taken into considera- 337  
 tion. In Table 3, we summarise the plastic distribution of 338  
 small microplastics found within the sampled volumes col- 339  
 lected around Okinawa. In total we have identified 282 parti- 340  
 cles by employing the OTRS method, of which 48 are small 341  
 microplastics. The small microplastic pollution observed 342

## Small microplastics Okinawa



**Figure 4:** Raman spectra of optically trapped small microplastics dispersed in seawater with their optical images: (a) Polyethylene (PE) spectra from different particles found in different locations. The red line (S10) has an organic matter overlay, while the purple (S4) and blue (S2) lines have additional peaks most likely from dyes or additives to the PE. (b) The black line indicates the Raman spectrum of polystyrene (PS) and the blue line of polypropylene (PP) found at Nago (S8) and Nakagusku (S2) areas, respectively. (c) Raman spectra of trapped sediment particles suspended in seawater with their optical images. In the purple line (S8-up) the calcite peaks are overlaid with organic matter, as observed on the optical image. The green line (S8-down) shows a rutile nanoparticle in which the Raman spectra is overlaid by the characteristic microscope slide Raman peaks.

343 within the sampled volumes follows the population gradi- 351  
 344 ent of the island [32]. There is a clear distinction between 352  
 345 the northern (Figure 1), less populated part of Okinawa, and 353  
 346 the southern part with high population density. While the 354  
 347 south west side with the capital Naha has the highest popu- 355  
 348 lation density, there is no bay on that side of the island. On 356  
 349 the south east side of Okinawa, on the other hand, the big 357  
 350 bay of Nakagusku (S2-Figure 1) is located. The cities of 358  
 Nanjō (2.98% of population), Urasoe (7.90% of population),  
 Ginowan (6.71% of population) and Okinawa city (9.74% of  
 population) are located along that bay. While only a handful  
 of rivers drain into this bay, these rivers have been found to  
 have the highest levels of inorganic nutrients [33] on Okinawa.  
 We analysed 44 particles in the sampled volume from that bay and  
 we calculated that 25.0% are plastics (8 of PE, 1 of PP, 1 of PS  
 and 1 of PVC). We conclude that the samples

## Small microplastics Okinawa

Table 3

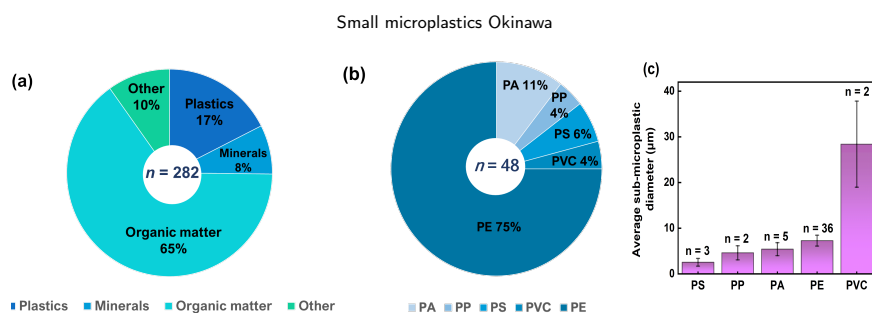
Small microplastic distribution around Okinawa: Station split for population and industry around Okinawa following the respective gradients.

Area name	Station names	Population distribution	Industry distribution	Volume checked [ $\mu\text{L}$ ]	Particles	Particles plastic (%)	Particles organic (%)
Nakagusku 2	S2	Sth2	E2	40	44	25.0	56.8
Kin 2	S4	Sth4	E4	60	56	17.9	66.1
Cape Hedo 1	S6	N2	E6	60	60	13.3	66.7
Cape Hedo 2	S7	N3	W1	60	13	15.4	61.5
Nago 1	S8	N4	W2	60	58	13.8	65.5
Naha 1	S10	Sth5	Naha1	40	51	19.6	58.8

359 coming from this area have the highest percentage of plas-  
 360 tics due to the high population density (2,838 people/km<sup>2</sup>)  
 361 found along the intake of the bay. The southern part of the  
 362 island has a high proportion of urban land use [32], which, in  
 363 combination with high traffic density [31], leads to high an-  
 364 thropogenic pressure on the coastal ecosystem [39]. This re-  
 365 sults in a significant increase of small microplastic particles  
 366 in sampled volumes from the southern half of the island (t-  
 367 test, two tailed  $p = 0.0147$ ). This is in reasonable agreement  
 368 with studies showing microplastic abundance in areas with  
 369 an increase of intensive anthropogenic activities such as: ur-  
 370 ban areas with high population density [40], tourist beaches  
 371 with high density of tourists [41], areas of intensive agricul-  
 372 ture [42], as well as fishing and shipping activities [43].

373 In the central part of the island, the land use shifts from  
 374 urban areas to more forest cover [32, 44]. Traffic density  
 375 goes down by between one third to about one half that found

376 in the southern part of the island [31]. On the east side, we  
 377 have a station at Kin (S4), while Nago (S8) is located on the  
 378 west side. Kin has a surrounding population of up to 1,386  
 379 people/km<sup>2</sup> while at Nago the population density is lower  
 380 at 296 people/km<sup>2</sup>. The anthropogenic pressure on the Kin  
 381 station is predicted to be high [39]. This difference in the  
 382 population density is reflected in the small microplastics dis-  
 383 tribution within the sampled volume, 17.9% (S4) and 13.8%  
 384 (S8), respectively, while the percentage of organic particles  
 385 within the sampled volume is reasonably stable (66.1% (S4)  
 386 and 65.5% (S8)). At Nago, we analysed 58 particles from the  
 387 sampled volume. PE was the only plastic type found there.  
 388 In Kin (S4) we characterised a similar number of particles  
 389 ( $n = 56$ ) but found a wider variety of plastic polymer types  
 390 (8 PE, one PS, and one PP small microplastic particle. The  
 391 particles in Nago bay ranged in size from 1.4  $\mu\text{m}$  to 27.2  $\mu\text{m}$ .  
 392 According to industrial density, which is higher on the east



**Figure 5:** (a) Percentage composition of all particles. (b) Polymer types of small microplastics collected in seawater around the main Okinawa island. (c) Average diameter of small microplastics where  $n$  indicates the number of polymers.

side of the island, the split of the stations into east (S2, S4, S6) and west (S10, S8, S7)) does not yield a significant difference (t-test,  $p = 0.7$ ) in small microplastic distribution from within the sampled volume, as most plastic is correlated with domestic activity, not industrial, on Okinawa.

Finally, in the north of Okinawa, Cape Hedo is located (Figure 1), with a low anthropogenic pressure prediction [39]. We collected particles from two stations (S6 and S7) located on both sides of the cape. In total, 60 particles were identified within the sampled volume at station S6, of which 8 are plastics (3 PE, 4 polyamide (PA) and 1 PS) while at station S7 we identified 13 particles within the sampled volume with two of them being plastics (1 PE and 1 PA). S6 is located on the east side of the cape, which has rivers draining into the ocean. Because of that, particulate organic matter content is comparable to the station located further south [45]. Polyamide is a family of polymers named Nylon. It is a ductile and strong polymer, permitting the fabrication of textile fibers and cordage. Based on Table 1, PA is the second most common plastic identified in the seawaters of Okinawa with

1.52% of all particles analysed.

Our analysis confirmed that 17% of particles were identified as small microplastic within the samples around Okinawa island, in which PE, PP, PVC, PA and PS are among the most abundant polymer types in aquatic environments (Figure 5(a) and (b)). Polyethylene (PE) was the most common plastic type, comprising of 75% of all the small microplastics polymers analysed (Figure 5(b)). The order of numerical dominance of small microplastic polymers was  $PE > PA > PS > PP = PVC$ . Generally, these polymers accounted for 74% of global plastic production and are commonly used in short life-cycle products [46]. Moreover, factors such as hydraulic conditions, salinity, temperature, wind, bio-flouring, as well as changes in surface to volume ratio may affect the distribution of small microplastics around Okinawa.

The source of small microplastics is related to the anthropogenic activities on the seawater, beaches, and in the trading centres in the area around Okinawa. In the fishing communities at the fish landing beaches, woven polymer sacks

## Small microplastics Okinawa

433 are used for storage and transport of a variety of products  
434 including fishes. Over 75% of the small microplastics are  
435 made of polyethylene and these may originate from broken  
436 fishing nets, lines or ropes, water bottle caps, household uten-  
437 sils, consumer carry bags, containers/packaging, etc. Re-  
438 cently, a study of the abundance of microplastics in road  
439 dust samples collected from several areas in Okinawa shows  
440 a high concentration of them in urban areas in which daily  
441 vehicle traffic, industrial activity, and high population den-  
442 sity are dominant [31]. In the road dust of Okinawa, PE was  
443 29% of the total microplastics [31], while in seawater it is  
444 75% of the total small microplastics. At the end, some of the  
445 road dust may be found in the oceans surrounding Okinawa,  
446 correlating the two findings via common high concentration  
447 areas.

448 Small microplastics were also classified based on their  
449 size as products of degradation of large plastic materials (op-  
450 tical images of each figure). The average size of all collected  
451 small microplastics is shown in Figure 5(c). The majority of  
452 small microplastics range from 1.4  $\mu\text{m}$  to 18.7  $\mu\text{m}$ , although  
453 we identified three microplastics with sizes of 27.2, 30.5,  
454 and 47.8  $\mu\text{m}$ . The smallest average size of  $2.53 \pm 0.85 \mu\text{m}$   
455 is identified for PS polymers while the largest average size  
456 of  $28.4 \pm 9.4$  is identified for PVC polymers. Likewise, the  
457 sampled small microplastics showed a wide range of sizes  
458 in various areas of Okinawa with the highest around Naha  
459 (S10).

460 Finally, we have demonstrated that the OTRS technique  
461 can be used for detecting small microparticles in a liquid en-

vironment; however, in order to use it to calculate the num- 462  
ber of particles per L, and to estimate the environmental mi- 463  
croplastic concentrations with high accuracy, some modifi- 464  
cations would be needed and these are beyond the scope of 465  
this study. As an example, a higher percentage of the to- 466  
tal sample volume would need to be checked using some 467  
form of through-put system. This technique has already been 468  
verified using commercial particles with different particle 469  
concentrations [24], whereas our work is applied to seawater 470  
samples from around Okinawa and the small microplas- 471  
tics contained therein. Summarising, the OTRS method pre- 472  
sented in this work permits a first study into how these very 473  
small particles are embedded within an organic matrix, while 474  
simultaneously providing a means of identifying the poly- 475  
mer type of the particle. No additional sample preparation is 476  
needed, thereby reducing both chemical and material waste. 477

#### 4. Summary 478

479 In recent years, much progress has been made in under- 479  
standing the sources, transport, fate, and biological implica- 480  
tions of the smallest plastic pollution particles. The public 481  
interest in plastic marine pollution and their ecological im- 482  
pacts have increased during the same time. Our results con- 483  
tribute to the knowledge about *in situ* analysis and iden- 484  
tification of microplastics and demonstrate that the seawater 485  
around Okinawa is polluted with micro and small microplas- 486  
tics. They were ubiquitously detected at all sites we sam- 487  
pled, present at different concentrations within each sampled 488  
volume, with a higher concentration found in samples from 489



## Small microplastics Okinawa

490 areas characterised by human activities. All the small mi-  
 491 croplastics were fragments of plastic materials used by the  
 492 community, with the major polymers being polyethylene and  
 493 polyamide materials. While some particles may have origi-  
 494 nated from and been transported over large distances, corre-  
 495 lation with population densities points to land-based sources  
 496 of the plastic particles. Being predominately found embed-  
 497 ded into organic matter, the resulting interactions between  
 498 marine planktonic organisms and the plastic particles are in-  
 499 evitable. One potential fate could be eventual sedimenta-  
 500 tion with the rest of the organic matter particle. Conclud-  
 501 ing, the risks that microplastics pose to fish and their natural  
 502 foods especially invertebrates, and the possible link to hu-  
 503 man health, need to be better understood. Strategies such as  
 504 proper waste management, plastic recycling, and penalties  
 505 for illegal dumping in areas close to water resources should  
 506 be promoted and implemented in the communities, to reduce  
 507 the land-based microplastics found in coastal waters.

## 508 5. Acknowledgements

509 This work was funded by Okinawa Institute of Science  
 510 and Technology Graduate University. DGK acknowledges  
 511 support from JSPS Grant-in-Aid for Scientific Research (C)  
 512 Grant Number GD1675001. We thank Elissaios Stavrou from  
 513 Lawrence Livermore National Laboratory (USA) for useful  
 514 comments on the Raman peak analysis. We also thank the  
 515 Captain and crew of the Okinawa Prefectural Fisheries and  
 516 Ocean Research Center ship, Tonan Maru, during the cruise  
 517 No.672 (FY2018 No.16) and the on-board team of Akinori

Murata and Marine Works Japan LTD technician, Shinsuke  
 Toyoda. The Engineering Support Section of OIST is also  
 acknowledged. 520

## References 521

- [1] Stephanie L. Wright, Richard C. Thompson, and Tamara S. Galloway. 522  
 The physical impacts of microplastics on marine organisms: a review. 523  
*Environmental Pollution*, 178:483–492, 2013. 524
- [2] Marcus Eriksen, Laurent C. Lebreton, Henry S. Carson, Martin Thiel, 525  
 Charles J. Moore, Jose C. Borerro, Francois Galgani, Peter G. Ryan, 526  
 and Julia Reisser. Plastic pollution in the world’s oceans: More than 5  
 trillion plastic pieces weighing over 250,000 tons afloat at sea. *PLoS* 528  
*One*, 9(12):e111913, 2014. 529
- [3] Edward J. Carpenter and Kenneth L. Smith. Plastics on the sargasso 530  
 sea surface. *Science*, 175(4027):1240–1241, 1972. 531
- [4] Anthony L. Andrady. Microplastics in the marine environment. *Mar.* 532  
*Pollut. Bull.*, 62(8):1596–1605, 2011. 533
- [5] David W. Laist. Overview of the biological effects of lost and dis- 534  
 carded plastic debris in the marine environment. *Marine Pollution* 535  
*Bulletin*, 18(6, Supplement B):319 – 326, 1987. 536
- [6] Matthew Cole, Pennie Lindeque, Claudia Halsband, and Tamara S. 537  
 Galloway. Microplastics as contaminants in the marine environment: 538  
 A review. *Mar. Pollut. Bull.*, 62(12):2588–2597, 2011. 539
- [7] Nikolai Maximenko, Jan Hafner, and Peter Niiler. Pathways of ma- 540  
 rine debris derived from trajectories of lagrangian drifters. *Marine* 541  
*Pollution Bulletin*, 65(1):51 – 62, 2012. 542
- [8] Erik van Sebille, Chris Wilcox, Laurent Lebreton, Nikolai Maxi- 543  
 menko, Britta Denise Hardesty, Jan A van Franeker, Marcus Eriksen, 544  
 David Siegel, Francois Galgani, and Kara Lavender Law. A global 545  
 inventory of small floating plastic debris. *Environmental Research* 546  
*Letters*, 10(12):124006, 2015. 547
- [9] David K. A. Barnes, Francois Galgani, Richard C. Thompson, and 548  
 Morton Barlaz. Accumulation and fragmentation of plastic debris in 549  
 global environments. *Philosophical Transactions of the Royal Society* 550

## Small microplastics Okinawa

- 551 *B: Biological Sciences*, 364(1526):1985–1998, 2009. 585
- 552 [10] Charles J. Moore. Synthetic polymers in the marine environment: a 586
- 553 rapidly increasing, long-term threat. *Environ. Res.*, 108(2):131–139, 587
- 554 2008. 2008. 588
- 555 [11] Joel E. Baker, Courtney Arthur, Holly A. Bamford, United States. 589
- 556 National Ocean Service. Office of Response, and Restoration. *Pro-* 590
- 557 *ceedings of the International Research Workshop on the Occurrence,* 591
- 558 *Effects, and Fate of Microplastic Marine Debris, September 9–11,* 592
- 559 *2008, University of Washington Tacoma, Tacoma, WA, USA.* U.S. De- 593
- 560 partment of Commerce, National Oceanic and Atmospheric Admin- 594
- 561 istration, National Ocean Service, Office of Response & Restoration, 595
- 562 2009. 596
- 563 [12] Julien Gigault, Alexandra ter Halle, Magalie Baudrimont, Pierre- 597
- 564 Yves Pascal, Fabienne Gauffre, Thuy-Linh Phi, Hind El Hadri, Bruno 598
- 565 Grassl, and Stéphanie Reynaud. Current opinion: What is a nanoplas- 599
- 566 tic? *Environmental Pollution*, 235:1030–1034, 2018. 600
- 567 [13] Richard E. Engler. The complex interaction between marine debris 601
- 568 and toxic chemicals in the ocean. *Environmental Science & Technol-* 602
- 569 *ogy*, 46(22):12302–12315, 2012. 603
- 570 [14] Valeria Hidalgo-Ruz and Martin Thiel. Distribution and abundance of 604
- 571 small plastic debris on beaches in the SE Pacific (Chile): A study sup- 605
- 572 ported by a citizen science project. *Marine Environmental Research*, 606
- 573 87-88:12–18, 2013. 607
- 574 [15] Laura Frère, Ika Paul-Pont, Moreau Jonathan, Soudant Philippe, Lam- 608
- 575 bert Christophe, Huvet Arnaud, and Emmanuel Rinnert. A semi- 609
- 576 automated Raman micro-spectroscopy method for morphological and 610
- 577 chemical characterizations of microplastic litter. *Marine Pollution* 611
- 578 *Bulletin*, 113(1):461–468, 2016. 612
- 579 [16] Martin Pivokonsky, Lenka Cermakova, Katerina Novotna, Petra Peer, 613
- 580 Tomas Cajthaml, and Vaclav Janda. Occurrence of microplastics in 614
- 581 raw and treated drinking water. *Science of The Total Environment*, 615
- 582 643:1644 – 1651, 2018. 616
- 583 [17] Matthew Cole and Tamara S. Galloway. Ingestion of Nanoplastics 617
- 584 and Microplastics by Pacific Oyster Larvae. *Environmental Science* 618
- & *Technology*, 49(24):14625–14632, 2015.
- [18] Lulu Lv, Lei He, Shiqi Jiang, Jinjun Chen, Chunxia Zhou, Junhao 586
- Qu, Yuqin Lu, Pengzhi Hong, Shengli Sun, and Chengyong Li. In 587
- situ surface-enhanced raman spectroscopy for detecting microplastics 588
- and nanoplastics in aquatic environments. *Science of The Total Envi-* 589
- ronment*, 728:138449, 2020. 590
- [19] Arthur Ashkin, Joseph M. Dziedzic, John E. Bjorkholm, and Steven 591
- Chu. Observation of a single-beam gradient force optical trap for 592
- dielectric particles. *Optics Letters*, 11(5):288–290, 1986. 593
- [20] Arthur Ashkin. Optical trapping and manipulation of neutral parti- 594
- cles using lasers. *Proceedings of the National Academy of Sciences*, 595
- 94(10):4853–4860, 1997. 596
- [21] Domna G. Kotsifaki and Sile Nic Chormaic. Plasmonic optical twee- 597
- zers based on nanostructures: fundamentals, advances and prospects. 598
- Nanophotonics*, 8(7):1227–1245, 2019. 599
- [22] Domna G. Kotsifaki, Mersini Makropoulou, and Alexandros A. Ser- 600
- afetinides. Efficient and low cost multiple optical trap, based on in- 601
- terference. *Optik*, 124(7):617–621, 2013. 602
- [23] Claudia Arbore, Laura Perego, Marios Sergides, and Marco Capi- 603
- tanio. Probing force in living cells with optical tweezers: from single- 604
- molecule mechanics to cell mechanotransduction. *Biophysical Re-* 605
- views*, 11(5):765–782, 2019. 606
- [24] Raymond Gillibert, Gireeshkumar Balakrishnan, Quentin Deshoules, 607
- Morgan Tardivel, Alessandro Magazzù, Maria Grazia Donato, 608
- Onofrio M. Maragò, Marc Lamy de La Chapelle, Florent Colas, Fa- 609
- bienne Lagarde, and Pietro G. Gucciardi. Raman Tweezers for Small 610
- Microplastics and Nanoplastics Identification in Seawater. *Environ-* 611
- mental Science & Technology*, 53(15):9003–9013, 2019. 612
- [25] Dan Buettner. *The Blue Zones, Second Edition: 9 Lessons for Living* 613
- Longer From the People Who've Lived the Longest*, 2012. 614
- [26] James L. Hench, James J. Leichter, and Stephen G. Monismith. 615
- Episodic circulation and exchange in a wave-driven coral reef and la- 616
- goon system. *Limnology and Oceanography*, 53(6):2681–2694, 2008. 617
- [27] Donald Craig Willcox, Giovanni Scapagnini, and Bradley J. Willcox. 618

## Small microplastics Okinawa

- 619 Healthy aging diets other than the mediterranean: A focus on the Ok- 653  
620 inawan diet. *Mechanisms of Ageing and Development*, 136-137:148– 654  
621 162, 2014. 655
- 622 [28] Google Earth. Okinawa island 26.2124°n, 127.6809°e, viewed June 656  
623 2020. 657
- 624 [29] Fes a De Scally. Historical Tropical Cyclone Activity and Impacts in 658  
625 the Cook Islands I. *Pacific Science*, 62(4):443–459, 2004. 659
- 626 [30] Delilah Lithner, Ake Larsson, and Göran Dave. Environmen- 660  
627 tal and health hazard ranking and assessment of plastic polymers 661  
628 based on chemical composition. *Science of the Total Environment*, 662  
629 409(18):3309–3324, 2011. 663
- 630 [31] Ken-Ichi Kitahara and Haruhiko Nakata. Plastic additives as tracers 664  
631 of microplastic sources in japanese road dusts. *Science of The Total 665  
632 Environment*, 736:139694, 2020. 666
- 633 [32] Samuel R.P.J. Ross, Nicholas R. Friedman, Kenneth L. Dudley, 667  
634 Masashi Yoshimura, Takuma Yoshida, and Evan P. Economo. Listen- 668  
635 ing to ecosystems: data-rich acoustic monitoring through landscape- 669  
636 scale sensor networks. *Ecological Research*, 33(1):135–147, 2018. 670
- 637 [33] Dativa J. Shilla, Izumi Mimura, Kimberly K. Takagi, and Makoto 671  
638 Tsuchiya. Preliminary survey of the nutrient discharge characteristics 672  
639 of Okinawa rivers, and their potential effects on inshore coral reefs. 673  
640 *Galaxea, Journal of Coral Reef Studies*, 15:172–181, 2013. 674
- 641 [34] Svetlana Wagner and Martin Schlummer. Legacy additives in a cir- 675  
642 cular economy of plastics: Current dilemma, policy analysis, and 676  
643 emerging countermeasures. *Resources, Conservation and Recycling*, 677  
644 158:104800, 2020. 678
- 645 [35] Young Kyoung Song, Sang Hee Hong, Mi Jang, Gi Myung Han, Se- 679  
646 ung Won Jung, and Won Joon Shim. Combined effects of uv expo- 680  
647 sure duration and mechanical abrasion on microplastic fragmentation 681  
648 by polymer type. *Environmental Science & Technology*, 51(8):4368– 682  
649 4376, 2017. 683
- 650 [36] Rappal S. Krishnan. Raman spectrum of quartz. *Nature*, 684  
651 155(3937):452–452, 1945. 685
- 652 [37] Zhaoyong Zou, Wouter J.E.M. Habraken, Galina Matveeva, An- 686  
653 ders C.S. Jensen, Luca Bertinetti, Matthew A. Hood, Chang-Yu Sun, 687  
654 Pupa U.P.A. Gilbert, Iryna Polishchuk, Boaz Pokroy, Julia Mahamid, 688  
655 Yael Politi, Stephen Weiner, Peter Werner, Sebastian Bette, Robert 689  
656 Dinnebier, Ute Kolb, Emil Zolotoyabko, and Peter Fratzl. A hydrated 690  
657 crystalline calcium carbonate phase: Calcium carbonate hemihydrate. 691  
658 *Science*, 363(6425):396–400, 2019. 692
- [38] Otakar Frank, Marketa Zukalova, Barbora Laskova, Jenö Kürti, János 693  
694 Koltai, and Ladislav Kavan. Raman spectra of titanium dioxide 695  
696 (anatase, rutile) with identified oxygen isotopes (16, 17, 18). *Phys. 697  
698 Chem. Chem. Phys.*, 14:14567–14572, 2012. 699
- [39] Joseph D. DiBattista, James D. Reimer, Michael Stat, Giovanni D. 700  
701 Masucci, Piera Biondi, Maarten De Brauwier, Shaun P. Wilkinson, 702  
703 Anthony A. Chariton, and Michael Bunce. Environmental DNA can 704  
705 act as a biodiversity barometer of anthropogenic pressures in coastal 706  
707 ecosystems. *Scientific Reports*, 10(1):8365, 2020. 708
- [40] Tomoya Kataoka, Yasuo Nihei, Kouki Kudou, and Hirofumi Hinata. 709  
710 Assessment of the sources and inflow processes of microplastics in the 711  
712 river environments of Japan. *Environmental Pollution*, 244:958–965, 713  
714 2019. 715
- [41] Raphael Bissen and Sakonvan Chawchai. Microplastics on beaches 716  
717 along the eastern Gulf of Thailand – a preliminary study. *Marine 718  
719 Pollution Bulletin*, 157:111345, 2020. 720
- [42] Minglong Chen, Meng Jin, Peiran Tao, Zheng Wang, Weiping Xie, 721  
722 Xubiao Yu, and Kan Wang. Assessment of microplastics derived 723  
724 from mariculture in Xiangshan Bay, China. *Environmental Pollution*, 725  
726 242:1146–1156, 2018. 727
- [43] Ulgen Aytan, Andre Valente, Yasemen Senturk, Riza Usta, 728  
729 Fatma Basak Esensoy Sahin, Rahsan Evren Mazlum, and Ertugrul 730  
731 Agirbas. First evaluation of neustonic microplastics in black sea wa- 732  
733 ters. *Marine Environmental Research*, 119:22–30, 2016. 734
- [44] Kwanchai Pakoksung, Anawat Suppasri, Kazuyo Matsubae, and Fu- 735  
736 mihiko Imamura. Estimating tsunami economic losses of Oki- 736  
737 nawa island with multi-regional-input-output modeling. *Geosciences 737  
738 (Switzerland)*, 9(8):1–21, 2019. 739

## Small microplastics Okinawa

- 687 [45] Sung-Yin Yang, Carine Bourgeois, Carey Denise Ashworth, and  
688 James Davis Reimer. Palythoa zoanthid 'barrens' in Okinawa: exami-  
689 nation of possible environmental causes. *Zoological Studies*, 52(1):1–  
690 11, 2013.
- 691 [46] PlasticsEurope. Plastics – the Facts 2015.

# Appendix B

## Genes that responded to nanoplastic exposure in *Symbiodinium tridacnidorum* and *Cladocopium* sp.

**Table B.1: Genes that responded to nanoplastic exposure in *Symbiodinium tridacnidorum*.** \*\*Annotations are available at the [genome browser](#). \*\*”up” and ”down” stand for ”upregulated” and ”downregulated”, respectively.

Gene IDs	Pfam protein domain*	Annotation by BLAST2GO*	Gene Ontology (GO)*	Response**
symbA_s719_g3	PARP			down
symbA_s7731_g3	ketoacyl-synt, Ketoacyl-synt_C, PP-binding, Thiolase_N	type i polyketide synthase	GO:0008152, GO:0003824	down
symbA_s4902_g5	Chloroa_b-bind	protein fucoxanthin chlorophyll a c protein	GO:0009579, GO:0044425, GO:0015979	down
symbA_s2605_g4	YchF-GTPase_C			down
symbA_s5873_g3				down
symbA_s236_g10	AAA, AAA_5, AAA_17, AAA_22, AAA_25, AAA_33, ACC_central, ATP-grasp_4, ATPgrasp_ST, ATPgrasp_Ter, Biotin_carb_C, Biotin_lipoyl, Carboxyl_trans, CP-Sase_L_chain, CPSase_L_D2, Dala_Dala_lig_C, IstB_IS21	acetyl-coa carboxylase	GO:0003824	down
symbA_s8212_g4	FA_desaturase,			down
symbA_s5495_g5	3HCDH_N, DAO, FAD_binding_2, FAD_binding_3, FAD_oxidored, GIDA, HI0933_like, Lycopene_cycl, NAD_binding_7, NAD_binding_8, NAD_binding_9, Pyr_redox, Pyr_redox_2, Pyr_redox_3, Thi4, Trp_halogenase	geranylgeranyl diphosphate chloroplastic	GO:0044249, GO:1901576, GO:0044763, GO:0016491, GO:0044711, GO:0016020, GO:0044434	down
symbA_s274_g14				down
symbA_s611_g22	Aminotran_5, Cys_Met_Meta_PP, DegT_DnrJ_EryC1, DUF883	cysteine desulfurase	GO:0042221, GO:0009058, GO:0006790, GO:0006520, GO:0016740	down
symbA_s9526_g3	CdCA1			down
symbA_s4600_g5	DNA_pol_A_exo1			down
symbA_s4045_g8	Fer4, RBB1NT			down
symbA_s2366_g6				down
symbA_s129_g11	Ank, Ank_2, Ank_3, Ank_4, Ank_5, Cupin_4, Cupin_8, JmjC, Pkinase, Pkinase_Tyr	ankyrin repeat-containing	GO:0003824	down
symbA_s7347_g2	Cortexin			down
symbA_s7664_g2	DUF1748			down
symbA_s3431_g3	Abhydrolase_6, NCD1, Ribosomal_L35p			down
symbA_s60_g36				down
symbA_s2301_g2	Ribosomal_L15e	60s ribosomal protein l15	GO:0005622	down
symbA_s2733_g13	Ank, Ank_2, Ank_3, Ank_4, Ank_5	ankyrin repeat-containing protein	GO:0003824	down
symbA_s2676_g10	Ank, Ank_2, Ank_3, Ank_4, Ank_5, Rad60-SLD, ubiquitin			down
symbA_s6597_g4	DUF2946, Glyco_transf_18			down
symbA_s250_g9				down
symbA_s7962_g3				down
symbA_s128_g31	ArfGap, SET	potential arf gap	GO:0044763, GO:0008152	down
symbA_s72_g14	Ank, Ank_2, Ank_3, Ank_4, Ank_5, DUF755			down
symbA_s1228_g15	DUF3584, Kinesin, V_ATPase_I			down
symbA_s177_g4	GBP, Miro, MMR_HSR1, Prok-RING_4	guanylate-binding protein 5	GO:0016021, GO:0007029, GO:0051260, GO:0042802, GO:0003924, GO:0008152, GO:0005783	down
symbA_s1596_g3	PDZ_1			down
symbA_s14930_g1	Gp_dh_N	glyceraldehyde-3-phosphate dehydrogenase	GO:0016620, GO:0044723, GO:0050662, GO:0000166	down
symbA_s2386_g5	PUF			down
symbA_s179_g4	DOMON, YHYH			down

Continued on next page

216 Genes that responded to nanoplastic exposure in *Symbiodinium tridacnidorum* and *Cladocopium* sp.

Table B.1 – Continued from previous page

Gene_IDs	Pfam protein domain*	Annotation by BLAST2GO*	Gene Ontology (GO)*	Response**
symbA_s4331_g2	TSP_1	thrombospondin-2 isoform x1	GO:0060089	down
symbA_s5216_g2	Filamin, fn3, PA14, TIG			up
symbA_s5819_g3				up
symbA_s527_g5	3Beta_HSD, adh_short, ketoacyl-synt, Ketoacyl-synt_C, KR, Polysacc_synt_2, PP-binding, PS-DH, ThiF, Thiolase_N	polyketide synthase type i	GO:0016747	up
symbA_s3252_g18				up
symbA_s3353_g1				up
symbA_s5559_g1				up
symbA_s4107_g1	DUF4381, Spexin, zf-C2H2_jaz, zf-met, zf-U1			up
symbA_s501_g13				up
symbA_s559_g9	AAA, AAA_5	serine threonine protein kinase	GO:0016740	up
symbA_s5819_g6	AAA_6	dynein heavy	GO:0006928, GO:0017111, GO:0036156, GO:0000166	up
symbA_s2756_g2	PAN_2, PAN_4, TGFb_propeptide			up
symbA_s5819_g4				up
symbA_s3643_g2	ADIP, APG6, ATP-synt_DE, DUF4201, Macoilin, Mnd1, PARP, Pijl, TMF_DNA_bd, V_ATPase_I, WEMBL, WWE			up
symbA_s1181_g14	zf-CCHC			up
s1738_g7				up
s148_g4	Apolipoprotein			up
s1791_g2				up
s122_g22	Ank, Ank_2, Ank_3, Ank_4, Ank_5			up
s1041_g1	Enkurin, PAF-AH_p_II, Val_tRNA-synt_C			up
s1038_g6				up
s2434_g9				up
s421_g46				up
s1286_g2				up
s4612_g2				up
s2533_g3				up
s3069_g7				up
s497_g5	DNA_pol3_gamma3, F5_F8_type_C, Laminin_G_3, RicinB_lectin_2			up
s3793_g9	AAA, AAA_5, AAA_16, AAA_22, ABC_tran, NACHT, RNA_helicase			up
s1020_g1	DUF2861, FNIP, LRR_5, Med31			up
s32_g20	HTH_psq			up
s3386_g3				up
s90_g48	RVT_1			up
s206_g39	rve, rve_3			up
s659_g5				up
s154_g41				up
s2157_g19	CotH, DUF2201, SecA_DEAD, VWA, VWA_2, VWA_CoxE			up
s1323_g1	Ypz1			up
s575_g23	OUT			up
s758_g32				up
s1290_g19	DUF3439, DUF4589, LPP20, SecD_SecF			up
s42_g4	FG-GAP, HD_5, TcdB_toxin_midN, UBA_4, VCBS			up
s1255_g43	CtIP_N, DUF2497			up
s1738_g8				up
s1016_g13	Flavi_M			up
s1845_g11	AAA_5			up
s573_g6	DUF1769, FNIP, LRR_5			up
s1429_g2	CMV_US, CobT, FAM176, SpoIIIAH, zf-DHHC			up
s1798_g12				up
s1141_g23	AGTRAP, NMN_transporter			up
s2515_g3	AhpC-TSA, DUF463, Redoxin,			up
s1066_g18				up
s467_g2	Fz			up
s2736_g7				up
s3717_g1				up
s288_g10				up
s884_g3				up
s5166_g8	Apc3, HAS, Lon_C, TPR_1, TPR_2, TPR_3, TPR_7, TPR_10, TPR_11, TPR_12, TPR_16, TPR_17, TraN	kinesin light chain 1	GO:0003676, GO:0003777, GO:0005524, GO:0005871, GO:0008152, GO:0043531, GO:0046872	up
s608_g16	DUF373			up
s1255_g30	DUF4215, fn3, IGFBP			up
s2491_g1	DUF1769, DUF2861, FNIP, LRR_5	fnip repeat-containing protein	GO:0016772	up
s172_g10				up
s4273_g7	DUF221			up
s1918_g9	DUF2087			up
s656_g13				up
s742_g15	Claudin_3, Ion_trans	voltage-gated ca2+ alpha subunit	GO:0044707, GO:0044765	up
s2564_g2	GTP_EFTU_D3	gtp-binding protein 1	GO:0000166	up
s4703_g2	ATP13			up
s4897_g6	LRR_1, LRR_4, LRR_7, LRR_8, ShK	clavata1 receptor kinase family protein	GO:0016740	up
s634_g8	AAA_5, AAA_6, DHC_N2, Intein_splicing			up
s2207_g2	AAA, AAA_5, AAA_6, AAA_7, AAA_16, AAA_17, AAA_18, AAA_19, AAA_22, AAA_30, DEAD, DUF853, FtsK_SpoIIIE, IstB_IS21, Mg_chelatase, Peptidase_C78, ResIII, RNA_helicase, Sigma54_activat, T2SE, Zeta_toxin	dynein heavy chain family protein	GO:0000166, GO:0007018, GO:0008152, GO:0017111, GO:0030286, GO:0044444	up
s2430_g6	DHC_N2, MRP-L27			up
s1254_g2				up

Continued on next page



Table B.1 – Continued from previous page

Gene IDs	Pfam protein domain*	Annotation by BLAST2GO*	Gene Ontology (GO)*	Response**
s1254_g3	AAA, AAA_5, AAA_6, AAA_17, DHC_N2, HMG_box, Nodulin-like, PseudoU_synth_2	dynein heavy chain partial	GO:000166, GO:0007018, GO:0017111, GO:0030286, GO:0043167	up
s1336_g15	AAA, AAA_5, AAA_6, AAA_10, AAA_16, AAA_17, AAA_18, AAA_19, AAA_22, AAA_24, AAA_28, AAA_30, AAA_33, ABC_tran, DHC_N1, DHC_N2, Mg_chelatase, Peripla_BP_5, RNA_helicase	flagellar outer dynein arm heavy chain beta	GO:0003777, GO:0005524, GO:0007018, GO:0008152, GO:0016887, GO:0030286	up
s26_g18	DHC_N1, DUF4455, IncA	dynein heavy chain family protein	GO:000166, GO:0017111	up
s634_g9	DHC_N2, DUF321, DUF1515, PAP_fibrillin			up
s634_g12	DHC_N1	heavy chain 2 family protein	GO:0005737, GO:0005929, GO:0044422	up
s38_g31	TIG			up
s83_g1	DUF3439, PAN_4, Sporozoite_P67, SRCR, SRCR_2			up
s2065_g2				up
s2358_g9	TIG			up
s2358_g5	TIG			up
s2358_g7	TIG			up
s1323_g2				up
s4606_g1				up
s3579_g5				up
s329_g12				up
s293_g7				up
s4112_g7	DUF4418			up
s1760_g18				down
s20_g20	CytochromB561_N			down
s592_g12				down
s556_g10	Armet, MAS20			down
s3382_g4	DUF667			down
s2119_g12	DUF4187, Noelin-1			down
s4797_g3	Lipocalin_7, Methyltransf_29, Nuc_N, RCC1_2, TPR_2, TPR_7, TPR_9, TPR_14, TPR_16, TPR_19			down
s4163_g1	Ank, Ank_2, Ank_3, Ank_4, Ank_5, DUF1843			down
s70_g17	PRKCSH-like			down
s1434_g24	LRR_1, LRR_4, LRR_6, LRR_7, LRR_8	protein nlrc3	GO:0000166, GO:0016772, GO:0044238, GO:0044260, GO:0044763, GO:0050794, GO:0050896	down
s1297_g5				down
s218_g4				down
s1348_g3				down
s912_g11	DUF1180			down
s1038_g5	DUF605			down
s4022_g1	PARP			down
s157_g15	PARP, Phage_integrase, PTS_2-RNA			down
s2131_g2				down
s309_g20	Clathrin, NT-C2, PPR, PPR_1, PPR_2, PPR_3			down
s1128_g5				down
s2448_g14				down
s5480_g1				down
s4414_g3	DUF4116, Pkinase	protein	GO:0004672, GO:0005524, GO:0006468, GO:0004672, GO:0016310, GO:0032550, GO:0032555, GO:0035639	down
s203_g50				down
s1161_g11	Apc3, Apc5, DSPn, Foie-gras_1, SMC_hinge, SNAP, TPR_12, TPR_14, TPR_15			down
s611_g26	rve, RVT_2, VWFD			down
s303_g34	PP-binding			down
s5215_g3	CDC45, Diety_REP, DUF3439			down
s630_g9	DENN			down
s1869_g2	PATI			down
s365_g10	EzrA, Laminin_II, Seryl_tRNA_N			down
s982_g14	Aldolase, LRR_1, LRR_4, LRR_5, LRR_6, LRR_7, LRR_8, LRR_9			down
s1162_g2	Crystall, DUF1914, Nuc_N, RCC1_2, YukD			down
s4916_g2	DUF2450, DUF4303, IncA			down
s4117_g1	LicD			down
s440_g18	AMP-binding, AMP-binding_C			down
s374_g51	DUF2614			down
s3619_g7	FMO-like, K_oxygenase, Pyr_redox, Pyr_redox_3, Shikimate_DH, Thi4			down
s1728_g9	Orbi_NS3			down
s347_g2	AAA_16, AAA_22, NACHT, T2SE	origin recognition complex subunit 4	GO:0097159, GO:1901363	down
s1823_g11	BBIP10, Trypsin_2			down
s3374_g7				down
s840_g20				down
s4414_g5	AfsA, APH, DBD_Tnp_Mut, DUF3049, DUF4116, NTPase_1, Pkinase, Reo_P9			down
s1495_g20				down
s399_g37				down
s3456_g1	UreD, UreF			down
s3148_g1	EGF_2, hEGF	tenascin isoform x1	GO:0009987, GO:0044699	down
s3282_g2	Abhydrolase_1, Abhydrolase_4, Abhydrolase_5, Chlorophyllase, Chlorophyllase2, DUF676, DUF915, PAF-AH_p_II			down
s1496_g1				down

Continued on next page

218 Genes that responded to nanoplastic exposure in *Symbiodinium tridacnidorum* and *Cladocopium* sp.

Table B.1 – Continued from previous page

Gene_IDs	Pfam protein domain*	Annotation by BLAST2GO*	Gene Ontology (GO)*	Response**
s3036_g2	Lge1, Methyltransf_11, Methyltransf_12, Methyltransf_18, Methyltransf_25, Methyltransf_26, Methyltransf_31, MTS, PCMT			down
s428_g19				down
s2458_g6	Crystall, Nuc_N, RCC1_2, YukD			down
s839_g36	Apc3, DUF2576, TPR_2, TPR_11, TPR_16, TPR_17, TPR_19			down
s2049_g7	Peptidase_C13			down
s628_g8	ADIP, Ax_dynein_light, HTH_Mga, Nsp1_C, Seryl_tRNA_N, SlyX, Tropomyosin_1, UCH			down
s112_g13	ALIX_LYPXL_bnd, Baculo_PEP_C, BLOC1_2, BRCA-2, OB3, CCDC155, DUF1798, FlaC_arch, Leu_zip, NPV_P10, Prefoldin, Spc7, Spectrin			down
s1471_g11				down
s138_g26	DUF2462, EF-1_beta_acid, MAGE_N, Ribosomal_60s, RRM_1, RRM_3, RRM_5, RRM_6			down
s971_g10	FmrO, Met_10, Methyltransf_18, Methyltransf_23, Methyltransf_26, MTS, PCMT, PrmA, PRMT5, Ubic_methyltran			down
s827_g1	zF-DBF			down
s5178_g3	FxsA			down
s286_g20	Kdo, Pkinase, Pkinase_Tyr	mitogen activated protein kinase kinase mekk3	GO:0004672, GO:0009628, GO:0016310, GO:0031323, GO:0033554, GO:0035556, GO:0044464, GO:0044710, GO:0071704	down
s1276_g9	Abhydrolase_1, Abhydrolase_5, Abhydrolase_6, DUF2048, DUF2974, Lipase_3, Thioesterase, TMEM125			down
s723_g1	Ank, Ank_2, Ank_3, Ank_4, Ank_5, PPR_2, Shigella_OspC			down
s2342_g6	Ank, Ank_2, Ank_3, Ank_4, Ank_5, Cupin_2			down
s888_g8	APH, Kdo, Kinase-like, Pkinase, Pkinase_Tyr			down
s373_g20	Alpha_kinase, Sel1, zF-NF-X1	eukaryotic elongation factor-2 isoform cra_b	GO:0004686, GO:0005516, GO:0005737, GO:0008135, GO:0031952	down
s2706_g2				down
s622_g15	DUF563, PG_binding_3, Pox_L5			down
s2256_g5				down
s1809_g7	Abhydrolase_5, Abhydrolase_6, AXE1, Esterase, Esterase_phd, Lipase_3, Peptidase_S9			down
s3095_g4				down
s1402_g26	DivIC, EF-hand_6, FUSC			down
s1005_g10	DUF4349			down
s1904_g2	Peptidase_C1, Peptidase_C1_2, RVT_1	papain family cysteine protease containing protein	GO:0016787	down
s232_g2	Zip			down
s519_g3	Apc3, PPR, PPR_1, PPR_2, PPR_3			down
s587_g10				down
s369_g22	DEAD			down
s1980_g9	Apc3, Rab5-bind, TPR_1, TPR_2, TPR_5, TPR_7, TPR_10, TPR_11, TPR_12, TPR_14, TPR_16, TPR_17, TPR_19			down
s507_g25				down
s186_g5	Bundlin			down
s2316_g17	Ank, Ank_2, Ank_3, Ank_4, Ank_5			down
s811_g5				down
s1013_g21	GILT, Thioredoxin_4			down
s2165_g1	PPR, PPR_1, PPR_2, PPR_3			down
s530_g16				down
s3303_g7				down
s1702_g11	His_Phos_2			down
s373_g3				down
s1897_g11				down
s3453_g13				down
s250_g32	DHODB_Fe-S_bind, Fer2, IRF-2BP1_2, Prim_Zn_Ribbon	chloroplast precursor	GO:0009536, GO:0009639, GO:0009767, GO:0051536	down
s243_g33				down
s165_g10	EF-hand_1, EF-hand_5, EF-hand_6, ScdA_N			down
s3839_g6	ADIP, Allexi_40kDa, APG6, CDC37_N, Cob_adoeno_trans, DUF4363, ERM, Exonuc_VII_L, FH2, Gtr1_RagA, IncA, Macoilin, Mod_r, PG_binding_4, Phyto_Pns9_10, Prominin, SPX, TBPIP, TMF_TATA_bd, TPR_MLP1_2, TraW_N, V_ATPase_I			down
s2313_g5				down
s288_g40	F-box-like			down
s756_g14	HpcH_Hpal			down
s1311_g9	BsuPI, FNIP, LRR_5			down
s165_g7	Ank, Ank_2, Ank_3, Ank_4, Ank_5, DNA_methylase, Nepo_coat_C			down
s2707_g3				down
s557_g8	AA_permease_C, rve, RVT_2, YfhO, ZZ			down
s1099_g9	WD40			down
s2161_g4				down
s3103_g2	DUF1469			down
s1464_g3	DUF2428, GCV_T, GCV_T_C			down
s1039_g1	Ank, Ank_2, Ank_3, Ank_4, Ank_5			down
s1645_g11	DnaJ			down
s4133_g1				down
s604_g13	DUF982, DUF2384, Nup54			down
s1587_g4				down

Continued on next page

Table B.1 – Continued from previous page

Gene IDs	Pfam protein domain*	Annotation by BLAST2GO*	Gene Ontology (GO)*	Response**
s607_g6	DUF4111			down
s267_g8	AAA_21, ABC_tran, ABC2_membrane_3, LON			down
s253_g2	CSD, OB_RNB, WW			down
s1130_g27	FANCL_C, PHD, Prok-RING_1, RINGv, zf-Apc11, zf-C3HC4, zf-C3HC4_2, zf-C3HC4_3, zf-C3HC4_4, zf-HC5HC2H, zf-Nse, zf-rbx1, zf-RING_2, zf-RING_5, zf-RING_UBOX			down
s1313_g1	Toxin-deaminase			down
s2581_g5	Fer4, Fer4_2, Fer4_3, Fer4_4, Fer4_6, Fer4_7, Fer4_8, Fer4_9, Fer4_10, Fer4_11, Fer4_13, Fer4_15, Fer4_16, Fer4_17, Fer4_18, Fer4_21	photosystem i subunit vii	GO:0009055, GO:0009522, GO:0009535, GO:0009773, GO:0016491, GO:0046872, GO:0051539	down
s141_g28	F_bp_aldolase	fructose-bisphosphate aldolase	GO:0004332, GO:0006096, GO:0008270	down
s1913_g7	Rotamase, Rotamase_2, Rotamase_3			down
s2092_g1	Glyco_transf_8, Glycos_transf_2			down
s3317_g8	PPR, PPR_2, PPR_3			down
s1811_g7				down
s501_g10	Phage_prot_Gp6, Syncollin			down
s601_g6				down
s274_g1	Lipase_3			down
s125_g13	Cys_Met_Meta_PP	o-succinylhomoserine sulphydrylase	GO:0003824	down
s4041_g2	Fun_ATP-synt_8, TctB	probable sugar phosphate phosphate translocator at3g14410 isoform x2	GO:0006810, GO:0044464	down
s64_g4				down
s629_g1	DUF937, LTXXQ, PPR, PPR_1, PPR_2, PPR_3, TPR_7, TPR_14			down
s403_g23	DUF3502, GRDA, Nuc_N, RCC1_2, YukD			down
s991_g26	AA_kinase	acetylglutamate chloroplastic-like	GO:0000166, GO:0009084, GO:0016301, GO:0016774	down
s85_g14				down
s342_g5	ADH_zinc_N_2, RCC1, RCC1_2			down
s2440_g8				down
s148_g7				down
s837_g13	DUF1759, Methyltransf_11, Methyltransf_25, Methyltransf_31, rve, UBN2_2, zf-CCHC, zf-CCHC_3, zf-CCHC_5			down
s1404_g18	3HCDH_N, adh_short, adh_short_C2, Epimerase, KR, NAD_binding_10			down
s576_g21	APH, Kdo, Kinase-like, Pkinase, Pkinase_Tyr	cell division control protein 2 homolog	GO:0004674, GO:0005515, GO:0005524, GO:0006468	down
s1989_g8	G_glu_transpept			down
s2682_g16				down
s188_g30	NifU	iron-sulfur cluster scaffold protein	GO:0005488	down
s3162_g8	AAA_16, AAA_17, AAA_21, AAA_22, AAA_23, AAA_25, AAA_29, ABC_membrane, ABC_tran, DUF258, SMC_N			down
s178_g6				down
s42_g1				down
s392_g25				down
s1580_g9	CIAPIN1, EF-hand_1, EF-hand_5, EF-hand_6, EF-hand_7, EF-hand_8, Ion_trans, Ion_trans_2	cytokine induced apoptosis inhibitor 1 family protein	GO:0005739, GO:0006915, GO:0051536	down
s740_g25	Crystall, DUF155, DUF2237, RCC1_2, TES, TFIIF_BTf_p62_N, YukD			down
s1143_g1	Dehydratase_MU, RAP			down
s694_g29				down
s250_g19	Ank, Ank_2, Ank_3, Ank_4, Ank_5, HEM4			down
s1854_g21	Aminotran_1_2			down
s247_g40				down
s196_g33				down
s3333_g8	Abhydrolase_1, Abhydrolase_3, Abhydrolase_5, Abhydrolase_6, DHquinase_I, DUF2974, Esterase, Lipase_3, Peptidase_S9, PGAP1, Thioesterase			down
s1138_g9	FdsD, Viral_Rep			down
s52_g10	YuzL			down
s30_g41	Ank, Ank_2, Ank_3, Ank_4, Ank_5			down
s1358_g8	adh_short, adh_short_C2, DUF1776, KR			down
s1070_g18				down
s834_g4	AIG1, SET			down
s821_g24	Ank, Ank_2, Ank_3, Ank_4, Ank_5, Glyco_hydro_10			down
s3795_g2	Armet, DUF1192, SAP			down
s4629_g2				down
s1017_g7	Dispanin			down
s1599_g2	2OG-FelI_Oxy, 2OG-FelI_Oxy_3	prolyl 4-hydroxylase alpha subunit	GO:0016705, GO:0046872, GO:0051213	down
s640_g18				down
s2860_g19				down

**Table B.2: Genes that responded to nanoplastic exposure in *Cladocodium* sp.** \*Annotations are available at the [genome browser](#). \*\*\*"up" and "down" stand for "upregulated" and "downregulated", respectively.

Gene IDs	Pfam protein domain*	Annotation by BLAST2GO*	Gene Ontology (GO)*	Response**
s1738_g7				up
s148_g4	Apolipoprotein			up
s1791_g2				up
s122_g22	Ank, Ank_2, Ank_3, Ank_4, Ank_5			up
s1041_g1	Enkurin, PAF-AH_p_II, Val_tRNA-synt_C			up
s1038_g6				up
s2434_g9				up
s421_g46				up
s1286_g2				up
s4612_g2				up
s2533_g3				up
s3069_g7				up
s497_g5	DNA_pol3_gamma3, F5_F8_type_C, Laminin_G_3, RicinB_lectin_2			up
s3793_g9	AAA, AAA_5, AAA_16, AAA_22, ABC_tran, NACHT, RNA_helicase			up
s1020_g1	DUF2861, FNIP, LRR_5, Med31			up
s32_g20	HTH_psq			up
s3386_g3				up
s90_g48	RVT_1			up
s206_g39	rve, rve_3			up
s659_g5				up
s154_g41				up
s2157_g19	CotH, DUF2201, SecA_DEAD, VWA, VWA_2, VWA_CoxE			up
s1323_g1	YpzI			up
s575_g23	OUT			up
s758_g32				up
s1290_g19	DUF3439, DUF4589, LPP20, SecD_SecF			up
s42_g4	FG-GAP, HD_5, TcdB_toxin_midN, UBA_4, VCBS			up
s1255_g43	CtIP_N, DUF2497			up
s1738_g8				up
s1016_g13	Flavi_M			up
s1845_g11	AAA_5			up
s573_g6	DUF1769, FNIP, LRR_5			up
s1429_g2	CMV_US, CobT, FAM176, SpoIIIAH, zF-DHHC			up
s1798_g12				up
s1141_g23	AGTRAP, NMN_transporter			up
s2515_g3	AhpC-TSA, DUF463, Redoxin,			up
s1066_g18				up
s467_g2	Fz			up
s2736_g7				up
s3717_g1				up
s288_g10				up
s884_g3				up
s5166_g8	Apc3, HAS, Lon_C, TPR_1, TPR_2, TPR_3, TPR_7, TPR_10, TPR_11, TPR_12, TPR_16, TPR_17, TraN	kinesin light chain 1	GO:0003676, GO:0003777, GO:0005524, GO:0005871, GO:0008152, GO:0043531, GO:0046872	up
s608_g16	DUF373			up
s1255_g30	DUF4215, fn3, IGFBP			up
s2491_g1	DUF1769, DUF2861, FNIP, LRR_5	fnip repeat-containing protein	GO:0016772	up
s172_g10				up
s4273_g7	DUF221			up
s1918_g9	DUF2087			up
s656_g13				up
s742_g15	Claudin_3, Ion_trans	voltage-gated ca2+ alpha subunit	GO:0044707, GO:0044765	up
s2564_g2	GTP_EFTU_D3	gtp-binding protein 1	GO:0000166	up
s4703_g2	ATP13			up
s4897_g6	LRR_1, LRR_4, LRR_7, LRR_8, ShK	clavata1 receptor kinase family protein	GO:0016740	up
s634_g8	AAA_5, AAA_6, DHC_N2, Intein_splicing			up
s2207_g2	AAA, AAA_5, AAA_6, AAA_7, AAA_16, AAA_17, AAA_18, AAA_19, AAA_22, AAA_30, DEAD, DUF853, FtsK_SpoIIIE, IstB_IS21, Mg_chelatase, Peptidase_C78, ResIII, RNA_helicase, Sigma54_activat, T2SE, Zeta_toxin	dynein heavy chain family protein	GO:0000166, GO:0007018, GO:0008152, GO:0017111, GO:0030286, GO:0044444	up
s2430_g6	DHC_N2, MRP-L27			up
s1254_g2				up
s1254_g3	AAA, AAA_5, AAA_6, AAA_17, DHC_N2, HMG_box, Nodulin-like, PseudoU_synth_2	dynein heavy chain partial	GO:0000166, GO:0007018, GO:0017111, GO:0030286, GO:0043167	up
s1336_g15	AAA, AAA_5, AAA_6, AAA_10, AAA_16, AAA_17, AAA_18, AAA_19, AAA_22, AAA_24, AAA_28, AAA_30, AAA_33, ABC_tran, DHC_N1, DHC_N2, Mg_chelatase, Peripla_BP_5, RNA_helicase	flagellar outer dynein arm heavy chain beta	GO:0003777, GO:0005524, GO:0007018, GO:0008152, GO:0016887, GO:0030286	up
s26_g18	DHC_N1, DUF4455, IncA	dynein heavy chain family protein	GO:0000166, GO:0017111	up
s634_g9	DHC_N2, DUF321, DUF1515, PAP_fibrillin			up
s634_g12	DHC_N1	heavy chain 2 family protein	GO:0005737, GO:0005929, GO:0044422	up
s38_g31	TIG			up
s83_g1	DUF3439, PAN_4, Sporozoite_P67, SRCR, SRCR_2			up
s2065_g2				up
s2358_g9	TIG			up

Continued on next page

Table B.2 – Continued from previous page

Gene IDs	Pfam protein domain*	Annotation by BLAST2GO*	Gene Ontology (GO)*	Response**
s2358_g5	TIG			up
s2358_g7	TIG			up
s1323_g2				up
s4606_g1				up
s3579_g5				up
s329_g12				up
s293_g7				up
s4112_g7	DUF4418			up
s1760_g18				down
s20_g20	CytochromB561_N			down
s592_g12				down
s556_g10	Armet, MAS20			down
s3382_g4	DUF667			down
s2119_g12	DUF4187, Noelin-1			down
s4797_g3	Lipoalain_7, Methyltransf_29, Nuc_N, RCC1_2, TPR_2, TPR_7, TPR_9, TPR_14, TPR_16, TPR_19			down
s4163_g1	Ank, Ank_2, Ank_3, Ank_4, Ank_5, DUF1843			down
s70_g17	PRKCSH-like			down
s1434_g24	LRR_1, LRR_4, LRR_6, LRR_7, LRR_8	protein nlrc3	GO:0000166, GO:0016772, GO:0044238, GO:0044260, GO:0044763, GO:0050794, GO:0050896	down
s1297_g5				down
s218_g4				down
s1348_g3				down
s912_g11	DUF1180			down
s1038_g5	DUF605			down
s4022_g1	PARP			down
s157_g15	PARP, Phage_integrase, PTS_2-RNA			down
s2131_g2				down
s309_g20	Clathrin, NT-C2, PPR, PPR_1, PPR_2, PPR_3			down
s1128_g5				down
s2448_g14				down
s5480_g1				down
s4414_g3	DUF4116, Pkinase	protein	GO:0004672, GO:0005524, GO:0006468, GO:0004672, GO:0016310, GO:0032550, GO:0032555, GO:0035639	down
s203_g50				down
s1161_g11	Apc3, Apc5, DSPn, Foie-gras_1, SMC_hinge, SNAP, TPR_12, TPR_14, TPR_15			down
s611_g26	rve, RVT_2, VWD			down
s303_g34	PP-binding			down
s5215_g3	CDC45, Dicty_REP, DUF3439			down
s630_g9	DENN			down
s1869_g2	PAT1			down
s365_g10	EzrA, Laminin_II, Seryl_tRNA_N			down
s982_g14	Aldolase, LRR_1, LRR_4, LRR_5, LRR_6, LRR_7, LRR_8, LRR_9			down
s1162_g2	Crystall, DUF1914, Nuc_N, RCC1_2, YukD			down
s4916_g2	DUF2450, DUF4303, IncA			down
s4117_g1	LicD			down
s440_g18	AMP-binding, AMP-binding_C			down
s374_g51	DUF2614			down
s3619_g7	FMO-like, K_oxygenase, Pyr_redox, Pyr_redox_3, Shikimate_DH, Thi4			down
s1728_g9	Orbi_NS3			down
s347_g2	AAA_16, AAA_22, NACHT, T2SE	origin recognition complex subunit 4	GO:0097159, GO:1901363	down
s1823_g11	BBIP10, Trypsin_2			down
s3374_g7				down
s840_g20				down
s4414_g5	AfsA, APH, DBD_Tnp_Mut, DUF3049, DUF4116, NTPase_1, Pkinase, Reo_P9			down
s1495_g20				down
s399_g37				down
s3456_g1	UreD, UreF			down
s3148_g1	EGF_2, hEGF	tenascin isoform x1	GO:0009987, GO:0044699	down
s3282_g2	Abhydrolase_1, Abhydrolase_4, Abhydrolase_5, Chlorophyllase, Chlorophyllase2, DUF676, DUF915, PAF-AH_p_II			down
s1496_g1				down
s3036_g2	Lge1, Methyltransf_11, Methyltransf_12, Methyltransf_18, Methyltransf_25, Methyltransf_26, Methyltransf_31, MTS, PCMT			down
s428_g19				down
s2458_g6	Crystall, Nuc_N, RCC1_2, YukD			down
s839_g36	Apc3, DUF2576, TPR_2, TPR_11, TPR_16, TPR_17, TPR_19			down
s2049_g7	Peptidase_C13			down
s628_g8	ADIP, Ax_dynectin_light, HTH_Mga, Nsp1_C, Seryl_tRNA_N, SlyX, Tropomyosin_1, UCH			down
s112_g13	ALIX_LYPXL_bnd, Baculo_PEP_C, BLOC1_2, BRCA-2_OB3, CCDC155, DUF1798, FlaC_arch, Leu_zip, NPV_P10, Prefoldin, Spc7, Spectrin			down
s1471_g11				down
s138_g26	DUF2462, EF-1_beta_acid, MAGE_N, Ribosomal_60s, RRM_1, RRM_3, RRM_5, RRM_6			down

Continued on next page

**Genes that responded to nanoplastic exposure in *Symbiodinium tridacnidorum* and *Cladocodium* sp.**

Table B.2 – Continued from previous page

Gene_IDs	Pfam protein domain*	Annotation by BLAST2GO*	Gene Ontology (GO)*	Response**
s971_g10	FmrO, Met_10, Methyltransf_18, Methyltransf_23, Methyltransf_26, MTS, PCMT, PrmA, PRMT5, Ubie_methyltran			down
s827_g1	zf-DBF			down
s5178_g3	FxsA			down
s286_g20	Kdo, Pkinase, Pkinase_Tyr	mitogen activated protein kinase kinase kinase mekk3	GO:0004672, GO:0009628, GO:0016310, GO:0031323, GO:0033554, GO:0035556, GO:0044464, GO:0044710, GO:0071704	down
s1276_g9	Abhydrolase_1, Abhydrolase_5, Abhydrolase_6, DUF2048, DUF2974, Lipase_3, Thioesterase, TMEM125			down
s723_g1	Ank, Ank_2, Ank_3, Ank_4, Ank_5, PPR_2, Shigella_OspC			down
s2342_g6	Ank, Ank_2, Ank_3, Ank_4, Ank_5, Cupin_2			down
s888_g8	APH, Kdo, Kinase-like, Pkinase, Pkinase_Tyr			down
s373_g20	Alpha_kinase, Sel1, zf-NF-X1	eukaryotic elongation factor-2 isoform cra_b	GO:0004686, GO:0005516, GO:0005737, GO:0008135, GO:0031952	down
s2706_g2				down
s622_g15	DUF563, PG_binding_3, Pox_L5			down
s2256_g5				down
s1809_g7	Abhydrolase_5, Abhydrolase_6, AXE1, Esterase, Esterase_phd, Lipase_3, Peptidase_S9			down
s3095_g4				down
s1402_g26	DivIC, EF-hand_6, FUSC			down
s1005_g10	DUF4349			down
s1904_g2	Peptidase_C1, Peptidase_C1_2, RVT_1	papain family cysteine protease containing protein	GO:0016787	down
s232_g2	Zip			down
s519_g3	Apc3, PPR, PPR_1, PPR_2, PPR_3			down
s587_g10				down
s369_g22	DEAD			down
s1980_g9	Apc3, Rab5-bind, TPR_1, TPR_2, TPR_5, TPR_7, TPR_10, TPR_11, TPR_12, TPR_14, TPR_16, TPR_17, TPR_19			down
s507_g25				down
s186_g5	Bundlin			down
s2316_g17	Ank, Ank_2, Ank_3, Ank_4, Ank_5			down
s811_g5				down
s1013_g21	GILT, Thioredoxin_4			down
s2165_g1	PPR, PPR_1, PPR_2, PPR_3			down
s530_g16				down
s3303_g7				down
s1702_g11	His_Phos_2			down
s373_g3				down
s1897_g11				down
s3453_g13				down
s250_g32	DHODB_Fe-S_bind, Fer2, IRF-2BP1_2, Prim_Zn_Ribbon	chloroplast precursor	GO:0009536, GO:0009639, GO:0009767, GO:0051536	down
s243_g33				down
s165_g10	EF-hand_1, EF-hand_5, EF-hand_6, ScdA_N			down
s3839_g6	ADIP, Allexi_40kDa, APG6, CDC37_N, Cob_adeno_trans, DUF4363, ERM, Exonuc_VII_L, FH2, Gtr1_RagA, IncA, Macoilin, Mod_r, PG_binding_4, Phyto_Pns9_10, Prominin, SPX, TBPIP, TMF_TATA_bd, TPR_MLP1_2, TraW_N, V_ATPase_I			down
s2313_g5				down
s288_g40	F-box-like			down
s756_g14	HpcH_Hpal			down
s1311_g9	BsuPI, FNIP, LRR_5			down
s165_g7	Ank, Ank_2, Ank_3, Ank_4, Ank_5, DNA_methylase, Nepo_coat_C			down
s2707_g3				down
s557_g8	AA_permease_C, rve, RVT_2, YfhO, ZZ			down
s1099_g9	WD40			down
s2161_g4				down
s3103_g2	DUF1469			down
s1464_g3	DUF2428, GCV_T, GCV_T_C			down
s1039_g1	Ank, Ank_2, Ank_3, Ank_4, Ank_5			down
s1645_g11	DnaJ			down
s4133_g1				down
s604_g13	DUF982, DUF2384, Nup54			down
s1587_g4				down
s607_g6	DUF4111			down
s267_g8	AAA_21, ABC_tran, ABC2_membrane_3, LON			down
s253_g2	CSD, OB_RNB, WW			down
s1130_g27	FANCL_C, PHD, Prok-RING_1, RINGv, zf-Apc11, zf-C3HC4, zf-C3HC4_2, zf-C3HC4_3, zf-C3HC4_4, zf-HC5HC2H, zf-Nse, zf-rbx1, zf-RING_2, zf-RING_5, zf-RING_UBOX			down
s1313_g1	Toxin-deaminase			down
s2581_g5	Fer4, Fer4_2, Fer4_3, Fer4_4, Fer4_6, Fer4_7, Fer4_8, Fer4_9, Fer4_10, Fer4_11, Fer4_13, Fer4_15, Fer4_16, Fer4_17, Fer4_18, Fer4_21	photosystem i subunit vii	GO:0009055, GO:0009522, GO:0009535, GO:0009773, GO:0016491, GO:0046872, GO:0051539	down
s141_g28	F_bp_aldolase	fructose-bisphosphate aldolase	GO:0004332, GO:0006096, GO:0008270	down
s1913_g7	Rotamase, Rotamase_2, Rotamase_3			down
s2092_g1	Glyco_transf_8, Glycos_transf_2			down

Continued on next page



Table B.2 – Continued from previous page

Gene IDs	Pfam protein domain*	Annotation by BLAST2GO*	Gene Ontology (GO)*	Response**
s3317_g8	PPR, PPR_2, PPR_3			down
s1811_g7				down
s501_g10	Phage_prot_Gp6, Syncollin			down
s601_g6				down
s274_g1	Lipase_3			down
s125_g13	Cys_Met_Meta_PP	o-succinylhomoserine sulfhydrylase	GO:0003824	down
s4041_g2	Fun_ATP-synt_8, TctB	probable sugar phosphate phosphate translocator at3g14410 isoform x2	GO:0006810, GO:0044464	down
s64_g4				down
s629_g1	DUF937, LTXXQ, PPR, PPR_1, PPR_2, PPR_3, TPR_7, TPR_14			down
s403_g23	DUF3502, GRDA, Nuc_N, RCC1_2, YukD			down
s991_g26	AA_kinase	acetylglutamate chloroplastic-like	GO:0000166, GO:0009084, GO:0016301, GO:0016774	down
s85_g14				down
s342_g5	ADH_zinc_N_2, RCC1, RCC1_2			down
s2440_g8				down
s148_g7				down
s837_g13	DUF1759, Methyltransf_11, Methyltransf_25, Methyltransf_31, rve, UBN2_2, zf-CCHC, zf-CCHC_3, zf-CCHC_5			down
s1404_g18	3HCDH_N, adh_short, adh_short_C2, Epimerase, KR, NAD_binding_10			down
s576_g21	APH, Kdo, Kinase-like, Pkinase, Pkinase_Tyr	cell division control protein 2 homolog	GO:0004674, GO:0005515, GO:0005524, GO:0006468	down
s1989_g8	G_glu_transpept			down
s2682_g16				down
s188_g30	NifU	iron-sulfur cluster scaffold protein	GO:0005488	down
s3162_g8	AAA_16, AAA_17, AAA_21, AAA_22, AAA_23, AAA_25, AAA_29, ABC_membrane, ABC_tran, DUF258, SMC_N			down
s178_g6				down
s42_g1				down
s392_g25				down
s1580_g9	CIAPIN1, EF-hand_1, EF-hand_5, EF-hand_6, EF-hand_7, EF-hand_8, Ion_trans, Ion_trans_2	cytokine induced apoptosis inhibitor 1 family protein	GO:0005739, GO:0006915, GO:0051536	down
s740_g25	Crystall, DUF155, DUF2237, RCC1_2, TES, TFIIH_BTf_p62_N, YukD			down
s1143_g1	Dehydratase_MU, RAP			down
s694_g29				down
s250_g19	Ank, Ank_2, Ank_3, Ank_4, Ank_5, HEM4			down
s1854_g21	Aminotran_1_2			down
s247_g40				down
s196_g33				down
s3333_g8	Abhydrolase_1, Abhydrolase_3, Abhydrolase_5, Abhydrolase_6, DHquinase_I, DUF2974, Esterase, Lipase_3, Peptidase_S9, PGAP1, Thioesterase			down
s1138_g9	FdsD, Viral_Rep			down
s52_g10	YuzL			down
s30_g41	Ank, Ank_2, Ank_3, Ank_4, Ank_5			down
s1358_g8	adh_short, adh_short_C2, DUF1776, KR			down
s1070_g18				down
s834_g4	AIG1, SET			down
s821_g24	Ank, Ank_2, Ank_3, Ank_4, Ank_5, Glyco_hydro_10			down
s3795_g2	Armet, DUF1192, SAP			down
s4629_g2				down
s1017_g7	Dispanin			down
s1599_g2	2OG-FelI_Oxy, 2OG-FelI_Oxy_3	prolyl 4-hydroxylase alpha subunit	GO:0016705, GO:0046872, GO:0051213	down
s640_g18				down
s2860_g19				down

## Statistics for RNA Expression Patterns

Genes that responded to nanoplastic exposure in *Symbiodinium tridacnidorum* and *Cladocopium* sp.

Table B.3: Differentially expressed genes with 2-fold difference between the controls and nP exposure (*Symbiodinium tridacnidorum* Clade A, TMM FPKM values, P<0.001)

gene_ID	100ng_rep1	100ng_rep2	100ng_rep3	100ng_mean	1000ng_rep1	1000ng_rep2	1000ng_rep3	1000ng_mean	10Mg_rep1	10Mg_rep2	10Mg_rep3	10Mg_mean	1000ng_rep1	1000ng_rep2	1000ng_rep3	1000ng_mean	10Mg_rep1	10Mg_rep2	10Mg_rep3	10Mg_mean	con_rep1	con_rep2	con_rep3	con_mean
s719_g3	10.281	8.743	9.811	9.612	7.587	10.165	11.039	9.597	6.436	7.994	8.706	7.712	15.185	13.403	19.122	15.903								
s7731_g3	19.112	20.230	17.347	18.896	13.772	21.005	24.863	19.880	10.054	15.591	13.244	12.963	26.641	22.492	35.478	28.204								
s4902_g5	48.766	53.929	47.379	48.321	35.181	47.435	47.830	47.830	38.333	39.913	36.315	36.513	94.307	75.123	89.733	86.817								
s2605_g4	25.723	18.647	18.195	20.835	16.598	21.184	30.840	22.874	14.788	18.120	12.453	15.120	34.516	31.581	44.355	36.877								
s5873_g3	4.811	5.438	4.941	5.063	3.067	5.167	8.831	5.688	2.412	2.946	3.416	2.925	6.420	7.324	10.255	8.000								
s236_g10	21.433	17.776	23.475	20.895	14.012	26.896	19.314	20.074	14.382	10.771	15.949	13.701	28.867	24.512	32.661	28.680								
s5495_g5	17.772	7.721	13.045	12.846	6.335	9.789	6.703	7.609	5.078	4.270	20.277	42.370	20.277	29.998	69.289	57.593	71.576	66.150	14.176	16.070	15.745	14.176		
s274_g14	6.181	5.839	6.058	6.026	4.671	5.484	4.446	4.867	6.487	4.096	6.732	5.772	12.119	8.471	13.912	11.501								
s611_g22	12.262	9.294	10.410	10.642	7.247	10.572	8.722	8.847	10.429	7.210	7.854	8.498	16.105	17.443	19.578	17.709								
s9526_g3	20.473	29.774	17.886	22.711	21.610	22.344	23.083	22.346	19.389	17.733	22.110	19.744	33.873	33.873	39.709	55.770	43.117	43.117	43.117	55.770	43.117	43.117	55.770	
s4600_g5	35.204	34.441	26.020	31.888	24.937	34.909	39.881	33.242	28.846	27.503	28.913	28.421	44.646	51.455	74.747	66.949								
s4045_g8	3.830	2.704	2.415	2.983	1.253	3.501	2.904	2.553	1.642	1.765	2.454	1.954	6.935	7.844	11.094	8.624								
s2366_g6	11.311	8.843	7.855	9.336	8.540	6.407	7.210	7.386	11.494	10.225	7.664	9.794	15.462	17.178	13.932	15.524								
s129_g11	3.270	2.894	2.665	2.943	2.215	1.983	2.218	2.139	2.199	2.618	2.675	2.497	5.174	4.049	4.786	4.670								
s7347_g2	17.762	13.800	16.069	15.877	10.073	12.992	13.108	12.058	19.815	16.692	13.996	16.834	19.736	24.316	29.625	24.559								
s7664_g2	7.791	9.053	7.985	8.276	6.254	7.676	6.474	6.801	10.784	11.356	10.770	10.970	12.247	12.247	15.285	15.572								
s3431_g3	29.694	33.519	22.238	28.484	15.045	19.597	16.728	17.123	28.805	29.377	30.235	29.472	39.700	33.316	49.462	41.493								
s60_g36	13.362	17.315	8.484	13.034	10.564	8.856	9.698	9.639	16.024	13.647	20.517	16.729	19.053	18.717	22.778	20.183								
s2301_g2	20.623	20.180	18.484	22.804	15.015	15.015	14.490	12.585	21.031	13.449	20.517	18.990	25.335	29.983	28.445	27.928								
s2733_g13	22.003	22.754	18.565	23.437	16.067	19.567	18.737	18.124	29.596	21.026	30.736	27.119	34.021	41.670	43.340	39.677								
s2676_g10	6.121	5.789	3.893	5.268	1.934	1.626	3.302	2.287	5.777	2.906	4.318	4.334	5.427	9.726	7.686	7.756								
s6597_g4	26.463	36.213	17.746	26.807	14.293	10.810	25.281	16.795	29.738	24.547	21.449	25.245	39.235	42.935	55.491	45.887								
s250_g9	55.957	53.859	34.614	48.143	30.420	33.789	42.128	35.446	39.680	42.826	47.975	46.677	68.329	51.955	73.877	73.877								
s7962_g3	26.703	21.532	20.291	22.842	13.371	16.780	18.200	16.117	15.325	17.952	22.862	18.713	31.459	32.473	46.427	36.786								
s128_g31	13.772	15.312	12.706	13.897	7.237	9.818	11.785	9.613	15.467	10.225	15.628	13.773	18.826	18.962	30.692	22.827								
s72_g14	9.571	16.574	9.013	11.653	3.588	6.843	5.341	5.257	8.037	7.528	8.964	8.184	16.590	11.560	14.978	14.376								
s1228_g15	3.040	2.153	2.276	2.490	2.466	3.134	3.013	2.871	1.976	2.094	2.034	2.094	5.857	5.638	4.775	5.423								
s177_g4	3.630	2.754	3.972	3.442	3.167	4.374	7.280	4.940	4.277	7.042	7.042	7.042	7.617	7.210	43.340	39.677								
s1596_g3	29.774	35.112	38.497	34.661	24.866	30.526	66.335	40.409	38.049	42.648	31.858	37.518	67.389	66.633	85.841	73.288								
s14930_g1	30.634	44.966	31.221	35.607	34.330	28.790	68.225	43.848	47.535	51.425	44.621	47.860	62.186	69.025	94.770	75.327								
s2386_g5	8.441	7.631	8.813	8.295	7.227	14.668	23.123	15.006	6.872	13.975	8.926	9.924	20.577	16.992	17.972	18.514								
s179_g4	5.151	5.879	8.244	6.425	4.861	11.415	19.910	12.062	5.463	11.287	5.700	7.483	14.018	13.050	12.254	13.107								
s4331_g2	1.210	3.495	5.240	3.315	3.298	3.550	4.167	3.672	1.307	1.448	1.733	1.733	6.054	9.373	6.764	7.397								
s5216_g2	10.031	9.324	9.861	9.739	15.005	12.794	16.837	14.879	7.237	10.126	10.048	9.137	7.924	6.550	5.304	6.294								
s5819_g3	13.492	11.026	11.026	12.338	18.212	13.924	17.574	17.574	8.818	14.768	13.214	12.267	8.854	7.050	7.230	7.711								
s527_g5	2.580	2.053	2.126	2.253	3.005	3.005	2.178	2.598	1.064	1.984	1.583	1.544	1.672	1.072	1.067	1.273								
s3252_g18	12.562	6.079	8.574	9.072	9.502	12.456	10.940	10.966	5.027	5.911	5.951	6.530	4.679	3.522	3.522	4.034								
s3533_g1	14.382	7.962	8.554	10.299	13.832	11.822	12.203	12.619	5.605	7.339	8.195	7.046	5.767	4.412	4.910	5.030								
s5559_g1	14.942	7.531	11.029	11.167	11.196	12.446	12.402	12.015	6.102	8.530	5.460	6.697	5.530	5.393	5.708	5.544								
s4107_g1	7.261	6.199	7.491	6.836	11.340	14.600	14.600	13.128	4.870	7.389	6.382	7.390	8.828	5.814	6.847	5.966								
s501_g13	25.873	21.231	38.706	28.693	10.304	41.963	43.491	40.508	24.457	39.533	18.363	27.451	20.874	24.414	15.559	20.282								
s559_g9	9.141	7.481	9.292	8.638	10.504	12.208	14.500	12.404	6.254	10.950	6.171	7.792	7.261	6.216	4.568	6.015								
s5819_g6	15.832	14.251	21.080	17.034	26.371	23.961	35.435	28.389	18.213	20.848	14.957	18.006	12.346	14.933	8.981	12.087								
s2756_g2	13.432	9.985	16.626	13.262	19.866	18.972	18.972	18.871	15.442	20.776	7.233	10.105	12.049	9.216	6.547	9.271								
s5819_g4	31.544	21.482	52.041	35.022	37.286	37.181	45.361	39.943	28.420	38.344	34.817	34.494	22.684	15.570	18.117	18.790								
s3643_g2	4.241	4.517	8.853	5.370	7.056	6.784	6.106	6.649	4.277	4.225	5.189	4.564	3.383	2.324	2.673	2.793								
s181_g14	13.812	13.109	25.491	17.471	30.781	26.668	29.697	29.049	16.936	20.550	20.968	19.485	13.959	15.423	12.410	13.951								

Table B.4: Differentially expressed genes with 2-fold difference between the controls and nP exposure *Cladocopium* sp. Clade C, TMM FPKM values,  $P < 0.001$

gene_ID	10ug_rep1	10ug_rep2	10ug_rep3	10ug_mean	100ug_rep1	100ug_rep2	100ug_rep3	100ug_mean	10MG_rep1	10MG_rep2	10MG_rep3	10MG_mean	con_rep1	con_rep2	con_rep3	con_mean
s1738_g7	5.502	8.133	7.775	7.137	8.95	8.318	7.603	8.672	7.274	6.072	7.575	6.974	2.875	1.973	4.664	3.171
s148_g4	14.93	19.734	22.266	18.798	21.336	33.706	24.131	24.131	29.301	28.094	10.336	25.577	12.749	10.826	10.616	11.397
s1791_g2	58.304	67.243	103.594	76.380	123.241	64.495	93.58	93.772	106.758	108.441	39.268	84.822	23.519	42.96	38.369	34.949
s122_g2	11.583	10.049	18.104	13.512	15.571	11.912	14.825	14.103	20.147	11.49	9.714	13.784	3.996	10.374	5.353	6.574
s1041_g1	11.583	11.875	11.797	11.751	13.58	10.31	18.291	14.060	17.972	18.528	10.42	15.640	7.066	7.901	3.515	6.161
s1038_g6	11.045	18.659	13.693	14.587	13.453	14.134	14.134	14.134	15.91	21.791	12.003	16.568	8.899	6.861	6.431	7.397
s421_g4	27.883	25.291	22.735	25.303	19.157	17.415	20.685	19.086	24.525	22.516	24.208	23.750	7.008	7.803	6.342	7.051
s1286_g2	7.329	6.054	6.447	6.610	5.081	2.985	4.638	4.235	10.444	10.785	12.437	11.222	5.634	2.866	5.023	4.508
s4612_g2	24.239	10.07	15.629	16.646	11.262	19.734	25.103	18.700	35.6	24.912	31.632	30.715	9.113	11.66	9.947	10.240
s2533_g3	10.15	7.007	5.06	7.406	9.846	8.867	9.446	9.386	4.978	4.038	8.342	5.786	3.597	4.613	5.463	4.558
s3069_g7	1.482	0.821	0.958	1.087	1.565	1.533	1.643	1.580	0.549	0.232	0.857	0.546	0.127	0.589	0.799	0.505
s497_g5	3.402	1.683	1.367	2.052	2.476	2.797	2.855	2.693	1.382	0.705	1.866	1.318	1.277	0.972	1.967	1.405
s3793_g9	1.117	0.72	0.22	0.686	0.664	0.557	0.992	0.738	0.274	0.272	0.431	0.431	0.214	0.196	0.479	0.296
s1020_g1	1.929	0.75	1.547	1.409	1.674	2.398	2.524	2.199	1.25	1.289	2.038	1.526	0.234	0.55	1.468	0.751
s32_g20	1.106	0.862	0.539	0.836	0.931	0.408	0.741	0.693	0.853	0.211	0.454	0.506	0	0.108	0.1	0.069
s3386_g3	3.441	1.724	2.056	2.407	3.635	2.627	2.965	3.076	1.961	1.057	1.846	1.621	0.819	0.324	1.338	0.827
s90_g48	0.173	0.142	0.429	0.248	0.327	0.269	0.29	0.295	0.193	0.121	0	0.105	0.049	0.128	0.04	0.072
s206_g39	0.376	0.162	0.689	0.409	0.753	0.468	0.531	0.584	0.366	0.363	0.438	0.330	0.195	0.088	0.26	0.181
s659_g5	0.162	0.112	0.03	0.101	0.248	0.249	0.18	0.226	0.183	0.161	0.272	0.205	0.039	0.029	0.06	0.043
s154_g41	0.315	0.355	0.25	0.307	0.941	0.955	0.571	0.822	0.284	0.06	0.262	0.202	0.136	0.059	0.3	0.165
s2157_g19	1.066	0.091	0.559	0.572	0.258	0.199	0.27	0.242	0	0.081	0	0.027	0	0	0.08	0.027
s1323_g1	0.954	0.477	0.719	0.717	1.575	1.98	1.893	1.816	0	0.806	0.736	0.514	0.673	0.815	0.489	0.659
s75_g23	7.623	4.634	7.725	6.661	14.372	14.549	9.206	12.709	5.374	6.082	6.364	5.907	3.947	5.064	4.913	4.641
s798_g52	487.311	581.151	434.398	500.953	677.587	783.638	809.551	756.925	327.051	635.156	708.073	556.760	328.316	263.833	430.169	340.839
s1290_g2	27.903	20.819	17.934	22.232	38.65	33.985	32.232	33.083	10.891	17.058	24.95	10.673	9.735	19.564	13.324	13.324
s42_g4	11.176	9.603	15.958	12.246	10.826	7.633	14.966	11.142	8.146	8.146	9.058	8.569	5.565	6.664	4.184	5.471
s1255_g43	9.206	8.467	11.797	9.823	14.937	10.648	15.056	13.547	8.798	12.889	9.754	10.480	6.316	5.781	5.153	5.750
s1738_g8	10.008	8.366	9.062	9.145	11.044	10.33	12.591	11.322	6.665	7.744	7.232	7.214	5.77	5.143	5.393	5.435
s1016_g13	33.923	16.489	30.499	26.970	34.52	27.75	28.689	30.328	14.64	20.321	23.472	19.478	9.337	18.825	12.873	13.678
s1845_g11	6.327	4.705	4.751	5.328	4.992	6.279	9.226	6.832	2.509	4.179	3.833	3.507	2.388	2.032	2.417	2.279
s73_g6	1.959	0.933	1.357	1.416	2.952	2.786	2.484	2.741	2.154	1.994	2.128	2.092	1.17	1.207	0.909	1.095
s1429_g2	3.096	1.47	3.423	2.663	3.487	4.379	2.444	3.437	3.15	4.179	2.744	3.358	1.842	1.06	1.428	1.443
s1798_g12	36.46	19.754	41.857	32.690	38.541	39.189	53.551	43.760	45.343	51.96	45.673	47.659	21.209	29.798	20.722	23.910
s1141_g23	29.142	23.141	18.863	23.715	24.753	21.246	26.886	24.295	16.215	32.807	25.499	24.840	8.46	14.644	8.359	10.488
s2515_g3	4.182	2.048	1.796	2.675	2.853	3.672	3.686	3.404	2.57	2.689	2.723	2.661	0.39	1.541	1.029	0.987
s1066_g18	3.603	1.663	2.615	2.627	4.735	5.931	5.96	5.542	2.286	5.095	4.126	3.836	1.248	1.718	0.829	1.265
s467_g2	7.572	7.747	5.639	6.986	8.261	8.936	9.306	8.854	4.765	6.868	7.202	6.278	6.063	4.161	2.956	4.393
s2736_g7	11.917	13.01	10.13	11.686	14.62	19.973	22.719	19.104	12.324	14.077	12.689	13.030	9.532	9.805	5.373	8.237
s288_g10	94.267	94.409	52.596	80.824	86.918	141.719	83.963	104.200	63.386	95.682	78.011	79.026	45.849	45.669	50.173	47.230
s884_g5	6.111	9.015	8.194	7.773	12.461	11.43	18.281	13.734	11.43	9.899	9.31	10.213	3.879	8.068	7.19	6.379
s5166_g8	5.248	7.859	5.968	6.358	8.419	11.802	10.704	10.704	4.236	7.732	7.844	6.604	3.207	5.585	4.834	4.542
s608_g16	1.888	4.178	8.204	4.757	6.924	9.693	13.493	10.037	4.105	7.693	5.175	5.658	2.944	4.79	4.923	4.219
s1255_g30	17.114	17.949	27.475	20.846	19.315	36.801	34.349	30.155	16.449	12.204	19.942	16.198	10.283	9.412	14.87	11.522
s2491_g1	0	0	0.489	0.163	0	0.985	1.052	0.679	0	0	0	0.000	0	0	0	0.000
s172_g10	56.751	17.726	30.44	34.972	49.16	61.142	50.186	53.496	73.942	23.12	12.659	36.574	22.096	23.055	23.249	22.800
s4273_g7	2.05	3.012	7.864	4.309	6.389	9.165	7.403	7.652	8.006	4.441	0.928	4.458	4.191	1.924	1.248	2.454
s1918_g9	1.807	1.582	2.136	1.842	2.734	3.861	2.154	2.916	1.842	1.722	1.069	1.831	1.491	1.492	0.599	1.194
s656_g13	1.472	0.284	0.689	0.815	1.02	1.761	1.362	1.381	0.711	0.675	0.353	0.580	0.604	0.746	0.479	0.610
s742_g15	5.867	3.245	2.834	3.982	10.767	6.777	3.786	8.399	4.379	3.786	3.52	3.895	4.181	4.525	2.027	3.578
s2664_g2	29.456	25.94	26.378	27.238	32.816	31.715	23.58	29.370	24.424	20.25	9.27	17.981	13.918	19.08	10.067	14.335

Continued on next page

Genes that responded to nanoplastic exposure in *Symbiodinium tridacnidorum* and *Cladocodium* sp.

Table B.4 – continued from previous page

gene ID	10ug_rep1	10ug_rep2	10ug_rep3	10ug_mean	100ug_rep1	100ug_rep2	100ug_rep3	100ug_mean	10MG_rep1	10MG_rep2	10MG_rep3	10MG_mean	con_rep1	con_rep2	con_rep3	con_mean
s4703_g2	2.142	3.803	1.946	2.630	3.467	2.836	3.646	3.316	3.15	2.306	1.584	2.347	1.501	2.473	0.929	1.634
s4897_g6	4.192	4.411	1.547	3.383	2.843	3.354	3.396	3.198	1.717	1.48	0	1.066	1.101	1.286	1.019	1.135
s634_g8	20.859	17.726	10.26	16.282	22.653	21.187	20.946	21.187	15.27	15.27	18.237	12.908	6.794	7.253	12.583	8.877
s2407_g6	34.095	30.473	18.863	27.810	36.639	30.269	35.861	34.490	24.983	9.314	27.93	20.742	9.152	11.415	22.24	14.269
s2430_g6	21.722	18.466	9.98	16.723	22.772	19.654	20.695	21.040	13.817	4.552	18.479	12.283	6.248	6.075	16.228	9.517
s1254_g2	2.103	19.298	14.97	18.457	35.5	30.451	29.6	31.850	19.781	8.227	25.177	17.728	9.99	7.911	18.485	12.129
s1254_g3	30.989	26.609	21.507	26.368	37.392	31.695	38.315	35.801	21.488	13.02	25.52	20.009	12.846	14.467	23.748	17.020
s1336_g15	41.941	31.73	27.935	33.869	41.226	38.91	46.339	42.158	26.141	17.139	34.033	25.771	15.4	18.167	26.195	19.921
s26_g18	34.156	21.61	18.254	24.673	30.657	32.82	34.879	32.785	17.028	10.15	25.035	17.404	8.46	14.673	21.242	14.792
s634_g9	12.617	9.289	4.521	8.809	13.045	9.086	9.005	10.379	8.189	2.266	8.08	6.178	1.667	2.424	7.5	3.864
s238_g12	6.151	4.006	1.198	3.785	7.617	5.573	4.989	6.060	3.779	0.755	4.136	2.890	0.37	0.677	3.415	1.487
s38_g31	9.785	7.18	3.653	6.873	5.403	6.581	6.548	6.081	3.15	3.857	6.548	4.138	3.033	3.206	2.869	2.669
s83_g1	24.98	22.401	13.882	20.421	16.482	19.415	20.826	18.908	10.058	10.15	18.106	12.771	8.187	9.815	10.786	9.596
s2065_g2	4.984	4.107	1.946	3.679	3.318	4.478	3.776	3.857	2.276	1.178	3.208	2.221	1.082	2.081	2.097	1.753
s238_g9	13.703	8.599	6.198	9.500	8.528	8.936	9.877	9.114	3.566	2.759	7.595	4.640	3.138	3.73	5.153	4.007
s238_g5	17.053	11.327	5.27	11.217	10.371	13.454	11.62	11.815	5.557	6.092	9.825	7.158	4.25	4.544	3.765	4.186
s238_g7	17.032	13.822	6.038	12.297	15.393	10.091	10.338	11.941	6.035	7.703	13.204	8.981	3.002	2.748	6.421	4.057
s1323_g2	1.756	1.947	1.916	1.873	2.546	2.179	2.184	2.303	0.721	0	1.513	0.745	0.458	0.422	0.609	0.496
s406_g1	6.202	2.971	5.469	4.881	3.714	5.075	3.436	4.075	2.794	0.534	2.915	2.081	1.179	2.032	2.477	1.896
s379_g5	14.637	68.064	116.459	66.387	89.959	104.56	55.965	83.495	53.115	36.523	61.6	50.413	13.178	30.112	30.799	24.696
s329_g12	8.049	0	9.351	5.800	24.228	25.953	6.231	18.804	4.023	3.575	5.235	4.278	3.918	8.951	0	4.290
s293_g7	1.583	8.599	5.938	5.373	9.638	11.275	9.937	10.283	0	0	0	0.000	4.698	4.289	9.927	6.305
s4112_g7	6.202	9.897	17.006	11.035	18.315	21.356	21.827	20.499	0	24.228	23.613	15.947	0	0	2.706	0.902
s1760_g18	4.558	5.02	4.371	4.650	6.092	0.796	7.062	4.650	1.392	1.208	2.653	1.751	11.998	9.147	3.575	8.240
s20_g20	9.247	34.752	14.96	19.653	6.914	10.371	14.194	10.625	4.572	20.381	5.971	10.308	20.108	40.791	30.609	30.503
s592_g12	6.344	11.886	12.959	9.638	13.146	11.6	11.461	11.461	12.893	12.809	8.342	11.348	21.901	27.158	26.944	25.334
s556_g10	1.868	5.03	2.325	3.074	3.932	4.956	2.655	3.848	2.337	2.266	0.736	1.780	5.293	3.573	8.139	5.668
s382_g4	1.421	3.472	3.214	2.684	3.249	1.761	1.957	1.447	1.957	1.447	1.957	1.447	3.631	3.725	4.184	3.812
s219_g12	1.655	1.572	2.285	1.837	2.972	1.164	1.302	1.813	0.772	0.886	0.646	0.768	3.938	2.925	4.574	3.812
s4797_g3	2.365	3.154	2.455	2.658	3.992	1.174	1.923	2.363	1.737	1.792	1.523	1.684	3.967	5.761	2.926	4.218
s4163_g1	4.456	6.804	7.565	6.275	7.053	5.991	5.149	6.064	4.897	4.219	3.329	4.148	7.378	9.795	9.787	8.987
s70_g17	4.405	6.186	7.106	5.899	6.171	6.896	5.975	6.575	3.84	3.877	2.824	3.514	8.256	8.961	6.501	7.906
s1434_g24	4.588	4.837	7.405	5.610	6.438	5.404	5.549	5.797	2.865	4.129	2.832	3.144	7.749	8.146	7.66	7.852
s1297_g5	0.711	0.998	0.833	0.833	0.587	1.322	1.322	0.831	0.528	0.222	0.222	0.324	1.082	1.296	2.417	1.598
s218_g4	4.984	5.527	5.389	5.300	5.26	7.424	8.374	7.019	4.856	4.048	4.721	4.542	7.008	8.892	11.195	9.032
s1348_g3	12.586	20.657	13.932	15.725	9.697	12.618	18.992	13.769	13.116	8.62	12.619	11.452	22.154	24.115	33.216	26.495
s912_g11	20.697	23.161	13.613	19.157	12.946	19.803	23.139	18.629	13.675	13.967	16.704	14.782	25.322	27.953	38.769	30.675
s1038_g5	6.933	6.754	5.09	6.259	5.091	6.508	9.065	6.888	3.911	4.773	7.535	5.406	10.751	9.059	12.813	10.874
s4022_g1	2.791	1.693	1.727	2.070	1.07	2.05	3.246	2.122	1.534	1.571	2.108	1.738	3.06	3.906	5.053	4.006
s157_g15	11.866	12.787	10.838	11.830	7.32	15.773	18.672	13.922	8.158	10.382	11.045	9.862	14.913	15.478	32.856	21.082
s2131_g2	6.466	5.101	6.218	5.928	4.338	5.662	4.037	4.679	4.978	5.186	3.783	4.649	8.1	8.294	13.981	10.125
s309_g20	3.187	2.312	3.333	2.944	2.385	3.652	2.454	2.897	2.428	2.558	1.866	2.284	3.86	5.064	7.151	5.358
s1128_g5	6.588	7.96	7.106	7.218	5.864	8.18	6.491	6.845	5.639	7.079	5.86	6.193	11.647	10.963	17.607	13.406
s2448_g14	18.971	15.708	12.845	15.841	13.947	13.584	12.131	13.221	9.753	10.372	7.242	9.122	18.841	14.212	26.804	19.952
s4414_g3	5.816	6.449	4.8	5.688	5.22	6.409	4.528	5.386	3.546	4.751	7.203	7.224	7.203	9.987	8.128	8.128
s203_g50	11.155	12.108	9.012	10.758	9.786	13.813	12.081	11.893	9.662	3.736	9.603	7.667	16.004	18.226	24.468	19.566
s1161_g11	17.56	15.16	12.086	14.935	13.194	15.813	13.443	14.130	9.733	10.382	11.045	10.387	17.651	19.865	24.428	20.648
s611_g26	2.03	1.511	1.886	1.809	2.1	2.538	1.873	2.098	0.965	1.41	1.311	1.229	1.813	3.092	2.876	2.594
s303_g34	2.111	0.548	1.327	1.329	2.1	0.824	2.074	1.803	1.097	0.826	1.029	0.984	2.602	2.149	2.986	2.579
s5215_g3	34.674	25.514	40.599	33.596	40.909	54.823	35.049	43.607	23.784	19.243	25.348	22.792	56.424	47.396	53	52.273
s630_g9	3.421	3.894	4.042	3.786	4.14	5.891	5.449	5.160	3.793	2.175	2.935	2.794	4.795	3.612	3.925	4.111
s1869_g2	12.13	10.84	11.767	11.579	11.54	16.519	15.506	14.522	7.031	6.868	7.212	7.037	13.041	11.797	13.242	12.693
s365_g10	1.766	1.115	1.277	1.386	1.716	1.026	1.637	1.271	1.026	1.279	1.099	1.134	2.328	2.13	2.367	2.344
s92_g14	1.766	1.115	1.277	1.386	1.716	1.026	1.637	1.271	1.026	1.279	1.099	1.134	2.328	2.13	2.367	2.344
s1162_g2	5.309	2.434	3.373	3.705	2.704	2.727	2.634	2.688	2.205	2.769	4.035	3.003	6.501	4.211	6.431	5.714

Continued on next page

Table B.4 - continued from previous page

gene_ID	10ug_rep1	10ug_rep2	10ug_rep3	10ug_mean	100ug_rep1	100ug_rep2	100ug_rep3	100ug_mean	10MG_rep1	10MG_rep2	10MG_rep3	10MG_mean	con_rep1	con_rep2	con_rep3	con_mean
s4976_g2	8.739	5.415	5.23	6.461	6.488	4.13	7.663	6.094	3.089	4.854	5.659	4.534	7.232	9.334	17.317	11.294
s4117_g1	3.796	3.113	3.842	3.584	4.873	5.533	6.782	5.729	3.81	3.917	5.931	4.553	6.91	8.087	8.858	7.952
s440_g18	2.72	2.434	1.617	2.257	2.556	4.14	5.72	4.139	2.174	3.524	4.075	3.258	4.445	6.302	6.302	4.724
s374_g51	11.348	11.418	9.781	10.849	6.864	7.812	4.888	6.521	8.29	4.572	6.95	6.604	12.953	19.119	19.224	17.099
s3619_g7	10.922	11.925	11.817	11.555	6.23	8.22	5.559	6.670	8.067	8.318	10.137	8.841	12.924	16.666	21.202	16.931
s1728_g9	8.384	9.482	9.252	9.039	6.755	7.344	6.537	6.219	7.772	6.545	6.377	6.965	13.421	11.042	17.177	13.880
s347_g2	7.024	9.056	6.098	7.393	5.171	6.667	4.458	5.499	6.502	4.411	6.94	5.951	14.347	10.021	16.388	13.585
s3374_g7	3.197	4.127	2.834	3.386	2.239	3.951	2.354	2.848	3.2	2.014	2.925	2.713	3.09	3.425	3.795	3.437
s1823_g11	1.705	1.886	1.277	1.623	1.149	1.642	1.382	1.391	1.626	1.18	1.18	1.378	3.09	3.425	3.795	3.437
s840_g20	5.217	4.249	3.044	4.170	2.387	3.185	3.276	3.616	3.82	1.984	3.359	3.054	6.374	6.841	6.921	6.712
s4414_g5	7.288	5.446	5.02	5.918	2.377	5.274	3.386	3.679	4.531	3.021	4.398	3.983	9.172	6.625	9.088	8.295
s14095_g20	27.376	24.784	24.97	25.710	11.51	21.445	17.65	16.868	22.92	15.115	17.672	18.569	26.667	43.323	35.723	35.238
s39_g37	75.986	49.557	75.121	66.888	37.174	59.848	40.93	45.984	43.534	33.039	34.769	37.114	85.255	89.364	90.1	88.240
s3456_g1	4.304	4.766	3.473	4.181	1.892	3.553	3.967	3.137	2.357	3.712	2.929	3.115	5.673	5.133	5.974	5.974
s3148_g1	3.086	2.484	2.176	2.582	1.179	3.115	2.360	2.785	2.753	2.376	2.708	2.611	7.885	5.614	6.471	6.637
s3282_g2	5.461	4.107	2.266	3.945	2.873	1.931	2.164	2.323	4.704	2.148	2.483	2.898	4.688	3.926	5.593	4.736
s1496_g1	9.349	9.786	5.03	8.055	3.001	5.463	4.297	4.254	5.11	2.699	4.64	4.150	9.474	6.448	9.827	8.583
s3036_g2	3.411	4.148	2.635	3.398	2.149	1.682	1.873	1.901	2.225	1.279	0.938	1.481	5.312	5.192	5.343	5.282
s428_g19	12.942	11.347	9.461	11.250	8.4	8.22	10.257	8.959	8.676	6.686	5.487	6.950	14.289	15.625	18.036	15.983
s2458_g6	3.136	1.541	0.669	1.782	0.733	0.856	1.152	0.914	0.376	1.964	0.958	1.099	3.606	1.983	6.092	3.894
s839_g36	2.72	0.75	1.487	1.652	0.713	1.692	2.264	1.556	2.621	0.806	1.412	1.613	2.671	4.24	3.306	3.406
s2049_g7	1.776	0.517	0.639	0.977	0.792	2.209	0.831	1.277	0.925	0.534	0	0.486	1.179	2.071	1.738	1.663
s628_g8	10.201	7.271	6.906	8.126	3.744	15.385	11.73	10.286	3.851	6.696	5.709	5.419	9.844	18.02	14.82	14.228
s112_g13	22.625	19.734	31.917	24.759	18.354	27.655	19.463	21.824	20.421	16.756	18.913	18.697	46.785	44.874	81.442	57.700
s1471_g11	11.236	8.741	8.563	9.513	7.043	12.429	5.81	8.427	7.061	5.196	5.265	5.841	11.716	24.675	42.803	26.398
s138_g26	16.423	8.285	9.172	11.293	6.389	10.827	11.84	9.685	5.1	3.172	4.63	4.301	9.084	12.151	19.364	13.533
s971_g10	2.436	3.144	1.956	2.512	1.704	2	2.224	1.976	0.884	0	0.295	1.274	2.306	2.986	2.206	2.605
s827_g1	7.613	7.96	7.106	7.560	8.954	8.538	8.284	8.592	4.511	7.22	8.291	6.674	16.55	16.302	17.876	16.909
s1778_g3	1.533	2.18	1.277	1.663	4.15	1.085	2.665	2.633	1.676	1.45	2.108	1.745	4.805	4.191	5.862	4.933
s286_g20	3.335	6.764	2.295	4.265	4.982	3.344	6.711	5.012	3.688	3.192	5.124	4.001	8.45	8.068	10.935	9.151
s723_g9	1.776	2.231	1.687	1.565	1.872	2.209	2.364	2.148	1.3	1.007	1.218	1.478	3.099	3.072	4.714	3.628
s733_g1	0.995	1.44	0.689	1.041	1.367	1.761	1.052	1.393	1.493	2.014	1.715	1.741	2.534	2.611	2.557	2.567
s2342_g6	0.944	1.44	0.579	0.988	1	1.174	0.521	0.898	1.565	1.128	0.978	1.224	1.735	2.051	2.407	2.064
s888_g8	2.639	2.921	1.816	2.459	4.348	4.18	2.895	3.808	5.314	4.249	4.65	4.738	6.248	8.588	7.28	7.372
s373_g20	2.852	2.201	1.687	2.247	3.665	3.553	2.755	3.324	3.962	1.772	4.287	3.340	5.078	4.299	5.173	4.850
s2706_g2	0.944	2.099	1.148	1.397	1.496	0.876	0.521	0.964	1.036	1.118	2.28	1.478	2.71	2.483	3.935	3.043
s622_g15	19.793	31.578	12.845	21.405	22.267	14.131	14.455	16.951	17.952	15.699	27.799	20.483	27.311	34.136	51.452	37.633
s256_g5	5.979	4.249	2.465	4.231	4.913	3.145	1.873	3.310	3.688	6.394	5.83	5.304	7.495	6.87	11.375	8.580
s1809_g7	3.208	3.894	4.002	3.701	4.665	4.737	4.067	4.490	3.861	4.562	5.053	4.748	7.992	6.154	8.609	7.585
s3095_g4	0.162	0.355	0.629	0.382	0.505	0.995	1.072	0.857	0.884	0.916	0.444	0.748	1.852	1.698	1.937	1.829
s1402_g26	0	0.193	0.329	0.174	0.357	0.846	0.942	0.715	1.118	1.128	0.706	0.984	1.959	0.491	2.517	1.656
s1005_g10	9.369	12.443	10.489	10.767	6.29	11.544	9.466	9.100	14.64	9.153	15.403	13.065	18.646	14.241	29.321	20.736
s1904_g2	4.091	7.687	5.519	5.766	4.705	5.025	5.82	5.183	8.849	7.663	7.273	7.928	10.994	6.978	17.287	11.753
s232_g2	4.923	1.592	1.986	2.834	6.26	5.085	4.319	5.294	4.501	6.852	4.319	6.291	8.339	8.441	8.339	7.877
s519_g3	1.401	0.314	0.14	0.618	1.179	0.866	0.311	0.785	0.62	0.534	0.585	0.580	1.618	2.149	2.207	1.991
s587_g10	0.7	0.254	0.898	0.617	2.199	1.443	2.054	1.899	1.016	1.319	1.604	1.313	3.148	6.007	5.363	4.839
s369_g22	1.015	0.75	0.659	0.808	3.041	2.946	3.195	3.061	2.428	2.9	1.644	2.324	2.222	2.601	2.507	2.531
s1980_g9	0.325	0.548	0.798	0.557	1.902	1.102	1.806	1.880	1.806	1.239	1.806	1.845	2.222	1.727	2.577	2.175
s507_g25	15.043	24.733	10.789	16.855	6.062	8.548	13.964	9.252	14.62	9.053	22.171	15.281	14.377	18.658	34.045	22.360
s186_g5	4.476	7.747	1.836	4.686	1.991	1.562	4.157	2.570	4.094	1.782	10.41	5.429	5.234	8.392	11.105	8.244
s2316_g17	3.959	6.236	1.088	3.761	1.179	2.767	5.529	3.158	3.637	1.057	2.31	2.335	6.384	6.91	12.424	8.573
s811_g5	39.292	81.926	47.017	56.078	13.838	24.232	35.491	24.520	37.784	22.415	38.784	39.466	60.313	32.634	75.5	56.149
s1013_g21	11.511	16.012	8.363	12.029	8.677	9.116	14.793	7.340	14.793	7.784	10.137	10.905	12.281	12.661	19.045	14.662
s2165_g1	1.502	2.14	1.248	1.630	0.901	1.065	0.471	0.812	2.113	1.218	1.473	1.601	1.569	3.69	2.766	2.675
s530_g16	32.39	63.186	21.607	39.061	28.874	22.52	17.059	22.818	58.205	29.283	41.104	42.864	38.919	60.096	58.213	52.409
s3303_g7	28.401	48.574	17.246	31.407	18.107	20.54	15.126	17.924	40.954	23.191	38.602	34.249	36.882	45.747	57.823	46.817

Continued on next page

Genes that responded to nanoplastic exposure in *Symbiodinium tridacnidorum* and *Cladocodium* sp.

Table B.4 – continued from previous page

gene ID	10ug_rep1	10ug_rep2	10ug_rep3	10ug_mean	100ug_rep1	100ug_rep2	100ug_rep3	100ug_mean	10MG_rep1	10MG_rep2	10MG_rep3	10MG_mean	con_rep1	con_rep2	con_rep3	con_mean
s1702_g11	3.817	5.415	2.465	3.899	1.119	2.627	2.344	2.030	4.419	3.011	3.803	3.744	2.661	6.291	7.25	5.401
s373_g3	21.082	31.426	17.505	23.338	10.093	11.842	19.213	13.716	20.756	25.466	21.697	22.640	19.308	26.255	36.521	27.361
s1897_g1	18.565	11.742	11.128	17.145	9.341	17.145	11.429	10.648	17.078	14.863	17.439	16.793	18.997	17.834	29.94	22.257
s3463_g13	129.316	121.039	64.003	104.786	65.83	85.712	68.106	73.216	106.474	74.355	107.818	96.216	136.299	102.624	205.158	148.027
s250_g32	62.019	67.871	33.334	54.408	30.795	43.328	37.613	37.613	87.323	44.387	59.442	63.717	69.69	63.718	108.825	80.744
s243_g33	7.207	5.983	4.651	5.947	1.575	2.966	2.645	2.395	5.557	4.249	6.597	5.468	7.183	6.007	10.516	7.902
s165_g10	7.674	7.595	5.449	6.906	2.536	4.468	3.095	3.366	5.037	3.786	4.082	5.742	8.363	5.742	12.993	9.033
s3839_g6	32.035	33.079	21.128	28.747	15.432	19.854	18.844	18.844	24.15	17.773	24.208	22.044	35.303	34.725	75.53	48.519
s2313_g5	131.712	132.305	76.678	113.565	66.415	91.882	82.761	80.353	102.146	68.172	126.912	99.077	124.262	105.834	296.087	175.394
s288_g40	7.521	9.441	4.92	7.294	4.309	5.284	5.99	5.194	6.289	6.354	8.352	6.998	9.932	10.679	12.104	10.905
s756_g14	22.717	23.648	17.475	21.280	13.233	13.872	21.437	16.181	22.402	18.075	25.59	22.022	28.217	30.298	40.137	32.884
s1311_g9	9.003	6.612	4.88	6.832	3.209	3.951	4.999	4.053	6.663	5.156	6.674	6.017	7.768	9.285	12.374	9.809
s165_g7	3.553	2.86	2.206	2.873	2.11	1.821	2.574	2.168	2.601	1.611	3.51	2.574	4.201	3.985	6.012	4.733
s2707_g3	11.399	12.078	11.387	11.621	9.152	7.175	8.484	8.270	10.658	7.099	14.323	10.693	15.848	15.341	19.045	16.745
s557_g8	1.583	1.612	1.218	1.471	0.971	0.697	0.952	0.873	1.382	0.695	1.463	1.180	1.248	1.688	2.716	1.884
s1099_g9	3.837	2.991	1.178	2.669	2.496	1.363	2.084	1.981	2.611	2.145	3.198	2.651	3.694	4.024	4.574	4.097
s2161_g4	5.633	4.949	2.505	4.362	2.962	1.742	2.855	2.520	4.115	3.333	5.497	4.315	5.634	6.517	5.852	6.001
s1303_g2	5.299	4.766	3.523	4.529	3.823	2.856	4.007	3.562	4.684	3.424	7.262	5.123	8.938	5.987	7.011	7.312
s1464_g3	4.436	4.34	2.784	3.853	3.298	3.871	3.456	3.542	4.562	3.454	4.67	4.229	6.53	8.48	8.429	7.813
s1039_g1	7.511	7.808	5.619	6.979	5.279	5.244	6.421	6.648	8.211	6.981	8.211	6.981	11.628	12.161	16.069	13.286
s1645_g11	9.48	7.149	6.068	7.566	4.992	7.523	7.773	6.763	9.987	8.473	9.149	8.473	13.675	11.817	15.779	13.757
s4133_g1	3.603	7.311	4.94	5.285	3.784	3.712	4.628	4.041	4.907	3.393	8.665	5.655	9.367	6.301	11.355	9.008
s604_g13	2.061	3.417	1.747	2.408	1.624	1.592	1.983	1.733	1.402	1.218	3.187	1.936	4.289	3.926	4.274	4.163
s1039_g4	11.531	19.024	11.707	14.087	7.469	7.882	12.451	9.267	15.29	9.999	18.363	14.599	18.363	20.17	20.363	19.632
s607_g8	1.127	1.693	0.549	1.123	0.654	0.851	0.851	0.737	1.158	0.886	0.981	0.981	2.203	1.443	1.887	1.844
s27_g2	4.05	5.466	3.323	4.280	3.021	2.966	3.887	3.291	4.734	2.87	4.509	4.038	7.427	5.516	7.071	6.671
s253_g2	9.856	20.454	7.785	12.698	9.658	7.792	8.194	8.548	13.035	11.328	14.182	12.848	22.008	17.971	21.222	20.400
s1130_g27	4.618	6.115	2.226	4.320	2.407	5.095	3.376	3.767	7.467	3.021	8.19	6.226	9.055	7.42	9.747	8.741
s1313_g1	2.903	3.559	1.776	2.746	1.773	2.846	1.863	1.621	4.023	3.661	6.361	4.268	3.675	3.661	6.212	4.516
s2581_g5	78.432	70.234	22.226	56.964	31.4	33.109	36.923	33.811	52.089	28.87	59.976	46.978	56.414	48.76	125.393	76.856
s141_g28	88.954	32.675	64.972	64.972	36.402	50.543	45.017	43.987	67.635	30.904	61.782	56.440	85.937	61.166	125.853	90.983
s1913_g7	9.034	7.433	1.747	6.071	3.804	4.468	3.706	3.993	6.208	4.973	5.026	6.988	9.891	9.767	8.215	8.215
s2092_g1	3.147	3.336	0.798	2.427	1.01	1.015	1.362	1.129	1.572	0.644	3.016	1.572	2.29	2.63	2.277	2.399
s3317_g8	4.07	1.886	1.816	2.591	0.535	1.473	3.015	1.674	3.729	2.739	4.922	3.797	4.084	5.212	3.765	4.354
s1811_g7	10.617	9.684	6.218	8.840	4.824	5.662	9.085	6.524	11.45	10.362	15.12	12.311	12.388	15.272	14.411	14.024
s501_g10	3.522	2.126	2.146	3.343	1.842	1.085	3.376	2.101	5.232	2.477	6.022	4.377	10.01	8.755	7.28	8.682
s601_g6	13.683	36.314	15.689	21.895	16.958	10.817	17.31	15.095	32.531	24.61	34.003	30.395	28.548	31.574	35.383	31.835
s274_g1	2.203	9.715	7.036	6.318	5.339	1.791	5.559	4.230	9.367	4.078	10.944	8.130	11.998	12.347	10.736	11.694
s125_g13	9.633	4.492	5.18	6.435	1.397	0	4.337	1.911	5.639	7.452	5.457	6.183	10.936	4.996	12.354	9.429
s4041_g2	3.4	3.722	2.146	3.089	2.328	0	1.202	1.177	4.704	6.193	3.026	4.641	10.234	4.152	10.236	8.207
s64_g4	5.41	1.186	2.046	2.881	1.109	0	2.304	1.138	9.001	1.974	4.337	5.104	8.694	4.966	8.798	7.486
s629_g1	2.314	2.018	2.725	2.352	1.04	0.816	2.013	1.290	3.993	2.034	1.594	2.540	5.01	2.856	2.746	3.537
s403_g23	1.147	2.545	4.072	2.588	1.605	0.468	0.841	0.971	2.906	2.155	2.098	2.386	3.577	5.094	4.234	4.302
s991_g26	2.348	2.15	1.527	2.075	1.535	1.811	1.212	1.519	2.276	2.417	2.179	2.291	3.938	2.562	3.256	3.252
s85_g14	6.476	6.47	4.561	5.836	3.754	4.627	3.055	3.812	4.45	5.065	6.93	5.482	3.754	7.312	7.79	7.692
s342_g5	1.502	2.211	1.776	1.830	1.05	1.861	1.292	1.401	3.218	2.054	3.218	2.245	3.83	2.719	2.617	3.055
s2440_g8	0	0.071	0.13	0.067	0	0.09	0.08	0.057	0.152	0	0.192	0.115	0.214	0.461	0.569	0.415
s148_g7	0.842	0.598	0.758	0.733	0.386	0.597	0.351	0.438	0.731	0.463	0.504	0.566	1.14	0.815	1.278	1.078
s837_g13	0.365	0.7	0.359	0.475	0.277	0.129	0.393	0.192	0.579	0.17	0.422	0.386	0.984	0.805	0.439	0.743
s1404_g18	1.655	1.044	2.745	1.815	0.743	0.876	1.042	0.887	1.036	2.004	1.301	1.447	2.953	3.602	1.738	2.764
s76_g21	35.293	35.279	40.26	36.944	29.884	20.918	31.213	27.338	39.623	35.969	36.766	37.453	56.103	62.265	59.092	59.153
s1989_g8	3.4	1.775	2.136	2.437	2.536	1.244	1.332	1.704	3.078	2.276	2.764	2.706	4.815	3.838	3.366	3.996
s2682_g16	6.953	6.328	8.274	7.185	5.993	3.015	4.348	4.348	9.733	9.969	7.947	9.350	8.031	10.845	10.526	9.801
s188_g30	11.545	9.522	7.086	9.254	4.348	4.329	3.857	4.188	10.538	7.502	11.368	9.643	10.263	8.49	11.744	10.166
s3162_g8	5.684	2.525	2.525	3.578	2.229	1.612	1.983	1.941	2.855	3.232	5.154	3.747	4.25	3.278	5.413	4.314
s178_g6	2.416	0.892	2.076	1.795	1.129	0	0	0.376	1.168	2.327	1.473	1.723	1.676	1.541	3.216	2.144

Continued on next page



Table B.4 – continued from previous page

gene_ID	10ug_rep1	10ug_rep2	10ug_rep3	10ug_mean	100ug_rep1	100ug_rep2	100ug_rep3	100ug_mean	10MG_rep1	10MG_rep2	10MG_rep3	10MG_mean	con_rep1	con_rep2	con_rep3	con_mean
s42_g1	2.101	1.359	1.707	1.722	1.852	1.304	0.581	1.246	2.692	1.662	0.726	1.693	3.489	3.366	5.193	4.016
s392_g25	2.578	2.839	3.713	3.043	2.011	2.358	1.402	1.924	3.444	3.595	1.755	2.931	3.967	8.46	6.491	6.306
s1580_g9	10.232	7.372	4.88	7.495	6.052	7.573	3.185	5.603	10.647	8.338	6.688	8.558	13.899	12.229	11.954	12.694
s740_g25	6.334	3.671	2.635	4.210	2.853	2.607	1.993	2.484	4.602	3.414	3.319	3.778	7.525	4.888	6.122	6.178
s1143_g1	5.075	3.022	2.635	3.577	2.456	2.886	2.144	2.495	8.046	4.038	2.673	4.919	6.072	5.565	6.112	5.916
s694_g29	80.483	60.499	45.29	62.091	27.675	32.173	27.988	29.279	86.307	60.881	17.601	54.930	59.309	96.343	80.074	78.575
s250_g19	3.339	3.083	4.321	3.581	1.951	1.841	1.643	1.812	3.871	1.752	3.581	3.068	2.719	4.976	6.172	4.622
s1854_g21	26.442	24.784	23.034	24.753	16.661	17.734	13.613	16.003	24.688	17.703	30.603	24.331	26.726	30.593	39.348	32.222
s247_g40	37.374	28.982	27.755	31.370	14.095	24.222	18.552	18.956	38.282	15.064	33.054	28.800	32.272	38.778	55.426	42.159
s196_g33	15.977	24.469	24.232	21.559	10.935	14.081	10.197	11.738	16.631	7.774	17.077	13.827	23.548	19.571	30.819	24.646
s3333_g8	9.196	11.936	11.337	10.823	6.656	9.394	5.93	7.327	11.734	6.565	10.45	9.583	14.172	12.082	17.537	14.597
s1138_g9	10.77	16.063	13.952	13.595	4.774	7.464	2.484	4.907	12.212	6.384	13.496	10.697	16.433	19.325	11.205	15.654
s52_g10	4.74	2.616	7.765	5.040	1.981	5.822	1.553	3.119	9.205	5.327	5.175	6.569	9.298	8.519	9.148	8.988
s30_g41	3.086	2.728	1.786	2.533	1.298	2.667	0.341	1.435	3.028	3.776	4.236	3.680	2.885	3.818	6.821	4.508
s1388_g8	9.298	12.787	7.625	9.903	5.913	6.618	4.347	5.626	8.605	11.157	11.227	10.330	12.31	7.793	19.224	13.109
s1070_g18	10.546	10.232	9.97	10.249	5.993	11.235	4.968	7.399	8.494	12.789	10.924	10.736	18.763	18.226	17.966	18.318
s834_g4	1.797	1.42	0.749	1.322	0	0.955	0	0.318	0.559	1.45	1.765	1.258	2.934	1.708	1.658	2.100
s821_g24	1.248	3.225	0.798	1.757	0.436	2.05	0.461	0.982	2.255	1.954	3.984	2.731	5.595	5.918	3.825	5.113
s3795_g2	86.684	42.094	29.551	52.776	42.394	37.059	10.808	30.087	34.573	24.912	36.363	31.949	71.386	52.755	128.499	84.213
s4629_g2	1.259	6.226	0.599	2.695	1.961	0.766	0	0.909	0.671	1.168	2.552	1.464	5.146	4.711	6.881	5.579
s1017_g7	5.725	7.778	0	4.501	4.358	1.702	0	2.020	5.852	10.321	1.886	6.020	12.768	6.478	11.545	10.264
s1599_g2	2.071	11.134	7.675	6.960	6.211	0	0	2.070	6.187	1.833	5.366	4.462	10.049	14.683	16.488	13.740
s640_g18	12.861	0	7.745	6.869	45.752	29.068	12.692	29.171	36.453	32.968	26.69	32.037	27.944	47.376	44.321	39.880
s2860_g19	9.612	0	8.413	6.008	62.799	31.248	9.045	34.364	42.752	39.463	22.715	34.977	59.592	62.285	47.976	56.618



## Appendix C

### Tables of Microplastics found and analyzed, with optical images

The table below shows all 73  $\mu\text{P}$  found around Okinawa, with optical images and closes up at 50x with the Raman microscopy system. The global and site numbering correspond to the plastics' numbering among all found and specific to a given site, respectively (see Columns 1 and 2).

Column 3 displays one optical image of the  $\mu\text{P}$ , an image was taken before Raman spectroscopy measurements at 50x with the Nanofinder 30. Columns 4 and 5 give the area and polymer type. Columns 6 - 8 correspond to the XRF analysis. 'XRF2', 'XRF4', and 'XRF6' correspond to a 2-fold, 4-fold, and 6-fold increased value of the respective element compared to the surrounding. While already a 2-fold increase shows the element's presence, the other two values give some indication of the abundance of the element. Columns 9 - 11 describes the particle according to [66]. Empty columns indicate that further analysis of the collected data remains to be done.

Table C.1: Station S1 (Nakagusku 1). 8 µP were present in samples from Manta Trawl.

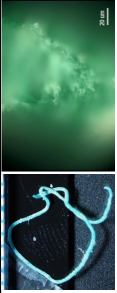
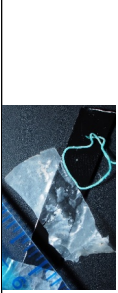

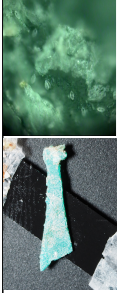
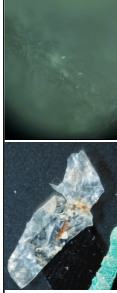
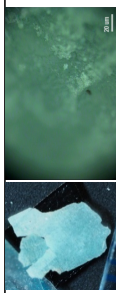
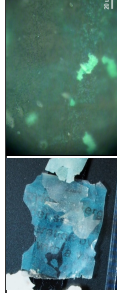
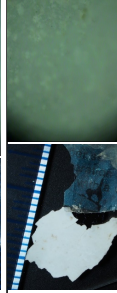
Numbering	Site	µP Images	Area (mm <sup>2</sup> )	Polymer Type	XRF			Hidalgo-Ruz2013		
					XRF 2	XRF 4	XRF 6	Shape	Erosion	Color
1	1		9.24	PE	no ID possible	no ID possible	no ID possible	Filament	Broken Edges	Blue
2	2		106.70	PE	no ID possible	no ID possible	no ID possible	Rectangular	Cracks in the surface, easy to tear, weathered	Light blue clear
3	3		35.37	PP	no ID possible	no ID possible	no ID possible	Rectangular	Cracks in the surface, easy to tear, weathered	Clear with blue marking
4	4		20.54	PE	As, Cl, Cr, Cu, Fe, Hg, Pb, S, Ti, Zn	Cr, S	Cr, S	Irregular, angular	Sharp edges, surface unbroken, surface coating weathered	Green
5	5		27.53	PP	Si, S, Cl, Ca, Ti, Fe, P, Cr, Mn, K	Si, S, Cl, Ca, Ti, Fe, P, Cr, Mn, K	Si, S, Cl, Ca, Ti, Fe, P, Cr, Mn, K	Rectangular	Broken film, tears, easy to disintegrate	Clear
6	6		19.91	PE				Irregular, subangular	Rounded edges, breaking more when handled, very weathered	Blue
7	7		159.94	PP				Irregular, breaking when handled	Folded part, rounded and sharp edges, depending on new break or old one	Clear blue, letters visible in black
8	8		99.75	PE	Si, Cl, Ti, Fe, V, Cd, S, K Nor all sites have the same things on them	Si, Cl, Ti, Fe, V, Cd, S, K Nor all sites have the same things on them	Si, Cl, Ti, Fe, V, Cd, S, K Nor all sites have the same things on them	Irregular, angular	Very thin with sharp edges	White, discoloration spots

Table C.2: Station S1 (Nakagusku 2). 9  $\mu\text{P}$  were present in samples from Manta Trawl.


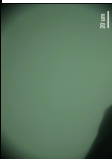

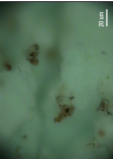

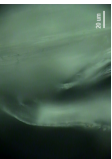

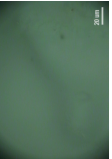

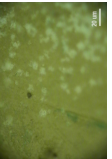

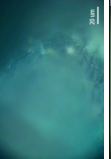
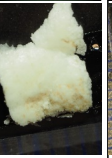
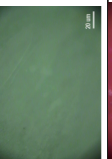

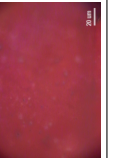
Numbering Global	Site	$\mu\text{P}$ Images		Area ( $\text{mm}^2$ )	Polymer Type	XRF				Hidalgo-Ruz2013	
						XRF 2	XRF 4	XRF 6	Shape	Erosion	Color
9	1				PP	Ca, Ti, V	Ti, V	Ti, V	Irregular, angular	Rounded edges	White
10	2				PP	C, Cl, Cu, Hg, Ti, Zn	Ti	Ti	Irregular, angular	Rounded edges	White
11	3				PP					Broken edges	White
12	4				PE	S, Ca, Cl, Cr, Ga, Hg, Ni, Pb, Si, S, Ti, V	Ca, Cl, Ni, S, Ti, V	Ca, Cl, S, Ti, V	Irregular, angular	Rounded edges	White
13	5				PE				Irregular, angular	Sharp edges	Yellow
14	6				PP				Filament	Broken edges	Blue
15	7				PS				Irregular, angular	Rounded edges, falling apart	White
16	8				(PVC)				Irregular	Breaking more, sharp edges	Mix





Table C.3: Station S2 (Kin 1). 6  $\mu\text{P}$  were present in samples from Manta Trawl.


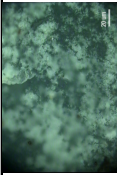

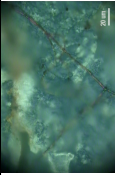



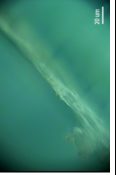
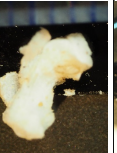
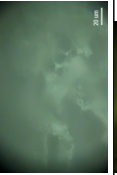

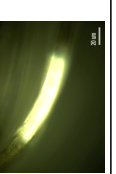
Numbering Global	Site	$\mu\text{P}$ Images		Area ( $\text{mm}^2$ )	Polymer Type	XRF			Hidalgo-Ruiz2013			
						XRF2	XRF 4	XRF 6	Shape	Erosion	Color	Color Type
18	1				PE	As, Bi, Ca, Cu, Ga, Ge, Hg, Mn, Ni, Pb, Ti, V, Zn	As, Bi, Ca, Cu, Ga, Ni, Pb, Ti, V, Zn	V	Irregular, angular	Rounded edges	Blue	Colored
19	2				PE	As, Cu, Pb, Bi, Ca, Cr, Ga, Ge, Hg, Mn, Ni, Ti, V, Zn	Ca, Ti	Ti	Irregular, angular	Sharp edges, still break- ing more	Blue	Colored
20	3				PS	Cl, S			Irregular, angular	Rounded edges	White	White
21	4				Unknown	As, Cl, Ca, Cu, Fe, Hg, Pb, S, Ti, Zn, Cr, Mn	Cl, Cr, Cu, Mn, Ca	Cl	Filament		Blue	Colored
22	5				PS	Ca, Si, S, Cl	Ca	Ca	Irregular, angular	Rounded edges	White	White
23	6				Unknown	Ca, Cl, S, Ti, V, Mn, Zn, As, Cl, Cu, Fe	Zn, Ti, S, Cl, Ca, Si	Ca, Si, Ti, Cl	Filament	Broken edges	Yellow	Colored

Table C.4: Station S4 (Kin 2). 5  $\mu$ P were present in samples from Manta Trawl.

Numbering		Hidalgo-Ruz2013		XRF			Erosion		Color	
Global	Site	Area (mm <sup>2</sup> )	Polymer Type	XRF2	XRF4	XRF6	Shape	Erosion	Color	Color Type
24	1	0.76	PE	As, Ca, Cl, Cu, Hg, Pb, Ti, V, Zn	Ca, Cl, Ti, V, Zn	Cl, Ti, V	Irregular, subangular	Less weathered, broken edges, rounded edges	White	White
25	2	0.96	PP	S, Cl, need to finish ID	S, Cl, need to finish ID	S, Cl, need to finish ID	Filament	Broken edges	Yellow	Colored
26	3	1.426	PE	As, Cl, Cu, Hg, Pb, Zn	S, Cl	S, Cl	Irregular, angular	Rounded edges	Opaque	White
27	4	1.81	PE	S, Cl, Fe hot spot, small amount of As and Pb	S, Cl, Fe hot spot, small amount of As and Pb	S, Cl, Fe hot spot, small amount of As and Pb	Irregular, subangular		Opaque	White
28	5		Unknown	Ca, Cl, Si, S, K	Ca, Cl, Si, S	Ca, Cl, S	Irregular, subangular		White	White

Table C.5: Station S4 (Oura). 2  $\mu\text{P}$  were present in samples from Manta Trawl.

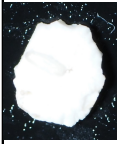
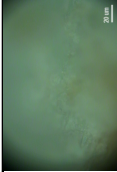

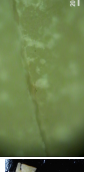
Numbering Global	Site	$\mu\text{P}$ Images		XRF			Hidalgo-Rutz2013			
				XRF2	XRF 4	XRF 6	Shape	Erosion	Color	Color Type
29	1			S, Ca, Ti, V, Bi, Cl	S, Ca, Ti, V, Bi, Cl	S, Ca, Ti, V, Bi, Cl	Irregular, subangular	Weathered, grooves, irregular surfaces, jagged fragments	White	White
30	2			Cl, Ti, Ca	Cl, Ti, Ca	Cl, Ti, Ca	Irregular, angular, broken edges	Weathered, splits	Yellow with bleached white dots	Colored

Table C.6: Station S4 (Cape Hedo 1). 4 µP were present in samples from Manta Trawl.

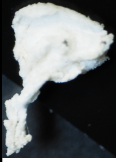
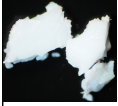
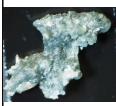

Numbering Global	Site	µP Images	Hidalgo-Ruz2013			XRF			Erosion	Color	Color Type
			Area (mm <sup>2</sup> )	Polymer Type	XRF2	XRF 4	XRF 6	Shape			
31	1		6.71	PS	Fe, K, Cl, Si, S	Cl, K	Cl, K	Irregular	Rounded edges	White	White
32	2		4.41	PE	V high, K, S, Ti, Ca, Cl, S in Hot spot, Si	S, Ca, Cl, K, Si, S, all in discolorations	S, K, Si, S	Irregular	Rounded edges	White	White
33	3		4.58	Unknown	Cl, Cu, K, S, Ti, Zn, Ca, Si	Ca, K, Si, S	Ca, Si, S	Irregular	Rounded edges	White weathered to green	White
34	4		23.83	PS	Ti hot spot, As, Cl, Cu, Hg, Pb, S, Zn, Ca, Si	Ti hot spot, Zn, Ca, Si	Ti hot spot, Ca	Irregular, round	Rounded edges	White	White

Table C.7: Station S8 (Nago 1). 2  $\mu\text{P}$  were present in samples from Manta Trawl.

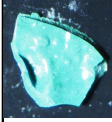
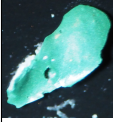
Numbering Global	Site	$\mu\text{P}$ Images	XRF			Hidalgo-Rutz2013					
			Area ( $\text{mm}^2$ )	Polymer Type	XRF 2	XRF 4	XRF 6	Shape	Erosion	Color	Color Type
35	1		0.85	Unknown	Ca, S, Ti, V, As, Cu, Fe, Pb, Tm, Zn	Ca, S, Ti, V	Ca, S, Ti, V	Irregular, subangular	Rounded edges	Green	Colored
36	2		1.49	Unknown	S, Cl, Ca, Fe, Ba, Tm, V, Ti, Cd, Cr	S, Cl, Ca, Fe, Ba, Tm, V, Ti, Cd, Cr	S, Cl, Ca, Fe, Ba, Tm, V, Ti, Cd, Cr	Irregular, subangular	Rounded edges	Green	Colored

Table C.8: Station S9 (Nago 2). 6 µP were present in samples from Manta Trawl.

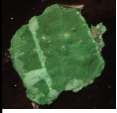
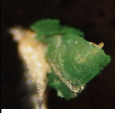

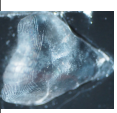
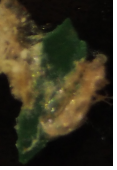
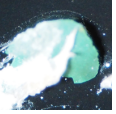
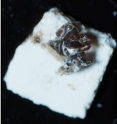
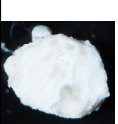
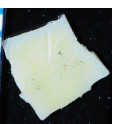

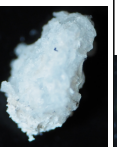

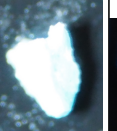
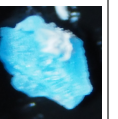
Numbering		µP Images	XRF				Hidalgo-Ruz2013				
Global	Site		Area (mm <sup>2</sup> )	Polymer Type	XRF2	XRF 4	XRF 6	Shape	Erosion	Color	Color Type
37	1			Unknown	S, Cl, Ca, Fe, Cu, Sr, Ti, V	S, Cl, Ca, Fe, Cu, Sr, Ti, V	S, Cl, Ca, Fe, Cu, Sr, Ti, V	Irregular, angular	Rounded edges	Green	Colored
38	2			Unknow	S, Cl, Ca, Fe, Cu, Sr, Ti, V	S, Cl, Ca, Fe, Cu, Sr, Ti, V	S, Cl, Ca, Fe, Cu, Sr, Ti, V	Irregular, subangular	Rounded edges	Green	Colored
39	3		5.79	Unknow	P, Ca	P, Ca	P, Ca	Irregular, round	Rounded edges	Clear	Transparent
40	4		7.58	Unknow	P, Ca	P, Ca	P, Ca	Irregular, round	Rounded edges	Clear	Transparent
41	5		0.5	Unknow	S, Cl, Ca, Fe, Cu, Sr, Ti, V	S, Cl, Ca, Fe, Cu, Sr, Ti, V	S, Cl, Ca, Fe, Cu, Sr, Ti, V	Irregular, angular	Rounded edges	Green	Colored
42	6		0.67	Unknow	S, Cl, Ca, Fe, Cu, Sr, Ti, V	S, Cl, Ca, Fe, Cu, Sr, Ti, V	S, Cl, Ca, Fe, Cu, Sr, Ti, V	Irregular, subangular	Rounded edges	Green	Colored



Table C.9: Station S10 (Naha 1). 24  $\mu\text{P}$  were present in samples from Manta Trawl.

Numbering	Global Site	$\mu\text{P}$ Images	Area ( $\text{mm}^2$ )	Polymer Type	XRF			Hidalgo-Ruiz2013			
					XRF2	XRF 4	XRF 6	Shape	Erosion	Color	Color Type
43	1		6.25	PP				Irregular, angular	Rounded edges, cracked surface	White	White
44	2		1.72	PP				Rounded	Rounded edges, cracked surface	White	White
45	3		11.88	PE				Irregular, angular	Sharp edges, discoloration	Yellow with white edges	Colored
46	4		5.64	PP	Zn, Ca, Cu	Cu, Ca		Rectangular	Rounded edges, cracked surface	White	White
47	5		3.06	PP				Rounded	Rounded edges, cracked surface	White	White
48	6		2.02	PP				Rounded	Rounded edges, cracked surface	White	White
49	7		0.32	PP				Irregular, subangular	Rounded edges	Blue	Colored
50	8		0.55	PP				Irregular, subangular	Rounded edges	Blue	Colored





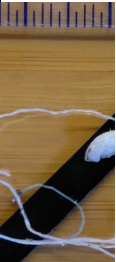


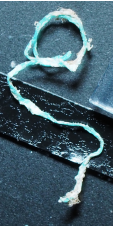
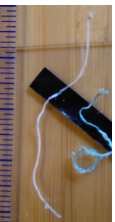

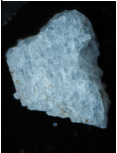

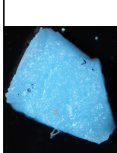



60	18								PE						Filament	Broken edges	White	White
61	19						16.53		PE						Irregular, subangular	Rounded edges, crystalline breakings	Opaque	White
62	20								PE						Filament	Broken edges	Blue	Colored
63	21								PE						Filament	Broken edges	White	White
64	22								PE						Filament	Broken edges	White	White
65	23								PE						Filament	Broken edges, discoloration	Clear	Transparent
66	24								PE						Filament	Broken edges	Blue	Colored

Table C.10: Station S11 (Naha 2). 7  $\mu$ P were present in samples from Manta Trawl.

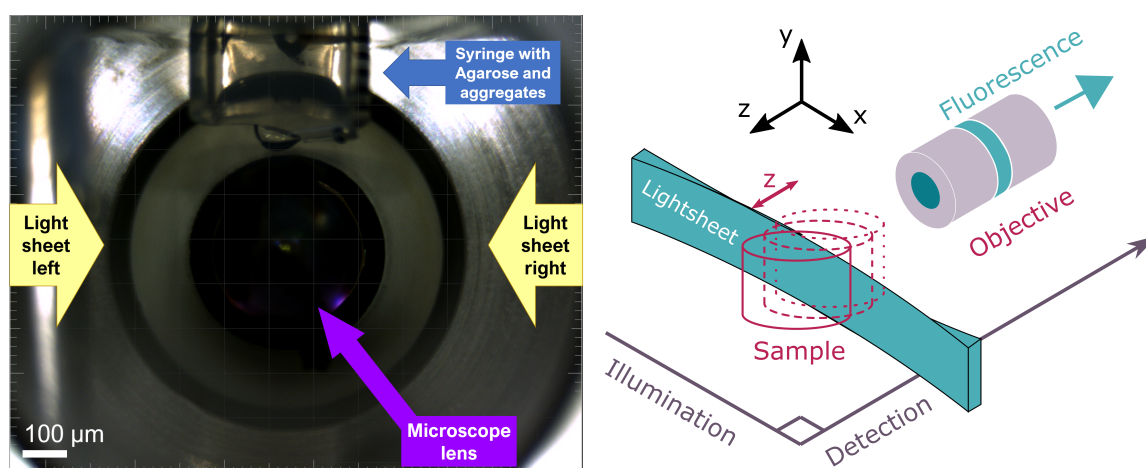
Numbering Global	Site	$\mu$ P Images	XRF				Hidalgo-Ruz2013				
			Area (mm <sup>2</sup> )	Polymer Type	XRF2	XRF 4	XRF 6	Shape	Erosion	Color	Color Type
67	1		0.85	PE	As, Cu, Hg, Pb, Si, S, Ti, Zn	Si, S, Ti	Si, S, Ti	Irregular, angular	Rounded edges, but sharp, breaks outside of the plane	White	White
68	2		1.47	PP				Irregular, angular	Breaks in parallel to the outer surfaces	Green	Colored
69	3		1.39	PE	As, Ca, Cr, Cu, Hg, Pb, Si, Ti, Zn	Ti	Ti	Irregular, subangular	Rounded edges, deep ridges, surface more weathered than ridges	Yellow	Colored
70	4		3.57	PE	As, Cu, Hg, Pb, S, Ti, Zn	S, Ti	S, Ti	Irregular, angular	straight breaks, surface weathered differently, bumpy	Blue	Colored
71	5		1.19	PE	As, Ca, Cu, Hg, Pb, Si, S, Ti, Zn	Ca, Si, S, Ti	Ca, Si, S, Ti	Irregular, angular	Rounded edges	White	White
72	6		5.2	PE				Irregular, angular	Long flat breaks, rounded edges	White	White
73	7		100.02	PE				Irregular, angular	Weathered and overgrown	Purple	Colored

## Appendix D

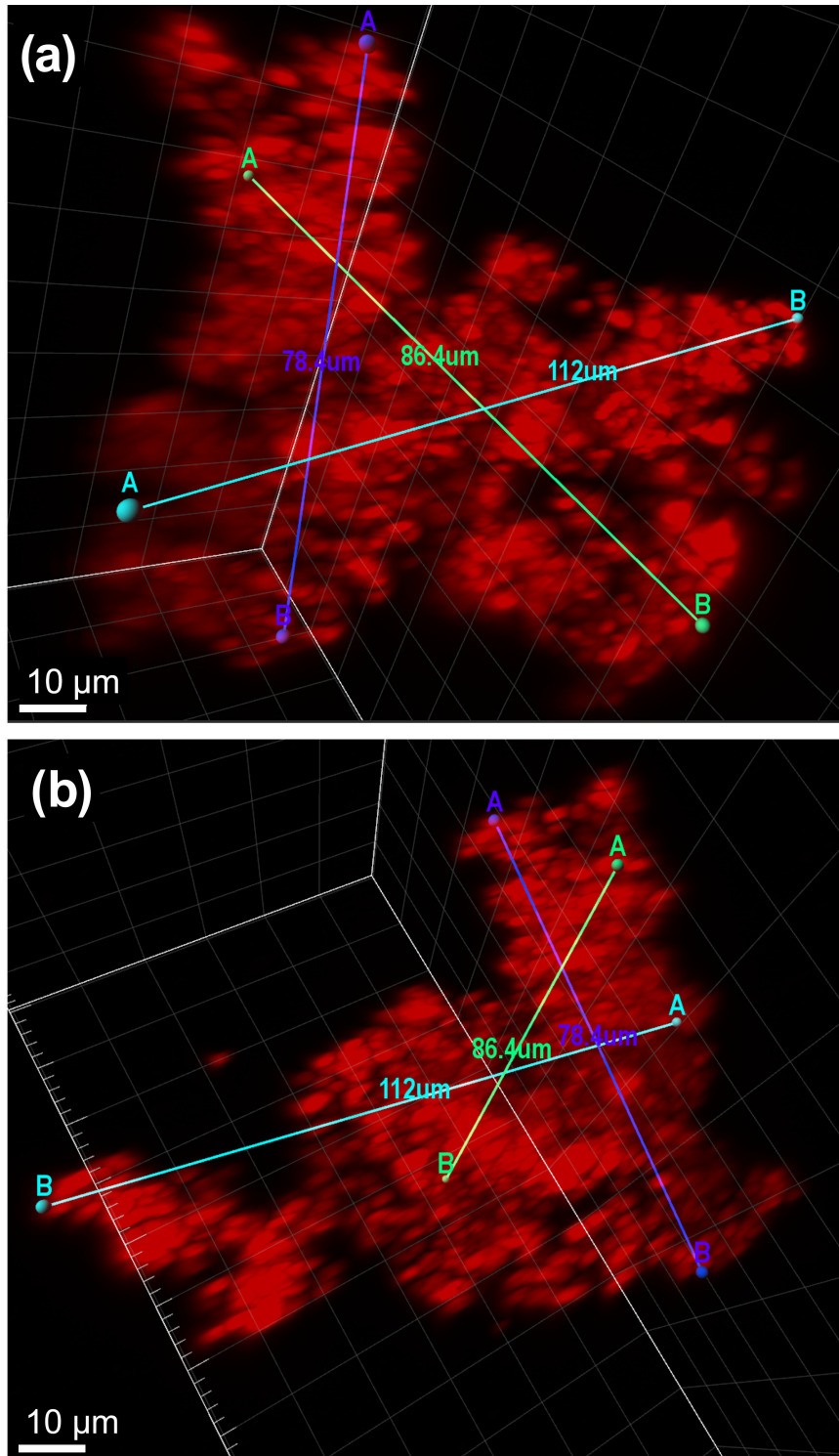
### 3D images for species in Chapter 2

In order to check the distribution of plastic in the aggregates and to get some insight into the cell packaging differences at different concentrations, 3D images were obtained using Zeiss Lightsheet Z.1 (Figure D.1). The lens movement in the  $z$ -direction artificially stretches the cells in this direction. This artifact is reduced by replacing the cells in the aggregates with spots of similar size which reveals the space between the cells. In these laser images, the plastic is green and the cells are red. Transparent extracellular polymers (TEP) are neither visible in the brightfield nor 3D images but can show up due to the trapped particles.

The fluorescent polystyrene beads were observed with band-pass filter (excitation: 405 nm; emission: 505-545 nm), and chloroplasts were visible using a long-pass red filter (excitation: 488 nm, emission: 660 nm). Z-stacks were analyzed using Imaris software (see Figures D.2 and D.3).

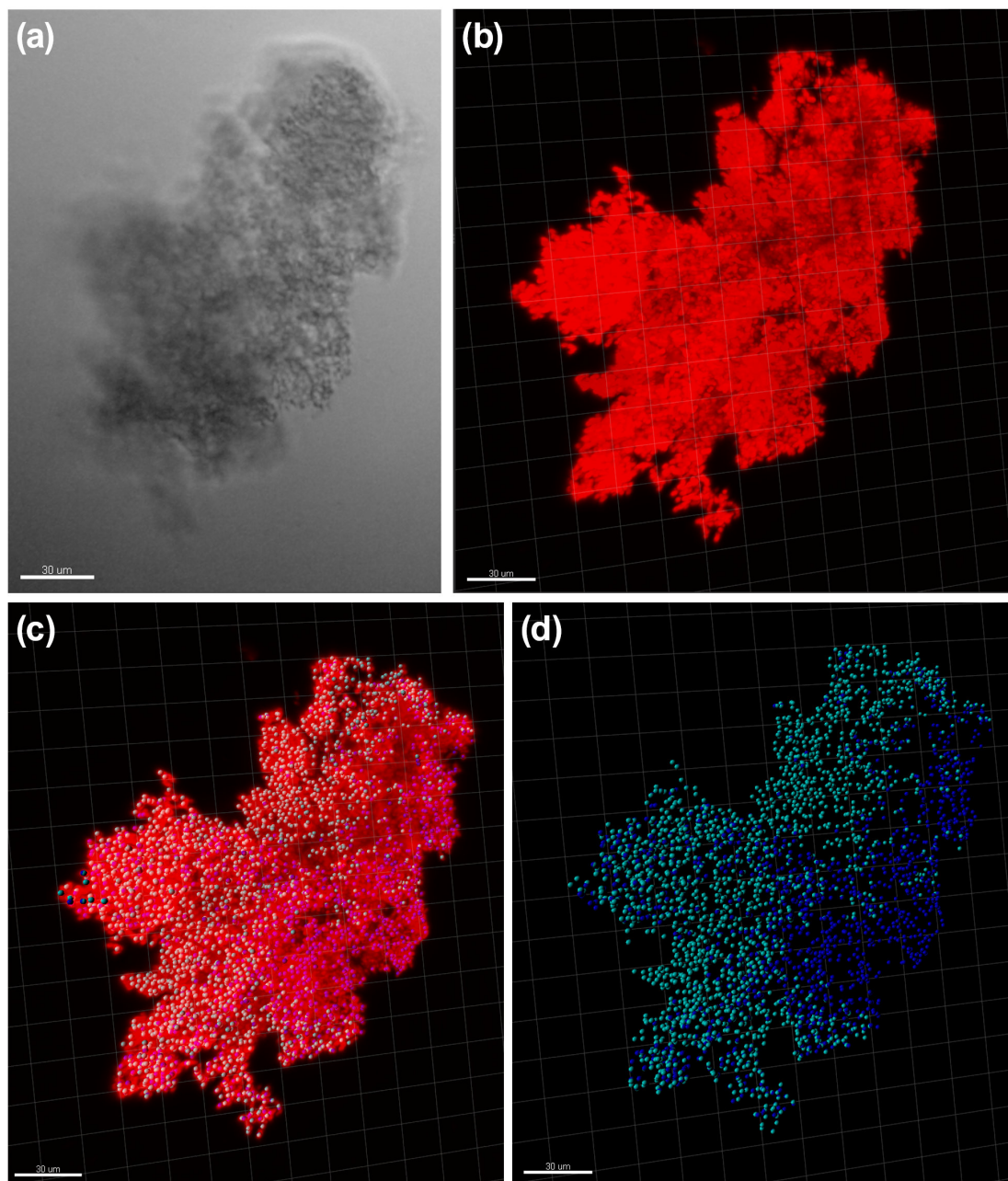


**Figure D.1: Zeiss Lightsheet Z.1 internal view and schematic of the set-up of the light sheet.** The left images shows the internal view of the lightsheet chamber, filled with seawater. The syringe with agarose is visible at the top of the picture (blue arrow) and the microscope lens at the back (purple arrow). The laser sheet direction is indicated with yellow arrows. The right image shows a set-up, indicating the  $x$ -,  $y$ - and  $z$ -directions. The movement of the lens in the  $z$ -direction introduces an artifact in the laser images which can be removed with the “spot tool” (see Figure D.4).

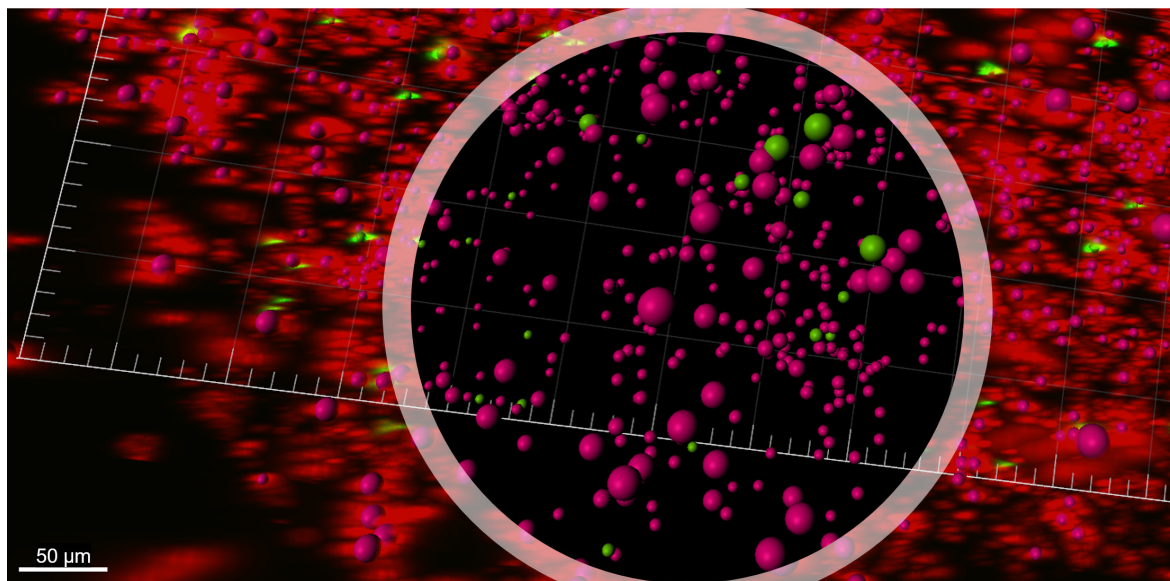


**Figure D.2: Internal structure through 3D fluorescent microscopy.** The images display a *Synechococcus elongatus* aggregate. Through 3D rotation, the measuring points for height, depth and width can be placed in the most suitable way. Aggregates were measured for size using the Imaris tools “Measurement Points”. (a) shows a frontal images of the the aggregate, while (b) has a rotation to see the back top view. Colors were chosen for maximum contrast and do not represent any additional information.

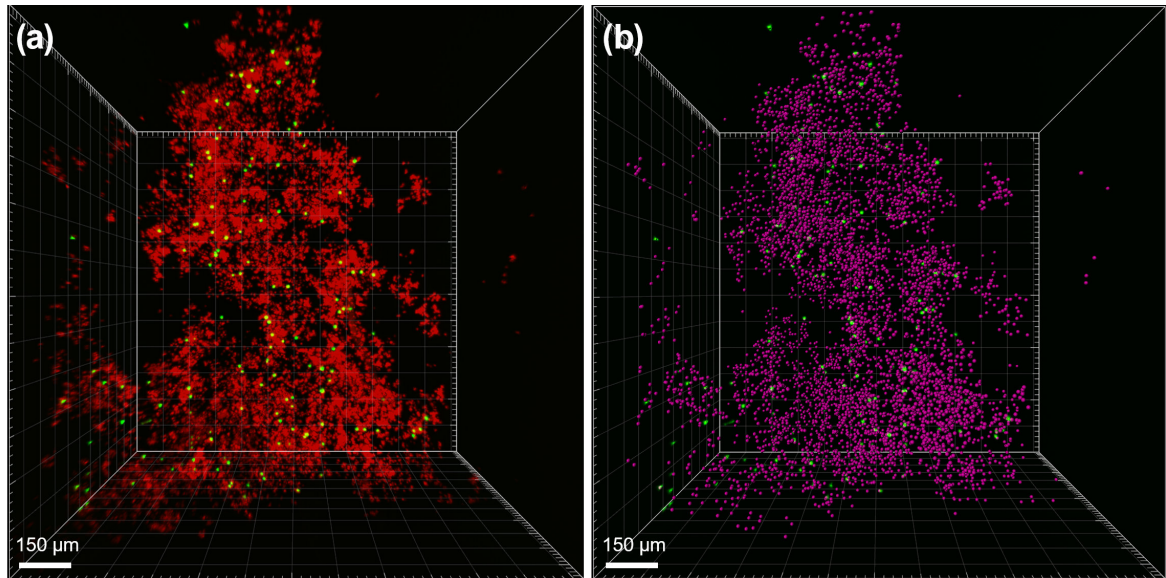




**Figure D.3: Cell counting through 3D fluorescent microscopy.** The images display a cyanobacteria *Synechococcus elongatus* aggregate with no plastic from a control tank. (a) is the optical image. The image shows that the aggregate is not dense, and as such, the laser can penetrate the entire aggregate. (b) is the 3D image with both laser channels displayed. Individual cells cannot be seen, due to the stretching of the cells in the  $z$ -direction and the consequent overlap of cells. The “spot tool” needs to be applied to every laser channel individually. (c) shows the laser channels with the “spot tool”. (d) shows the right laser in blue and the left laser in cyan, without the laser image overlay. Comparing images (c) and (d), it is interesting to see how much the overlap of the  $z$ -direction’s artificial stretching of the cells by the laser sheets blurs up the aggregate, making it appear much denser than it actually is (see Figure D.4). Colors were chosen for maximum contrast and do not represent any additional information.



**Figure D.4: Imaris spot tool.** The image displays a *Skeletonema grethae* aggregate with microPS<sub>2</sub> at a concentration of 0.01 mg/L. The outside shows how the laser lights up the cell (red) and microPS<sub>2</sub> (green). The “spot tool” displays cells in pink and the microPS<sub>2</sub> in green. The comparison between the pink spots and the red laser ellipsoids shows that this technique stretches the image of the cells in the  $z$ -direction. The spot tool allows in addition to counting cells and plastic to remove this stretching. Spot diameter can be adjusted to match the cells or plastics diameter; in this image, the microPS<sub>2</sub> is displayed with a 6 μm diameter for better visualization. The inner circle of the image shows the image without the laser created volume for better analysis of the plastics’ location within the aggregate. Not all red laser cells in this image have a complimentary spot, as spots are generated per laser and in this image only two laser channels are displayed for illustrative purposes, making the image better suited for 2D representation. Same images as shown in Section 2.2.5.

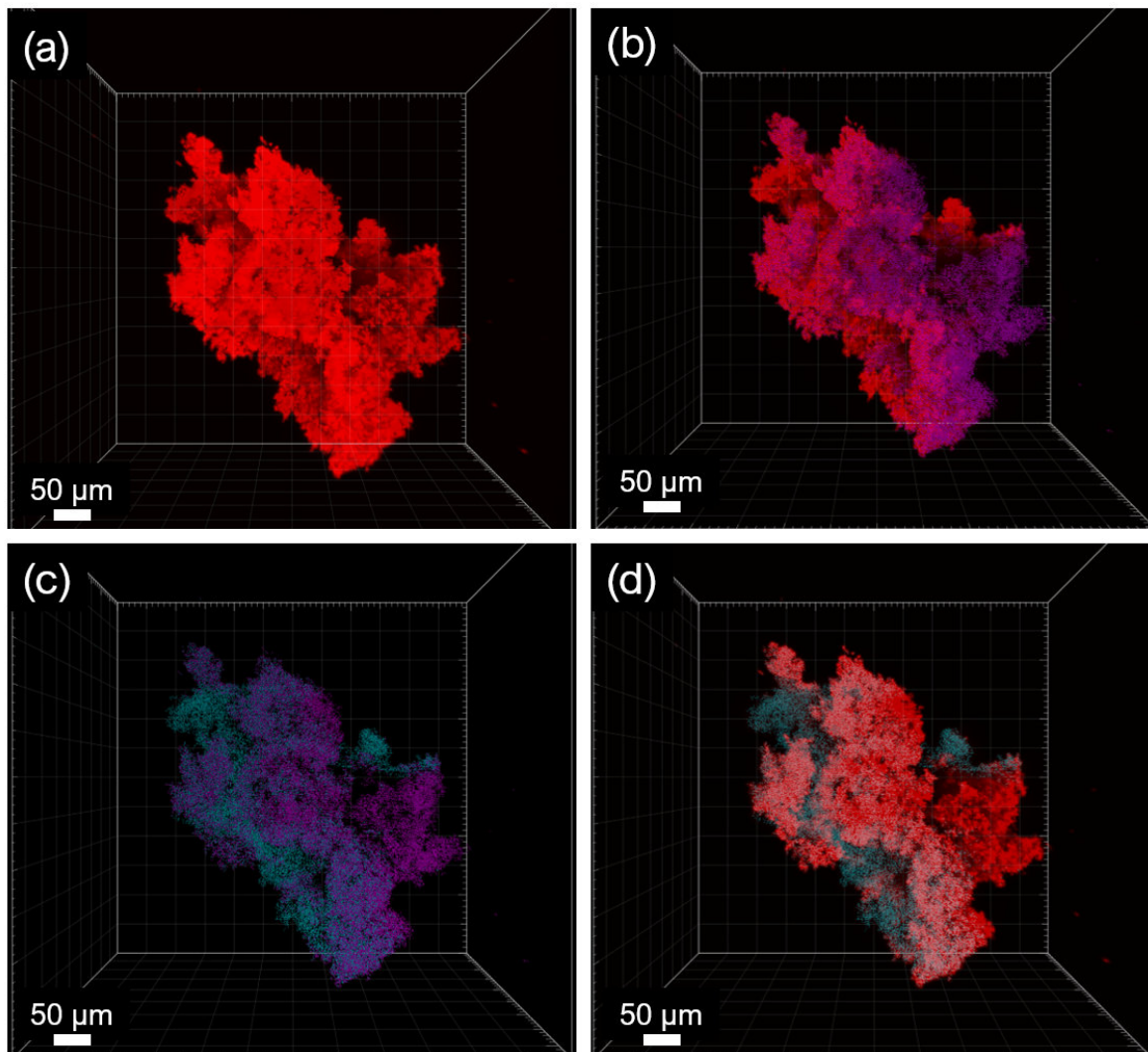


**Figure D.5: Imaris spot tool.** The images display a *Skeletonema grethae* aggregate with microPS<sub>2</sub> at a concentration of 0.01 mg/L, same as in D.3. (a) shows how the laser lights up the cell (red) and microPS<sub>2</sub> (green). The “spot tool” displays cells in pink and the microPS<sub>2</sub> in green (b). While the green microPS<sub>2</sub> in the laser image on the left appeared bigger, this is due to their high fluorescence. In the size adjusted spot image on the right, some green spots representing the microPS<sub>2</sub> are hardly visible next to the bigger *Skeletonema grethae* cells, presenting a more realistic appearance of the aggregate. Colors were chosen for maximum contrast and do not represent any additional information.

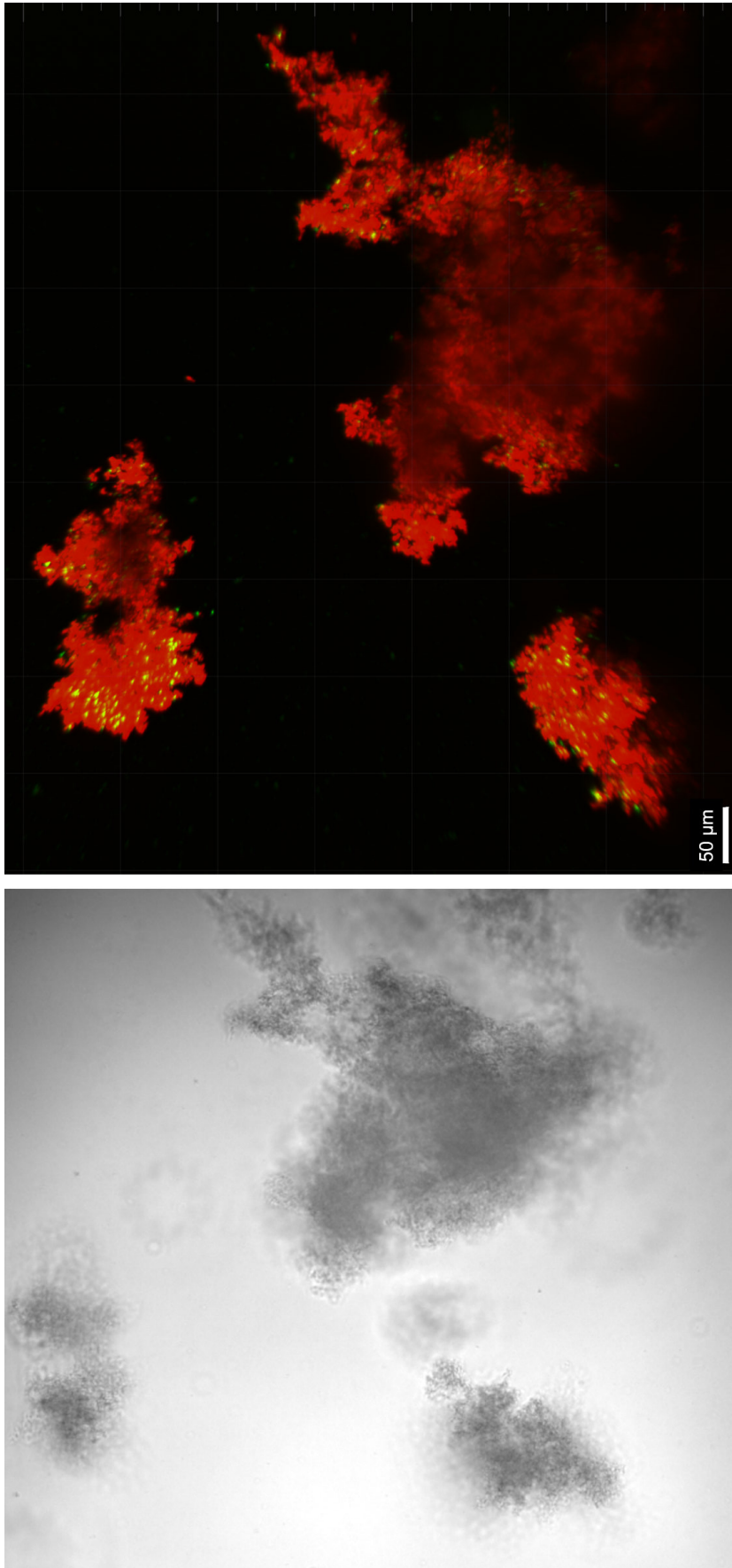
## D.1 3D images in *Synechococcus elongatus*

The *Synechococcus elongatus* cells are notably smaller ( $\sim 1 \mu\text{m}$ ) than the diatoms (see D.2 and D.3) and the dinoflagellates in Section 4.4.4. This makes aggregates look different in the 3D images. Cells were counted with  $1 \mu\text{m}$  in diameter.

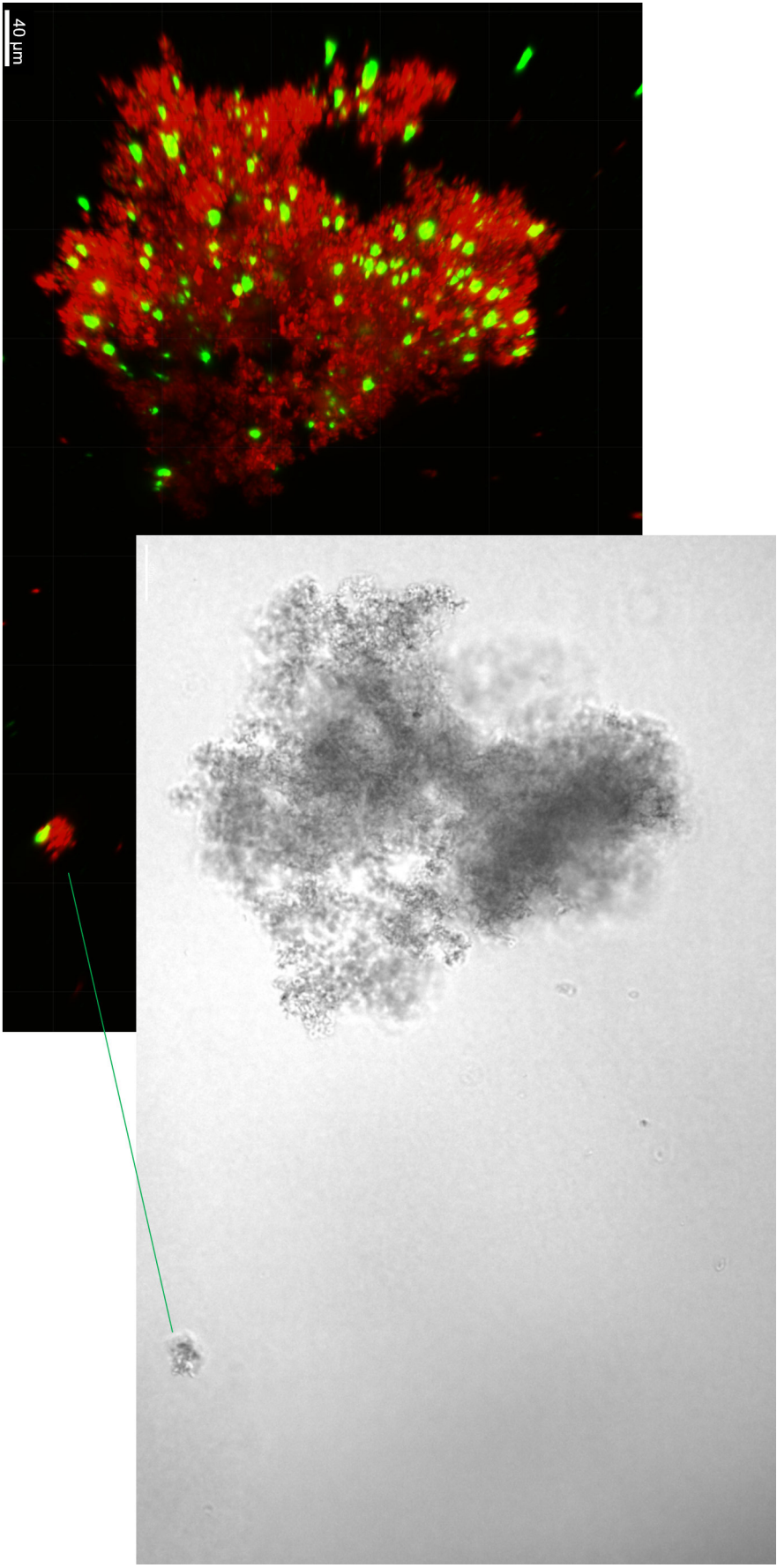


NanoPS<sub>194</sub> Experiment in *Synechococcus elongatus*

**Figure D.6: 3D images of a *Synechococcus elongatus* control aggregate in the nanoPS<sub>194</sub> experiment.** The images display a control aggregate with the following dimensions: 469  $\mu\text{m}$  height, 548  $\mu\text{m}$  width, and 316  $\mu\text{m}$  depth (total volume of  $4.25 \times 10^7 \mu\text{m}^3$ ). There are about 200,000 cells found in this dense aggregate leading to a total bio-volume of 104,720  $\mu\text{m}^3$ . This means that the bio-volume represents only 0.246% of the total aggregate volume. (a) Laser image of the control aggregate, only, the green channel does not show up as there was no nanoPS<sub>194</sub>. (b) shows the right laser being replaced by cell count (pink). (c) shows the cell counts with left and right laser counts in different colors. The space between the cells becomes visible in this image, making the difference between bio-volume and aggregate volume apparent. The space is most likely filled with water and extracellular polymeric substances (EPS). (d) shows the left laser being replaced by cell counts (cyan). While the laser image (a) shows a very dense aggregate, this is due to the  $z$ -axis stretching from the laser sheets. In the other three images ((b), (c) or (d)), where the laser has been replaced, the aggregate is not as dense.

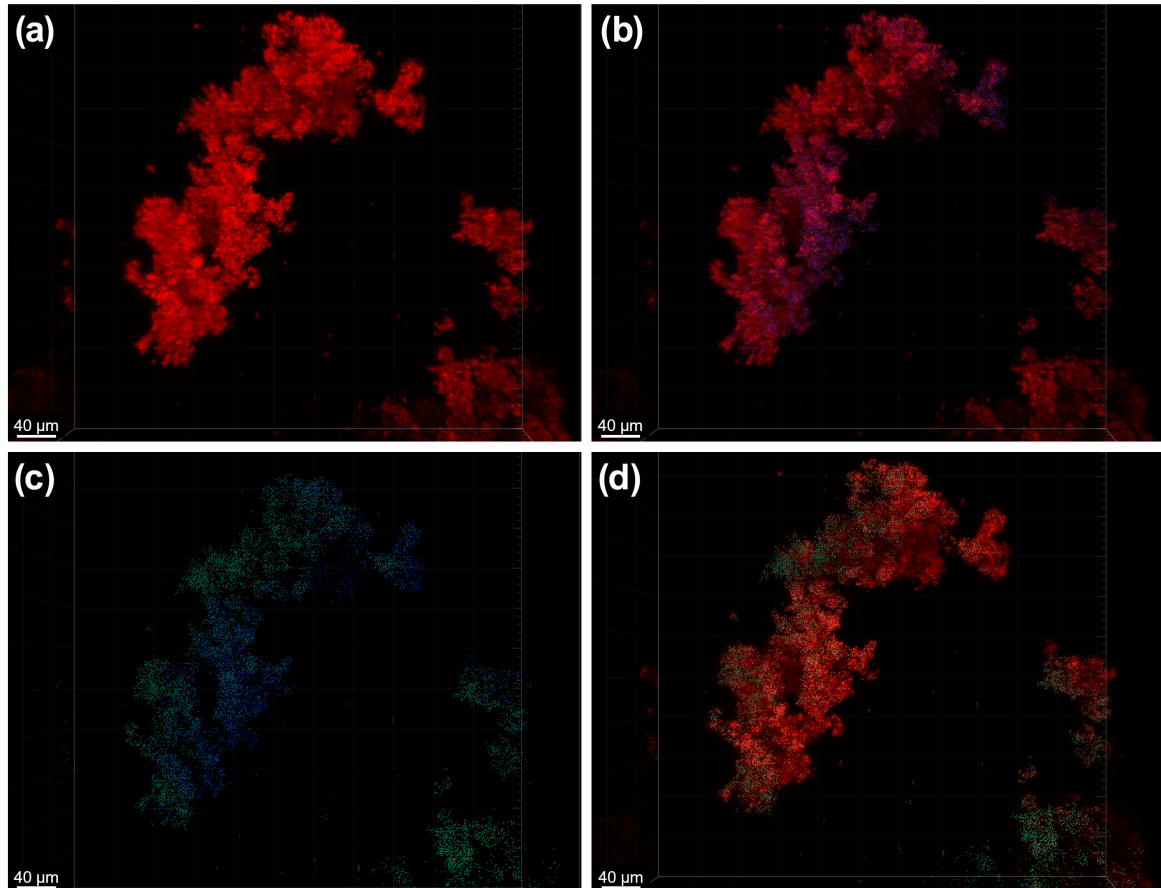


**Figure D.7: Optical and 3D images of *Synechococcus elongatus* aggregates with 0.01 mg/L nanoPS<sub>194</sub>.** The images display three separate aggregates with the top one measuring 245  $\mu\text{m}$  height, 118  $\mu\text{m}$  width and 219  $\mu\text{m}$  depth. The smaller lower one was 99  $\mu\text{m}$  height, 122  $\mu\text{m}$  width and 215  $\mu\text{m}$  depth and the large lower one was 235  $\mu\text{m}$  height, 451  $\mu\text{m}$  width and 415  $\mu\text{m}$  depth. The total volume of all the aggregates is  $2.77 \times 10^7 \mu\text{m}^3$ . There are about 68,000 cells found in these aggregates combined leading to a total bio-volume of 35,605  $\mu\text{m}^3$ . This means that the bio-volume represents only 0.129% of the total aggregate volume. The green spots show the nanoPS<sub>194</sub> and while individual beads can not be seen, agglomerates of beads are visible.

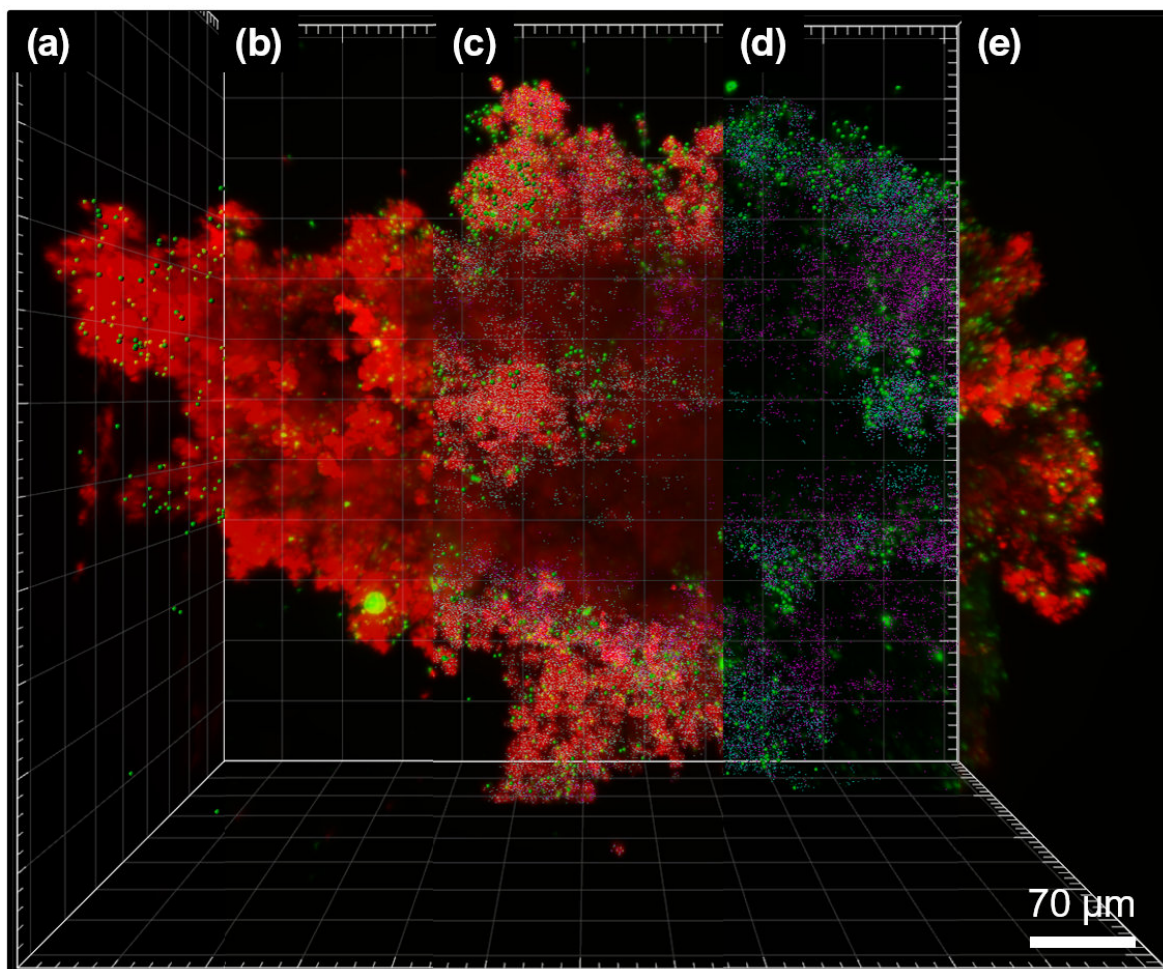


**Figure D.8:** Optical and 3D images of *Synechococcus elongatus* aggregate with 1 mg/L nanoPS<sub>194</sub>. The images display an aggregate with the following dimensions: 374 μm height, 321 μm width and 297 μm depth (total volume  $1.87 \times 10^7 \mu\text{m}^3$ ). There are about 64,000 cells found in this aggregate leading to a total bio-volume of 33, 510 μm<sup>3</sup>. This means that the bio-volume represents only 0.18% of the total aggregate volume.. The green spots show the nanoPS<sub>194</sub> and while individual beads can not be seen, agglomerates of beads are visible. In comparison to Figure D.7 of the lower plastic treatment many more such agglomerates are visible.



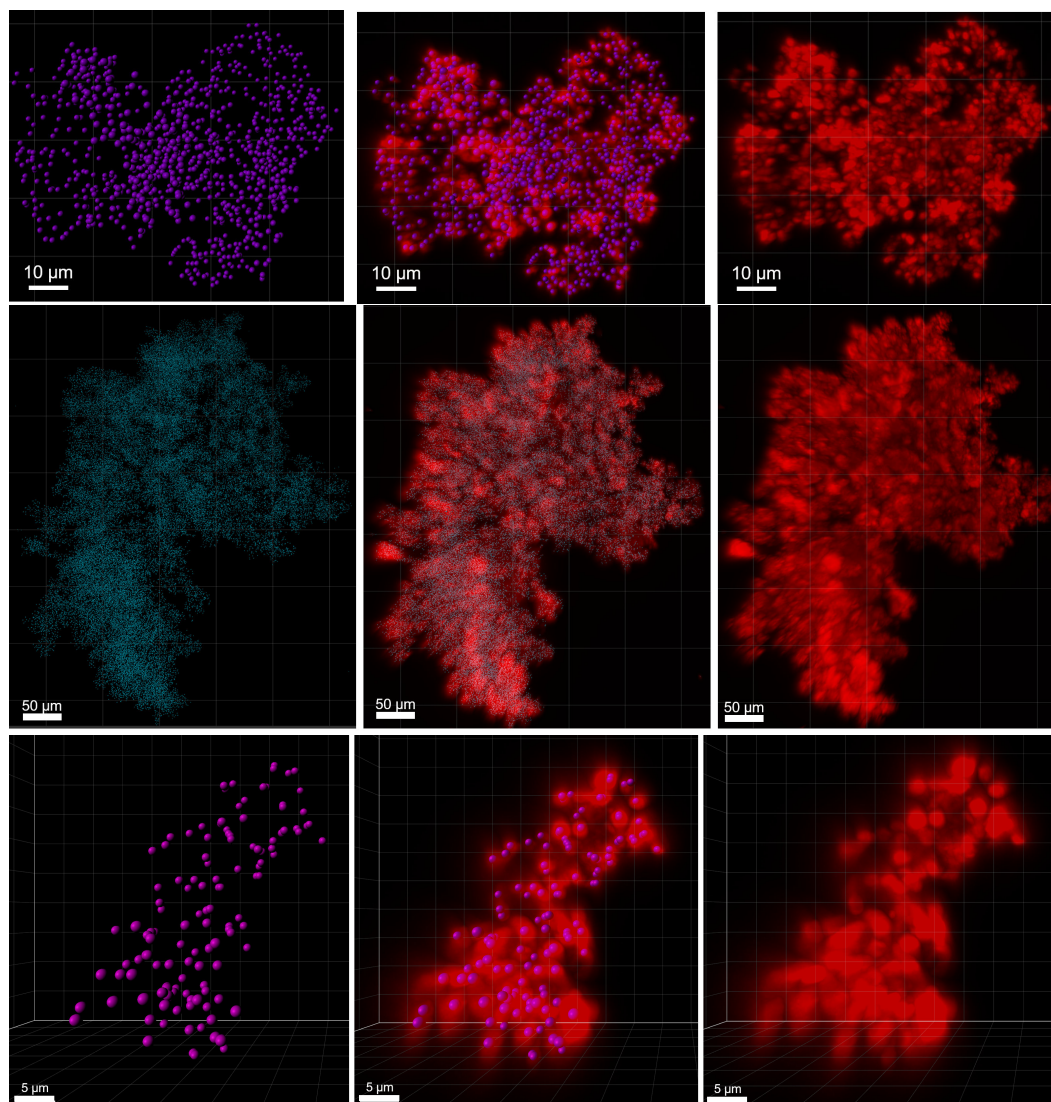
NanoPS<sub>42</sub> Experiment in *Synechococcus elongatus*

**Figure D.9:** 3D images of a control aggregate in the nanoPS<sub>42</sub> experiments with *Synechococcus elongatus*. The images display an aggregate with 407  $\mu\text{m}$  height, 219  $\mu\text{m}$  width and 177  $\mu\text{m}$  depth with a total volume of  $8.26 \times 10^6 \mu\text{m}^3$ . There are about 17,000 cells found in this aggregate leading to a total bio-volume of  $8901 \mu\text{m}^3$ . This means that the bio-volume represents only 0.108% of the total aggregate volume. (a) displays the aggregate in the laser image, (b) shows the right laser substituted by cell counts, (c) is the combination of the cell counts without the laser image overlay and (d) shows the left laser substituted by cell count. In the comparison of (a) and (c) the water and EPS filled space between the cells is becomes apparent, as (c) shows the much less dense aggregate without the z direction overlap of the cells..



**Figure D.10: 3D image collage for the nanoPS<sub>42</sub> experiment in *Synechococcus elongatus* for the 1 mg/L treatment.** The image displays an aggregate with 523  $\mu\text{m}$  height, 608  $\mu\text{m}$  width and 422  $\mu\text{m}$  depth (total volume  $7 \times 10^7 \mu\text{m}^3$ ). There are about 80,000 cells found in this aggregate leading to a total bio-volume of 41,888  $\mu\text{m}^3$ . This means that the bio-volume represents only 0.596% of the total aggregate volume. The plastic could not be counted due to its small size, but there are 1330 agglomerates of plastic in sizes between 0.4  $\mu\text{m}$  and 19.2  $\mu\text{m}$ . (a) displays the laser channel of the cells with the plastic as agglomerates replaced by green spots. (b) is just the laser, making the individual agglomerates much less visible, while (c) has the laser with all overlay of spot counts for cells in purple and plastics in green. In (d) the laser is removed and the gaps between the cells becomes visible. (e) has the laser with an overlay of the plastic in green. When (e) is compared to (a) and (b), it is much easier to see how the plastic is located within the aggregate: in (a), the plastic laser channel was more removed than in the other two sections. Comparing (d) and (e) directly, the blur in the laser due to the  $z$  stacking becomes apparent.

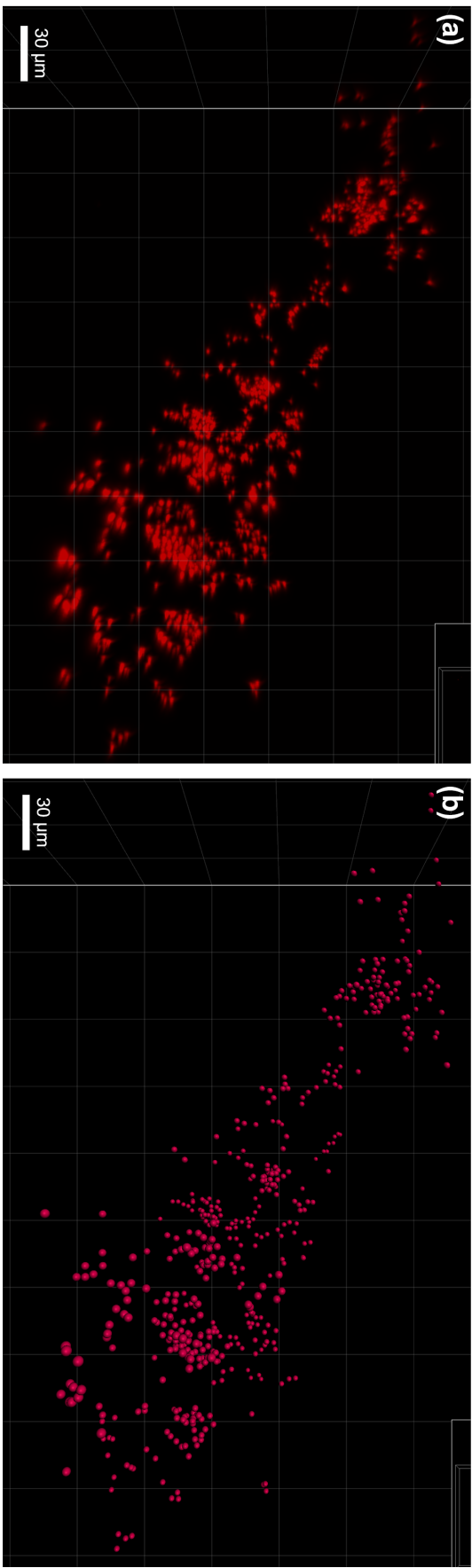
Acrylic Microfiber Experiment in *Synechococcus elongatus*



**Figure D.11: 3D images for the dust aggregates in aMF experiments of *Synechococcus elongatus*.** The top row: 1 mg/L aMF aggregate ( $72.4 \times 86.4 \times 112 \mu\text{m}$ , total volume  $366,833 \mu\text{m}^3$ ). There are  $\sim 1025$  cells found in this aggregate leading to a total bio-volume of  $536.69 \mu\text{m}^3$ . This means that the bio-volume represents only 0.146% of the total aggregate volume. The middle row: 0.1 mg/L aMF aggregate ( $629 \times 427 \times 349 \mu\text{m}$ , total volume  $4.91 \times 10^7 \mu\text{m}^3$ ), with  $\sim 58,700$  cells found in this aggregate leading to a total bio-volume of  $30,735 \mu\text{m}^3$ . This means that the bio-volume represents only 0.626% of the total aggregate volume. The bottom row: control aggregate ( $38.0 \times 19.7 \times 31.7 \mu\text{m}$ , total volume  $12,425 \mu\text{m}^3$ ). There are  $\sim 126$  cells found in this aggregate leading to a total bio-volume of  $66 \mu\text{m}^3$ . This means that the bio-volume represents only 0.531% of the total aggregate volume. Fibers were not integrated into these aggregates. The dust aggregates from the control and 1 mg/L treatment were smaller than those found in the 0.1 mg/L treatment. This might have been due to the significantly more TEP found in the 0.1 mg/L treatment (see Figure 2.35). The left column shows just the spot cells and the right column displays just the laser image. The middle column is an overlay of both images. This comparison shows big EPS filled space becoming apparent within the aggregate, especially visible in the bottom row. Colors were chosen for maximum contrast and do not represent any additional information.

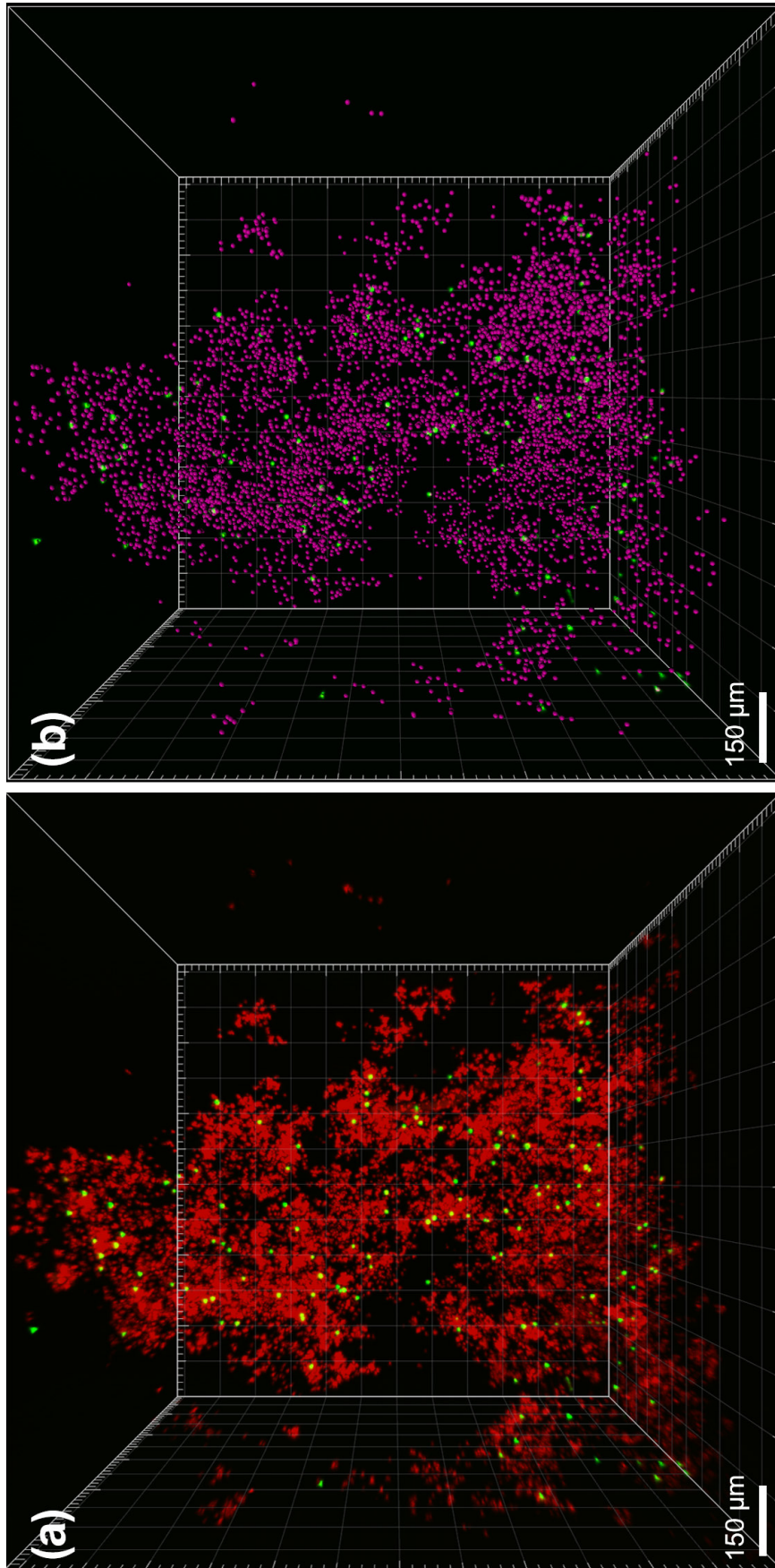
## D.2 3D images of *Skeletonema grethae*

MicroPS<sub>2</sub> Experiment in *Skeletonema grethae*

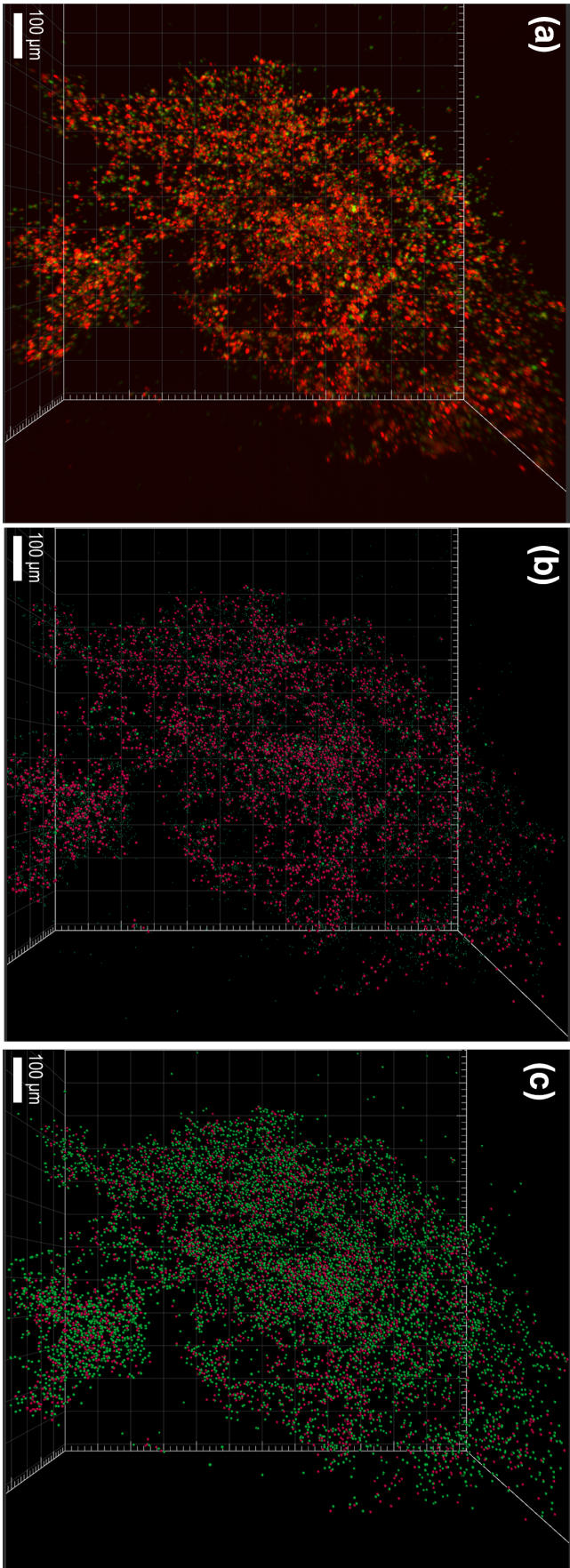


**Figure D.12: 3D images of microPS<sub>2</sub> aggregate in *Skeltonemna grethae* in the control.** The image displays an aggregate with 174 μm height, 417 μm width, and 257 μm depth (total volume of  $9.76 \times 10^6 \mu\text{m}^3$ ). There are about 513 cells found in this aggregate leading to a total bio-volume of 58, 019 μm<sup>3</sup>. This means that the bio-volume represents 0.594% of the total aggregate volume. (a) displays the laser channel of the cells with the plastic. In (b) cells have been substituted with magenta spots. Big gaps between the cells are visible in both images,





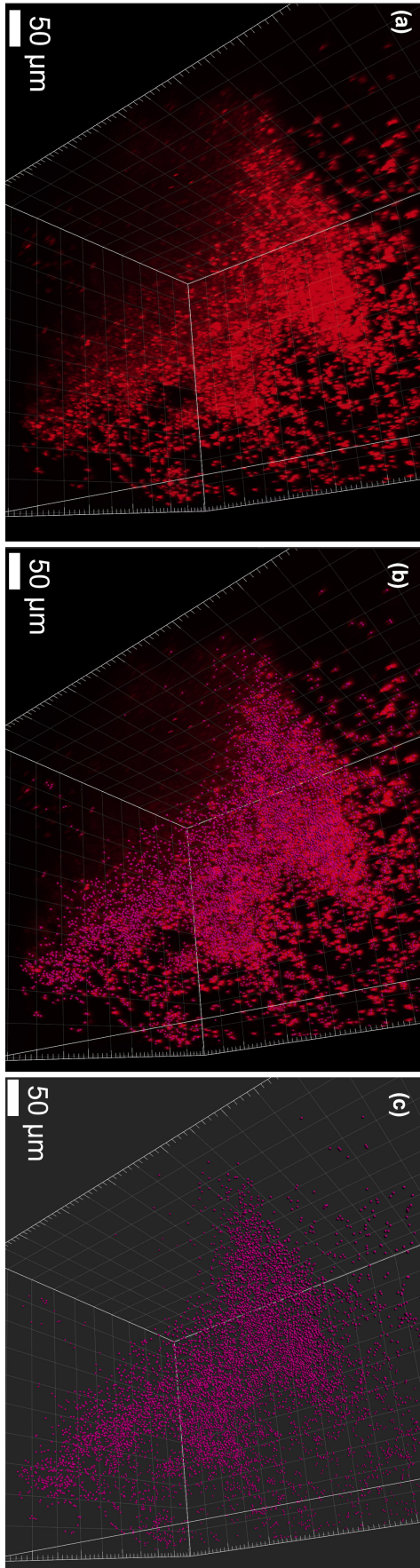
**Figure D.13: 3D images of microPS<sub>2</sub> aggregate in *Skeletonema grethae* at 0.01 mg/L treatment.** The image displays an aggregate with 1221 µm height, 915 µm width, and 1000 µm depth (total volume of  $5.85 \times 10^8 \mu\text{m}^3$ ). There are about 5538 cells found in this aggregate leading to a total bio-volume of  $626,333 \mu\text{m}^3$ . This means that the bio-volume represents 0.107% of the total aggregate volume. There are 120 microPS<sub>2</sub>. (a) displays the laser channel of the cells with the plastic. In (b) cells (magenta) and plastic (green) have been substituted with spots of equivalent diameter.



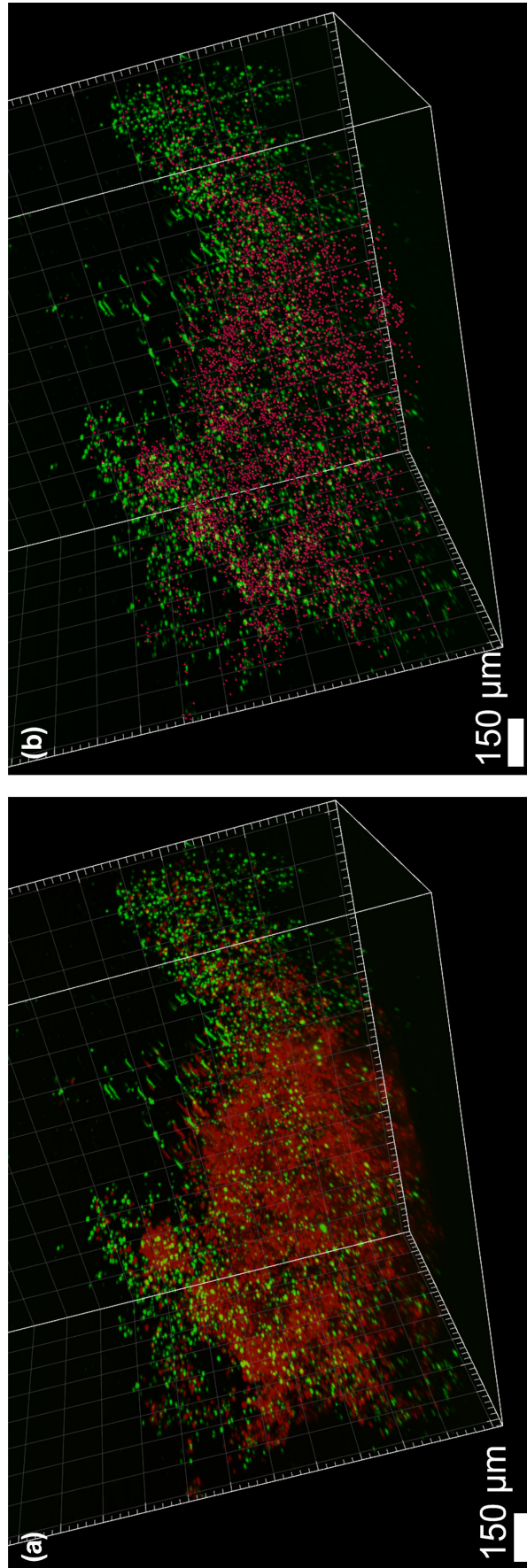
**Figure D.14: 3D images of microPS<sub>2</sub> aggregate in *Skeltonema grethae* in 10 mg/L treatment.** The image displays an aggregate with 1242 μm height, 1023 μm width and 1037 μm depth (total volume of  $6.9 \times 10^8 \mu\text{m}^3$ ). There are about 7469 cells found in this aggregate leading to a total bio-volume of  $844,724 \mu\text{m}^3$ . This means that the bio-volume represents 0.122% of the total aggregate volume. There are 18,500 microPS<sub>2</sub> beads in the aggregate, with 192 bigger agglomerates at 6 μm diameter, where the microPS<sub>2</sub> stuck together. (a) displays the laser channel of the cells with the plastic. In (b) cells have been substituted for magenta spheres and only the bigger agglomerates of microPS<sub>2</sub> are shown in green. (c) shows the single microPS<sub>2</sub> added back in. Comparing (b) and (c) it can be seen that the 18,500 single microPS<sub>2</sub> beads drown out the magenta cell spots at a 1 to 2.5 ratio.

NanoPS<sub>194</sub> Experiment in *Skeletonema grethae*

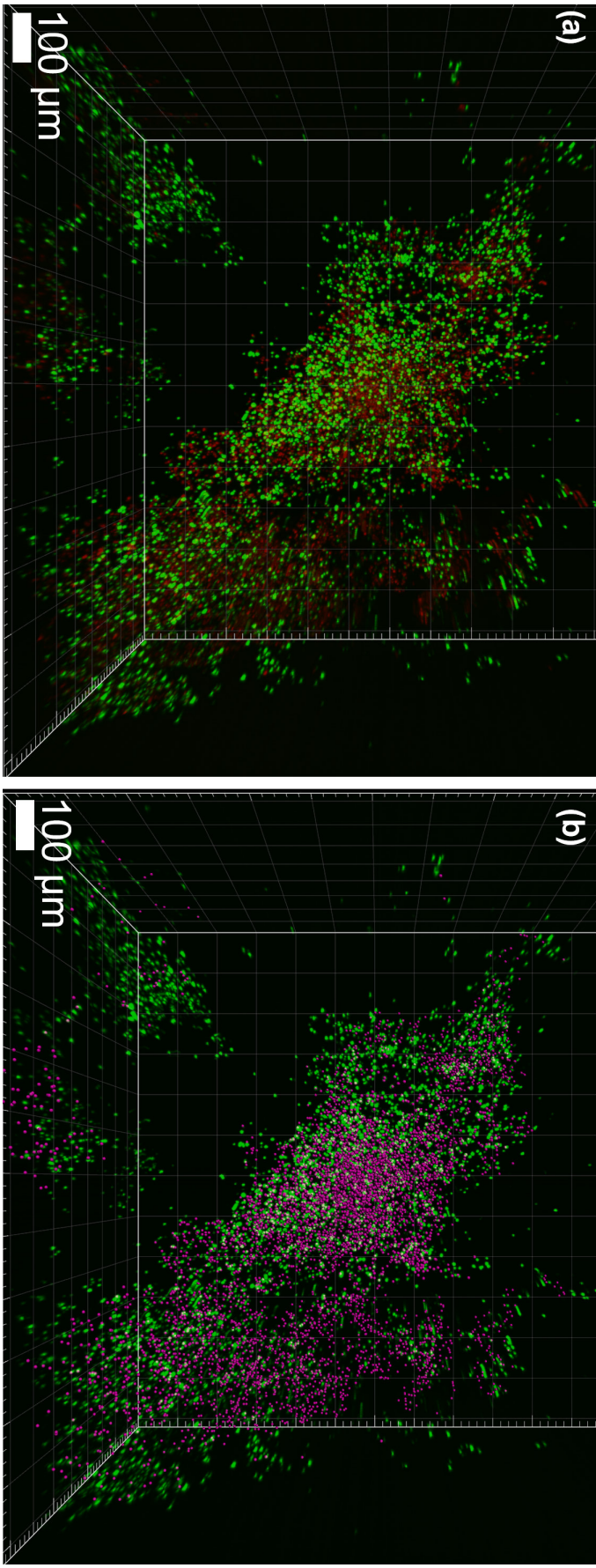




**Figure D.15: 3D images of nanoPS<sub>194</sub> aggregate in *Skeltonema grethae* control.** The image displays an aggregate with 173 µm height, 529 µm width and 463 µm depth (total volume of  $2.22 \times 10^7 \mu\text{m}^3$ ). There are about 10,400 cells found in this aggregate leading to a total bio-volume of  $1.18 \times 10^6 \mu\text{m}^3$ . This means that the bio-volume represents 5.3% of the total aggregate volume. (a) shows the laser channel, (b) the laser channel overlay with magenta cell spots and (c) just the cell spots. In comparing the images, the dense core of the aggregate is easier seen in (c), while in the laser image the individual cells at the sides of the aggregate distract from that.

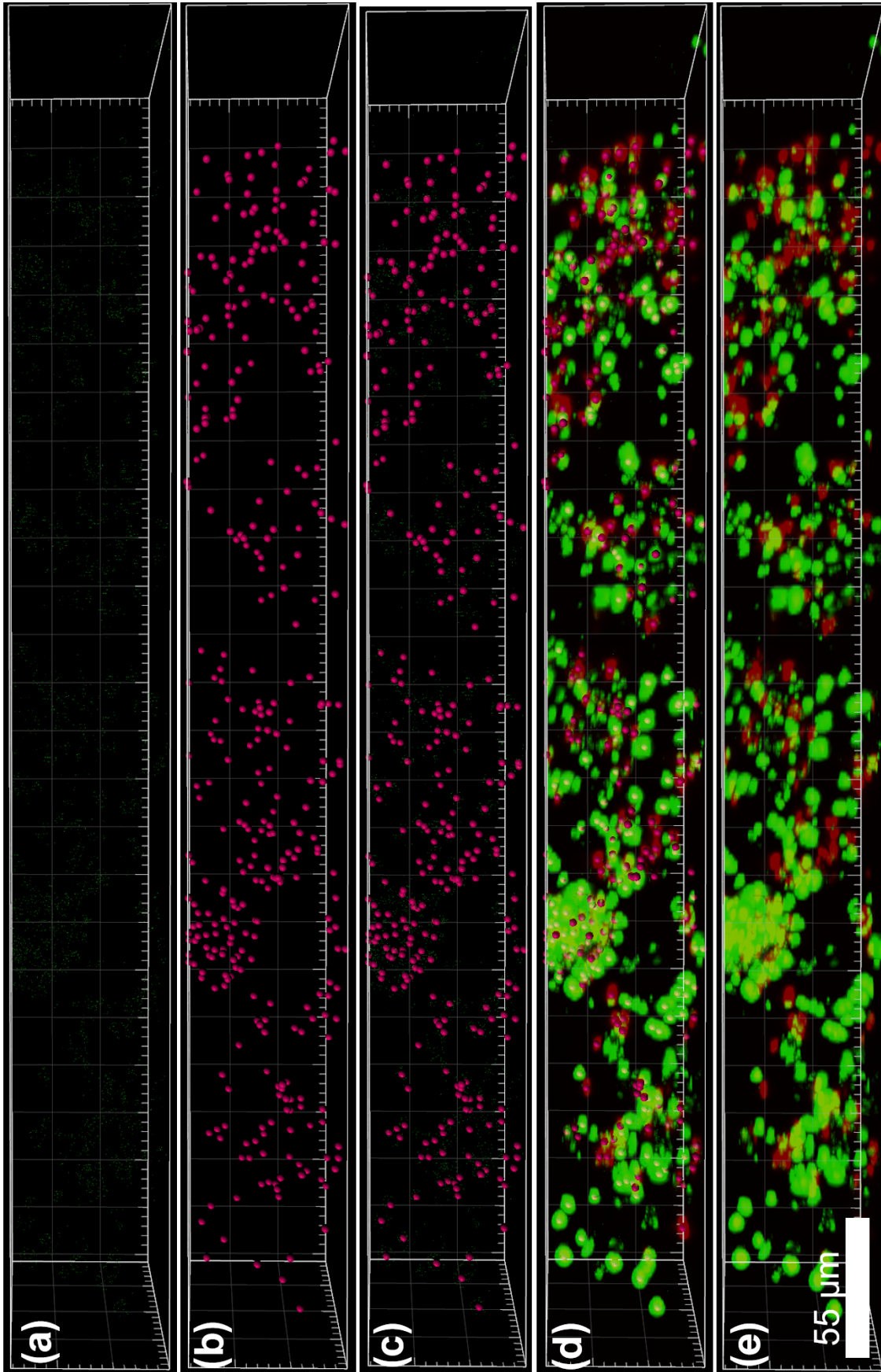


**Figure D.16: 3D images of nanoPS<sub>194</sub> aggregate in *Skeletonema grethae* in the 0.01 mg/L treatment.** The image displays an aggregate with 1218 μm height, 621 μm width and 868 μm depth (total volume of  $3.44 \times 10^8 \mu\text{m}^3$ ). There are about 6885 cells found in this aggregate leading to a total bio-volume of 778, 675 μm<sup>3</sup>. This means that the bio-volume represents 0.227% of the total aggregate volume. (a) displays the laser image while in (b) cells have been substituted for magenta spots. The nanoPS<sub>194</sub> could not be counted due to the *z*-stretch visible at the back of both images (long green strips).

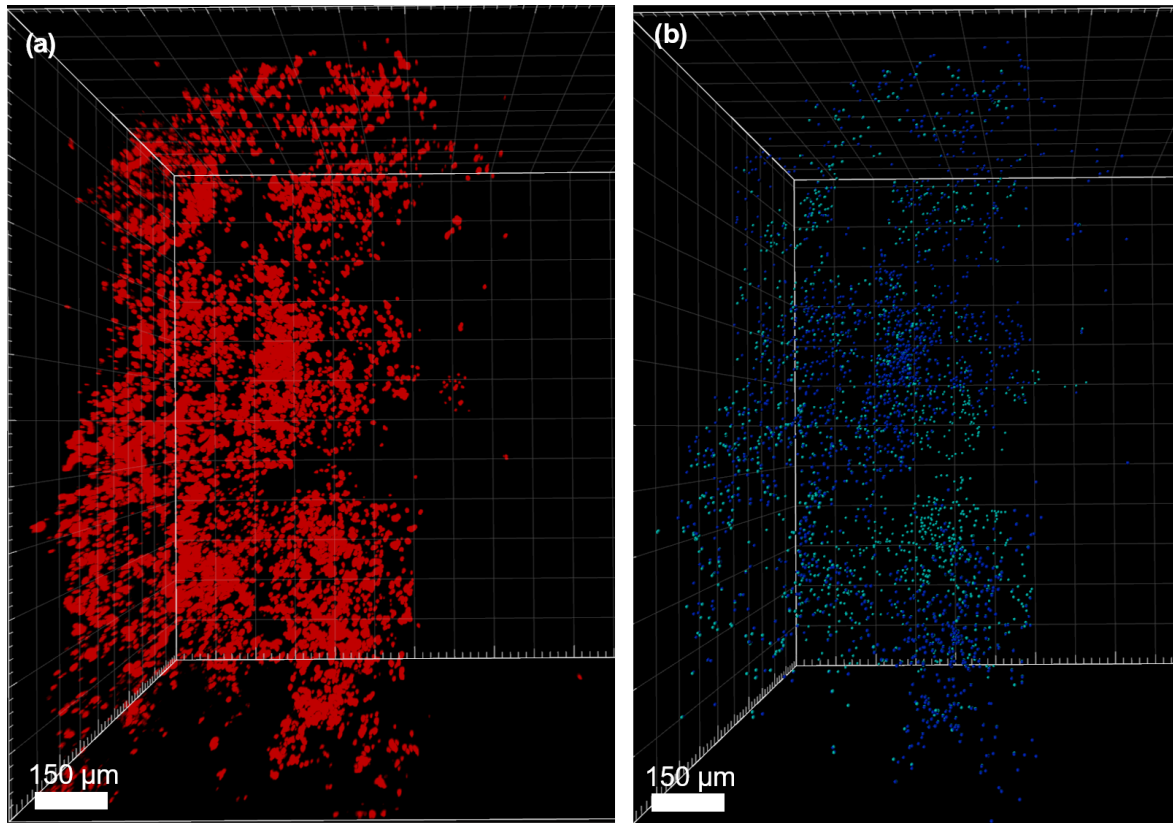


**Figure D.17: 3D images of nanoPS<sub>194</sub> aggregate in *Skeltonema grethae* in the 1 mg/L treatment.** The image displays an aggregate with 1424 μm height, 820 μm width and 1045 μm depth (total volume  $6.39 \times 10^8 \mu\text{m}^3$ ). There are about 6006 cells found in this aggregate leading to a total bio-volume of 679, 263 μm<sup>3</sup>. This means that the bio-volume represents 0.106% of the total aggregate volume. (a) shows the laser image and in (b) the cells are replaced by magenta spots. The core of the aggregate can be better seen in (b), as the magenta spots give a better contrast to the overwhelming green nanoPS<sub>194</sub> beads.

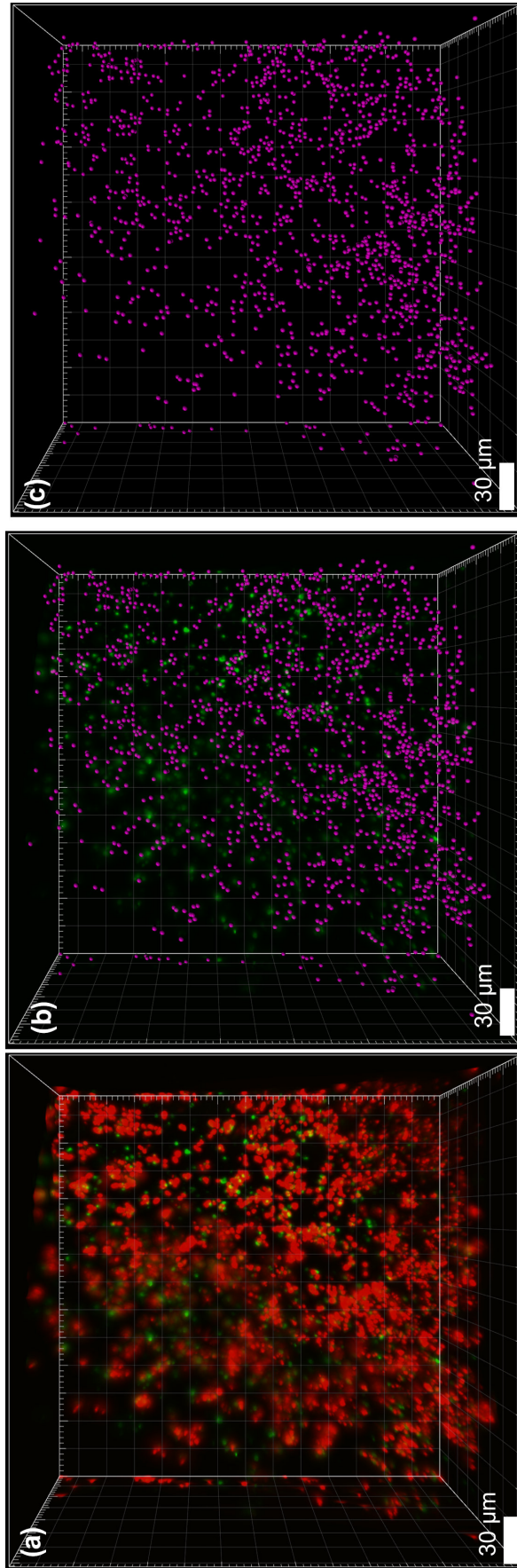




**Figure D.18:** 3D images of cross section through a nanoPS<sub>194</sub> aggregate in the 10 mg/L treatment. The aggregate has a depth of 481 µm, and the section (54.5 × 77.2 µm) has a volume of 1.06 × 10<sup>6</sup> µm<sup>3</sup>. There are about 356 cells found in this section, leading to a total bio-volume of 40, 263 µm<sup>3</sup>. This means that the bio-volume represents 3.8% of the total aggregate volume of the section. The different images display: (a) just plastic agglomerates of nanoPS<sub>194</sub>, (b) just spots replacing cells, (c) plastic and cell replacements, (d) laser image overlay with spots of cells and plastic, (e) laser image.

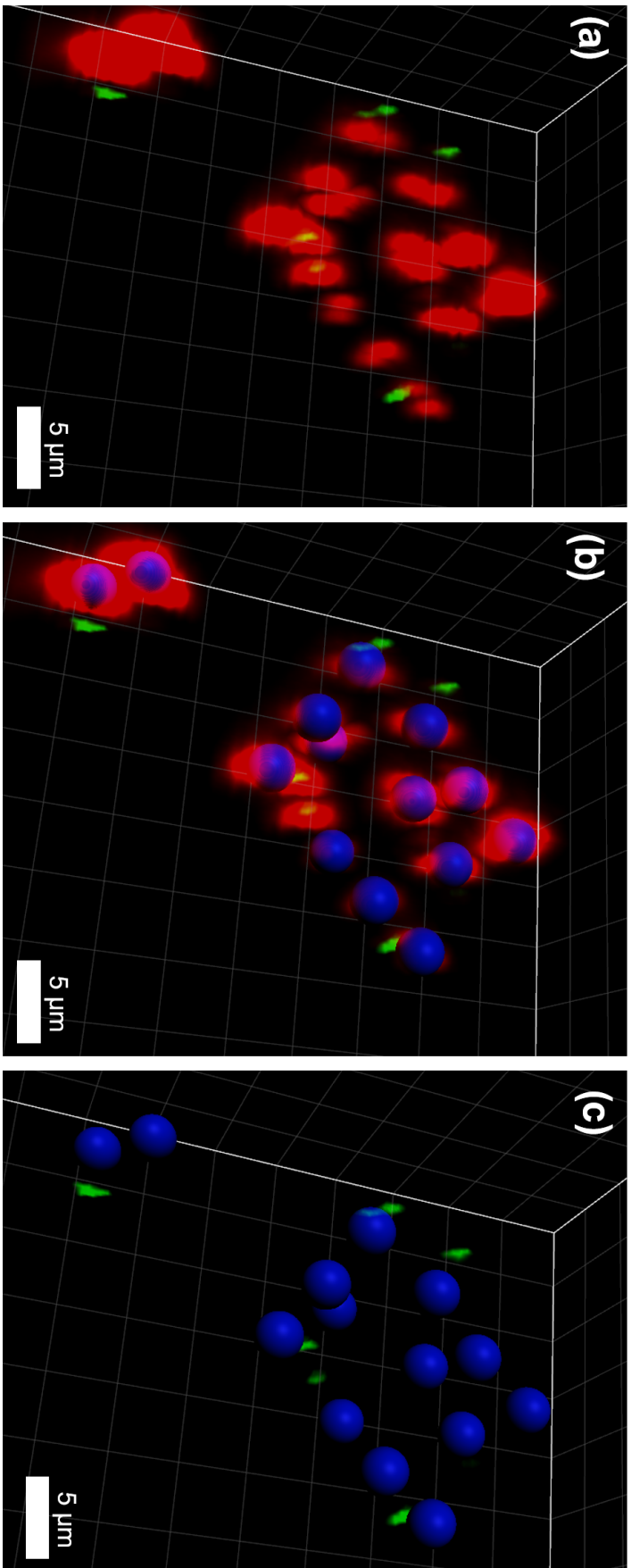
nanoPS<sub>42</sub> Experiment in *Skeletonema grethae*

**Figure D.19: 3D images of nanoPS<sub>42</sub> aggregate in *Skeletonema grethae* control.** The image displays an aggregate with 1232 μm height, 805 μm width and 753 μm depth (total volume  $3.91 \times 10^8 \mu\text{m}^3$ ). There are about 4540 cells found in this aggregate leading to a total bio-volume of 513,462 μm<sup>3</sup>. This means that the bio-volume represents 0.131% of the total aggregate volume. (a) is the original laser image, with overlapping *z*-stretch leading to a visually dense aggregate. (b) in blue and cyan cells are replaced. This make the EPS filled space between the cells visible.

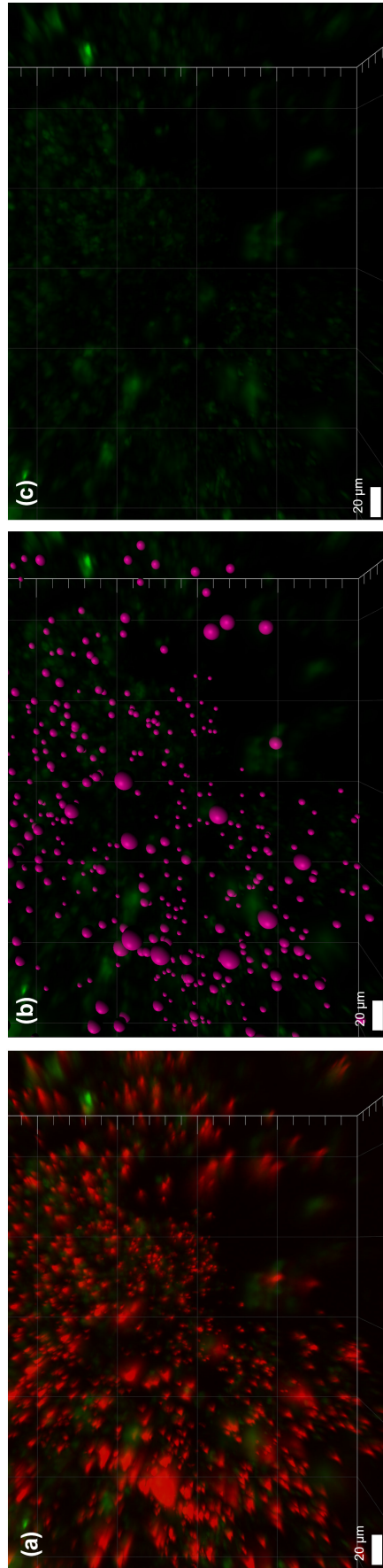


**Figure D.20: 3D images of nanoPS<sub>42</sub> aggregate in *Skeletonema grethae* in 0.01 mg/L treatment.** The image displays an aggregate with 263  $\mu\text{m}$  height, 202  $\mu\text{m}$  width and 25.1  $\mu\text{m}$  depth (total volume 698, 199  $\mu\text{m}^3$ ). There are 14 cells found in this aggregate leading to a total bio-volume of 1583  $\mu\text{m}^3$ . This means that the bio-volume represents a 0.227% of the total aggregate volume. Individual nanoPS<sub>42</sub> cannot be seen, the green spots are agglomerates of nanoPS<sub>42</sub>. Because the nanoPS<sub>42</sub> could not be counted, there is no replacement with spots of the nanoPS<sub>42</sub> in the image. (a) laser image with cells and plastic. (b) cells are replaced with magenta spots, plastic is still from the laser channel. (c) plastic has been removed to make a big gaps between the cells more visible, filled in (b) with nanoPS<sub>42</sub>.





**Figure D.21: 3D images of nanoPS<sub>42</sub> aggregate in *Skeltonemena grethae* in 1 mg/L treatment.** The image displays an aggregate with 21 μm height, 20 μm width and 12 μm depth (total volume 2639 μm<sup>3</sup>). There are 14 cells found in this aggregate leading to a total bio-volume of 1583 μm<sup>3</sup>. This means that the bio-volume represents a very high 60% of the total aggregate volume. While individual nanoPS<sub>42</sub> cannot be seen, the green spots correspond to agglomerates of nanoPS<sub>42</sub>. (a) is the laser image and in (b) the cells are overlaid with the spot tool (blue). The  $z$ -stretch is pretty clear as the diameter of the spots fit in two dimensions with the red laser image and in the third ( $z$ -direction) the laser image is much longer. Two cells at the lower left corner of the image are wider than the spots, while three cells at the upper right are smaller than the blue spot. This shows the natural variation in cell size, demonstrating that the spot tool can identify both smaller and bigger cells correctly. (c) shows only the replaced cells and the plastic. The cells are not closely linked. The bio-volume in the aggregate is higher compared to what is usually observed in the other aggregates of this species and literature [99]. The small size of the aggregate could display an aggregate in the early stages of formation, with the hypothesis that with addition of more cells, the total bio-volume would go down as the aggregates grows.

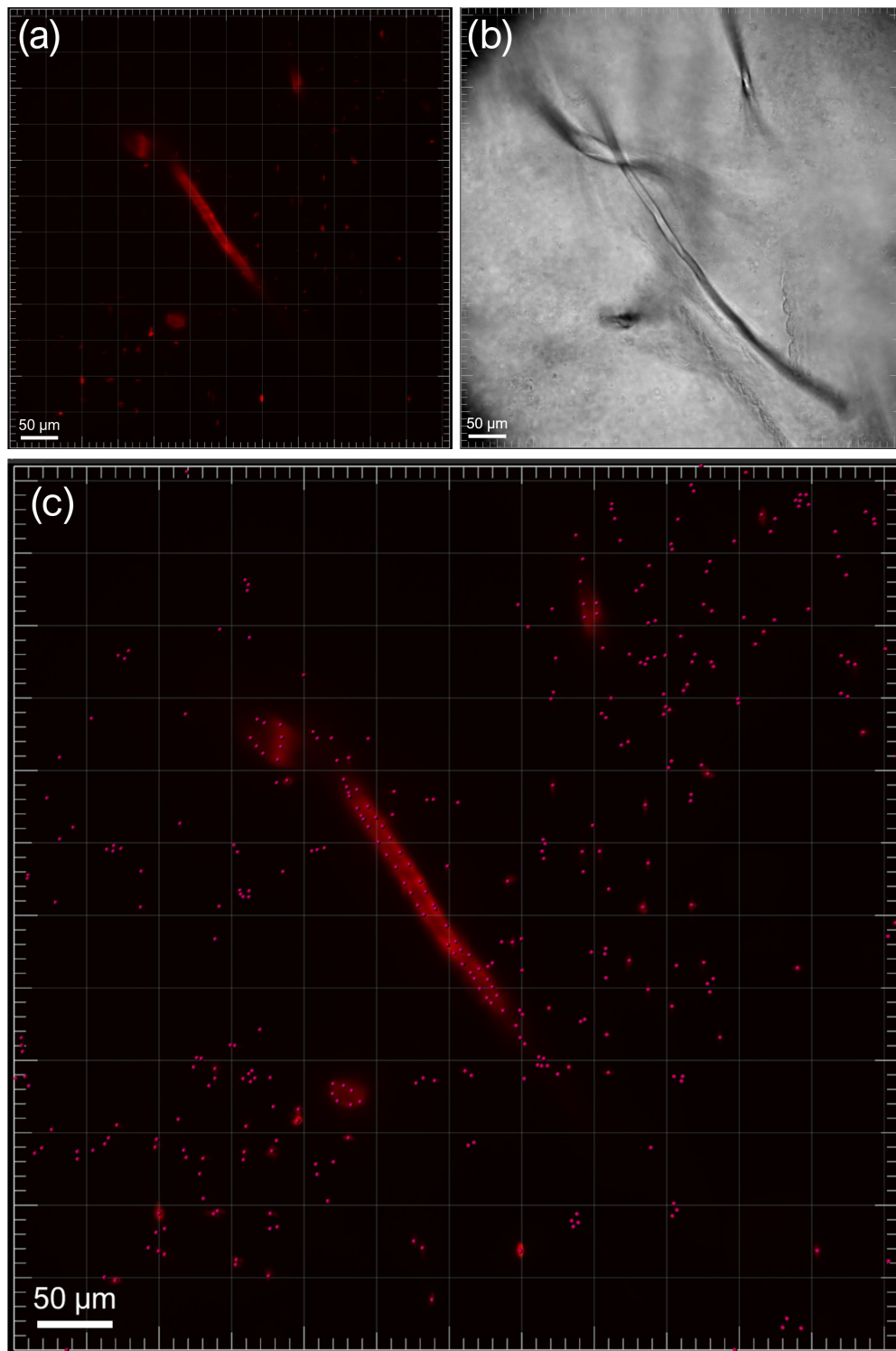


**Figure D.22: 3D images of corner of nanoPS<sub>42</sub> aggregate in *Skeletonema grethae* in the 10 mg/L treatment.** The image displays the lower right corner of an aggregate. (a) is the laser image, and in (b) the cells have been substituted for magenta spots while the plastic is still displayed via the laser. It is easier to see that cells are not connected when the *z*-axis distortion is removed and cells are replaced with spots. In (c) the fine dust in green are small agglomerates of nanoPS<sub>42</sub> caught in the TEP of the aggregate.

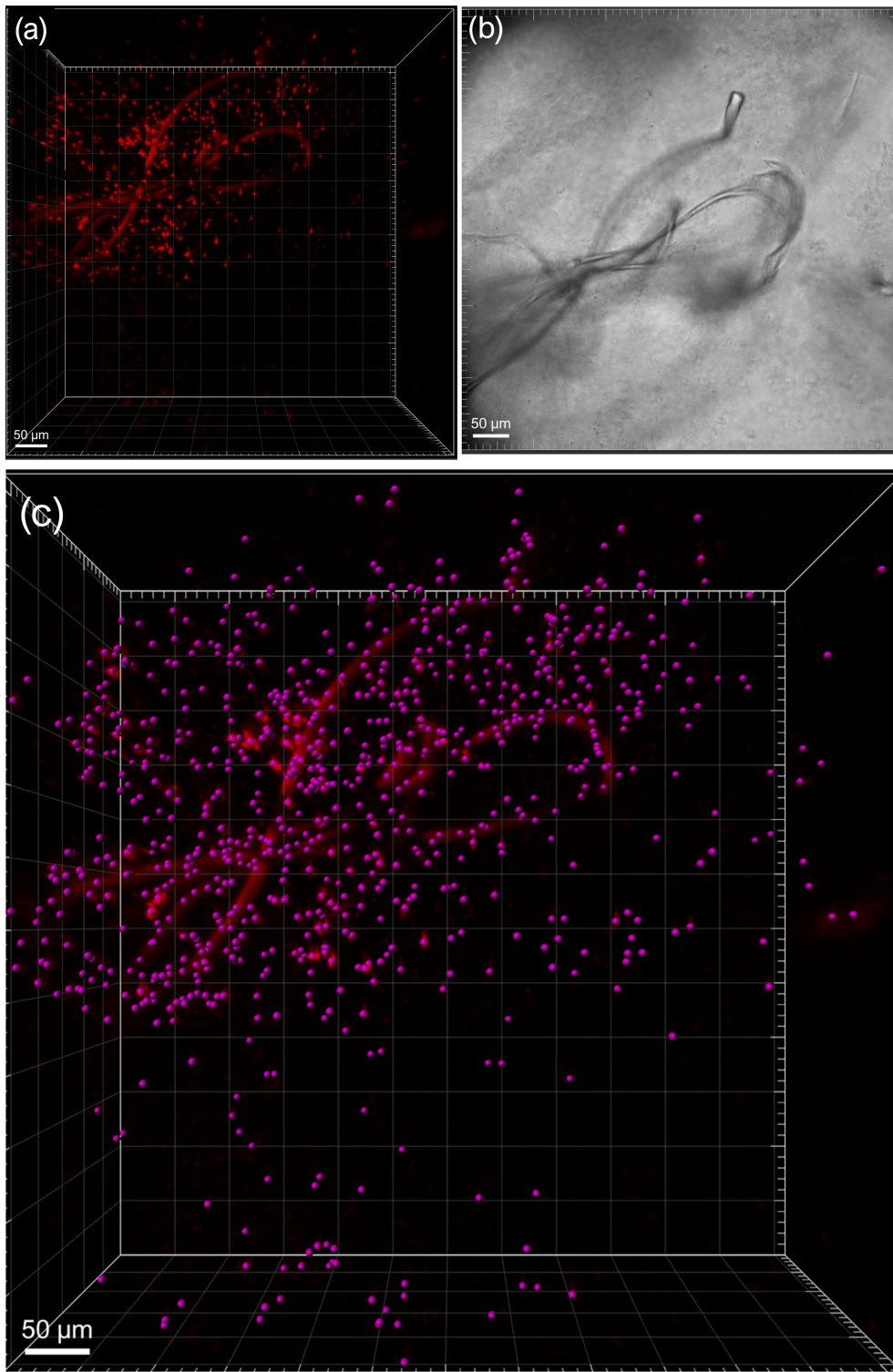
### Polyester Microfiber Experiment in *Skeletonema grethae*

As the MF are not visible in the 3D images without overexposure, no systematic imaging of the aggregates was done. Below, two different aggregates are displayed to give some idea of the internal structure. Aggregates are from the 0.01 mg/L treatment.





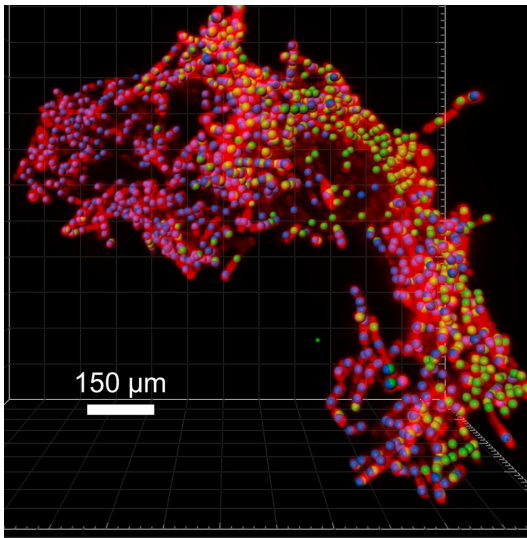
**Figure D.23:** 3D images of pMF aggregate in *Skeletonema grethae*. Only 298 cells were found in the aggregate, none were directly attached to the pMF. It is harder to image with the pMF, as the same overexposure that makes the fiber visible also over counts the cells. (a) is the laser image, (b) shows the brightfield image of the aggregate and in (c) the cells have been counted and overlay the laser image. The 61 spots seen within the fibers are subtracted from the original spot count. (c) is not a 3D image, but a 3D image projected into a plane, making the spots appear different than in the 3D image (see Figure D.24(c)).



**Figure D.24:** 3D images of part of a pMF aggregate in *Skeletonema grethae*. (a) is the laser image, (b) shows the brightfield image of the aggregate and in (c) the cells have been counted and overlay the laser image. More cells can be seen closer to the pMF. No definitive cell count can be given, as not all fibers seen in the brightfield image could be clearly localized within the laser images even under highest overexposure. Thus, spots might correspond to pMF rather than to *Skeletonema grethae* cells.

### D.3 3D images in *Odontella aurita*

The replacement of cells in the *Odontella aurita* images was done by approximating them as spheres with a 20  $\mu\text{m}$  diameter, as *Odontella aurita*'s ellipsoid shape was not seen as individual cells by the software. Rather the chloroplasts within the cells were recognized when sizes in the spot tool were selected to be smaller (see Figure D.25). The cell count is thus not as accurate as for *Skeletonema grethae* and *Synechococcus elongatus*.



**Figure D.25: Method for cell counting in 3D images in *Odontella aurita*.** Blue and green sphere represent the cell. While enough cells were estimated, it is clear that the sphere is smaller than the actual cell in depth.

Differences in the structure of the *Odontella aurita* aggregates compared to the other two species is due to the chain that *Odontella aurita* forms. The control aggregate displayed in Figure D.26 shows how densely the chains are intermingled. In the infected control shown in Figure D.27, small cells are visible in red, indicated between the two blue bars.

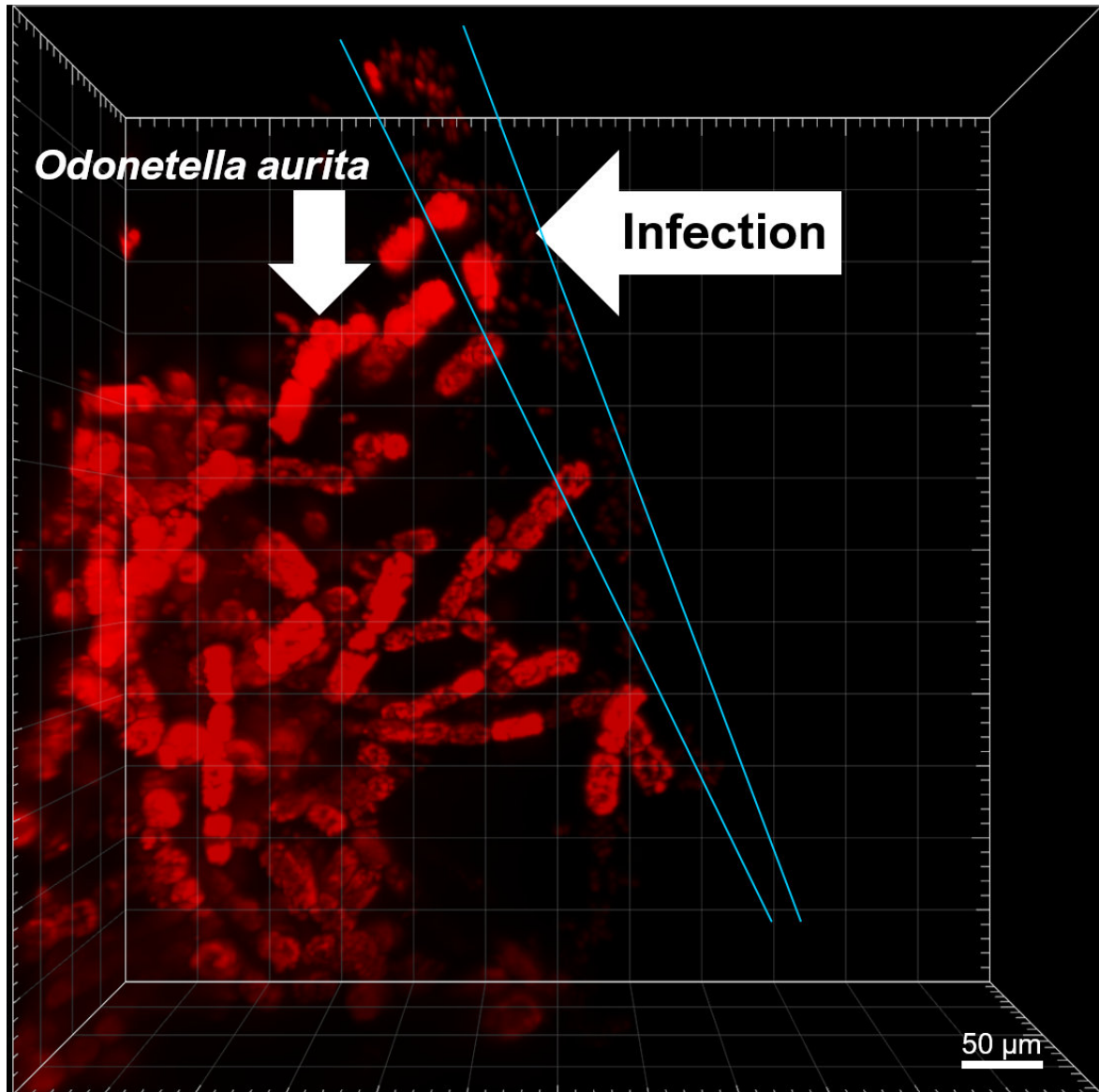
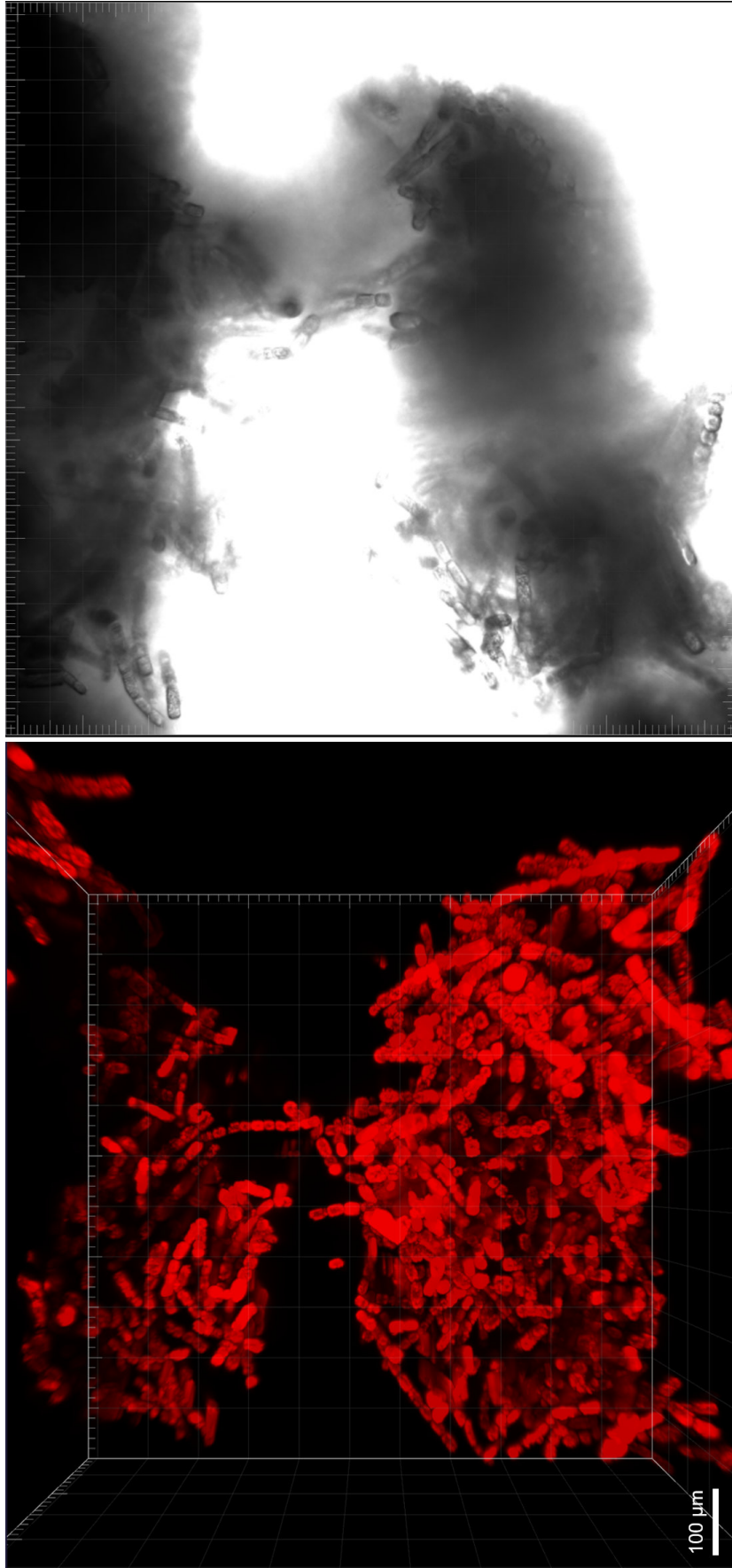
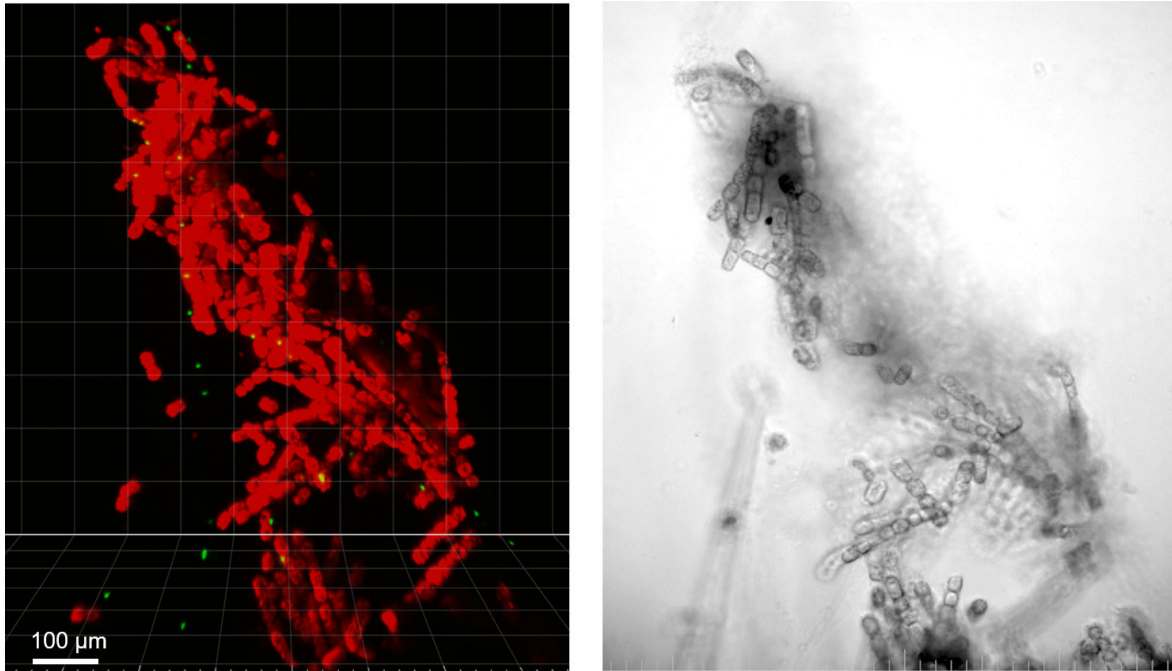


Figure D.27: 3D Image of infected control aggregate of *Odontella aurita*. The small red cells are faintly visible along the outer edge of the *Odontella aurita* aggregate (between the blue bars) from the infected control tank.



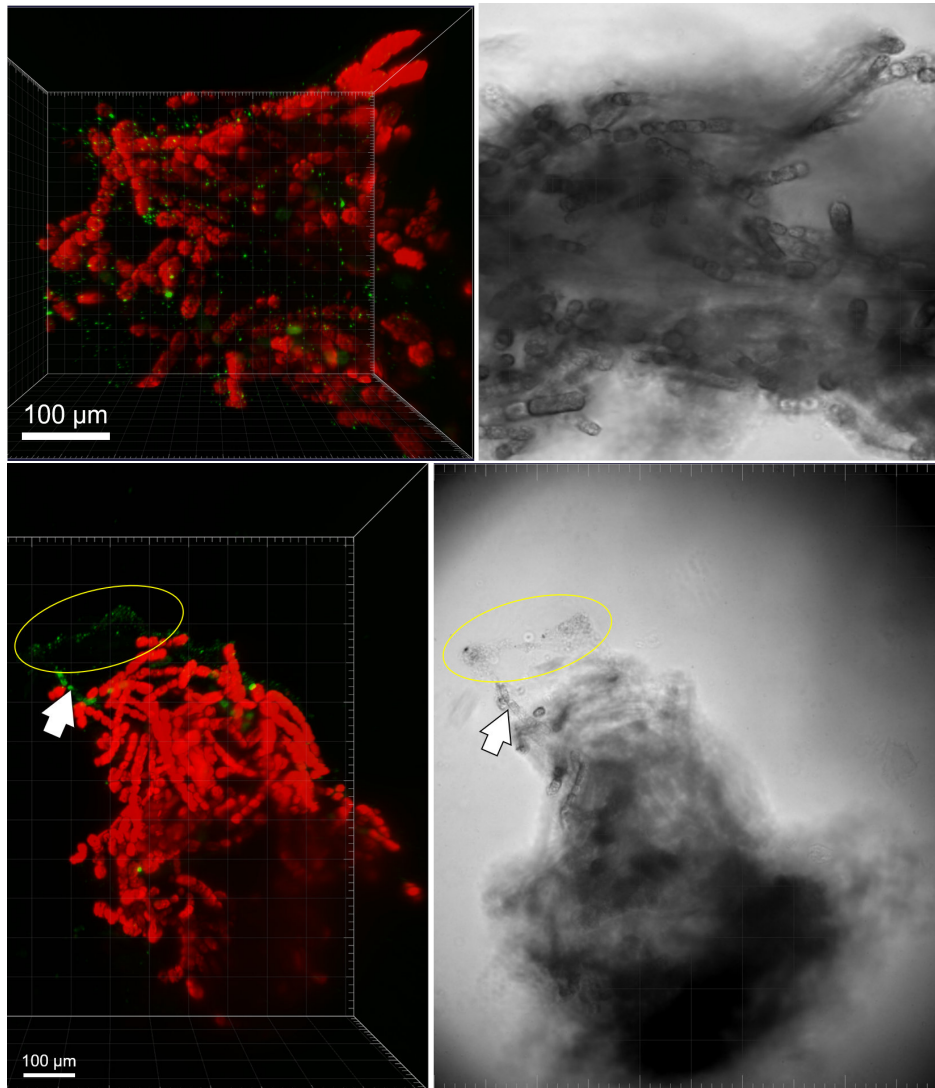
**Figure D.26: Images of a clean control aggregate of *Odontella aurita*.** The dense intermingled cell chains are clearly visible on the 3D image but only on the outside of the aggregate in the brightfield image on the right. The image displays an aggregate with 962  $\mu\text{m}$  height, 966  $\mu\text{m}$  width, and 772  $\mu\text{m}$  depth (total volume of  $3.76 \times 10^8 \mu\text{m}^3$ ). There are about 1158 cells found in this aggregate leading to a total bio-volume of  $9.7 \times 10^6 \mu\text{m}^3$ . This means that the bio-volume represents 2.6% of the total aggregate volume.



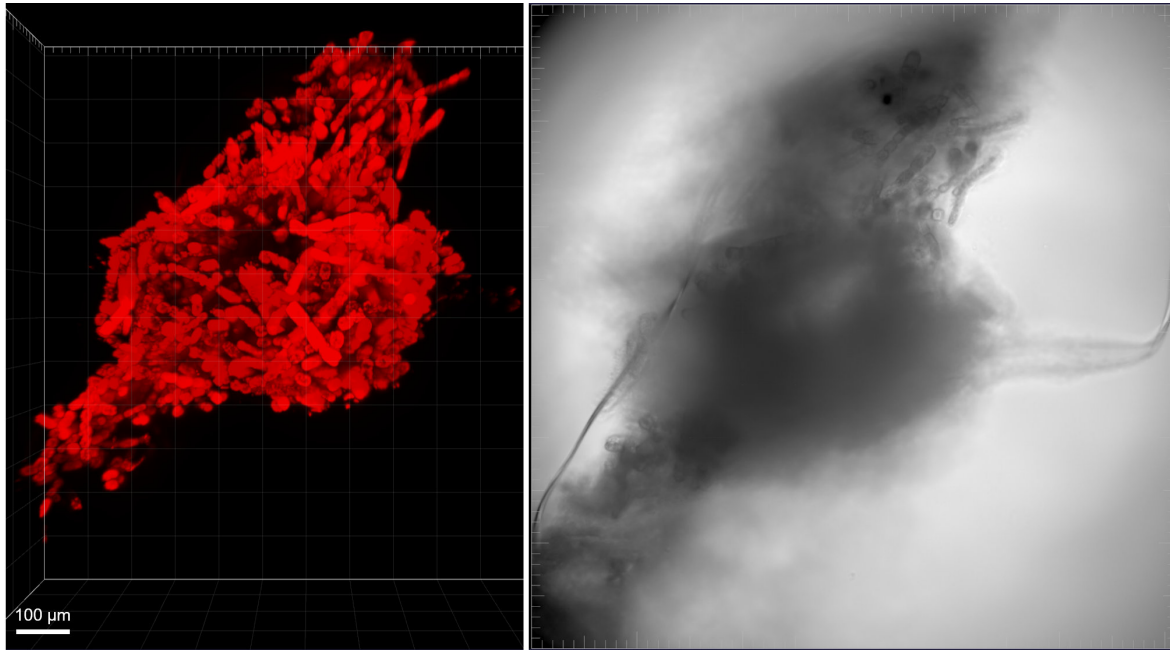


**Figure D.28:** Images of *Odontella aurita* with microPS<sub>2</sub> incorporated into the aggregate. The image displays an aggregate with 854 µm height, 266 µm width, and 310 µm depth (total volume of  $3.69 \times 10^7 \mu\text{m}^3$ ). There are about 569 cells found in this aggregate leading to a total bio-volume of  $4.77 \times 10^6 \mu\text{m}^3$ . This means that the bio-volume represents 12.9% of the total aggregate volume. There are 26 microPS<sub>2</sub> trapped in this aggregate. From the close up it is visible that microPS<sub>2</sub> does not directly attach to the cells but gets trapped in the TEP.

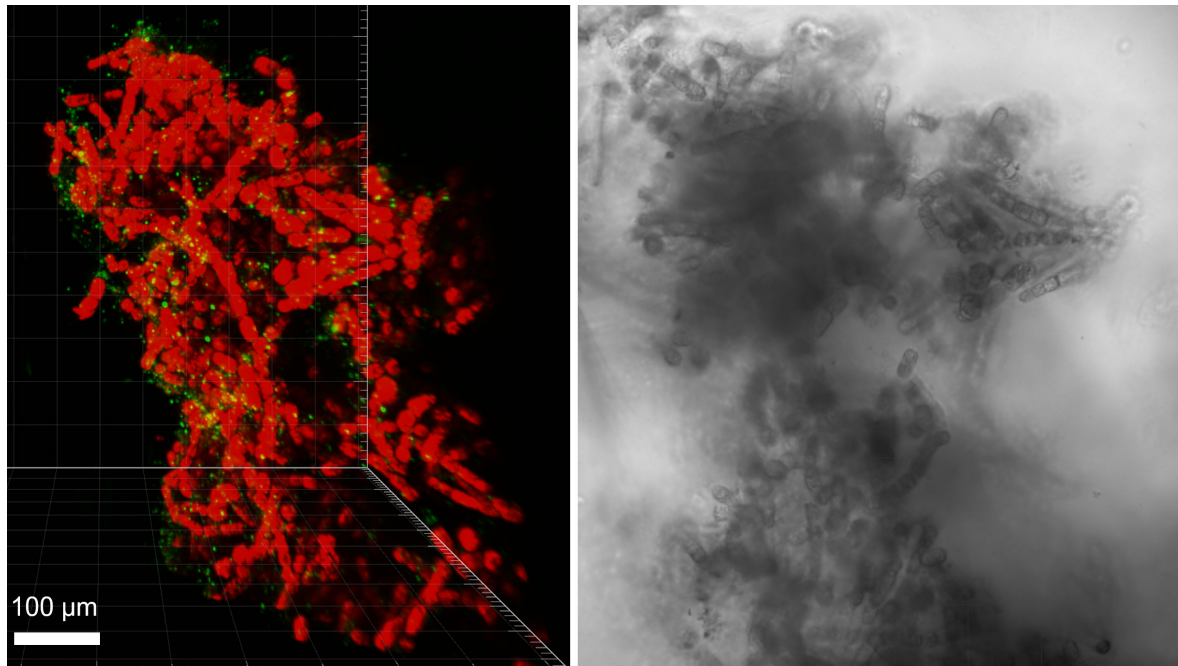




**Figure D.29:** Images of *Odontella aurita* with nanoPS<sub>194</sub> (top) and nanoPS<sub>42</sub> (bottom) incorporated into the aggregate. No individual particles can be seen, but nanoplastic agglomerates are visible in green. Again, these clusters are not directly attached to cells but trapped in the TEP. The direction of the aggregate is slightly rotated between the two images. Top image: The image displays an aggregate with 1066  $\mu\text{m}$  height, 915  $\mu\text{m}$  width, and 906  $\mu\text{m}$  depth (total volume of  $4.63 \times 10^8 \mu\text{m}^3$ ). There are about 1237 cells found in this aggregate leading to a total bio-volume of  $1.04 \times 10^7 \mu\text{m}^3$ . This means that the bio-volume represents 2.24% of the total aggregate volume. Bottom image: the white arrow points to dead *Odontella aurita* cells, which appear green in the 3D image. The yellow circle shows nanoPS<sub>42</sub> trapped in TEP. The image displays an aggregate with 799  $\mu\text{m}$  height, 511  $\mu\text{m}$  width, and 512  $\mu\text{m}$  depth (total volume of  $1.09 \times 10^8 \mu\text{m}^3$ ). There are about 445 cells found in this aggregate leading to a total bio-volume of  $3.73 \times 10^6 \mu\text{m}^3$ . This means that the bio-volume represents 3.4% of the total aggregate volume.



**Figure D.30: Images of *Odontella aurita* with acrylic fibers incorporated into the aggregate.** The fibers are visible in the brightfield but not in the 3D image as they are not fluorescent. The image displays an aggregate with 1321  $\mu\text{m}$  height, 554  $\mu\text{m}$  width, and 695  $\mu\text{m}$  depth (total volume of  $2.66 \times 10^8 \mu\text{m}^3$ ). There are about 674 cells found in this aggregate leading to a total bio-volume of  $5.65 \times 10^6 \mu\text{m}^3$ . This means that the bio-volume represents 2.12% of the total aggregate volume.



**Figure D.31:** Images of infected *Odontella aurita* with nanoPS<sub>42</sub> incorporated into the aggregate. Individual nanoPS<sub>42</sub> cannot be seen but the beads clump together and are trapped within the TEP. No ciliate cells are visible in this image. The image displays an aggregate with 1192  $\mu\text{m}$  height, 899  $\mu\text{m}$  width, and 1084  $\mu\text{m}$  depth (total volume of  $6.08 \times 10^8 \mu\text{m}^3$ ). There are about 1158 cells found in this aggregate leading to a total bio-volume of  $9.7 \times 10^6 \mu\text{m}^3$ . This means that the bio-volume represents 1.6% of the total aggregate volume.